SYSTEM DESCRIPTION AND PERFORMANCE DATA FOR THE USAF/CAL VARIABLE STABILITY T-33 AIRPLANE

G. WARREN HALL
RONALD W. HUBER

FOREWORD

This report was prepared by the Flight Research Department of the Cornell Aeronautical Laboratory, Inc. (CAL), Buffalo, New York, under USAF Contract No. F33615-69-C-1664. The contract was initiated under Project No. 8219, "Stability and Control Investigations," Task No. 821905, "Flying Qualities Design Requirements for Military Airplanes." The work was administered by the Air Force Flight Dynamics Laboratory, Wright-Patterson Air Force Base, Ohio, Mr. David K. Bowser (FDCC), Project Engineer.

Mr. F.D. Newell was the T-33 Program Manager for CAL.

This report was submitted by the authors in May 1970.

The contractor's report number is CAL Report BM-2821-F-2.

This technical report has been reviewed and is approved.

C.B. Westbrook
Chief, Control Criteria Branch
Air Force Flight Dynamics Laboratory

ABSTRACT

The USAF/CAL variable stability T-33 airplane is a jet trainer which has been extensively modified for use as a research vehicle. A response-feedback system allows the normal T-33 derivatives to be augmented so that handling qualities of existing airplanes, future airplanes, or hypothetical configurations may be simulated in flight or in a fixed-base ground simulator. This report has been prepared to provide an updated functional description of the variable stability T-33. The information is presented for setting up a simulation program and for performing calibration procedures. A brief description of the equipment and airplane systems is also included.

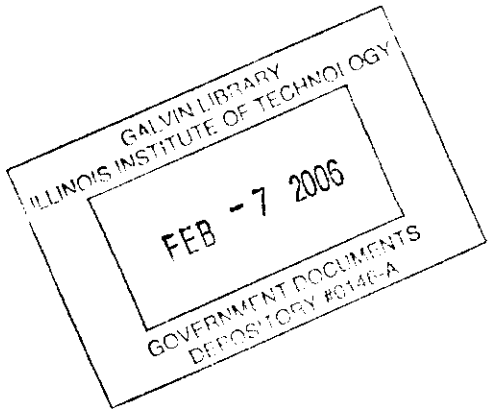

TABLE OF CONTENTS

TABLE OF CONTENTS (CONT.)

TABLE OF CONTENTS (CONCLUDED)

LIST OF FIGURES

LIST OF TABLES

LIST OF SYMBOLS

I. AIRCRAFT GEOMETRY, MASS AND INERTIA

AR - b^2/S - wing aspect ratio

b - reference span, ft

c - wing chord, ft

$\bar{c}$ - mean aerodynamic chord, ft

$c.g.$ - center of gravity

$\mathbb{C}$ - center line

g - gravitational constant, 32.17 ft/sec^2

h_x - moment of momentum about the x axis, slug/sec-ft^3, ft^2-lb sec

h_y - moment of momentum about the y axis, slug/sec-ft^3, ft^2-lb sec

h_z - moment of momentum about the z axis, slug/sec-ft^3, ft^2-lb sec

I_{xx} - moment of inertia about x-body axis, slug-ft^2, ft-lb sec^2

I_{yy} - moment of inertia about y-body axis, slug-ft^2, ft-lb sec^2

I_{zz} - moment of inertia about z-body axis, slug-ft^2, ft-lb sec^2

I_{xz} - product of inertia, body axes, slug-ft^2, ft-lb sec^2

ℓ - distance from c.g. to cockpit, ft

$m = \frac{W}{g}$ - aircraft mass, slugs,

RFS - response feedback system

S - reference area, ft^2

W - aircraft weight, lb

W/S - wing loading, lb/ft^2

x - distance from c.g. to arbitrary point along x-body axis, ft

$\bar{x}$ - c.g. location ahead of position for which basic data applies, ft

$\bar{y}$ - distance from c.g. to arbitrary point along y body axis, ft

$\bar{z}$ - distance from c.g. to arbitrary point along z body axis, ft

z_i - perpendicular distance from c.g. to thrust line

ξ - angle between x axis and thrust line, radian or deg

II. AIRCRAFT MOTION VARIABLES

a - speed of sound, ft/sec

h_p - pressure altitude, ft

M - Mach number

n_x - longitudinal acceleration, g's, positive along + x-wind axis

n_y - lateral acceleration, g's, positive along + y-body axis

n_z - normal acceleration, g's, positive along +z-body axis

p - roll rate, component of angular velocity about x-body axis, rad/sec or deg/sec

p_g - incremental roll rate due to gusts, rad/sec or deg/sec

q - pitch rate, component of angular velocity about y-body axis, rad/sec or deg/sec

q_g - incremental pitch rate due to gusts, rad/sec or deg/sec

$\bar{q}$ - dynamic pressure, $\frac{1}{2}\rho V^2$

r - yaw rate, component of angular velocity about z-body axis, rad/sec or deg/sec

u - velocity along x axis

V - total velocity of c.g., ft/sec

v - velocity along y axis

w - velocity along z axis

x, y, z - stability axes (i.e., a right hand orthogonal body axis system with origin at the c.g., the z axis in the plane of symmetry and the x axis aligned with the relative wind at zero sideslip trim flight).

α - airplane angle of attack from trim level flight, radians or degrees

α_G - incremental angle of attack due to gusts, radian or degrees

α_o - airplane trim angle of attack

β - angle of sideslip, radian or degrees

β_G - incremental sideslip angle due to gusts, radians or degrees

$\dot{\beta}$ - sideslip rate, radians/sec or degrees/sec

γ - flight path angle from horizontal, radians or degrees

θ - pitch angle from trim level flight, radians or degrees

η - angle between thrust line and fuselage reference line

ϕ - bank angle, radians or degrees

ψ - heading angle, radians or degrees

θ, ϕ, ψ - Euler angles defining orientation of body axes, radians or degrees

ρ - air density, slugs/ft^3

$\rho_o, \rho_h, \rho_{h^2}$ - coefficients in polynominal expression for density as a function of altitude

III. AIRCRAFT DYNAMIC MODE PROPERTIES

ζ_d - Dutch roll damping ratio

ζ_{FS} - feel system damping ratio

ζ_p - phugoid damping ratio

ζ_{RS} - roll spiral damping ratio

ζ_{SP} - short period damping ratio

ζ_β - damping ratio of numerator quadratic in sideslip to aileron input transfer function

ζ_ϕ - damping ratio of numerator quadratic in roll to aileron input transfer function

ζ_r - damping ratio of numerator quadratic in yaw rate to aileron input transfer function

τ - time constant, seconds

τ_R - roll mode time constant, seconds

τ_S - spiral mode time constant, seconds

$\lambda_{r_{1,2,3}}$ - real roots of numerator cubic in yaw-rate-to-aileron input transfer function

$\lambda_{\beta_{1,2,3}}$ - real roots of numerator cubic in sideslip-to-aileron-input transfer function

$\lambda_{\phi_{1,2,3}}$ - real roots of numerator quadratic in bank-angle-to-aileron-input transfer function

$|p/r|$ - magnitude of roll rate to yaw rate ratio

$|\phi/r|$ - magnitude of roll to yaw rate ratio

$|\phi/\beta|$ - magnitude of roll to sideslip ratio

ω - imaginary part of $s = \sigma + j\omega$

ω_d - Dutch roll undamped natural frequency, radians/sec

ω_{FS} - feel system undamped natural frequency, radians/sec

ω_p - phugoid undamped natural frequency, radians/sec

ω_r - undamped natural frequency of numerator quadratic in yaw rate to aileron input transfer function, radians/second

ω_{RS} - roll spiral undamped natural frequency, radians/sec

ω_β - undamped natural frequency of numerator quadratic in sideslip to aileron input transfer function, radians/sec

ω_ϕ - undamped natural frequency of numerator quadratic in bank angle to aileron input transfer function, radians/sec

IV. FORCES AND MOMENTS

D - drag, lb

L - lift, lb

$\mathcal{L}$ - rolling moment about x-body axis, ft-lb

M - pitching moment about y-body axis, ft-lb

N - yawing moment about z-body axis, ft-lb

T - thrust, lb

X - component of aerodynamic forces along x-body axis, lb

C_C - coefficient of axial force along x-body axis

C_{D_0} - drag coefficient at zero angle of attack

C_{D_p} - drag coefficient of tip tank petals

C_{L_0} - lift coefficient at zero angle of attack

C_{m_0} - pitching moment coefficient at zero angle of attack

C_N - coefficient of normal force along z-body axis

V. NONDIMENSIONAL STABILITY DERIVATIVES

$C_D = \frac{D}{\bar{q}S}$ drag coefficient

$C_{D_u} = \frac{u}{2}\frac{\partial C_D}{\partial u}$ change in drag coefficient with variation in forward speed

$C_{D_\alpha} = \frac{\partial C_D}{\partial \alpha}$ change in drag coefficient with variation in angle of attack, rad^{-1} or deg^{-1}

$C_{D_{\delta_e}} = \frac{\partial C_D}{\partial \delta_e}$ change in drag coefficient with a change in elevator deflection, rad^{-1} or deg

$C_L = \frac{L}{\bar{q}S}$ lift coefficient

$C_{L_u} = \frac{u}{2}\frac{\partial C_L}{\partial u}$ change in lift coefficient with variation in forward speed

$C_{L_\alpha} = \frac{\partial C_L}{\partial \alpha}$ change in lift coefficient with variation in angle of attack, lift curve slope, rad^{-1}

$C_{L_{\dot{\alpha}}} = \frac{2u}{\bar{c}} \frac{\partial C_L}{\partial \dot{\alpha}}$ change in lift coefficient with variation in time rate of change of angle of attack, rad^{-1}

$C_{L_q} = \frac{2u}{\bar{c}} \frac{\partial C_L}{\partial q}$ change in lift coefficient with no change of angle of attack with varying pitching velocity, rad^{-1}

$C_{L_{\delta_e}} = \frac{\partial C_L}{\partial \delta_e}$ change in lift coefficient with change in elevator deflection, rad^{-1}

$C_m = \frac{M}{\bar{q} S \bar{c}}$ pitching moment coefficient

$C_{m_u} = \frac{u}{2} \frac{\partial C_m}{\partial u}$ change in pitching moment coefficient with variation in forward speed

$C_{m_\alpha} = \frac{\partial C_m}{\partial \alpha}$ change in pitching moment coefficient with variation in angle of attack, longitudinal static stability derivative, rad^{-1}

$C_{m_{\dot{\alpha}}} = \frac{2u}{\bar{c}} \frac{\partial m}{\partial \dot{\alpha}}$ change in pitching moment coefficient with variation in time rate of change of angle of attack, rad^{-1}

$C_{m_q} = \frac{2u}{q} \frac{\partial C_m}{\partial q}$ change in pitching moment coefficient with variation in pitch rate. The pitch damping derivative, rad^{-1}

$C_{m_{\delta_e}} = \frac{\partial C_m}{\partial \delta_e}$ change in pitching moment coefficient with change in elevator deflection, elevator effectiveness or control power, rad^{-1}

$C_n = \frac{N}{\bar{q} S b}$ yawing moment coefficient

$C_{n_\beta} = \frac{\partial C_n}{\partial \beta}$ change in yawing moment coefficient with variation in sideslip angle, static directional derivative, rad^{-1}

$C_{n_{\dot{\beta}}} = \frac{2u}{b} \frac{\partial C_n}{\partial \dot{\beta}}$ change in yawing moment coefficient with variation in time rate of change in sideslip angle, rad^{-1}

$C_{n_p} = \frac{2u}{b} \frac{\partial C_n}{\partial p}$ change in yawing moment coefficient with variation in rolling velocity

$C_{n_r} = \frac{2u}{b}\frac{\partial C_n}{\partial r}$ change in yawing moment coefficient with variation in yawing velocity. The yaw damping derivative, rad^{-1}

$C_{n_\beta} = \frac{\partial C_n}{\partial \beta}$ change in yawing moment coefficient with variation in sideslip angle. The static directional derivative, rad^{-1}

$C_{n_{\dot\beta}} = \frac{2u}{b}\frac{\partial C_n}{\partial \dot\beta}$ change in yawing moment coefficient with variation in rate of change of sideslip angle, rad^{-1}

$C_{n_{\delta_a}} = \frac{\partial C_n}{\partial \delta_a}$ change in yawing moment coefficient with change of aileron deflection, rad^{-1}

$C_{n_{\delta_r}} = \frac{\partial C_n}{\partial \delta_r}$ change in yawing moment coefficient with change of rudder deflection, rad^{-1}

$C_y = \frac{Y}{\bar{q}S}$ side force coefficient

$C_{y_\beta} = \frac{\partial C_y}{\partial \beta}$ change in side force coefficient with variation in sideslip angle, rad^{-1}

$C_{y_{\dot\beta}} = \frac{2u}{b}\frac{\partial C_y}{\partial \dot\beta}$ change in side force coefficient with variation in time rate of change of sideslip angle. The side force damping derivative, rad^{-1}

$C_{y_p} = \frac{2u}{b}\frac{\partial C_y}{\partial p}$ change in side force coefficient with variation in rolling velocity, rad^{-1}

$C_{y_r} = \frac{2u}{b}\frac{\partial C_y}{\partial r}$ the change in side force coefficient with variation in yawing velocity, rad^{-1}

$C_{y_{\delta_a}} = \frac{\partial C_y}{\partial \delta_a}$ change in side force coefficient with variation in aileron deflection, rad^{-1}

$C_{y_{\delta_r}} = \frac{\partial C_y}{\partial \delta_r}$ change in side force coefficient with variation in rudder deflection, rad^{-1}

$C_\ell = \frac{L}{\bar{q}Sb}$ rolling moment coefficient

$C_{l_\beta} = \frac{\partial C_l}{\partial \beta}$ change in rolling moment coefficient with variation in sideslip angle. The effective dihedral derivative, rad^{-1}

$C_{l_{\dot\beta}} = \frac{2u}{b}\frac{\partial C_l}{\partial \dot\beta}$ change in rolling moment coefficient with variation in time rate of change of sideslip angle, rad^{-1}

$C_{l_p} = \frac{2u}{b}\frac{\partial C_l}{\partial p}$ change in rolling moment coefficient with variation in rolling velocity, the roll damping derivative, rad^{-1}

$C_{l_r} = \frac{2u}{b}\frac{\partial C_l}{\partial r}$ change in rolling moment coefficient with variation in yawing velocity, rad^{-1}

$C_{l_{\delta_a}} = \frac{\partial C_l}{\partial \delta_a}$ change in rolling moment coefficient with variation in aileron deflection, aileron effectiveness or aileron power, rad^{-1}

$C_{l_{\delta_r}} = \frac{\partial C_l}{\partial \delta_r}$ change in rolling moment coefficient with variation in rudder deflection, rad^{-1}

VI. DIMENSIONAL DERIVATIVES

L - rolling moment about x-body axis, ft-lb

$L_\beta = \frac{1}{I_{xx}}\frac{\partial L}{\partial \beta} = \frac{\rho S U^2 b}{2I_{xx}} C_{l_\beta}$ - changes in rolling moment, L, due to a variation in sideslip angle, sec^{-2} rad^{-1}

$L_{\dot\beta} = \frac{1}{I_{xx}}\frac{\partial L}{\partial \dot\beta} = \frac{\rho S U b^2}{4I_{xx}} C_{l_{\dot\beta}}$ - change in rolling moment, L, due to a variation in time rate of change of sideslip angle, sec^{-1} rad^{-1}

$L_p = \frac{1}{I_{xx}}\frac{\partial L}{\partial p} = \frac{\rho S U b^2}{4I_{xx}} C_{l_p}$ - change in rolling moment, L, due to a variation in rolling velocity, sec^{-1} rad^{-1}

$L_r = \frac{1}{I_{xx}}\frac{\partial L}{\partial r} = \frac{\rho S U b^2}{4I_{xx}} C_{l_r}$ - change in rolling moment, L, due to a variation in yawing velocity, sec^{-1} rad^{-1}

$L_{\delta_a} = \frac{1}{I_{xx}}\frac{\partial L}{\partial \delta_a} = \frac{\rho S U b^2}{2I_{xx}} C_{l_{\delta_a}}$ - change in rolling moment, L, due to a variation in aileron deflection, sec^{-2} rad^{-1}

$L_{\delta_r} = \frac{1}{I_{xx}}\frac{\partial L}{\partial \delta_r} = \frac{\rho S U b^2}{2I_{xx}} C_{l_{\delta_r}}$ - change in rolling moment, L, due to a variation in rudder deflection, sec^{-2} rad^{-1}

$$L'_i = \left(1 - \frac{I_{xz}^2}{I_{xx} I_{zz}}\right)^{-1} \left(L_i + \frac{I_{xz}}{I_{xx}} N_i\right)$$ $i = \beta, \dot{\beta}, p, r, \delta_a, \delta_r$ - Primed rolling moment derivatives

M - pitching moment about y-body axis, ft-lb

$M_u = \frac{1}{I_{yy}} \frac{\partial M}{\partial u} = \frac{\rho S U \bar{c}}{I_{yy}} C_m + C_{m_u}$ - change in pitching moment, M, due to a variation in forward speed, sec^{-1} ft^{-1}

$M_\alpha = \frac{1}{I_{yy}} \frac{\partial M}{\partial \alpha} = \frac{\rho U^2 S \bar{c}}{I_{yy}} C_{m_\alpha}$ - change in pitching moment, M, due to a variation in angle of attack, sec^{-2}

$M_{\dot{\alpha}} = \frac{1}{I_{yy}} \frac{\partial M}{\partial \dot{\alpha}} = \frac{\rho U S c^2}{I_{yy}} C_{m_{\dot{\alpha}}}$ - change in pitching moment, M, due to a variation in time rate of change of angle of attack, sec^{-1}

$M_w = \frac{1}{I_{yy}} \frac{\partial M}{\partial w} = \frac{\rho S U c}{2 I_{yy}} C_{m_\alpha}$ - change in pitching moment, M, due to a variation in speed along in z-axis, sec^{-1} ft^{-1}

$M_{\dot{w}} = \frac{1}{I_{yy}} \frac{\partial M}{\partial \dot{w}} = \frac{\rho S c^2}{4 I_{yy}} C_{m_{\dot{\alpha}}}$ - change in pitching moment, M, due to a variation in the time rate of change of speed along the y-axis, ft^{-1}

$M_q = \frac{1}{I_{yy}} \frac{\partial M}{\partial q} = \frac{\rho S c^2}{4 I_{yy}} C_{m_q}$ - change in pitching moment, M, due to a variation in pitch velocity, sec^{-1} rad^{-1}

$M_{\delta_e} = \frac{1}{I_{yy}} \frac{\partial M}{\partial \delta_e} = \frac{\rho S U^2 c}{2 I_{yy}} C_{m_{\delta_e}}$ - change in pitching moment, M, due to a variation in elevator deflection, sec^{-2} rad^{-1}

N - yawing moment about z-body axis, ft-lb

$N_\beta = \frac{1}{I_{zz}} \frac{\partial N}{\partial \beta} = \frac{\rho S U^2 b}{2 I_{zz}} C_{n_\beta}$ - change in yawing moment, N, due to a variation in sideslip angle, sec^{-2} rad^{-1}

$N_{\dot{\beta}} = \frac{1}{I_{zz}} \frac{\partial N}{\partial \dot{\beta}} = \frac{\rho S U b^2}{4 I_{zz}} C_{n_{\dot{\beta}}}$ - change in yawing moment, N, due to a variation in time rate of change of sideslip angle, sec^{-1} rad^{-1}

$N_p = \frac{1}{I_{zz}} \frac{\partial N}{\partial p} = \frac{\rho S U b^2}{4 I_{zz}} C_{n_p}$ - change in yawing moment, N, due to a variation in rolling velocity, sec^{-1} rad^{-1}

$N_r = \frac{1}{I_{zz}} \frac{\partial N}{\partial r} = \frac{\rho S U b^2}{4 I_{zz}} C_{n_r}$ - change in yawing moment, N, due to a variation in yawing velocity, sec^{-1} rad^{-1}

$N_{\delta_a} = \frac{1}{I_{zz}} \frac{\partial N}{\partial \delta_a} = \frac{\rho S U^2 b}{2 I_{zz}} C_{n_{\delta_a}}$ - change in yawing moment, N, due to a variation in aileron deflection, sec^{-2} rad^{-1}

$N_{\delta_r} = \frac{1}{I_{zz}} \frac{\partial N}{\partial \delta_r} = \frac{\rho S U^2 b}{2 I_{zz}} C_{n_{\delta_r}}$ - change in yawing moment, N, due to a variation in rudder deflection, sec^{-2} rad^{-1}

$N'_i = \left(1 - \frac{I_{xz}^2}{I_{xx} I_{zz}}\right)^{-1} \left(N_i + \frac{I_{xz}}{I_{zz}} L_i\right)$ $i = \beta, \dot{\beta}, p, r, \delta_a, \delta_r$ - Primed yawing moment derivation

$X_u = \frac{1}{mU} \frac{\partial X}{\partial u} = \frac{\rho S U}{m} (-C_D - C_{D_u})$ - change in X force due to a variation in forward speed, sec^{-1}

$X_w = \frac{1}{mU} \frac{\partial X}{\partial w} = \frac{\rho S U}{2m} (C_L - C_{D_\alpha})$ - change in X force due to a variation in speed along the z-axis, sec^{-1}

$X_{\delta_e} = \frac{1}{mU} \frac{\partial X}{\partial \delta_e} = \frac{\rho S U^2}{2m} (-C_{D_{\delta_e}})$ - change in X force due to a variation in elevator deflection

$Y_\beta = Y_v = \frac{1}{mU} \frac{\partial Y}{\partial \beta} = \frac{\rho S U}{2m} (C_{Y_\beta})$ - change in Y force due to a variation in sideslip angle, sec^{-1} rad^{-1}

$Y_{\dot{\beta}} = Y_{\dot{v}} = \frac{1}{mU} \frac{\partial Y}{\partial \dot{\beta}} = \frac{\rho S b}{4m} (C_{Y_{\dot{\beta}}})$ - change in Y force due to a variation in time rate of change of sideslip angle, rad^{-1}

$Y_p = \frac{1}{mU} \frac{\partial Y}{\partial p} = \frac{\rho S b}{4m} (C_{Y_p})$ - change in Y force due to a variation in rolling velocity, rad^{-1}

$Y_r = \frac{1}{mU} \frac{\partial Y}{\partial r} = \frac{\rho S b}{4m} (C_{Y_r})$ - change in Y force due to a variation in yawing velocity, rad^{-1}

$Y_{\delta_a} = \frac{1}{mU} \frac{\partial Y}{\partial \delta_a} = \frac{\rho S U}{2m} (C_{Y_{\delta_a}})$ - change in Y force due to a variation in aileron deflection, sec^{-1} rad^{-1}

$Y_{\delta_r} = \frac{1}{mU} \frac{\partial Y}{\partial \delta_r} = \frac{\rho S U}{2m} (C_{Y_{\delta_r}})$ - change in Y force due to a variation in rudder deflection, sec^{-1} rad^{-1}

$Z_\alpha = -L_\alpha = \frac{\rho S U}{2m} (-C_{L_\alpha})$ - change in Z force due to a variation in angle of attack, sec^{-1}

$Z_u = \frac{1}{m} \frac{\partial Z}{\partial u} = \frac{\rho S U}{m} (-C_L - C_{L_u})$ - change in Z force due to a variation in forward speed, sec^{-1}

$Z_w = Z_{\frac{\alpha}{u_o}} = \frac{1}{m} \frac{\partial Z}{\partial w} = \frac{\rho S U}{2m} (-C_{L_\alpha} - C_D)$ - change in Z force due to a variation in speed along the z-axis, sec-1

$Z_{\dot{w}} = \frac{1}{m} \frac{\partial Z}{\partial \dot{w}} = \frac{\rho S \bar{c}}{4m} (-C_{L_{\dot{\alpha}}})$ - change in Z force due to a variation in time rate of change of speed along the z-axis

$Z_q = \frac{1}{m} \frac{\partial Z}{\partial q} = \frac{\rho S U \bar{c}}{4m} (-C_{L_q})$ - change in Z force due to a variation in pitching velocity, ft sec^{-1} rad^{-1}

$Z_{\delta_e} = -L_{\delta_e} = \frac{1}{m} \frac{\partial Z}{\partial \delta_e} = \frac{\rho S U^2}{2m} (-C_{L_{\delta_e}})$ - change in Z force due to a variation in elevator deflection, sec^{-2} rad^{-1}

VII. CONTROL SYSTEM VARIABLES

δ_a - aileron deflection, positive right aileron trailing edge down, rad or deg

δ_{aT} - total aileron deflection, rad or deg

δ_{AS}, δ_{AW} - aileron stick or wheel rotation, positive stick right or wheel rotation clockwise when observed along the positive x axis, rad or deg

δ_e - elevator deflection, positive trailing edge down, rad or deg

δ_{ES} - elevator stick or wheel deflection, positive stick or wheel deflection aft, rad or deg

δ_r - rudder deflection, positive trailing edge left, rad or deg

δ_{RP} - rudder pedal deflection, positive right rudder pedal forward

F_{AS}, F_{AW} - aileron stick or wheel force, positive stick right or wheel rotation clockwise when observed along the positive x axis, lbs

F_{ES} - elevator stick or wheel force, positive aft, lbs

F_{RP} - rudder pedal force - positive right rudder pedal forward, lbs

δ_T - throttle deflection, positive throttle forward

δ_a/δ_{AS} - aileron gear ratio

δ_a/δ_r - aileron rudder interconnect

F_{AS}/δ_{AS} - aileron stick or wheel force gradient, lbs/in. or lbs/deg

δ_a/β - RFS sideslip angle to aileron gain, deg/deg

$\delta_a/\dot{\beta}$ - RFS sideslip angle rate to aileron gain, sec

δ_a/p - RFS roll rate to aileron gain, sec

$\delta_a/\dot{p}$ - RFS roll acceleration to aileron gain, sec^2

δ_a/r - RFS yaw rate to aileron gain, sec

$\delta_a/\dot{r}$ - RFS yaw acceleration to aileron gain, sec^2

δ_a/X - RFS variable feedback to aileron gain, where X may be replaced by any desired parameter

$\delta_e/_{IN}$ - automatic and random noise input to aileron gain

δ_e/δ_{ES} - elevator gear ratio

F_{ES}/δ_{ES} - elevator stick or wheel force gradient lbs/in. or lbs/deg

δ_e/α - RFS angle of attack to elevator gain, deg/deg

$\delta_e/\dot{\alpha}$ - RFS angle of attack rate to elevator gain, sec

δ_e/q - RFS pitch rate to elevator gain, sec

$\delta_e/\dot{q}$ - RFS pitch acceleration to elevator gain, sec^2

δ_e/u - RFS perturbation velocity to elevator gain, deg sec/ft

$\delta_e/\dot{u}$ - RFS rate of change of speed to elevator gain, deg-sec^2/ft

δ_e/x - RFS variable feedback to elevator gain, where x may be replaced by any desired parameter

$\delta_E/_{IN}$ - automatic and random noise input to elevator gain

δ_p/α - RFS angle of attack to drag petal gain, deg/deg

δ_p/u - RFS perturbation velocity to drag petal gain, deg/deg

δ_r/δ_{RP} - rudder gear ratio

δ_r/δ_a - rudder aileron interconnect

F_{RP}/δ_{RP} - rudder pedal force gradient, lbs/in. or lbs/deg

δ_r/β - RFS sideslip angle to rudder gain, deg/deg

$\delta_r/\dot{\beta}$ - RFS sideslip angle rate to rudder gain, sec

δ_r/p - RFS roll rate to rudder gain, sec

$\delta_r/\dot{p}$ - RFS roll acceleration to rudder gain, sec^2

δ_r/r - RFS yaw rate to rudder gain, sec

$\delta_r/\dot{r}$ - RFS yaw acceleration to rudder gain, sec^2

δ_r/x - RFS variable feedback to rudder gain, where x may be replaced by any desired parameter

δ_r/IN - automatic and random noise input to rudder

α_V - angle of attack vane position, deg or rad

β_V - sideslip probe position, deg or rad

$\bar{q}_c$ - dynamic pressure command, $lb/in.^2$

VIII. SUBSCRIPTS

a - aileron

AS - aileron stick or wheel

$c.g.$ - measured at center of gravity

d - Dutch roll

d - damped

e - equivalent

e - elevator

ES - elevator stick or wheel

FS - feel system

IN - input

MAX - maximum

MIN - minimum

n_d - refers to pitch angle, pitch velocity, and pitch acceleration including feel system dynamics, to initial pitch acceleration, excluding feel system dynamics

0 - initial value, or value at time zero

p - phugoid

r - rudder

R - roll mode

RP - rudder pedal

RS - roll spiral, pedal forward

S - spiral mode

SA - simulated airplane

SP - longitudinal short period

SS - steady state

T - throttle

$T\text{-}33$ - basic, unaugmented T-33 airplane

ϵ - error

x - positive x direction

xx - along x body axis

y - positive y direction

yy - along y body axis

z - positive z direction

zz - abong z body axis

IX. ABBREVIATIONS

AF - Air Force

CAL - Cornell Aeronautical Laboratory

CAP - control anticipation parameter

CAS - calibrated airspeed

cps - cycles per second

deg - degrees

FR - fuel remaining

ft - feet

IAS - indicated airspeed

in. - inch

kt - knots

lb - pounds

LSF - least-squares-fit

PIO - pilot-induced oscillation

PIOR - pilot induced oscillation rating

PR - pilot rating

rad - radians

rad/sec - radians per second

RFS - response-feedback system

RMS - root mean square

VSS - variable stability system

X. ADDITIONAL SYMBOLS

$(\dot{}) = \frac{d()}{dt}$ - first derivative with respect to time, sec^{-1}

$(\ddot{}) = \frac{d^2()}{dt^2}$ - second derivative with respect to time, sec^{-2}

$j = \sqrt{-1}$

s - Laplace operator

t - time, sec

Δ - small incremental change

σ - real part of $s = \sigma + j\omega$

SECTION I
INTRODUCTION

The NT-33A variable stability airplane (Serial No. 51-4120) is an extensively modified T-33 jet trainer. The elevator, aileron and rudder controls in the front cockpit are disconnected from their respective control surfaces and have been connected to separate servomechanisms that make up an "artificial feel" system. In addition, the elevator, aileron and rudder control surfaces have been connected to individual servos which can be driven by a number of different inputs. These servos receive their electrical inputs from the artificial feel system (pilot's commands, position or force), attitude and rate gyros, accelerometers, dynamic pressure, α vane and β probe. This arrangement, through a response-feedback system, allows the normal T-33 derivatives to be augmented to the extent that the handling qualities of many existing airplanes, future airplanes or hypothetical research configurations, can be simulated. The original T-33 nose section has been replaced with the larger nose of an F-94 to provide the volume required for the electronic components of the response-feedback system and the recording equipment.

The rear seat pilot, or "safety" pilot, takes off and lands the airplane as a near normal T-33. At test altitude the safety pilot and the "evaluation" pilot perform a sequence of operations necessary to engage the variable stability system. When the system is engaged the evaluation pilot has control of the airplane through the artificial feel system. Since the dynamics and statics of both the feel system and airplane can be varied by the changing of a set of gain controls located in the rear cockpit, many different airplanes or configurations can be simulated on a single flight.

Historically, the T-33A was delivered to CAL in October 1954 by the Air Force's Air Research and Development Command for the purpose of having it outfitted as a variable stability airplane. Design and installation of the variable stability system reached the ground checkout stage in 1956. The flight checkout started in January 1957 and continued into 1958. Since then, the aircraft has been used in a continuing series of handling qualities investigations.

This report has been prepared with the intent of providing an updated functional description of the T-33 variable stability airplane. It presents the information necessary to set up a simulation program, calibration procedures, and a brief description of the airplane systems.

SECTION II
FUNCTIONAL DESCRIPTION OF THE VARIABLE STABILITY SYSTEM

This section presents a brief description of the T-33 variable stability system as it presently exists. The system uses the normal T-33 control surfaces in the variable stability operation. The evaluation pilot's cockpit controls are only electrohydraulically connected to the T-33 flight controls; however, the safety pilot's cockpit controls, in the rear seat, are connected in the normal manner. Because of the direct mechanical connection, the safety pilot's controls move with the inputs applied to the controls by the evaluation pilot and the variable stability system. Since the T-33 responds in a normal manner to these control motions, the safety pilot is afforded some advance information concerning the impending airplane motions by the control positions. Thus, he can anticipate dangerous situations before they develop and take control of the airplane. Also, he can evaluate noise in the system and decide if the control system is being subjected to excessive vibrations or loads. On the other hand, the evaluation pilot is not directly connected to the control system and he does not feel any of the variable stability system inputs in his controls since his cockpit control movements and feel characteristics are controlled only by the variable feel system.

Functionally, the variable stability system may be divided into two independent parts. The first part, the variable feel system, provides the evaluation pilot with the stick and rudder pedal feel forces, gradients and displacements. The second part, the response-feedback flight control system, augments the normal T-33 dynamics to represent those of the vehicle being simulated. Figure 1 shows a block diagram of the variable stability system.

Both the variable feel system and the response-feedback flight control systems are controlled by the gain controls located in the rear cockpit and shown in Figures 2 and 3. These gain controls allow the airplane and feel system dynamics to be varied in flight without the evaluation pilot knowing what changes are being made. The gain controls are connected in series with a set of nose gains located on a chassis in the nose of the airplane and shown in Figure 4. These nose gains can only be set on the ground and are designed primarily to expand the scale of the safety pilot-controlled gain settings. The nose gains permit a greater number of digits per unit gain, hence the error that can result from imprecise gain settings by the safety pilot is minimized.

The various electronic chasses that make up the major parts of the variable stability system are shown in Figures 2 through 8.

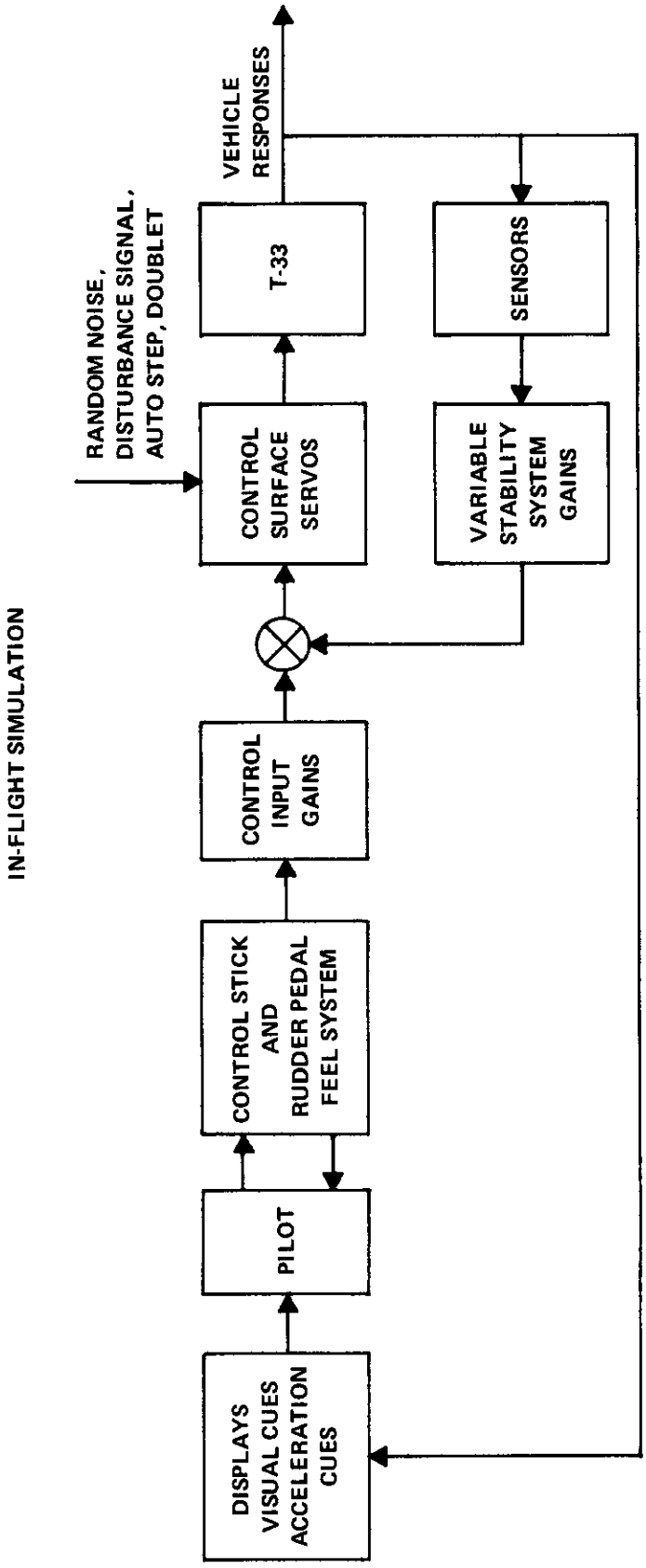

Figure 1 VARIABLE STABILITY T-33 BLOCK DIAGRAM

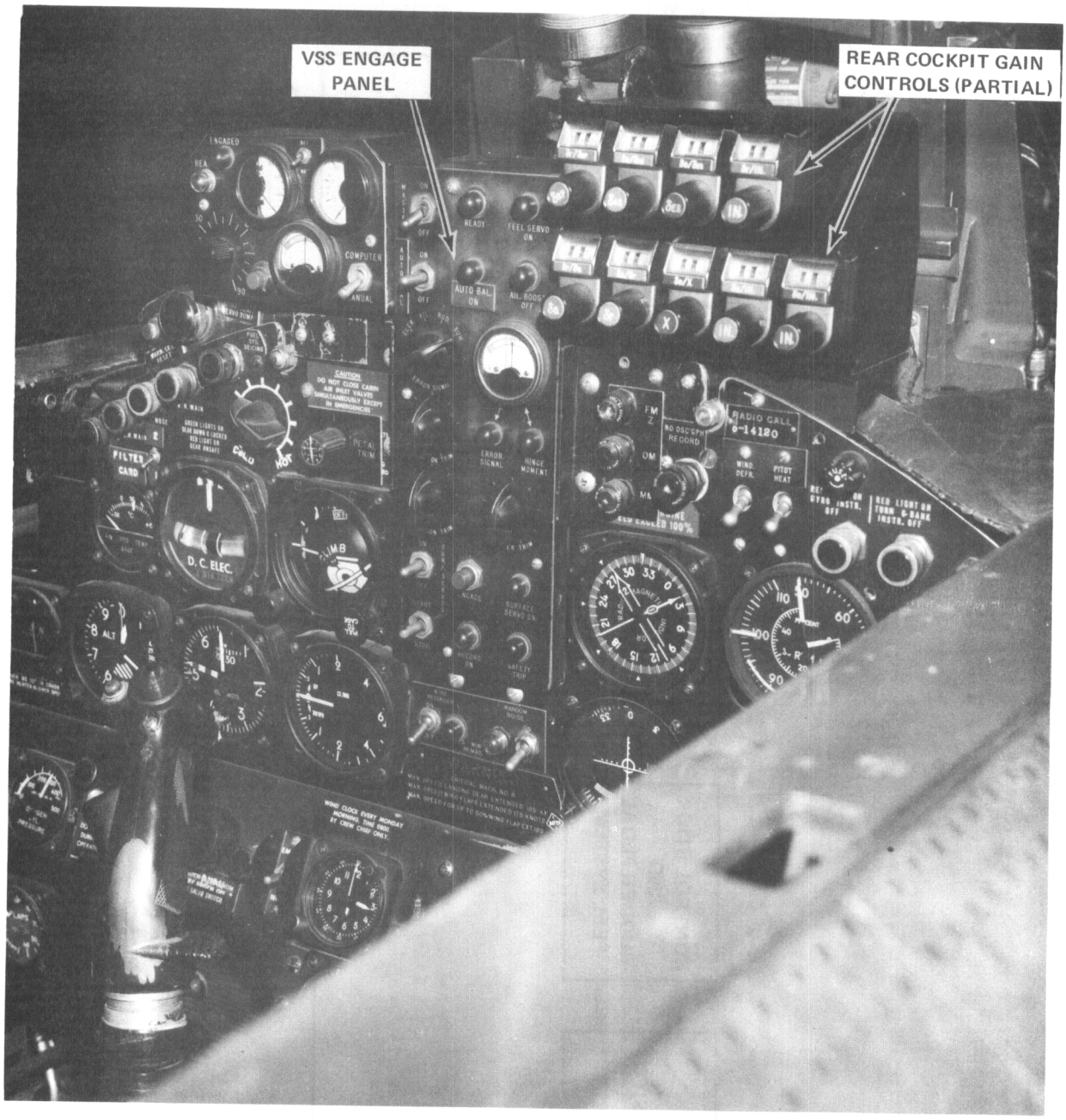

Figure 2 REAR COCKPIT VSS GAIN CONTROLS (INSTRUMENT PANEL)

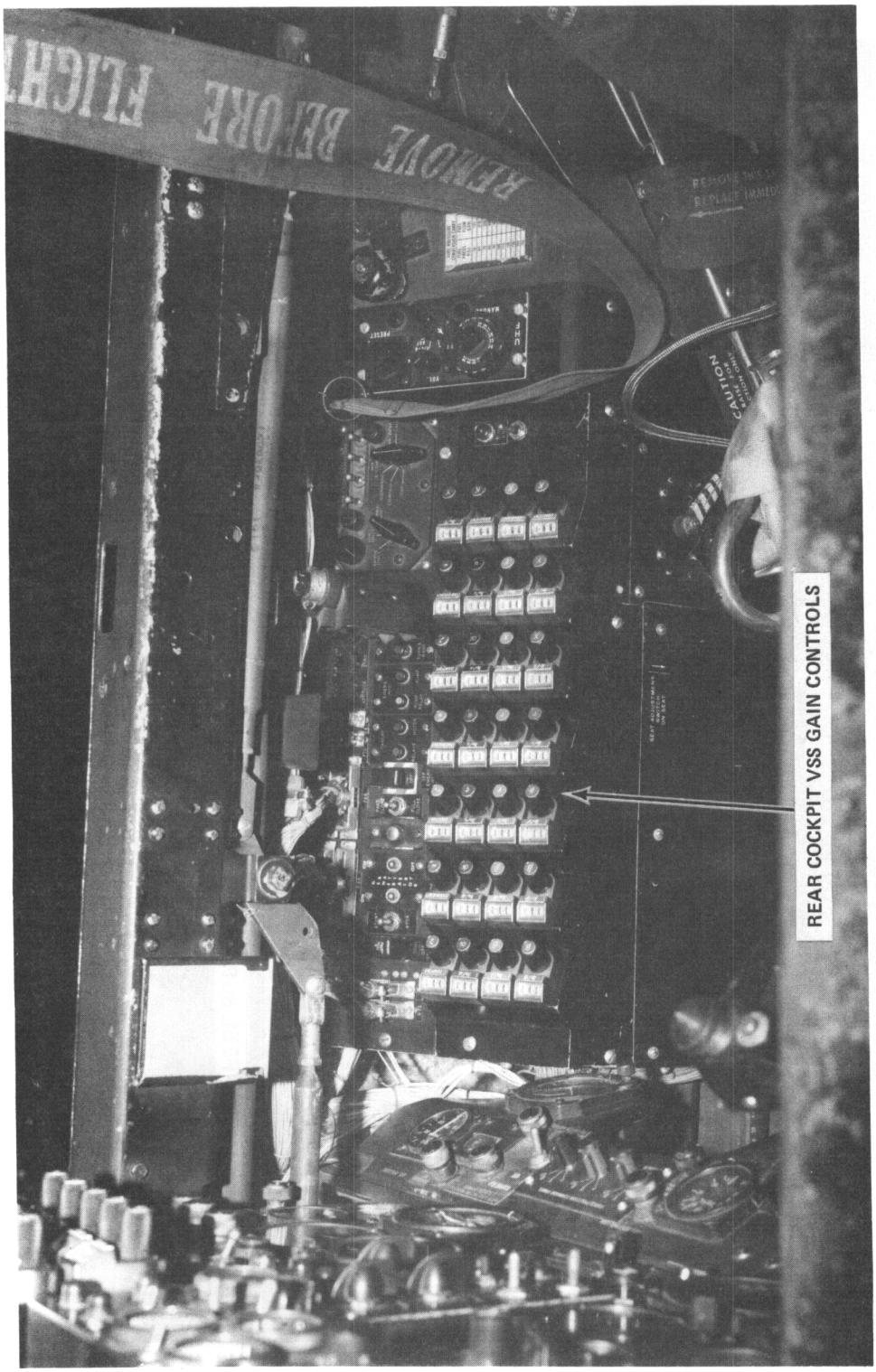

Figure 3 REAR COCKPIT VSS GAIN CONTROLS (SIDE PANEL)

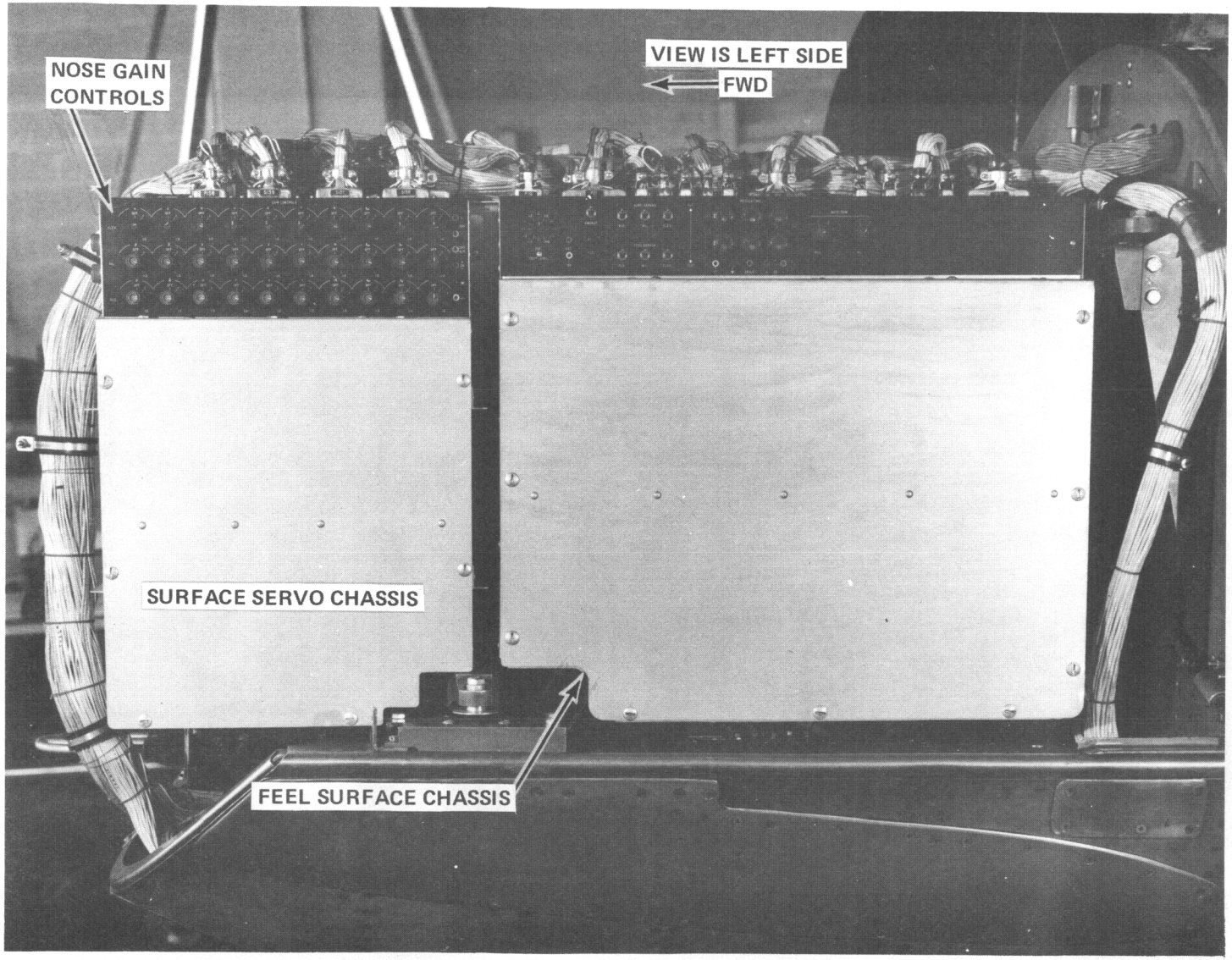

Figure 4 SURFACE SERVO CHASSIS AND FEEL SYSTEM CHASSIS

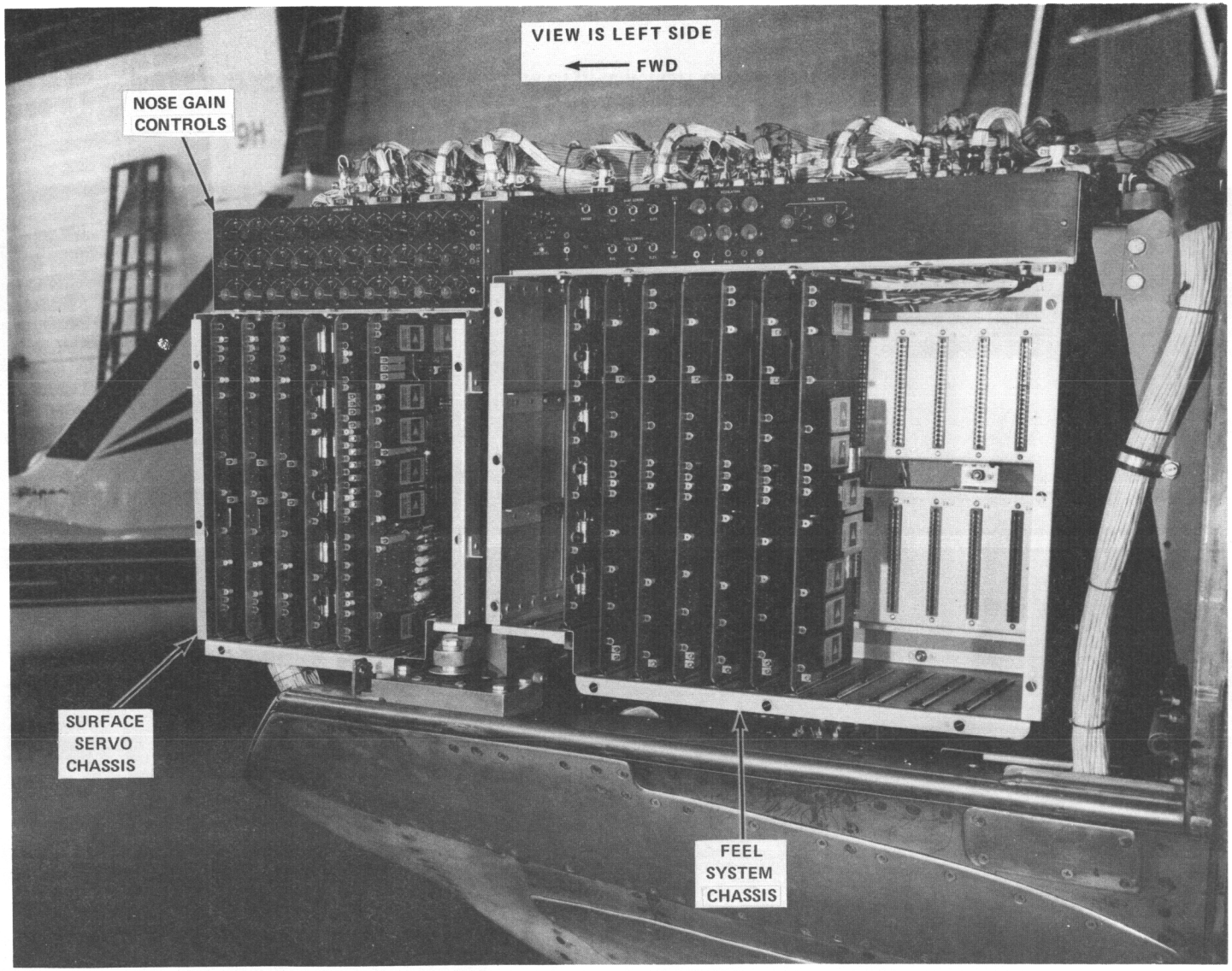

Figure 5 SURFACE & FEEL CHASSIS WITH COVERS REMOVED TO SHOW PRINTED CIRCUIT CARDS

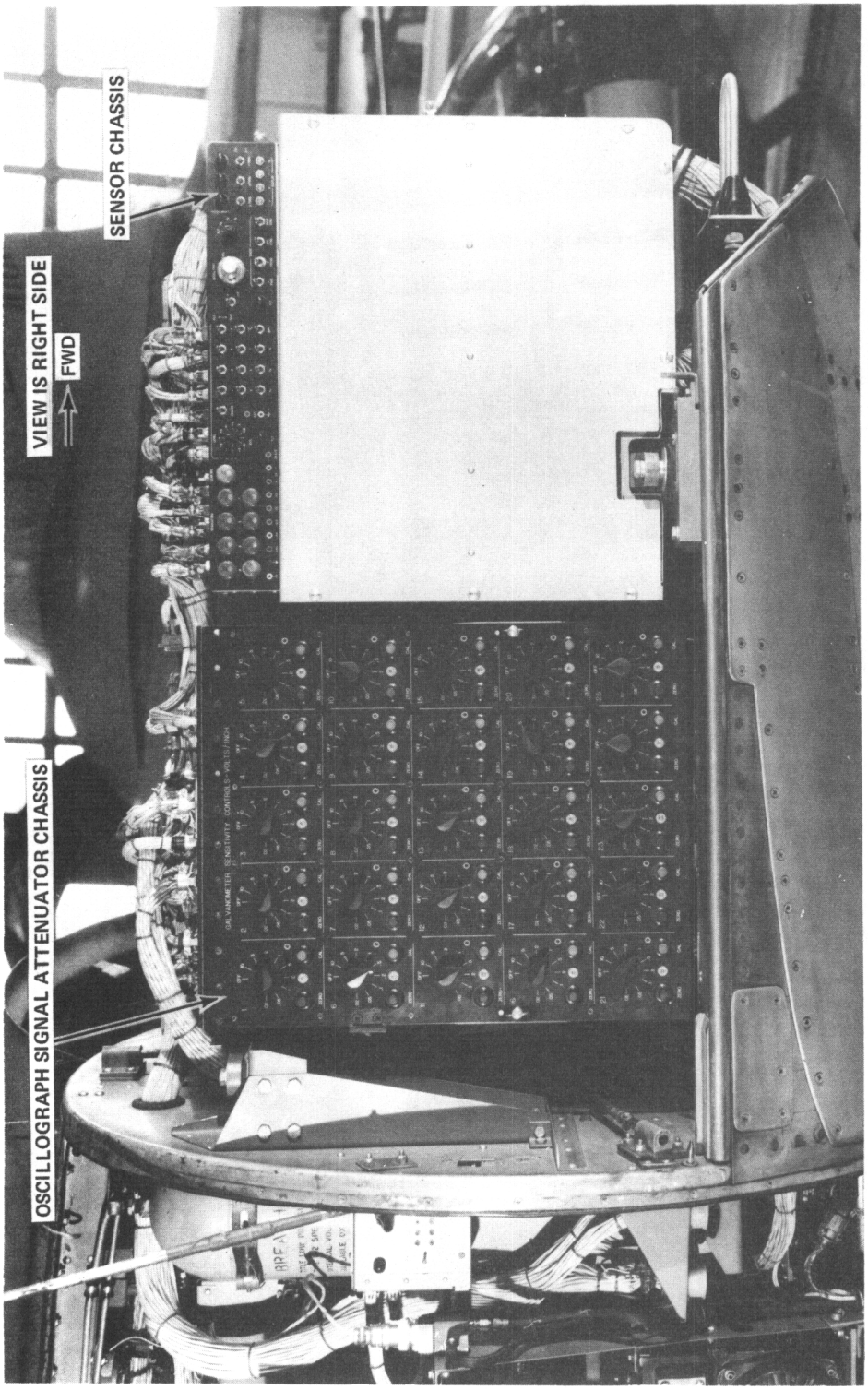

Figure 6 OSCILLOGRAPH SIGNAL ATTENUATOR CHASSIS AND SENSOR CHASSIS

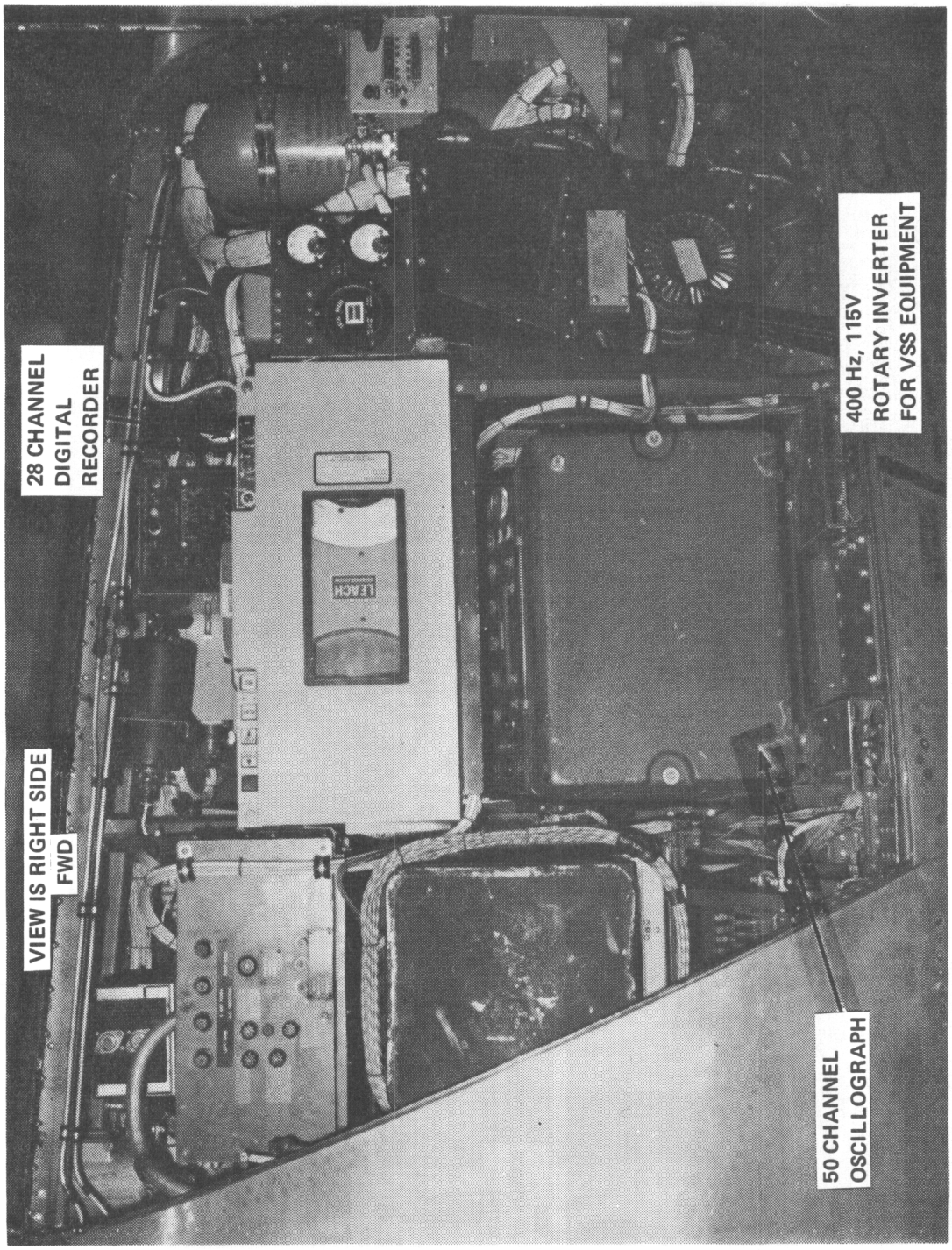

Figure 7 DATA RECORDERS

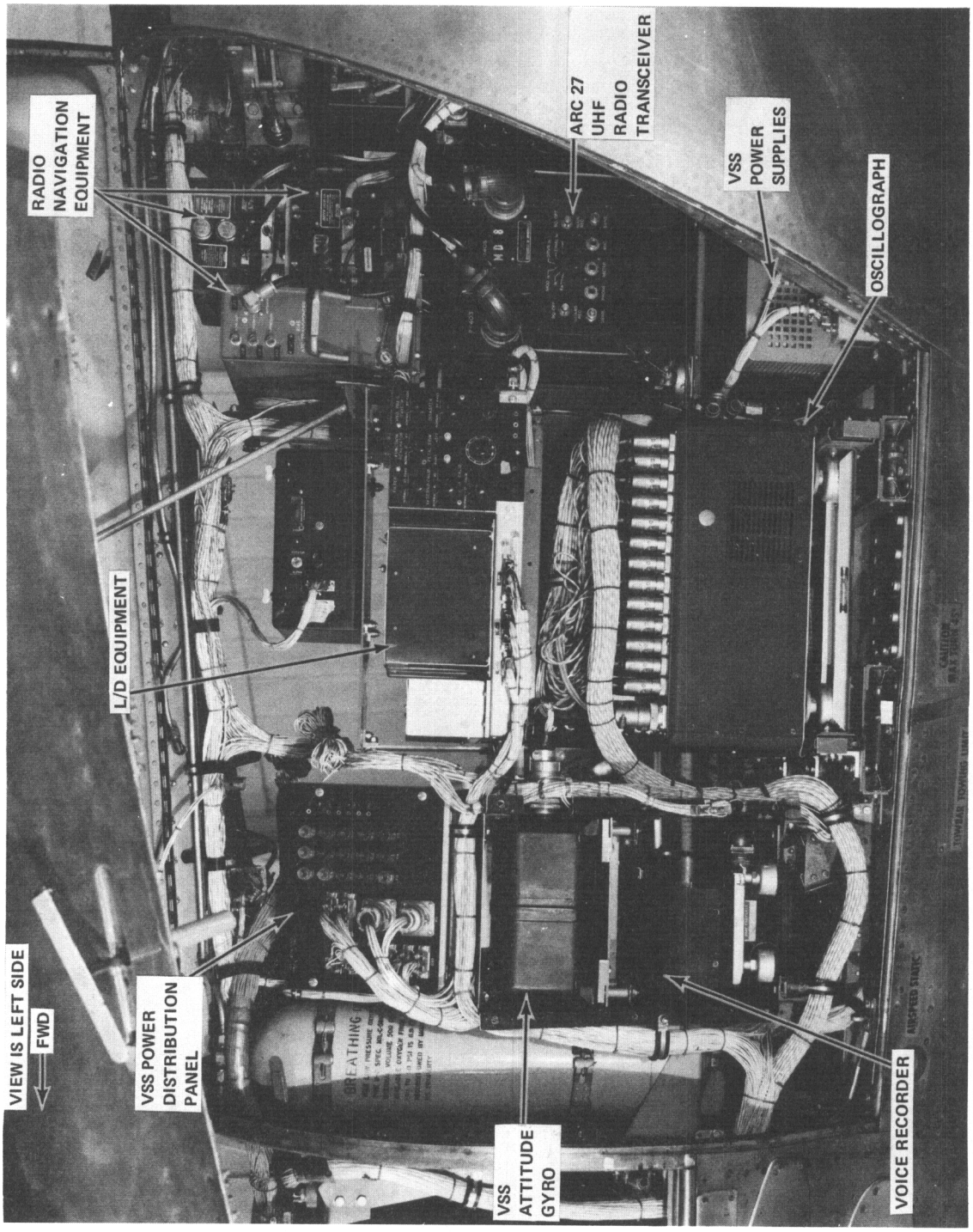

Figure 8 NAVIGATION, COMMUNICATION EQUIPMENT, VOICE RECORDER, VSS ATTITUDE GYRO, L/D CHASSIS

SECTION III
VARIABLE STABILITY RESPONSE-FEEDBACK FLIGHT CONTROL SYSTEM

The response-feedback flight control system uses the T-33 control surfaces to augment the normal T-33 stability derivatives to obtain those desired for a specific simulation. Therefore, the system includes enough feedback loops so that most of the stability derivatives and control parameters in the equations of motion can be independently varied over wide ranges. Although one gain often changes more than one stability derivative, and a single derivative can change more than one significant flying qualities parameter, the use of the proper combination of feedback loops can allow accurate determination of the stability and control characteristics to be simulated.

Briefly, the pilot input is fed into the flight control system through the feel system and the resulting control surface movement causes the airplane to respond. The loop is closed by sensing the airplane's motion and feeding back a signal proportional to this motion, thus modifying the response to the pilot's input. This principle is shown in the sketch below.

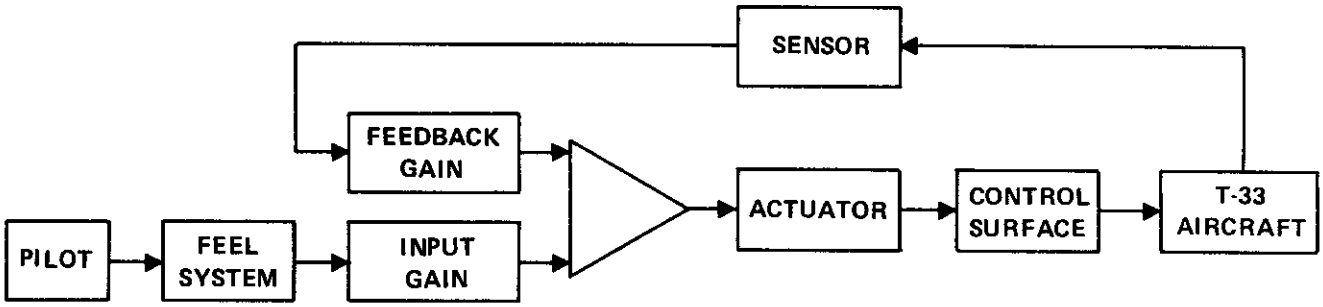

An angle of attack vane, a sideslip probe, accelerometers, rate and attitude gyros, and dynamic pressure pickups are used as the sensor elements.

The physical layout of the control system is shown in Figure 9 and a schematic of the T-33 servo hydraulic system is shown in Figure 10. Each control surface has an electrohydraulic position servo which receives its inputs from the variable stability system. These servos operate independent of, but in parallel with, the normal T-33 control surfaces actuating mechanisms. Each of the surface position servo actuators is operated by a flow control servo valve which receives its electrical input from the variable stability system. Each of the surface position actuators has a hydraulic limiting circuit operating in parallel with it. This limiting circuit restricts the amount of supply pressure differential that can occur across the servo piston, thus limiting the maximum hinge moment that can be generated. In addition to the pressure limiter circuit, there is an electrically operated servo bypass valve which allows the servo actuator to be bypassed completely so that manual control

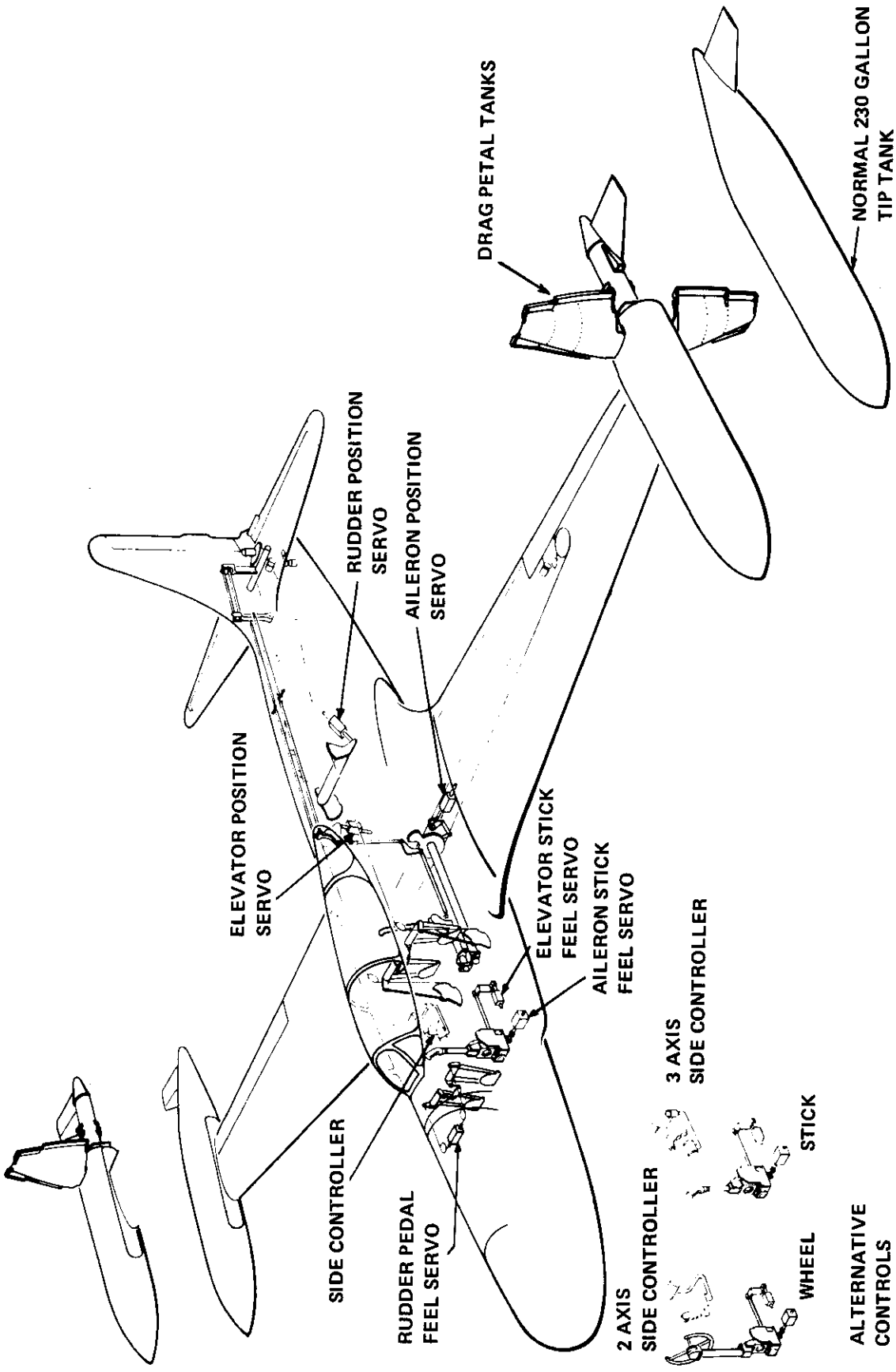

Figure 9 CONTROL SYSTEM LAYOUT

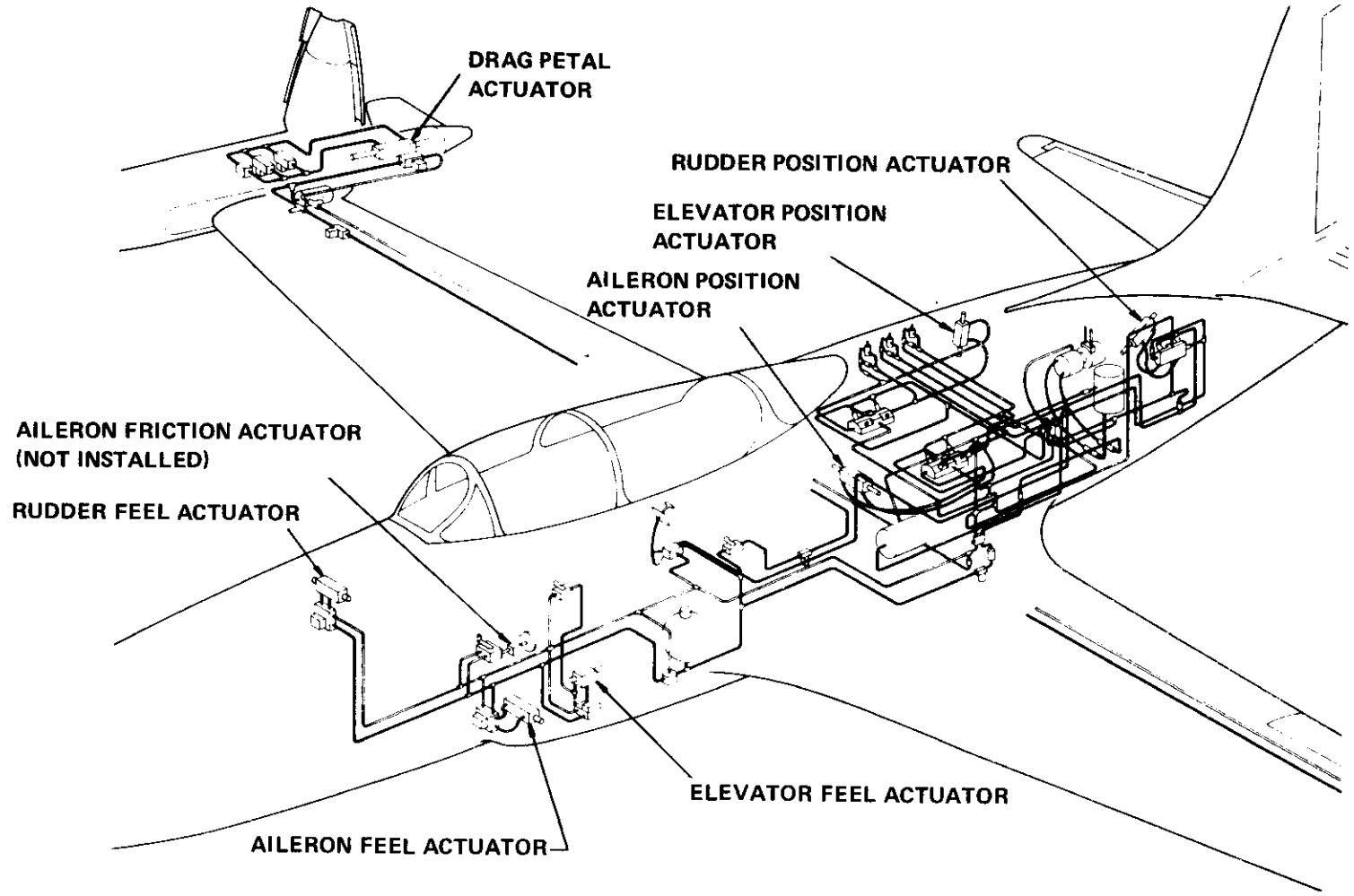

NOTE FOR COMPLETE NOMENCLATURE OF ALL HYDRAULIC COMPONENTS SEE DRAWING NO. FRS-835-016-IC & FDS-C09-007-26C

Figure 10 SCHEMATIC DRAWING - T-33 SERVO HYDRAULIC SYSTEM

of the airplane is possible. Figure 11 illustrates the pressure limiting and bypass circuit. It will be noticed that the elevator requires two different limiting pressures, one for up elevator and one for down elevator. These pressures correspond to the hinge moments required to produce the safety limit load factors established for the system in the positive and negative g directions respectively. Both the rudder and aileron have symmetrical requirements for their limiting hinge moment; hence the simpler arrangement.

The variable stability system also includes an L/D (lift to drag) system which consists basically of a set of movable petals located on a set of specially modified tip tanks. This system allows the lift to drag ratio of the T-33 to be varied. The L/D system includes its own response-feedback loops. Since this is a special simulation device, the L/D system will be discussed in a separate section later in the report.

Block diagrams for the aileron, rudder, and elevator response-feedback systems are shown in Figures 12, 13, and 14, respectively.

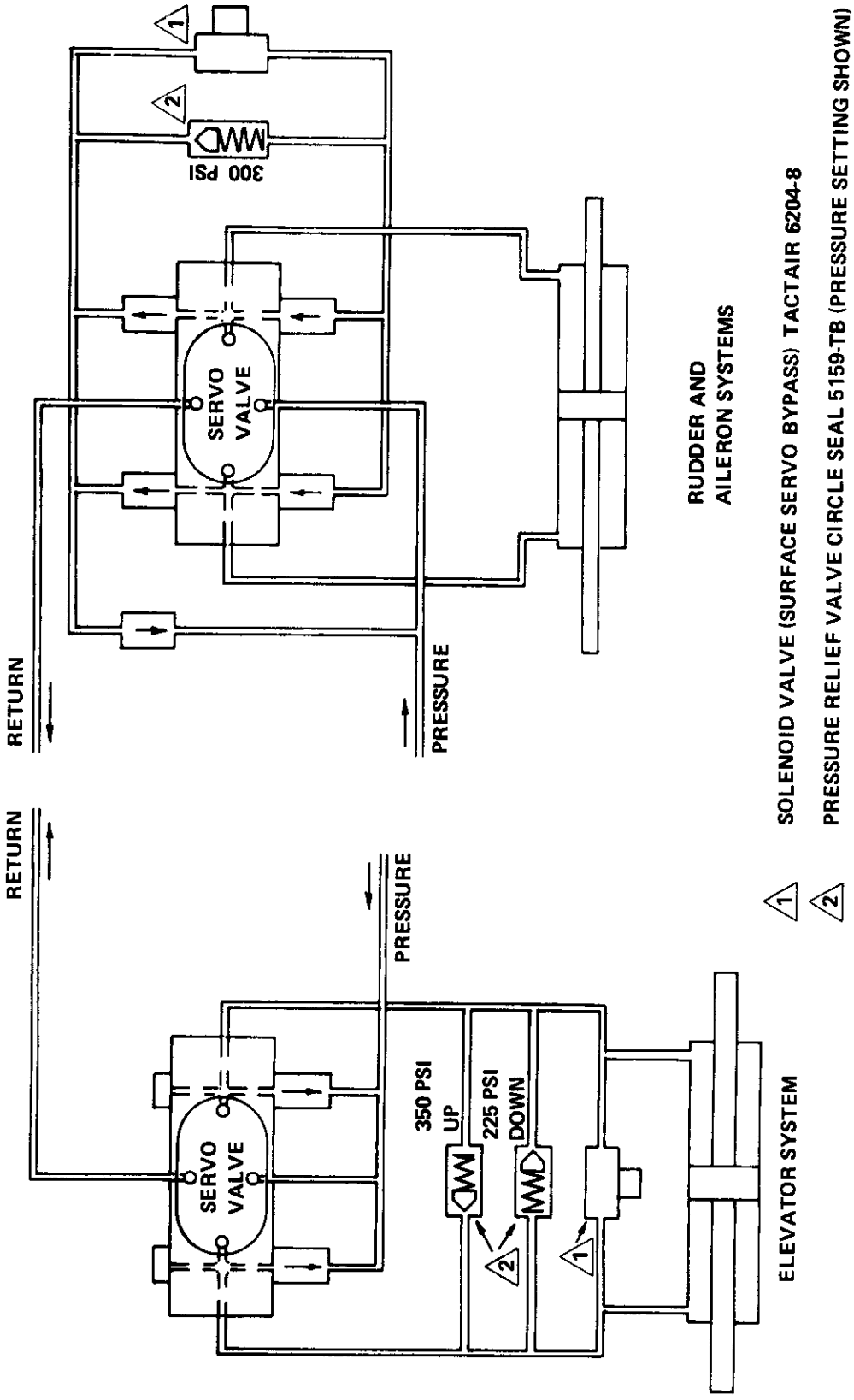

Figure 11 HYDRAULIC PRESSURE LIMITING CIRCUITS

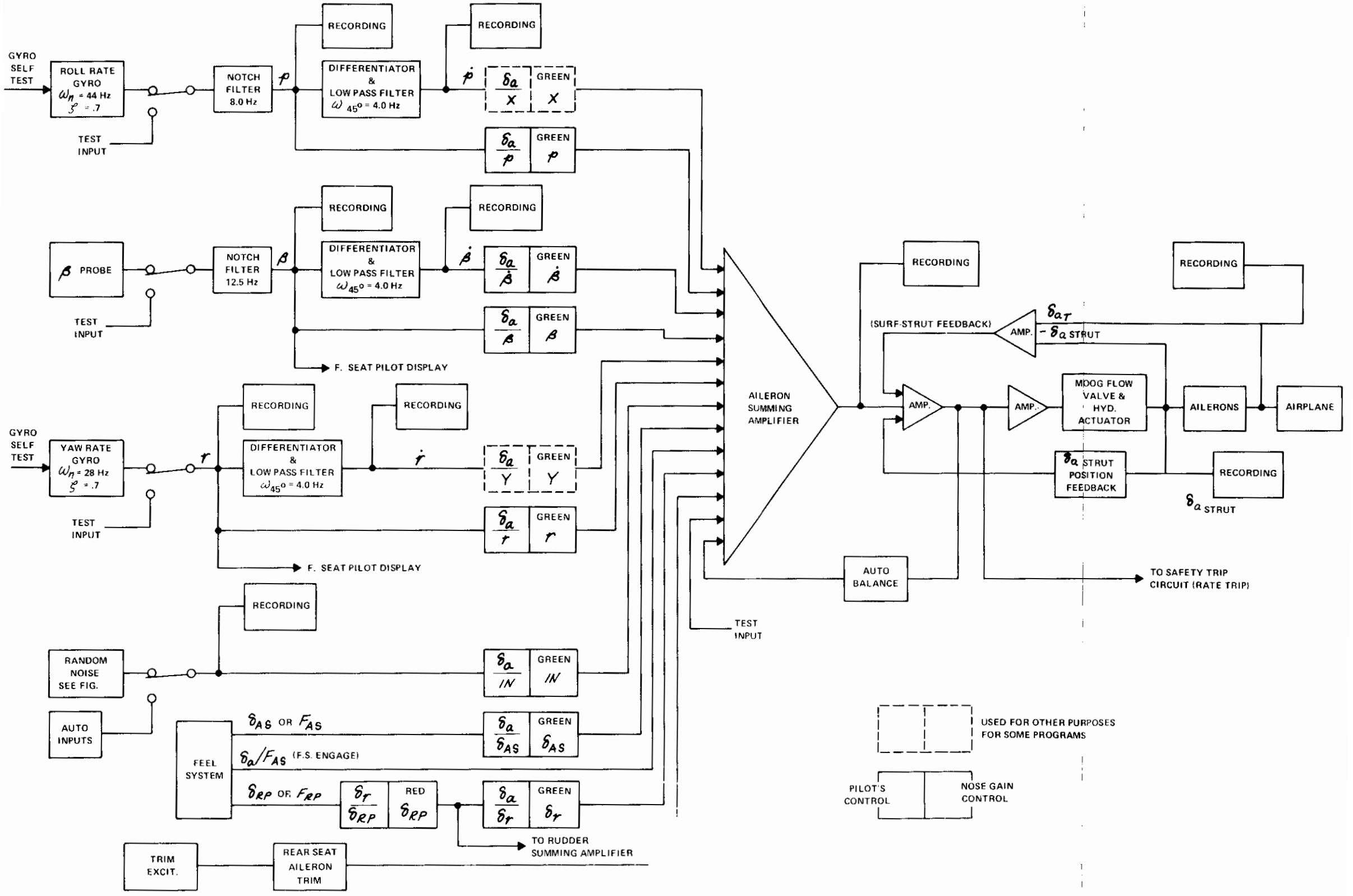

Figure 12 BLOCK DIAGRAM OF RESPONSE FEEDBACK CONTROL LOOPS, AILERON CHANNEL

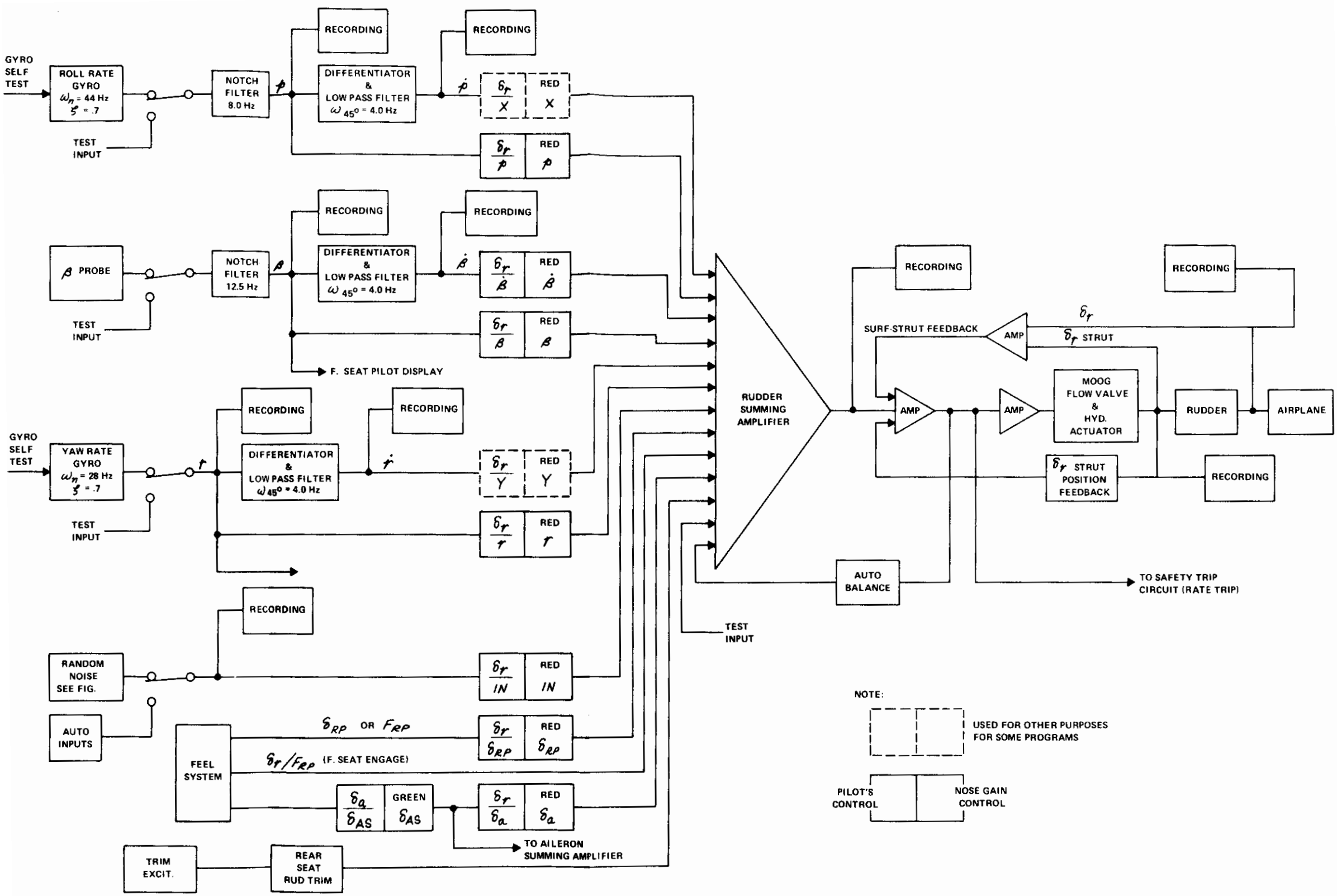

Figure 13 BLOCK DIAGRAM RESPONSE OF RESPONSE FEEDBACK CONTROL LOOPS, RUDDER CHANNEL

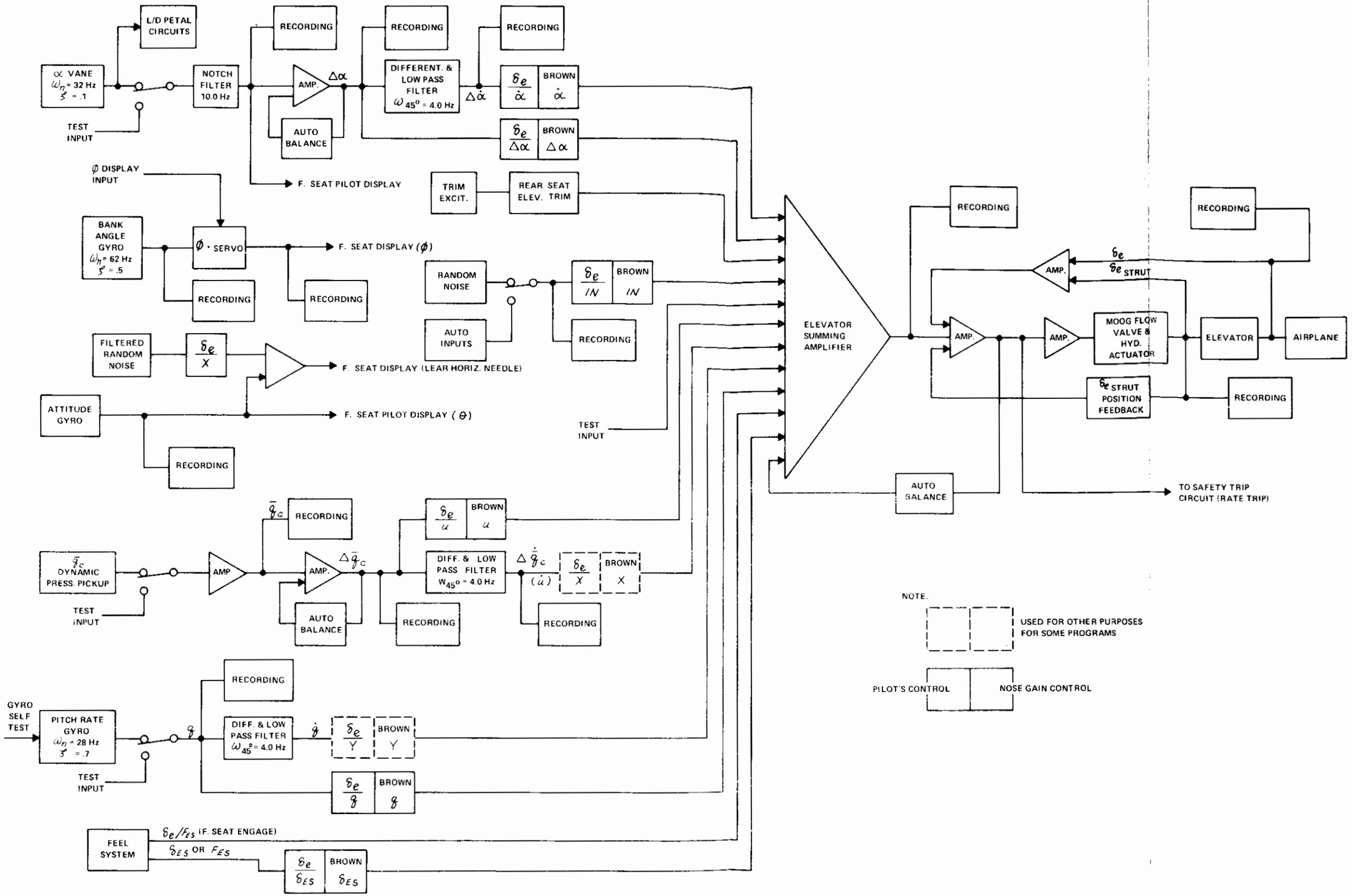

Figure 14 BLOCK DIAGRAM OF RESPONSE FEEDBACK CONTROL LOOPS, ELEVATOR CHANNEL

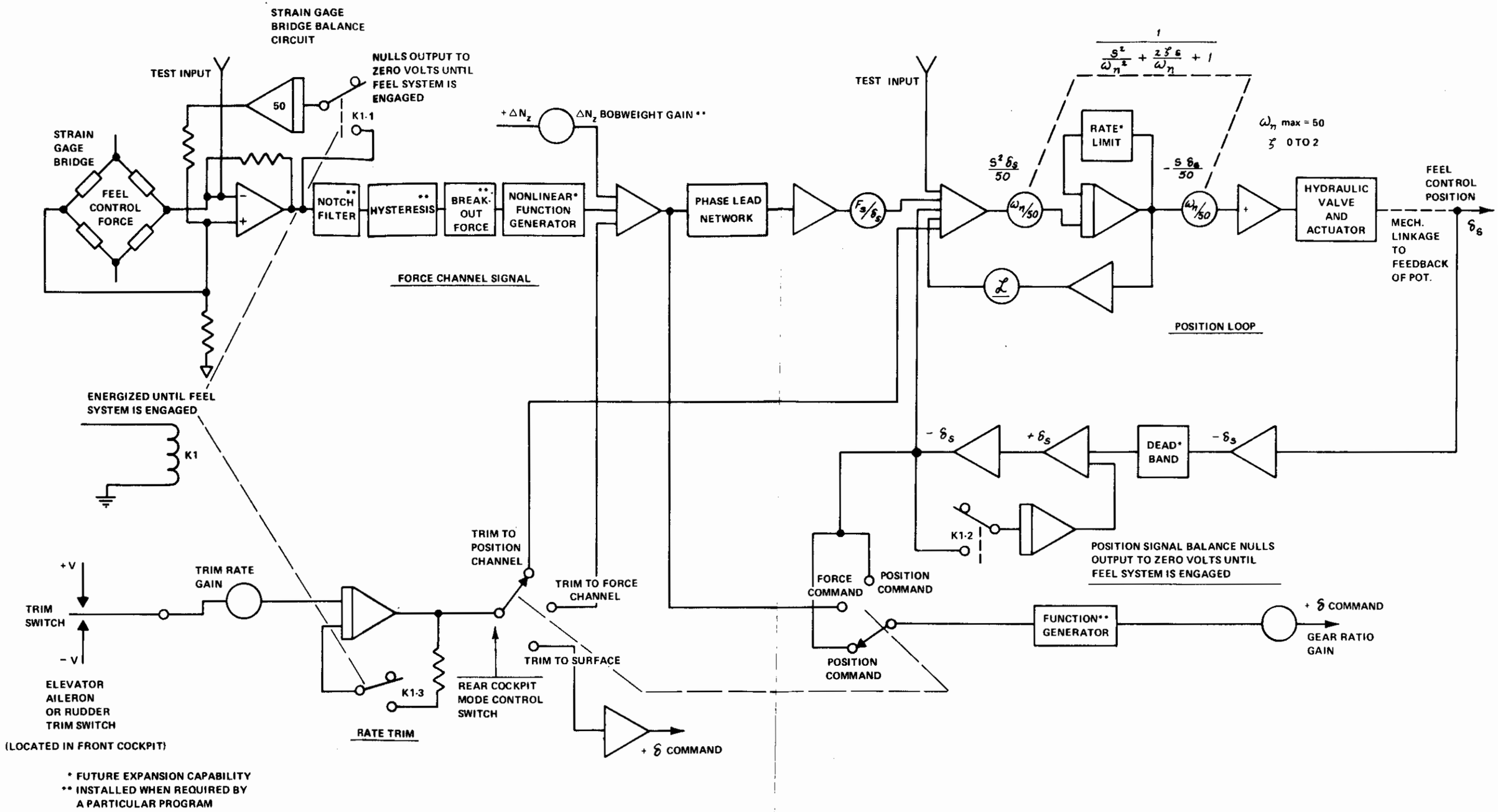

* FUTURE EXPANSION CAPABILITY
** INSTALLED WHEN REQUIRED BY A PARTICULAR PROGRAM

Figure 15 FEEL SYSTEM BLOCK DIAGRAM – TYPICAL FOR ELEVATOR, AILERON, RUDDER

SECTION IV
VARIABLE STABILITY FEEL SYSTEM

The variable feel system is a very important part of the variable stability system. Since the evaluation pilot's controls are not mechanically connected to the control surfaces of the airplane, the variable feel system must provide the pilot with the proper or desired forces, deflections and feel characteristics of the cockpit controls. Figure 15 presents a block diagram of the feel system.

The feel system uses electrohydraulic servos which can receive a wide variety of inputs, thus the feel characteristics of the cockpit controls can be made to vary in a number of different ways. For example, the variable feel system can be made to behave like a system having aerodynamic feel, like an irreversible control system or a zero-deflection pure force control system. The standard control stick can be replaced by a wheel or by either a two or three-axis side controller (see Figures 16 and 17). The effective gearing between the cockpit control motion or force and control surface deflection can be altered. The addition of shaping filters between the feel system and the flight control system allows the shape of the control surface motion following a cockpit control input to be changed.

The system is designed so that the frequency, damping ratio and force gradients for each of the cockpit controls can be varied independently and directly. Provisions are also made so that hysteresis, breakout force, nonlinear inputs and bobweight effects can be incorporated in the feel system.

HYSTERESIS AND BREAKOUT FORCE CIRCUITS

Hysteresis and breakout forces are often required for better simulation of actual aircraft control systems. Provisions have been made to provide hysteresis, breakout force and combined hysteresis and breakout force in the feel system force channels or in the feel system displacement or force output signals that are used to drive the elevator, aileron or rudder control surface servos. The following sketches show typical wave forms for the hysteresis and breakout force circuits. The amount of hysteresis and breakout force obtained with these circuits can be changed by controls in the rear cockpit.

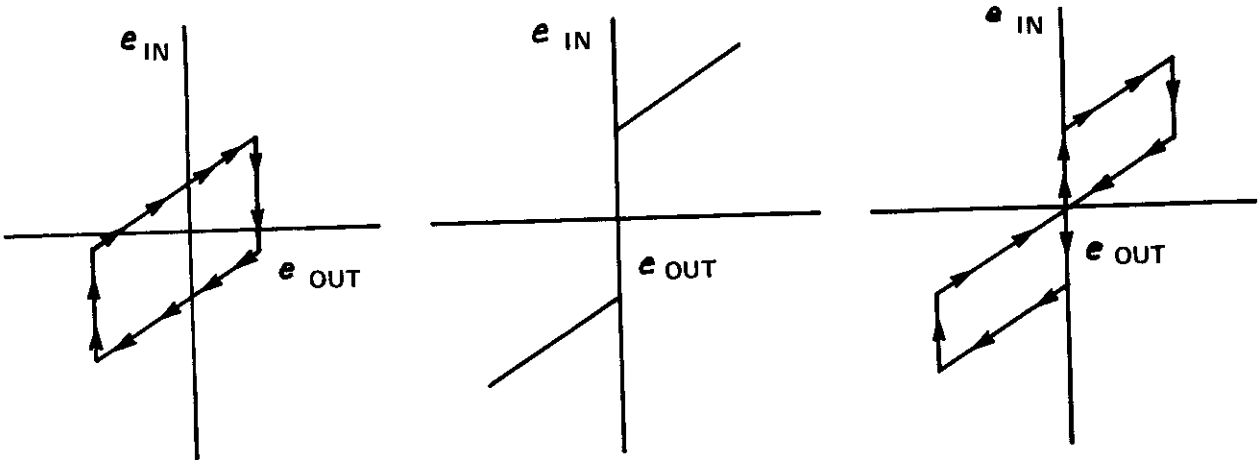

HYSTERESIS | BREAKOUT FORCE | HYSTERESIS AND BREAKOUT FORCE

The position loop portions of the T-33 elevator, aileron and rudder feel systems are second order and can be described by a second-order transfer function

$$\frac{\delta_s}{F_s} = \frac{1}{\frac{s^2}{\omega_n^2} + \frac{2\zeta}{\omega_n} s + 1}$$

where F_s is the force command input and δ_s is the stick or rudder displacement. Lead network circuits have been installed in the force command channels in all three feel servos to make the feel systems more stable with high force gains (light feel system gradients). Consequently the overall feel system from force command input to stick or rudder displacement is not exactly second order.

In the data taken on the feel systems and presented in Figures 18 through 26, it was convenient to treat the overall feel system as second order, so that second-order parameters ω_n, ζ could be used in describing the feel systems. The feel servo input signal was applied at the strain gage amplifier. Figures 18, 19, and 20 are plots of elevator, aileron, and rudder feel servo natural frequency ω_n versus the feel servo frequency cockpit gain control (ω) settings. ω_n is defined as the servo frequency in radians per second where the stick or rudder displacement signals lag the force command by 90 degrees. Data are given for three different values of damping ratio, ζ = 1.0, 0.7, 0.5, however, it can be seen that ω_n is essentially independent of ζ for ω_n over the range of 0 to 30 radians per second which is the range normally used.

Figures 21, 22 and 23 present elevator, aileron and rudder feel system damping ratio ζ versus cockpit ζ control settings. ζ was measured by matching feel system step response records with typical response curves of a second-order system.

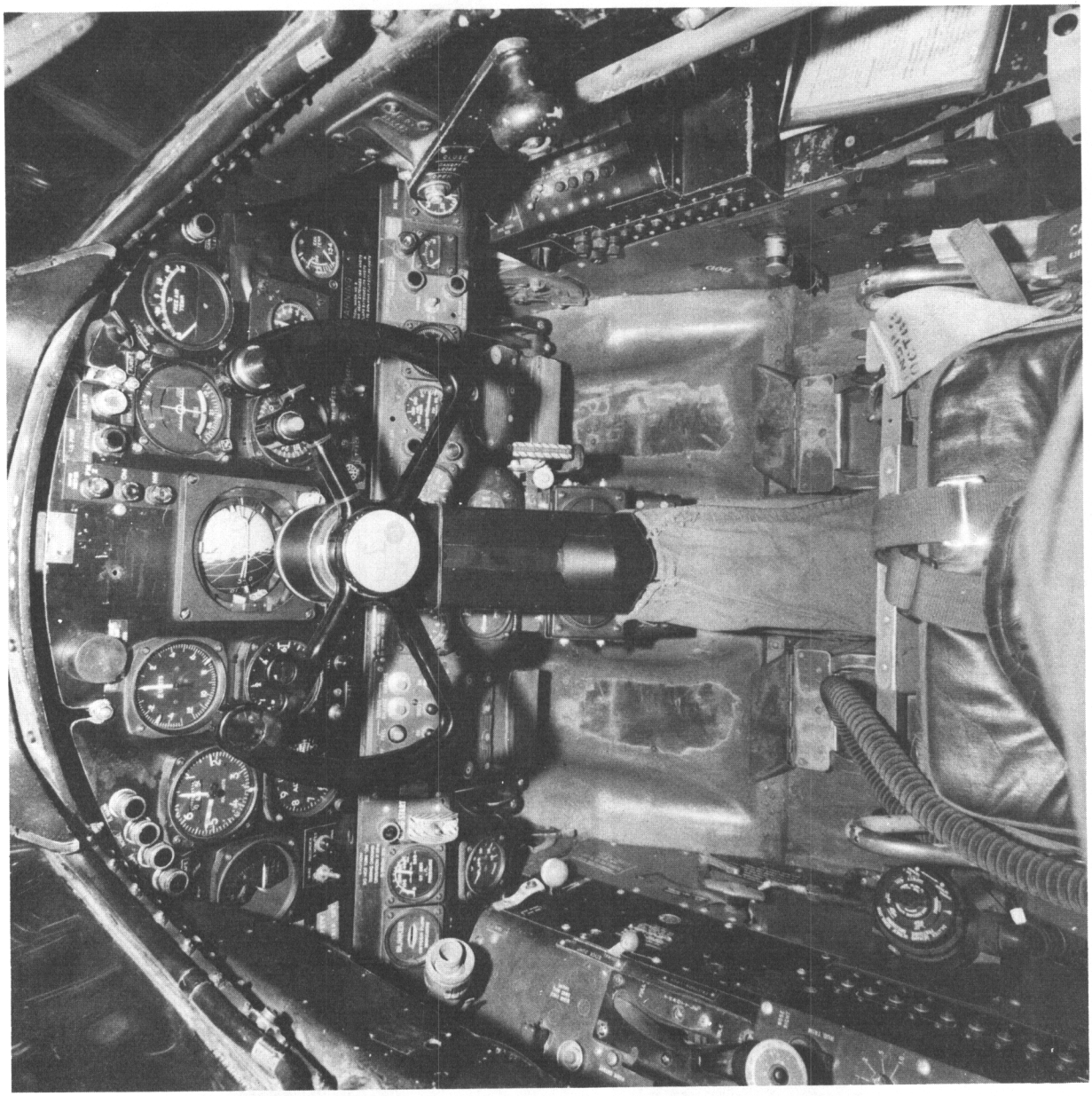

Figure 16 FRONT COCKPIT SHOWING CONTROL WHEEL INSTALLATION

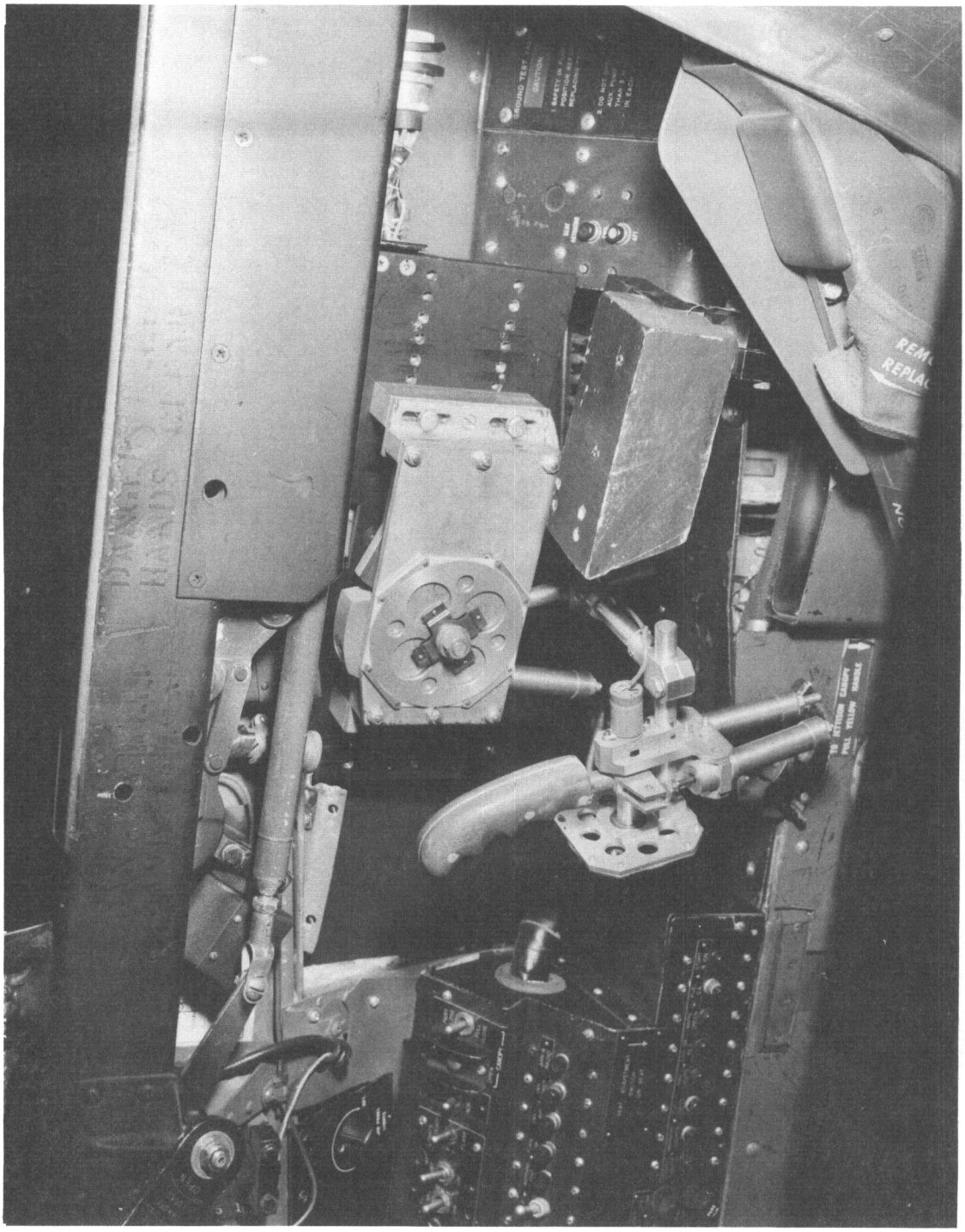

Figure 17 TWO-AXIS SIDE CONTROLLER (RIGHT HAND SIDE, FRONT COCKPIT)

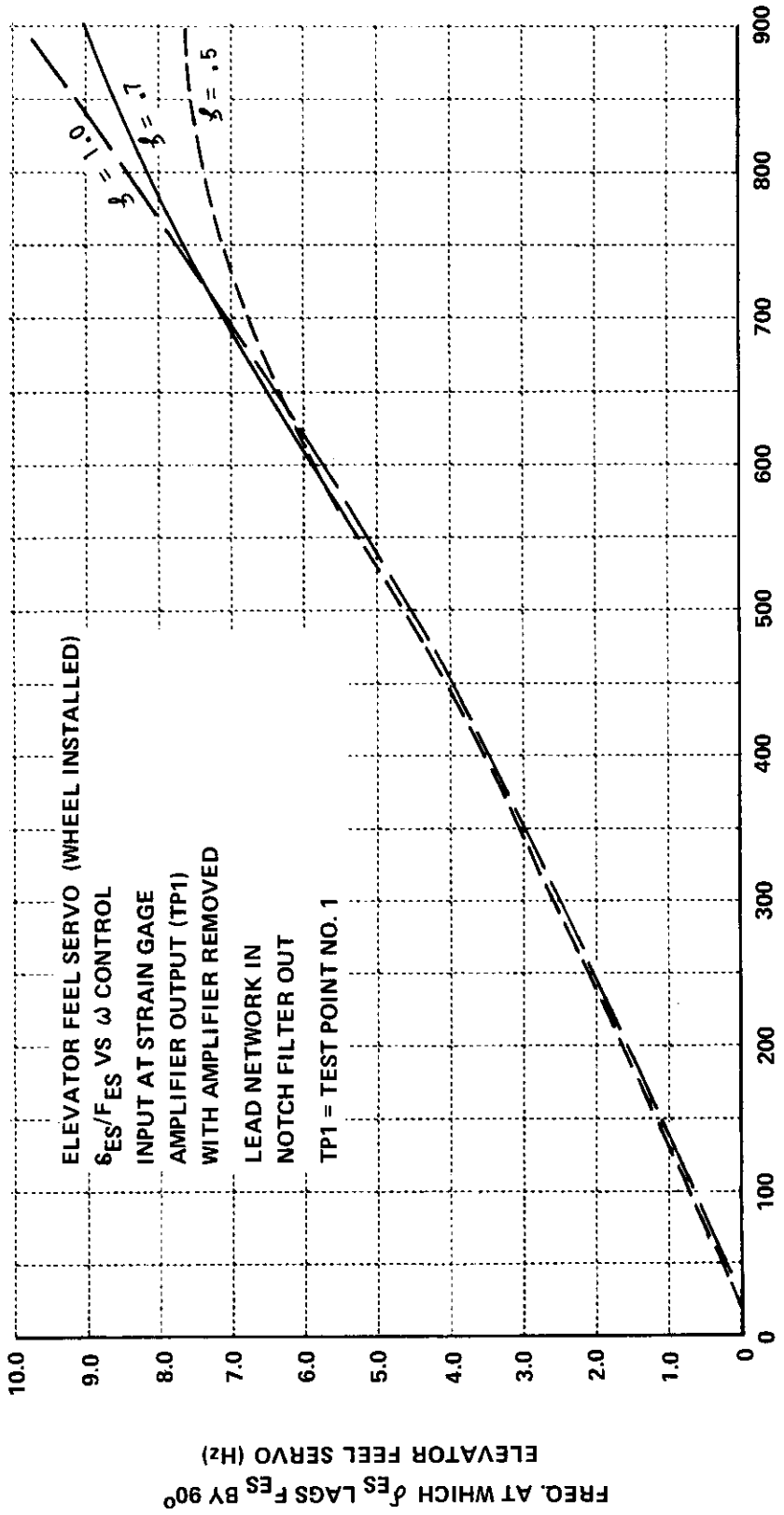

Figure 18 ω_n 90° VERSUS BROWN ω CONTROL SETTING, ELEVATOR FEEL SERVO

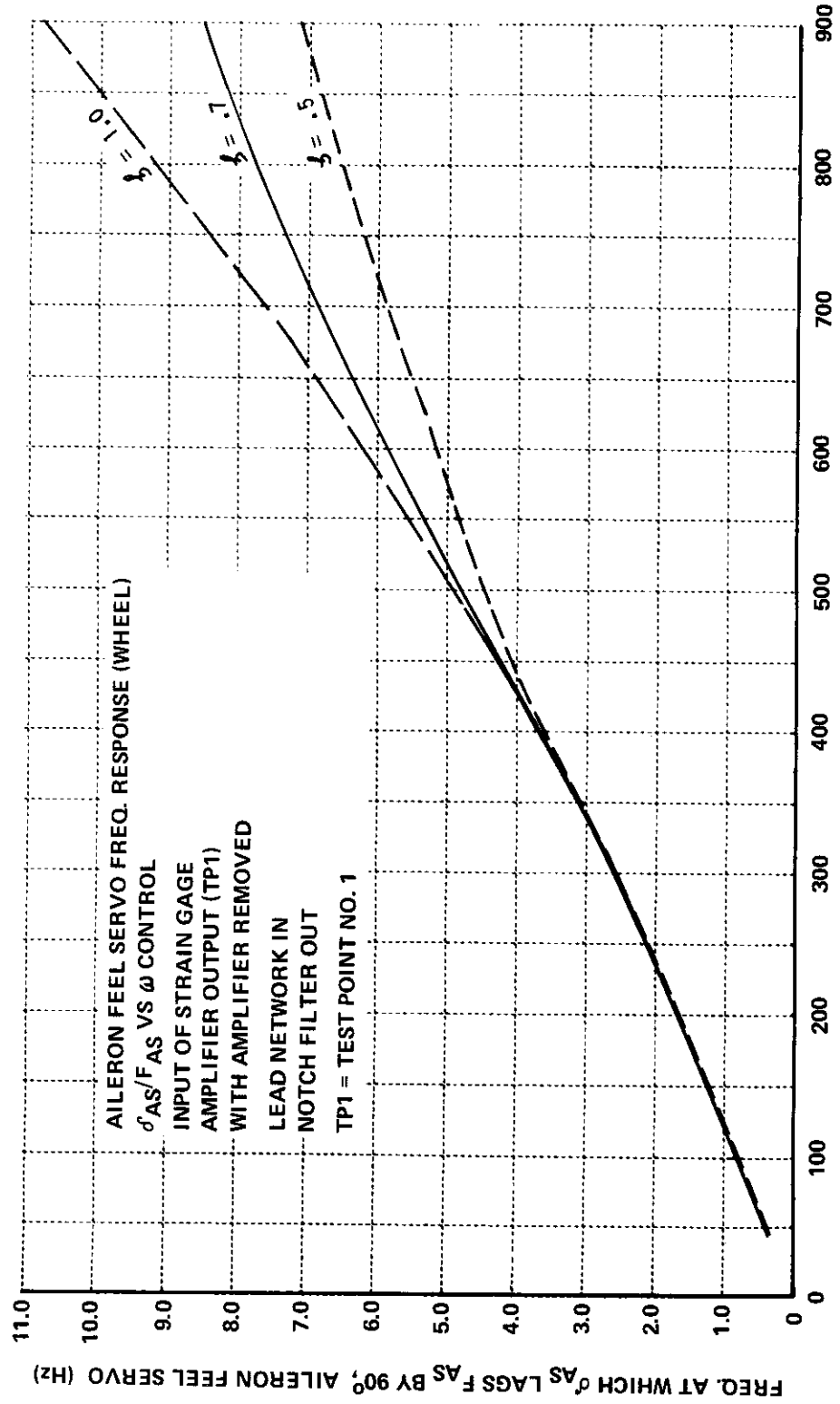

Figure 19 ω_n 90° VERSUS GREEN ω CONTROL SETTING, AILERON FEEL SERVO

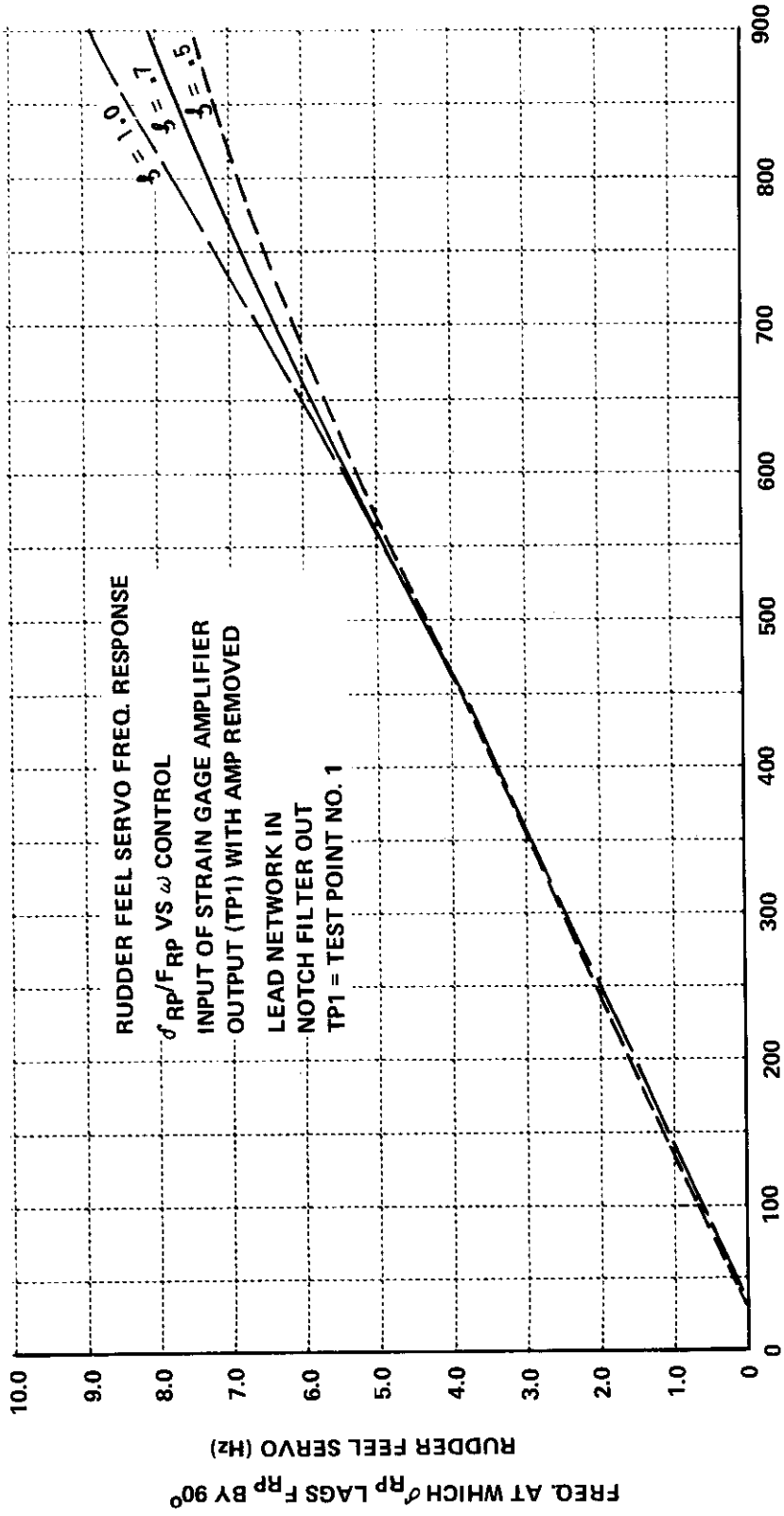

Figure 20 ω_n 90° VERSUS RED ω CONTROL SETTING, RUDDER FEEL SERVO

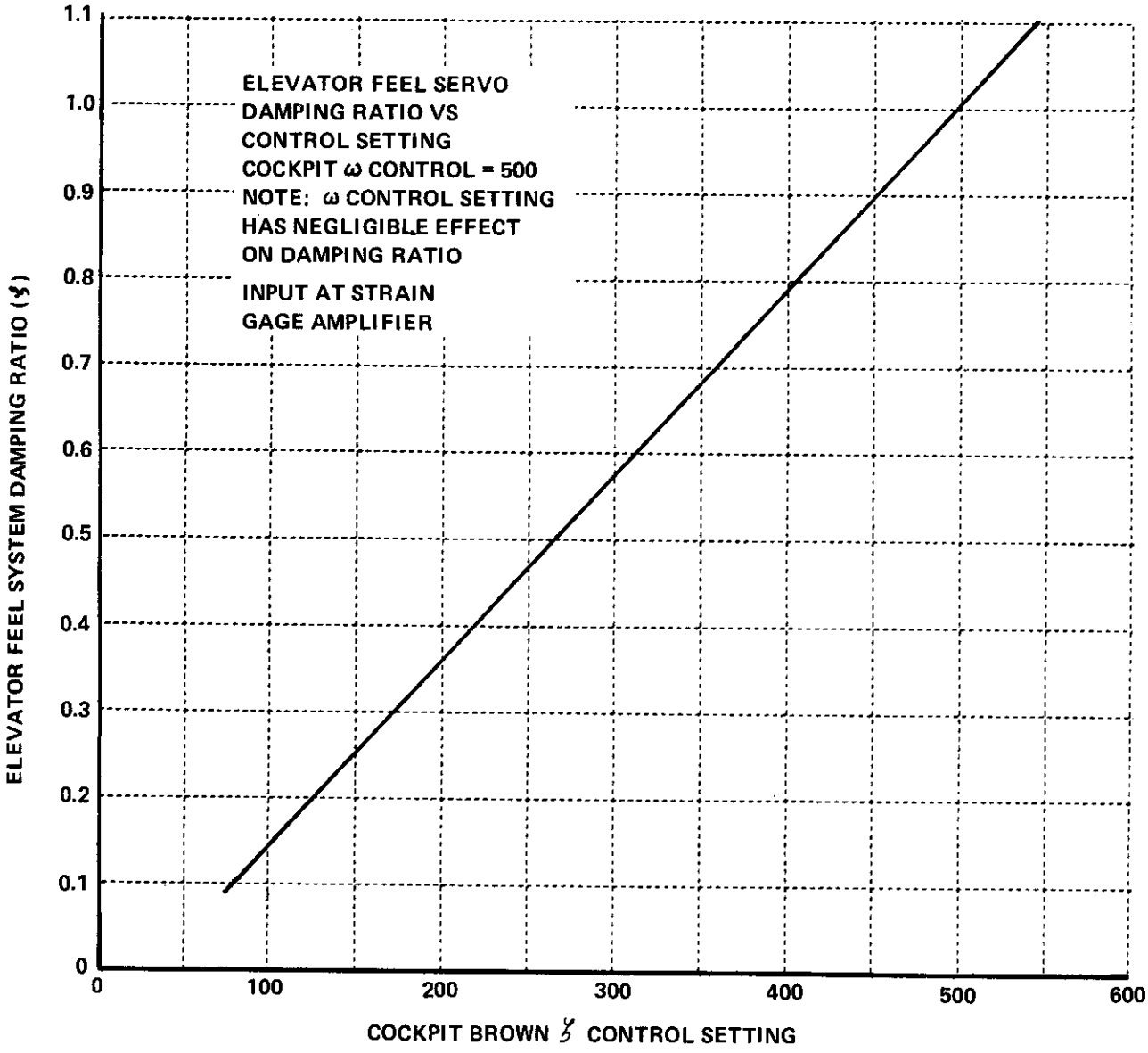

Figure 21 DAMPING RATIO VERSUS BROWN ζ CONTROL SETTING, ELEVATOR FEEL SERVO

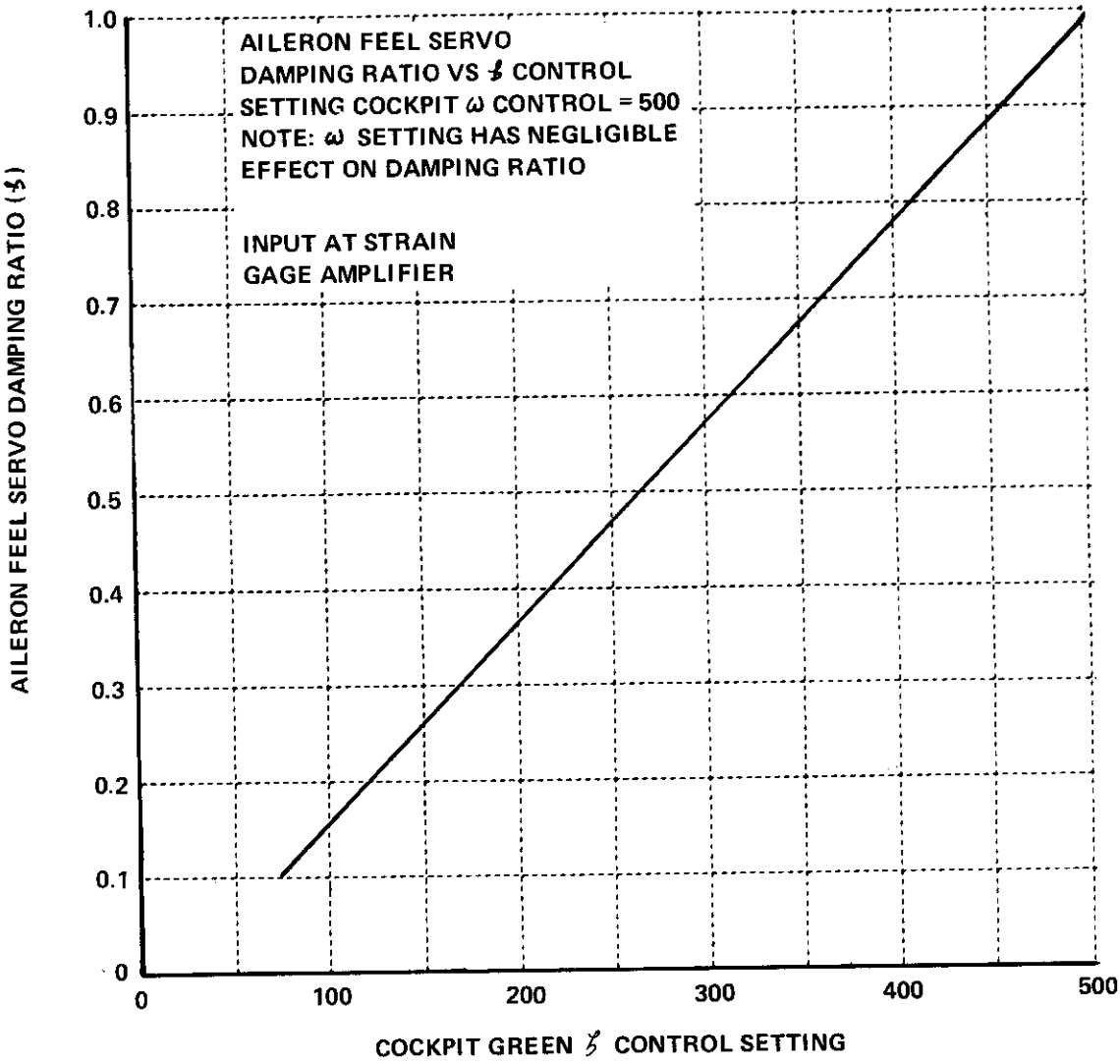

Figure 22 DAMPING RATIO VERSUS GREEN ζ CONTROL SETTING, AILERON FEEL SERVO

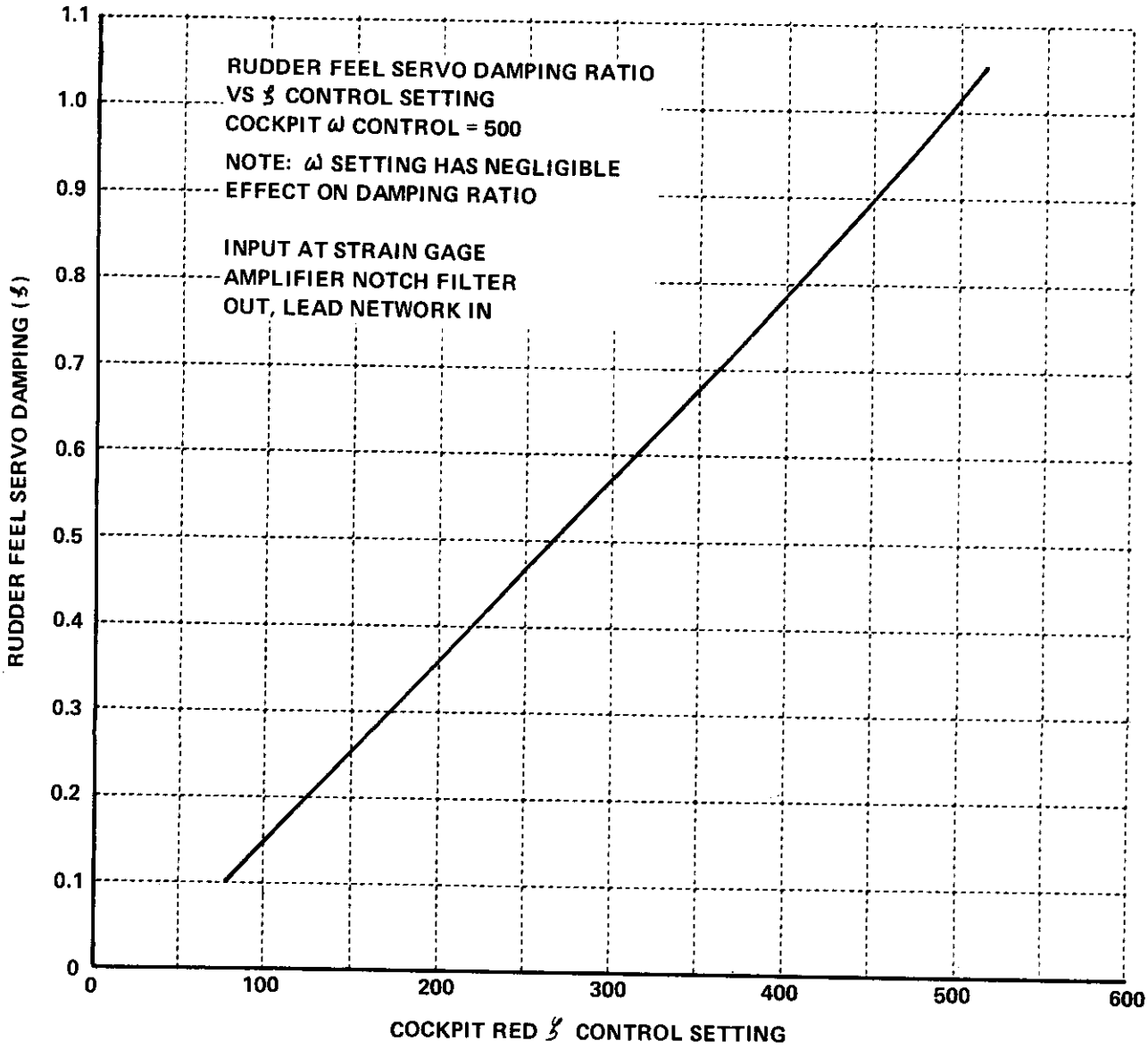

Figure 23 DAMPING RATIO VERSUS RED ζ CONTROL SETTING, RUDDER FEEL SERVO

Figures 24, 25 and 26 present control force gradients versus cockpit gradient control (K) settings.

NOTE: The above data (Figures 18 through 26) were taken with the control wheel installed, but the data are applicable for the stick installation as well.

RANGE OF ADJUSTMENT FOR FEEL SYSTEM PARAMETERS

Elevator

ω_n	0 to 50 rad/sec		
ζ	0 to 2.0		
F_{ES}/δ_{ES}	∞ lb/in. to 12 lb/in. MAX GAIN (See Note 1)		
δ_e /rate trim front cockpit (See Note 2)	pos	0.5 in./sec	authority ± 5. in.
	force	4 lb/sec	±40. lb.
	surf	2 deg/sec	±10 deg
δ_e /rate trim front seat engage (normal T-33)	surf 2 deg/sec (pos and force not used)		±10 deg
δ_e/F_{ES} front seat engage (normal T-33)	-0.446 deg/lb	Not adjustable Fixed resistors	
F_{ES}/δ_{ES} front seat engage (normal T-33)	22.5 lb/in.	Not adjustable Fixed resistors	
δ_e /trim rear cockpit	±10 deg		

Note 1. With fixed gain resistor = 249K (Other ranges available by changing fixed gain resistor.)

Note 2. Values are for front cockpit δ_e/rate trim gain control set at 1.0. Other settings available are 0.5, 0.2, and 0.1.

Aileron

ω_n	0 to 50 rad/sec		
ζ	0 to 2.0		
F_{AS}/δ_{AS}	∞ lb/deg to 0.2 lb/deg (wheel installed) MAX GAIN		
δ_{a_T} /rate trim front cockpit	pos	0.25 in./sec	authority ± 2.5 in.
	force	2.5 lb/sec	25 lb
	$surf_T$	2.0 deg/sec	±20 deg
δ_{a_T} /rate trim front seat engage (normal T-33)	$surf_T$	2 deg/sec	±20 deg
	(pos and force not used)		
δ_{a_T}/F_{AS} front seat engage (normal T-33)	3.92 deg/lb	Not adjustable Fixed resistors	
F_{AS}/δ_{AS} front seat engage (normal T-33)	0.5 lb/deg	Not adjustable Fixed resistors	
δ_{a_T} /trim rear cockpit	±20 deg		

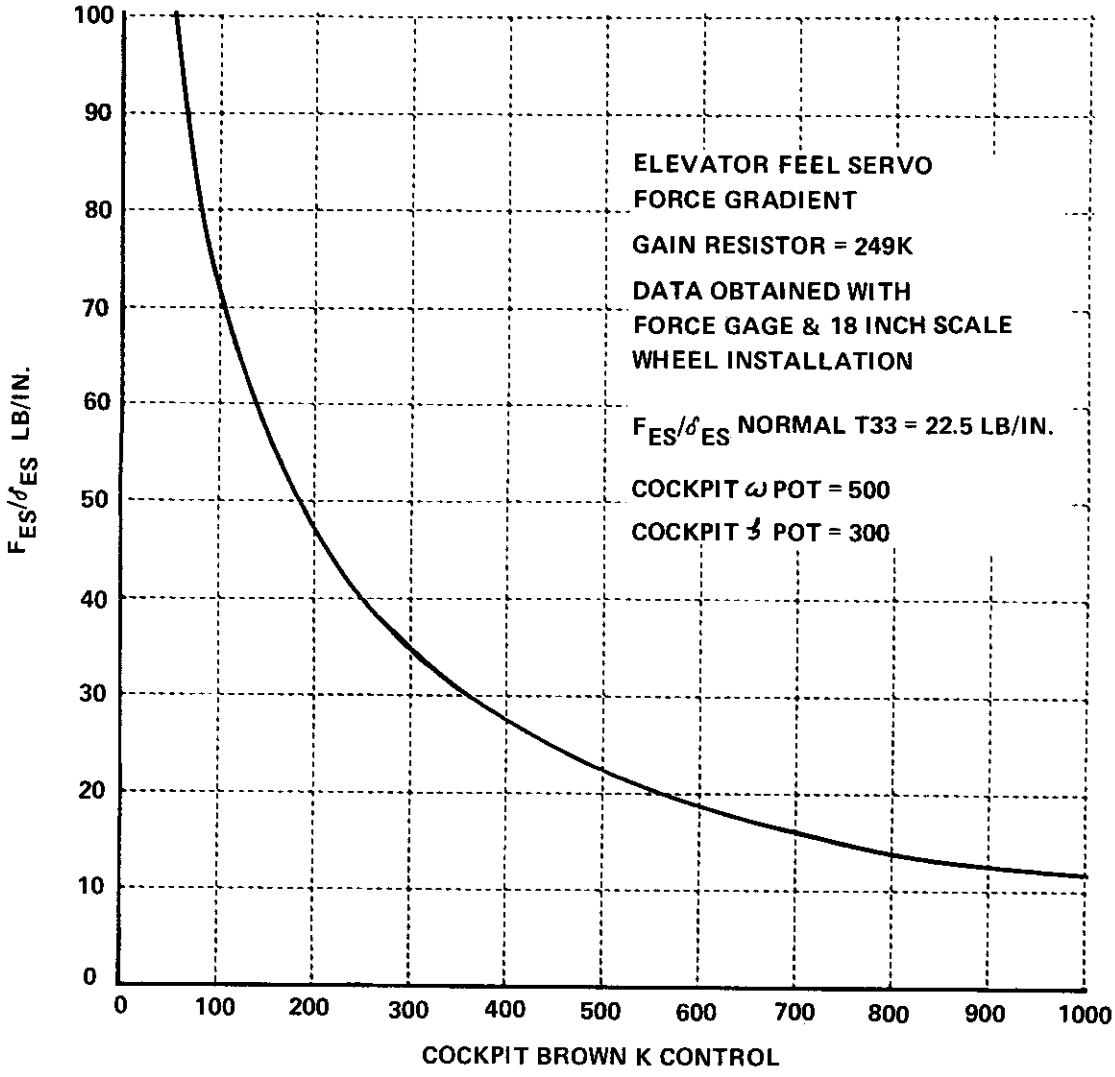

Figure 24 F_{ES}/δ_{ES} VERSUS BROWN K CONTROL SETTING

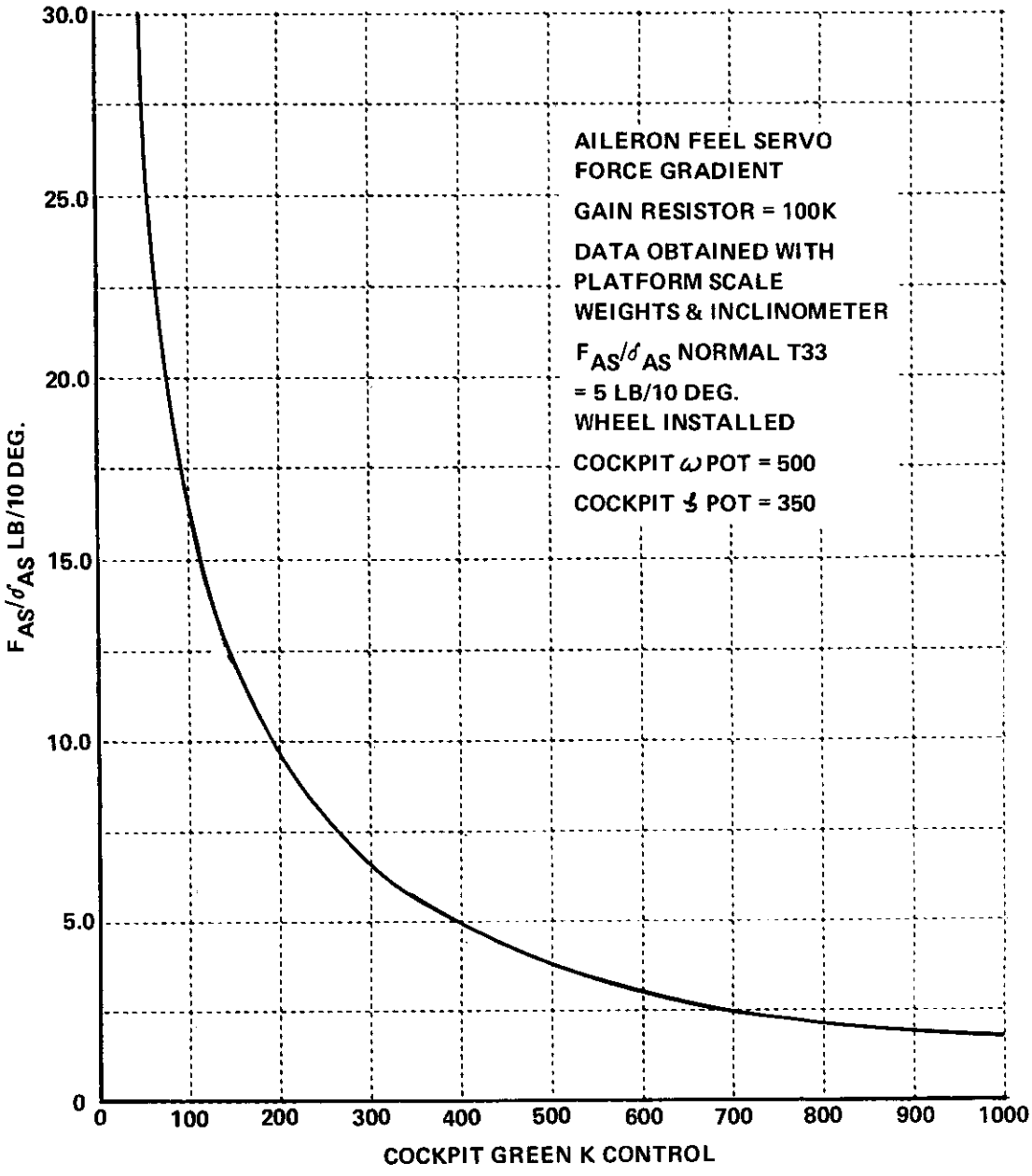

Figure 25 F_{AS}/δ_{AS} VERSUS GREEN K CONTROL SETTING

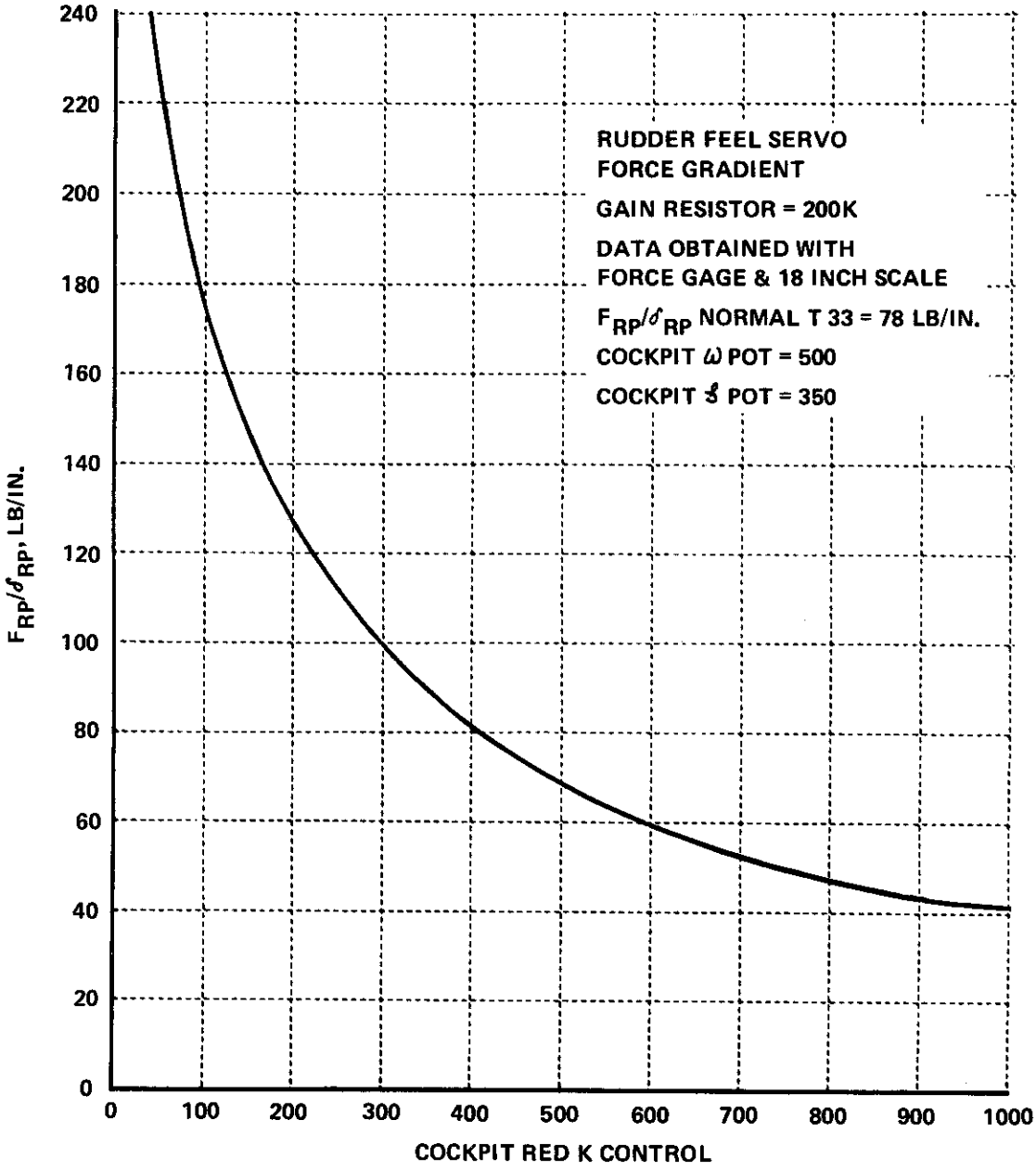

Figure 26 F_{RP}/δ_{RP} VERSUS RED K CONTROL SETTING

Rudder

ω_n	0 to 50 rad/sec		
ζ	0 to 2.0		
F_{RP}/δ_{RP}	∞ lb/in. to 40 lb/in. MAX GAIN		
δ_r /rate trim front cockpit	pos	.2 in./sec	authority ±2 in.
	force	20. lb/sec	200 lb
	surf	1.0 deg/sec	±10.0 deg
δ_r /rate trim front seat engage (normal T-33)	surf	0.4 deg/sec	±4.0 deg
δ_r/F_{RP} front seat engage (normal T-33)	-.031 deg/lb	Not adjustable Fixed Resistors	
F_{RP}/δ_{RP} front seat engage (normal T-33)	78 lb/in.	Not adjustable Fixed Resistors	
δ_r /trim rear cockpit	±20 deg		

FEEL SYSTEM SIGN CONVENTION

Sign convention for the feel system is: control forces and displacements normally used to execute a climbing right turn are considered positive (see below).

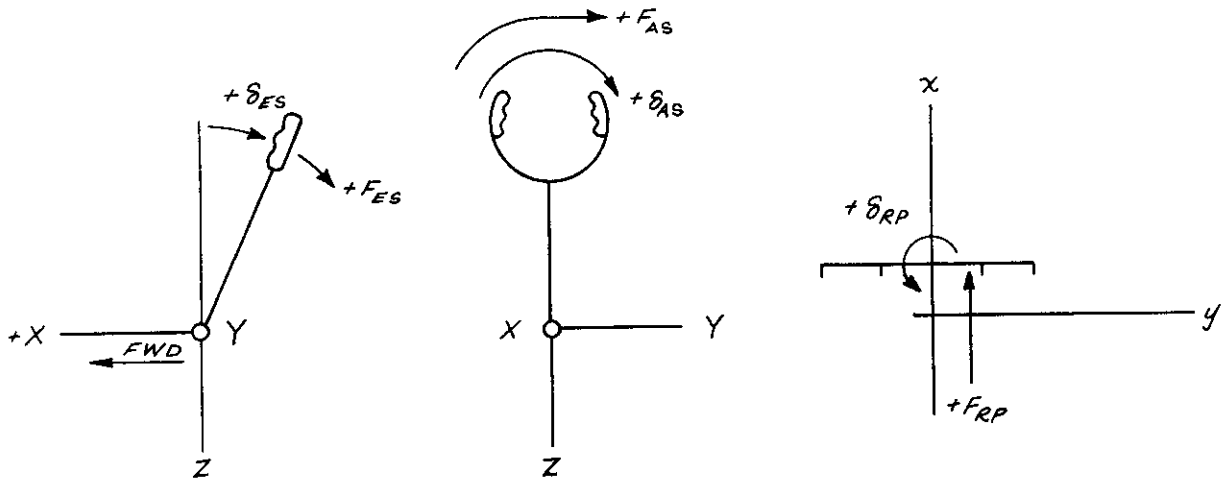

ELEVATOR **AILERON** **RUDDER**

TWO-AXIS SIDE CONTROLLER

The two-axis side controller inputs, elevator and aileron, to the control surface servos are applied directly to the elevator and aileron surface servo summing amplifiers through cockpit gain control and nose gain potentiometers. Consequently, the side controller inputs do not go through the normal feel system.

Aircraft trim from the front cockpit with the side controller installed is achieved with side-panel-mounted trim switches. Control force gradients are achieved through mechanical springs (adjustable) built into the side controller. A block diagram of the side controller elevator channel is shown below.

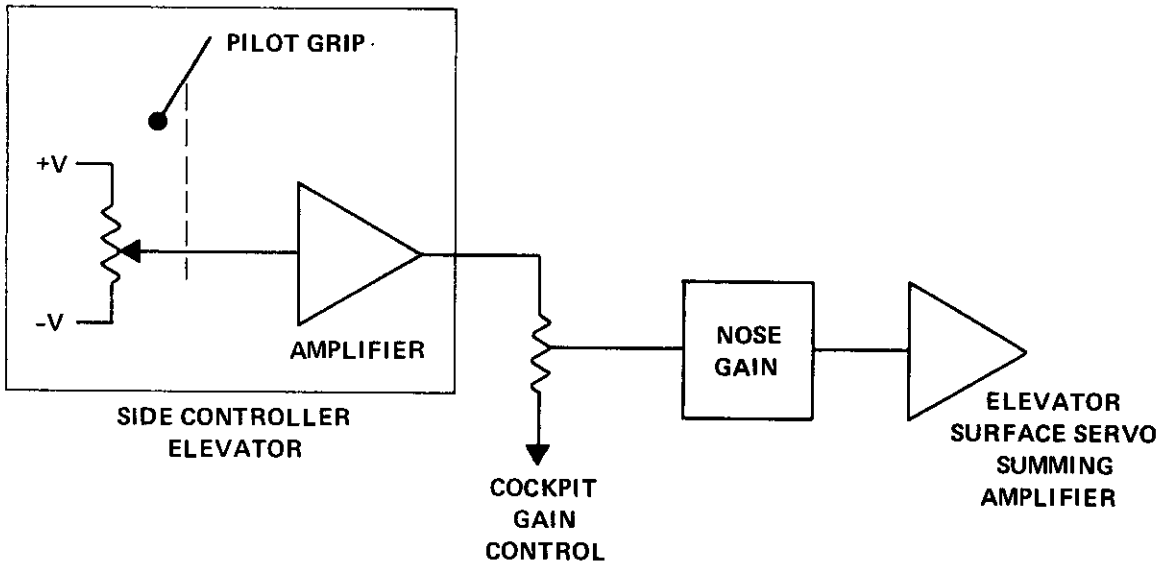

SECTION V
SAFETY PROVISIONS

A general description of the variable stability system safety provisions is given below.

DESIGN OF CONTROL AND INTERLOCK CIRCUITRY

The T-33 variable stability installation has been equipped with a system of control and interlock features which are designed to provide a maximum of operational safety. By control and interlock we mean the control by the pilot of the various functions of the variable stability system (VSS) by manipulation of various cockpit switches and push buttons. Interlocking means that the control buttons and switches are wired so that the proper sequence of operation of these controls must be observed to energize the various parts of the VSS. No action will result from a button or switch activated out of sequence. Control interlocking prevents an out of sequence portion of the VSS from being energized. For example, interlocking circuits prevent servo engage prior to auto balance engage.

The system energizing and servo-engage process advances in a sequence of steps. Those functions which least affect safety of flight are brought into operation first. The power supply equipment and the data recording systems are energized first; then the feel servo system is put into operation. Next, the position servo system variable stability inputs are automatically balanced to zero (to prevent engaged transients), the servo circuits pressurized and finally, the actuator bypasses are closed, thus completing the engagement process.

Extensive use is made of holding circuits in the design of the control and interlock system. Through use of these holding circuits and momentary switches, the system will automatically revert to the OFF position in the event of a malfunction or normal servo shutoff without the necessity of repositioning a number of switches. To re-engage the servos, it is necessary to repeat the entire engage procedure.

The holding circuits are also well suited to the use of interlock arrangements and indicator lights. Properly designed and arranged interlocks and indicators prevent omitting steps in the operating procedures and also serve as automatic safety guards in the event of a malfunction of some electronic components such as control relays (open windings or contacts), control switches or push buttoms (open contacts or broken wires). If this type of malfunction does occur, the VSS system will revert to OFF condition and remain that way until the malfunction is corrected.

AUTOMATIC SAFETY TRIP

The automatic safety trip monitors the servo-valve amplifier error signals and the normal and lateral accelerometer output signals. If these signals exceed preset values, the VSS is automatically shut off. Monitoring the servo-valve amplifier error signals provides protection against a malfunction in the VSS such as an open-loop control surface servo or a large step input to the servo caused by an amplifier failure. Protection is also provided against an inadvertent control stick motion which would produce a dangerous control surface deflection. Monitoring the accelerometer signals prevents maneuvers which would cause the airplane's structural limits to be exceeded.

Safety trip accelerometer limits have been set as follows:

n_z pushover (-1g on g meter)

n_z pullout (+4g on g meter)

$\pm n_y$ 0.25 g

These settings can be changed on the ground with a screwdriver.

CONTROL SURFACE SERVO-VALVE ERROR SIGNAL LIMITS

The limits on the servo-valve amplifier monitoring circuits have been set to allow normal step and doublet inputs to be applied to the control surface servos without shutting off the system, yet providing protection against dangerously large control surface deflections.

The maximum deflections without shutoff are:

δ_e ±6 deg

δ_r ±18 deg

δ_{a_r} ±24 deg

These limits were set using a doublet type input. These limits can also be changed on the ground with a screwdriver.

HYDRAULIC PRESSURE DUMP CONTROLS

The feel servo system has two control valves. One is a solenoid actuated selector valve which either pressurizes, or opens to return, the feel servo hydraulic lines. The control switch for this valve is located on the front cockpit instrument panel, lower left side. This switch is the "FEEL" button shown in Figure 27. This is a fail-safe type valve, i.e., in the event of electrical failure it assumes the "open to return" configuration which depressurizes the actuator.

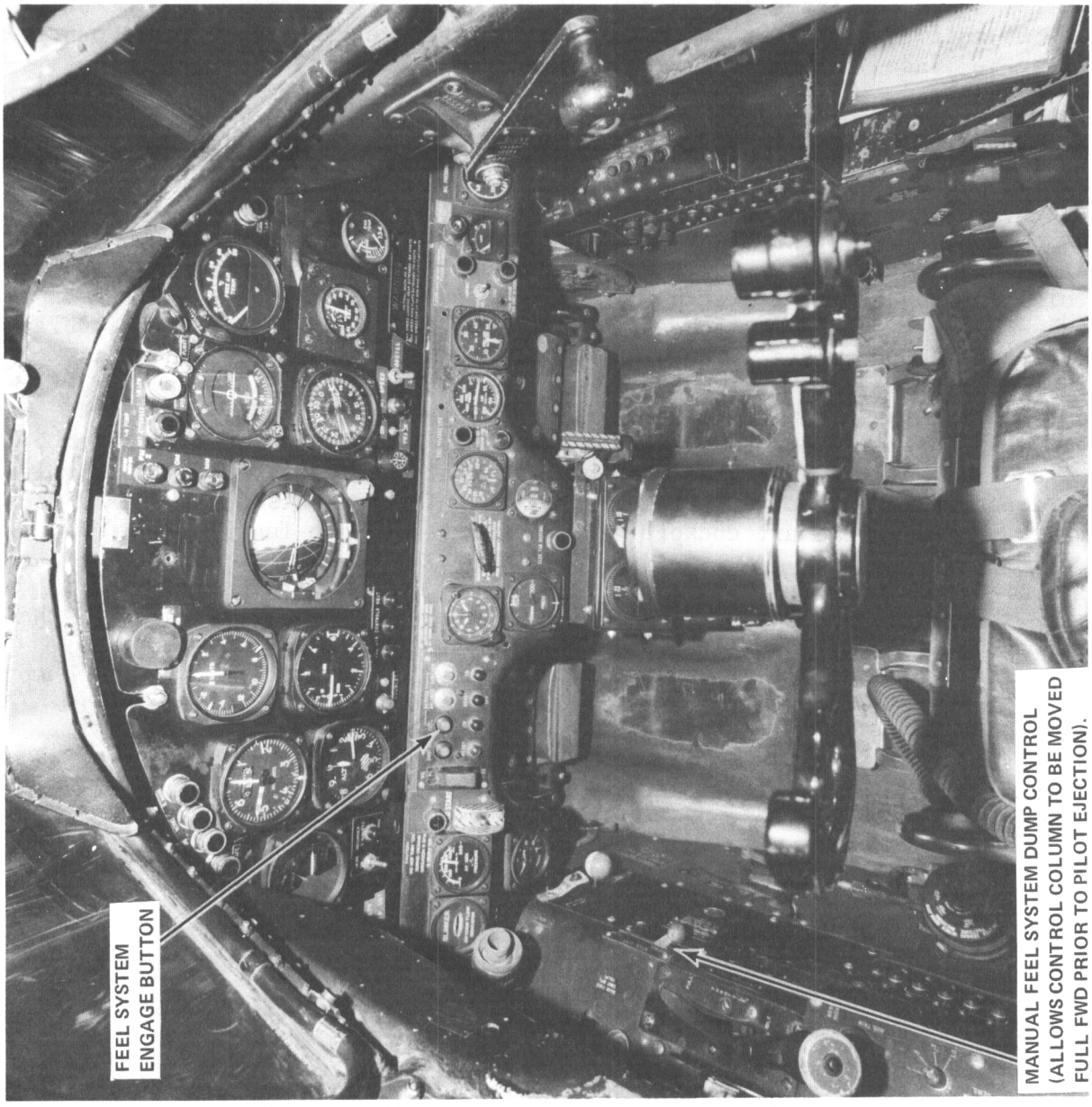

Figure 27 FRONT COCKPIT SHOWING FEEL SYSTEM ENGAGE/DISENGAGE CONTROLS

The second control valve in the feel servo system permits the pressure on one side of the elevator feel servo to be released and the control column to be moved forward. Moving the control column forward is essential with the wheel configuration installed to provide the necessary clearance in the event the pilot must eject. A bungee cord is bolted to the front instrument panel that can be placed around the wheel to insure that it will be held in the forward position.

Toggle switches and push button switches are used to control the hydraulic pressure valves for the control surface servos. These control switches, located in the aft cockpit, are operated by the safety pilot. The location of these switches is shown in Figure 28 (VSS Engage Panel). A single solenoid actuated selector valve which pressurizes all three position servo circuits is operated by a switch ("PRESSURE" toggle switch) on the aft cockpit switch console. Another switch on this console ("ENGAGE" push button) operates the three solenoid valves which bypass the three position servo actuators. These valve installations are also of the fail-safe type. The bypass and pressurization functions can also be done from the front cockpit with a single push button switch (Surface "ON"). There are also switches on both front and rear sticks, the wheel and on the front control panel (shutoff valve) which deactivate the feel and position servos. There is also a hand held "pickle" switch in the aft cockpit that performs the same function (see Figure 29).

In addition to the electrical valve controls, used for control of the electrohydraulic control surface servos, there is a manually operated valve in the aft cockpit. This manually operated valve is actuated by the red dump handle below the hydraulic pressure indicator (see Figure 29). This valve permits the releasing of the pressure on both sides of the pistons of all three position servos. Thus, in an emergency, the position servos can be depressurized and manual control of the airplane regained by operating one mechanically controlled valve.

The normal aileron boost control in the rear cockpit (see Figure 29) is safety wired in the "BOOST ON" position. This manually operated hydraulic boost control is no longer used in the VSS engage procedure to turn off aileron boost before engaging the VSS. The aileron boost is now automatically turned off electrically at the proper point in the VSS engage process.

HINGE MOMENT LIMITS

Each of the position servos is equipped with pressure relief valves which limit the maximum force or hinge moment output of the servo actuator. The servo actuators and valves were selected to provide the required dynamic performance, frequency response and limit linear displacement rates. Unfortunately this design criterion is not necessarily compatible with the structural integrity of the airplane. Therefore, for reasons of safety, it was necessary to limit the maximum differential hydraulic pressure which could occur across any of the servo pistons to a fraction of the supply pressure. An important reason for limiting the maximum hinge moments from the actuators is to prevent excessive horizontal or vertical tail loads which might occur

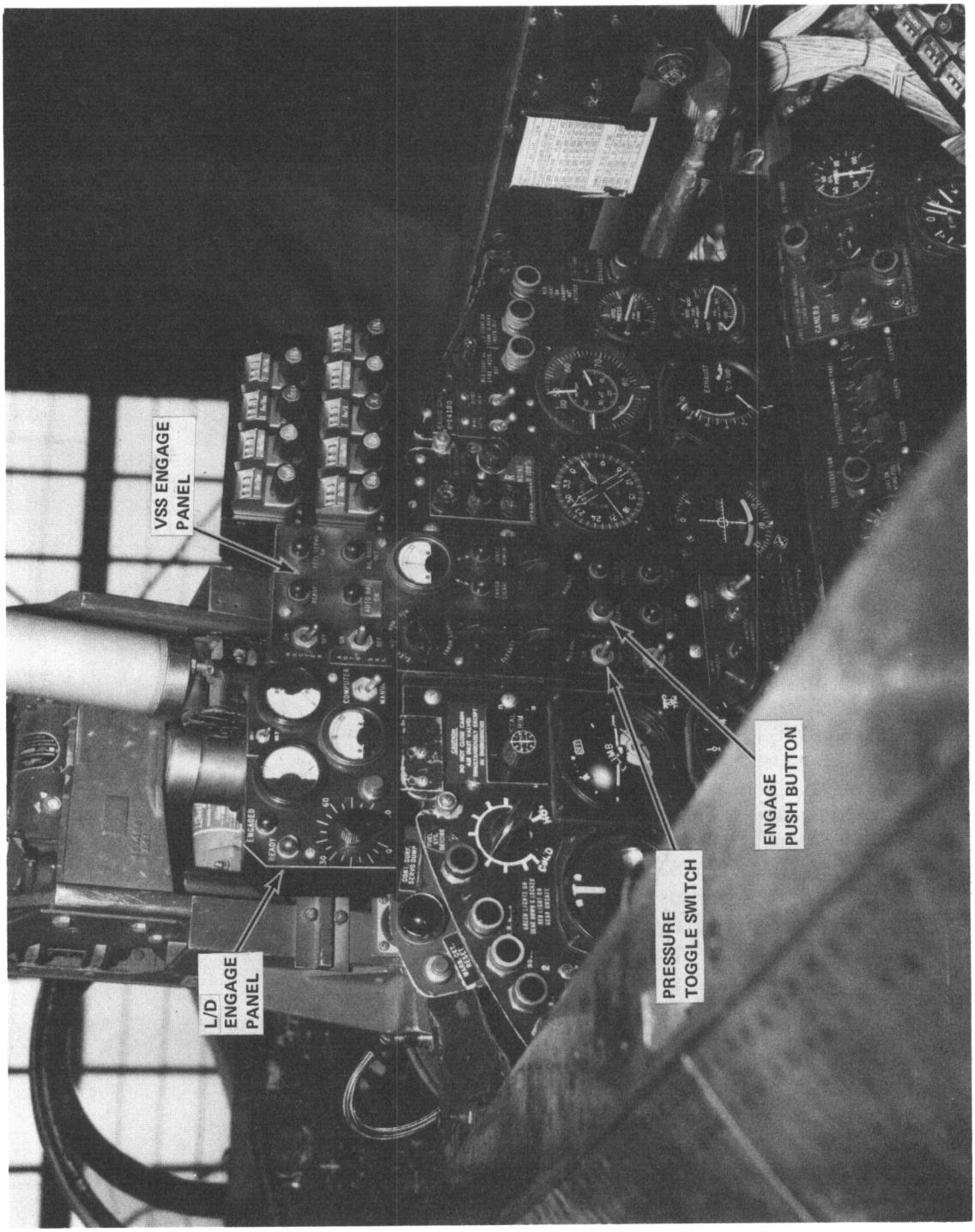

Figure 28 AFT COCKPIT SHOWING VSS ENGAGE PANEL

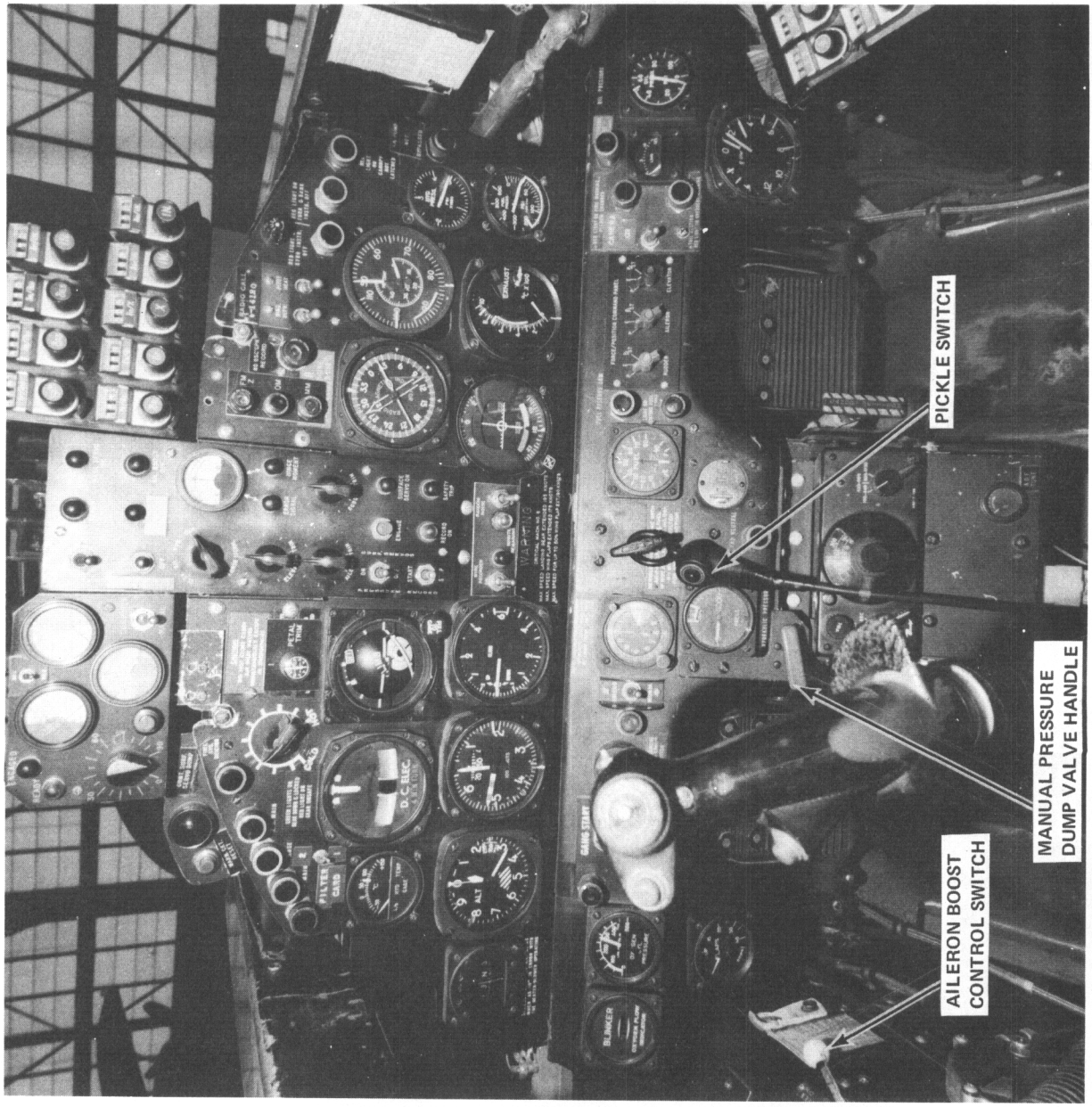

Figure 29 AFT COCKPIT SHOWING CONTROL SURFACE SERVO DISENGAGE CONTROLS

when simulating airplane dynamics different from the normal T-33. Hinge moment limiting is also quite effective in limiting the maneuvering loads on the airplane.

AUDIO/VISUAL SHUTOFF WARNING CIRCUIT

If the VSS or L/D system is automatically shut off, then it is essential that the safety pilot recognize the situation and take control of the airplane as quickly as possible. This is particularly important during low level approaches. To help the pilot recognize when the systems are dumped, a one-inch diameter red light has been provided in the top left side of the rear cockpit instrument panel. An audio signal resembling "beep, beep, beep" is also heard in both front and rear headsets.

FRONT SEAT ENGAGE

The variable stability equipment can be engaged from the front cockpit in two ways; (1) variable stability engage and (2) normal T-33 engage. The variable stability engage energizes the same equipment as a rear seat engage. To get this mode of engage, it is necessary to set a guarded toggle switch to VSS (unguarded position) and perform the proper front seat engage sequence.

The normal T-33 mode of engage is a safety feature provided to enable the front seat pilot to fly the airplane and land it in the event of incapacitation of the rear seat pilot. The T-33 mode of engage can also be used to allow the front seat pilot to fly the airplane while the rear seat pilot's attention is diverted to other duties such as setting gain controls for a configuration, taking notes, etc. When the front seat pilot engages the aircraft with the toggle switch in the guarded position (T-33 position), he gets, in effect a normal T-33 airplane. Force commands are used as control inputs. All the variable stability inputs are locked out except the control inputs from the front stick. A set of fixed feel system characteristics is provided except for frequency and damping which are determined by whatever the ζ and ω_n pots are set to in the rear cockpit.

The T-33 engage feel system characteristics are:

Wheel Installed		Stick Installed	
F_{EW}/δ_{EW}	= 22.5 lb/in.	F_{ES}/δ_{ES}	= 22.5 lb/in.
F_{AW}/δ_{AW}	= 5 lb/10 deg	F_{AS}/δ_{AS}	= 2.5 lb/in.
F_{RP}/δ_{RP}	= 78 lb/in.	F_{RP}/δ_{RP}	= 78 lb/in.

T-33 engage trim rates are:

δ_e surface movement 2 deg/sec

δ_a surface movement 2 deg/sec

δ_r surface movement 0.4 deg/sec

NOTE: Trim commands in the T-33 engage position do not move the stick or rudder pedal positions. Trim commands go directly to control surface servo summing amplifiers. Gains of control surface movements per front seat control force inputs are set to approximately simulate the normal T-33 in the landing approach configuration.

The control gains are:

$$\delta_e/F_{ES} = 2.5 \text{ deg}/5 \text{ lb}$$

$$\delta_a/F_{AS} = 10 \text{ deg}/2.5 \text{ lb}$$

$$\delta_r/F_{RP} = 3 \text{ deg}/100 \text{ lb}$$

These settings result in a very sensitive airplane configuration at high speeds, but in the interest of safety, the greater consideration was given to the handling characteristics in the landing approach configuration. This was done in the event it became necessary to land the airplane from the front seat under emergency conditions.

SPECIAL CIRCUITS

Due to their frequent use, certain test signal inputs have been made a permanent installation in the T-33. These are the doublet, step and random noise signals, and sine wave generator signal. See Figures 30 through 34.

Auto Input Circuits - Step or Doublet

The doublet and step are applied through the δ_e/IN, δ_r/IN and δ_a/IN gain controls (which control amplitude and sign) to the control surface summing amplifiers. A toggle switch in the front cockpit selects either step or doublet and a pushbutton applies the signal for as long as it is pressed. Both halves of the doublet are generated automatically once the pushbutton is pressed. The width of the doublet is adjustable on the ground and can be adjusted from 0.8 to 1.2 seconds.

Random Noise

The basic random signal source used in the T-33 noise generator consists of four Zener diodes arranged in a bridge circuit (see Figure 31). The bridge circuit is used, rather than a single diode, in order to minimize output variations due to temperature changes. Since the low frequency portion of the diode output spectrum is not flat, i.e., of constant spectral density, the desired spectrum could not be obtained directly. However, the diode's spectrum is flat over narrow bands at higher frequencies. To produce a flat low frequency spectrum, the signal from the diode bridge is passed through a band-pass filter and then a modulator, both of which are tuned to 400 Hz. This circuitry is followed by a high-pass filter (ω_n = 0.1 rad/sec) to remove d.c. drift and a low-pass filter (ω_n = 18.8 rad/sec) which attenuates undesirable high frequencies (see Figure 32). The signal out of the low-pass filter is then used to drive the elevator, aileron and rudder servos through the δ_e/IN, δ_a/IN and δ_r/IN cockpit gain controls to produce random variations in the pitching, yawing and rolling motions of the airplane.

Tests for the characteristics of the signal being fed to the elevator servo have yielded the following results:

a. Average value was within + 1 and -1/2 volts for 1000 second time interval. Average value = $\frac{1}{T}\int_0^{1000} e_o \, dt$ where e_o = output of noise generator.

b. RMS value was found to be temperature dependent with an average value of 0.28 volts. Temperature dependence noted but was not measured.

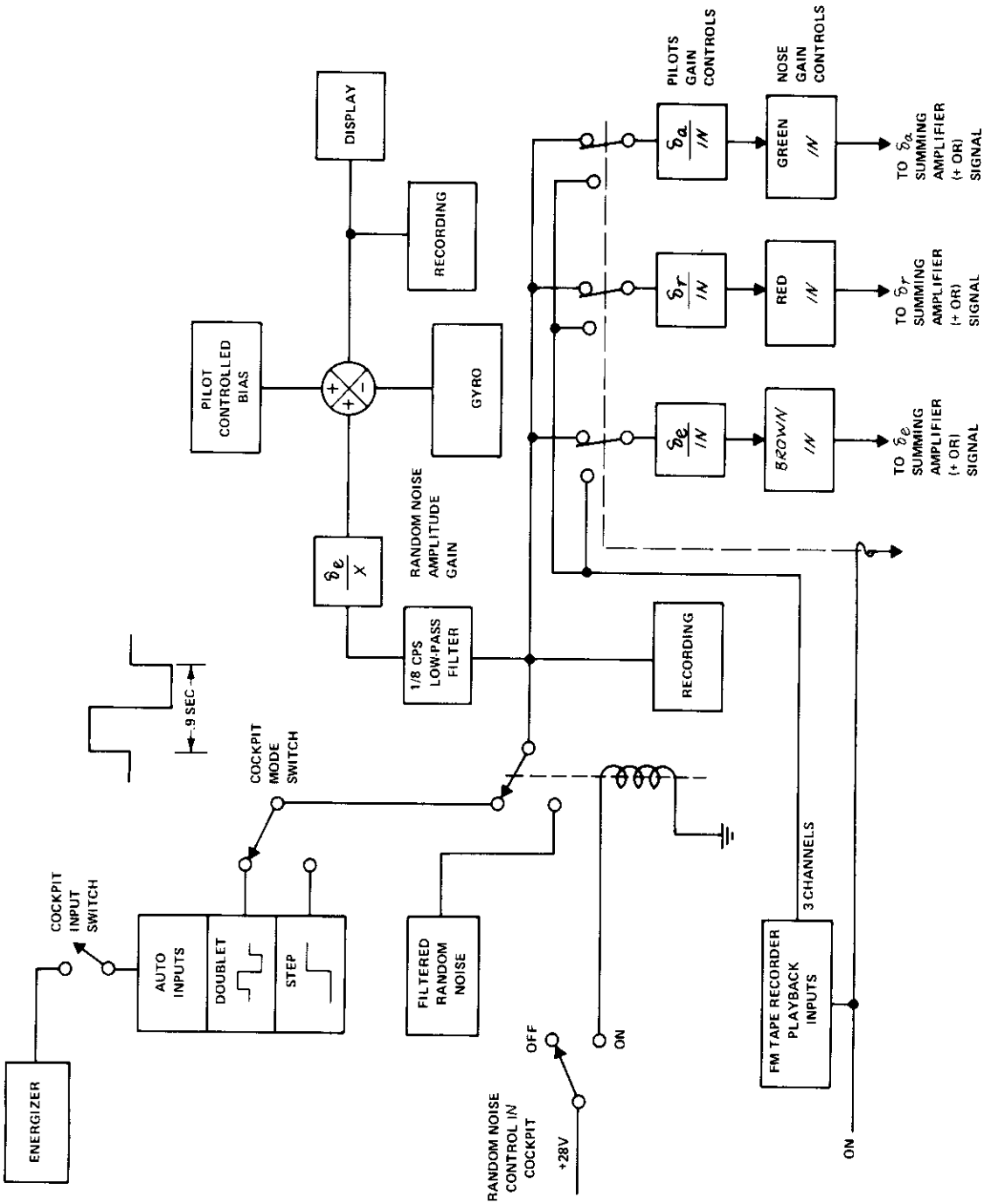

Figure 30 AUTOMATIC DOUBLET OR STEP INPUTS AND RANDOM NOISE SOURCE

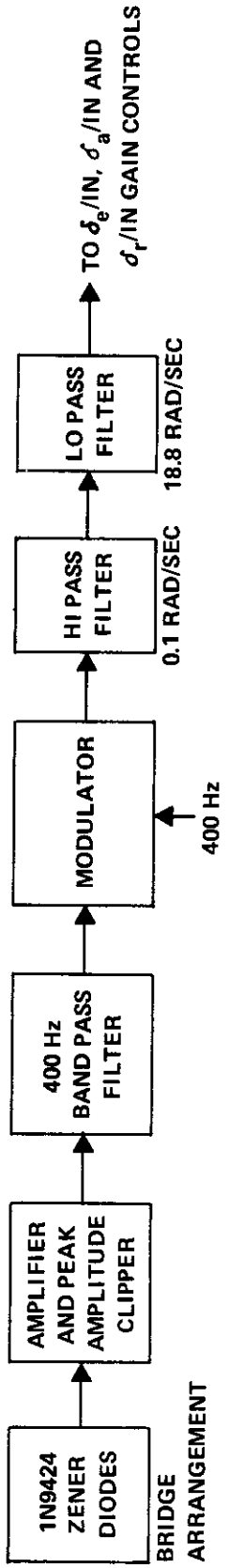

NOTE: MODULATOR OUTPUT IS SUM AND DIFFERENCE FREQUENCIES OF THE TWO INPUTS. THE DIFFERENCE FREQUENCIES ONLY PASS THROUGH THE LOW PASS FILTER AND ARE FED TO THE δ_e/IN, δ_r/IN, AND δ_a/IN POTS.

Figure 31 BLOCK DIAGRAM – RANDOM NOISE (ROUGH AIR SIMULATION)

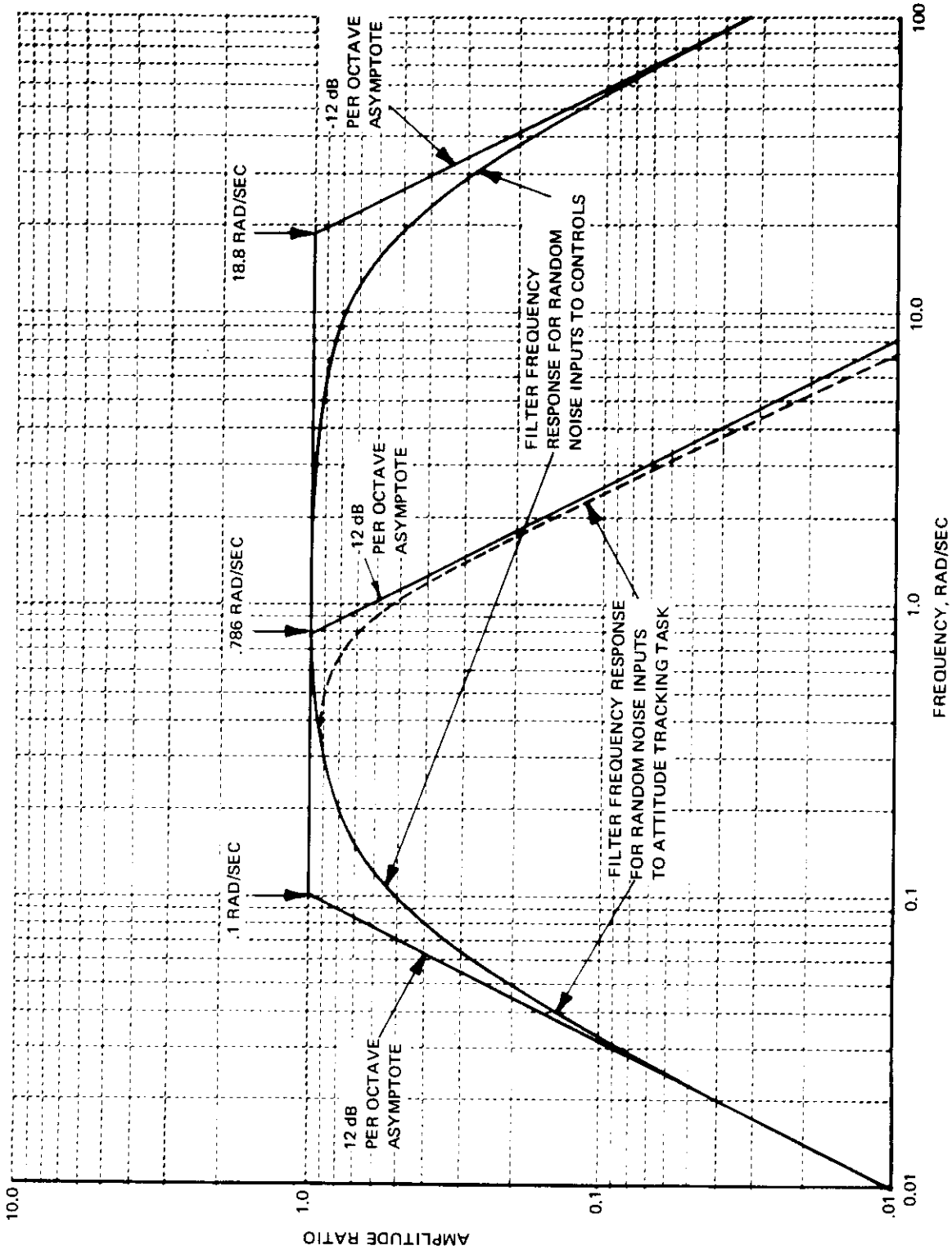

Figure 32 RANDOM NOISE FILTER FREQUENCY RESPONSE

c. By measuring the percentage of time the output is above a given value, the distribution function can be closely fit by a normal curve. The distribution function is a continuous curve, therefore the total number of points required to fill out the curve would approach infinity. For a quick check, the Gaussian shaped density function curve was divided into ten sections and data taken at each section. This was adequate to fill out a curve which closely approximated the normal Gaussian shaped density function curve.

d. The power spectral density at 0.10, 0.20, 0.50, and 1.0 cps is within 1 dB of being flat and then follows the asymptote of the low-pass filter. For an rms of 0.28, the value for the spectral density below the filter corner frequency should be 3.8×10^{-3} volts^2/rad/sec.

Sine Wave Generator

A sine wave signal source has been added as a permanent installation in the T-33 airplane. The circuit consists of a motor driven sin/cos potentiometer. See Figures 33 and 34. The frequency and amplitude of the sinusoidal output are controlled from two gain controls "SIN FREQ" and "F_{ES}/SIN" in the rear cockpit.

The generator output can be connected to provide an input as dictated by a particular program requirement. If desired a sine wave input can be made into the force channel (F_{ES}) of the elevator feel system. The sine wave generator output can also be displayed in the front cockpit on the horizontal needle of the Lear attitude indicator.

The frequency of the sine wave output is varied with the "SIN FREQ" potentiometer control in the rear cockpit. To provide a larger or different range of frequency adjustment, the gearing between the d.c. motor and sin/cos potentiometer can also be changed on the ground between flights.

Sampler Circuit

The sampling circuit in the T-33 is a device which checks the configuration of the variable stability and control system as set up by the rear seat pilot. This is done by sampling the setting of each rear cockpit gain control potentiometer and the setting of Force/Position Command Panel switches. This information is recorded in the form of voltage steps or pulses on the oscillograph and on the digital recorder at the beginning of each data record. The height of a pulse indicates the potentiometer setting. A special recording channel is reserved for this purpose on both oscillograph (Galvanometer 49) and digital recorder.

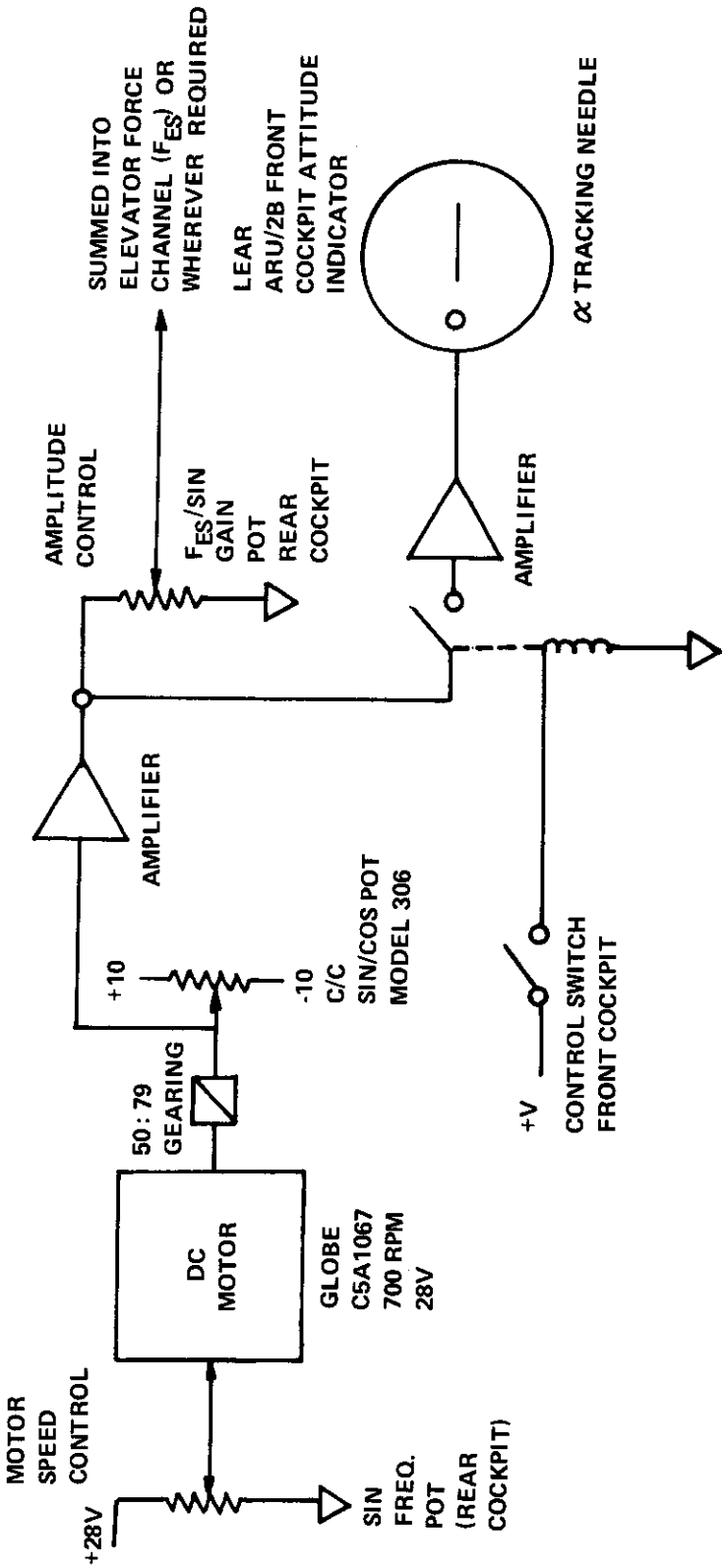

Figure 33 SINE WAVE GENERATOR SCHEMATIC

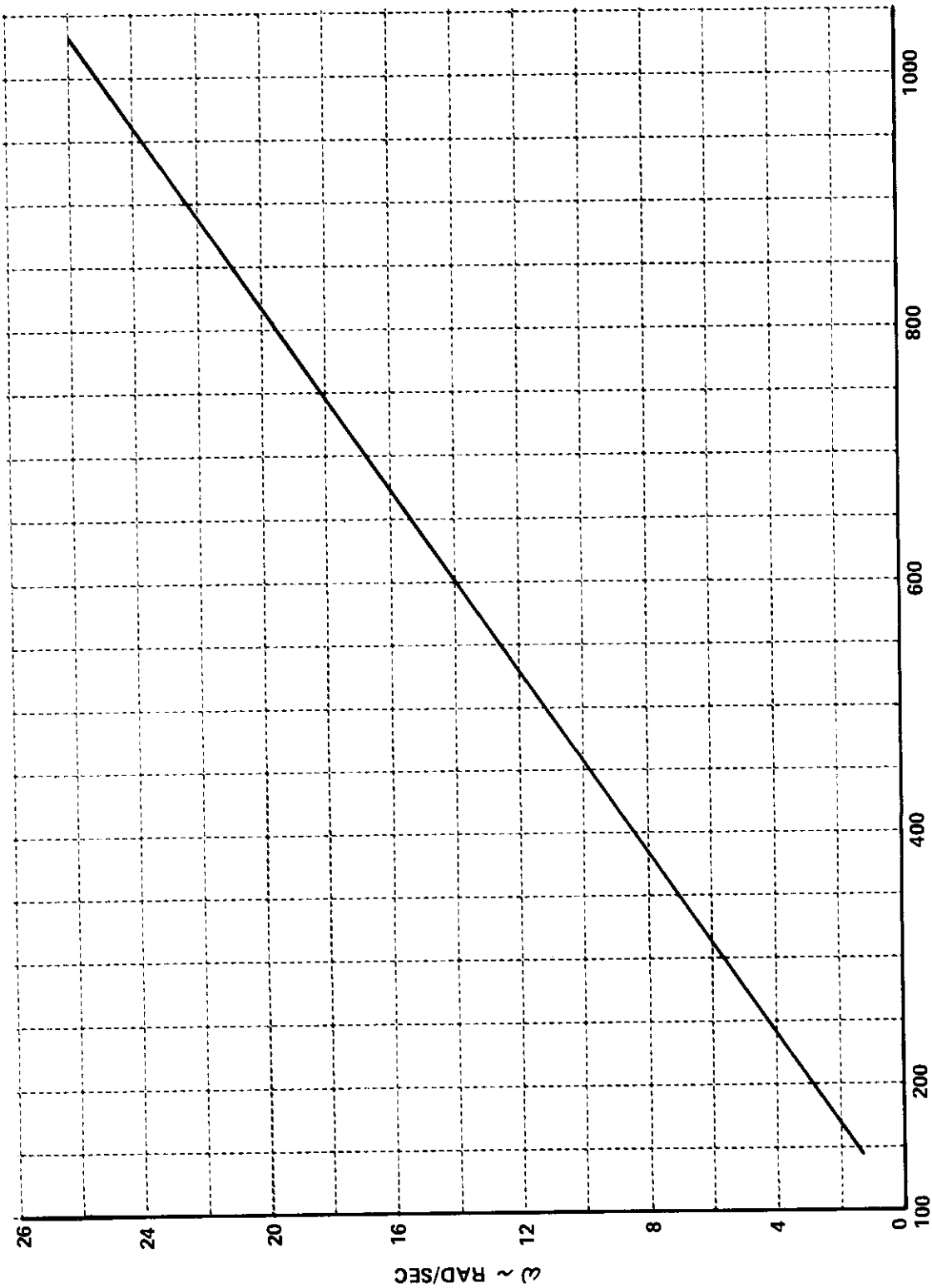

Figure 34 SINE WAVE GENERATOR FREQUENCY VS. COCKPIT POT SETTING

The rudder, aileron and elevator switch positions on the Force/Position Command Panel are sampled first. (These switches are located on the rear cockpit instrument panel. They select force or position commands from the front stick to control surfaces.) The gain control potentiometers are then sampled. This includes all the gain control pots in the rear cockpit; 9 on the instrument panel and 28 on the right-hand console. Figure 35 is a diagram of the sampler circuit for 2 of the 37 gain control pots. Table I, The Sampling Circuit Code, lists each sample pulse number and the parameter associated with it.

A sampling period requires approximately 13 seconds for completion. The recording equipment is designed such that minimum recording time is 13 seconds to allow a complete sampling cycle. Each parameter is sampled for

$$\frac{13 \text{ sec}}{52 \text{ position}} = 0.25 \text{ sec}$$

A time delay relay provides zero output (ground) for the first half of each sample pulse. The voltage present at the output of the sample circuit amplifier is shown in Figure 36.

For example, the elevator, aileron and rudder Force/Position Command Panel switch positions are given below along with the sample circuit voltages for each of the switch positions. Sample circuit voltages obtained for several gain control potentiometer settings are also given below.

Force/Position Command Panel

Switch Position	Function	Sample Circuit Output
1	Position Command	+ 10.00 V
2	Force Command	+ 5.00 V
3	Position Command (Surface trim - stick does not move.)	- 5.00 V
4	Unassigned - future use	- 10.00 V

NOTE: The sampling sequence is elevator, aileron and then rudder corresponding to the sample steps 6, 7 and 8 in Table I.

Cockpit Gain Control Potentiometers

Potentiometer Setting	
000	-10.00 V
500	0.00 V
1000	+ 10.00 V

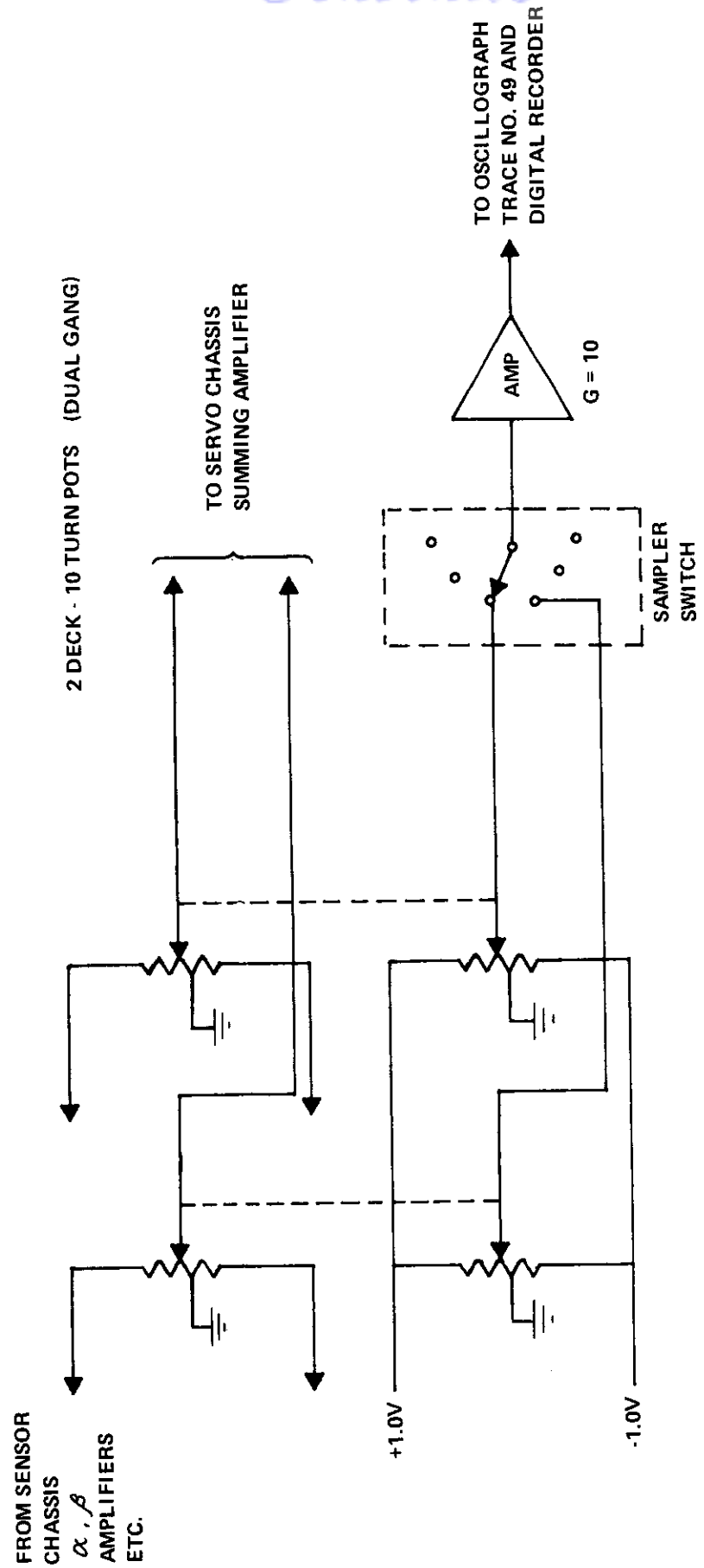

Figure 35 SAMPLING CIRCUIT SCHEMATIC SHOWN FOR TWO GAIN CONTROL POTENTIOMETERS

Table I
SAMPLING CIRCUIT CODE

SAMPLE NUMBER	PARAMETER SAMPLED
1	SIGNAL GROUND
2	+1.0 V IDENTIFICATION
3	- 1.0 V
4	UNASSIGNED
5	UNASSIGNED
6	ELEVATOR COMMAND MODE
7	AILERON COMMAND MODE
8	RUDDER COMMAND MODE
9	δ_r/β
10	$\delta_r/\dot{\beta}$
11	δ_r/p
12	δ_r/r
13	$\delta_r/x\ (\dot{p})$
14	$\delta_r/y\ (\dot{r})$
15	RUDDER FEEL SYSTEM K (GRADIENT)
16	RUDDER FEEL SYSTEM ω (FREQUENCY)
17	RUDDER FEEL SYSTEM ζ (DAMPING)
18	δ_r/δ_{RP}
19	δ_r/δ_a
20	δ_r/IN
21	+1.0 V } IDENTIFICATION
22	- 1.0 V }
23	UNASSIGNED
24	δ_a/β
25	$\delta_a/\dot{\beta}$
26	δ_a/p
27	δ_a/r
28	$\delta_a/x\ \ (\dot{p})$
29	$\delta_a/y\ \ (\dot{r})$
30	AILERON FEEL SYSTEM K (GRADIENT)
31	AILERON FEEL SYSTEM ω (FREQUENCY)
32	AILERON FEEL SYSTEM ζ (DAMPING)
33	δ_a/δ_{AS}
34	δ_a/r
35	δ_a/IN
36	+1.0 V } IDENTIFICATION
37	1.0 V }
38	δ_e/IN
39	δ_e/α

Table I (Cont.)

SAMPLE NUMBER	PARAMETER SAMPLED
40	$\delta_e/\dot{\alpha}$
41	δ_e/q
42	δ_e/u
43	δ_e/y $(\dot{q})$
44	ELEVATOR FEEL SYSTEM K (GRADIENT)
45	ELEVATOR FEEL SYSTEM ω (FREQUENCY)
46	ELEVATOR FEEL SYSTEM ζ (DAMPING)
47	δ_e/δ_{ES}
48	δ_e/x $(\dot{u})$
49	δ_p/α
50	δ_p/u
51	SIGNAL GROUND
52	SIGNAL GROUND

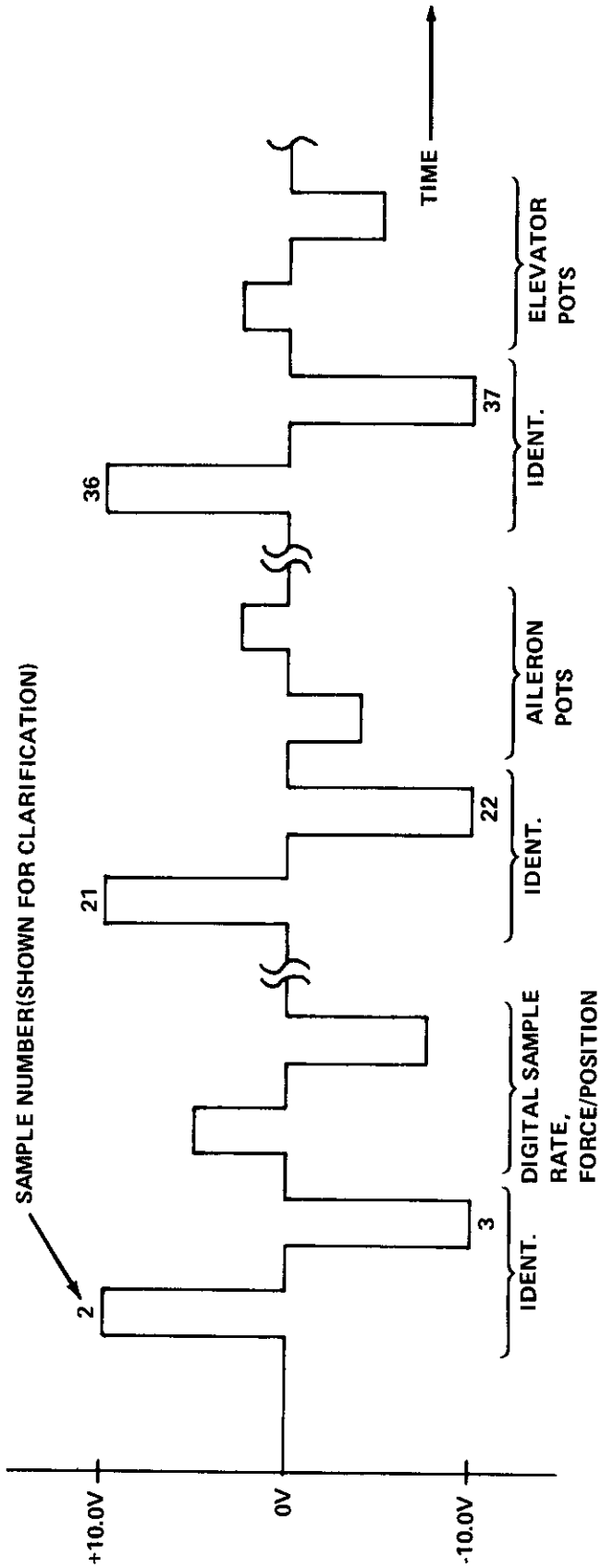

Figure 36 TYPICAL SAMPLING CIRCUIT OUTPUT VS TIME

Identification Samples

The potentiometer samples for each axis, elevator, aileron and rudder are separated by identification samples.

Identification Sample Number	Sample Circuit Output
2	+10.00 V
3	-10.00 V
21	+10.00 V
22	-10.00 V
36	+10.00 V
37	-10.00 V

A typical sampling sequence recorded on the oscillograph (trace No. 49) is shown in Figure 36. Galvanometer deflection is adjusted for a convenient scale, e.g., ±10.0 V = ±2.0 inches on the oscillograph. The digital data processing equipment can be programmed to print out the actual dial setting of the cockpit gain control.

To determine a particular gain control or switch position setting used during an oscillograph record, it is first necessary to locate the sampling trace (trace No. 49) on the oscillograph record and then the pulse which is associated with the wanted gain control setting or control switch setting.

The location of the desired pulse is most easily done by using a strip of paper approximately 24 inches long which is especially made up for this purpose. The paper has marks spaced along it identifying the pulses. The paper strip is laid down adjacent to the sampling trace and the desired gain control pulse or switch position pulse can easily be located.

To convert pulse amplitude to cockpit gain control dial setting, the pulse amplitude is measured and converted to dial settings. The current scale factor is 250 digits of dial setting per inch of trace deflection. A dial setting of 500 is zero inches of deflection. A pulse deflection "up" paper (toward side of paper where oscillograph number is printed) of 1 inch equals a dial setting of 250, etc. A dial setting versus amplitude scale is provided on the above noted paper strip.

SPECIAL SIMULATION DEVICES AVAILABLE

Each T-33 research program normally has some special instrumentation requirements. These are special VSS inputs, recordings, or front cockpit instrument displays. These special circuits/devices are listed below for reference:

PEMCO Magnetic Tape Recorder-Playback Unit

This is a small 3-channel FM magnetic tape recorder/reproducer which can be mounted in the T-33 and used to play back 3 channels of prerecorded analog data into the VSS system when airborne.

1. Playback time: 88 minutes
   (825 ft at 1 7/8 inches per second)

2. Type of playback - FM analog DC to 300 Hz
   FM center frequency: 1.68 KC IRIG

Airspeed Error Indicator Lights

On certain programs, such as landing-approach handling qualities studies, it is often desirable to provide the T-33 evaluation pilot with a remote or "heads up" airspeed display. This display, mounted on the top right-hand side of the front instrument panel, is within the pilot's field of vision during the VFR portion of the landing approach. The pilot gets a high, low, or "on" airspeed indication without having to look down at the instrument panel.

A visual presentation of the speed relative to a given datum is displayed. This display is analogous to the Navy's remote angle of attack display. The T-33 display consists of three lights (green, amber, red) in a vertical column (see Figure 37). The center light (green) glows at datum speed plus or minus 5 knots. The top light (red) glows at datum speed plus 2.5 knots (i.e., α low). The bottom light (amber) glows at datum minus 2.5 knots (i.e., α high). The alternate display presented is the same as the Navy's angle of attack display.

Displayed Bank Angle Tracking

On some lateral-directional T-33 programs, it is desirable to have the evaluation pilot perform some exacting tracking task utilizing aileron control surface inputs. This is done to aid the pilot in assessing the lateral-directional handling qualities of the configuration as set up by the safety pilot. For this reason, a bank angle tracking circuit was designed for presentation of a bank angle tracking task. The bank angle tracking circuit causes an artificial bank angle error signal to be displayed to the evaluation pilot which he must null out with actual bank angle inputs through aileron control inputs.

True bank angle is sensed by an attitude gyro and fed through a ϕ display servo to the front cockpit bank angle instrument (see Figure 38). The ϕ display servo is driven by an auxiliary input and thus the displayed bank angle is the combined input of the gyro and the auxiliary input signal.

The auxiliary input signal is usually the output of the disturbance generator described in this section or a random noise type analog signal which can be obtained from either the random noise generator or from a prerecorded tape played back on the PEMCO tape machine.

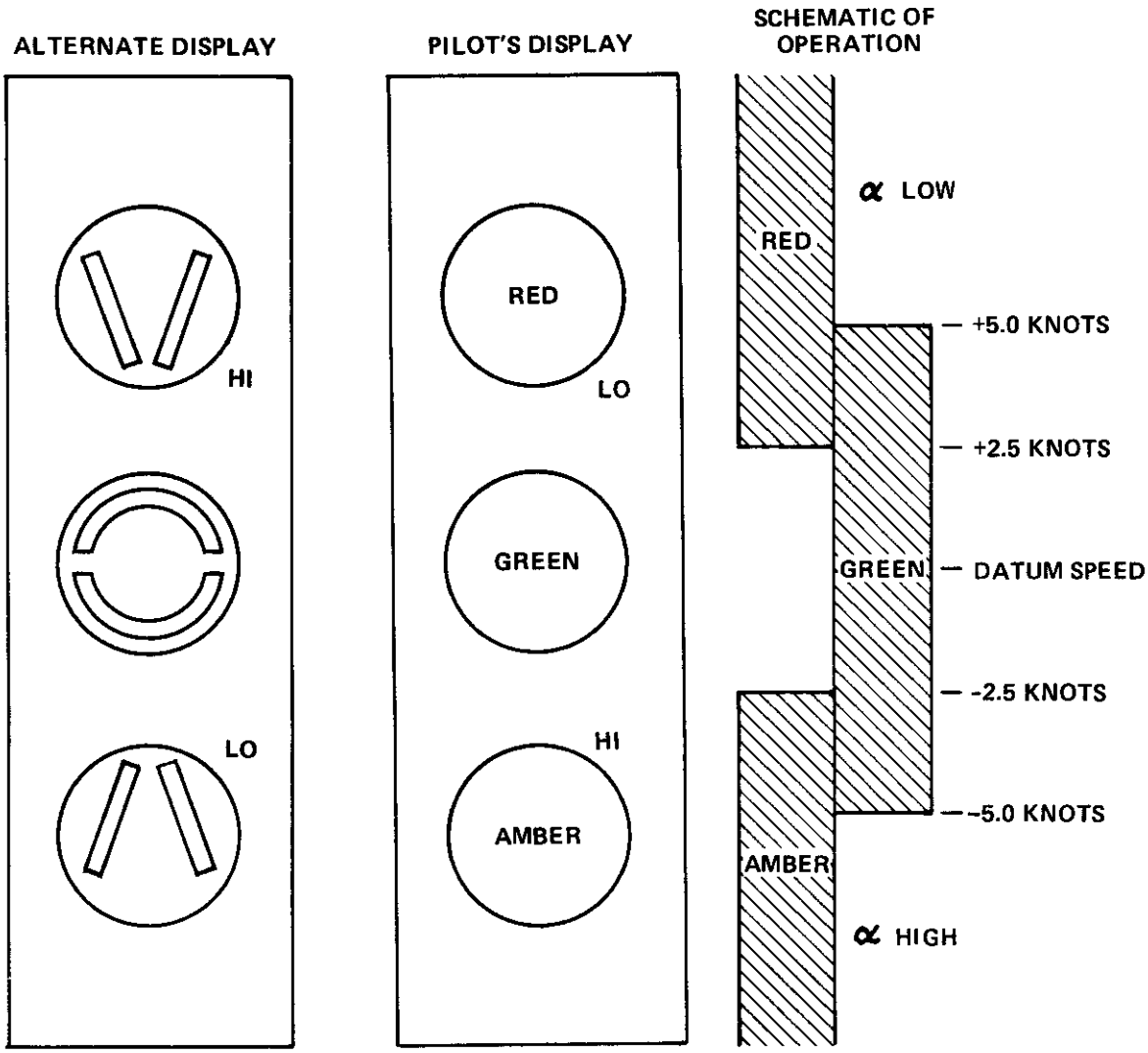

Figure 37 AIRSPEED ERROR BAND INDICATOR LIGHTS

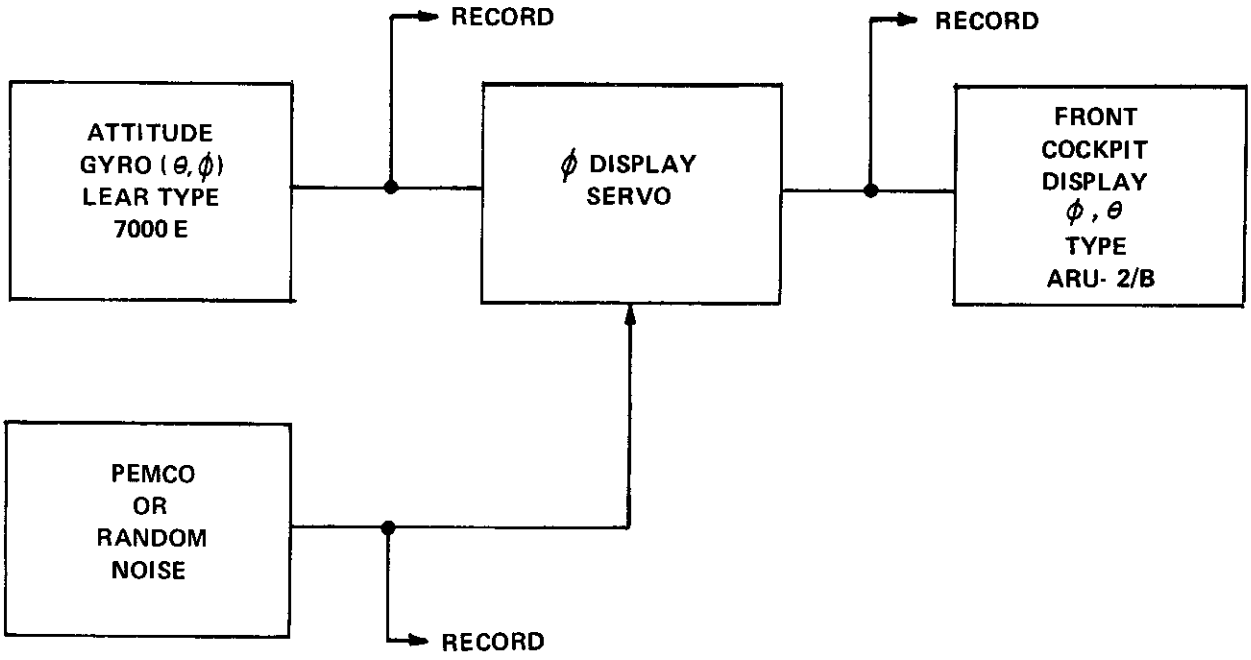

Figure 38 BANK ANGLE SENSOR AND DISPLAY CIRCUITS

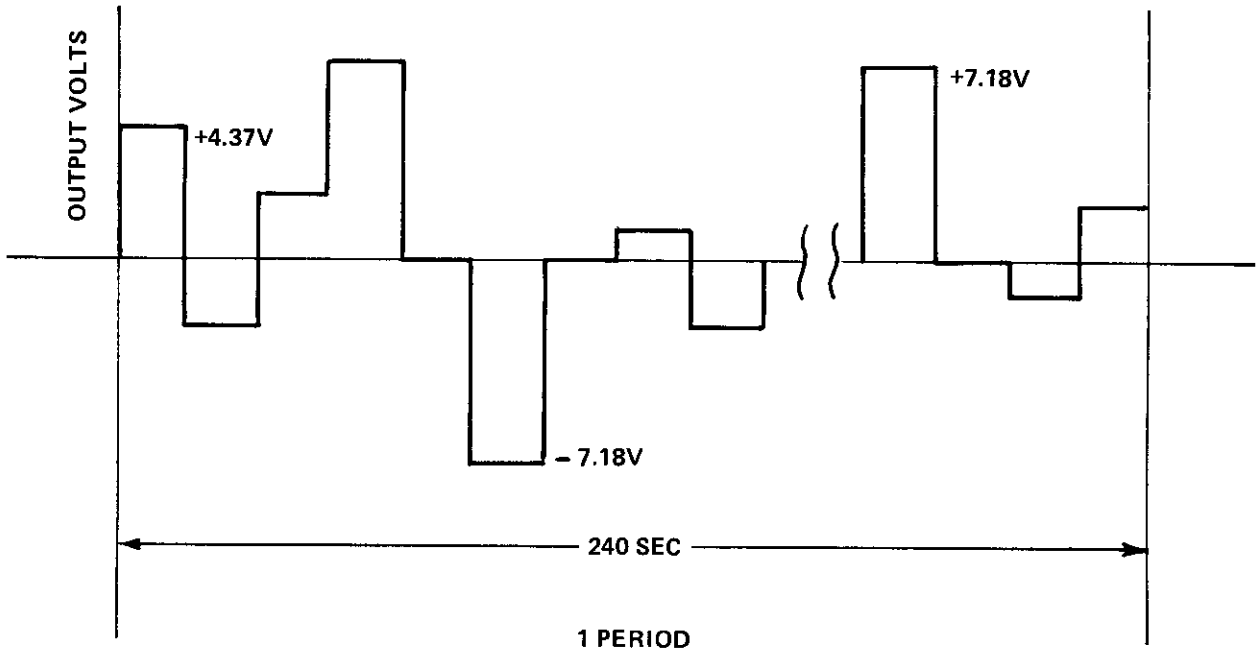

Figure 39 TYPICAL DISTURBANCE GENERATOR WAVEFORM

Disturbance Generator

The disturbance generator is an airborne unit and is used frequently enough to be classified as a permanent installation in the T-33. The disturbance generator is used to provide inputs for longitudinal and also lateral-directional tracking tasks.

It consists of a small dc motor, adjustable from 0 - 1 rpm, which drives 10 cams mounted on a common shaft through a 4:1 gear reduction. An arrangement of microswitches, potentiometers and relays is used to provide the desired amplitude and type of output. A typical output waveform is shown in Figure 39. The waveform shown is periodic and repeats every 240 seconds.

Random Noise Tracking

The output of the random noise generator is sometimes used as a tracking task input, however there is usually too much high frequency content for the signal to be useful without additional filtering. A second-order, low-pass filter has been used which has the characteristics of -3 dB at 1/8 Hz. The filtered output is then amplitude controlled (δ_e/x) from the rear cockpit and fed to a summing amplifier along with a θ signal. The summed output of θ and filtered random noise can be displayed on a horizontal needle of the front cockpit θ, ϕ display unit (ARU-2/B). The pilot task is to keep the horizontal needle centered in the display which requires a pitch attitude signal of the proper amplitude and sign to cancel the random noise input.

Low-Pass Filters (Butterworth Second-, Third-, Fourth-, and Fifth-Order)

Occasionally, special signal conditioning circuits are required for T-33 programs. For one program a set of low-pass Butterworth filters was required, each filter having different frequency break points and filter order. Five printed circuit boards were used for the filter circuits. The filters were used one at a time, with two filter configurations per card. The configurations were selected by switches from the rear cockpit and were used to filter the feel system elevator stick displacement signal that is used to drive the elevator control surface servo.

These filter cards can be modified to suit the needs of future programs and can be used in the elevator, aileron or rudder feel systems. These filter cards can also be used to filter sensor signals in the sensor chassis if required.

DATA RECORDING EQUIPMENT

There are three basic data recording systems in the T-33 airplane. They are a 50-channel oscillograph, a 28-channel digital recorder, and a one-channel voice recorder for pilot comments.

50 Channel Oscillograph

The 50 channel oscillograph is a Consolidated Electrodynamics Corporation (CEC) type 5-119P3-50 with a 5-006A magazine. The magazine capacity is a 475 foot roll of 12 inch wide paper. A CEC processor is used to wet process the recorded oscillograph data. Figures 7 and 8 show the oscillograph as installed in the T-33 airplane.

A block diagram of a typical oscillograph recording channel is shown below.

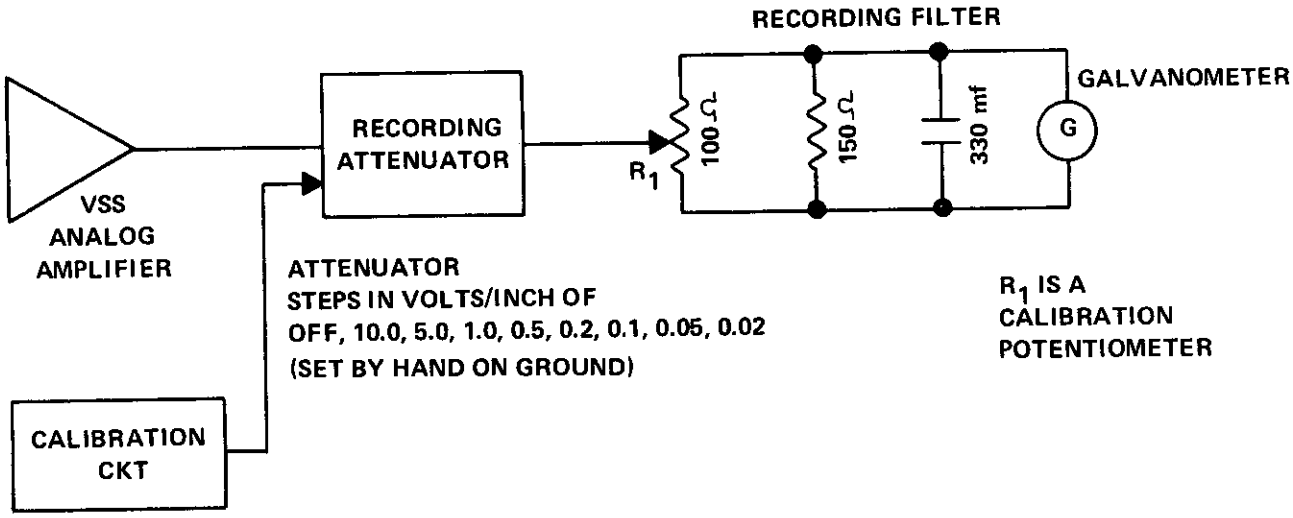

There are 44 oscillograph channels that go through recording attenuators. There are 6 channels that do not have attenuators or recording filters. These 6 channels are used for special instrumentation tests.

The 44 channels with attenuators are hard wired to amplifier outputs and thus have permanent recording parameters assigned to them. The remaining 6 channels are assigned as required.

Two types of galvanometers are used with the recording system. These are the CEC 7-339 and 7-315 galvanometer types. The majority of the galvanometers are 7-339 types. Figure 40 shows frequency response plots (amplitude and phase) for the 7-339 and 7-315 galvanometers as used with the recording filters. The response is typically 3 dB down at 10 Hz for the 7-339 and 3 dB down at 15 Hz for the 7-315 type.

Since there is a difference in the response of the two types of galvanometers, the galvanometer type 7-339 was assigned to all parameters where phase measurements between parameters might be of interest on oscillograph records. It was desirable to have all the parameters between which one might be interested in obtaining phase measurements, assigned the same type of galvanometer. The 7-339 type galvanometer was used because it has a slightly better amplitude response characteristic (no overshoot) than the 7-315 type galvanometer.

The calibration circuit provides a means (2 push buttons per channel) of injecting a signal ground and a d.c. voltage in place of the VSS signal to check the galvanometer for proper deflections.

Table II provides the important characteristics of the 7-339, 7-315 galvanometers. It can be seen that the 7-315 galvanometer is less sensitive and has a higher frequency response than the 7-339.

Table II

7-315, 7-339 GALVANOMETER CHARACTERISTICS WITHOUT RECORDING FILTERS

TYPE	EXT. DAMPING RESISTOR	UNDAMPED NATURAL FREQUENCY	FLAT (5%) FREQUENCY RANGE	UNDAMPED DC SENSITIVITY 11.5 IN. OPTICAL ARM	MAX. SAFE CURRENT
7-339	350 OHM	50 Hz	0 - 30 Hz	4.61 MA/IN.	15 MA
7-315	350 OHM	100 Hz	0 - 60 Hz	12.2 MA/IN.	15 MA

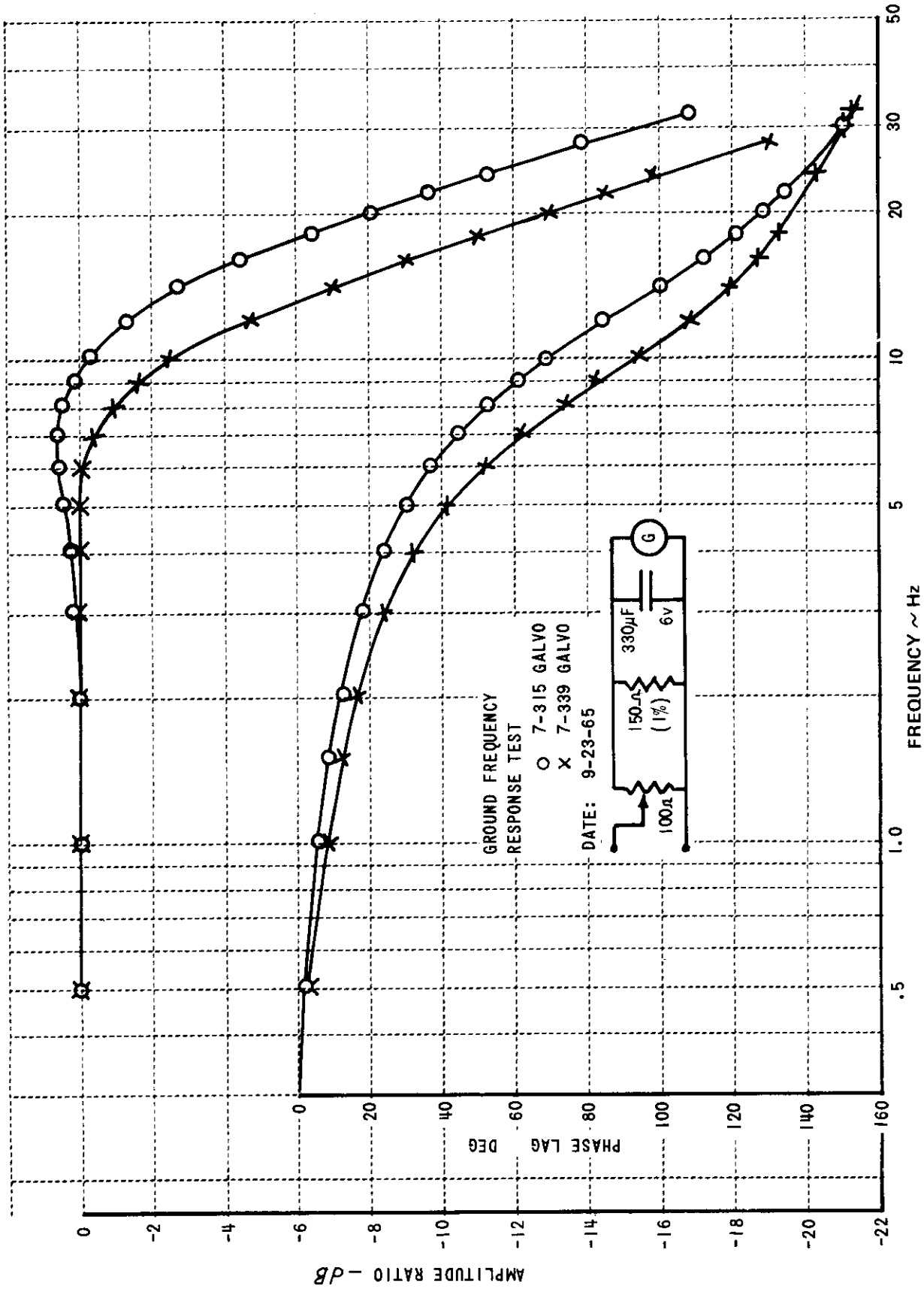

Figure 40 FREQUENCY RESPONSE OF RECORDING GALVANOMETER FILTERS

Accuracy

The long term (1 - 2 months) accuracy and repeatability of the recording attenuators is about 1%. Attenuator settings are selected during the ground calibration phase of a program based on the anticipated range of each parameter. Normally these attenuator settings are used throughout the program, however, the trace sensitivity can be increased or decreased at least one step without changing the calibration accuracy by more than 1%.

The normal oscillograph paper speed used on T-33 programs is 1.0 or 1.6 inches per second. Other speeds available are 10.0, 6.3, 4.0, 2.5, .63, .4, .25, .16 and .10 inches per second. Any of these speeds are obtained by changing gears which drive the oscillograph magazine. A Hi/Low speed switch is provided in the front cockpit to increase the speed by a factor of 10 for special records.

28 Channel Digital Recorder

The T-33 digital recorder consists of a Leach MTR 3200 tape transport with data processing electronics added by Interland Electronics Company (formerly Aeroscience Incorporated). The system consists of 28 channels of high level (0 to ±5.116 V) analog data which are multiplexed into 10-bit-plus-sign binary code. This binary information is arranged according to IBM format and recorded on 1/2 inch magnetic tape.

The system consists of the recorder, power supply unit and a remote control unit mounted in the rear T-33 cockpit. A record counter is also located in the rear cockpit (0 to 99) and updates as each record is taken.

Each of the 28 data channels is sampled 200 (Hi speed) or 100 (Lo speed) times per second.

The magnetic tapes made on this recorder are compatible with the 2400 series tape machines used with the IBM/360 data processing system. A 9 track, 1/2 inch, 800 byte-per-inch configuration is used. Recorder tape speed is 7.5 inches per second (Lo speed) or 15 inches per second (Hi speed) which is selectable in the rear cockpit.

Calibration and Display Box

A portable digital checkout box is provided which can be connected by cable to the recorder during ground calibrations. This unit can be used to control the record sequence and also displays any of the 28 channels (selectable by thumb switches) of analog data after they have been converted to digital data. This unit provides a calibration check on the data on any of the 28 analog channels as they are being converted to digital format and recorded on tape. The display is digital and consists of the 10 binary bits plus the sign bit. Each bit location is represented by a lamp which is illuminated when that particular bit is present.

Figure 41 shows the digital recorder and the calibration/checkout unit.

A block diagram of a typical recording channel is given below.

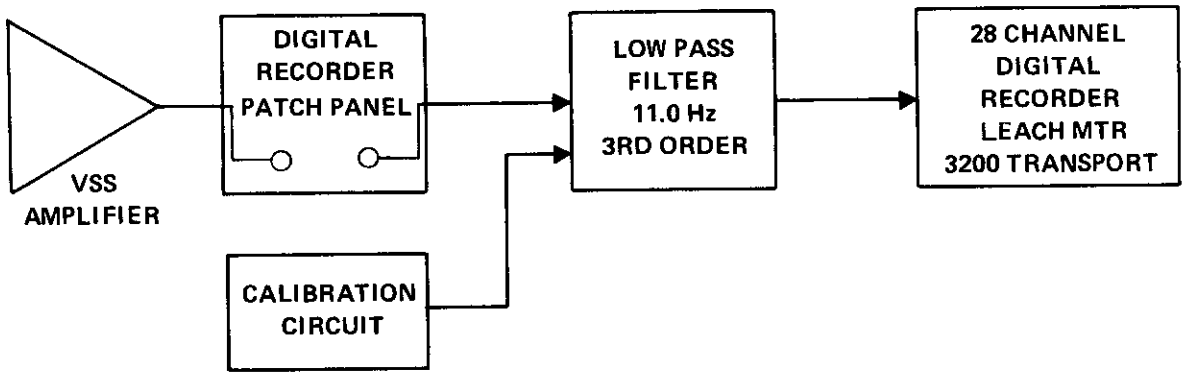

At the beginning and end of each record a calibration circuit provides a ground and then a +1.00 V d.c. signal, each for 1/2 second duration. This occurs on each of the 28 analog channels. The normal VSS signal is switched out and the calibration signal switched in the channel during the calibration period.

As shown on the block diagram, a patch panel is provided which allows easy reassignment of VSS signals to recorder channels if desired.

Each of the 28 analog channels passes through a third-order low pass filter (3 dB down at 11.0 Hz), see Figures 42 and 43. These filters normally have a gain of -0.5, however, 12 of these channels (No. 1 - No. 12) have an extra operational amplifier in front of the filter. These amplifiers have step adjustable gains of +10, +5, +2, +1 and are used to provide increased resolution of recorded parameters where desired.

Full scale input at the recorder is ±5.116 V. Typical accuracy is 0.2% of full scale.

28-CHANNEL DIGITAL RECORDER

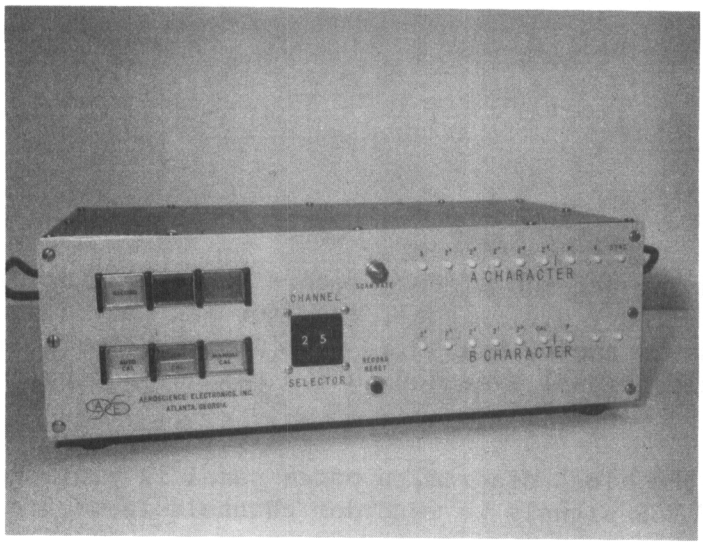

CALIBRATION/CHECKOUT UNIT FOR DIGITAL RECORDING SYSTEM

Figure 41 DIGITAL RECORDER AND CALIBRATION/CHECKOUT UNIT

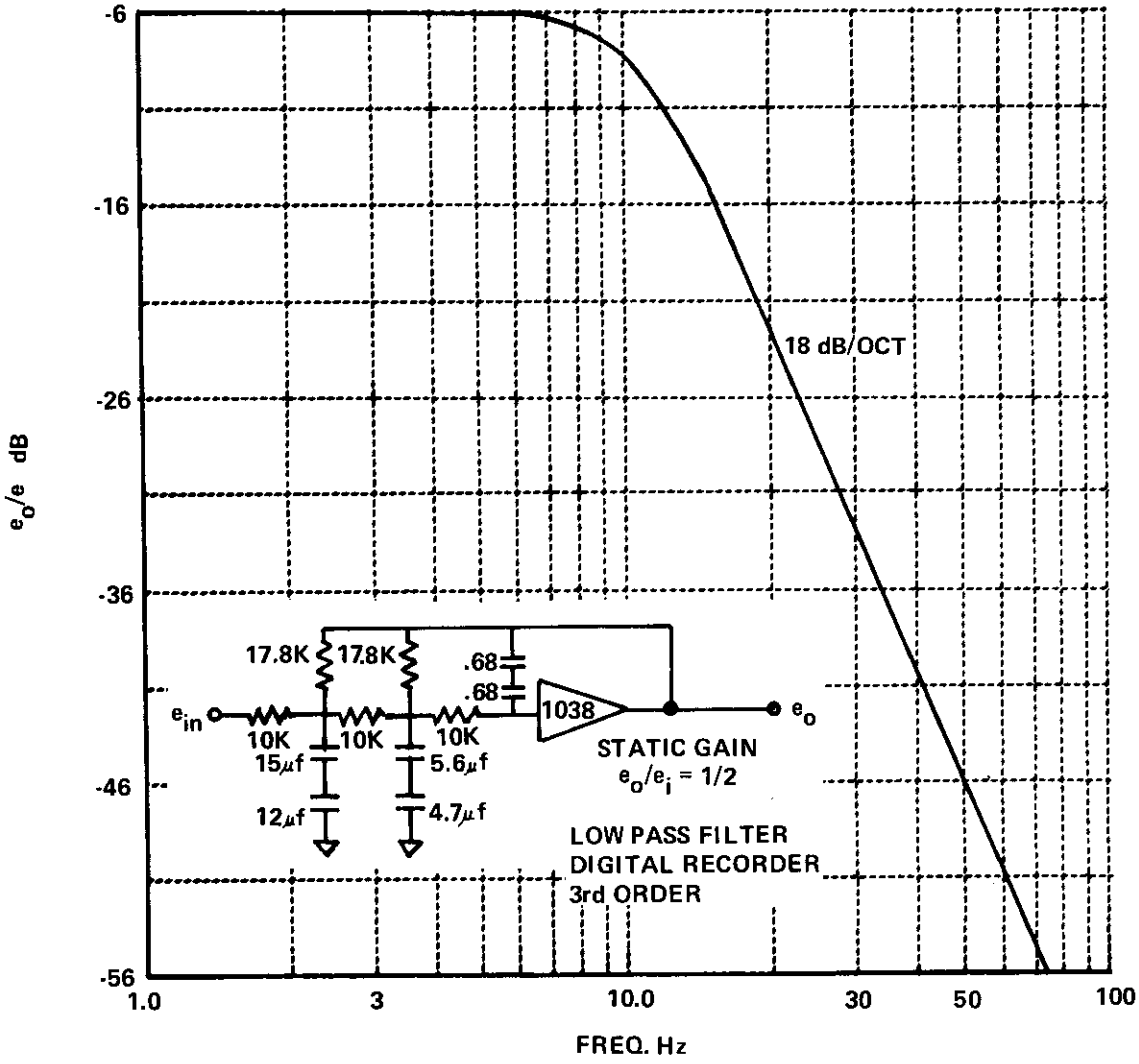

Figure 42 DIGITAL RECORDER LOW PASS FILTER AMPLITUDE VS FREQUENCY

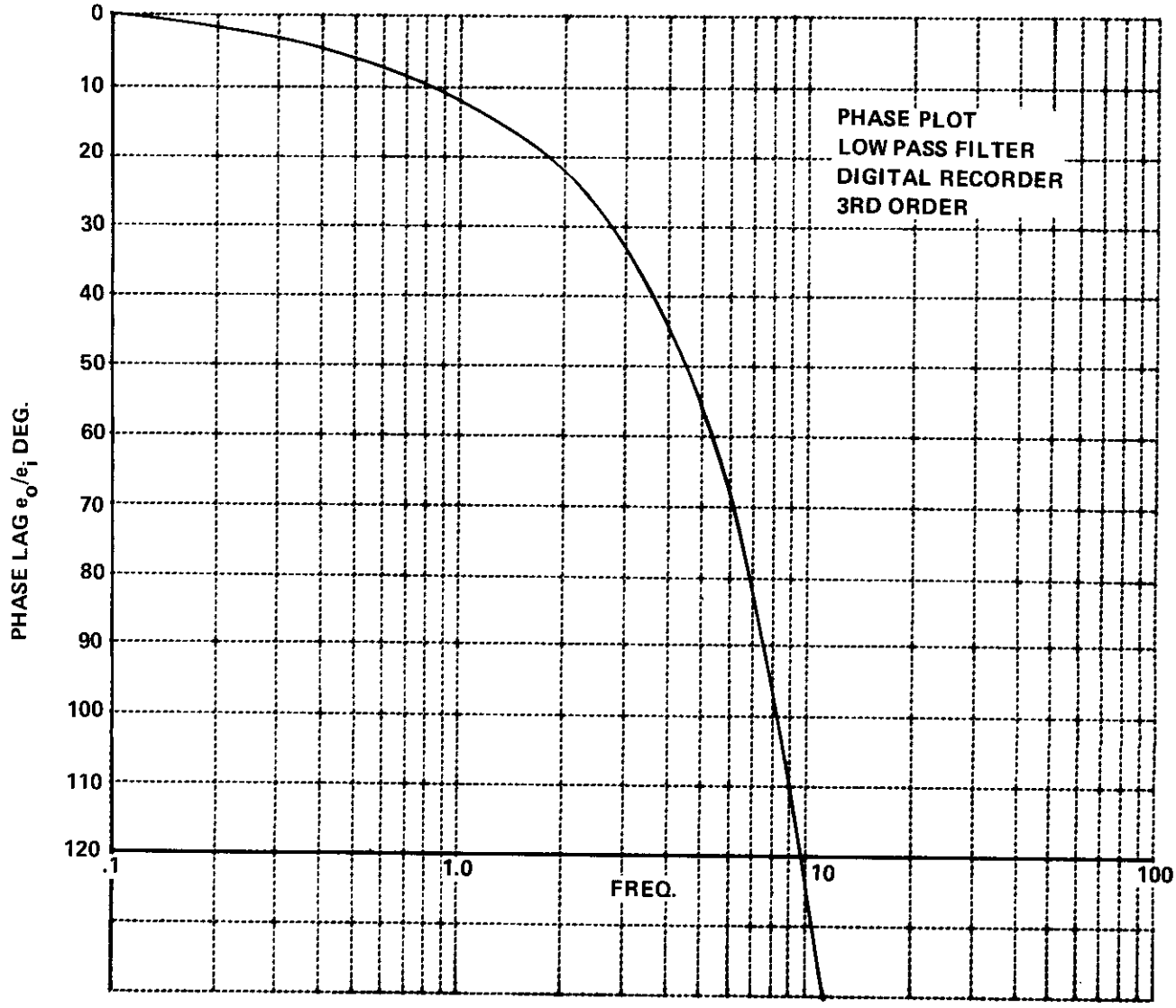

Figure 43 DIGITAL RECORDER LOW PASS FILTER PHASE SHIFT VS FREQUENCY

Typical maximum recording times are 26 minutes at low speed and 13 minutes at high speed.

Ground Playback System (Quick Look System)

In conjunction with the T-33 Airborne Digital Data Recording System, a complete functional ground playback system is provided. This digital-to-analog playback system will accept magnetic tapes recorded on either the T-33 30-channel digital tape recording system or the 60-channel Total In-Flight Simulator (TIFS) recorders and will automatically synchronize to either format. The playback system is contained in a single 19 inch equipment rack on casters and provides eight analog outputs, expandable to sixteen. There is a provision (i.e., thumbwheel switches) to independently select any eight channels of recorded information for conversion to analog signals and provision made to connect a strip chart recorder such as a Brush Instruments Mark 200 recorder to the ground playback unit. The analog outputs are brought out to a connector mounted on the back panel of the equipment rack. For a +5.000 volt signal on the tape, a -10.000 ±0.010 volt signal output to the strip chart recorder is provided. The ground playback system will accept the standard 9-track 800 byte per inch tapes compatible with IBM 2400 tape machines and the IBM 360 computer. Two playback speeds are provided, 15 and 30 inches per second, which will permit playback at speeds faster than those at which the tapes are recorded. For either airborne system, (30 or 60 channel) playback will take place two or four times the recording speed when recording at 7.5 inches per second and at the same or two times recording speed when recording at 15 inches per second. (This will provide a time compression capability in a precise ratio to simplify any data reduction accomplished from the strip chart record.) The speed at which the airborne tape was recorded will be detected from the tape format and displayed by the system as HI or LO speed. If a parity error is detected, a properly identified indicator will be energized. In addition, the system will light a display indicating which frame length (30 to 60 channels) was recorded, and it will display the record number from the recorded data.

The tape transport used for ground playback is the Ampex Model TM 7293. Figure 44 shows the ground playback system.

Oscillograph and Digital Recorder Record Taking

Both oscillograph and digital records are taken from the rear cockpit by activation of a single toggle switch. A toggle switch (digital slave) is provided. With this slave switch "ON" it causes both oscillograph and digital recorder to run. With the slave switch off, only the oscillograph runs when the record switch is activated.

Record and record malfunction lights are provided in the rear cockpit for both oscillograph and digital recorder. High and low speed switches are provided for both oscillograph and digital recorders.

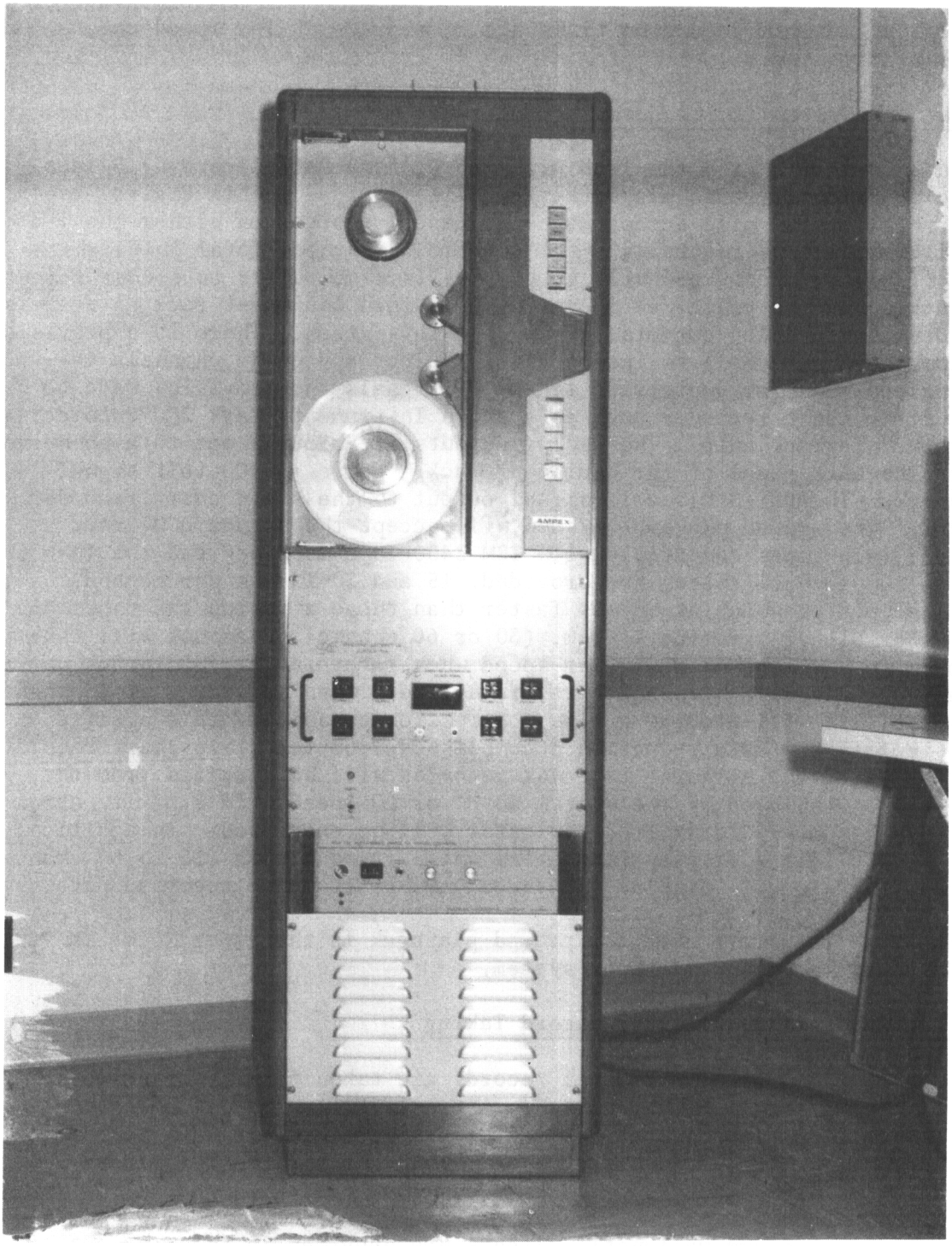

Figure 44 GROUND PLAYBACK (QUICK LOOK) SYSTEM FOR AIRBORNE DIGITAL RECORDER

A green light is provided in the front cockpit which, when "ON", indicates that the digital recorder is not in the calibration mode of the record sequence and that a pilot input is permissible.

Voice Recorder

A sound (voice) recorder set AN/ANH-2 manufactured by the Pierce Wire Recorder Corporation, Chicago, Illinois is provided in the T-33 to allow recording of both front and rear cockpit pilot comments.

The recorder is connected to the T-33 intercom system and any comments made by either pilot will be recorded when the wire recorder toggle switch in either cockpit is "ON".

The magazines contain enough wire for 60 minutes of recording time and a blue light in the rear cockpit will light when all but 5 minutes of a magazine have been used.

Figure 8 shows the voice recorder installed in the T-33 and Figure 45 shows the components of the sound recorder system.

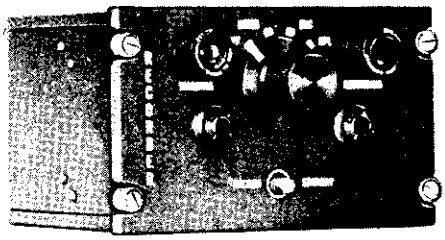

RECORDER CONTROL
C-1051/ANH-2

SOUND RECORDER RD-106/ANH-2

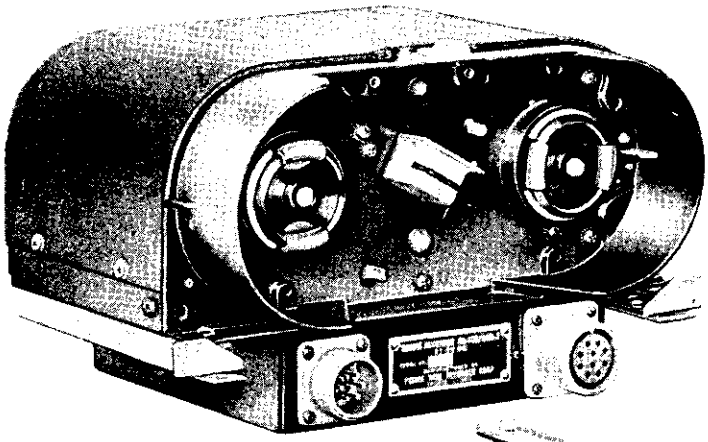

SOUND RECORDER
MAGAZINE MX-1330/ANH-2

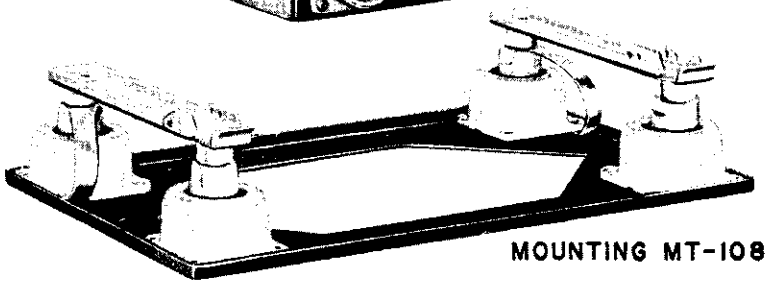

MOUNTING MT-1081/ANH-2

Figure 45 COMPONENTS OF SOUND RECORDER SET AN/ANH-2 (T-33 VOICE RECORDER)

SECTION VI
VARIABLE L/D SYSTEM

The variable Lift to Drag (L/D) system is discussed in detail in Reference 2. Briefly, the L/D system includes two 230-gallon T-33 tip tanks, shown in Figure 46, each of which has been modified to include two movable petals. The L/D system includes a separate 3000-psi hydraulic system and additional electronics that allow the petals to be programmed as functions of various airplane responses.

The method for varying L/D is evident in Figure 46. The hydraulically operated drag petals can be opened to an included angle of 164° by either manual or computed command. Simulation of the lift-to-drag ratio of other vehicles is accomplished by fixing the petals at a predetermined angle or using a computed command to position the petals according to equivalent airspeed and/or angle of attack.

At a given equivalent airspeed, or given angle of attack, the basic drag of the T-33 can be augmented by the drag petals, as well as wing flaps, dive brakes and landing gear. The effective lift-drag ratio can be held below 4 for all speeds greater than 140 knots, provided the engine is throttled to approximately 60% rpm. A minimum L/D value of 2.2 to 2.5 can be achieved.

L/D ELECTRONICS

The L/D electronic instrumentation consists of a versatile computer with inputs from the petals, the angle of attack vanes, the wing flaps, the equivalent airspeed and the landing gear. It is used to control the petals and the elevator according to known, programmed functions. It can be used to program any L/D profile (L/D vs V_e) that is within the drag capability of the modified airplane. It can be used to vary drag versus angle of attack and drag versus airspeed independently of each other while varying both of them at the same time.

A block diagram of the L/D system is given in Figure 47.

The pilot can also manually control the petal deflections. Figure 48 shows the pilot's L/D control box and main L/D electronics chassis. The manual control can be used to establish an initial petal position. The output of the computer can then be nulled with respect to the manual control setting, and the signal command switched over to the computer. Both left and right petal positions are indicated on the meters on the control panel. The null meter indicates the difference between the manually called-for petal position and the computer called-for petal position when the petals are driven manually. When the petals are operating in the computer mode, the null meter indicates the difference between the left and right petal position. If the petals are being operated from the computer signal, and it is desirable to disengage the L/D system, the pilot can rotate the manual control knob until it agrees with the existing petal angle. Then he can switch to manual control and rotate the knob to close the petals. A controlled disengage circuit is

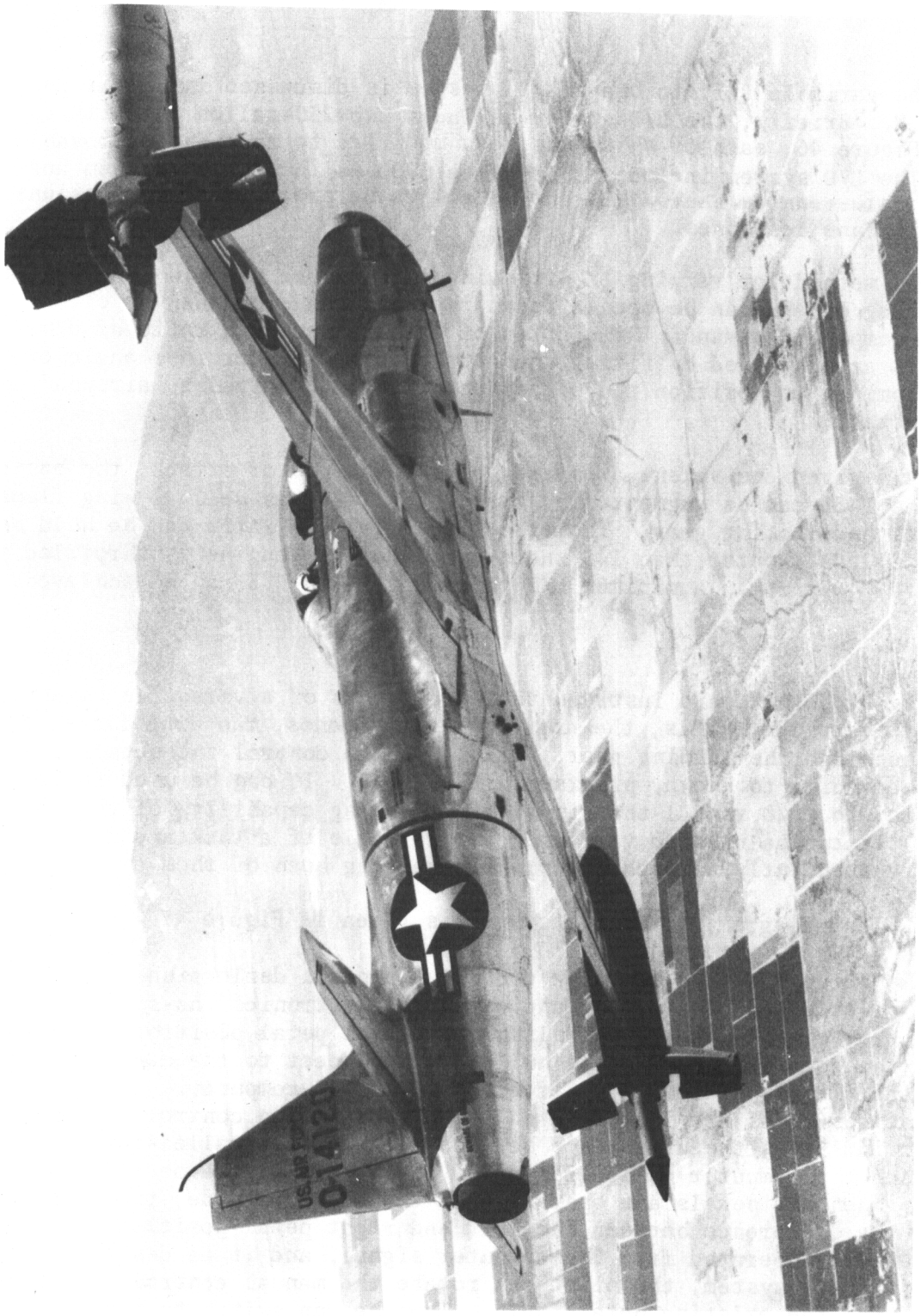

Figure 46 T-33 AIRPLANE WITH L/D DRAG PETALS EXTENDED TO FULL OPEN POSITION (164 DEGREES INCLUDED ANGLE)

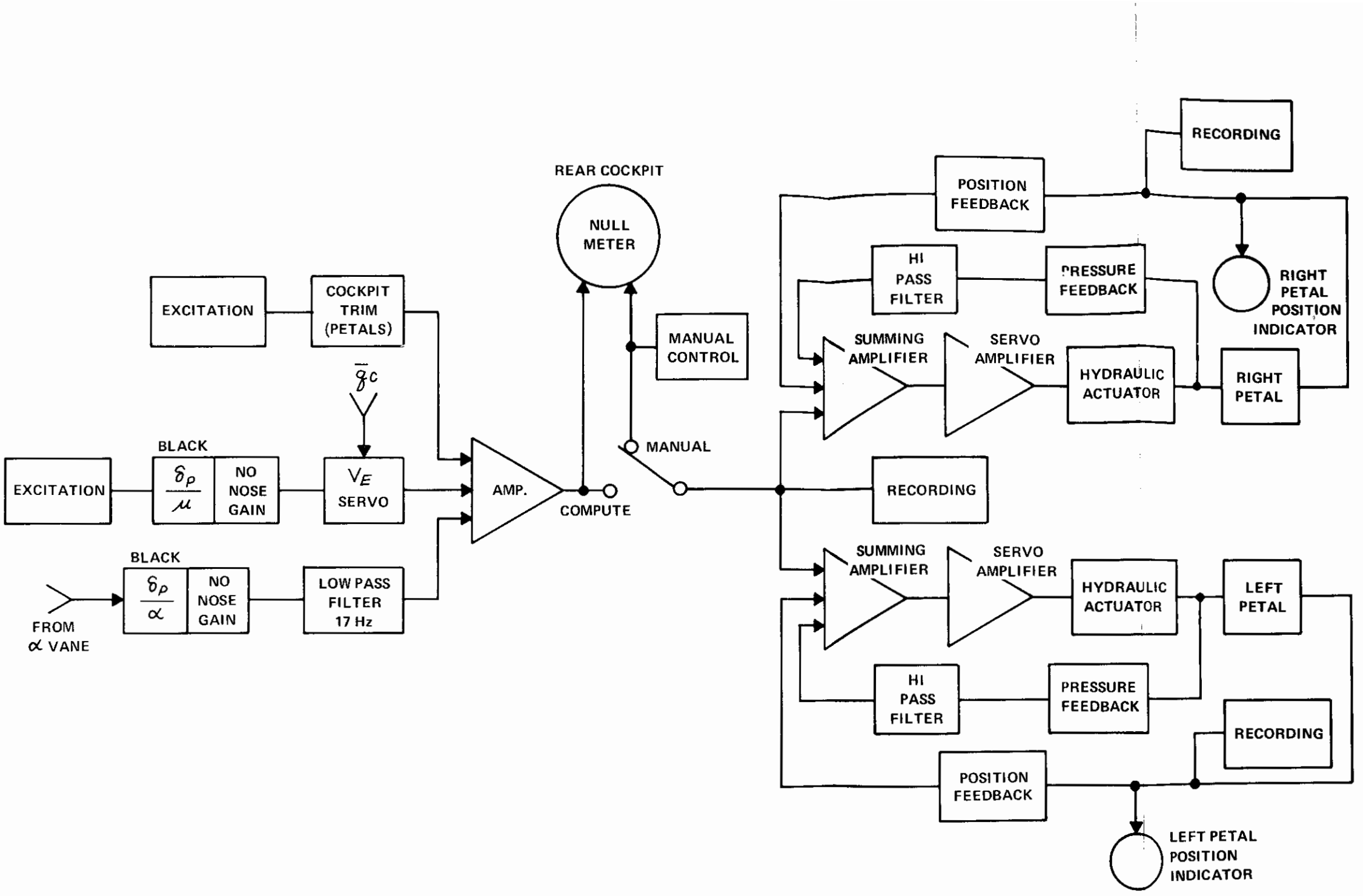

Figure 47 FUNCTIONAL BLOCK DIAGRAM, L/D SYSTEM

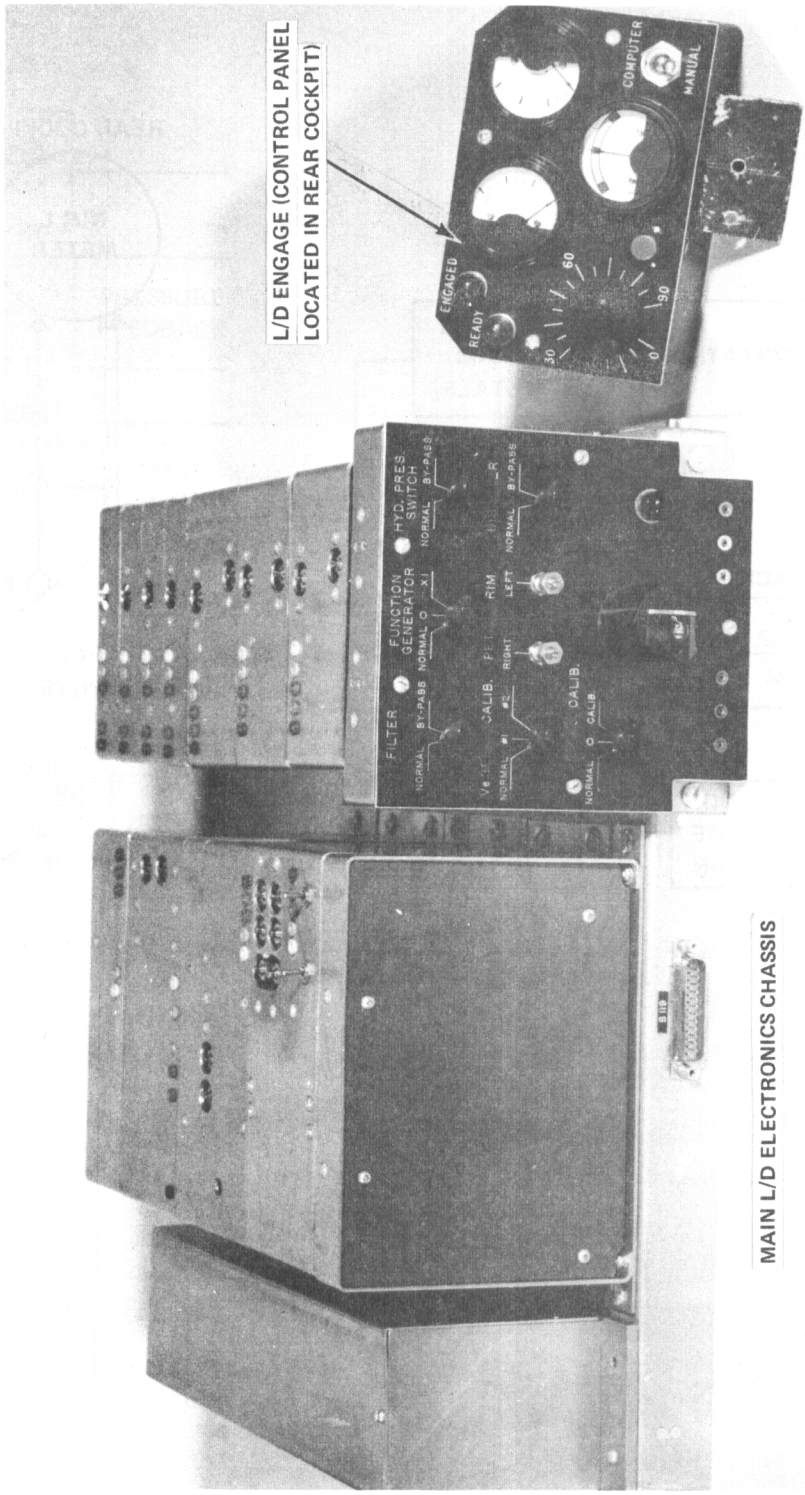

Figure 48 L/D ELECTRONIC CHASSIS

built into the system. The pilot can actuate the push button on the control panel at any time, and the petals will be driven closed at a rate determined by an R-C circuit that has a time constant of approximately 5 seconds.

L/D ELECTRONIC SAFETY TRIPS

For safety of flight purposes, a safety trip system removes excitation from the L/D hydraulic dump solenoids whenever one, or more, of the following abnormalities occur:

1. The petal deflections differ by approximately 7° to 12° (adjustable),
2. Either petal rate exceeds approximately 30°/sec (adjustable),
3. The regulated power supply voltages are interrupted,
4. The 400 cps carrier voltage is interrupted, or
5. The variable stability system automatic safety trip system operates.

Whenever the excitation to the hydraulic dump valves is interrupted, the valves will open and hydraulically short circuit the actuators, and the petals will close because of the air loads on them. The L/D system can also be dumped manually by the pilot with the existing variable stability safety trip push buttons.

THE L/D HYDRAULIC SYSTEM

The schematic of the hydraulic system is given in Figure 49.

The hydraulic power source is a Kellog through-shaft, variable displacement pump type AP6V-S7, mounted directly on the engine accessory pad. The pump supplies a regulated pressure of 3000 psi. A Vickers relief valve that opens at 3150 psi protects the system from over-pressures. The airplane and variable stability systems hydraulic pump (NYAB type 67WS300) is mounted on the back end of the Kellog pump.

The high pressure hydraulic oil leaves the Kellog pump, and whenever the system is engaged it passes through a Republic selector valve, a solenoid valve, and out to the L/D servo actuators mounted in each tip tank. The high pressure of the oil is expended in the servo actuator and the oil is returned at low pressure, through a filter, to the hydraulic reservoir. Whenever the L/D system is engaged, the oil supply to the Kellog pump is from the upper half of the reservoir and is approximately one gallon of oil.

Whenever the L/D system is not engaged, then the Republic selector valve returns the pump output to the reservoir, thus providing a system by-pass. Also, with the system in this "by-pass" position the entire capacity (approximately 2.5 gallons) of the reservoir is in the by-pass hydraulic circuit by

virtue of the position of the Parker T-drilling selector valve. The Republic and Parker selector valves are mechanically fastened together and are operated simultaneously through a Teleflex cable connected to a hydraulic selector lever in the rear cockpit.

Safety Considerations

The hydraulic selector lever can be in either of two positions: "L/D" or "By-pass." If the selector lever is in the "L/D" position, but if the Tactair solenoid valve (no. 6204-8) is not open at the same time, then the output flow from the pump is blocked. Whenever this situation occurs a red light in each cockpit blinks to warn the pilots of the situation. Upon noting this warning, the rear-seat pilot must immediately take corrective action, because if the pump is blocked for more than a minute or two it will overheat. The pilot can either engage the electronic equipment which will open the Tactair solenoid valve, or he can put the hydraulic selector lever in the "By-pass" position.

As long as the L/D system is engaged, the petals need not be operated to obtain sufficient flow through the pump to keep it lubricated and prevent overheating. The leakage flow through the Moog flow control valves is sufficient to keep the pump lubricated and cool.

Cavitation will occur in the pump whenever the head pressure at the pump inlet is less than 5 psi (gauge). The required head pressure is obtained by pressurizing the reservoir with pressure that is bled from the engine compressor. At 100% engine rpm the reservoir is pressurized to approximately 20 psi (gauge). If engine rpm falls below 80% the bleed pressure is very low, but a check valve in the reservoir pressure line helps maintain the reservoir pressure at a substantial value.

Hydraulic oil temperature and pressure can be read on rear cockpit instruments. Oil temperature is sensed by a thermocouple mounted in the reservoir. Oil pressure is measured, essentially, at the pump outlet. The pressure sensor is protected from valving surge pressures by the Hydrodyne "snubber" accumulator.

Whenever the L/D system is not engaged the Tactair solenoid valve (6204-8) is closed and the Tactair dump valves (6104-6), which are in parallel across each actuator, are open. If the system is engaged, then the solenoid valve is open and the dump valves are closed.

Two dump valves are paralleled to short circuit each actuator upon system disengagement. Such reliability is very necessary for if, when the system were disengaged, one actuator was short circuited, but the other was not, due to a malfunction of the dump valve, then one set of petals would blow shut, but the other set would be hydraulically locked open - perhaps wide open. The resulting yawing moment on the airplane might well result in uncontrollability. To ensure against this, two dump valves are paralleled across each actuator.

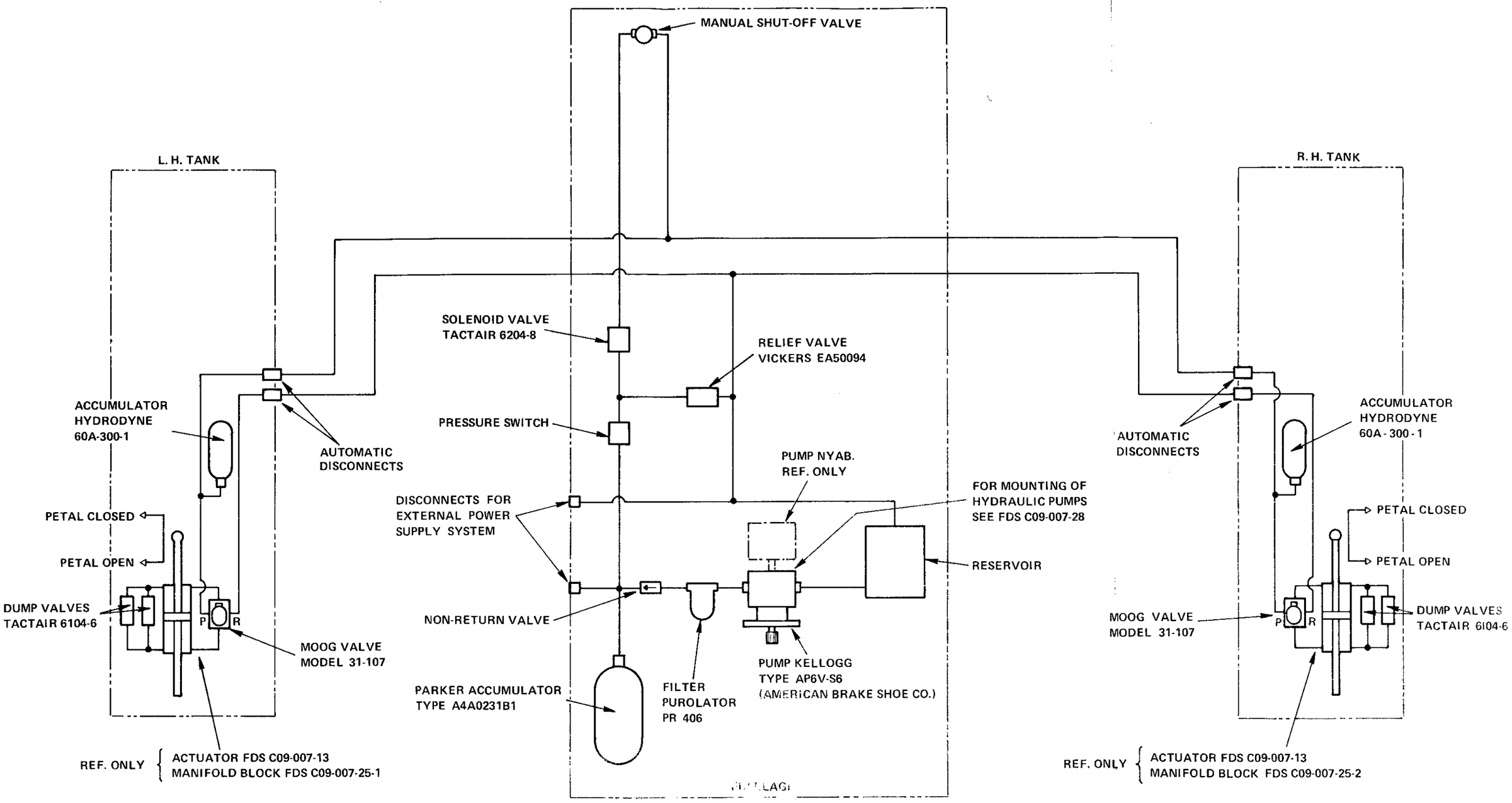

Figure 49 SCHEMATIC OF L/D HYDRAULIC SYSTEM

The last-ditch safety precaution designed into the system allows for jettisoning the tip tanks. The hydraulic lines leading into the tip tanks are continuous 3/8 in. steel tubing. Each hydraulic line passes through an explosive cutter developed by the Conax Company expressly for this application. To prevent losing hydraulic oil, if a tip tank is jettisoned, each hydraulic pressure line passes through an explosive shut-off valve. Each set of three explosive devices per wing tip is actuated by microswitches which close and fire the devices whenever a tip tank leaves the wing tip by 3/16 inch. This amount of motion cannot occur unless the tank has been jettisoned or has inadvertently become detached from the airplane. The firing sequence of the explosive devices can be chosen by the pilot so that if one tank should fall free then the other tank will automatically be jettisoned and the respective explosive devices will fire. This automatic feature can also be disarmed by the pilot so that if one tank is jettisoned or falls free, then only that tank is lost.

When a tip tank is jettisoned, the L/D system electrical circuits to that tank are disrupted by a pull-apart connector. The electronic equipment senses the disruption and automatically disengages the whole L/D system.

The remaining items of the hydraulic circuit are the General Controls Company pressure switch and the Borg-Warner differential-pressure transducers. The pressure switch makes it impossible to engage the system if the hydraulic pressure is below 2600 psi and automatically disengages the system if pressure falls below 2300 psi. Note: after extensive use of the L/D system, the rate limit and system engage shutoff portions of the pressure monitoring circuits have been considered unnecessary and are currently deactivated. The differential pressure transducers are to make the servo system stable above frequencies of 15 cycles per second.

CALIBRATION OF THE L/D SYSTEM

The following calibration procedures are taken from Reference 2. Several aerodynamic calibrations of the L/D system are required. The drag of the petals, flaps, and landing gear must be determined. Because the landing gear and the flaps can be used with the petals, the pitching moment contributions of these must be accurately known. A flight test program was designed and conducted to obtain the data. The results of the tests are presented and discussed here.

Petal drag is determined from flight test data by using Newton's Second Law of Motion, $F = ma$. First of all, trimmed straight and level flight is established with the petals closed. The petals are then opened, and the resulting deceleration measured with an accelerometer. This recorded deceleration, multiplied by the mass of the airplane, yields the drag that the petals produce. However, the analysis becomes complicated if changes in attitude, angle of attack and velocity occur. Such changes (though small) do occur because the airplane does not remain in precise trim, and because the velocity drops due to deceleration. Therefore, it was necessary to develop the perturbation equation to account for these changes.

The perturbation equation was obtained by subtracting the X-force equation of motion for the reference flight condition from the X-force equation of motion for the petals-open condition. The equation of motion in the body axis system for the reference flight condition is:

$$L \sin \alpha_o + T \cos \eta - D \cos \alpha_o - mg \sin \theta_o = 0$$

where L and D are the wind axis lift and drag forces respectively; α_o and θ_o are reference angle of attack and pitch angle respectively; T is the thrust; η is the angle between the thrust vector and the x-body axis; and mg is the weight of the airplane. The equation of motion after the petals are opened is:

$$L \sin(\alpha+\alpha_o) + T \cos \eta - D \cos(\alpha+\alpha_o) - mg \sin(\theta+\theta_o) - D_p \cos(\alpha+\alpha_o) = ma_x$$

where α and θ are perturbation quantities; D_p is the drag of the petals; and a_x is the resulting acceleration. Note that the change in flight path angle is included. Therefore, after standard small angle assumptions are made, subtracting the petal-open equation from the reference equation yields the perturbation equation:

$$\alpha L - \theta mg - D_p = ma_x$$

Extreme care is required when using this equation. In any particular flight test evaluation the relative magnitudes of the small quantities must be assessed before any small quantities are discarded. For example, the terms αL and θmg will cancel under certain conditions, but care must be used to verify that these conditions exist before any terms are dropped.

The drag of the petals, for various petal angles, obtained by the above procedure is shown in Figure 50. A linear variation of petal drag with petal angle is seen to exist throughout the full range of petal angles. Data are presented at 160 and 180 knots and there is no indication that the drag coefficient of the petals has changed; therefore, it is implied that an angle of attack change from approximately 4.5 to 6.5 degrees, which is the change in trim angle of attack for speed changes from 180 knots to 160 knots, has not significantly changed the drag coefficient of the petals.

A second procedure can also be used to measure petal drag. In this case, after the petals are opened, a steady state of descent is established at the same velocity and power setting as the trimmed, level-flight reference condition. The flight path angle is then measured and used to compute petal drag. The results appear in Figure 51. The straight line shown in Figure 50 is the same straight line that appears in Figure 51. Good agreement exists between both flight test techniques. The increased scatter in Figure 51 is attributed to the difficulty in measuring the flight path angle precisely and the difficulty in establishing a well-stabilized trim.

FLIGHT TEST TECHNIQUE ~ D_p = ma (a MEASURED AFTER PETALS WERE OPENED IN STRAIGHT AND LEVEL FLIGHT) PRESSURE ALTITUDE = 16,500 FT

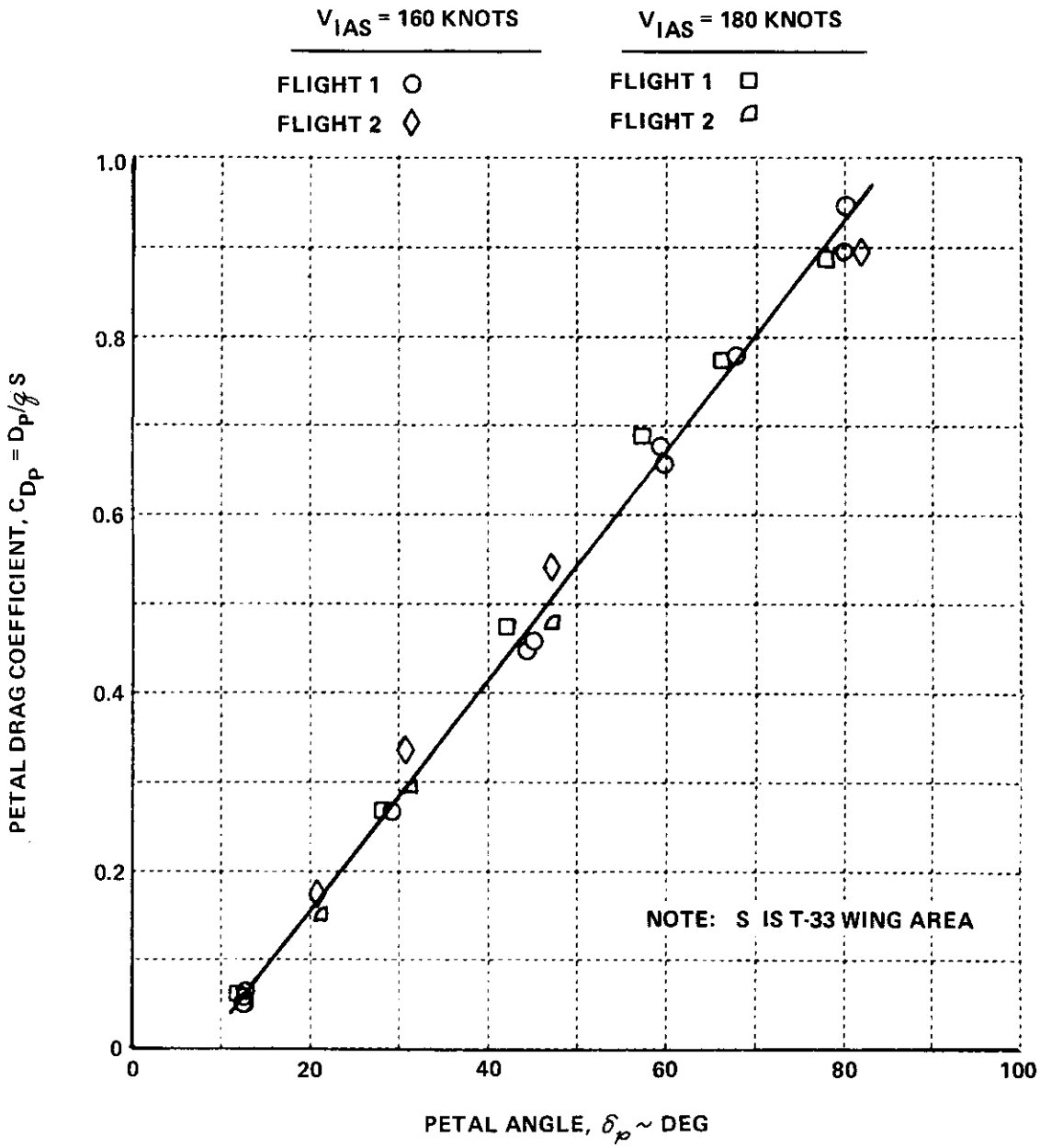

Figure 50 PETAL DRAG DETERMINED FROM D_p = ma

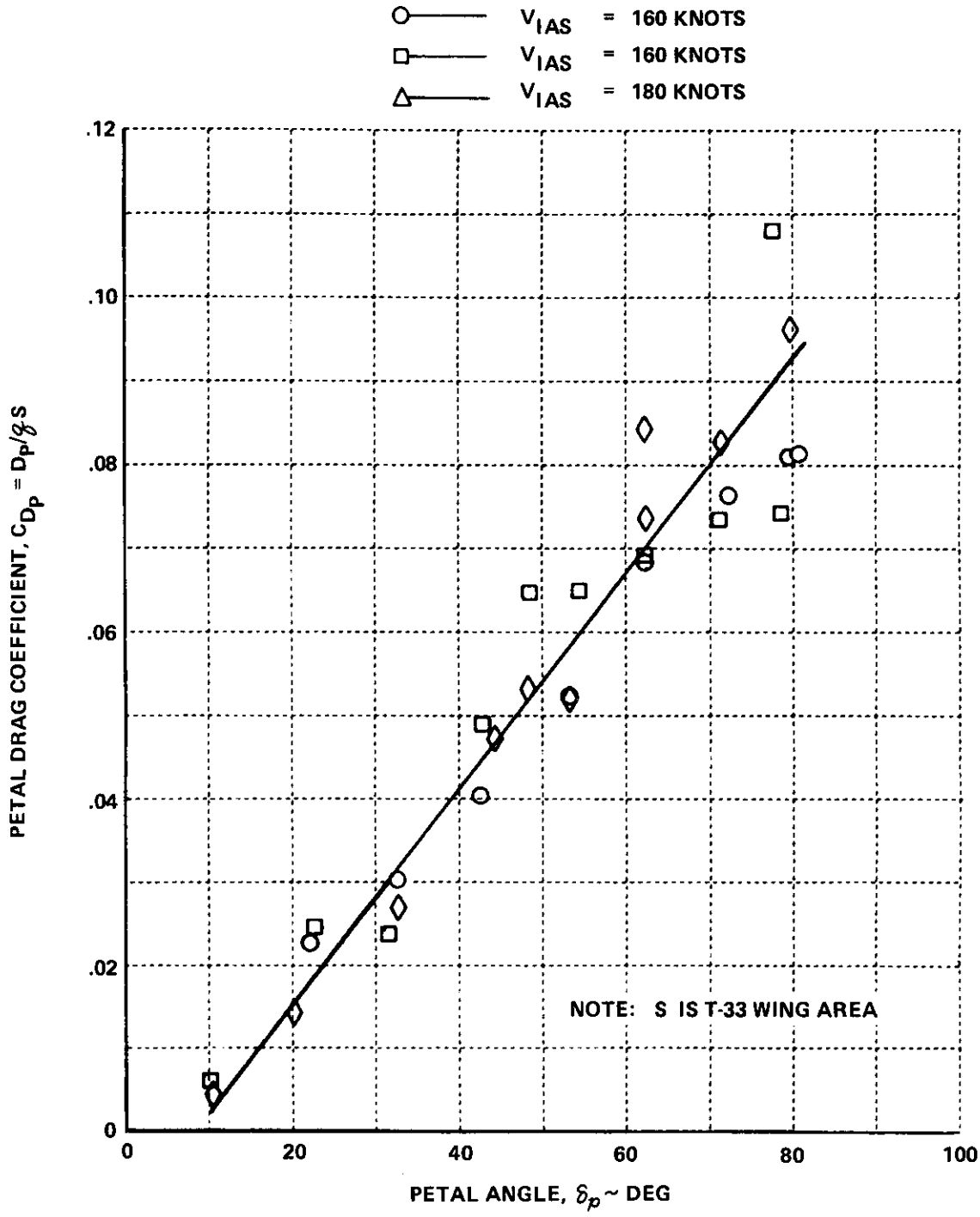

Figure 51 PETAL DRAG DETERMINED FROM CHANGE IN FLIGHT PATH ANGLE

The experiments to determine petal drag revealed that the petals produce a significant pitching moment. Therefore, it was necessary to determine the change in elevator angle required to re-establish trim when the petals are opened. The required change in elevator angle for petal angle is shown in Figure 52.

If the flaps must be lowered during a simulated L/D profile to attain low values of effective L/D at low indicated airspeed, it is undesirable for the evaluation pilot to sense the deceleration due to lowering flaps. Therefore, flap drag must be compensated by a reduction in petal drag. To establish the petal angle change required to produce no net increase in drag, the drag of the flaps for various flap deflections can be determined from a brief flight test.

The flight test consists of establishing trimmed straight and level flight at 16,500 feet pressure altitude and 160 knots IAS with the flaps deflected at some angle. The flaps are then retracted and the petals deflected until the reference flight condition is again attained with constant thrust. Thus, the petal drag is equal to flap drag during the reference flight condition. Since petal drag was previously established, as shown in Figure 51, flap drag can be calculated from the change in petal position.

Figure 53 illustrates flap drag determined in this manner; it is seen to be nearly linear with flap deflection angle. Full flap yields an increase in drag coefficient of 0.055. An auxiliary scale on the figure indicates the petal angle change required to produce drag equal to the corresponding flap drag. If the flaps are fully lowered, then the petals must be retracted 50° to maintain the same reference total drag.

The change in zero-lift angle of attack as a function of flap deflection can also be obtained from flight testing. The angles of attack are recorded for stabilized straight and level flight at 160 knots indicated airspeed for various angles of flap deflection. These angles are compared to the angle of attack for zero flap angle. Figure 54 shows the change in zero lift angle of attack as a function of flap deflection.

The flap drag flight test also provided the data from which the elevator angle required to trim out the flap pitching moment was determined. The elevator compensation for the pitching moment that is produced by the flaps is shown in Figure 55.

If both the landing gear and the speed brakes are used to achieve the low values of effective L/D, the drag and pitching moment produced can be obtained by the same procedure used in the case of the flaps.

The drag data for the various devices are used to show the obtainable values of effective L/D in a series of summary graphs shown in Figures 56 through 61. A family of curves is plotted that shows the drag force per petal as a function of indicated airspeed for a given petal angle. This family of

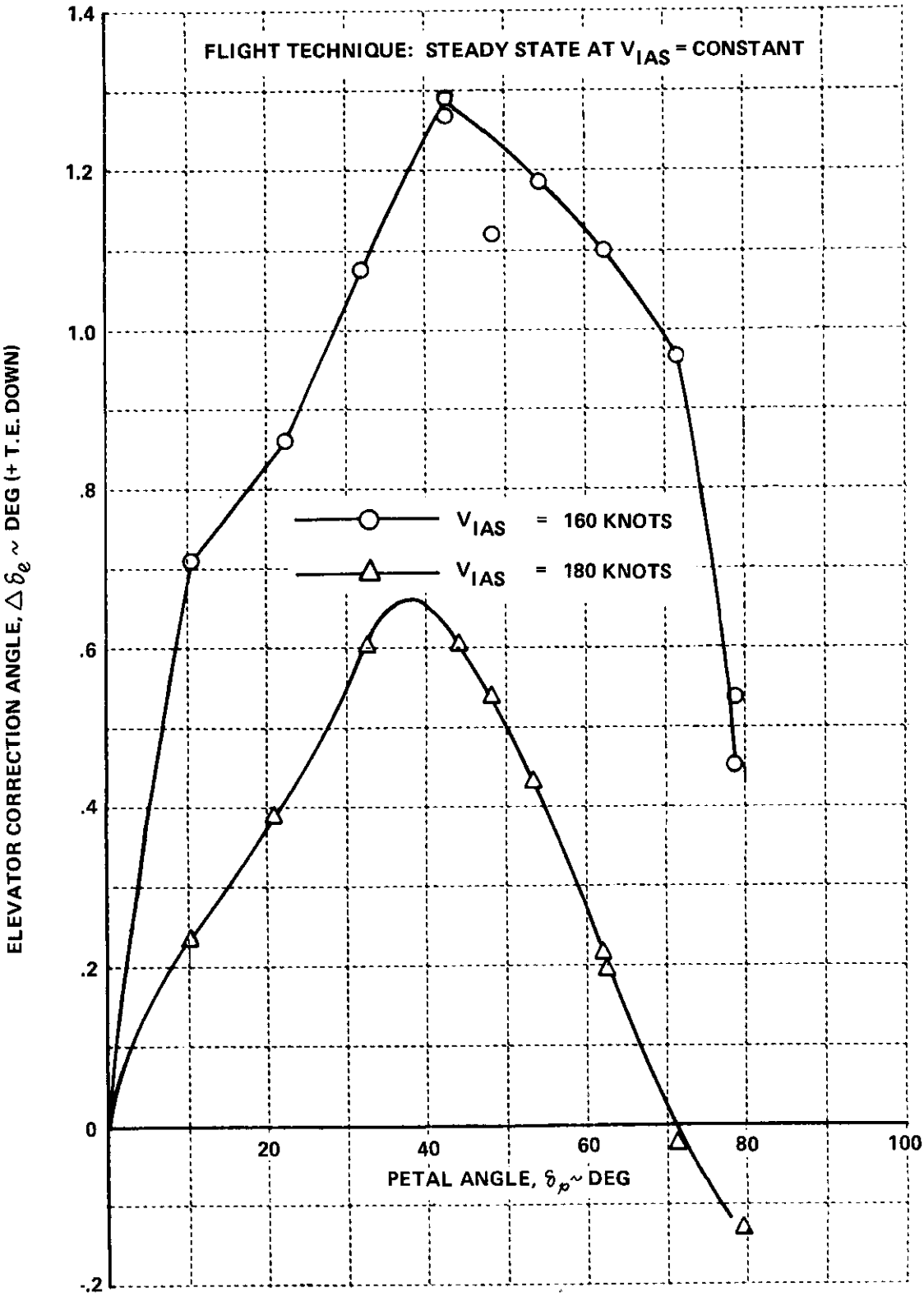

Figure 52 ELEVATOR REQUIRED TO TRIM PITCHING MOMENT DUE TO DRAG PETAL OPERATION

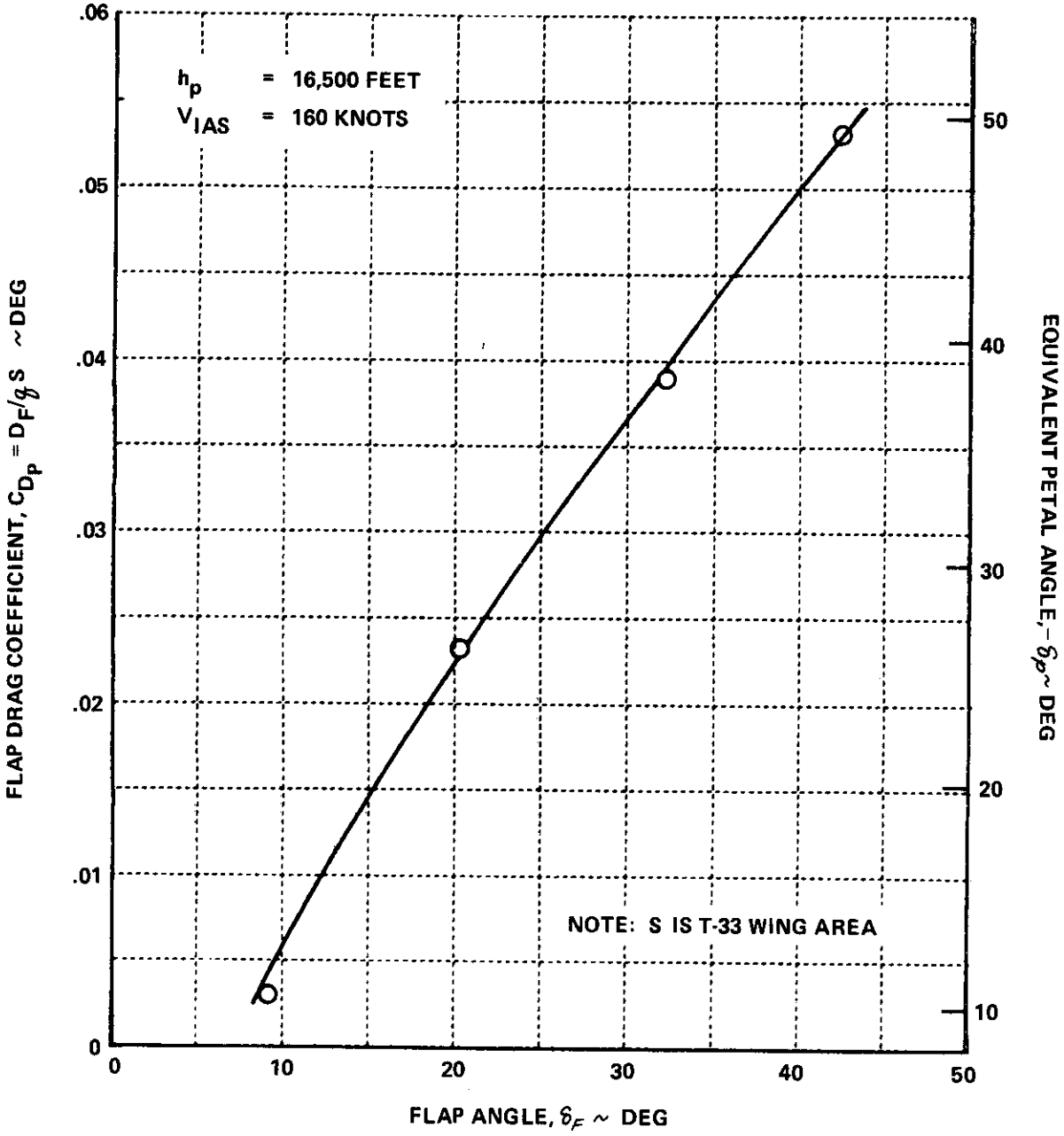

Figure 53 DRAG DUE TO T-33 FLAP DEFLECTION

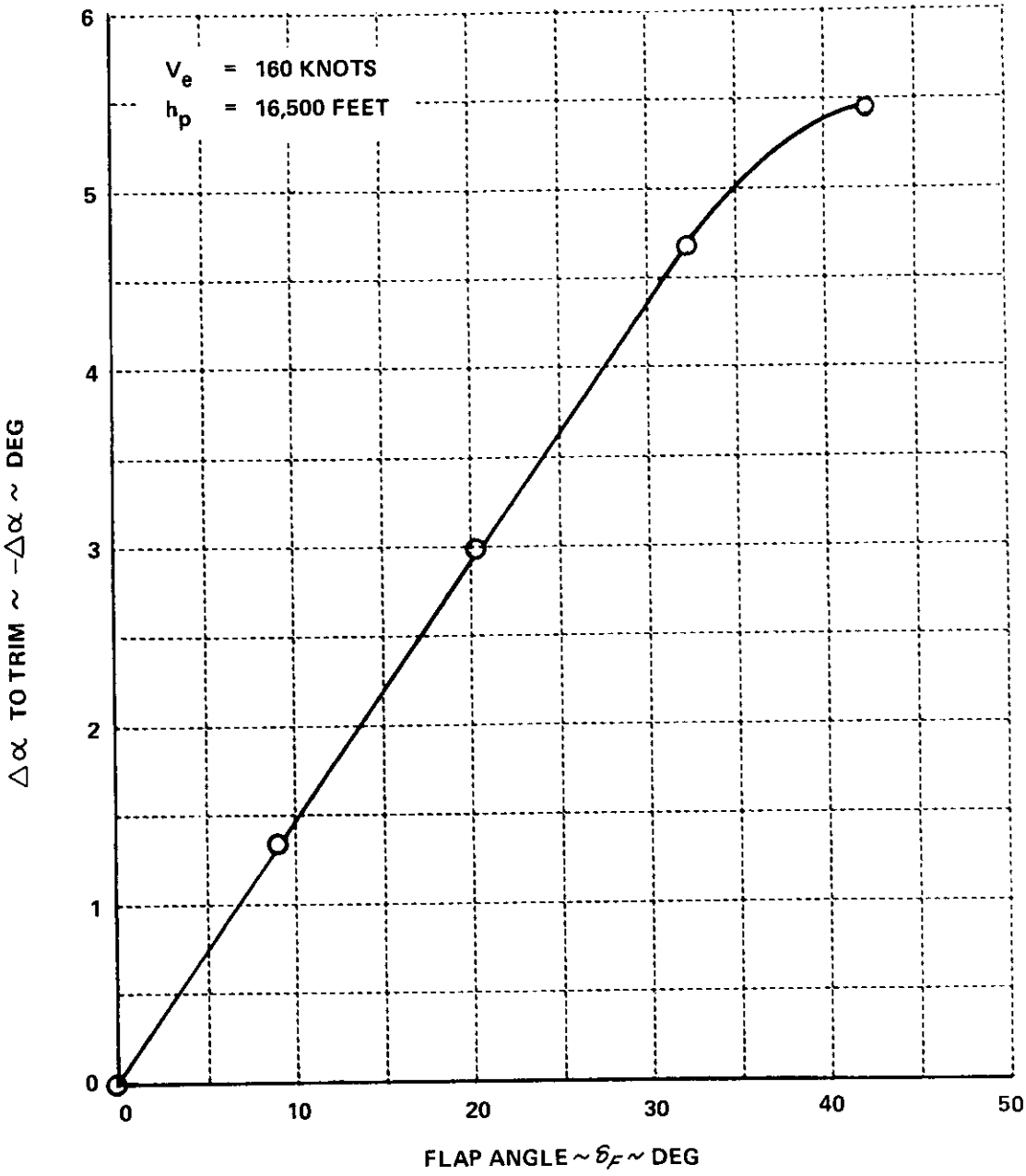

Figure 54 CHANGE IN ZERO-LIFT ANGLE OF ATTACK AS A FUNCTION OF FLAP DEFLECTION

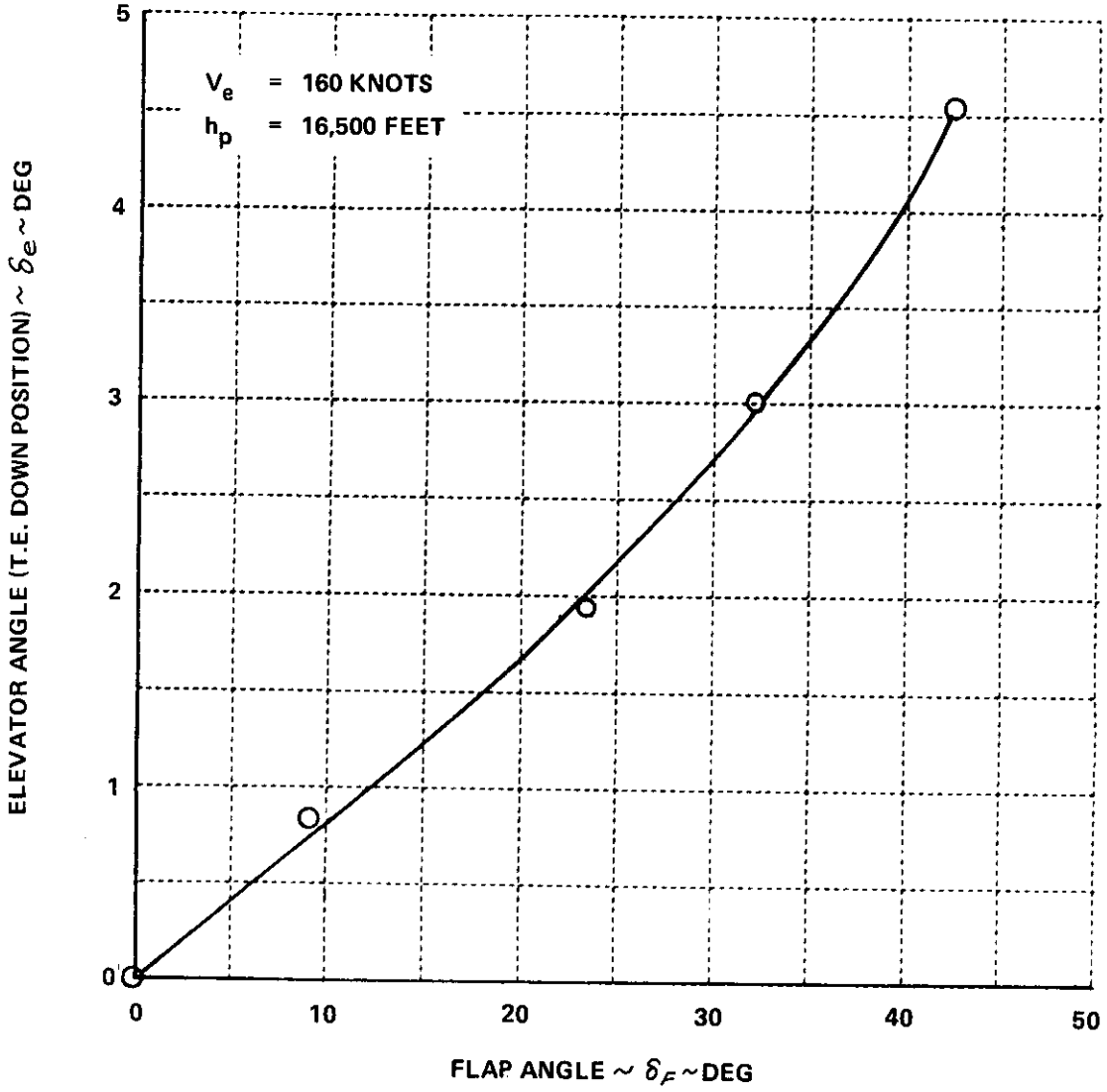

Figure 55 ELEVATOR ANGLE REQUIRED TO TRIM PITCHING MOMENT DUE TO FLAP DEFLECTION

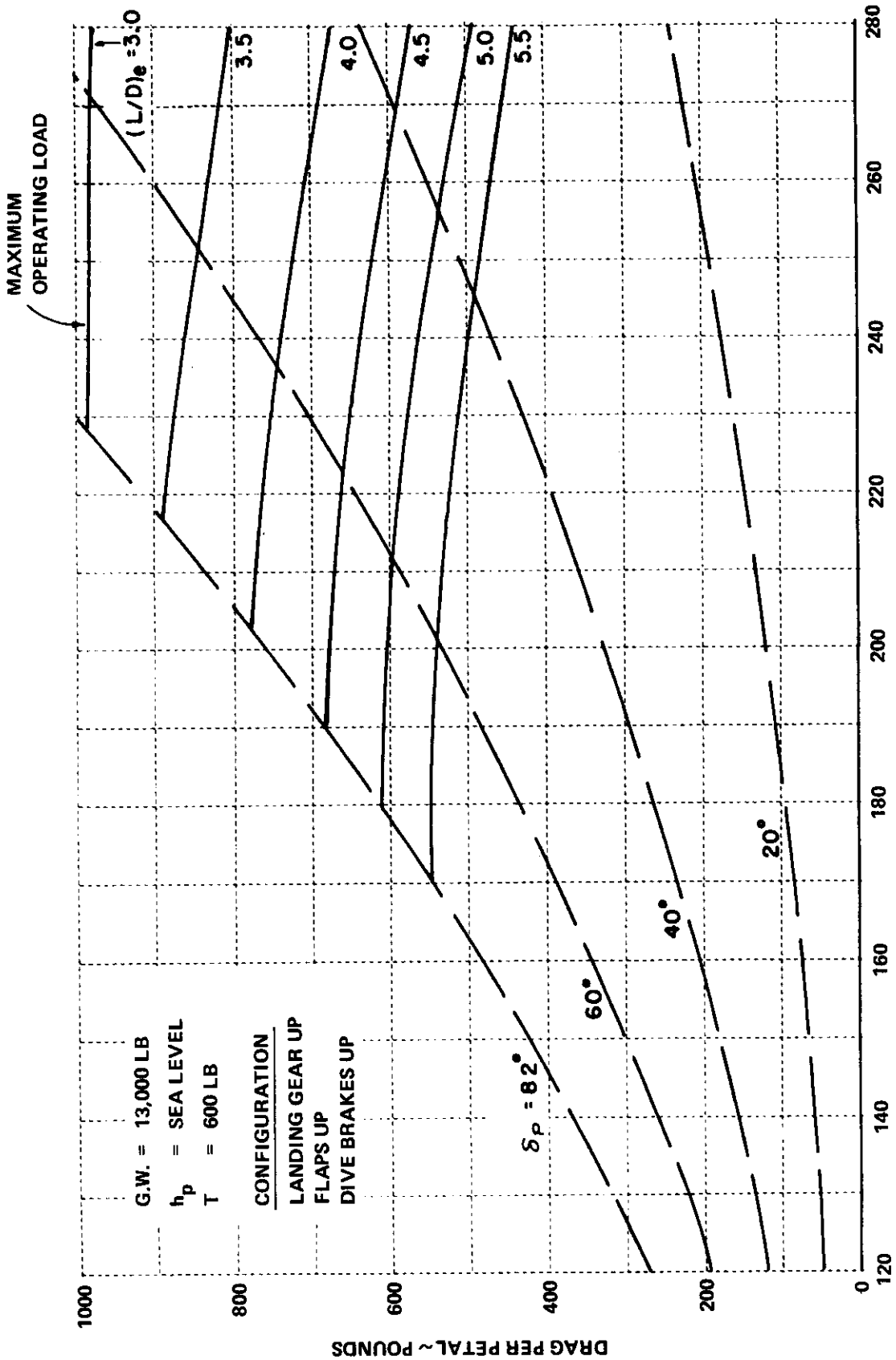

Figure 56 L/D CALIBRATION CHART (CLEAN AIRPLANE)

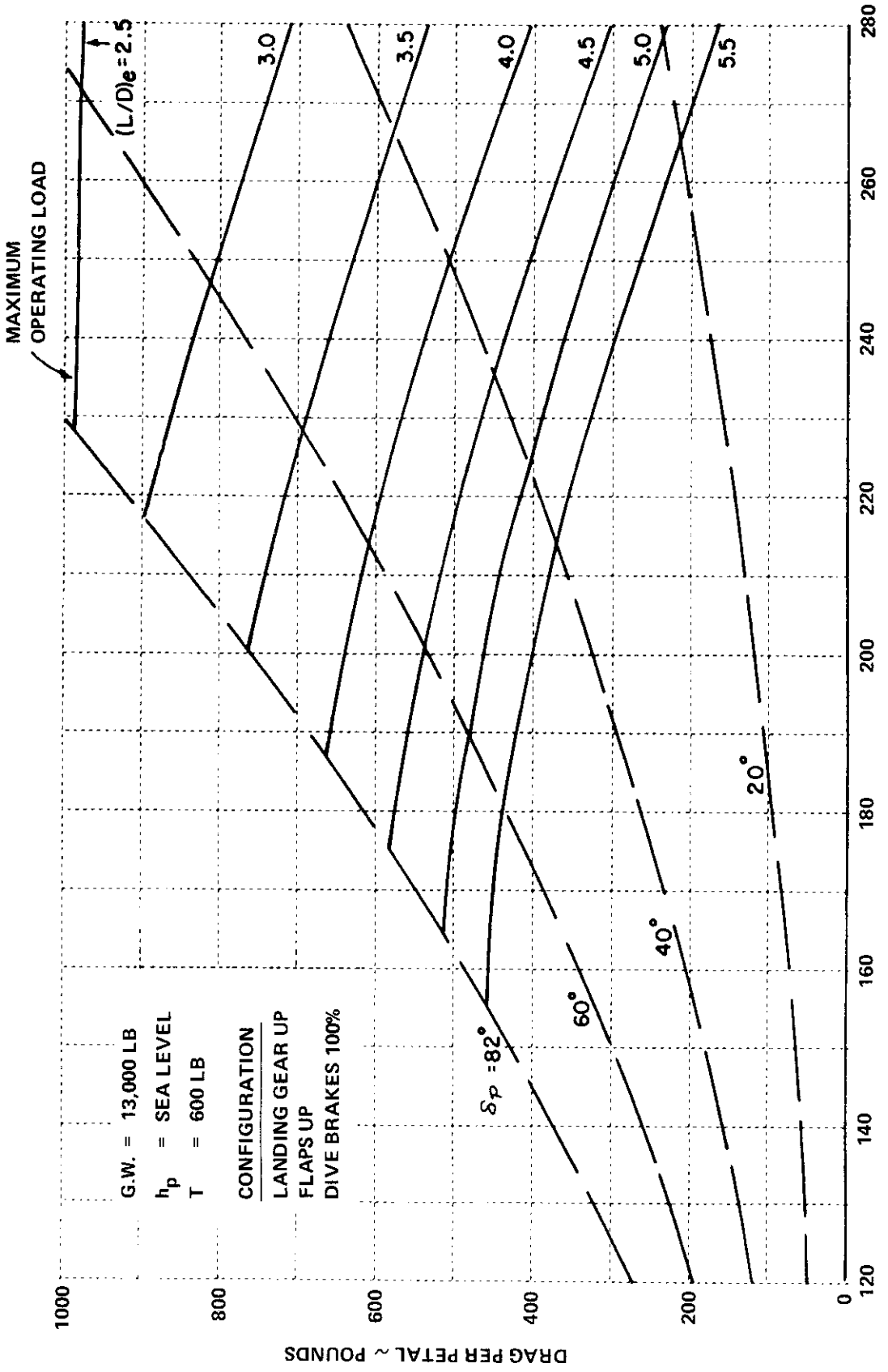

Figure 57 L/D CALIBRATION CHART, DIVE BRAKES EXTENDED (SEA LEVEL)

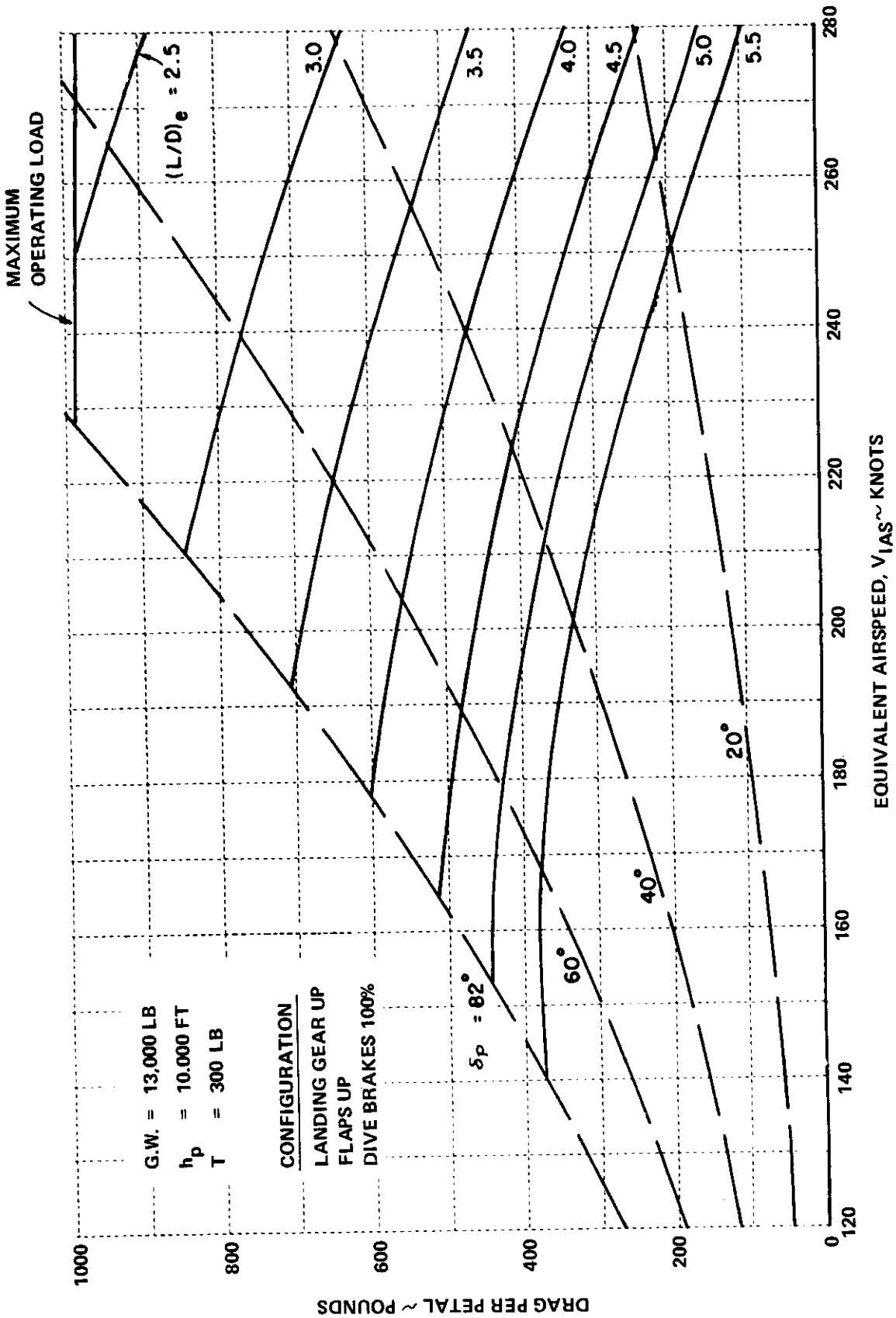

Figure 58 L/D CALIBRATION CHART, DIVE BRAKES EXTENDED (10,000 FT)

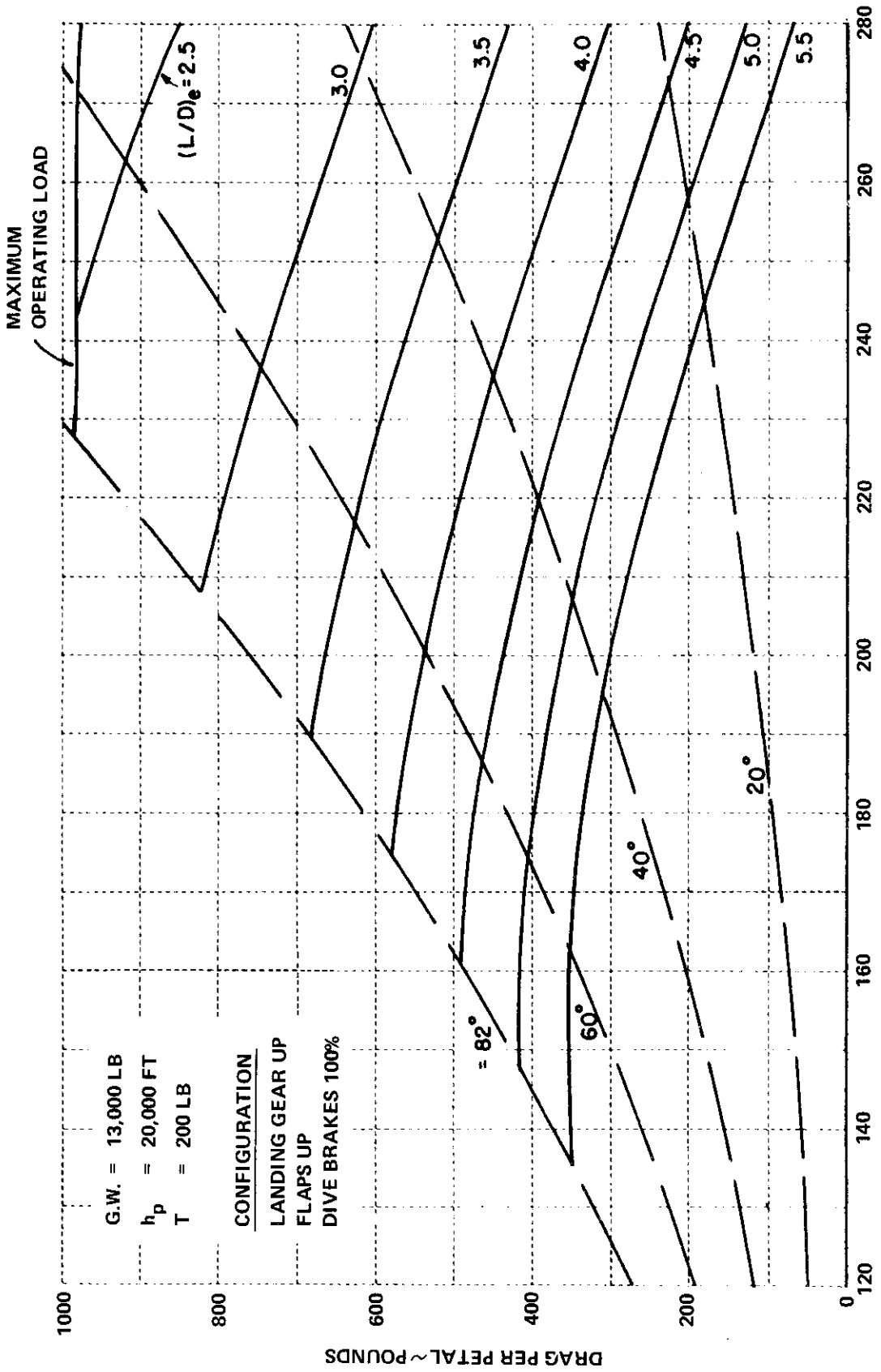

Figure 59 L/D CALIBRATION CHART, DIVE BRAKES EXTENDED (20,000 FT)

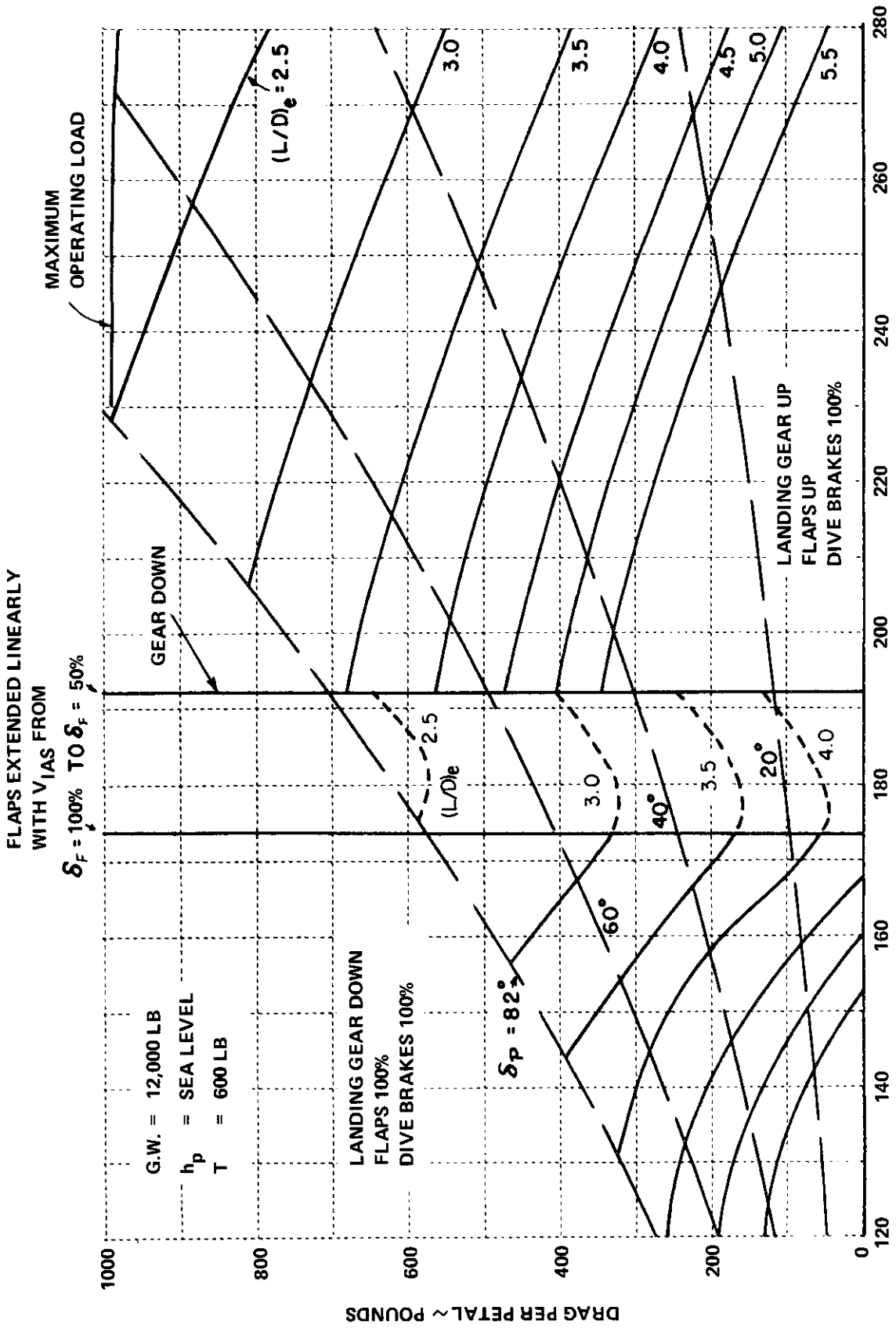

Figure 60 SEA LEVEL SUMMARY PLOT (GROSS WEIGHT = 12,000 LBS)

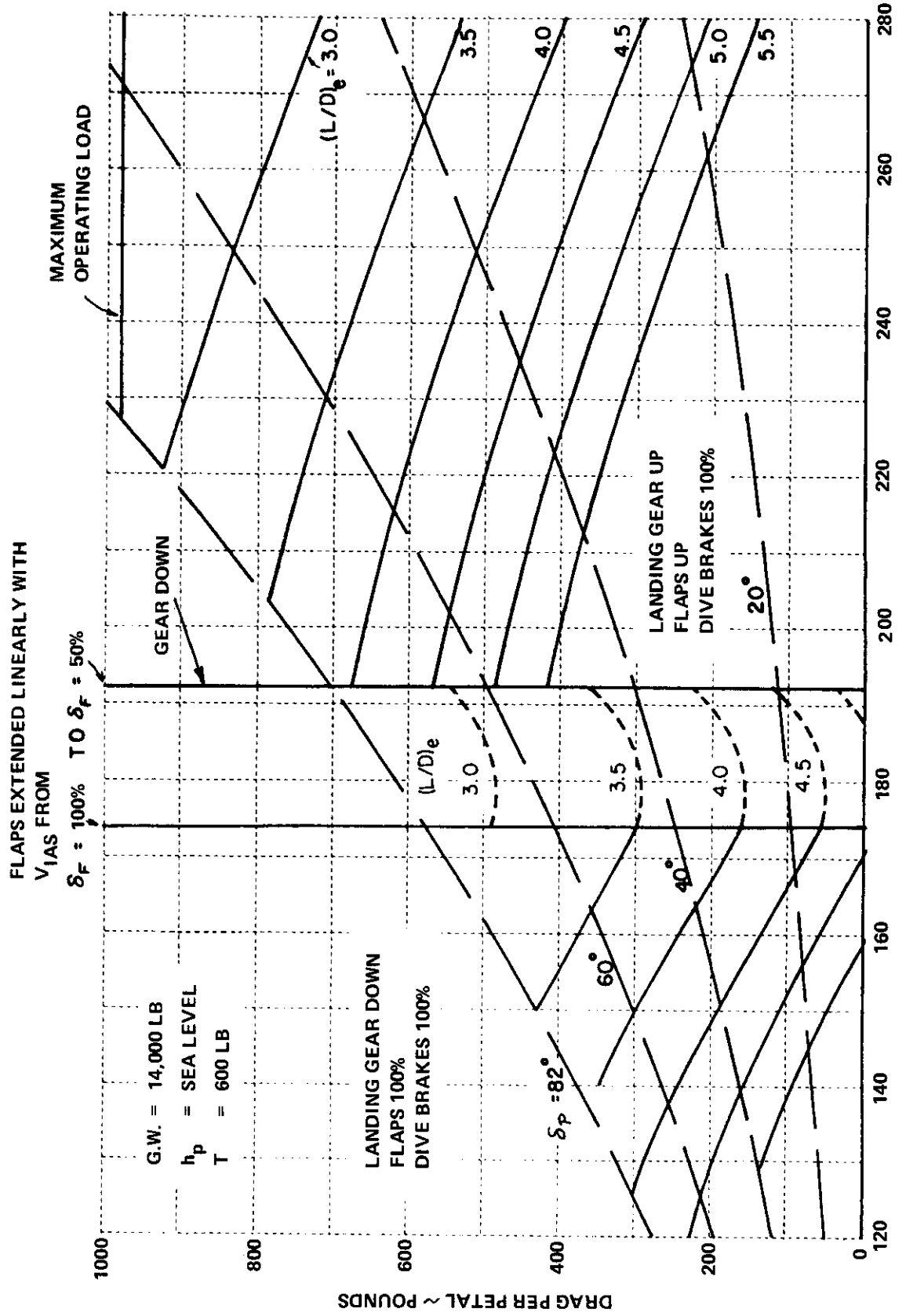

Figure 61 SEA LEVEL SUMMARY PLOT (GROSS WEIGHT = 14,000 LBS)

curves shown in the summary graphs indicates the drag per petal required to achieve a given effective L/D as a function of indicated airspeed. All the data used to establish the drag was determined from the series of flight tests previously described with the exception of the drag for the clean airplane. The drag of the clean T-33 was obtained from Reference 3 .

Because it is often desirable to use different configurations and flight conditions in the various L/D system experiments, the effects of landing gear, flap, speed brake positions, altitude, and gross weight are shown in the summary graphs. Figure 56 shows the effective L/D's obtainable for the clean airplane plus petals at sea level and a gross weight of 13,000 lb. The engine thrust is assumed to be 600 pounds, which corresponds to approximately 55% engine rpm at sea level. It is noted that an effective L/D of less than 4 can be obtained only at indicated airspeeds greater than 203 knots. This fact indicates the importance of the landing gear, speed brake and flaps if lower $(L/D)_e$ is desired. The next four summary plots, Figures 56, 57, 58 and 59 show the effects of altitude and configuration variations.

The variation of effective L/D ratio with altitude is a result of thrust variation. The thrust at 55% rpm is 600, 300, and 200 pounds at sea level, 10,000 ft, and 20,000 ft, respectively. With the speed brakes extended and a gross weight of 13,000 pounds, an effective L/D ratio of 4 can be obtained at 187 knots at sea level, whereas an effective L/D equal to 4 can be obtained at 178 knots at 10,000 ft, and 175 knots at 20,000 ft. A comparison of Figures 56 and 57 shows clearly the importance of using the dive brakes in conjunction with the petals. By opening the dive brakes, the airspeed to achieve an effective L/D of 4 was reduced from 203 to 187 knots.

Figures 60 and 61 illustrate the lowest values of effective L/D ratio that are obtainable at sea level with the L/D system. In these figures, values of effective L/D are shown with the flaps and landing gear extended at the respective limit speeds. The limit speed for the landing gear is 192 knots. The flaps may be extended 50% at 192 knots and 100% at 174 knots. The calculations shown are based on the assumption that the flaps are lowered linearly with indicated airspeed in the region from 192 to 174 knots. The large effects of the landing gear and flaps in producing drag is apparent from the large discontinuity in the curves. The effect of gross weight is also seen from a comparison of Figures 60 and 61. In general, an increase in gross weight increases the effective L/D at a given indicated airspeed. Furthermore, as the effective L/D decreases, gross weight changes become more important. It is seen that an effective L/D of 4 can be obtained for airspeeds above 130 knots for 12,000 pounds gross weight and above 137 knots for 14,000 pounds.

The summary graphs may be conveniently used to determine the functions for any L/D profile that is to be evaluated. If the L/D profile vs. velocity is superimposed on the appropriate summary graph, then the petal angle vs. velocity function can be read directly. This function is then programmed in the function generator. Although many calibrations were required to determine the various functions for the L/D system, only the petal angle vs. velocity function must be changed from time to time. The compensating functions for drag, pitching moment, and angle of attack from the flaps, landing gear and petals will not fluctuate.

SECTION VII
METHOD OF SIMULATION

The essence of in-flight simulation with a response-feedback variable stability airplane is to use the airplane's control surfaces to apply moments (and in some cases forces) to the airplane as functions of the various airplane responses such that the augmented variable stability airplane's stability derivatives or mode characteristics match those of the airplane to be simulated. This method uses a feedback control system to move the variable stability airplane's control surfaces proportional to measured airplane response variables. The moving control surfaces generate incremental derivatives which are effectively added to, or subtracted from, the stability derivatives inherent to the airplane. Thus, once the stability derivatives of both the T-33 and the airplane to be simulated are known, the required increment in each T-33 stability derivative can be calculated.

At this point, it is in order to look at how many parameters are required to describe the dynamics of an airplane and to see how many are controllable using the T-33 variable stability airplane.

The lateral-directional motions for an airplane that is considered as a rigid body with conventional rudder and aileron controls and fixed elevator control, are adequately described as a three-degree-of-freedom, fourth-order system. The total number of independent coefficients in the homogeneous set of equations is:

Independent Coefficients = Degrees of Freedom x Order of System
= 3 x 4 = 12.

For rudder and aileron controls, the total number of coefficients in the control set is:

Independent Coefficient = Degrees of Freedom x Number of Controls
= 3 x 2 = 6.

Thus, a total of 18 independent coefficients is required to describe the lateral-directional motions for a conventional airplane. With only two independent controls available, there are only two degrees of freedom which can be independently controlled. Thus, the number of coefficients in the homogeneous set which can be specified is:

Specifiable Coefficient = Controllable Degrees of Freedom x Order of System = 2 x 4 = 8.

The number of coefficients in the control set which can be specified is:

Specifiable Coefficient = Controllable Degrees of Freedom X Number of Controls = 2 x 2 = 4.

From the above discussion, it can be seen that the T-33 variable stability airplane using rudder and aileron controls has 12 parameters available with which to simulate the lateral-directional behavior of an airplane described by 18 parameters. The independent coefficients which cannot be directly controlled are (for equations written in terms of β , p , and r):

$$Y_\beta, Y_{\dot\beta}, Y_p, Y_r, Y_{\delta_{RP}}, Y_{\delta_{AS}}$$

The twelve parameters which can be specified with the variable stability airplane are expressed either in terms of stability derivatives or in terms of mode characteristics, or a combination of the two.

To determine the dimensional derivatives of the basic T-33 at a chosen flight condition, the mode characteristics are measured from flight records. A digital program, based on a technique similar to that described in NASA TN4066 (Reference 4) is used to calculate the set of stability derivatives which would produce the measured mode characteristics.

The T-33 control derivatives are calculated from in-flight measurements of the angular accelerations produced by sharp control inputs and by the angular rate responses to sinusoidal control inputs.

It is also necessary to know the T-33 stability derivatives as a function of fuel remaining. The effects of fuel usage are calculated from the corresponding mode responses obtained at different fuel loads. The variation of the moments of inertia is especially significant during the time the tip tank fuel is being consumed.

The T-33 lateral-directional stability derivatives are shown as a function of fuel remaining in Appendix III.

For the purpose of calculating the variable stability system gains, it is convenient to express the stability derivatives in primed, dimensional form, referenced to T-33 body axes. Therefore, it is necessary to compute the stability derivatives in the same form for the airplane to be simulated. A method is presented in Section VIII that allows stability derivatives to be transformed from one axis system to another and conversion to dimensional and primed derivatives.

LATERAL-DIRECTIONAL REPRESENTATION OF THE SIMULATED VEHICLE

As pointed out earlier in this section, it is beyond the capability of the T-33 to independently vary the side force derivatives. Thus, it is generally not possible to match exactly the stability derivatives of a simulated vehicle. Also, it is not always possible to select a flight condition where the speed of the T-33 can match the speed of the vehicle being simulated. Therefore, it is necessary to select which parameters will be matched and which will not. If, for instance, it is decided to match the important mode characteristics of the simulated vehicle, a set of stability derivatives different from the actual set must be used to calculate the variable stability system gains. These derivatives are termed "pseudo" derivatives in the sense that they result in flying qualities similar to those of the vehicle being simulated.

When the true airspeed of the simulated vehicle cannot be matched, the problem is more complicated because it is not possible to match both the bank angle and steady yaw rate in a steady coordinated turn. If the side force terms are neglected, these quantities are approximately related by:

$$r = \frac{g}{V}\phi \tag{1}$$

If it is decided to attempt to match the bank angle response to aileron control and to scale the yaw rate response proportional to g/V, an approach similar to the following can be used:

The equations of motion for a coordinated turn ($\beta = \dot{\beta} = 0$) are:

$$(1 - Y_r)r = \frac{g}{V}\phi + Y_{\delta_{AS}}\delta_{AS} + Y_{\delta_{RP}}\delta_{RP} \tag{2}$$

$$N'_r r = -N'_{\delta_{AS}}\delta_{AS} - N'_{\delta_{RP}}\delta_{RP} \tag{3}$$

$$L'_r r = -L'_{\delta_{AS}}\delta_{AS} - L'_{\delta_{RP}}\delta_{RP} \tag{4}$$

If the side force terms $Y_r r$, $Y_{\delta_{AS}}\delta_{AS}$, $Y_{\delta_{RP}}\delta_{RP}$ are neglected, the side force equation becomes:

$$r = \frac{g}{V}\phi \tag{5}$$

Substituting this expression for the yaw rate, r, in the two moment equations, an expression for rudder pedal deflection as a function of bank angle can be written:

$$\frac{\delta_{RP}}{\phi} = \frac{g}{V}\left[\frac{L'_{\delta_{AS}}N'_r - N'_{\delta_{AS}}L'_r}{N'_{\delta_{AS}}L'_{\delta_{RP}} - L'_{\delta_{AS}}N'_{\delta_{RP}}}\right] \tag{6}$$

From this expression, it can be seen that by matching $\frac{g}{V} N'_r$ and $\frac{g}{V} L'_r$ rather than N'_r and L'_r, it is possible to match the steady rudder deflection required as a function of bank angle in coordinated turns when the control derivatives are matched.

If the roots of the characteristic equation are to be matched, the following equation can be obtained by equating the last coefficient of the quartic with the product of the roots:

$$\frac{\omega_d^2}{\tau_R \tau_S} = \frac{g}{V}\left[L'_\beta N'_r - N'_\beta L'_r\right] \tag{7}$$

From this expression it can be seen that matching $\frac{g}{V} N'_r$ and $\frac{g}{V} L'_r$ permits satisfying this equation by matching the sideslip derivatives L'_β and N'_β.

If, for example, the following procedure is to be used:

a. Match the roll response to aileron stick inputs. This requires that the following parameters be specified:

$$\omega_d, \zeta_d, \tau_R, \tau_S$$
$$\omega_\phi, \zeta_\phi$$
$$L_{\delta_{AS}}$$

b. Match the steady rudder pedal deflection as a function of bank angle required to coordinate a turn. This can be done by the following:

$$\left(\frac{g}{V} L'_r\right)_{\substack{\text{SIMULATED}\\ \text{AIRCRAFT}}} = \left(\frac{g}{V}\right)_{T\text{-}33} L'_r)_{\text{PSEUDO}} \tag{8}$$

$$\left(\frac{g}{V} N'_r\right)_{\substack{\text{SIMULATED}\\ \text{AIRCRAFT}}} = \left(\frac{g}{V}\right)_{T\text{-}33} N'_r)_{\text{PSEUDO}} \tag{9}$$

$$L'_{\delta_{RP}})_{\substack{\text{SIMULATED}\\ \text{AIRCRAFT}}} = L'_{\delta_{RP}})_{\text{PSEUDO}} \tag{10}$$

$$N'_{\delta_{RP}})_{\substack{\text{SIMULATED}\\ \text{AIRCRAFT}}} = N'_{\delta_{RP}})_{\text{PSEUDO}} \tag{11}$$

c. Since a total of twelve parameters can be specified and only eleven were selected in a. and b. above, one remaining parameter could be specified. A good choice would be to specify the magnitude of the bank angle to sideslip ratio in the Dutch roll mode

$$\left|\frac{\phi}{\beta}\right|_{\substack{\text{SIMULATED}\\ \text{AIRCRAFT}}} = \left|\frac{\phi}{\beta}\right|_{\text{PSEUDO}} \qquad (12)$$

A digital computer program similar to that mentioned in Section VII can be used to compute the pseudo derivatives which will satisfy the constraints listed above. This program is reported in Reference 11. However, with this program, it is not possible to directly specify ζ_ϕ as an input. Instead, the phase angle between bank angle and sideslip in the Dutch roll mode can be specified and ζ_ϕ calculated. Several values of $\angle \frac{\phi}{\beta}$ can be run and the one which best satisfies the ζ_ϕ requirement selected.

With respect to the digital program, the following input data (Figures 62-65) are required and should be presented on the sample **data** sheet shown. The output will be compensated knob (cockpit gain control) settings.

Inputs Required (LTD/SUDO)

Options

1. Iterate side forces (y's)

2. Iterate to match simulated airplane parameter

   a) ζ_ϕ c) $N'_p)_{SA} - \frac{g}{V_{SA}}$

   b) $N'_p)_{SA}$ d) $\angle \frac{\phi}{\beta}$ or series $\angle \frac{\phi}{\beta}$

3. Compute $\zeta_{\phi_{PSEUDO}}$

   a) given $\omega_{\phi_{SA}}$, $\dot{p}/\delta_{AS}$

   b) given $L'_{\delta_{AS}}$, $N'_{\delta_{AS}}$

4. For "pseudo" airplane

   a) compute equations of motion

   b) print equations of motion, roots, ζ , ω , transfer functions and phase angles

   c) compute transient responses to δ_a , δ_r , ξ

   d) list transient response parameters (β , p , ϕ , r)

   e) plot transient responses (need Δt , t_o , t_f and length of axis and size of increments)

(MAY REPLACE)
τ_R, τ_S

CONFIG.	F_R	ζ_d	ω_d	τ_R	τ_S	V_{SA} (fps)	ζ_p	ω_p	$\left\lvert \frac{\phi}{\beta} \right\rvert$	$\angle \frac{\phi}{\beta}$	ζ_{RS}	ω_{RS}
	650	231	232	237	238	6	369	370	262	263	233	234
CONFIG.	F_R	$L'_{\dot{\beta}}$	$N'_{\dot{\beta}}$	L'_r	N'_r	$L'_{\delta_{RP}}$	$N'_{\delta_{RP}}$	N'_p	$Y_{\dot{\beta}}$	$L'_{\dot{\beta}}$	$Y_{\delta_{AS}}$	$L'_{\delta_{AS}}$ or p/δ_{AS}
		256	257	258	259	225	226	87	82	83	91	92

Figure 62a COMPUTER PROGRAM INPUTS REQUIRED FOR THE SIMULATED AIRPLANE

CONFIG.	F_R	V_{VSA} (fps)	L'_{δ_a}	N'_{δ_a}	L'_{δ_r}	N'_{δ_r}	L'_β	N'_β	$L'_{\dot\beta}$	$N'_{\dot\beta}$	L'_p	N'_p
	650	274	239	240	241	242	243	244	245	246	247	248
CONFIG.	F_R	L'_r	N'_r	Y_β	$Y_{\dot\beta}$	Y_p	Y_r	Y_{δ_a}	Y_{δ_r}	$\alpha_{o\ VSA}$ (deg)		
		249	250	251	252	253	254	260	261	22		

Figure 62b COMPUTER PROGRAM INPUTS REQUIRED FOR THE VARIABLE STABILITY AIRPLANE

CONFIGURATION NUMBER: FUEL REMAINING:

SUB-TITLES: FOR "PSEUDO" AIRPLANE

EQUATIONS OF MOTION

$$\begin{array}{cccccccccccc} & \underline{\dot{\beta}} & \underline{\beta} & \underline{\dot{p}} & \underline{p} & \underline{\phi} & \underline{\ddot{r}} & \underline{\dot{r}} & \underline{r} & & \underline{\delta_a} & \underline{\delta_r} & \underline{\xi} \\ \underline{Y} & Y_{\dot{\beta}} & + Y_{\beta} & + Y_{\dot{p}} & + Y_{p} & + Y_{\phi} & + Y_{\ddot{r}} & + Y_{\dot{r}} & + Y_{r} & = & Y_{\delta_a} & + Y_{\delta_r} & + Y_{\xi} \\ \underline{L} & L_{\dot{\beta}} & + L_{\beta} & + L_{\dot{p}} & + L_{p} & + L_{\phi} & + L_{\ddot{r}} & + L_{\dot{r}} & + L_{r} & = & L_{\delta_a} & + L_{\delta_r} & + L_{\xi} \\ \underline{N} & N_{\dot{\beta}} & + N_{\beta} & + N_{\dot{p}} & + N_{p} & + N_{\phi} & + N_{\ddot{r}} & + N_{\dot{r}} & + N_{r} & = & N_{\delta_a} & + N_{\delta_r} & + N_{\xi} \end{array}$$

CHARACTERISTIC EQUATION:

$$a_5 s^5 + a_4 s^4 + a_3 s^3 + a_2 s^2 + a_1 s + a_0$$

ROOTS, ETC.

REAL	IMAG	ZETA	OMEGA	PHI/BETA PHASE (DEG)		R/BETA PHASE (DEG)		TAU
$(a$	$+ bi)$	ζ_d	ω_d	ϕ/β	$\angle\ \phi/\beta$	r/β	$\angle\ r/\beta$	
a				ϕ/β	$\angle\ \phi/\beta$	r/β	$\angle\ r/\beta$	τ_R, τ_S

Figure 63 GENERAL FORM FOR EQUATIONS OF MOTION

BETA/DELTA-A
(BASIC EQUATION) $a_4 s^4 + a_3 s^3 + a_2 s^2 + a_1 s + a_0$

COMPLEX ROOTS ARE	REAL	IMAG	ZETA	OMEGA
	$(a$	$+ bi)$	ζ	ω
REAL ROOTS ARE			a_1	a_2
TAU			τ_1	τ_2

REPEAT GENERAL FORM OF BASIC EQUATION & ROOTS FOR:

PHI/DELTA-A
R/DELTA-A
BETA/DELTA-R
R/DELTA-R
BETA/XI
PHI/XI
R/XI

PHI/DELTA-R

TRANSFER FUNCTIONS FOR "PSEUDO" AIRPLANE

Figure 64 GENERAL FORM FOR TRANSFER FUNCTION NUMERATORS

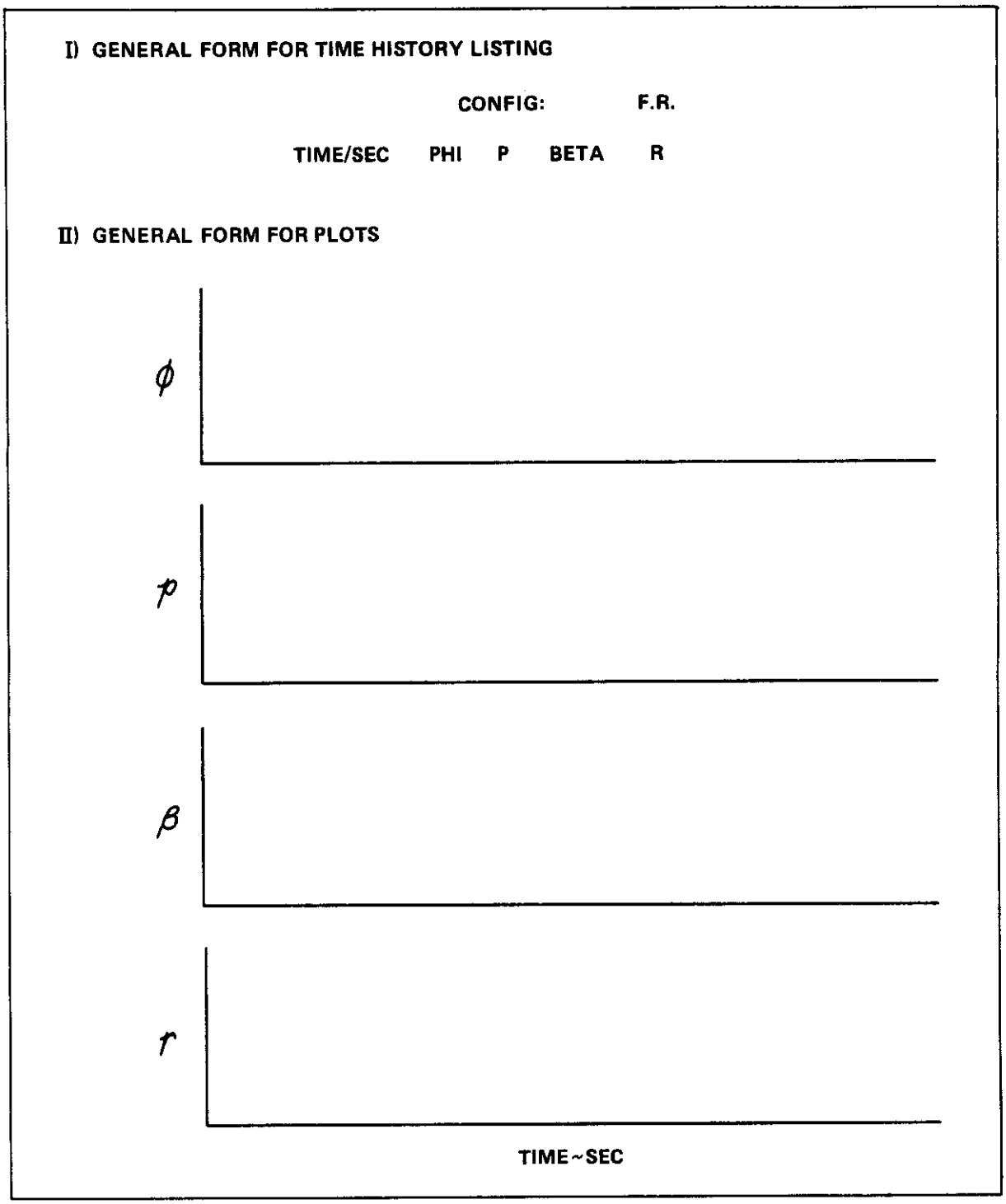

Figure 65 GENERAL FORM FOR TIME HISTORY LISTING AND PLOTS FOR "PSEUDO" AIRPLANE

The longitudinal motions, for a rigid-body airplane with a conventional elevator and fixed aileron and rudder controls are adequately described as a three-degree-of-freedom fourth-order system.

The total number of independent coefficients in the homogeneous set of equations is:

Independent coefficients = Degrees of Freedom x Order of System
= 3 x 4 = 12

For elevator control only, the total number of coefficients in the control set is:

Independent Coefficients = Degrees of Freedom x Number of Controls
= 3 x 1 = 3

Thus a total of 15 independent coefficients is required to describe the longitudinal motions for a conventional airplane. With only one independent controller, there is only one degree of freedom which can be independently controlled. The L/D system provides an additional independent controller in the x-axis, but the remaining discussion will assume only elevator control is available. Thus, the number of coefficients in the homogeneous set which can be specified is:

Specifiable Coefficients = Controllable Degree of Freedom x
Order of System = 1 x 4 = 4

The number of coefficients in the control set which can be specified is:

Specifiable Coefficients = Controllable Degrees of Freedom x
Number of Controls = 1 x 1 = 1

From the above discussion, it can be seen that the T-33 variable stability airplane using elevator control only has 5 parameters available with which to simulate the longitudinal behavior of an airplane described by 15 parameters. The independent coefficients which cannot be directly controlled are (for equations written in u, α and q);

$$X_u, X_\alpha, X_{\dot{\alpha}}, X_q, X_{\delta_e}, Z_u, Z_\alpha, Z_{\dot{\alpha}}, Z_q, Z_{\delta_e}$$

Thus, the 5 parameters which can be specified with the variable stability airplane using only the elevator are the pitching moment coefficients:

$$M_u, M_\alpha, M_{\dot{\alpha}}, M_q, M_{\delta_e}$$

This is not as serious a handicap as it might first appear because it is usually assumed that

$$X_{\dot{\alpha}} = X_q = X_{\delta_e} = Z_{\dot{\alpha}} = Z_q = 0 \tag{13}$$

The L/D system adds another controller which raises the number of degrees of freedom which can be independently controlled to two. Thus, the specifiable coefficients = controllable degrees of freedom x order of system = 2 x 4 = 8, however, the number of coefficients in the control set which can be controlled is controllable degrees of freedom x number of controls = 2 x 1 = 2. Thus with the L/D system, the number of parameters which can be independently controlled is raised to 10. This includes both the χ force and pitching moment, M, coefficients.

LONGITUDINAL REPRESENTATION OF THE SIMULATED VEHICLE

The T-33 does not have the capability of varying lift directly and therefore cannot directly control the z force coefficients.

The following approximate transfer functions indicate the functional relationships that exist between the various longitudinal response variables when the airplane is disturbed through the elevator: (These approximate expressions are used here to simplify the presentation of the ideas. In actual simulation, the more complete expressions in Section VIII should be used.)

$$\frac{n_z}{\alpha} \approx \frac{V}{g} L_\alpha \;,\; \frac{n_z}{q} \approx \frac{V}{g}\frac{1}{\left(\frac{1}{L_\alpha}s+1\right)} \;,\; \dot{\gamma} \approx q - \dot{\alpha} \;,\; n_z \approx \frac{V}{g}\dot{\gamma} \;,\; \frac{\dot{\gamma}}{\alpha} \approx L_\alpha \qquad (14)$$

From these relationships, it can be seen that the steady-state normal acceleration is related to the steady-state pitch rate by V/g and to angle of attack by $\frac{V}{g} L_\alpha$. The steady-state pitch rate and rate of change of flight path are related to the angle of attack by L_α.

Because of the inability to vary the lift, the value of L_α for any given altitude and speed in the T-33 is fixed. This allows three possible choices to obtain the best combination of steady-state pitch rate, normal acceleration and angle of attack responses.

1. If the speed of the simulated vehicle is within the speed capability of the T-33, it may be possible to match L_α by selecting the altitude at which the density is such that the following relationship is satisfied:

$$L_\alpha = \frac{g\rho VS}{2W} C_{L_\alpha} \qquad (15)$$

for the desired speed.

If this is possible, within the restrictions imposed by not being able to match the Z coefficients directly, the n_z/α, q and $\dot{\gamma}$ responses should be adequately simulated.

2. If the speed of the simulated vehicle is not within the speed capability of the T-33, a good choice is to match the steady-state n_z/α response.

The reason for this, as demonstrated below, is that for short period frequencies $\omega > L_\alpha$, the n_z/α and $\dot{\theta}/n_z$ responses will have the proper relationship.

The $\dot{\theta}/n_z$ relationship can be written in approximate form as:

$$\frac{\dot{\theta}}{n_z} \approx \frac{g}{V}\left(\frac{1}{L_\alpha}s + 1\right) \tag{16}$$

which allows us to write:

$$\frac{\theta}{n_z} \approx \frac{g}{V}\frac{\left(\frac{1}{L_\alpha}s + 1\right)}{s} \approx \frac{g}{VL_\alpha}\left(\frac{s + L_\alpha}{s}\right) \tag{17}$$

we recognize that:

$$\frac{g}{VL_\alpha} \approx \frac{\alpha}{n_z} \quad thus \quad \frac{\theta}{n_z} \approx \frac{\alpha}{n_z}\left(\frac{s + L_\alpha}{s}\right) \tag{18}$$

thus for high frequencies the θ/n_z response is approximately equal to the α/n_z response both of which provide important longitudinal handling qualities cues for the evaluation pilot.

Since $\frac{n_z}{\alpha} \approx \frac{V}{g}L_\alpha$ and $L_\alpha = \frac{g\rho VS}{2W}C_{L_\alpha}$, then $\frac{n_z}{\alpha} = \frac{\rho V^2 S}{2W}C_{L_\alpha}$ (19)

this allows the choice of altitude and speed that will allow the n_z/α response of the simulated vehicle to be matched.

3. If the speed of the simulated vehicle is within the speed capability of the T-33, or even if it is not, but there is no combination of speed and/or altitude that will allow the L_α of the simulated vehicle to be matched, another criterion must be selected. A possible choice is to match the ratio of initial pitch acceleration response to steady-state normal acceleration response for a step input which has been shown (Reference 5) to be an important longitudinal handling qualities parameter. Thus, the primary short term handling qualities can be simulated by simulating the control anticipation parameter (CAP) and the steady-state stick force per g (F_{ES}/n_z). These two expressions can be written as:

$$CAP = \frac{\ddot{\theta}_o}{n_{z_{ss}}} = \frac{\omega_{sp}^2}{(n_z/\alpha)_{ss}} \tag{20}$$

$$\frac{\ddot{\theta}_o}{F_{ES}} = \frac{\omega_{sp}^2}{(n_z/\alpha)_{ss}(F_{ES}/n_z)_{ss}} \tag{21}$$

NOTE: $\ddot{\theta}_o$ is the initial pitch acceleration to a step elevator input.

Thus it is possible to match the initial pitch response to a control force input, F_{Es}, and the steady-state maneuver forces, F_{Es}/n_z, by simulating $\omega_{sp}^2/(n_z/\alpha)_{ss}$ and $(F_{Es}/n_z)_{ss}$. If the desired $(n_z/\alpha)_{ss}$ is less than that which can be attained by the T-33, higher ω_{sp} can be simulated and if the desired $(n_z/\alpha)_{ss}$ is greater than that which can be attained by the T-33, lower ω_{sp} can be simulated to keep $\omega_{sp}^2/(n_z/\alpha)_{ss}$ at the desired value. Thus at this time it appears that the short term longitudinal handling characteristics are best simulated by matching CAP, ζ_{sp}, $(F_{Es}/n_z)_{ss}$, and F_{Es}/δ_{Es}.

CALCULATION OF THE GAINS REQUIRED

Once the pseudo derivatives are determined, the variable stability system gains required to match the pseudo derivatives can be calculated from the following matrix equations:

$$\begin{bmatrix} \frac{\delta_a}{\beta} & \frac{\delta_a}{\dot{\beta}} & \frac{\delta_a}{p} & \frac{\delta_a}{r} \\ \frac{\delta_r}{\beta} & \frac{\delta_r}{\dot{\beta}} & \frac{\delta_r}{p} & \frac{\delta_r}{r} \end{bmatrix} = \begin{bmatrix} L'_{\delta_a} & L'_{\delta_r} \\ N'_{\delta_a} & N'_{\delta_r} \end{bmatrix}^{-1}_{T-33} \begin{bmatrix} \Delta L'_\beta & \Delta L'_{\dot{\beta}} & \Delta L'_p & \Delta L'_r \\ \Delta N'_\beta & \Delta N'_{\dot{\beta}} & \Delta N'_p & \Delta N'_r \end{bmatrix}_{PSEUDO} \tag{22}$$

where for example $$L'_{\beta_{PSEUDO}} = L'_{\beta_{T-33}} + \Delta L'_\beta = L'_{\beta_{T-33}} + L'_{\delta_{r_{T-33}}} \frac{\delta_r}{\beta} + L'_{\delta_{a_{T-33}}} \frac{\delta_a}{\beta}$$

$$\begin{bmatrix} \frac{\delta_a}{\delta_{AS}} & \frac{\delta_a}{\delta_{RP}} \\ \frac{\delta_r}{\delta_{AS}} & \frac{\delta_r}{\delta_{RP}} \end{bmatrix} = \begin{bmatrix} L'_{\delta_a} & L'_{\delta_r} \\ N'_{\delta_a} & N'_{\delta_r} \end{bmatrix}^{-1}_{T-33} \begin{bmatrix} L'_{\delta_{AS}} & L'_{\delta_{RP}} \\ N'_{\delta_{AS}} & {}'_{\delta_{RP}} \end{bmatrix}_{PSEUDO} \tag{23}$$

where $L'_{\delta_{AS}} = L'_{\delta_{AS}})_{PSEUDO}$

Table III is a display card used by the safety pilot as an aid in setting the variable stability system gains in flight.

Table III

T-33 VARIABLE STABILITY GAIN CONTROLS

δ_{RP}	δ_r/δ_{RP} 000→999 INCREASE GEAR RATIO	δ_{AS}	δ_a/δ_{AS} 000→999 INCREASE GEAR RATIO	δ_{ES}	δ_e/δ_{ES} 000→999 INCREASE GEAR RATIO	IN	δ_r/IN AUTO INPUT R.N. ← 5 → 0 0	COLOR CODE Red-Rudder Green-Aileron Brown-Elevator Black-Drag Petals
δ_a	δ_r/δ_a INTERCON. (-)← 5 →(+) 0 PRO. 0 ADV. YAW YAW	δ_r	δ_a/δ_r INTERCON. (-)← 5 →(+) 0 POS. 0 NEG. DIHD. DIHD.	X	$\delta_e/X(\dot{u})$ PHUGOID DAMPING (-)← 5 →(+) 0 DEC. 0 INC.	IN	δ_a/IN AUTO INPUT R.N. (-)← 5 →(+) 0 RT. 0 LEFT	IN δ_e/IN AUTO INPUT R.N. (-)← 5 →(+) 0 UP 0 DOWN
β	δ_r/β DUTCH ROLL FREQUENCY (-)← 5 →(+) 0 INC. 0 DEC.	β	δ_a/β AND DIHEDRAL (-)← 5 →(+) 0 DEC. 0 INC.	α	δ_e/α SHORT PERIOD FREQUENCY (-)← 5 →(+) 0 DEC. 0 INC.	ζ	RUDDER FEEL SYSTEM DAMPING 000→999 INCREASE DAMPING	
$\dot{\beta}$	$\delta_r/\dot{\beta}$ DUTCH ROLL DAMPING (-)← 5 →(+) 0 INC. 0 DEC.	$\dot{\beta}$	$\delta_a/\dot{\beta}$ DUTCH ROLL DAMPING (-)← 5 →(+) 0 DEC. 0 INC.	$\dot{\alpha}$	$\delta_e/\dot{\alpha}$ SHORT PERIOD DAMPING (-)← 5 →(+) 0 DEC. 0 INC.	ω	RUDDER FEEL SYSTEM FREQUENCY 000→999 INCREASE FREQUENCY	
p	δ_r/p YAW DUE TO ROLL (-)← 5 →(+) 0 PRO. 0 ADV. YAW 0 YAW	p	δ_a/p ROLL DAMPING (-)← 5 →(+) 0 DEC 0 INC.	q	δ_e/q SHORT PERIOD DAMPING (-)← 5 →(+) 0 DEC. 0 INC.	ζ	AILERON FEEL SYSTEM DAMPING 000→999 INCR. DAMPING	
r	δ_r/r DUTCH ROLL DAMPING (-)← 5 →(+) 0 DEC. 0 INC.	r	δ_a/r ROLL DUE TO YAW RATE (-)← 5 →(+) 0 INC. 0 DEC.	u	δ_e/u PHUGOID FREQUENCY (-)← 5 →(+) 0 INC. 0 DEC.	ω	AILERON FEEL SYSTEM FREQUENCY 000→999 INCREASE FREQUENCY	
X	$\delta_r/X(\dot{p})$ PRODUCT OF INERTIA (-)← 5 →(+) 0 DEC. 0 INC.	X	$\delta_a/X(\dot{p})$ INERTIA (-)← 5 →(+) 0 DEC. 0 INC.	α	δ_p/α DRAG DUE TO ANG. OF ATTACK (-)← 5 →(+) 0 DEC. 0 INC.	ζ	ELEVATOR FEEL SYSTEM DAMPING 000→999 INCREASE FREQUENCY	
Y	$\delta_r/Y(\dot{r})$ INERTIA (-)← 5 →(+) 0 DEC. 0 INC.	Y	$\delta_a/Y(\dot{r})$ PRODUCT OF INERTIA (-)← 5 →(+) 0 DEC. 0 INC.	u	δ_p/u DRAG DUE TO Δ VELOCITY (-)← 5 →(+) 0 DEC. 0 INC.	ω	ELEVATOR FEEL SYSTEM FREQUENCY 000→999 INCREASE FREQUENCY	
K	F_{RP}/δ_{RP} 000→999 INCREASE GRADIENT	K	F_{AS}/δ_{AS} 000→999 INCREASE GRADIENT	K	F_{ES}/δ_{ES} 000→999 INCREASE GRADIENT	Y	$\delta_e/Y(\dot{q})$ INERTIA (-)← 5 →(+) 0 DEC. 0 INC.	

SECTION VIII
DEFINITIONS OF AXIS SYSTEMS

The equations of motion for an airplane can be written with respect to a number of axis systems. Also, flight test data is often obtained in one axis system and will require transformation to a different axis system. Therefore, it is important to understand these reference systems and know what axis system is being employed. Figure 66 shows the various axis systems. The choice of the axis system to be used is primarily a function of the problem one is attempting to solve. Definitions of the more commonly employed axis systems are given below:

(a) Earth Axes (x_e , y_e , z_e) are generally used to describe the motion of the airplane with respect to time for short intervals. This axis system is assumed to be fixed with respect to the earth and the earth is assumed to be fixed in space. Therefore this axis system is an inertial, space-fixed system from which the orientation of the airplane may be described. This axis system is an orthogonal triad with the origin at the center of gravity of the airplane at time t = 0. The x_e and y_e axes are tangent to the earth's surface and the z_e axis is directed toward the center of the earth. The orientation of the x_e axis is somewhat arbitrary, however, two conventions are in general use. One convention is to have the x_e axis point in the direction of North and the second is to have the x_e axis point in the direction of the fuselage reference line at time t = 0.

(b) Eulerian Axes (x , y , z) are also defined as a right-hand system of orthogonal coordinate axes which has its origin fixed with respect to the airplane and moves with the airplane. At any instant of time, the airplane can have linear and angular velocities and accelerations with respect to Eulerian axes but can never have any displacement. The velocities of the airplane are absolute velocities, since at any instant of time the Eulerian axes are considered fixed in space. Moments and products of inertia are independent of time because the axis system does not move with respect to the airframe. These moments and products of inertia are, however, functions of the weight distribution of the airplane and the orientation of the axes with respect to the airframe.

(c) Principal Axes (x_o , y_o , z_o) are defined as the axes about which the products of inertia are zero and define the natural axes of rotation of the airplane. Since the product of inertia is zero for an axis of symmetry, it follows that axes of symmetry are principal axes. The assumption is usually made that airplanes have a vertical plane of mirror symmetry, in which case the y_o axis will coincide with the y body axis and be a principal axis. The x_o and z_o axes will then lie in the plane of symmetry. Principal axes have little use in flight test data reduction techniques.

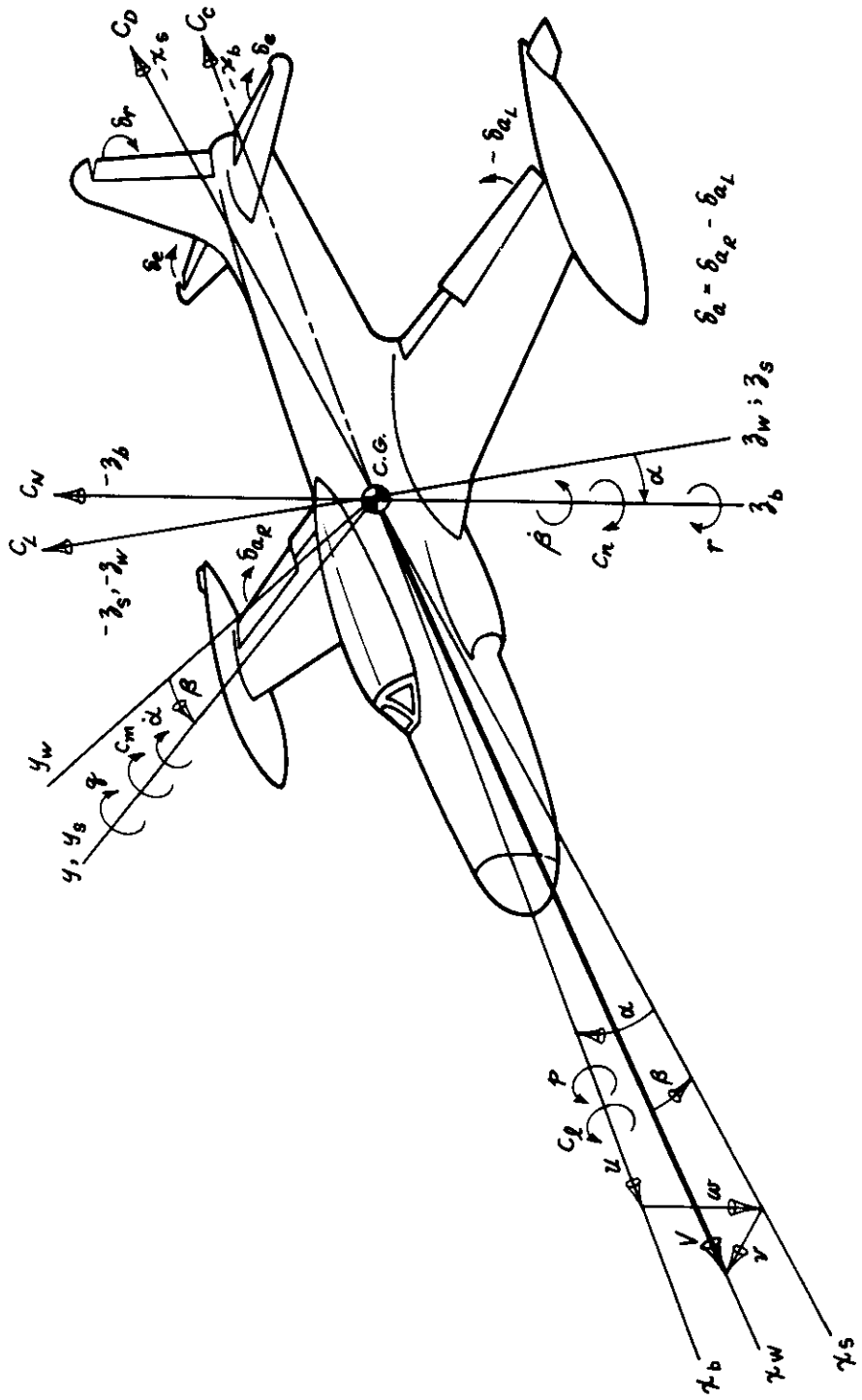

Figure 66 AXIS SYSTEMS

(d) Body Axes (x_b , y_b , z_b) are defined as a right-hand system of orthogonal coordinate axes fixed in the body of the airplane with its origin at the center of gravity. The x_b and z_b axes are fixed in the plane of symmetry and therefore the y_b axis is perpendicular to it. The exact alignment of the x_b axis is somewhat arbitrary; however, it is conventional to have it aligned with the reference line of the airplane. The x_b axis is positive forward and the z_b axis positive downward. Since this axis system is fixed in the airframe, it is the logical reference about which flight test data will be determined from flight test instruments. Since the pilot is also fixed in this reference system, many stability and control parameters concerned with handling qualities studies are given in this reference system.

(e) Wind Axes (x_w , y_w , z_w) are likewise a right-handed orthogonal triad whose origin is fixed at the airplane center of gravity. It has the additional requirements that the z_w axis lie in the plane of symmetry and x_w axis be coincident with the relative wind. The orientation of the wind axes relative to the body axes determines another coordinate system known as the stability axes.

(f) Stability Axes (x_s , y_s , z_s) are a right-hand orthogonal triad whose origin is fixed at the center of gravity of the airplane with the x_s and z_s axes in the plane of symmetry. The x stability axis, x_s , is the projection of the x wind axis, x_w , on the airplane plane of symmetry. Therefore, the x_s and z_s are angular-variant with respect to the fuselage reference line. The angle between the x stability axis, x_s , and the x body axis, x_b , is defined as the angle of attack, α . The angle between the x stability axis, x_s, and the x wind axis, x_w , is defined as the sideslip angle, β . The z stability axis, z_s , is coincident with the z wind axis, z_w, and the y stability axis, y_s , is coincident with the y body axis, y_b .

Euler Angles (ψ , θ , ϕ) are defined as the angles through which one axis system must be successively rotated (about its own axes) to superimpose it upon another, having an initial angular displacement from the first. Care must be exercised when using Eulerian Angles because the order of rotation must be maintained. The sequence of rotation can be arbitrary provided the same order of rotation is always maintained. The following convention is generally used:

1. A rotation of ψ about the z axis, which rotates both x and y axes.

2. A rotation of θ about the new position of the y axis, which rotates both the x and z axes.

3. A rotation of ϕ about the new position of the x axis.

Thus the airplane is yawed, pitched, and then rolled.

It is further possible to express the airplane angular velocity components (p, q, r) in terms of the Euler velocity components $(\dot{\psi}, \dot{\theta}, \dot{\phi})$ and the Euler angles (ψ, θ, ϕ) as follows:

$$p = \dot{\phi} - \dot{\psi} \sin\theta \tag{24}$$

$$q = \dot{\theta} \cos\phi + \dot{\psi} \cos\theta \sin\phi \tag{25}$$

$$r = \dot{\psi} \cos\theta \cos\phi - \dot{\theta} \sin\phi \tag{26}$$

It should be pointed out that, although the quantities, p, q and r are orthogonal, the quantities $\dot{\psi}$, $\dot{\theta}$ and $\dot{\phi}$ are not.

Coordinate transformations are frequently required between the various axis systems. The transformations are most conveniently expressed in terms of the direction cosine matrices.

TRANSFORMATION OF AXIS SYSTEMS

Transformation from Earth Axes to Body Axes

The transformation from earth to body axes is obtained by rotating the earth axes successively through the Euler angles ψ, θ and ϕ.

Symbolically, the transformation is:

$$\begin{bmatrix} x_b \\ y_b \\ z_b \end{bmatrix} = [\phi][\theta][\psi] \begin{bmatrix} x_e \\ y_e \\ z_e \end{bmatrix} \tag{27}$$

where

$$[\phi] = \begin{bmatrix} 1 & 0 & 0 \\ 0 & \cos\phi & \sin\phi \\ 0 & -\sin\phi & \cos\phi \end{bmatrix} \tag{28}$$

$$[\theta] = \begin{bmatrix} \cos\theta & 0 & -\sin\theta \\ 0 & 1 & 0 \\ \sin\theta & 0 & \cos\theta \end{bmatrix} \tag{29}$$

$$[\psi] = \begin{bmatrix} \cos\psi & \sin\psi & 0 \\ -\sin\psi & \cos\psi & 0 \\ 0 & 0 & 1 \end{bmatrix} \tag{30}$$

$$\begin{bmatrix} x_b \\ y_b \\ z_b \end{bmatrix} = \begin{bmatrix} \cos\theta\cos\psi & \cos\theta\sin\psi & -\sin\theta \\ \sin\phi\sin\theta\cos\psi - \sin\psi\cos\phi & \sin\psi\sin\theta\sin\phi + \cos\psi\cos\phi & \sin\phi\cos\theta \\ \cos\psi\cos\phi\sin\theta + \sin\psi\sin\phi & \sin\psi\cos\phi\sin\theta - \cos\psi\sin\phi & \cos\phi\cos\theta \end{bmatrix} \begin{bmatrix} x_e \\ y_e \\ z_e \end{bmatrix} \tag{31}$$

Transformation from Body Axes to Earth Axes

This transformation is simply the inverse of the transformation above. Since all that has taken place is a series of rotations between orthogonal axis systems, the transformation matrix is orthogonal and therefore the inverse of the matrix is equal to its transpose.

$$\begin{bmatrix} x_e \\ y_e \\ z_e \end{bmatrix} = \begin{bmatrix} \cos\theta\cos\psi & \sin\phi\sin\theta\cos\psi - \sin\psi\cos\phi & \cos\psi\cos\phi\sin\theta + \sin\psi\sin\phi \\ \cos\theta\sin\psi & \sin\psi\sin\theta\sin\phi + \cos\psi\cos\phi & \sin\psi\cos\phi\sin\theta - \cos\psi\sin\phi \\ -\sin\theta & \sin\phi\cos\theta & \cos\phi\cos\theta \end{bmatrix} \begin{bmatrix} x_b \\ y_b \\ z_b \end{bmatrix} \tag{32}$$

Transformation from Body Axes to Stability Axes

This transformation is defined as a rotation of the body axes through the angle $-\alpha$. The negative sign is dictated by convention. The angle is defined as the angle between the x body axis and the x stability axis and is positive when x_b is above x_s.

Where

$$[\alpha] = \begin{bmatrix} \cos\alpha & 0 & -\sin\alpha \\ 0 & 1 & 0 \\ \sin\alpha & 0 & \cos\alpha \end{bmatrix}$$

Therefore

$$[-\alpha] = \begin{bmatrix} \cos\alpha & 0 & \sin\alpha \\ 0 & 1 & 0 \\ -\sin\alpha & 0 & \cos\alpha \end{bmatrix} \tag{33}$$

Thus

$$\begin{bmatrix} x_s \\ y_s \\ z_s \end{bmatrix} = \begin{bmatrix} \cos\alpha & 0 & \sin\alpha \\ 0 & 1 & 0 \\ -\sin\alpha & 0 & \cos\alpha \end{bmatrix} \begin{bmatrix} x_b \\ y_b \\ z_b \end{bmatrix} \tag{34}$$

Transformation from Stability Axes to Wind Axes

This transformation is defined as a rotation of the stability axes through the angle α . This is once again just the transpose of the transformation matrix due to its orthogonality.

$$\begin{bmatrix} x_b \\ y_b \\ z_b \end{bmatrix} = \begin{bmatrix} \cos\alpha & 0 & -\sin\alpha \\ 0 & 1 & 0 \\ \sin\alpha & 0 & \cos\alpha \end{bmatrix} \begin{bmatrix} x_s \\ y_s \\ z_s \end{bmatrix} \tag{35}$$

Transformation from Stability Axes to Body Axes

This transformation is defined as a rotation of the stability axes through the angle $-\beta$.

Where

$$[\beta] = \begin{bmatrix} \cos\beta & -\sin\beta & 0 \\ \sin\beta & \cos\beta & 0 \\ 0 & 0 & 1 \end{bmatrix}$$

and

$$[-\beta] = \begin{bmatrix} \cos\beta & \sin\beta & 0 \\ -\sin\beta & \cos\beta & 0 \\ 0 & 0 & 1 \end{bmatrix} \tag{36}$$

$$\begin{bmatrix} x_w \\ y_w \\ z_w \end{bmatrix} = \begin{bmatrix} \cos\beta & \sin\beta & 0 \\ -\sin\beta & \cos\beta & 0 \\ 0 & 0 & 1 \end{bmatrix} \begin{bmatrix} x_s \\ y_s \\ z_s \end{bmatrix} \tag{37}$$

Transformation from Wind Axes to Stability Axes

This transformation is defined as a rotation of the wind axes through the angle β .

$$\begin{bmatrix} x_s \\ y_s \\ z_s \end{bmatrix} = \begin{bmatrix} \cos\beta & -\sin\beta & 0 \\ \sin\beta & \cos\beta & 0 \\ 0 & 0 & 1 \end{bmatrix} \begin{bmatrix} x_w \\ y_w \\ z_w \end{bmatrix} \tag{38}$$

Transformation from Body Axes to Wind Axes

This transformation is defined as a rotation of the body axes through the angle $-\alpha$ followed by a rotation through the angle $-\beta$.

$$\begin{bmatrix} x_w \\ y_w \\ z_w \end{bmatrix} = \begin{bmatrix} \cos\beta & \sin\beta & 0 \\ -\sin\beta & \cos\beta & 0 \\ 0 & 0 & 1 \end{bmatrix} \begin{bmatrix} \cos\alpha & 0 & \sin\alpha \\ 0 & 1 & 0 \\ -\sin\alpha & 0 & \cos\alpha \end{bmatrix} \begin{bmatrix} x_b \\ y_b \\ z_b \end{bmatrix} \tag{39}$$

$$\begin{bmatrix} x_w \\ y_w \\ z_w \end{bmatrix} = \begin{bmatrix} \cos\alpha\cos\beta & \sin\beta & \sin\alpha\cos\beta \\ -\cos\alpha\sin\beta & \cos\beta & -\sin\alpha\sin\beta \\ -\sin\alpha & 0 & \cos\alpha \end{bmatrix} \begin{bmatrix} x_b \\ y_b \\ z_b \end{bmatrix} \tag{40}$$

Transformation from Wind Axes to Body Axes

This transformation is defined as a rotation of the wind axes through the the angle β to the stability axis system followed by a rotation of the stability axis system through the angle α .

$$\begin{bmatrix} x_b \\ y_b \\ z_b \end{bmatrix} = \begin{bmatrix} \cos\alpha & 0 & -\sin\alpha \\ 0 & 1 & 0 \\ \sin\alpha & 0 & \cos\alpha \end{bmatrix} \begin{bmatrix} \cos\beta & -\sin\beta & 0 \\ \sin\beta & \cos\beta & 0 \\ 0 & 0 & 1 \end{bmatrix} \begin{bmatrix} x_w \\ y_w \\ z_w \end{bmatrix} \tag{41}$$

$$\begin{bmatrix} x_b \\ y_b \\ z_b \end{bmatrix} = \begin{bmatrix} \cos\alpha\cos\beta & -\cos\alpha\sin\beta & -\sin\alpha \\ \sin\beta & \cos\beta & 0 \\ \sin\alpha\cos\beta & -\sin\alpha\sin\beta & \cos\alpha \end{bmatrix} \begin{bmatrix} x_w \\ y_w \\ z_w \end{bmatrix} \tag{42}$$

Transformation of Coordinate Axes

Earth Axes to Body Axes

$$\begin{aligned} x_b &= x_e\cos\theta\cos\psi + y_e\cos\theta\sin\psi - z_e\sin\theta \\ y_b &= x_e(\sin\phi\sin\theta\cos\psi - \sin\psi\cos\phi) + y_e(\sin\psi\sin\theta\sin\phi \\ &\quad + \cos\psi\cos\phi) + z_e\sin\phi\cos\theta \\ z_b &= x_e(\cos\psi\cos\phi\sin\theta + \sin\psi\sin\phi) + y_e(\sin\psi\cos\phi\sin\theta \\ &\quad - \cos\psi\sin\phi) + z_e\cos\phi\cos\theta \end{aligned} \tag{43}$$

Body Axes to Earth Axes

$$\begin{aligned} x_e &= x_b\cos\theta\cos\psi + y_b(\sin\phi\sin\theta\cos\psi - \sin\psi\cos\phi) \\ &\quad + z_b(\cos\psi\cos\phi\sin\theta + \sin\psi\sin\phi) \\ y_e &= x_b\cos\theta\sin\psi + y_b(\sin\psi\sin\theta\sin\phi + \cos\psi\cos\phi) \\ &\quad + z_b(\sin\psi\cos\phi\sin\theta - \cos\psi\sin\phi) \\ z_e &= -x_b\sin\theta + y_b\sin\phi\cos\theta + z_b\cos\phi\cos\theta \end{aligned} \tag{44}$$

Body Axes to Stability Axes

$$\begin{aligned} x_s &= x_b\cos\alpha + z_b\sin\alpha \\ y_s &= y_b \\ z_s &= -x_b\sin\alpha + z_b\cos\alpha \end{aligned} \tag{45}$$

Stability Axes to Body Axes

$$\begin{aligned} x_b &= x_s \cos\alpha - z_s \sin\alpha \\ y_b &= y_s \\ z_b &= x_s \sin\alpha + z_s \cos\alpha \end{aligned} \tag{46}$$

Stability Axes to Wind Axes

$$\begin{aligned} x_w &= x_s \cos\beta + y_s \sin\beta \\ y_w &= -x_s \sin\beta + y_s \cos\beta \\ z_w &= z_s \end{aligned} \tag{47}$$

Wind Axes to Stability Axes

$$\begin{aligned} x_s &= x_w \cos\beta - y_w \sin\beta \\ y_s &= x_w \sin\beta + y_w \cos\beta \\ z_s &= z_w \end{aligned} \tag{48}$$

Body Axes to Wind Axes

$$\begin{aligned} x_w &= x_b \cos\alpha \cos\beta + y_b \sin\beta + z_b \sin\alpha \cos\beta \\ y_w &= -x_b \cos\alpha \sin\beta + y_b \cos\beta - z_b \sin\alpha \sin\beta \\ z_w &= -x_b \sin\alpha + z_b \cos\alpha \end{aligned} \tag{49}$$

Wind Axes to Body Axes

$$\begin{aligned} x_b &= x_w \cos\alpha \cos\beta - y_w \cos\alpha \sin\beta - z_w \sin\alpha \\ y_b &= x_w \sin\beta + y_w \cos\beta \\ z_b &= x_w \sin\alpha \cos\beta - y_w \sin\alpha \sin\beta + z_w \cos\alpha \end{aligned} \tag{50}$$

TRANSFORMATIONS OF AERODYNAMIC COEFFICIENTS

Aerodynamic forces, in the Eulerian axis system, are designated by the letters X, Y, and Z corresponding to the individual axis along which they act. Moments about the x, y and z Eulerian axes are designated as L, M and N, respectively. Two additional quantities, Lift, $\mathcal{L}$, and Drag, D, are defined. Lift is the force acting perpendicular to the relative wind and drag is the force acting parallel to the relative wind. Each of these forces can be expressed:

$$X = \tfrac{1}{2}\rho V^2 S C_x$$

$$Y = \tfrac{1}{2}\rho V^2 S C_Y$$

$$Z = \tfrac{1}{2}\rho V^2 S C_z$$

$$\mathcal{L} = \tfrac{1}{2}\rho V^2 S C_{\mathcal{L}}$$

$$D = \tfrac{1}{2}\rho V^2 S C_D$$

$$L = \tfrac{1}{2}\rho V^2 S b C_\ell$$

$$M = \tfrac{1}{2}\rho V^2 S \bar{c} C_m$$

$$N = \tfrac{1}{2}\rho V^2 S b C_n$$

where ρ = density

V = velocity

S = wing area

b = wing span

$\bar{c}$ = mean aerodynamic chord

C_i = dimensionless aerodynamic coefficient ($i = x, y, z$ etc.)

Since principal, body and stability axis systems are Eulerian axis systems, the above forces may be originally expressed in either of these axis systems. They transform from one axis system to another according to the equations shown in the section on transformation of axes. Accordingly, the aerodynamic coefficients can be transformed according to the following transformations.

As a result of the definitions of lift, drag and the Eulerian axis systems, it follows that:

$$(C_x)_s = -C_D \qquad (C_x)_b = -C_c$$

$$(C_Y)_s = (C_Y)_a = (C_Y)_b$$

$$(C_z)_s = -C_L \qquad (C_z)_b = -C_N$$

therefore

$$\begin{aligned} C_c &= C_D \cos\alpha - C_L \sin\alpha \\ C_N &= C_D \sin\alpha + C_L \cos\alpha \end{aligned} \tag{51}$$

and

$$\begin{aligned} C_D &= C_c \cos\alpha + C_N \sin\alpha \\ C_L &= -C_c \sin\alpha + C_N \cos\alpha \end{aligned} \tag{52}$$

If we define the positive directions for the moment equations about the Eulerian axis according to the right-hand rule:

$$\begin{aligned} L_b &= L_s \cos\alpha - N_s \sin\alpha \\ M_b &= M_s \\ N_b &= L_s \sin\alpha + N_s \cos\alpha \end{aligned} \tag{53}$$

To transform aerodynamic coefficients from body axes to stability axes.

$$\begin{aligned} C_D &= C_c \cos\alpha + C_N \sin\alpha \\ C_L &= -C_c \sin\alpha + C_N \cos\alpha \\ (C_Y)_s &= (C_Y)_b \\ (C_\ell)_s &= (C_\ell)_b \cos\alpha + (C_n)_b \sin\alpha \\ (C_m)_s &= (C_m)_b \\ (C_n)_s &= -(C_\ell)_b \sin\alpha + (C_n)_b \cos\alpha \end{aligned} \tag{54}$$

To transform aerodynamic coefficients from stability axes to body axes.

$$
\begin{aligned}
C_c &= C_D \cos\alpha - C_L \sin\alpha \\
(C_Y)_b &= (C_Y)_s \\
C_N &= C_D \sin\alpha + C_L \cos\alpha \\
(C_\ell)_b &= (C_\ell)_s \cos\alpha - (C_n)_s \sin\alpha \\
(C_m)_b &= (C_m)_s \\
(C_n)_b &= (C_\ell)_s \sin\alpha + (C_n)_s \cos\alpha
\end{aligned}
\tag{55}
$$

To transform the aerodynamic coefficients from body axes to wind axes.

$$
\begin{aligned}
(C_x)_w &= -C_c \cos\alpha \cos\beta + (C_Y)_b \sin\beta - C_N \sin\alpha \cos\beta \\
(C_Y)_w &= C_c \cos\alpha \sin\beta + (C_Y)_b \cos\beta + C_N \sin\alpha \sin\beta \\
(C_z)_w &= C_c \sin\alpha - C_N \cos\alpha = -C_L \\
(C_\ell)_w &= (C_\ell)_b \cos\alpha \cos\beta + (C_m)_b \sin\beta + (C_n)_b \sin\alpha \cos\beta \\
(C_m)_w &= -(C_\ell)_b \cos\alpha \sin\beta + (C_m)_b \cos\beta - (C_n)_b \sin\alpha \sin\beta \\
(C_n)_w &= -(C_\ell)_b \sin\alpha + (C_n)_b \cos\alpha
\end{aligned}
\tag{56}
$$

To transform the aerodynamic coefficients from wind axes to body axes.

$$
\begin{aligned}
C_c &= -(C_x)_w \cos\alpha \cos\beta - (C_Y)_w \cos\alpha \sin\beta + (C_z)_w \sin\alpha \\
(C_Y)_b &= (C_x)_w \sin\beta + (C_Y)_w \cos\beta \\
-C_N &= -(C_x)_w \sin\alpha \cos\beta - (C_Y)_w \sin\alpha \sin\beta + (C_z)_w \cos\alpha \\
(C_\ell)_b &= (C_\ell)_w \cos\alpha \cos\beta - (C_m)_w \cos\alpha \sin\beta + (C_n)_w \sin\alpha \\
(C_m)_b &= (C_m)_w \sin\beta + (C_m)_w \cos\beta \\
(C_n)_b &= (C_\ell)_w \sin\alpha \cos\beta - (C_m)_w \sin\alpha \sin\beta + (C_n)_w \cos\alpha
\end{aligned}
\tag{57}
$$

To transform the aerodynamic coefficients from stability axes to wind axes.

$$
\begin{aligned}
(C_x)_w &= -C_D \cos\beta + (C_Y)_s \sin\beta \\
(C_Y)_w &= C_D \sin\beta + (C_Y)_s \cos\beta \\
(C_z)_w &= -C_L \\
(C_\ell)_w &= (C_\ell)_s \cos\beta + (C_m)_s \sin\beta \\
(C_m)_w &= -(C_\ell)_s \sin\beta + (C_m)_s \cos\beta \\
(C_n)_w &= (C_n)_s
\end{aligned}
\tag{58}
$$

To transform the aerodynamic coefficients from wind axes to stability axes.

$$
\begin{aligned}
C_D &= -(C_x)_w \cos\beta + (C_Y)_w \sin\beta \\
(C_Y)_s &= (C_x)_w \sin\beta + (C_Y)_w \cos\beta \\
C_L &= -(C_z)_w \\
(C_\ell)_s &= (C_\ell)_w \cos\beta - (C_m)_w \sin\beta \\
(C_m)_s &= (C_\ell)_w \sin\beta + (C_m)_w \cos\beta \\
(C_n)_s &= (C_n)_w
\end{aligned}
\tag{59}
$$

Body Axes to Stability Axes

$$
\begin{aligned}
C_D &= -(C_x)_b \cos\alpha - (C_z)_b \sin\alpha \\
C_L &= (C_x)_b \sin\alpha - (C_z)_b \cos\alpha \\
(C_Y)_s &= (C_Y)_b \\
(C_\ell)_s &= (C_\ell)_b \cos\alpha + (C_n)_b \sin\alpha \\
(C_m)_s &= (C_m)_b \\
(C_n)_s &= -(C_\ell)_b \sin\alpha + (C_n)_b \cos\alpha
\end{aligned}
\tag{60}
$$

Stability Axes to Body Axes

$$
\begin{aligned}
(C_x)_b &= -C_D \cos\alpha + C_L \sin\alpha \\
(C_Y)_b &= (C_Y)_s \\
(C_z)_b &= -C_D \sin\alpha - C_L \cos\alpha \\
(C_\ell)_b &= (C_\ell)_s \cos\alpha - (C_n)_s \sin\alpha \\
(C_m)_b &= (C_m)_s \\
(C_n)_b &= (C_\ell)_s \sin\alpha + (C_n)_s \cos\alpha
\end{aligned}
\tag{61}
$$

Body Axes to Wind Axes

$$
\begin{aligned}
(C_x)_w &= (C_x)_b \cos\alpha\cos\beta + (C_Y)_b \sin\beta + (C_z)_b \sin\alpha\cos\beta \\
(C_Y)_w &= -(C_x)_b \cos\alpha\sin\beta + (C_Y)_b \cos\beta - (C_z)_b \sin\alpha\sin\beta \\
(C_z)_w &= -(C_x)_b \sin\alpha + (C_z)_b \cos\alpha = -C_L \\
(C_\ell)_w &= (C_\ell)_b \cos\alpha\cos\beta + (C_m)_b \sin\beta + (C_n)_b \sin\alpha\cos\beta \\
(C_m)_w &= -(C_\ell)_b \cos\alpha\sin\beta + (C_m)_b \cos\beta - (C_m)_b \sin\alpha\sin\beta \\
(C_n)_w &= -(C_\ell)_b \sin\alpha + (C_n)_b \cos\alpha
\end{aligned}
\tag{62}
$$

Wind Axes to Body Axes

$$
\begin{aligned}
(C_x)_b &= (C_x)_w \cos\alpha\cos\beta - (C_Y)_w \cos\alpha\sin\beta + (C_z)_w \sin\alpha \\
(C_Y)_b &= (C_x)_w \sin\beta + (C_Y)_w \cos\beta \\
(C_z)_b &= (C_x)_w \sin\alpha\cos\beta - (C_Y)_w \sin\alpha\sin\beta + (C_z)_w \cos\alpha \\
(C_\ell)_b &= (C_\ell)_w \cos\alpha\cos\beta - (C_m)_w \cos\alpha\sin\beta + (C_n)_w \sin\alpha \\
(C_m)_b &= (C_\ell)_w \sin\beta + (C_m)_w \cos\beta \\
(C_n)_b &= (C_\ell)_w \sin\alpha\cos\beta - (C_m)_w \sin\alpha\sin\beta + (C_n)_w \cos\alpha
\end{aligned}
\tag{63}
$$

Stability Axes to Wind Axes

$$
\begin{aligned}
(C_x)_w &= -C_D \cos\beta + (C_Y)_s \sin\beta \\
(C_Y)_w &= C_D \sin\beta + (C_Y)_s \cos\beta \\
(C_z)_w &= -C_L \\
(C_\ell)_w &= (C_\ell)_s \cos\beta + (C_m)_s \sin\beta \\
(C_m)_w &= -(C_\ell)_s \sin\beta + (C_m)_s \cos\beta \\
(C_n)_w &= (C_n)_s
\end{aligned}
\tag{64}
$$

Wind Axes to Stability Axes

$$
\begin{aligned}
C_D &= -(C_x)_w \cos\beta + (C_Y)_w \sin\beta \\
C_L &= -(C_z)_w \\
(C_Y)_s &= (C_x)_w \sin\beta + (C_Y)_w \cos\beta \\
(C_\ell)_s &= (C_\ell)_w \cos\beta - (C_m)_w \sin\beta \\
(C_m)_s &= (C_\ell)_w \sin\beta + (C_m)_w \cos\beta \\
(C_n)_s &= (C_n)_w
\end{aligned}
\tag{65}
$$

TRANSFORMATIONS OF STABILITY DERIVATIVES

Transformation of the longitudinal derivatives can be accomplished by direct differentiation of the coefficient equations, however, the lateral-directional derivatives cannot be transformed in this manner.

Transformation of the longitudinal stability derivatives from the body axis system to the stability axis system.

$$
\begin{aligned}
(C_{D_\alpha})_s = \frac{\partial C_D}{\partial \alpha} &= -\left(\frac{\partial C_x}{\partial \alpha}\right)_b \cos\alpha + (C_x)_b \sin\alpha - \left(\frac{\partial C_z}{\partial \alpha}\right)_b \sin\alpha - (C_z)_b \cos\alpha \\
&= -\left(\frac{\partial C_x}{\partial \alpha}\right)_b \cos\alpha - \left(\frac{\partial C_z}{\partial \alpha}\right)_b \sin\alpha + C_L \\
(C_{L_\alpha})_s = \frac{\partial C_L}{\partial \alpha} &= \left(\frac{\partial C_x}{\partial \alpha}\right)_b \sin\alpha + (C_x)_b \cos\alpha - \left(\frac{\partial C_z}{\partial \alpha}\right)_b \cos\alpha + (C_z)_b \sin\alpha \\
&= \left(\frac{\partial C_x}{\partial \alpha}\right)_b \sin\alpha - \left(\frac{\partial C_z}{\partial \alpha}\right)_b \cos\alpha - C_D \\
(C_{m_\alpha})_s = \left(\frac{\partial C_m}{\partial \alpha}\right)_s &= \left(\frac{\partial C_m}{\partial \alpha}\right)_b = (C_{m_\alpha})_b
\end{aligned}
\tag{66}
$$

The following relationships are required to transform the lateral-directional stability derivatives from the body axis system to the stability axis system.

$$(C_\ell)_b = \left(\frac{\partial C_\ell}{\partial \beta}\right)_b \beta_b + \left(\frac{\partial C_\ell}{\partial \dot{\beta}}\right)_b \dot{\beta}_b + \left(\frac{\partial C_\ell}{\partial p}\right)_b p_b + \left(\frac{\partial C_\ell}{\partial r}\right)_b r_b + \left(\frac{\partial C_\ell}{\partial \delta}\right)_b \delta_b$$

$$(C_n)_b = \left(\frac{\partial C_n}{\partial \beta}\right)_b \beta_b + \left(\frac{\partial C_n}{\partial \dot{\beta}}\right)_b \dot{\beta}_b + \left(\frac{\partial C_n}{\partial p}\right)_b p_b + \left(\frac{\partial C_n}{\partial r}\right)_b r_b + \left(\frac{\partial C_n}{\partial \delta}\right)_b \delta_b \qquad (67)$$

$$(C_Y)_b = \left(\frac{\partial C_Y}{\partial \beta}\right)_b \beta_b + \left(\frac{\partial C_Y}{\partial \dot{\beta}}\right)_b \dot{\beta}_b + \left(\frac{\partial C_Y}{\partial p}\right)_b p_b + \left(\frac{\partial C_Y}{\partial r}\right)_b r_b + \left(\frac{\partial C_Y}{\partial \delta}\right)_b \delta_b$$

The following relationships are used in the transformation from body axes to stability axis.

$$\begin{aligned}
(C_\ell)_s &= (C_\ell)_b \cos\alpha + (C_n)_b \sin\alpha \\
(C_n)_s &= -(C_\ell)_b \sin\alpha + (C_n)_b \cos\alpha \\
(C_Y)_s &= (C_Y)_b \\
\beta_b &= \beta_s \\
\dot{\beta}_b &= \dot{\beta}_s \\
p_b &= p_s \cos\alpha - r_s \sin\alpha \\
r_b &= p_s \sin\alpha + r_s \cos\alpha \\
\delta_b &= \delta_s
\end{aligned} \qquad (68)$$

using the following relationships.

$$\begin{aligned}
(C_{\ell_\beta})_s = {} & \left[\left(\frac{\partial C_\ell}{\partial \beta}\right)_b \cos\alpha + \left(\frac{\partial C_n}{\partial \beta}\right)_b \sin\alpha\right] \beta_s + \left[\left(\frac{\partial C_\ell}{\partial \dot{\beta}}\right)_b \cos\alpha + \left(\frac{\partial C_n}{\partial \dot{\beta}}\right)_b \sin\alpha\right] \dot{\beta}_s \\
& + \left[\left(\frac{\partial C_\ell}{\partial p}\right)_b \cos^2\alpha + \left(\frac{\partial C_\ell}{\partial r} + \frac{\partial C_n}{\partial p}\right)_b \sin\alpha\cos\alpha + \left(\frac{\partial C_n}{\partial r}\right)_b \sin^2\alpha\right] p_s \\
& + \left[\left(\frac{\partial C_\ell}{\partial r}\right)_b \cos^2\alpha + \left(\frac{\partial C_n}{\partial r} - \frac{\partial C_\ell}{\partial p}\right)_b \sin\alpha\cos\alpha - \left(\frac{\partial C_n}{\partial p}\right)_b \sin^2\alpha\right] r_s \\
& + \left[\left(\frac{\partial C_\ell}{\partial \delta}\right)_b \cos\alpha + \left(\frac{\partial C_n}{\partial \delta}\right)_b \sin\alpha\right] \delta_s
\end{aligned} \qquad (69)$$

$$(C_n)_s = \left[\left(\frac{\partial C_n}{\partial \beta}\right)_b \cos\alpha - \left(\frac{\partial C_\ell}{\partial \beta}\right)_b \sin\alpha\right] \beta_s + \left[\left(\frac{\partial C_n}{\partial \dot{\beta}}\right)_b \cos\alpha - \left(\frac{\partial C_\ell}{\partial \dot{\beta}}\right)_b \sin\alpha\right] \dot{\beta}_s$$

$$+ \left[\left(\frac{\partial C_n}{\partial p}\right)_b \cos^2\alpha + \left(\frac{\partial C_n}{\partial r} - \frac{\partial C_\ell}{\partial p}\right)_b \sin\alpha\cos\alpha - \left(\frac{\partial C_\ell}{\partial r}\right)_b \sin^2\alpha\right] p_s$$

$$+ \left[\left(\frac{\partial C_n}{\partial r}\right)_b \cos^2\alpha - \left(\frac{\partial C_n}{\partial p} + \frac{\partial C_\ell}{\partial r}\right)_b \sin\alpha\cos\alpha + \left(\frac{\partial C_\ell}{\partial p}\right)_b \sin^2\alpha\right] r_s$$

$$+ \left[\left(\frac{\partial C_n}{\partial \delta}\right)_b \cos\alpha - \left(\frac{\partial C_\ell}{\partial \delta}\right)_b \sin\alpha\right] \delta_s \qquad (70)$$

$$(C_Y)_s = \left(\frac{\partial C_Y}{\partial \beta}\right)_b \beta_s + \left(\frac{\partial C_Y}{\partial \dot{\beta}}\right)_b \dot{\beta}_s + \left[\left(\frac{\partial C_Y}{\partial p}\right)_b \cos\alpha + \left(\frac{\partial C_Y}{\partial r}\right)_b \sin\alpha\right] p_s$$

$$+ \left[\left(\frac{\partial C_Y}{\partial r}\right)_b \cos\alpha - \left(\frac{\partial C_Y}{\partial p}\right)_b \sin\alpha\right] r_s + \left(\frac{\partial C_Y}{\partial \delta}\right)_b \delta_s \qquad (71)$$

Transformation of longitudinal stability derivatives from stability axes to body axes.

$$(C_{x_\alpha})_b = \left(\frac{\partial C_x}{\partial \alpha}\right)_b = -\left(\frac{\partial C_D}{\partial \alpha}\right)_s \cos\alpha + C_D \sin\alpha + \left(\frac{\partial C_L}{\partial \alpha}\right)_s \sin\alpha + C_L \cos\alpha$$

$$= -\left(\frac{\partial C_D}{\partial \alpha}\right)_s \cos\alpha + \left(\frac{\partial C_L}{\partial \alpha}\right)_s \sin\alpha - (C_z)_b$$

$$(C_{z_\alpha})_b = \left(\frac{\partial C_z}{\partial \alpha}\right)_b = -\left(\frac{\partial C_D}{\partial \alpha}\right)_s \sin\alpha - C_D \cos\alpha - \left(\frac{\partial C_L}{\partial \alpha}\right)_s \cos\alpha + C_L \sin\alpha \qquad (72)$$

$$= -\left(\frac{\partial C_D}{\partial \alpha}\right)_s \sin\alpha - \left(\frac{\partial C_L}{\partial \alpha}\right)_s \cos\alpha + (C_x)_b$$

$$(C_{m_\alpha})_b = \left(\frac{\partial C_m}{\partial \alpha}\right)_b = \left(\frac{\partial C_m}{\partial \alpha}\right)_s = (C_{m_\alpha})_s$$

The following relationships are used in the transformation of the lateral-directional stability derivatives from stability axes to body axes.

$$
\begin{aligned}
(C_\ell)_b &= (C_\ell)_s \cos\alpha - (C_n)_s \sin\alpha \\
(C_n)_b &= (C_\ell)_s \sin\alpha + (C_n) \cos\alpha \\
(C_Y)_b &= (C_Y)_s \\
\beta_s &= \beta_b \\
\dot{\beta}_s &= \dot{\beta}_b \\
p_s &= p_b \cos\alpha + r_b \sin\alpha \\
r_s &= -p_b \sin\alpha + r_b \cos\alpha \\
\delta_s &= \delta_b
\end{aligned}
\tag{73}
$$

Thus

$$
\begin{aligned}
(C_\ell)_b = {} & \left[\left(\frac{\partial C_\ell}{\partial \beta}\right)_s \cos\alpha - \left(\frac{\partial C_n}{\partial \beta}\right)_s \sin\alpha\right] \beta_s + \left[\left(\frac{\partial C_\ell}{\partial \dot{\beta}}\right)_s \cos\alpha - \left(\frac{\partial C_n}{\partial \dot{\beta}}\right)_s \sin\alpha\right] \dot{\beta}_s \\
& + \left[\left(\frac{\partial C_\ell}{\partial p}\right)_s \cos^2\alpha - \left(\frac{\partial C_\ell}{\partial r} + \frac{\partial C_n}{\partial p}\right)_s \cos\alpha \sin\alpha + \left(\frac{\partial C_n}{\partial r}\right)_s \sin^2\alpha\right] p_b \\
& + \left[\left(\frac{\partial C_\ell}{\partial r}\right)_s \cos^2\alpha + \left(\frac{\partial C_\ell}{\partial p} - \frac{\partial C_n}{\partial r}\right)_s \sin\alpha \cos\alpha - \left(\frac{\partial C_n}{\partial p}\right)_s \sin^2\alpha\right] r_b \\
& + \left[\left(\frac{\partial C_\ell}{\partial \delta}\right)_s \cos\alpha - \left(\frac{\partial C_n}{\partial \delta}\right)_s \sin\alpha\right] \delta_s
\end{aligned}
\tag{74}
$$

$$
\begin{aligned}
(C_n)_b = {} & \left[\left(\frac{\partial C_\ell}{\partial \beta}\right)_s \sin\alpha + \left(\frac{\partial C_n}{\partial \beta}\right)_s \cos\alpha\right] \beta_b + \left[\left(\frac{\partial C_\ell}{\partial \dot{\beta}}\right)_s \sin\alpha + \left(\frac{\partial C_n}{\partial \dot{\beta}}\right)_s \cos\alpha\right] \dot{\beta} \\
& + \left[\left(\frac{\partial C_n}{\partial p}\right)_s \cos^2\alpha + \left(\frac{\partial C_\ell}{\partial p} - \frac{\partial C_n}{\partial r}\right)_s \sin\alpha \cos\alpha - \left(\frac{\partial C_\ell}{\partial r}\right)_s \sin^2\alpha\right] p_b \\
& + \left[\left(\frac{\partial C_n}{\partial r}\right)_s \cos^2\alpha + \left(\frac{\partial C_\ell}{\partial r} + \frac{\partial C_n}{\partial p}\right)_s \sin\alpha \cos\alpha + \left(\frac{\partial C_\ell}{\partial p}\right)_s \sin^2\alpha\right] r_b \\
& + \left[\left(\frac{\partial C_\ell}{\partial \delta}\right)_s \sin\alpha + \left(\frac{\partial C_n}{\partial \delta}\right)_s \cos\alpha\right] \delta_b
\end{aligned}
\tag{75}
$$

$$(C_Y)_b = \left(\frac{\partial C_Y}{\partial \beta}\right)_b \beta_b + \left(\frac{\partial C_Y}{\partial \dot{\beta}}\right)_b \dot{\beta}_b + \left[\left(\frac{\partial C_Y}{\partial p}\right)_s \cos\alpha - \left(\frac{\partial C_Y}{\partial r}\right)_s \sin\alpha\right] p_b$$
$$+ \left[\left(\frac{\partial C_Y}{\partial p}\right)_s \sin\alpha + \left(\frac{\partial C_Y}{\partial r}\right)_s \cos\alpha\right] r_b + \left(\frac{\partial C_Y}{\partial \delta}\right)_s \delta_b \qquad (76)$$

Body Axes to Stability Axes

$$\begin{aligned}
(C_{D_\alpha})_s &= (C_{X_\alpha})_b \cos\alpha - (C_{Z_\alpha})_b \sin\alpha + C_L \\
(C_{L_\alpha})_s &= (C_{X_\alpha})_b \sin\alpha - (C_{Z_\alpha})_b \cos\alpha - C_D \\
(C_{m_\alpha})_s &= (C_{m_\alpha})_b \\
(C_{\ell_\beta})_s &= (C_{\ell_\beta})_b \cos\alpha + (C_{n_\beta})_b \sin\alpha \\
(C_{\ell_{\dot\beta}})_s &= (C_{\ell_{\dot\beta}})_b \cos\alpha + (C_{n_{\dot\beta}})_b \sin\alpha \\
(C_{\ell_p})_s &= (C_{\ell_p})_b \cos^2\alpha + (C_{\ell_r} + C_{n_p})_b \sin\alpha\cos\alpha + (C_{n_r})_b \sin^2\alpha \\
(C_{\ell_r})_s &= (C_{\ell_r})_b \cos^2\alpha + (C_{n_r} - C_{\ell_p})_b \sin\alpha\cos\alpha - (C_{n_p})_b \sin^2\alpha \\
(C_{\ell_\delta})_s &= (C_{\ell_\delta})_b \cos\alpha + (C_{n_\delta})_b \sin\alpha \\
(C_{n_\beta})_s &= (C_{n_\beta})_b \cos\alpha - (C_{\ell_\beta})_b \sin\alpha \\
(C_{n_{\dot\beta}})_s &= (C_{n_{\dot\beta}})_b \cos\alpha - (C_{\ell_{\dot\beta}})_b \sin\alpha \\
(C_{n_p})_s &= (C_{n_p})_b \cos^2\alpha + (C_{n_r} - C_{\ell_p})_b \sin\alpha\cos\alpha - (C_{\ell_r})_b \sin^2\alpha \\
(C_{n_r})_s &= (C_{n_r})_b \cos^2\alpha - (C_{n_p} + C_{\ell_r})_b \sin\alpha\cos\alpha + (C_{\ell_p})_b \sin^2\alpha \\
(C_{n_\delta})_s &= (C_{n_\delta})_b \cos\alpha - (C_{\ell_\delta})_b \sin\alpha \\
(C_{Y_\beta})_s &= (C_{Y_\beta})_b \\
(C_{Y_{\dot\beta}})_s &= (C_{Y_{\dot\beta}})_b \\
(C_{Y_p})_s &= (C_{Y_p})_b \cos\alpha + (C_{Y_r})_b \sin\alpha \\
(C_{Y_r})_s &= (C_{Y_r})_b \cos\alpha - (C_{Y_p})_b \sin\alpha \\
(C_{Y_\delta})_s &= (C_{Y_\delta})_b
\end{aligned} \qquad (77)$$

Stability Axes to Body Axes

$$
\begin{aligned}
(C_{x_\alpha})_b &= -(C_{D_\alpha})_s \cos\alpha + (C_{L_\alpha})_s \sin\alpha - (C_z) \\
(C_{z_\alpha})_b &= -(C_{D_\alpha})_s \sin\alpha - (C_{L_\alpha})_s \cos\alpha + (C_x) \\
(C_{m_\alpha})_b &= (C_{m_\alpha})_s \\
(C_{\ell_\beta})_b &= (C_{\ell_\beta})_s \cos\alpha - (C_{n_\beta})_s \sin\alpha \\
(C_{\ell_{\dot\beta}})_b &= (C_{\ell_{\dot\beta}})_s \cos\alpha - (C_{n_{\dot\beta}})_s \sin\alpha \\
(C_{\ell_p})_b &= (C_{\ell_p})_s \cos^2\alpha - (C_{\ell_r} + C_{n_p})_s \cos\alpha \sin\alpha + (C_{n_r})_s \sin^2\alpha \\
(C_{\ell_r})_b &= (C_{\ell_r})_s \cos^2\alpha + (C_{\ell_p} - C_{n_r})_s \sin\alpha \cos\alpha - (C_{n_p})_s \sin^2\alpha \\
(C_{\ell_\zeta})_b &= (C_{\ell_\zeta})_s \cos\alpha - (C_{n_\zeta})_s \sin\alpha \\
(C_{n_\beta})_b &= (C_{\ell_\beta})_s \sin\alpha + (C_{n_\beta})_s \cos\alpha \\
(C_{n_{\dot\beta}})_b &= (C_{\ell_{\dot\beta}})_s \sin\alpha + (C_{n_{\dot\beta}})_s \cos\alpha \\
(C_{n_p})_b &= (C_{n_p})_s \cos^2\alpha + (C_{\ell_p} - C_{n_r})_s \sin\alpha \cos\alpha - (C_{\ell_r})_s \sin^2\alpha \\
(C_{n_r})_b &= (C_{n_r})_s \cos^2\alpha + (C_{\ell_r} + C_{n_p})_s \sin\alpha \cos\alpha + (C_{\ell_p})_s \sin^2\alpha \\
(C_{\ell_\zeta})_b &= (C_{\ell_\zeta})_s \sin\alpha + (C_{n_\zeta})_s \cos\alpha \\
(C_{Y_\beta})_b &= (C_{Y_\beta})_s \\
(C_{Y_{\dot\beta}})_b &= (C_{Y_{\dot\beta}})_s \\
(C_{Y_p})_b &= (C_{Y_p})_s \cos\alpha - (C_{Y_r})_s \sin\alpha \\
(C_{Y_r})_b &= (C_{Y_r})_s \sin\alpha + (C_{Y_p})_s \cos\alpha \\
(C_{Y_\beta})_b &= (C_{Y_\zeta})_s
\end{aligned}
\tag{78}
$$

TRANSFORMATIONS OF MOMENTS OF INERTIA

The following definitions apply.

$$I_x = \int (Y^2 + Z^2)\, dm \qquad I_z = \int (X^2 + Y^2)\, dm$$

$$I_y = \int (X^2 + Z^2)\, dm \qquad I_{xz} = \int (X Z)\, dm$$

To transform from body axes to stability axes, the following equations apply:

$$
\begin{aligned}
X_s &= X_b \cos\alpha + Z_b \sin\alpha \\
Y_s &= Y_b \\
Z_s &= -X_b \sin\alpha + Z_b \cos\alpha
\end{aligned}
\tag{79}
$$

$$I_{x_s} = \int (Y_s^2 + Z_s^2)\,dm = \int \left[(Y_b)^2 + (-X_b \sin\alpha + Z_b \cos\alpha)^2 \right] dm$$

$$= \int \left[(Y_b)^2 + X_b^2 \sin^2\alpha + Z_b^2 \cos^2\alpha - 2X_b Z_b \sin\alpha \cos\alpha \right] dm \qquad (80)$$

USING $\sin^2\alpha + \cos^2\alpha = 1$

$$I_{x_s} = \left[\int (Y_b^2 + Z_b^2)dm\right] \cos^2\alpha + \left[\int (Y_b^2 + X_b^2)dm\right] \sin^2\alpha - 2\left[\int X_b Z_b\, dm\right] \sin\alpha \cos\alpha$$

$$= I_{x_b} \cos^2\alpha + I_{z_b} \sin^2\alpha - 2I_{x_b z_b} \sin\alpha \cos\alpha \qquad (81)$$

USING $\cos^2\alpha = \frac{1}{2}(1+\cos 2\alpha)$, $\sin^2\alpha = \frac{1}{2}(1-\cos 2\alpha)$, and $\sin\alpha\cos\alpha = \frac{1}{2}\sin\alpha$:

$$I_{x_s} = \frac{1}{2}(I_{x_b} + I_{z_b}) + \frac{1}{2}(I_{x_b} - I_{z_b})\cos 2\alpha - I_{x_b z_b} \sin 2\alpha \qquad (82)$$

A similar development for I_z and I_{xz} gives:

$$I_{z_s} = \frac{1}{2}(I_{x_b} + I_{z_b}) - \frac{1}{2}(I_{x_b} - I_{z_b})\cos 2\alpha + I_{x_b z_b} \sin 2\alpha \qquad (83)$$

$$I_{x_s z_s} = \frac{1}{2}(I_{x_b} - I_{z_b})\sin 2\alpha + I_{x_b z_b} \cos 2\alpha \qquad (84)$$

Since $y_s = y_b$, it follows that:

$$I_{y_s} = I_{y_b}$$

Transformation of moments of inertia from body axes to stability axes.

$$\begin{aligned} I_{x_s} &= \frac{1}{2}(I_{x_b} + I_{z_b}) + \frac{1}{2}(I_{x_b} - I_{z_b})\cos 2\alpha - I_{x_b z_b} \sin 2\alpha \\ I_{y_s} &= I_{y_b} \\ I_{z_s} &= \frac{1}{2}(I_{x_b} + I_{z_b}) - \frac{1}{2}(I_{x_b} - I_{z_b})\cos 2\alpha + I_{x_b z_b} \sin 2\alpha \\ I_{x_s z_s} &= \frac{1}{2}(I_{x_b} - I_{z_b})\sin 2\alpha + I_{x_b z_b} \cos 2\alpha \end{aligned} \qquad (85)$$

Transformation of moments of inertia from stability axes to body axes.

$$
\begin{aligned}
I_{x_b} &= \tfrac{1}{2}\left(I_{x_s}+I_{z_s}\right)+\tfrac{1}{2}\left(I_{x_s}-I_{z_s}\right)\cos 2\alpha + I_{x_s z_s}\sin 2\alpha \\
I_{y_b} &= I_{y_s} \\
I_{z_b} &= \tfrac{1}{2}\left(I_{x_s}+I_{z_s}\right)-\tfrac{1}{2}\left(I_{x_s}-I_{z_s}\right)\cos 2\alpha - I_{x_s z_s}\sin 2\alpha \\
I_{x_b z_b} &= I_{x_s z_s}\cos 2\alpha - \tfrac{1}{2}\left(I_{x_s}-I_{z_s}\right)\sin 2\alpha
\end{aligned}
\tag{86}
$$

Transformation of moments of inertia from principal axes to body axes.

If we define the angle between the x and z body axes and the x and z principal axes as ϵ, then the following equations apply:

$$
\begin{aligned}
X_b &= X_o\cos\epsilon - Z_o\sin\epsilon \\
Y_b &= Y_o \\
Z_b &= X_o\sin\epsilon + Z_o\cos\epsilon
\end{aligned}
\tag{87}
$$

It follows from the development for stability axes to body axes, in which $I_{y_b} = I_{y_s}$ and $I_{x_b} I_{z_b} = I_{x_s} I_{z_s}$

that:

$$
\begin{aligned}
I_{x_b} &= \tfrac{1}{2}\left(I_{x_o}+I_{z_o}\right)+\tfrac{1}{2}\left(I_{x_o}-I_{z_o}\right)\cos 2\epsilon \\
I_{y_b} &= I_{y_s} \\
I_{z_b} &= \tfrac{1}{2}\left(I_{x_o}+I_{z_o}\right)-\tfrac{1}{2}\left(I_{x_o}-I_{z_o}\right)\cos 2\epsilon \\
I_{x_b z_b} &= -\tfrac{1}{2}\left(I_{x_o}-I_{z_o}\right)\sin 2\epsilon
\end{aligned}
\tag{88}
$$

Transformation of moments of inertia from body axes to principal axes.

It follows from the development for body axes to stability axes, in which $\alpha = \epsilon$, that:

$$
\begin{aligned}
I_{x_o} &= \tfrac{1}{2}\left(I_{x_b}+I_{z_b}\right)+\tfrac{1}{2}\left(I_{x_b}-I_{z_b}\right)\cos 2\epsilon - I_{x_b} I_{z_b}\sin 2\epsilon \\
I_{y_o} &= I_{y_b} \\
I_{z_o} &= \tfrac{1}{2}\left(I_{x_b}+I_{z_b}\right)-\tfrac{1}{2}\left(I_{x_b}-I_{z_b}\right)\cos 2\epsilon + I_{x_b z_b}\sin 2\epsilon \\
I_{x_o z_o} &= \tfrac{1}{2}\left(I_{x_b}-I_{z_b}\right)\sin 2\epsilon + I_{x_b z_b}\cos 2\epsilon = 0
\end{aligned}
\tag{89}
$$

Body Axes to Stability Axes

$$
\begin{aligned}
I_{x_s} &= \tfrac{1}{2}\left(I_{x_b}+I_{z_b}\right)+\tfrac{1}{2}\left(I_{x_b}-I_{z_b}\right)\cos 2\alpha - I_{x_b z_b}\sin 2\alpha \\
I_{y_s} &= I_{y_b} \\
I_{z_s} &= \tfrac{1}{2}\left(I_{x_b}+I_{z_b}\right)-\tfrac{1}{2}\left(I_{x_b}-I_{z_b}\right)\cos 2\alpha + I_{x_b z_b}\sin 2\alpha \\
I_{x_s z_s} &= \tfrac{1}{2}\left(I_{x_b}-I_{z_b}\right)\sin 2\alpha + I_{x_b z_b}\cos 2\alpha
\end{aligned}
\tag{90}
$$

Stability Axes to Body Axes

$$
\begin{aligned}
I_{x_b} &= \tfrac{1}{2}\left(I_{x_s}+I_{z_s}\right)-\tfrac{1}{2}\left(I_{x_s}-I_{z_s}\right)\cos 2\alpha - I_{x_s z_s}\sin 2\alpha \\
I_{y_b} &= I_{y_s} \\
I_{z_b} &= \tfrac{1}{2}\left(I_{x_s}+I_{z_s}\right)-\tfrac{1}{2}\left(I_{x_s}-I_{z_s}\right)\cos 2\alpha - I_{x_s z_s}\sin 2\alpha \\
I_{x_b z_b} &= I_{x_s z_s}\cos 2\alpha - \tfrac{1}{2}\left(I_{x_s}-I_{z_s}\right)\sin 2\alpha
\end{aligned}
\tag{91}
$$

Principal Axes to Body Axes

$$
\begin{aligned}
I_{x_b} &= \tfrac{1}{2}\left(I_{x_o}+I_{z_o}\right)+\tfrac{1}{2}\left(I_{x_o}-I_{z_o}\right)\cos 2\epsilon \\
I_{y_b} &= I_{y_o} \\
I_{z_b} &= \tfrac{1}{2}\left(I_{x_o}+I_{z_o}\right)-\tfrac{1}{2}\left(I_{x_o}-I_{z_o}\right)\cos 2\epsilon \\
I_{x_b z_b} &= -\tfrac{1}{2}\left(I_{x_o}-I_{z_o}\right)\sin 2\epsilon
\end{aligned}
\tag{92}
$$

Body Axes to Principal Axes

$$
\begin{aligned}
I_{x_o} &= \tfrac{1}{2}\left(I_{x_b}+I_{z_b}\right)+\tfrac{1}{2}\left(I_{x_b}-I_{z_b}\right)\cos 2\epsilon - I_{x_b z_b}\sin 2\epsilon \\
I_{y_o} &= I_{y_b} \\
I_{z_o} &= \tfrac{1}{2}\left(I_{x_b}+I_{z_b}\right)-\tfrac{1}{2}\left(I_{x_b}-I_{z_b}\right)\cos 2\epsilon + I_{x_b z_b}\sin 2\epsilon \\
I_{x_o z_o} &= \tfrac{1}{2}\left(I_{x_b}-I_{z_b}\right)\sin 2\epsilon + I_{x_b z_b}\cos 2\epsilon = 0
\end{aligned}
\tag{93}
$$

AIRPLANE EQUATIONS OF MOTION

Longitudinal Equations

The following equations are written in Laplace notation for a set of body axes using the following basic assumptions:

(1) The airplane is a rigid body.

(2) The mass of the airplane does not change during the period of dynamic analysis.

(3) The airplane is initially in unaccelerated flight.

(4) The earth is considered to be a flat, inertial, nonrotating, space fixed body and the incremental effects of gravity and density are neglected.

(5) The XZ plane is considered to be a plane of symmetry.

(6) The perturbations from the equilibrium or steady state condition are small enough that the products and squares of the variations are small in comparison with the variations themselves and can be neglected. Also, the perturbation angles are small enough that the sines of these angles may be set equal to the angles and the cosines equal to one. Products of these angles are also negligibly small.

(7) In the steady flight condition, the airplane is in wings level, symmetric flight with no angular velocity.

(8) The elevators and ailerons are symmetrically located with respect to the XZ plane and the rudder is located parallel to the XZ plane.

(9) The control surfaces are movable rigid components attached to a rigid body.

(10) The airflow around the airplane is quasi-steady.

The longitudinal equations may be written in the airplane body axis system as follows:

$$\left[\left(X_u - \frac{s}{U_0}\right) + T_u \cos(\eta)\right] u + \left[X_{\dot{\alpha}}\, s + X_\alpha\right] \alpha + \left[(X_q - \alpha_0)\right] s - \frac{g}{U_0} \cos\theta_0\ \theta$$
$$= -X_{\delta_e} \delta_e - X_{\delta_F} \delta_F - X_{\delta_B} \delta_B - T_{\delta_{RPM}} \delta_{RPM} \cos(\eta)$$

$$\left[Z_u - T_u \sin(\eta)\right] u + \left[(Z_{\dot\alpha} - 1)\, s + Z_\alpha\right] \alpha + \left[(1 + Z_q)\, s - \frac{g}{U_0} \sin\theta_0\right] \theta$$
$$= -Z_{\delta_e} \delta_e - Z_{\delta_F} \delta_F - Z_{\delta_B} \delta_B + T_{\delta_{RPM}} \delta_{RPM} \sin(\eta)$$

$$\left[M_u + \frac{m T_u \gamma_\eta}{I_{yy}}\right] u + \left[M_{\dot\alpha}\, s + M_\alpha\right] \alpha + \left[s\,(M_q - s)\right] \theta \qquad (94)$$
$$= -M_{\delta_e} \delta_e - M_{\delta_F} \delta_F - M_{\delta_B} \delta_B - \frac{m T_{\delta_{RPM}} \delta_{RPM}}{I_{yy}} (\gamma_\eta)$$

Assuming the contributions due to thrust (T), flaps (δ_F), and speed brakes (δ_B) are negligible, then: assuming that $T_u = T_{\delta_{RPM}} = \delta_F = \delta_B = 0$

$$\begin{bmatrix} X_u - \frac{s}{U_0} & X_{\dot\alpha}\, s + X_\alpha & (X_q - \alpha) s - \frac{g}{U_0} \cos\theta_0 \\ Z_u & (Z_{\dot\alpha} - 1) s + Z_\alpha & (1 - Z_q) s - \frac{g}{U_0} \sin\theta_0 \\ M_u & M_{\dot\alpha}\, s + M_\alpha & s(M_q - s) \end{bmatrix} \begin{bmatrix} u \\ \alpha \\ \theta \end{bmatrix} = - \begin{bmatrix} X_{\delta_e} \\ Z_{\delta_e} \\ M_{\delta_e} \end{bmatrix} \begin{bmatrix} \delta_e \end{bmatrix} \qquad (95)$$

The longitudinal characteristic equation may be written:

$$|\Delta_{Long}| = \left[\frac{Z_{\dot\alpha}}{U_0} - \frac{1}{U_0}\right] s^4 + \left[-M_q \frac{Z_{\dot\alpha}}{U_0} + \frac{M_q}{U_0} - X_u Z_{\dot\alpha} + X_u + \frac{Z_\alpha}{U_0} + \frac{M_{\dot\alpha}}{U_0} + \frac{M_{\dot\alpha} Z_q}{U_0} + Z_u X_{\dot\alpha}\right] s^3$$
$$+ \left[M_q X_u Z_{\dot\alpha} - M_q X_u - \frac{M_q Z_\alpha}{U_0} - X_u Z_\alpha + M_u X_{\dot\alpha} + M_u X_{\dot\alpha} Z_q + Z_u M_{\dot\alpha} X_q\right.$$
$$- Z_u M_{\dot\alpha} \alpha_0 - M_u Z_{\dot\alpha} X_q + M_u Z_{\dot\alpha} \alpha_0 + M_u Z_q - M_u \alpha_0 - M_{\dot\alpha} X_u - M_{\dot\alpha} X_u Z_q$$
$$\left. - M_{\dot\alpha} \frac{g}{U_0^2} \sin\theta_0 + \frac{M_\alpha}{U_0} + \frac{M_\alpha Z_q}{U_0} - Z_u M_q X_{\dot\alpha} + Z_u X_\alpha\right] s^2$$
$$+ \left[M_q X_u Z_\alpha - M_u X_{\dot\alpha} \frac{g}{U_0} \sin\theta_0 + M_u X_\alpha + M_u X_\alpha Z_q + Z_u M_\alpha X_q - M_\alpha Z_u \alpha_0\right.$$
$$- Z_u \frac{g}{U_0} M_{\dot\alpha} \cos\theta_0 + M_u Z_{\dot\alpha} \frac{g}{U_0} \cos\theta_0 - M_u \frac{g}{U_0} \cos\theta_0 - M_u Z_\alpha X_q + M_u Z_\alpha \alpha_0$$
$$\left. + M_{\dot\alpha} X_u \frac{g}{U_0} \sin\theta_0 - M_\alpha X_u - M_\alpha X_u Z_q - M_\alpha \frac{g}{U_0^2} \sin\theta_0 - Z_u M_q X_\alpha\right] s$$
$$+ \left[-M_u X_\alpha \frac{g}{U_0} \sin\theta_0 - Z_u M_\alpha \frac{g}{U_0} \cos\theta_0 + M_u Z_\alpha \frac{g}{U_0} \cos\theta_0 + M_\alpha X_u \frac{g}{U_0} \sin\theta_0\right] \qquad (96)$$

The following longitudinal transfer functions were obtained using Cramer's Rule. The change in forward velocity per elevator input can be written as follows:

$$\frac{u}{\delta_e} = \frac{1}{\Delta_{long}} \left\{ \left[X_{\delta_e} Z_{\dot{\alpha}} - X_{\delta_e} - Z_{\delta_e} X_{\dot{e}} \right] s^3 + \left[-X_{\delta_e} M_q Z_{\dot{\alpha}} + X_{\delta_e} M_q + X_{\delta_e} Z_\alpha - M_{\delta_e} X_{\dot{\alpha}} \right.\right.$$

$$- M_{\delta_e} X_{\dot{\alpha}} Z_q - Z_{\delta_e} M_{\dot{\alpha}} X_q + Z_{\delta_e} M_{\dot{\alpha}} \alpha_o + M_{\delta_e} Z_{\dot{\alpha}} X_q - M_{\delta_e} Z_{\dot{\alpha}} \alpha_o - M_{\delta_e} X_q + M_{\delta_e} \alpha_o$$

$$\left. + X_{\delta_e} M_{\dot{\alpha}} + X_{\delta_e} M_{\dot{\alpha}} Z_q + Z_{\delta_e} M_q X_{\dot{\alpha}} - Z_{\delta_e} X_\alpha \right] s^2$$

$$+ \left[-X_{\delta_e} Z_\alpha M_q + M_{\delta_e} X_{\dot{\alpha}} \frac{g}{U_o} \sin\theta_o - M_{\delta_e} X_\alpha - M_{\delta_e} X_\alpha Z_q - Z_{\delta_e} M_\alpha X_q + Z_{\delta_e} M_\alpha \alpha_o \right.$$

$$+ Z_{\delta_e} \frac{g}{U_o} M_{\dot{\alpha}} \cos\theta_o - M_{\delta_e} Z_{\dot{\alpha}} \frac{g}{U_o} \cos\theta_o + M_{\delta_e} \frac{g}{U_o} \cos\theta_o + M_{\delta_e} Z_\alpha X_q$$

$$\left. - M_{\delta_e} Z_\alpha \alpha_o - X_{\delta_e} M_{\dot{\alpha}} \frac{g}{U_o} \sin\theta_o + X_{\delta_e} M_\alpha + X_{\delta_e} M_\alpha Z_q + Z_{\delta_e} M_q X_\alpha \right] s$$

$$\left. + \left[M_{\delta_e} X_\alpha \frac{g}{U_o} \sin\theta_o + Z_{\delta_e} M_\alpha \frac{g}{U_o} \cos\theta_o - M_{\delta_e} Z_\alpha \frac{g}{U_o} \cos\theta_o - X_{\delta_e} M_\alpha \frac{g}{U_o} \sin\theta \right] \right\} \qquad (97)$$

The change in angle of attack per elevator input can be written as follows:

$$\frac{\alpha}{\delta_e} = \frac{1}{\Delta_{long}} \left\{ \left[-\frac{Z_{\delta_e}}{U_o} \right] s^3 + \left[Z_{\delta_e} X_u + \frac{Z_{\delta_e}}{U_o} M_q - \frac{M_{\delta_e}}{U_o} - \frac{M_{\delta_e} Z_q}{U_o} - Z_u X_{\delta_e} \right] s^2 \right.$$

$$+ \left[-Z_{\delta_e} X_u M_q - M_u X_{\delta_e} - M_u X_{\delta_e} Z_q - Z_u M_{\delta_e} X_q + Z_u M_{\delta_e} \alpha_o + M_u Z_{\delta_e} X_q \right.$$

$$\left. - M_u Z_{\delta_e} \alpha_o + M_{\delta_e} X_u + M_{\delta_e} X_u Z_q + \frac{M_{\delta_e}}{U_o} g \sin\theta_o + Z_u M_{\delta_e} M_q \right] s$$

$$\left. + \left[M_u X_{\delta_e} \frac{g}{U_o} \sin\theta_o + Z_u M_{\delta_e} \frac{g}{U_o} \cos\theta_o - M_u Z_{\delta_e} \frac{g}{U_o} \cos\theta_o - M_{\delta_e} X_u \frac{g}{U_o} \sin\theta_o \right] \right\} \qquad (98)$$

The pitch angle per elevator input can be written as follows:

$$\frac{\theta}{\delta_e} = \frac{1}{\Delta_{long}} \left\{ \left[\frac{M_{\delta_e} Z_{\dot{\alpha}}}{U_o} - \frac{M_{\delta_e}}{U_o} - \frac{Z_{\delta_e} M_{\dot{\alpha}}}{U_o} \right] s^2 + \left[-M_{\delta_e} X_u Z_{\dot{\alpha}} + M_{\delta_e} X_u + M_{\delta_e} \frac{Z_\alpha}{U_o} \right.\right.$$

$$- Z_{\delta_e} M_u X_{\dot{\alpha}} - X_{\delta_e} Z_u M_{\dot{\alpha}} + M_u X_{\delta_e} Z_{\dot{\alpha}} - M_u X_{\delta_e} + Z_{\delta_e} M_{\dot{\alpha}} X_u - Z_{\delta_e} \frac{M_\alpha}{U_o} + M_{\delta_e} Z_u X_{\dot{\alpha}} \left. \right] s$$

$$\left. + \left[-M_{\delta_e} X_u Z_\alpha - Z_{\delta_e} M_u X_\alpha - X_{\delta_e} Z_u M_\alpha + M_u X_{\delta_e} Z_\alpha + Z_{\delta_e} M_\alpha X_u + M_{\delta_e} Z_u X_\alpha \right] \right\} \qquad (99)$$

With the additional assumptions:

1. Constant speed
2. $\theta_o \approx 0$
3. $Z_{\dot{\alpha}} \approx Z_q \approx 0$
4. $\dot{\theta} = s\theta$
5. $n_z = \frac{U_o}{g}(\dot{\theta} - \dot{\alpha})$

and making the following conventional substitutions:

1. $L_\alpha = -Z_\alpha$
2. $L_{\delta_e} = -Z_{\delta_e}$

the characteristic equation becomes

$$|\Delta_{long}| = \frac{s^2}{U_o}\left\{s^2 + \left[M_q - L_\alpha + M_{\dot{\alpha}}\right]s + \left[M_q L_\alpha + M_\alpha\right]\right. \tag{100}$$

and the longitudinal transfer functions can be written as $\frac{u}{\delta_e} = 0$.

$$\frac{\dot{\theta}(s)}{\delta_e(s)} = \frac{(M_{\delta_e} - L_{\delta_e} M_{\dot{\alpha}})s + (M_{\delta_e} L_\alpha - M_\alpha L_{\delta_e})}{s^2 + (L_\alpha - M_q - M_{\dot{\alpha}})s - (M_\alpha + M_q L_\alpha)} \tag{101}$$

$$\frac{\alpha(s)}{\delta_e(s)} = \frac{-L_{\delta_e} s + (M_{\delta_e} + M_q L_{\delta_e})}{s^2 + (L_\alpha - M_q - M_{\dot{\alpha}})s - (M_\alpha + M_q L_\alpha)} \tag{102}$$

$$\frac{n_z(s)}{\delta_e(s)} = \frac{V}{g}\,\frac{L_{\delta_e} s^2 + (-L_{\delta_e} M_q - L_{\delta_e} M_{\dot{\alpha}})s + (M_{\delta_e} L_\alpha - M_\alpha L_{\delta_e})}{s^2 + (L_\alpha - M_q - M_{\dot{\alpha}})s - (M_\alpha + M_q L_\alpha)} \tag{103}$$

Assuming that the product of small terms is negligible ($L_{\delta_e} M_q \approx L_{\delta_e} M_{\dot{\alpha}} \approx 0$)

$$\frac{\dot{\theta}(s)}{\delta_e(s)} = \frac{M_{\delta_e}\left(s + \left[\frac{M_{\delta_e} L_\alpha - M_\alpha L_{\delta_e}}{M_{\delta_e}}\right]\right)}{s^2 + (L_\alpha - M_q - M_{\dot{\alpha}})s - (M_\alpha + M_q L_\alpha)} \tag{104}$$

$$\frac{\alpha(s)}{\delta_e(s)} = \frac{M_{\delta_e}\left[-\frac{L_{\delta_e}}{M_{\delta_e}}s+1\right]}{s^2+(L_\alpha - M_q - M_{\dot\alpha})s-(M_\alpha + M_q L_\alpha)} \tag{105}$$

$$\frac{n_z(s)}{\delta_e(s)} = \frac{V}{g}\,\frac{\left[M_{\delta_e}L_\alpha - M_\alpha L_{\delta_e}\right]\left[\frac{L_{\delta_e}}{M_{\delta_e}L_\alpha - M_\alpha L_{\delta_e}}s^2+1\right]}{s^2+(L_\alpha - M_q - M_{\dot\alpha})s-(M_\alpha + M_q L_\alpha)} \tag{106}$$

The short-period natural frequency and damping ratio can be expressed:

$$\omega_{sp}^2 = -M_\alpha - M_q L_\alpha \tag{107}$$

$$2\zeta_{sp}\omega_{sp} = L_\alpha - M_q - M_{\dot\alpha} \tag{108}$$

$$\zeta_{sp} = \frac{L_\alpha - M_q - M_{\dot\alpha}}{2\sqrt{-M_\alpha - M_q L_\alpha}} \tag{109}$$

$$\frac{1}{T_{\theta_2}} = \frac{M_{\delta_e}L_\alpha - M_\alpha L_{\delta_e}}{M_{\delta_e}} \tag{110}$$

$$\tau_\alpha = -\frac{L_{\delta_e}}{M_{\delta_e}} \tag{111}$$

$$\tau_{n_z} = \pm\sqrt{\frac{L_{\delta_e}}{M_{\delta_e}L_\alpha - M_\alpha L_{\delta_e}}} \tag{112}$$

Making these substitutions

$$\frac{\dot\theta(s)}{\delta_e(s)} = \frac{M_{\delta_e}\left(s+1/T_{\theta_2}\right)}{s^2+2\zeta_{sp}\omega_{sp}s+\omega_{sp}^2} \tag{113}$$

$$\frac{\alpha(s)}{\delta_e(s)} = \frac{M_{\delta_e}(\tau_\alpha s+1)}{s^2+2\zeta_{sp}\omega_{sp}s+\omega_{sp}^2} \tag{114}$$

$$\frac{n_z(s)}{\delta_e(s)} = \frac{V}{g}\,\frac{1}{T_{\theta_2}}\,\frac{M_{\delta_e}(\tau_{n_z}s+1)(-\tau_{n_z}s+1)}{s^2+2\zeta_{sp}\omega_{sp}s+\omega_{sp}^2} \tag{115}$$

For almost all conventional airplanes, τ_α is quite small and can usually be neglected. τ_{n_z} is likewise negligible for most conventional airplanes, however, it increases in importance for airplanes on which M_{δ_e} is large and/or the tail length is quite short. In this experiment, the tail length was sufficient to make τ_{n_z} negligible. Thus assuming, $\tau_\alpha \approx \pm \tau_{n_z} \approx 0$ and making the above substitutions, we have:

$$\frac{\dot{\theta}(s)}{\delta_e(s)} = \frac{M_{\delta_e}\left(s + 1/T_{\theta_2}\right)}{s^2 + 2\zeta_{sp}\omega_{sp}\, s + \omega_{sp}^2} \tag{116}$$

$$\frac{\alpha(s)}{\delta_e(s)} = \frac{M_{\delta_e}}{s^2 + 2\zeta_{sp}\omega_{sp}\, s + \omega_{sp}^2} \tag{117}$$

$$\frac{n_z(s)}{\delta_e(s)} = \frac{V}{g}\,\frac{1}{T_{\theta_2}}\,\frac{M_{\delta_e}}{s^2 + 2\zeta_{sp}\omega_{sp}\, s + \omega_{sp}^2} \tag{118}$$

The following relationships are derived from the above transfer functions:

$$\frac{n_z(s)}{\alpha(s)} = \frac{n_z(s)/\delta_e(s)}{\alpha(s)/\delta_e(s)} = \frac{V}{g}\,\frac{1}{T_{\theta_2}} \tag{119}$$

$$\frac{n_z(s)}{\dot{\theta}(s)} = \frac{n_z(s)/\delta_e(s)}{\dot{\theta}(s)/\delta_e(s)} = \frac{V}{g}\,\frac{1}{T_{\theta_2}}\left(\frac{1}{s + 1/T_{\theta_2}}\right) \tag{120}$$

$$\frac{\ddot{\theta}(s)}{\delta_e(s)} = s\,\frac{\dot{\theta}(s)}{\delta_e(s)} = \frac{s\,M_{\delta_e}\left(s + 1/T_{\theta_2}\right)}{s^2 + 2\zeta_{sp}\omega_{sp}\, s + \omega_{sp}^2} \tag{I-24}$$

The initial pitch acceleration, $\ddot{\theta}_0$, for a step elevator input can be obtained by the initial value theorem:

$$\frac{\ddot{\theta}_0}{\delta_e} = \lim_{s\to\infty}\left[s\left(\frac{\ddot{\theta}(s)}{s\delta_e(s)}\right)\right] = \lim_{s\to\infty}\left[\frac{M_{\delta_e}\left(1 + \frac{1}{T_{\theta_2}s}\right)}{1 + \frac{2\zeta_{sp}\omega_{sp}}{s} + \frac{\omega_{sp}^2}{s^2}}\right] \tag{121}$$

$$\frac{\ddot{\theta}_0}{\delta_e} = M_{\delta_e} \tag{122}$$

By the final value theorem, the steady state pitch rate to a step input is obtained:

$$\frac{\dot{\theta}_{ss}}{\delta_e} = \lim_{s \to 0} \left[s \left(\frac{\dot{\theta}(s)}{s\delta_e(s)} \right) \right] = \lim_{s \to 0} \left[\frac{M_{\delta_e}(s + 1/T_{\theta_2})}{s^2 + 2\zeta_{sp}\omega_{sp}s + \omega_{sp}^2} \right] \tag{123}$$

$$\frac{\dot{\theta}_{ss}}{\delta_e} = \frac{M_{\delta_e}}{T_{\theta_2}\omega_{sp}^2} \tag{124}$$

The time history for the $\dot{\theta}$ response to a unit elevator step input ($\delta_e = 1$) can be described as:

$$\dot{\theta}_{\delta_{e_{step}}} = \frac{M_{\delta_e}}{T_{\theta_2}\omega_{sp}^2} - \frac{M_{\delta_e}}{\omega_{sp}\sqrt{1-\zeta_{sp}^2}} \sqrt{\frac{\omega_{sp}^2(1-\zeta_{sp}^2) + (1/T_{\theta_2} - \zeta_{sp}\omega_{sp})^2}{\omega_{sp}^2}}\, e^{-\zeta_{sp}\omega_{sp}t} \sin\left(\omega_{sp}\sqrt{1-\zeta_{sp}^2}\, t + \psi_{\dot{\theta}_{sp}}\right) \tag{125}$$

where

$$\psi_{\dot{\theta}_{sp}} = \tan^{-1}\left(\frac{\sqrt{1-\zeta_{sp}^2}}{\zeta_{sp}}\right) + \tan^{-1}\left(\frac{\omega_{sp}\sqrt{1-\zeta_{sp}^2}}{1/T_{\theta_2} - \zeta_{sp}\omega_{sp}}\right)$$

$$\ddot{\theta}_{\delta_{e_{step}}} = \frac{d\dot{\theta}}{dt} = \frac{M_{\delta_e}\zeta_{sp}}{\sqrt{1-\zeta_{sp}^2}} \sqrt{\omega_{sp}^2(1-\zeta_{sp}^2) + (1/T_{\theta_2} - \zeta_{sp}\omega_{sp})^2}\, e^{-\zeta_{sp}\omega_{sp}t} \sin\left(\omega_{sp}\sqrt{1-\zeta_{sp}^2}\, t + \psi_{\dot{\theta}_{sp}}\right)$$

$$- M_{\delta_e}\sqrt{\omega_{sp}^2(1-\zeta_{sp}^2) + (1/T_{\theta_2} - \omega_{sp}\zeta_{sp})^2}\, e^{-\zeta_{sp}\omega_{sp}t} \cos\left(\omega_{sp}\sqrt{1-\zeta_{sp}^2}\, t + \psi_{\dot{\theta}_{sp}}\right) \tag{126}$$

The time at which the maximum pitch rate overshoot, $\dot{\theta}_{MAX}$, will occur can be obtained from the conditions for $\ddot{\theta} = 0$:

$$\sin\left(\omega_{sp}\sqrt{1-\zeta_{sp}^2}\, t + \psi_{\dot{\theta}_{sp}}\right) = \frac{\sqrt{1-\zeta_{sp}^2}}{\zeta_{sp}} \cos\left(\omega_{sp}\sqrt{1-\zeta_{sp}^2}\, t + \psi_{\dot{\theta}_{sp}}\right)$$

$$\tan\left(\omega_{sp}\sqrt{1-\zeta_{sp}^2}\, t + \psi_{\dot{\theta}_{sp}}\right) = \frac{\sqrt{1-\zeta_{sp}^2}}{\zeta_{sp}}$$

$$t = \frac{1}{\omega_{sp}\sqrt{1-\zeta_{sp}^2}}\left[\tan^{-1}\left(\frac{\sqrt{1-\zeta_{sp}^2}}{\zeta_{sp}}\right) - \psi_{\dot{\theta}_{sp}}\right]$$

$$t = \frac{-1}{\omega_{sp}\sqrt{1-\zeta_{sp}^2}}\left[\tan^{-1}\left(\frac{\omega_{sp}\sqrt{1-\zeta_{sp}^2}}{1/T_{\theta_2} - \omega_{sp}\zeta_{sp}}\right)\right]$$

Thus we can define

$$\frac{\dot{\theta}_{MAX}}{\dot{\theta}_{ss}} = 1 - \frac{T_{\theta_2}}{\sqrt{1-\zeta_{sp}^2}}\sqrt{\omega_{sp}^2\left(1-\zeta_{sp}^2\right)+\left(1/T_{\theta_2}-\zeta_{sp}\omega_{sp}\right)^2}\; e^{\frac{\zeta_{sp}}{\sqrt{1-\zeta_{sp}^2}}\left[\tan^{-1}\left(\frac{\omega_{sp}\sqrt{1-\zeta_{sp}^2}}{1/T_{\theta_2}-\zeta_{sp}\omega_{sp}}\right)\right]}\sin\left[\tan^{-1}\left(\frac{\sqrt{1-\zeta_{sp}^2}}{\zeta_{sp}}\right)\right] \qquad (127)$$

which reduces to:

(128)

$$\frac{\dot{\theta}_{MAX}}{\dot{\theta}_{ss}} = 1 - \frac{1}{\sqrt{1-\zeta_{sp}^2}}\sqrt{1-2\zeta_{sp}\left(\omega_{sp}T_{\theta_2}\right)+\left(\omega_{sp}T_{\theta_2}\right)^2}\; e^{\frac{\zeta_{sp}}{\sqrt{1-\zeta_{sp}^2}}\left[\tan^{-1}\left(\frac{\omega_{sp}\sqrt{1-\zeta_{sp}^2}}{1/T_{\theta_2}-\zeta_{sp}\omega_{sp}}\right)\right]}\sin\left[\tan^{-1}\left(\frac{\sqrt{1-\zeta_{sp}^2}}{\zeta_{sp}}\right)\right]$$

Lateral-Directional Equations

The lateral-directional equations of motion, for an input, δ, may be written in stability axes as follows:

$$\begin{bmatrix} Y_\beta + \left(Y_{\dot\beta}-1\right)s & Y_r - 1 & \frac{g}{U_o} + \left(Y_p + \alpha_o\right)s \\ N'_\beta + N'_{\dot\beta}\,s & N'_r - s & N'_p s \\ L'_\beta + L'_{\dot\beta}\,s & L'_r & s\left(L'_p - s\right) \end{bmatrix} \begin{bmatrix} \beta \\ r \\ \phi \end{bmatrix} = -\begin{bmatrix} Y_\delta \\ N'_\delta \\ L'_\delta \end{bmatrix} \delta \qquad (129)$$

The characteristic equation, $\Delta(s)$ is:

$$\Delta_{lat} = \left[Y_{\dot\beta} - 1\right] s^4 + \left[Y_\beta - (Y_{\dot\beta} - 1)(N'_r + L'_p) + N'_{\dot\beta}(Y_r - 1) + L'_{\dot\beta}(Y_p + \alpha_o)\right] s^3$$
$$+ \left[-Y_\beta (N'_r + L'_p) + (Y_{\dot\beta} - 1)(N'_r L'_p - L'_r N'_p) + N'_\beta (Y_r - 1) - N'_{\dot\beta}(Y_r - 1) L'_p + N'_{\dot\beta} L'_r (Y_p + \alpha_o)\right.$$
$$\left. + L'_\beta (Y_p + \alpha_o) + L'_{\dot\beta} N'_p (Y_r - 1) + L'_{\dot\beta}\left(\frac{g}{U_o} - N'_r (Y_p + \alpha_o)\right)\right] s^2 \left[+ Y_\beta (N'_r L'_p - L'_r N'_p)\right.$$
$$- N'_\beta (Y_r - 1) L'_p + N'_\beta L'_r (Y_p + \alpha_o) + N'_{\dot\beta} L'_r \left(\frac{g}{U_o}\right) + L'_\beta N'_p (Y_r - 1) + L'_\beta \left(\frac{g}{U_o} - N'_r (Y_p + \alpha_o)\right)$$
$$\left. - L'_{\dot\beta} N'_r \frac{g}{U_o}\right] s + \left[N'_\beta L'_r \frac{g}{U_o} - L'_\beta N'_r \frac{g}{U_o}\right] \qquad (130)$$

The bank angle per aileron stick input transfer function can be written as follows:

$$\frac{\phi}{\delta_{AS}} = \frac{-1}{\Delta_{lat}} \left\{ \left[Y_{\delta_{AS}} L'_{\dot\beta} - L'_{\delta_{AS}} (Y_{\dot\beta} - 1)\right] s^2 + \left[Y_{\delta_{AS}} (N'_{\dot\beta} L'_r - L'_{\dot\beta} N'_r + L'_\beta) + N'_{\delta_{AS}} (L'_{\dot\beta} [Y_r - 1]\right.\right.$$
$$\left. - L'_r [Y_{\dot\beta} - 1]) + L'_{\delta_{AS}} (N'_r [Y_{\dot\beta} - 1] - Y_\beta) - N'_{\dot\beta} [Y_r - 1]\right] s + \left[Y_{\delta_{AS}} (N'_\beta L'_r - L'_\beta N'_r)\right.$$
$$\left.\left. + N'_{\delta_{AS}} (L'_\beta [Y_r - 1] - L'_r Y_\beta) + L'_{\delta_{AS}} (N'_r Y_\beta - N'_\beta [Y_r - 1])\right]\right\} \qquad (131)$$

The transfer function can be written as:

$$\frac{\phi}{\delta_{AS}} = \frac{A_{\phi_{\delta_{AS}}} (s^2 + 2\zeta_\phi \omega_\phi s + \omega_\phi^2)}{\left(s + \frac{1}{\tau_s}\right)\left(s + \frac{1}{\tau_2}\right)(s^2 + 2\zeta_d \omega_d s + \omega_d^2)} \qquad (132)$$

where

$$A_{\phi_{\delta_{AS}}} = \frac{L'_{\delta_{AS}} (Y_{\dot\beta} - 1) - Y_{\delta_{AS}} L'_{\dot\beta}}{(Y_{\dot\beta} - 1)}$$

The sideslip per aileron stick input transfer function can be written as follows:

$$\frac{\beta}{\delta_{AS}} = \frac{-1}{\Delta_{lat}} \left\{ \left[Y_{\delta_{AS}}\right] s^3 + \left[-Y_{\delta_{AS}} (N'_r + L'_p) + N'_{\delta_{AS}} (Y_r - 1) + L'_{\delta_{AS}} (Y_p + \alpha_o)\right] s^2 \right.$$
$$+ \left[Y_{\delta_{AS}} (N'_r L'_p - L'_r N'_p) - N'_{\delta_{AS}} L'_p (Y_r - 1) + N'_{\delta_{AS}} L'_r (Y_p + \alpha_o) + L'_{\delta_{AS}} N'_p (Y_r - 1)\right.$$
$$\left.\left. + L'_{\delta_{AS}} \left(\frac{g}{U_o} - N'_r (Y_p + \alpha_o)\right)\right] s + \left[N'_{\delta_{AS}} L'_r \frac{g}{U_o} - L'_{\delta_{AS}} N'_r \frac{g}{U_o}\right]\right\} \qquad (133)$$

The transfer function can be written in the form:

$$\frac{\beta}{\delta_{AS}} = \frac{A_{\beta\delta_{AS}}\left(s+\lambda_{\beta_1}\right)\left(s^2+2\zeta_\beta\omega_\beta s+\omega_\beta^2\right)}{\left(s+\frac{1}{\tau_s}\right)\left(s+\frac{1}{\tau_R}\right)\left(s^2+2\zeta_d\omega_d s+\omega_d^2\right)} \tag{134}$$

where

$$A_{\beta\delta_{AS}} = \frac{Y_{\delta_{AS}}}{1-Y_{\dot\beta}}$$

For $Y_{\delta_{AS}} = 0$, the following equation applies

$$\frac{\beta}{\delta_{AS}} = \frac{A_{\beta\delta_{AS}}\left(s^2+2\zeta_\beta\omega_\beta s+\omega_\beta^2\right)}{\left(s+\frac{1}{\tau_s}\right)\left(s+\frac{1}{\tau_R}\right)\left(s^2+2\zeta_d\omega_d s+\omega_d^2\right)} \tag{135}$$

where

$$A_{\beta\delta_{AS}} = \frac{L'_{\delta_{AS}}}{(1-Y_{\dot\beta})}\left[\frac{N'_{\delta_{AS}}}{L'_{\delta_{AS}}}\left(Y_r-1\right)+\left(Y_p+\alpha_0\right)\right]$$

The yaw rate per aileron stick input transfer function can be written as follows:

$$\begin{aligned}\frac{r}{\delta_{AS}} = \frac{-1}{\Delta_{Lat}}\Bigg\{&\left[Y_{\delta_{AS}}N'_{\dot\beta}-N'_{\delta_{AS}}\left(Y_{\dot\beta}-1\right)\right]s^3+\Big[-Y_{\delta_{AS}}\left(N'_{\dot\beta}L'_p-N'_\beta-N'_pL'_{\dot\beta}\right)+N'_{\delta_{AS}}\Big(L'_p\left[Y_{\dot\beta}-1\right]\\&-Y_\beta-L'_{\dot\beta}\left(Y_p+\alpha_0\right)\Big)-L'_{\delta_{AS}}\left(N'_p\left[Y_{\dot\beta}-1\right]-N'_{\dot\beta}\left(Y_p+\alpha_0\right)\right)\Big]s^2+\Big[-Y_{\delta_{AS}}\left(N'_\beta L'_p-N'_pL'_\beta\right)\\&+N'_{\delta_{AS}}\left(Y_\beta L'_p-L'_{\dot\beta}\frac{g}{U_o}-L'_\beta\left(Y_p+\alpha_0\right)\right)-L'_{\delta_{AS}}\left(Y_\beta N'_p-N'_{\dot\beta}\frac{g}{U_o}-N'_\beta\left(Y_p+\alpha_0\right)\right)\Big]s\\&+\left[-N'_{\delta_{AS}}L'_\beta\frac{g}{U_o}+L'_{\delta_{AS}}N'_\beta\frac{g}{U_o}\right]\Bigg\}\end{aligned} \tag{136}$$

The transfer function can be written as:

$$\frac{r}{\delta_{AS}} = \frac{A_{r_{\delta_{AS}}}\left(s+\lambda_{r_1}\right)\left(s^2+2\zeta_r\omega_r s+\omega_r^2\right)}{\left(s+\frac{1}{\tau_s}\right)\left(s+\frac{1}{\tau_R}\right)\left(s^2+2\zeta_d\omega_d s+\omega_d^2\right)} \tag{137}$$

where:

$$A_{r_{\delta_{AS}}} = \frac{Y_{\delta_{AS}} N'_{\dot{\beta}} - N'_{\delta_{AS}} (Y_{\dot{\beta}} - 1)}{(1 - Y_{\dot{\beta}})}$$

For $N_{\delta_{AS}} = N'_{\beta} = L'_{\dot{\beta}} = 0$, the following equation applies:

$$\frac{r}{\delta_{AS}} = \frac{A_{r_{\delta_{AS}}} \left(s^2 + 2\zeta_r \omega_r s + \omega_r^2\right)}{\left(s + \frac{1}{\tau_s}\right)\left(s + \frac{1}{\tau_R}\right)\left(s^2 + 2\zeta_d \omega_d s + \omega_d^2\right)} \tag{138}$$

where

$$A_{r_{\delta_{AS}}} = \frac{L'_{\delta_{AS}}}{1 - Y_{\dot{\beta}}} \left[\frac{Y_{\delta_{AS}}}{L'_{\delta_{AS}}} N'_{\beta} - N'_{p} (Y_{\dot{\beta}} - 1) \right]$$

From Equation 104,

$$\frac{p}{\delta_{AS}} = \frac{\dot{\phi}}{\delta_{AS}} = \frac{A_{\phi_{\delta_{AS}}} s \left(s^2 + 2\zeta_\phi \omega_\phi s + \omega_\phi^2\right)}{\left(s + \frac{1}{\tau_s}\right)\left(s + \frac{1}{\tau_R}\right)\left(s^2 + 2\zeta_d \omega_d s + \omega_d^2\right)} \tag{139}$$

where

$$A_{\phi_{\delta_{AS}}} = \frac{L'_{\delta_{AS}} (Y_{\dot{\beta}} - 1) - Y_{\delta_{AS}} L'_{\dot{\beta}}}{(Y_{\dot{\beta}} - 1)}$$

With the assumption that the spiral mode is at the origin, i.e., $\tau_s = \infty$, the above equation can be written:

$$\frac{p}{\delta_{AS}} = \frac{A_{\phi_{\delta_{AS}}} \left(s^2 + 2\zeta_\phi \omega_\phi s + \omega_\phi^2\right)}{\left(s + \frac{1}{\tau_R}\right)\left(s^2 + 2\zeta_d \omega_d s + \omega_d^2\right)} = \left(\frac{A_{\phi_{\delta_{AS}}} \omega_\phi^2}{\frac{\omega_d^2}{\tau_R}} \right) \frac{\left(\frac{s^2}{\omega_\phi^2} + \frac{2\zeta_\phi s}{\omega_\phi} + 1\right)}{(\tau_R s + 1)\left(\frac{s^2}{\omega_d^2} + \frac{2\zeta_d s}{\omega_d} + 1\right)} \tag{140}$$

Thus the steady-state roll rate per step aileron stick input becomes:

$$\frac{p_{ss}}{\delta_{AS}} = \tau_R \left(A_{\phi_{\delta_{AS}}}\right) \left(\frac{\omega_\phi}{\omega_d}\right)^2 = \tau_R \left[L'_{\delta_{AS}}\right] \left(\frac{\omega_\phi}{\omega_d}\right)^2 \tag{141}$$

SECTION IX
T-33 FIXED-BASE GROUND SIMULATOR

The T-33 can be quickly converted to a ground-based simulator by connecting analog computer equipment to the T-33 VSS equipment (see Figure 67).

To convert to ground-based simulation operation, the following changes are required:

1. Connect the large external hydraulic pump to the T-33 1000 psi hydraulic system.

2. Connect quick disconnect type cables to VSS equipment from computer equipment.

3. Replace air-driven instruments in front cockpit, i.e., altimeter, rate of climb, airspeed, with electrical instruments.

4. Install throttle and thrust meter in front cockpit.

5. Cover front cockpit canopy and windshield with translucent covering.

Six-degree-of-freedom equations of motion representing the configurations of aircraft to be simulated are set up on the computer. The configurations can be changed either with the T-33 rear seat gain controls or by potentiometers on the analog equipment. The choice is determined by the particular experiment design.

Present computer equipment consists of three Electronic Associates type TR-10 analog computers and one TR-20. Four instrument servos, pitch attitude (θ), bank angle (ϕ), heading (ψ), and altitude (h) are mounted in an equipment rack located next to the analog computers. The instrument servos have d.c. inputs from the analog equipment and drive synchros which are connected to front cockpit instruments.

Inputs to the analog equipment from the VSS equipment are control surface deflections (d.c. signals) or in some cases front cockpit control deflection or force signals. The throttle is another input to the analog equipment. Outputs from analog equipment to the VSS are cockpit displays, and all of the signals that normally come from the VSS sensors in flight, e.g., r, p, q rate gyro signals and their derivatives; α , β , $\bar{q}_c$ and their derivatives; as well as the accelerometer signals n_x , n_y , n_z .

The same recording equipment is used for ground simulations as for flight experiments and, in addition to VSS signals, analog signals of interest are recorded. In addition, an 8-channel Brush strip line pen recorder is used to record analog signals.

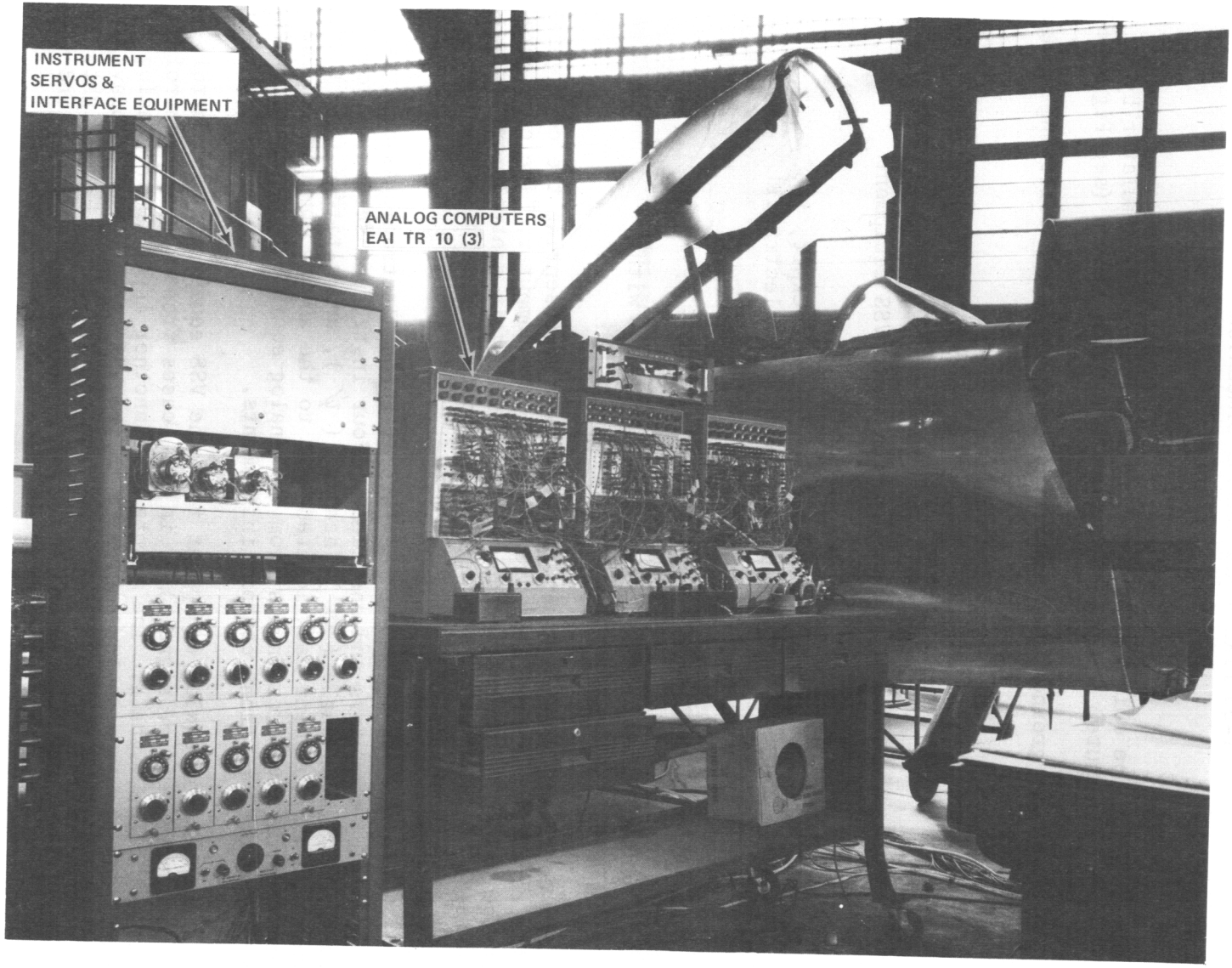

Figure 67 T-33 GROUND SIMULATOR EQUIPMENT HOOK UP

Evaluations are conducted with the canopy covered and closed to simulate IFR conditions. An intercom is used for communications between the computer operator and evaluation pilot.

The equations of motion used for the ground simulation are given below.

EQUATIONS OF MOTION USED FOR T-33 GROUND SIMULATIONS

The equations of motion, the aerodynamic data, and the simplifications assumed for the simulations are listed and the resulting approximate equations are given.

Full six-degree-of-freedom equations are given in Reference 6. The moment equations are in terms of body axes, the force equations in terms of body axes, the force equations in terms of stability axes and the body axes are referenced to earth axes by Euler angles. This choice of axis systems is the most economical in the amount of analog equipment required for simulations incorporating the small perturbation approximations and not requiring all three earth-referenced velocity components. For more sophisticated simulations, it may be advantageous to use wind axes for the force equations rather than stability axes, see Reference 6.

Moment Equations in Body Axes

$$L_b = I_x \dot{p}_b + (I_z - I_y) q_b r_b - I_{xz} (p_b q_b + \dot{r}_b)$$

$$M_b = I_y \dot{q}_b + (I_x - I_z) p_b r_b - I_{xz} (r_b^2 - p_b^2)$$

$$N_b = I_z \dot{r}_b + (I_y - I_x) p_b q_b - I_{xz} (\dot{p}_b - r_b q_b) \qquad (143)$$

Where L_b , M_b , N_b are the aerodynamic rolling, pitching and yawing moments about the x , y , z body axes respectively.

These are the complete equations. It is assumed that there are no gyroscopic effects or moments from thrust misalignments.

Euler Angles

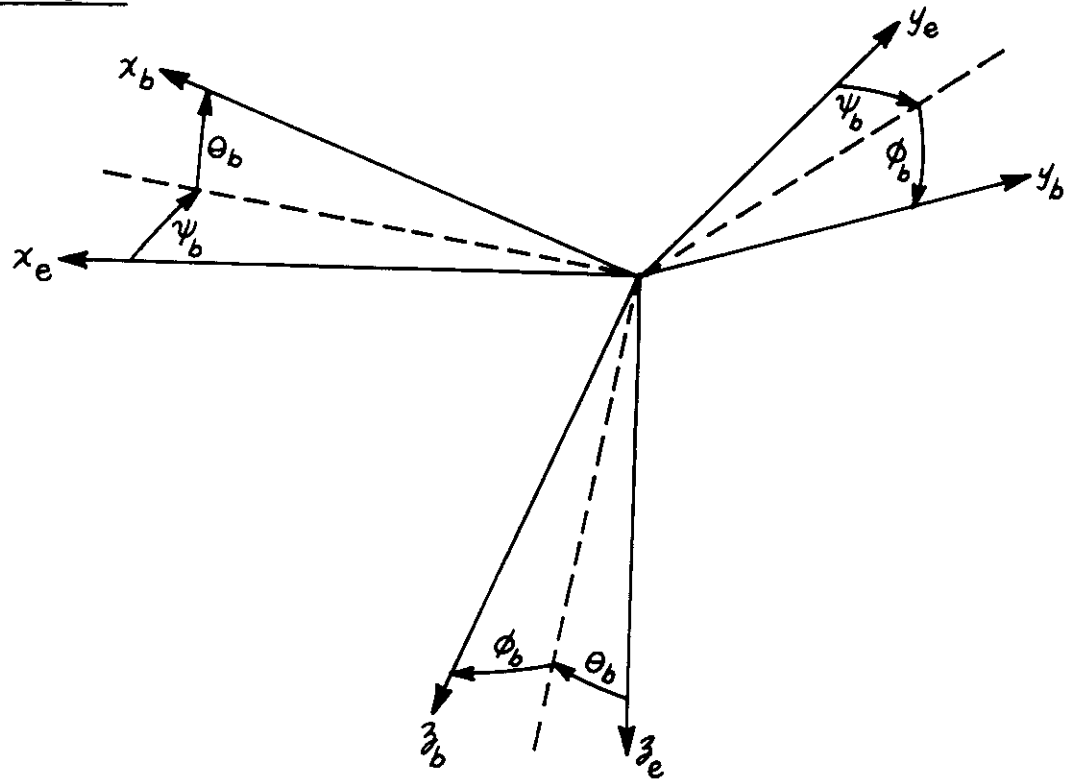

Euler angles describing the orientation of body axes relative to the earth axes are shown above.

Displacements are in the order: yaw ψ_b, pitch θ_b, roll ϕ_b. In terms of the body axis angular rates we get:

$$\dot{\phi}_b = p_b + \tan\theta_b \left(q_b \sin\phi_b + r\cos\phi_b\right)$$

$$\dot{\theta}_b = q_b \cos\phi_b - r_b \sin\phi_b$$

$$\dot{\psi}_b = \frac{q_b \sin\phi_b + r_b \cos\phi_b}{\cos\theta_b} \qquad (144)$$

Earth-Referenced Velocities

For most simulations, only the height above the earth is of interest. This is given by:

$$-\dot{h} = w_e = -u_s \cos\alpha \sin\theta_b + v_s \sin\phi \cos\theta + u_s \sin\alpha \cos\phi \cos\theta \qquad (145)$$

However, for completeness, the two translational components of velocity are given by:

$$u_e = u_s \cos\alpha \cos\theta_b \cos\psi_b + v_s (\sin\phi_b \sin\theta_b \cos\psi_b - \cos\phi_b \sin\psi_b)$$
$$+ u_s \sin\alpha (\sin\phi_b \sin\psi_b + \cos\phi_b \cos\psi_b \sin\theta_b)$$
$$v_e = u_s \cos\alpha \cos\theta_b \sin\psi_b + v_s (\cos\phi_b \cos\psi_b + \sin\phi_b \sin\theta_b \sin\psi_b)$$
$$+ u_s \sin\alpha (\cos\phi_b \sin\theta_b \sin\psi_b - \sin\phi_b \cos\psi_b) \qquad (146)$$

Force Equations in Stability Axes

$$X_s = m\left[\dot{u}_s - v_s(r_b \cos\alpha - p_b \sin\alpha) + g(\sin\theta_b \cos\alpha \right.$$
$$\left. - \cos\theta_b \cos\phi_b \sin\alpha)\right] - T\cos(\alpha + \eta_T)$$
$$Y_s = m\left[\dot{v}_s + u_s(r_b \cos\alpha - p_b \sin\alpha) - g\cos\theta_b \sin\phi_b\right]$$
$$Z_s = m\left[v_s(p_b \cos\alpha + r_b \sin\alpha) - (q_b - \dot{\alpha})\right.$$
$$\left. - g(\cos\theta_b \cos\phi_b \cos\alpha + \sin\theta_b \sin\alpha)\right] + T\sin(\alpha + \eta_T) \qquad (147)$$

Where X_s, Y_s and Z_s are the aerodynamic forces along the x, y and z stability axes respectively and T is the engine thrust.

The equations are complete, (i.e., they have no approximations) and include gravitational and thrust components.

Simplifications Assumed for Simulations

(1) Assume α, β, θ are small so that

$$\sin\alpha \approx \alpha, \quad \sin\beta \approx \beta, \quad \sin\theta \approx \theta$$
$$\cos\alpha \approx \cos\beta \approx \cos\theta \approx 1$$

(2) Products and squares among α , β , p , q , r are negligible.

(3) Assume $u_s \approx V$ and $\tan\beta \approx \beta$

so that $\frac{v_s}{u_s} \approx \beta$

(4) Thrust component, $T \sin(\alpha + \eta_T)$ is negligible.

Collection of Simplified Equations Used in the Simulation

Moments:

$$\frac{L_b}{I_x} = \dot{p}_b - \frac{I_{xz}}{I_x}\dot{r}_b$$
$$\frac{M_b}{I_y} = \dot{q}_b$$
$$\frac{N_b}{I_z} = \dot{r}_b - \frac{I_{xz}}{I_z}\dot{p} \qquad (148)$$

Forces:

$$\dot{V} = \frac{X_s}{m} - g(\theta_b - \alpha\cos\phi_b) + \frac{P}{m}$$
$$V(\dot{\beta} + r_b - p_b\alpha) = \frac{Y_s}{m} - g\sin\phi_b$$
$$V(\dot{\alpha} - q_b) = \frac{Z_s}{m} + g\cos\phi_b \qquad (149)$$

Euler Angle Rates:

$$\dot{\phi}_b = p_b + \theta_b\dot{\psi}_b$$
$$\dot{\theta}_b = q_b\cos\phi_b - r\sin\phi_b$$
$$\dot{\psi}_b = q_b\sin\phi_b + r\cos\phi_b \qquad (150)$$

Height:

$$\dot{h} = V(\theta_b - \alpha\cos\phi_b - \beta\sin\phi_b)$$
$$h = \int \dot{h}\,dt \qquad (151)$$

For the T-33 airplane, an adequate representation of the aerodynamic forces and moments is given by the following expressions:

Aerodynamic Moment Equations in Body Axes

$$\frac{L_b}{I_x} = L_\beta \beta + \frac{\partial L_\beta}{\partial \alpha} \alpha\beta + L_p p + L_r r + \frac{\partial L_r}{\partial \alpha} \alpha r + L_{\delta_a} \delta_a + L_{\delta_r} \delta_r$$

$$\frac{M_b}{I_y} = M_\alpha \alpha + M_{\dot{\alpha}} \dot{\alpha} + M_q q + M_{\delta_e} \delta_e \qquad (152)$$

$$\frac{N_b}{I_z} = N_\beta \beta + N_p p + \frac{\partial N_p}{\partial \alpha} \alpha p + N_r r + N_{\delta_a} \delta_a + N_{\delta_r} \delta_r + \frac{\partial N_{\delta_a}}{\partial \alpha} \alpha \delta_a$$

Aerodynamic Force Equations in Stability Axes

$$X_s = q_o S \left(C_{D_o} + C'_{D_\alpha} \alpha + C'_{D_{\alpha^2}} \alpha^2\right) - q_o S \frac{2}{V_o} \left(C_{D_o} \Delta V + C'_{D_\alpha} \alpha \Delta V + C'_{D_{\alpha^2}} \alpha^2 \Delta V\right)$$

$$\frac{Y_s}{mV} = Y_\beta \beta + Y_{\delta_r} \delta_r \qquad (153)$$

$$Z_s = -q_o S \left(C_{L_o} + C_{L_\alpha} \alpha + C_{L_{\delta_e}} \delta_e\right) - q_o S \frac{2}{V_o} \left(C_{L_o} \Delta V + C_{L_\alpha} \alpha \Delta V\right)$$

Note: C'_{D_α}, $C'_{D_{\alpha^2}}$ are curve-fitting coefficients for a second-order polynomial approximation of the drag polar.

T-33 Aerodynamic Data

V = 250 kt IAS, = 590 ft/sec, M = .595
h_p = 23,000 ft Standard Day
W = 12,400 lb 200 Gal. Fuel Remaining

I_x = 17,000 slug-ft^2	q = 200 lb/ft^2
I_y = 20,700 slug-ft^2	S = 234.8 ft^2
I_z = 36,400 slug-ft^2	c = 6.72 ft
I_{xz} = 490 slug-ft^2	b = 37.54 ft

The following data are referred to body axes for moments and stability axes for the forces.

L_β	= -9.6	$1/sec^2$-rad	N_β	= +3.4	$1/sec^2$-rad
$\partial L_\beta/\partial\alpha$	= -87.3	$1/sec^2$-rad^2	$N_{\dot\beta}$	= 0	
$L_{\dot\beta}$	= 0		N_p	= -.032	1/sec-rad
L_p	= -2.1	1/sec-rad	$\partial N_p/\partial\alpha$	= -1.64	1/sec-rad^2
L_r	= .76	1/sec-rad	N_r	= -.27	1/sec-rad
$\partial L_r/\partial\alpha$	= +3.58	1/sec-rad^2	N_{δ_a}	= +.125	$1/sec^2$-rad
L_{δ_a}	= -11.5	$1/sec^2$-rad	$\partial N_{\delta_a}/\partial\alpha$	= -2.3	$1/sec^2$-rad^2
L_{δ_r}	= 2.0	$1/sec^2$-rad	N_{δ_r}	= -3.8	$1/sec^2$-rad
Y_β	= -.14	1/sec-rad	Y_{δ_r}	= .038	1/sec-rad
M_α	= -6.75	$1/sec^2$-rad			
$M_{\dot\alpha}$	= -.731	1/sec-rad			
M_q	= -.736	1/sec-rad			
M_{δ_e}	= -13.18	$1/sec^2$-rad			
α_o	= .60°	Measured from Fuselage Reference			
C_{L_o}	= .264				
C_{L_α}	= 6.47	1/rad			
$C_{L_{\delta_e}}$	= .368	1/rad			

The drag coefficient, C_D, was represented by a polynomial of the form:

$$C_D = C_{D_o} + C'_{D_\alpha}\,\alpha + C'_{D_{\alpha^2}}\,\alpha^2$$

where the coefficients of α and α^2 were

C'_{D_α}	= .172	1/rad
$C'_{D_{\alpha^2}}$	= .057	$1/rad^2$
C_{D_o}	= .0217	For the level flight cases.
C_{D_o}	= .1055	For the spiral descents with L/D = 2.5

SECTION X
SENSOR DYNAMICS AND POSITION ERROR CORRECTIONS

To close the loop with the variable stability system, it is necessary to measure the motion and attitude of the aircraft. The loop consists of sensors, sensor amplifiers, control surface servos and motions of the aircraft caused by the control surface movements. This measurement is done with the following sensors:

1. β probe - probe angle of sideslip
2. α vane - vane angle of attack
3. Normal, n_z, lateral, n_y, and longitudinal, n_x, accelerometers
4. Attitude gyros for pitch, θ, and bank angle ϕ
5. Rate gyros for rate of yaw, r, pitch, q, and roll, p
6. Pitot-static-dynamic pressure, $\bar{q}_c$

SENSOR POSITION ERRORS

There are two types of sensor position errors. One type of error occurs because the sensor which is being used to measure the motion of the aircraft about its own center of gravity (c.g.) and also the motion of the c.g. itself in earth coordinates, is not located at the c.g. Sensors exhibiting this type of error are the β probe, α vane and n_x, n_y, n_z accelerometers.

The other error occurs because the sensor is located within the disturbed flow field of the aircraft. Sensors having this type of error are the α vane, β probe and $\bar{q}_c$ pitot-static tube. Corrections have to be made in the appropriate equations for both types of errors. Figure 68 shows the location of all the sensors relative to the reference datum line.

The position error corrections are calculated with respect to the center of gravity and since the center of gravity changes as a function of fuel remaining, it is necessary to take into account the effect of fuel remaining on position error corrections. Table IV is presented which gives the distance measurements to be used as a function of fuel remaining.

SIDESLIP ANGLE PROBE (β_v) AND ANGLE OF ATTACK (α_v) POSITION ERROR CORRECTIONS

The T-33 β probe is mounted on the top of the fuselage and the α vane is mounted on the side of the fuselage forward of the cockpit as shown in Figure 68.

The sideslip measured by the probe and the angle of attack measured by the vane will lag the true sideslip and angle of attack, respectively, by

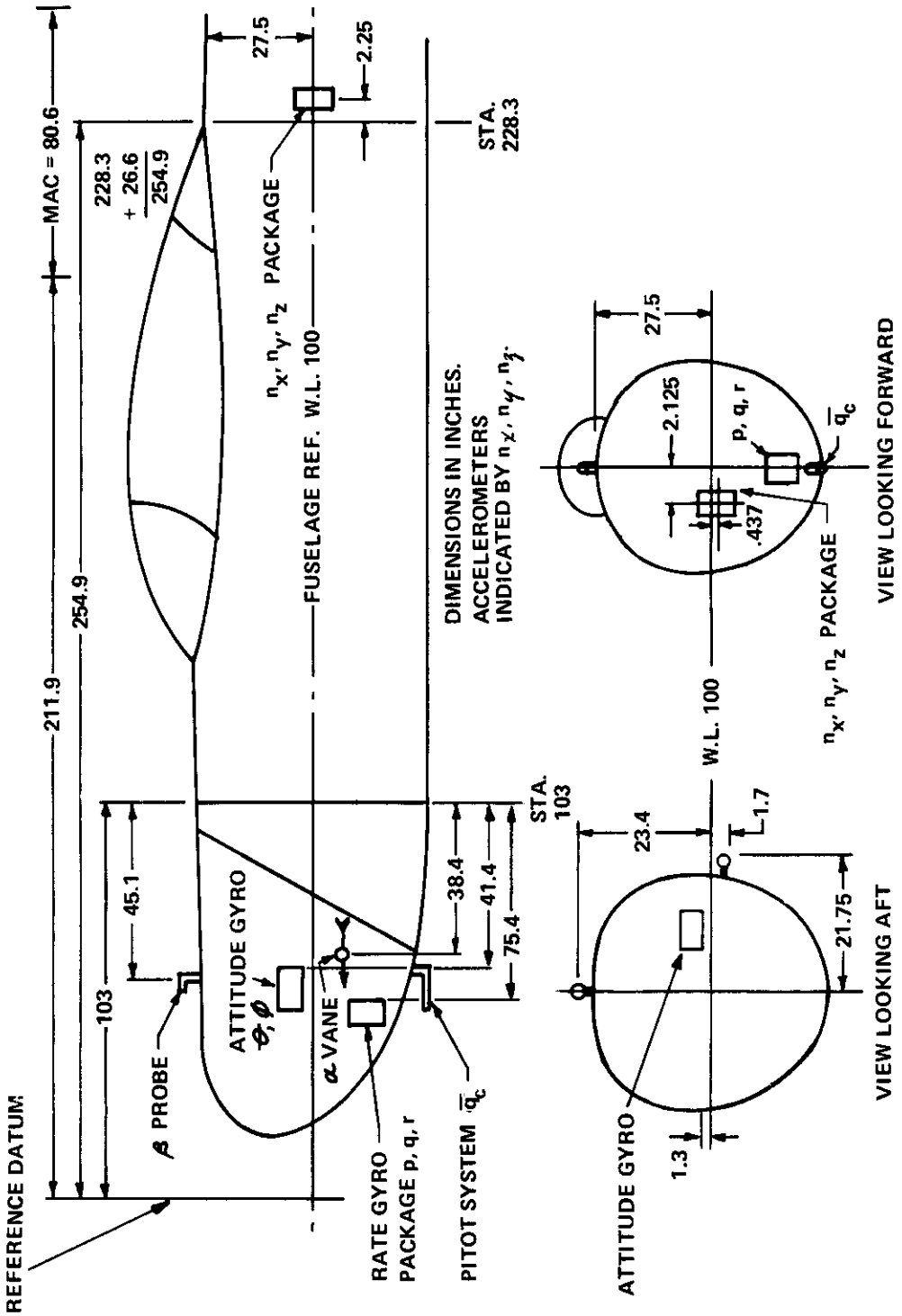

Figure 68 LOCATION OF LINEAR ACCELEROMETERS, α VANE, β PROBE, ATTITUDE GYRO, RATE GYROS & PITOT SYSTEM

Table IV

DISTANCE MEASUREMENTS TO BE USED TO DETERMINE THE POSITION ERROR CORRECTIONS AS A FUNCTION OF FUEL LOADING

BASED ON C.G. MEASUREMENTS BY G.W. HALL ON 17 MAY 1967.

FUEL LOAD / POSITION	FULL INTERNAL PLUS FULL 230 GALLON TIP TANKS	FULL INTERNAL	FULL FUSELAGE PLUS FULL MAIN WING TANKS	FULL FUSELAGE TANK	NO FUEL
C.G. % MAC	28.26	26.64	27.30	24.85	24.75
C.G. STATION	234.68	233.37	233.90	231.93	231.85
$\bar{x}$	22.78	21.47	22.00	20.03	19.95
x_α	170.08	168.77	169.30	167.33	167.25
x_β	176.78	175.47	176.00	174.03	173.95
$x_{n_y}, x_{n_z}, x_{n_x}$	-22.47	-23.78	-23.25	-25.22	-25.30

NOTE: INCLUDES FULL OIL PLUS CREW OF TWO.

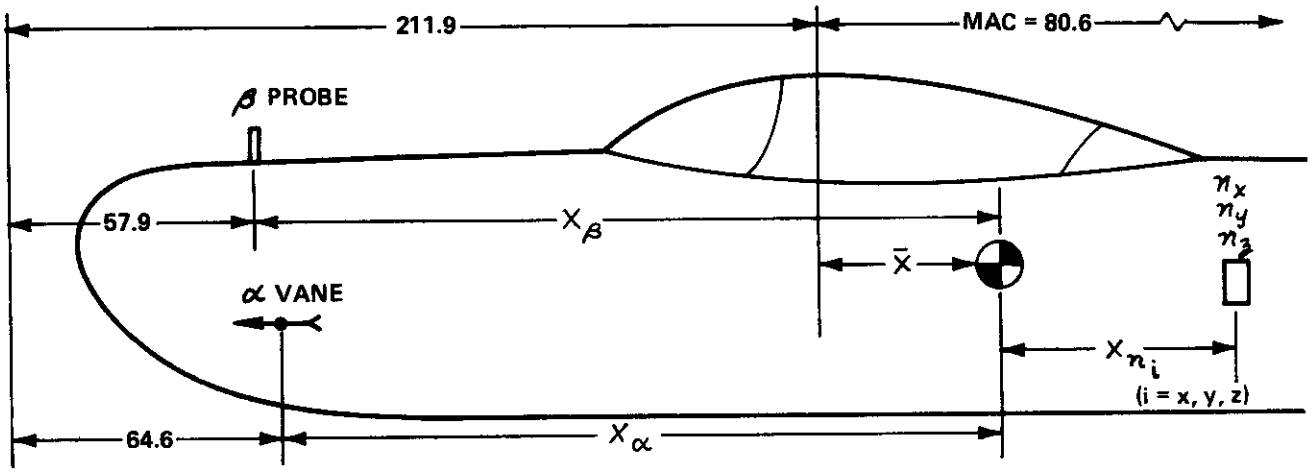

an amount dependent on the probe and vane dynamics and also on the speed and altitude of the airplane. Also the measured amplitudes of the sideslip angle and angle of attack will be different from the true values for the airplane due to the induced flow caused by the shape of the fuselage and the effective side and vertical velocities caused by the locations of the probe and vane with respect to the center of gravity of the airplane. It is probable that the correction for induced flow will show a variation with Mach number equal to 0.5 or greater.

ESTIMATION OF SIDESLIP PROBE POSITION ERROR CORRECTION FACTOR

The following expression can be used to represent the output of the sideslip probe in the steady state. The coordinates of the probe from the c.g. (x, z) are shown on Figure 68 and Table IV.

$$\beta_{\substack{PROBE \\ MEAS.}} = \left[\frac{\beta_{PROBE}}{\beta_{TRUE}}\right]_{c.g.} \left[\beta_{\substack{TRUE \\ AT\ c.g.}} + \frac{rx}{V_o}\right] - \frac{pz}{V_o} \tag{154}$$

This equation can be solved for the true sideslip at the c.g. as follows:

$$\beta_{TRUE} = \frac{1}{\left[\frac{\beta_{PROBE}}{\beta_{TRUE}}\right]} \left[\beta_{\substack{PROBE \\ MEAS.}} + \frac{pz}{V_o}\right] - \frac{rx}{V_o} \tag{155}$$

In order to calculate β_{true} the ratio $\beta_{probe}/\beta_{true}$ is first determined by making use of the following equations and oscillograph trace measurements.

Consider the side force equation:

$$Y = m(\dot{V} - pw + ru) - mg\phi = mgn_y$$

$$\text{or} \quad \dot{\beta} - p\alpha + r - \left(\frac{g}{V_o}\right)\phi = \frac{g}{V_o} n_y \tag{156}$$

Assume $\alpha \approx 0$ and $\dot{\beta} = s\beta$, $\dot{\phi} = p = s\phi$. For a Dutch roll maneuver,

$$s = \zeta\omega_{n_d} \pm i\omega_{nd}\sqrt{1-\zeta_d^2}$$

Divide Equation 156 by p:

$$\frac{s\beta}{p} + \frac{r}{p} - \frac{g}{sV_o} = \frac{g}{V_o}\frac{n_y}{p} \tag{157}$$

$$\text{or} \quad \left[\frac{\beta}{p}\right] = \frac{1}{s}\left\{\frac{g}{V_o}\left(\left[\frac{n_y}{p}\right] + \frac{1}{s}\right) - \left[\frac{r}{p}\right]\right\}$$

Consider measuring the parameters n_y, p, r, β, etc.

$$\left.\begin{aligned} \frac{p_{TRACE}}{p_{TRUE}} &= \frac{K_p}{\tau_p s+1}, \qquad \frac{r_{TRACE}}{r_{TRUE}} = \frac{K_r}{\tau_r s+1} \\ \frac{n_{y_{TRACE}}}{n_{y_{TRUE}}} &= \frac{K_{n_y}}{\tau_{n_y} s+1}, \qquad \frac{\beta_{TRACE}}{\beta_{TRUE}} = \frac{K_\beta}{\tau_\beta s+1} \end{aligned}\right\} \tag{158}$$

where K = gain in inches of trace per deg/sec, etc.

τ = total equivalent first-order lag of circuit including response of measuring sensor and any filters and the recorder

s = frequency of Dutch roll maneuver

Since the accelerometers are not at the c.g.,

$$n_y = n_{y_{MEAS}} - (pq + \dot{r})x + (r^2 + p^2)y - (rq - \dot{p})z$$

For the T-33, $y = z = 0$ (see Figure 68).
Assuming $q = 0$, we have

$$n_y = n_{y_{MEAS}} - x\dot{r} \tag{159}$$

Substituting Equation 159 into 157 gives:

$$\left[\frac{\beta}{p}\right]_{TRUE} = \frac{1}{s}\left\{\frac{g}{V_0}\left(\frac{n_{y_{MEAS}}}{p_{TRUE}} - sxr + \frac{1}{s}\right) - \left[\frac{r}{p}\right]_{TRUE}\right\} \tag{160}$$

and from Equations 158:

$$\left.\begin{aligned} \left[\frac{r}{p}\right]_{TRUE} &= \frac{K_p}{K_r}\left(\frac{\tau_r s+1}{\tau_p s+1}\right)\left[\frac{r}{p}\right]_{TRACE} \\ \frac{n_{y_{MEAS}}}{p_{TRUE}} &= \frac{K_p}{K_{n_y}}\left(\frac{\tau_{n_y} s+1}{\tau_p s+1}\right)\left[\frac{n_y}{p}\right]_{TRACE} \end{aligned}\right\} \tag{161}$$

hence 160 becomes:

$$\left[\frac{\beta}{p}\right]_{TRUE} = \frac{1}{s}\left\{\frac{g}{V_0}\left[\frac{K_p}{K_{n_y}}\left(\frac{\tau_{n_y} s+1}{\tau_p s+1}\right)\left[\frac{n_y}{p}\right]_{TRACE} - sx\,r_{TRACE}\,\frac{\tau_r s+1}{K_r} + \frac{1}{s}\right] - \frac{K_p}{K_r}\left(\frac{\tau_r s+1}{\tau_p s+1}\right)\left[\frac{r}{p}\right]_{TRACE}\right\} \tag{162}$$

We have seen earlier (Equation 155)

$$\beta_{\substack{PROBE \\ MEAS}} = \left[\frac{\beta_{PROBE}}{\beta_{TRUE}}\right]_{c.g.}\left[\beta_{\substack{TRUE \\ c.g.}} + \frac{rx}{V_0}\right] - \frac{pz}{V_0}$$

$$= \beta_{TRACE}\left(\frac{\tau_\beta s+1}{K_\beta}\right) \qquad \text{from Equation 158.}$$

Dividing by p_{TRACE}, we get

$$\left[\frac{\beta}{p}\right]_{TRACE}\left(\frac{\tau_\beta s+1}{K_\beta}\right)=\left\{\left[\frac{\beta_{PROBE}}{\beta_{TRUE}}\right]_{c.g.}\left(\left[\frac{\beta}{p}\right]_{TRUE}+\frac{v}{V_0}\left[\frac{r}{p}\right]_{TRUE}\right)-\frac{y}{V_0}\right\}\frac{p_{TRUE}}{p_{TRACE}} \tag{163}$$

Solving for $\left[\frac{\beta_{PROBE}}{\beta_{TRUE}}\right]_{c.g.}$, we have

$$\left[\frac{\beta_{PROBE}}{\beta_{TRUE}}\right]_{c.g.}=\left\{\left[\frac{\beta}{p}\right]_{TRACE}\left(\frac{\tau_\beta s+1}{K_\beta}\right)\frac{p_{TRACE}}{p_{TRUE}}+\frac{y}{V_0}\right\}\left\{\frac{1}{\left[\frac{\beta}{p}\right]_{TRUE}+\frac{v}{V_0}\left[\frac{r}{p}\right]_{TRUE}}\right\} \tag{164}$$

This can be evaluated using

$\left[\frac{\beta}{p}\right]_{TRACE}$ as measured from the β and p traces

$\frac{p_{TRACE}}{p_{TRUE}}$ from Equation 158

$\left[\frac{\beta}{p}\right]_{TRUE}$ from Equation 162

$\left[\frac{r}{p}\right]_{TRUE}$ from Equation 161

together with the estimated τ values and calibration factors, K.

AN ALTERNATE TECHNIQUE FOR DETERMINING $\beta_{VANE}/\beta_{TRUE}$ POSITION ERROR CORRECTION FACTOR

The following is an alternate method used to determine the $\frac{\beta_{VANE}}{\beta_{TRUE}}$ position error correction factor. It disregards the dynamics of the sensor, assumes linearity of the system and minimizes the effect of the probe not being at the c.g.

1. Obtain a high frequency, zero-damped, low $|\phi/\beta|_d$ Dutch roll record. For this condition $|\phi/\beta|_d \approx 0$, $\zeta_d \approx 0$, $p \approx 0$ and the center of gravity of the airplane essentially tracks a straight line through the air so that $n_{y_{c.g.}} \approx 0$.

   From $\dot{\beta}-p\alpha+r-\left(\frac{g}{V_0}\right)\phi=\left(\frac{g}{V_0}\right)n_{y_{c.g.}}$

   and $\dot{\beta}=\beta\omega_d$ for $\zeta_d \approx 0$

$$\dot{\beta}_T=\frac{\dot{\beta}_T}{\omega_d}=\frac{p\alpha}{\omega_d}-\frac{r}{\omega_d}+\left(\frac{g}{V_0}\right)\frac{\phi}{\omega_d}+\left(\frac{g}{V_0}\right)n_{y_{c.g.}} \tag{165}$$

since $n_y \approx \phi \approx p \approx 0$

$$\beta_T \approx -\frac{r}{\omega_d} \approx -\psi$$

Therefore

$$\left|\frac{\beta_{VANE}}{\beta_{TRUE}}\right| \approx \left|\frac{\beta_{VANE}}{\psi}\right| \approx \left|\frac{\beta_{VANE}\,\omega_d}{r}\right| \tag{166}$$

2. Measure the double amplitude of the β trace and r trace and ω_d from the Dutch roll record

$$\frac{\beta_{VANE}}{\beta_{TRUE}} \approx \frac{|\beta_{TRACE}|\left(\frac{\beta_{VANE}}{\beta_{TRACE}}\right)}{|r_{TRACE}|\left(\frac{r_{TRUE}}{r_{TRACE}}\right)}$$

A third method that can be used to determine the $\left(\frac{\beta_{VANE}}{\beta_{TRUE}}\right)$ position error correction factor is to use the terms of Equation 156.

$$\dot{\beta}_I = \frac{57.3g}{V} n_{y_{c.g.}} + \frac{g}{V}\phi - r + \frac{\alpha_I}{57.3} p \tag{167}$$

determine the values of $n_{y_{c.g.}}$, ϕ, r, p, and use average trim value for α_I, $\alpha_I = \alpha_{TRIM}$ and calculate $\dot{\beta}_I$.

Then

$$\left[\frac{\beta_{VANE}}{\beta_{TRUE}}\right] = \frac{\Delta\beta_V}{\Delta\beta_I} = \frac{\Delta\dot{\beta}_V}{\Delta\dot{\beta}_I} \tag{168}$$

Two further methods for estimating the position error correction factor are available. The first, described by Bradley in Reference 7, involves flight test work, and has not been done.

The other method, described in Reference 8, presents parametric curves of flow around various fineness ratio ellipsoids of revolution. The correction factor is determined from the curves by estimating the equivalent shape of the airplane nose and by a knowledge of the sensor location. Because of the difficulty in defining the equivalent nose shape, the results cannot be considered as reliable as those obtained by the flight test methods. However, they do give a first-order estimate which may be of use on a new airplane, or if the probe needs relocating.

The value currently in use for the β probe position error correction (at 250 knots IAS, 23,000 feet, M = 0.6) is:

$$\left[\frac{\beta_{PROBE}}{\beta_{TRUE}}\right]_{c.g.} = 2.1$$

This value was obtained using the high frequency, zero damped, low $|\phi/\beta|_d$ technique described on page 10-6.

Figure 69 shows the estimated Mach number variation for the correction factor $\left(\frac{\beta_{PROBE}}{\beta_{TRUE}}\right)_{c.g.}$ which is based on the flow around an ellipsoid of revolution, factored to pass through the known point at M = 0.6.

Angle-of-Attack Position Error Corrections

The incidence measured by the vane is

$$\alpha_{\substack{VANE \\ MEAS}} = \left[\frac{\alpha_{VANE}}{\alpha_{TRUE}}\right]_{c.g.} \left[\alpha_{\substack{TRUE \\ c.g.}} - \frac{qx}{V}\right] + \frac{py}{V} \tag{169}$$

This can be solved for α_{TRUE} at the c.g.

$$\alpha_{\substack{TRUE \\ c.g.}} = \frac{1}{\left[\frac{\alpha_{VANE}}{\alpha_{TRUE}}\right]_{c.g.}} \left[\alpha_{\substack{VANE \\ MEAS.}} - \frac{py}{V}\right] + \frac{qx}{V} \tag{170}$$

The coordinates x and y are given on Table IV.

$\left[\frac{\alpha_{VANE}}{\alpha_{TRUE}}\right]$ is determined as outlined below.

Trim is established at high fuel remaining and again with low fuel remaining. The angle of attack is measured and plotted versus C_L for the appropriate weight, thus giving a plot of C_L vs. α_{VANE}. Since $C_{L_{\alpha_{TRUE}}}$ is known from wind tunnel data, the vane correction factor can be found from the expression:

$$\Delta C_{L_{\alpha_{VANE}}} \Delta\alpha_{VANE} = \Delta C_{L_{\alpha_{TRUE}}} \Delta\alpha_{TRUE}$$

$$\left[\frac{\alpha_{VANE}}{\alpha_{TRUE}}\right]_{c.g.} = \frac{\Delta C_{L_{\alpha_{TRUE}}}}{\Delta C_{L_{\alpha_{VANE}}}} \tag{171}$$

The estimated variation of this correction factor with Mach number is shown on Figure 69.

The value currently in use for the α vane position error correction (at 250 KIAS, 23,000 feet, M = 0.6) is

$$\left[\frac{\alpha_{VANE}}{\alpha_{TRUE}}\right]_{c.g.} = 1.7$$

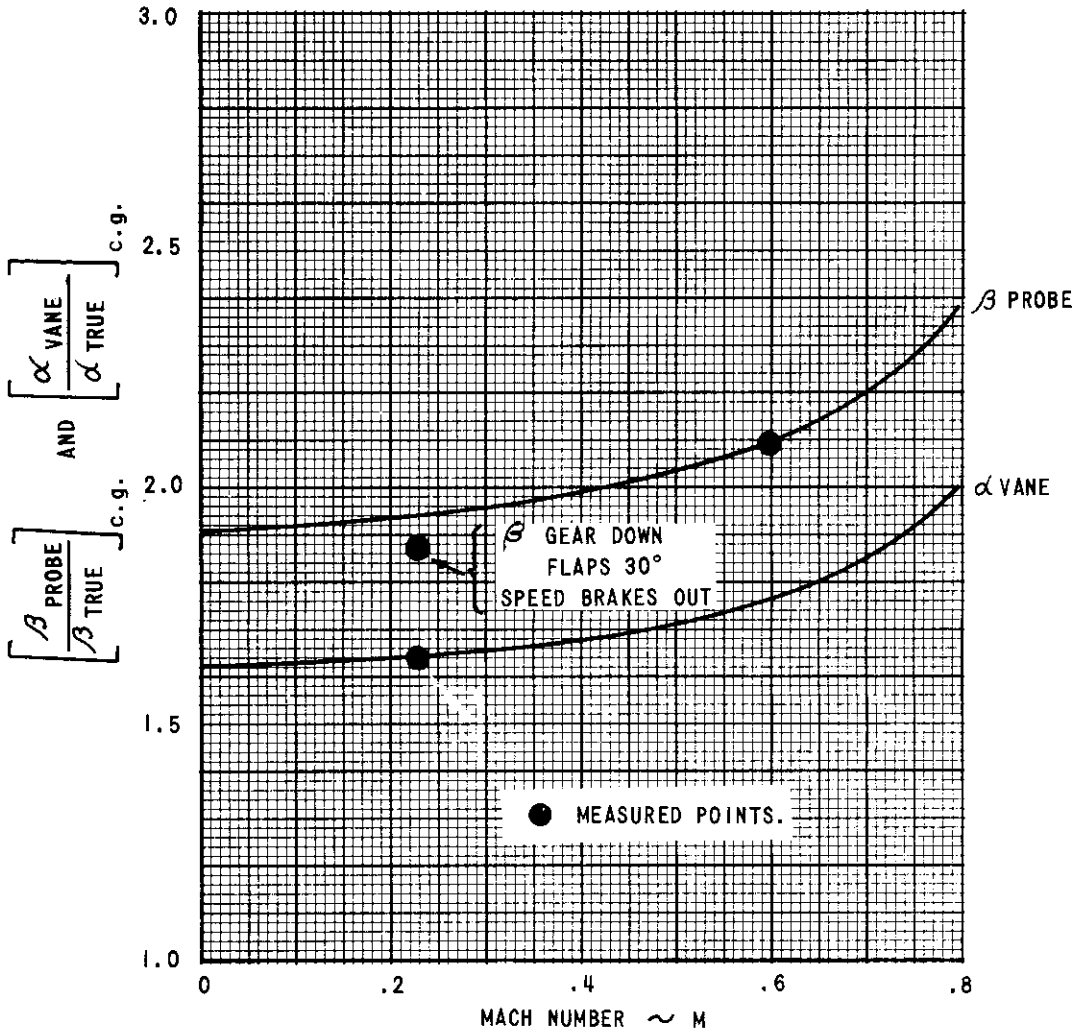

ESTIMATED MACH NUMBER VARIATION CORRESPONDS TO FLOW AROUND AN ELLIPSOID OF REVOLUTION REF: SHAPIRO, COMPRESSIBLE FLOW, VOL I. PG 399

Figure 69 α VANE AND β PROBE CORRECTION FACTORS VARIATIONS WITH MACH NUMBER.

ACCELEROMETER POSITION ERROR CORRECTIONS

The normal (n_z), lateral (n_y) and longitudinal (n_x) linear accelerometers are aligned with the aircraft's reference axes and located relative to the c.g. as shown on Figure 68.

The position error corrections are calculated with respect to the center of gravity and since the center of gravity changes as a function of fuel remaining, it is necessary to take into account the effect of fuel remaining on position error corrections. Table IV, page 10-3 is presented which gives the distance measurements to be used as a function of fuel remaining.

Expressions for the acceleration of the c.g. in terms of the accelerometer coordinates and the aircraft rates of rotation about aircraft reference body axes are:

$$n_{x_{c.g.}} = n_{x_{MEAS}} + \frac{1}{g}\left[x(q^2+r^2) - y(qp-\dot{r}) - z(rp+\dot{q})\right] \tag{172}$$

$$n_{y_{c.g.}} = n_{y_{MEAS}} + \frac{1}{g}\left[-x(pq+\dot{r}) + y(r^2+p^2) - z(rq-\dot{p})\right] \tag{173}$$

$$n_{z_{c.g.}} = n_{z_{MEAS}} + \frac{1}{g}\left[-x(pr-\dot{q}) - y(rq+\dot{p}) + z(p^2+q^2)\right] \tag{174}$$

where x, y, z are the coordinates of the accelerometer measured from the c.g. (Figure 68 and Table IV).

ATTITUDE AND RATE GYRO POSITION ERRORS

The attitude and rate gyros are aligned with the appropriate aircraft reference and therefore have zero position error.

PITOT-STATIC-DYNAMIC PRESSURE ($\bar{q}_c$) POSITION ERROR

The pitot static system is calibrated on the ground by applying known increments of pressure to the pitot tube. Readings are taken on the front and rear cockpit airspeed indicator and recorded on oscillograph records. Airspeed position error correction factors from the T-33 Flight Manual (T.O. IT-33A-1) can be applied to indicated airspeed readings if dictated by the needs of a particular flight program being conducted.

SENSOR DYNAMICS

Amplitude and phase response characteristics of the variable stability channels have a significant effect on the success of accurate simulation work

done with the T-33 airplane. Therefore, it is important to have the various channel responses and feedback loop responses defined as accurately as possible.

The best way to determine the response of a particular VSS channel (e.g., δ_r/β) is to perform a frequency response test on it so that all the components are included. This has been done on some channels for some programs and more of this will be done in the future.

In lieu of measured channel lag data for a particular channel, another technique can be used. It consists of representing the dynamics of each individual component (sensor, filter, etc.) as a lag which can be added to all the other lags in the loop to give an overall equivalent lag. These component lags are determined using measured amplitude and phase response data whenever possible. When no measured data on a component is available, an equivalent lag can be estimated based on knowledge of the natural frequency and damping of the component obtained from the manufacturer's data sheet.

Data on sensor dynamics and lags is presented in this section. Included in the lag of the various sensors is the lag of the demodulator (if the sensor output is a.c.) and the demodulator third-order low-pass filter. It is convenient to combine the demodulator and filter lags with the sensor lags since none of these components is subject to change due to program requirements. Data on other portions of the channel such as filters and differentiators are presented in Appendix VI.

PROBE DYNAMICS DUE TO ELECTRONICS

The dynamics of the β probe (from probe input to 80 Hz third-order low-pass filter output) have been the determined by digitally analyzing the response to an electrical step change to the probe excitation. See Appendix VI. for data and procedure.

DETERMINATION OF SIDESLIP PROBE LAG IN ALIGNING WITH RELATIVE WIND

The time lag of the rudder and aileron servos in response to the output of the sideslip probe was determined by mechanically driving the probe with an oscillating table and recording the output of the probe and the servo strut feedback signal on the oscillograph. This technique, of course, does not evaluate the lag of the probe in aligning itself with the relative wind and neglects the small effect which the airloads will have on the servo response. The following indirect technique was used to estimate the total channel lag for the δ_r/β_{TRUE} channel.

For a Dutch roll free oscillation, the β_T and $\dot{\beta}_T$ signals can be represented by the following diagram.

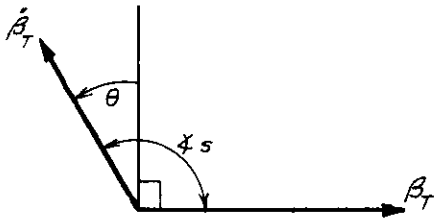

$$\dot{\beta}_T = s\beta_T$$

$$|\dot{\beta}_T| e^{i\angle s} = |s||\beta_T| e^{i\angle s}$$

$$s = \omega_n e^{i(90+\theta)}$$

$$\zeta = \sin\theta$$

Force and moment diagrams can be obtained by multiplying the β_T and $\dot{\beta}_T$ vectors by the appropriate stability derivatives. Also in the diagrams, the magnitude of $\dot{\beta}_T$ has been written in terms of ω_n and β_T.

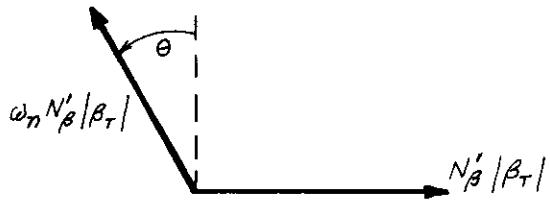

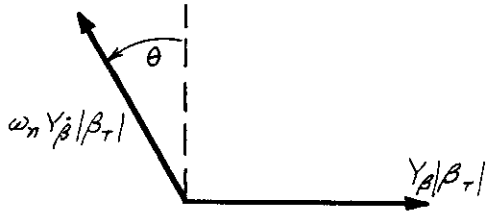

The effect of the variable stability gain δ_r/β_v is to add a force and a moment to the airplane which lag the β_T variations. The following expressions represent the force and moment produced by the artificial stability system.

$$Y = Y_{\delta_r} \left|\frac{\delta_r}{\beta_v}\right| \left|\frac{\beta_v}{\beta_T}\right| |\beta_T| e^{-i\phi} = |Y||\beta_T| e^{-i\phi} \tag{175}$$

$$N = N_{\delta_r} \left|\frac{\delta_r}{\beta_v}\right| \left|\frac{\beta_v}{\beta_T}\right| |\beta_T| e^{-i\phi} = |N||\beta_T| e^{-i\phi} \tag{176}$$

If these force and moment vectors are added to the diagrams, we have:

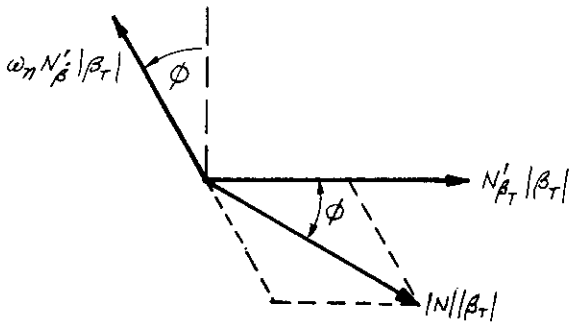

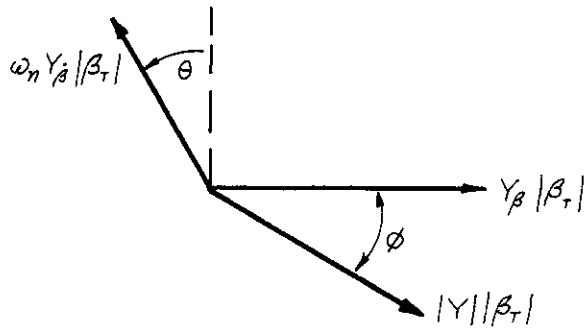

If the artificial stability force and moment vectors are resolved into components along β_T and $\dot{\beta}_T$, we get the following expressions for the incremental forces and moments in phase with β_T and $\dot{\beta}_T$

$$\Delta N'_{\beta_T} |\beta_T| = |N||\beta_T| [\cos\phi - \sin\phi \tan\theta]$$

$$\omega_n \Delta N'_{\dot{\beta}_T} |\beta_T| = -|N||\beta_T| \sin\phi/\cos\theta \tag{177}$$

$$\omega_n \Delta Y_{\dot{\beta}} |\beta_T| = -|Y||\beta_T| \sin\phi/\cos\theta$$

$$\Delta Y_{\beta} |\beta_T| = |Y||\beta_T| [\cos\phi - \sin\phi \tan\theta]$$

Consider next the following approximate equations for the Dutch roll mode characteristics. The Dutch roll frequency can be approximated by

$$\omega_n^2 = N'_{\beta_T} + Y_{\beta_T} N'_r \tag{178}$$

For the T-33 airplane, the second term is negligible; thus

$$\omega_n^2 \approx N'_{\beta_T} \tag{179}$$

The Dutch roll damping can be approximated for the T-33 by the following expression:

$$2\zeta_d \omega_d = N'_{\beta_T} - Y_{\beta_T} - N'_r \tag{180}$$

As discussed above, the δ_r/β variable stability gain causes increments in Y_{β_T} and also N'_{β_T} because of the system lags. Writing Equation 177 for two values of δ_r/β gain and subtracting, we get:

$$2\zeta_{d_1} \omega_{n_1} - 2\zeta_{d_0} \omega_{n_0} = \Delta N'_{\dot{\beta}_T} - \Delta Y_{\beta_T} \tag{181}$$

Next, from the ratio

$$\frac{2\zeta_{d_1} \omega_{n_1} - 2\zeta_{d_0} \omega_{n_0}}{\omega_{n_1}^2 - \omega_{n_0}^2} = \frac{\Delta N'_{\dot{\beta}_T} - \Delta Y_{\beta_T}}{\Delta N'_{\beta_T}} \tag{182}$$

and substitute for the $\Delta N'_{\beta_T}$, $\Delta N'_{\dot{\beta}_T}$ and ΔY_{β_T} terms from Equations 177:

$$\frac{2\zeta_{d_1}\omega_{n_1} - 2\zeta_{d_o}\omega_{n_o}}{\omega_{n_1}^2 - \omega_{n_o}^2} = \frac{\frac{-1}{\omega_{n_1}}|N|\frac{\sin\phi}{\cos\theta} - |Y|[\cos\phi - \sin\phi\tan\theta]}{|N|[\cos\phi - \sin\phi\tan\theta]}$$

$$= \frac{-\frac{1}{\omega_{n_1}}\frac{\sin\phi}{\cos\theta} + \frac{Y_{\delta_r}}{N'_{\delta_r}}[\cos\phi - \sin\phi\tan\theta]}{[\cos\phi - \sin\phi\tan\theta]}$$

$$= \frac{-\frac{1}{\omega_{n_1}}\frac{1}{\cos\theta} + \frac{Y_{\delta_r}}{N'_{\delta_r}}\left[\frac{1}{\tan\phi} - \tan\theta\right]}{\left(\frac{1}{\tan\phi} - \tan\theta\right)} \qquad (183)$$

$$= A$$

Then, rearranging to solve for ϕ:

$$A\left[\frac{1}{\tan\phi} - \tan\theta\right] = \frac{-1}{\omega_{n_1}\cos\theta} - \frac{Y_{\delta_r}}{N'_{\delta_r}}\left[\frac{1}{\tan\phi} - \tan\theta\right]$$

$$\omega_{n_1}\cos\theta\left[\frac{1}{\tan\phi} - \tan\theta\right]\left[A + \frac{Y_{\delta_r}}{N'_{\delta_r}}\right] = -1$$

$$\left[\frac{1}{\tan\phi} - \tan\theta\right] = \frac{-1}{\omega_{n_1}\cos\theta\left[A + \frac{Y_{\delta_r}}{N'_{\delta_r}}\right]} \qquad (184)$$

$$\frac{1}{\tan\phi} = \tan\theta - \frac{1}{\omega_{n_1}\cos\theta\left[A + \frac{Y_{\delta_r}}{N'_{\delta_r}}\right]}$$

$$\tan\phi = \left(\frac{1}{\tan\theta - \frac{1}{\omega_{n_1}\cos\theta\left[A + \frac{Y_{\delta_r}}{N'_{\delta_r}}\right]}}\right)$$

If $\zeta_{d_1} = 0$, then $\theta = 0$, and the expression reduces to

$$\tan\phi = \omega_{n_1}\left(\frac{2\zeta_o\omega_{n_o}}{\omega_{n_1}^2 - \omega_{n_o}^2} - \frac{Y_{\delta_r}}{N'_{\delta_r}}\right) \qquad (185)$$

If the lag can be represented as a linear phase shift up to the frequencies of interest (see Appendix VII), then the total channel lag, τ, between the β probe and rudder strut is given by

$$\omega_{n_0} \tau_{\beta,\delta_r} = \phi \tag{186}$$

and $$\tau_{\beta,\delta_r} = \frac{\phi}{\omega_{n_0}}$$

The lag of the probe to rudder system, τ_{β_p,δ_r}, can be determined by mechanically driving the probe with an oscillating table and recording the output of the probe and rudder surface position pickoff. The actual probe lag is given by the difference between the two lags $\tau_{\beta,\delta_r} - \tau_{\beta_p,\delta_r} = \tau_{\beta_p}$.

An example of this method has been calculated using the data from a calibration flight to determine δ_r/β versus RD knob setting. The frequency and damping ratio are plotted versus RD on Figure 70. From this data, ϕ was calculated and plotted versus ω_{n_0}, (also on Figure 70). The slope of this line gives $\tau_{\beta,\delta_r} = 0.098$ seconds.

NOTE: These probe lag data were taken with variable stability electronics which have since been replaced by equipment using solid state electronics. Data using the old system are presented here to show technique.

ANGLE OF ATTACK VANE (α VANE) DYNAMICS

To determine the in-flight dynamic characteristics of the α vane, the vane output was recorded with a special oscillograph galvanometer (CEC type 7-315 with proper damping but no filtering). The response of this galvanometer was flat out to 60 Hertz. The recorded signal characteristically showed a high frequency lightly damped oscillation at approximately 32 Hz and $\zeta = 0.1$ (at 250 KIAS) for the range of frequencies of interest (i.e., $\omega/\omega_n \leq 1/60$). This can be represented by a linear phase shift with a lag of 0.002 sec, see Appendix VII.

ANGLE OF ATTACK VANE DYNAMICS DUE TO ELECTRONICS

The dynamics of the α vane (from vane input to 60 Hz third-order low-pass filter output) have been determined by digitally analyzing the response to an electrical step change to the vane excitation. See Appendix VI for data and procedure.

ACCELEROMETER (n_x, n_y , n_z) DYNAMICS

The dynamics of the n_x, n_y , n_z linear accelerometers were determined by digitally analyzing the response of the accelerometer to a step input. The

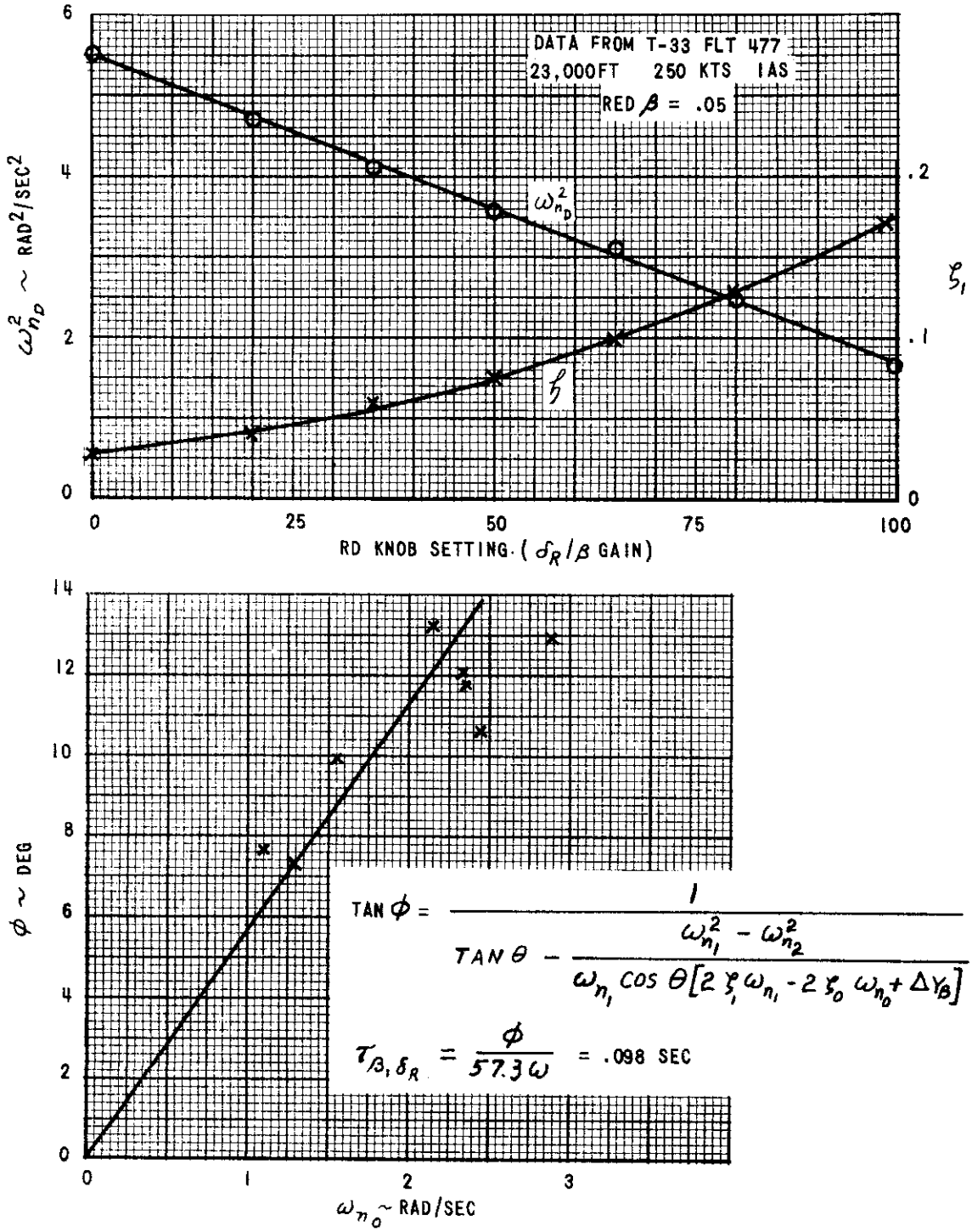

Figure 70 DETERMINATION OF β PROBE LAG

electrical step was applied through the accelerometer self-test input to the accelerometer and the response was recorded at the output of the 25 Hz second-order low-pass filter. The data were then analyzed and are presented as amplitude and phase response data in Appendix VI.

RATE GYRO DYNAMICS

The dynamics of the p, q and r rate gyros were determined by analyzing the response of the gyros to a step input. The electrical step was applied through the gyro self-test input to the gyro and the response was recorded at the output of the 80 Hz third-order low-pass filter. The data were then analyzed and are presented as amplitude and phase response data in Appendix VI.

ATTITUDE GYRO (ϕ, θ) DYNAMICS

The dynamics of the Lear model 7000E attitude gyro (ϕ, θ) were not measured primarily due to the difficulty of not having a rate table or other means large enough to mount and properly excite a package the size of the attitude gyro.

Published data on the gyro indicate, however, that the response is second order in nature and very fast (-3db at 100 Hertz). This is very much faster than the frequencies of interest (airplane and servo frequencies) which are normally 10 Hertz or less.

SECTION XI
CALIBRATION OF THE VARIABLE STABILITY GAINS

GROUND CALIBRATIONS

Sensor Calibrations

The VSS equipment contains the following sensors α, β, ϕ, θ, r, p, q, $\bar{q}_c$, n_x, n_y, n_z and front cockpit control inputs F_{ES}, δ_{ES}, F_{RP}, δ_{RP}, F_{AS}, δ_{AS}. Each of these sensors and control inputs to the VSS is an input to an operational amplifier. For a given sensor or control input change, there is a corresponding predictable voltage change at a designated amplifier output (e.g., ±20 degrees of α_v equals ±10.0 V). These calibration (scale factors) factors are verified at periodic intervals (usually at the beginning and end of a flight program). Each sensor and control input scale factor is checked by comparing measured sensor movements to the sensor output which is a d.c. signal measured with a digital voltmeter. This is done one sensor at a time, by using the calibration fixtures provided for this purpose.

Each sensor and control signal output is recorded on both the oscillograph and digital recorder. The recording system is calibrated by taking records with the sensor set at known values of the parameter with the calibration fixtures provided. Enough data points are taken to define an actual slope. The oscillograph data is plotted on graph paper with the parameter increments plotted against oscillograph trace movement. The plots are kept in a notebook used by the T-33 project engineer and the slopes obtained from the plots are recorded on a "T-33 Oscillograph/Digital Recording Data Sheet." (See Figure 71). Copies of this sheet are placed in each flight folder.

Parameter changes versus d.c. voltage are also plotted and slopes obtained. This data which also appears on the recording data sheet noted above is used in data analysis using the digital recording system.

Provisions have been made to conveniently substitute known test signals in place of sensor signals. Once the sensor and control scale factors are known, the test signals can be used for checking VSS channel gains and all other calibrations throughout the remainder of VSS equipment. The VSS, which is a d.c. system having operational amplifiers, can then be treated as an analog computer.

Self-Test of Sensors

Some of the sensors have self-test capability. These are the p, q, r rate gyros, and the n_x, n_y, n_z accelerometers. By actuating a toggle switch on the VSS chassis, a sensor can be checked easily and quickly for proper output over a range of values.

T-33 OSCILLOGRAPH/DIGITAL RECORDING SYSTEM

LANDING APPROACH PROGRAM, WINTER 1969

DIGITAL RECORDER

DIGITAL CHANNEL NO. SEE NOTE (4)	GAIN SEE NOTE (5)	SCALE FACTOR (X PER VOLT) DIG. RECORDER-FULL SCALE = ±10.23V	GALV. NO.	RECORDED VARIABLE	RECORDING MASTER UNIT VOLTS/INCH	CALIBRATION FACTOR (X PER INCH)
1		+1.0 DEG	1	$\Delta\alpha_v$	2.0	+1.96 DEG
2		+2.53 DEG	2	δ_e	1.0	+2.53 DEG
3		+.051 PSI	3	$\Delta\bar{q}_c$	1.0 (250 KT.)	+.051 PSI (+3.89 KT)
4		+4.96 DEG/SEC	4	q	1.0	+5.96°/SEC
13		+1.00 DEG	5	β_v	5.0	+4.785 DEG
6		+5.25 DEG/SEC	6	r	.5	+2.50°/SEC
23		+5.17 DEG/SEC^2	7	$\dot{\beta}_v$	1.0	+4.84°/SEC
14		+24.82 DEG/SEC^2	8	$\dot{r}$	1.0	+26.53°/SEC^2
15		+50.63 DEG/SEC^2	9	$\dot{p}$	1.0	+50.0°/SEC^2
			10	SINE WAVE GEN	OFF	--
11		+10.00 DEG	11	ϕ	.5	+4.68 DEG
12		+10.00 DEG/SEC	12	p	.5	+4.76°/SEC
		+26.66 DEG/SEC^2	13	q	.5	+12.50°/SEC
		--	14	n_x	1.0	--
		+4.78 DEG/SEC	15	$\dot{\omega}_v$	1.0	+4.78°/SEC
16		+.5g	16	n_z	1.0	+4.88g
17		+.05g	17	n_y	1.0	+.0476g
			18	$\delta_{y_{ST}}$	1.0	--
			19	ϕ	0.1	+1.01 DEG
20		+5.19 DEG	20	δ_r	1.0	+4.40 DEG
21		+4.0 DEG	21	δ_{at}	1.0	+3.83 DEG
			22	$\delta_{e_{COM}}$	1.0	+2.0 DEG
7		+8.94 LBS	23	F_{AS}	.5	+4.18 LB
			24	--	OFF	--
			25	--	OFF	--
6		+23.0 LBS	26	F_{ES}	.5	+11.3 LB

Figure 71 TYPICAL RECORDING SYSTEM CALIBRATION DATA SHEET

Sensor Calibration Techniques and Equipment

Rate Gyro Package Calibration - p, q, r in One Unit

Equipment: Inland Control model 722 rate table.

Procedure:

The rate gyro package is removed from the aircraft and mounted on the Inland Control rate table such that motions will occur in the desired plane (p, q, or r). A test cable connects the gyro package to the VSS. The rate gyro is driven at specified rates and measurements are made with a digital voltmeter and oscillograph records are taken.

α Vane, β Probe Calibration

Equipment: Special calibrated vane and probe fixtures.

Procedure:

These special calibrated fixtures fasten to the fuselage at the vane and probe. The vane and probe can then be moved in known increments of degrees and the vane and probe voltages measured at appropriate amplifier outputs.

NOTE: The α vane and β probe correction factors must be applied then to get α_{TRUE} and β_{TRUE}.

Alternate α Vane, β Probe Calibration Technique

Equipment: Micro Gee oscillating rate table.

Procedure:

Alternate and less suitable technique (due to the complexity of the equipment set up) is as follows:

The Micro Gee table is positioned under the α vane and is connected to the vane using the special α calibration hardware provided. The vane position is read, in degrees, directly off the table position indicator. The β probe calibration is similar except that the table is positioned in front of the airplane and different calibration hardware, a system of channel irons, pulleys, cord, and weights, translates table movement into β probe movement. β probe rotation is read directly off the table position indicator.

Linear Accelerometer (n_x, n_y, n_z) Calibration

Equipment: Calibrated tilt table and level

Procedure:

The accelerometer package is removed from the aircraft and mounted on a calibrated tilt table. The table is calibrated in 0.1 g steps with a maximum of ±1.0 g. The accelerometer package position on the table is different for each of the three accelerometers. A test cable connects the accelerometer package to the VSS. The table is moved in steps and voltage and oscillograph records taken. The level is used to adjust the table for a level condition in respect to earth since earth gravity is used in calibrating the accelerometers.

Attitude Gyro (ϕ, θ) Calibration

Equipment: Inclinometer and tilt plate.

Procedure:

The attitude gyro is removed from the aircraft and placed on a metal plate approximately 1 foot square. The plate is then tilted and the inclination measured with the inclinometer positioned on the plate next to the attitude gyro. Voltage and oscillograph records are taken at each increment of inclination. The inclination steps are done both in the bank angle (ϕ) and pitch (θ) axis of the gyro.

Control Surface (δ_a, δ_e) Calibration

Equipment: Inclinometer

Procedure:

Elevator and aileron surface position measurements are made with an inclinometer placed on the control surface. The VSS hydraulic system is off and the surface is positioned by hand. Voltage and oscillograph records are taken at each increment of surface travel. For the aileron surface, one surface (δ_{a_L} or δ_{a_R}) is measured; however, the data is plotted in terms of total included aileron angle travel δ_{a_T} which is δ_{a_L} or δ_{a_R} increments times 2.

Control Surface (δ_r) Calibration

Equipment: Template Protractor

Procedure:

A template protractor is used for the rudder surface. The protractor is attached to the fuselage at the base of the rudder surface and rudder position is read directly off the protractor in degrees. Hydraulics are turned off and the surface is positioned in increments by hand.

Front Cockpit Control Stick (δ_{AS}, δ_{ES}) Calibration

Equipment: Calibration fixture

Procedure:

The calibration fixture which consists of a piece of plexiglass with a grid network graduated to read inches at the pilot's hand grip is mounted in the front cockpit. Stick movement in inches is read off the calibration fixture using a pointer taped to the stick at the pilot's grip. Control Wheel Configuration: (δ_{EW}) is measured with a ruler using the front instrument panel as a reference. (δ_{AW}) is measured with an inclinometer and is in degrees rather than inches. An angle bracket is fastened across the top of the control wheel and the inclinometer is placed on the angle bracket. For aileron (F_{AW}) measurements, the wheel is first centered by aligning a mark on the wheel with a mark on the control column. This is defined as F_{AW} = 0 degrees.

Front Cockpit Rudder Pedal (δ_{RP}) Calibration

Equipment: Six foot steel tape

Procedure:

A steel tape is used to measure front cockpit pedal displacement. Measurements are made from each rudder pedal to some convenient point aft of the rudder pedals (a screw head on the oxygen regulator valve is normally used for the left rudder pedal and a screw head on the seat for the right rudder pedal).

NOTE: δ_{ES}, δ_{AS}, δ_{RP} measurements should be accomplished with the hydraulic system energized and with the feel system spring rates set up as they will be used in the flight program. Use of the proper spring rates minimizes δ_{AS}, δ_{ES}, δ_{RP} calibration errors due to control column bending and control cable stretching.

Front Cockpit Stick and Rudder Force (F_{AS}, F_{ES}, F_{EP}) Calibration

Equipment: Force gage.

Procedure:

The VSS is engaged electrically and hydraulically and a hand-held force gage is used for the F_{ES}, F_{AS} calibrations. For F_{RP} the gage is placed between the rudder pedal and the foot. Known increments of force are applied and voltage and oscillograph records are taken.
Wheel Configuration: F_{EW} - a hand-held force gage is used. F_{AW} - this calibration is done by hanging a set of weights (1 - 5 lb range) on the outside edge of the control wheel, first on one side and then the other. Voltage and oscillograph records are taken as increments of force are applied.

Pitot System ($\bar{q}_c$) Calibration

Equipment: Air tank, accurate pressure gage, rubber hoses

Procedure:

This channel is calibrated with an air tank and an accurate pressure gage. The air tank and gage are connected to the aircraft pitot tube. Readings are taken on the front airspeed indicator as well as on the pressure gage for each voltage reading and oscillograph record.

Derivative Signal ($\dot{\alpha}$, $\dot{\beta}$, $\dot{r}$, $\dot{p}$, $\dot{q}$, $\dot{\bar{q}}_c$) Calibration

Equipment: Sine wave signal generator

Procedure:

These channels are calibrated by substituting a test signal instead of a sensor movement. A signal generator is used to generate a sine wave as the input to the differentiator network. The output of the differentiator is oscillograph recorded. The oscillograph data is plotted against the calculated differentiator output. Enough points are taken to provide a slope with calculated differentiator output as the ordinate and oscillograph deflections in inches as the abscissa.

Calibration of Channel Gains

Rear cockpit gain controls are potentiometers with dials (000 to 999 with zero volts output at 500). These potentiometers control the amplitude of sensor and feel system control inputs that drive the control surfaces.

Sign convention has been established such that for potentiometer settings between 500 and 999 (for the sensors) a "+" sensor movement results in a positive control surface deflection and for potentiometer numbers below 500, i.e., 000 to 500 a "+" sensor movement results in a negative control surface movement. Feel system control inputs have only one sign and 000 setting is null (zero volts output). Figure 72 shows the control surface, feel system and angular rate sense notation used in T-33 program work.

Another set of gain controls adjustable in steps is connected electrically in series with these rear cockpit gain controls. These step adjustable gain controls are located in the nose of the airplane on the control surface servo chassis and are commonly called nose gains. These nose gains can only be set on the ground and are designed primarily to expand the scale of the safety pilot controlled gain settings.

The VSS channels are calibrated one at a time by selecting a convenient nose gain setting and then moving the appropriate sensor a known amount. Oscillograph records are taken with the appropriate rear cockpit gain control changed in increments of 100 digits starting at 500 (null) and increasing toward 999 and also decreasing to 000.

The ratio of oscillograph trace deflections of surface to sensor is then plotted versus gain control setting. Calibration factors for a particular surface and sensor, taken from the oscillograph/digital recording system sheets (see Figure 71) are applied when the data is used by the Project Engineer. Table V contains a list of the maximum gains available for the variable stability channels.

FLIGHT CALIBRATIONS

In-Flight Calibration of Variable Stability Channels

Occasionally it is desirable to do in-flight calibration of the VSS channels. This is done by turning up one gain at a time and applying a control input to the airplane that would excite the response variable being calibrated. The flight data is then used to make calibration plots of system gain from sensor output to surface deflection as functions of knob settings in the aft cockpit and nose gains settings.

Compliance Elimination Circuits

The T-33 VSS has special electrical circuits (Reference 9) which eliminate the compliance effect and thus keeps the ratio of control surface movement to control surface strut movement constant regardless of the varying air loads caused by different altitudes or airspeeds. As a result, in-flight single channel calibrations are normally not required.

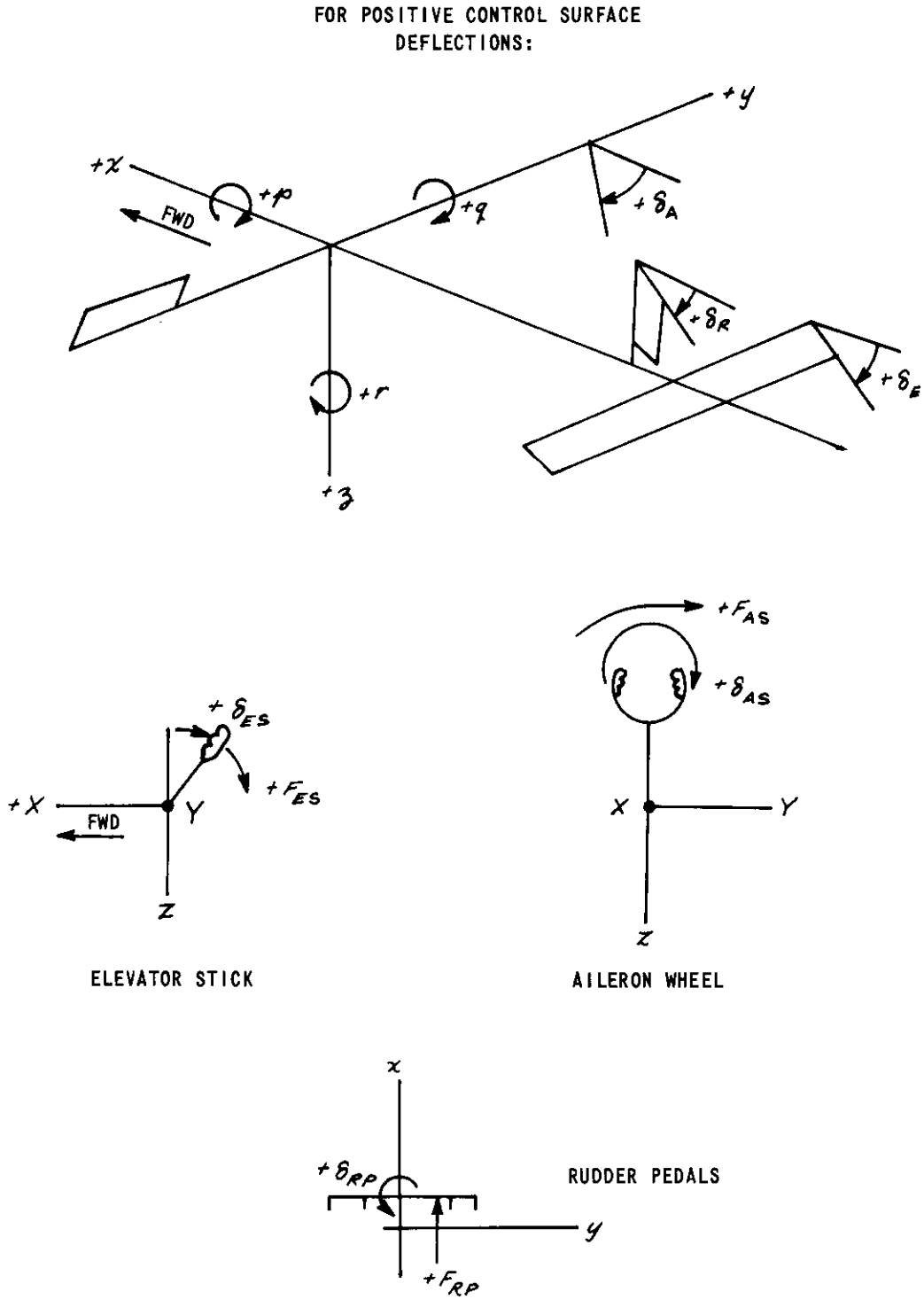

Figure 72 T-33 SENSE NOTATION FOR CONTROL SURFACES, FEEL SYSTEM AND ANGULAR RATES

Table V

VARIABLE STABILITY MAXIMUM CHANNEL GAINS

PARAMETERS	± MAX GAIN AVAILABLE
$\delta_e/\Delta\alpha$	10°/DEG
$\delta_e/\dot{\alpha}$	2°/DEG/SEC
δ_e/q	5°/DEG/SEC
$\delta_e/\bar{q}_c$	500°/PSI (5.65°/KT @ 250 KT)
$\delta_e/\dot{\bar{q}}_c$	2500°/PSI/SEC (28.3°/KT/SEC @ 250 KT)
$\delta_e/\dot{q}$ $(\delta_e/\ddot{\alpha})$	0.5°/DEG/SEC^2
δ_e/δ_{ES}	20°/IN.
δ_e/F_{ES}	2°/LB
δ_e/IN RANDOM NOISE AUTO DOUBLET	2°/VOLT
δ_e /RATE TRIM FRONT COCKPIT	POS 0.5IN./SEC AUTHORITY ±5 IN. FORCE 4 LB/SEC ±40 LB SURF 2°/SEC ±10°
δ_e /TRIM REAR COCKPIT	±10°
δ_a/β_V	10°/DEG
$\delta_a/\dot{\beta}_V$	2°/DEG/SEC
δ_a/r	5°/DEG/SEC
δ_a/p	2°/DEG/SEC
$\delta_a/\dot{p}$ $(\delta_a/\ddot{\alpha})$	0.2°/DEG/SEC^2
$\delta_a/\dot{r}$ $(\delta_{a_T}/\ddot{\beta})$	0.5°/DEG/SEC
δ_a/δ_{AS}	50°/IN.
δ_a/δ_y COMMAND	2°/DEG
δ_{a_T}/F_{AS}	5°/LB
δ_{a_T}/IN RANDOM NOISE AUTO DOUBLET	4°/VOLT
δ_{a_T} /RATE TRIM FRONT COCKPIT	POS 0.25IN./SEC AUTHORITY ±2.5 IN. FORCE 2.5 LB/SEC 25 LB SURF$_T$ 2.0°/SEC ±20°
δ_{a_T} /TRIM REAR COCKPIT	±20°
δ_r/β	10°/DEG
$\delta_r/\dot{\beta}$	2°/DEG/SEC
δ_r/r	5°/DEG/SEC
δ_r/p	2°/DEG/SEC

Table V (Cont.)

	PARAMETERS	± MAX GAIN AVAILABLE
	$\delta_r/\dot{p}$ (δ_r/w)	0.2°/DEG/SEC^2
	$\delta_r/\dot{r}$ (δ_r/y)	0.5°/DEG/SEC^2
	δ_r/δ_{RP}	50°/IN.
δ_r/δ_{a_T}	COMMAND	2°/DEG
	δ_r/F_{RP}	0.5°/LB
δ_r/IN	RANDOM NOISE AUTO DOUBLET	5°/VOLT
δ_r /RATE TRIM FRONT COCKPIT		POS .2IN./SEC AUTHORITY ±2 IN. FORCE 20 LB/SEC 200 LB SURF 1.0°/SEC ±10.0°
δ_r /TRIM REAR COCKPIT		±20°

APPENDIX I

T-33 DIMENSIONAL DATA

TABLE I-I

(Taken from Reference 1)

HYDRAULIC FLOW CHARACTERISTICS

FEEL SERVOS	PISTON AREA A (in.^{2})	GEAR RATIO δ_c/δ_p (in./in.)
AILERON	.76	7.7
ELEVATOR	.78	3.67
RUDDER	1.284	4.16

POSITION SERVOS	PISTON AREA A (in.^{2})	GEAR RATIO δ_s/δ_p (deg./in.)
AILERON	4.13	11.4
ELEVATOR	.78	12.0
RUDDER	1.173	20.0

Maximum Total Flow Requirement $\sum Q = 45.89$ in.^{3}/sec

Valve Leakage Flow $= 4.0$ in.^{3}/sec

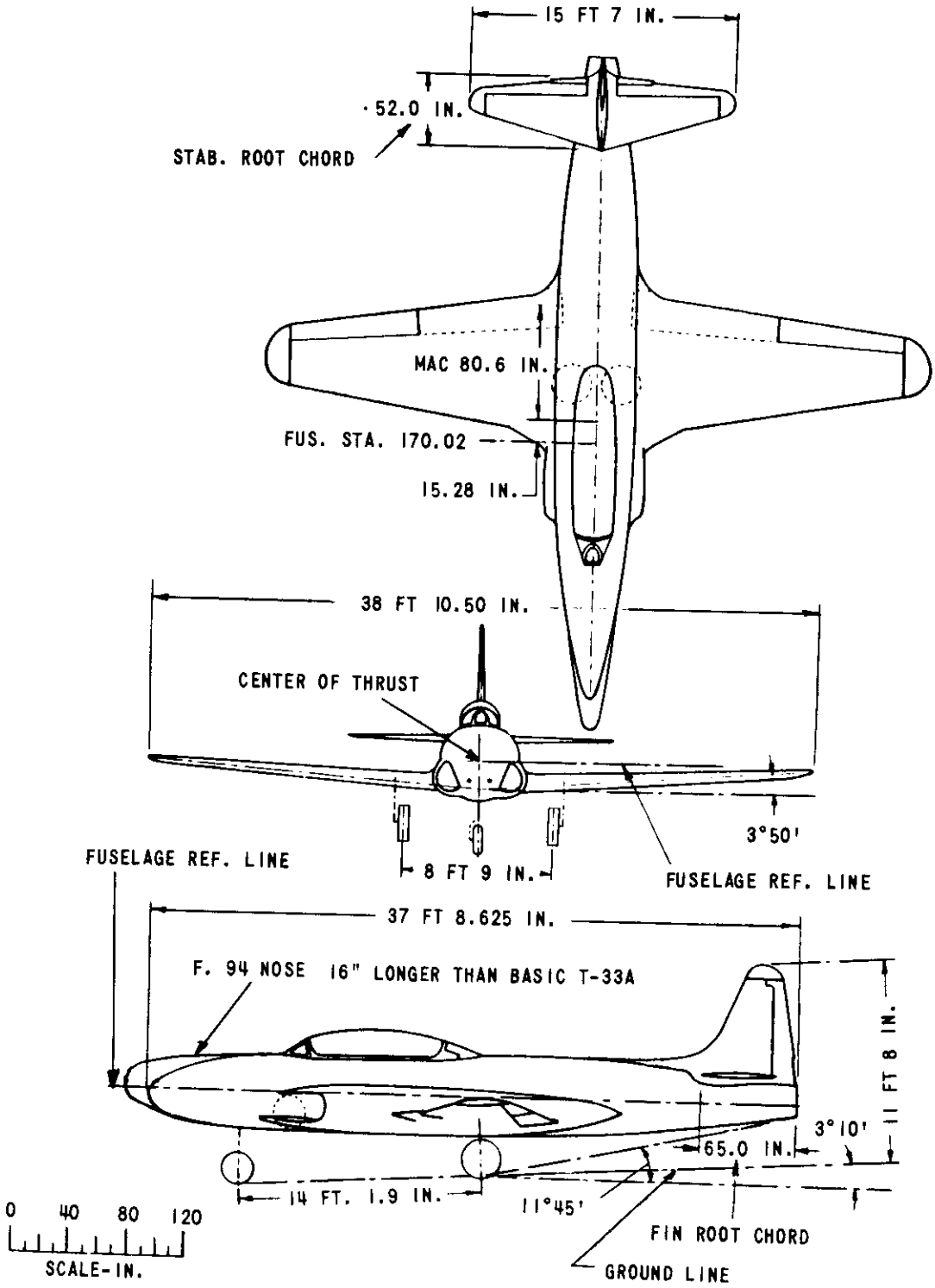

Figure I-1 THREE VIEW DRAWING OF T-33A AIRPLANE WITH F-94 NOSE

Table I-II

DIMENSIONAL DATA FOR THE T-33A AIRPLANE

BASIC DATA

A. WING

AREA, S	234.8 SQ FT
SPAN, b	37.54 FT
MAC, $\bar{c}$	80.6 IN. = 6.72 FT
ASPECT RATIO, AR	6.00
TAPER RATIO	0.355
SWEEPBACK (L.E.)	9.31°
SWEEPBACK ($\bar{c}$ 0.25)	5.0°
UNSWEPT CHORD LINE,	.52 $\bar{c}$ (FUS. STA. 227.2)
DIHEDRAL (WING REF.PLANE)	3.83°
INCIDENCE (ROOT)	1.0°
GEOMETRIC TWIST (ROOT STA. TO W.S. 222)	-1.5°
AIRFOIL SECTION	NACA 65_1-213, a = 0.5
CHORDS	
ROOT (W.S. -0)	110.0 IN.
TIP (W.S. 216)	41.89 IN.
LOCATION OF 25% $\bar{c}$	FUS. STA. 205.45

B. AILERON (EACH SIDE)

AREA, S_a	8.75 SQ FT
MEAN CHORD, $\bar{c}_a$	1.17 FT
DEFLECTION LIMITS, δ_a	±20°
TAB AREA, S_{at}	0.399 SQ FT
TAB MEAN CHORD, c_{at}	3.86 IN.
TAB DEFLECTION LIMITS	±20°

C. WING FLAPS (EACH SIDE)

TYPE	SPLIT
AREA, S_f	15.32 SQ FT
MEAN CHORD, c_f	1.8 FT
MAXIMUM DEFLECTION	45°

D. HORIZONTAL TAIL

AREA, S_t	43.5 SQ FT
SPAN, b_t	15.58 FT
MEAN CHORD, $\bar{c}_t$	3.12 FT
ASPECT RATIO, A_t	5.58
TAPER RATIO	0.319
AIRFOIL SECTION	NACA 65_2-010
INCIDENCE ROOT	+1.5°
CHORDS	
ROOT	4.33 FT
TIP (EQUIV.)	1.38 FT
$\bar{Y}/\frac{b}{2}$ (SPANWISE MAC LOCATION)	0.412

Table I-II (Cont.)

DIMENSIONAL DATA FOR THE T-33A AIRPLANE (Cont.)

D. HORIZONTAL TAIL (Cont.)	
UNSWEPT CHORD LINE,	$.75\,\bar{c}$
$[(S_t/S)(\ell_t/\bar{c})] = \bar{V}_H$	0.438
$(.25\,\bar{c}$ to $.25\,\bar{c}_t) = \ell_H$	15.9 FT
$\ell_t/\bar{c}$	2.37
E. ELEVATOR	
AREA (BOTH SIDES)	8.70 SQ FT
MEAN CHORD, $\bar{c}_e$	0.708 FT
DEFLECTION LIMITS	25° T.E. UP TO 15° T.E. DOWN
F. VERTICAL TAIL	
AREA, S_V	22.5 SQ FT
SPAN, b_V	6.42 FT
ASPECT RATIO, A_V	1.83
MEAN CHORD, $\bar{c}_V$	3.89 FT
TAPER RATIO	0.309
AIRFOIL SECTION	NACA 65_2-010
CHORDS	
ROOT	5.42 FT
TIP (EQUIV.)	1.79 FT
$(0.25\,\bar{c}$ TO $0.25\,\bar{c}_V) = \ell_T$	16.08 FT
$[(S_t/S)(\ell_t/b)] = \bar{V}_T$	0.041
ℓ_t/b	0.428
HEIGHT OF C.P. $\bar{z}/b$	$-.1112 + .00748\alpha$
G. RUDDER	
AREA, S_r	5.3 SQ FT
MEAN CHORD, $\bar{c}_r$	1.09 FT
DEFLECTION LIMITS, δ_r	$\pm 30°$
H. DIVE FLAPS (EACH SIDE)	
AREA, S_{df}	2.95 SQ FT
MEAN CHORD, $\bar{c}_{df}$	2.22 FT
MAXIMUM DEFLECTION, δ_{df}	45°
J. DRAG PETALS	
AREA (EACH OF 4)	7.0 SQ FT
MAXIMUM DEFLECTION, δ_p	82°

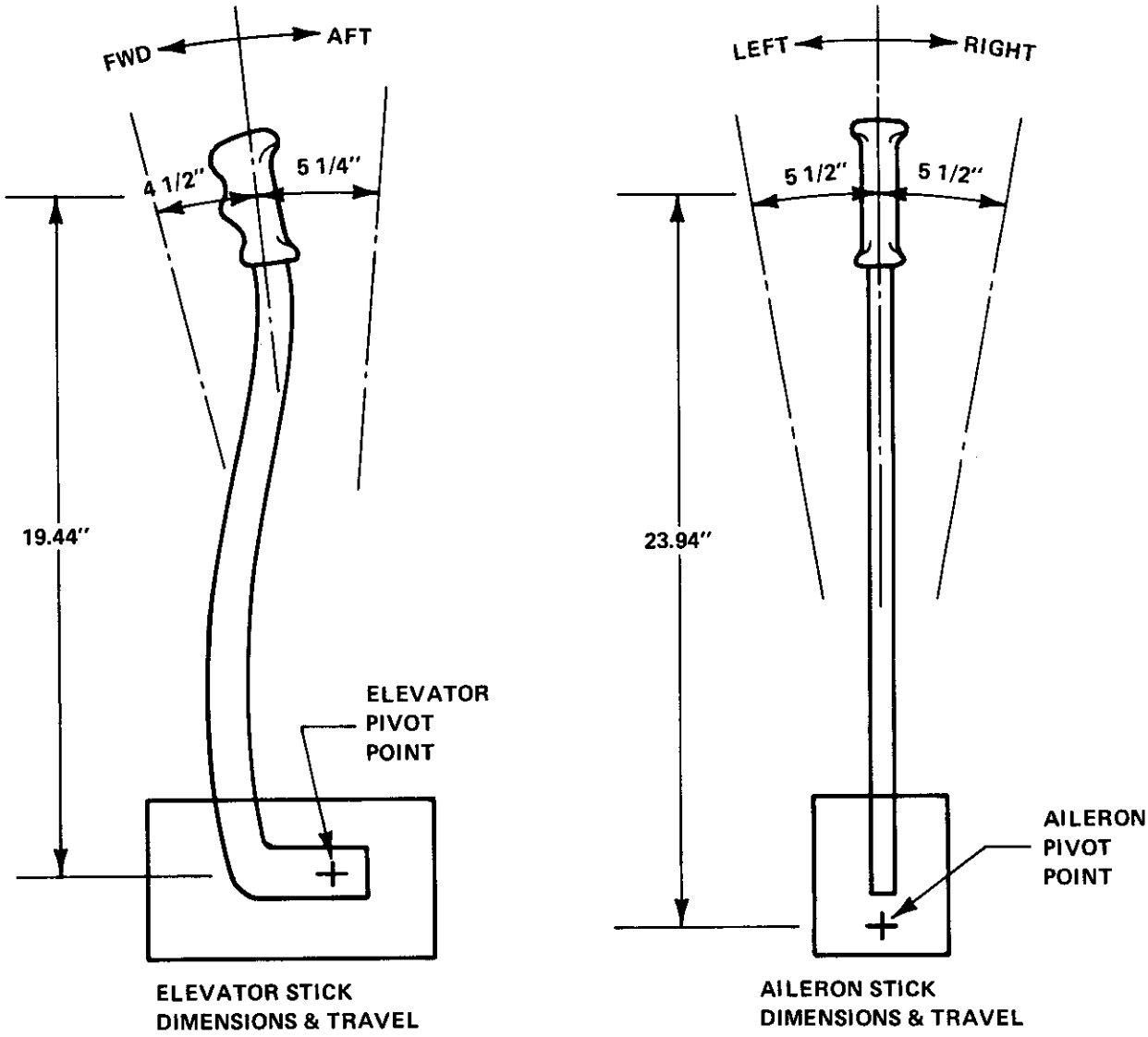

Figure I-2 T-33 FRONT COCKPIT STICK DIMENSIONS AND TRAVEL

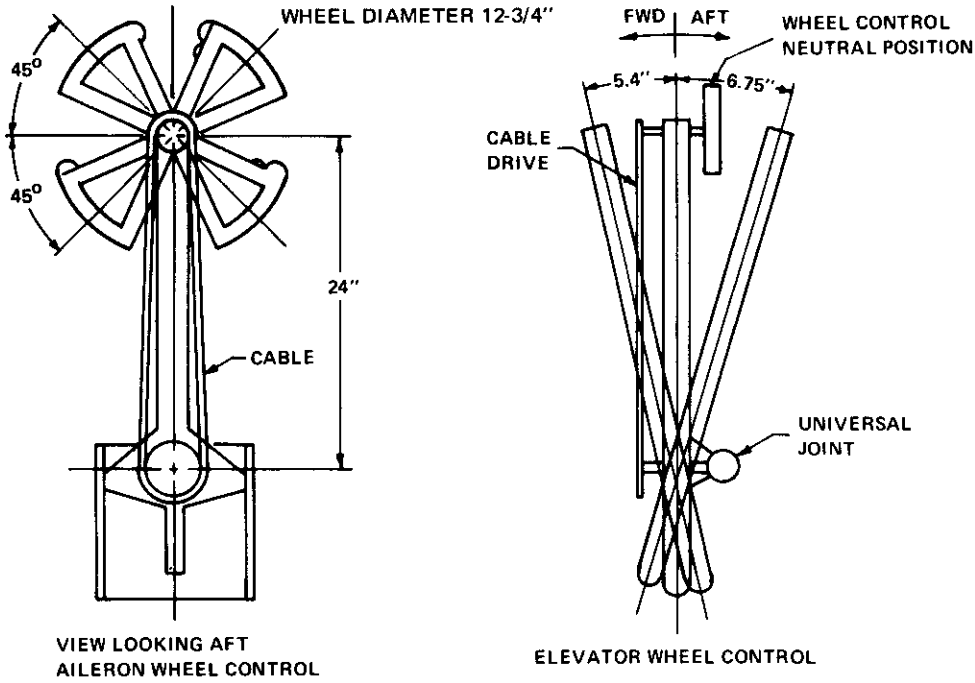

Figure 1-3 WHEEL INSTALLATION IN VARIABLE STABILITY T-33 COCKPIT

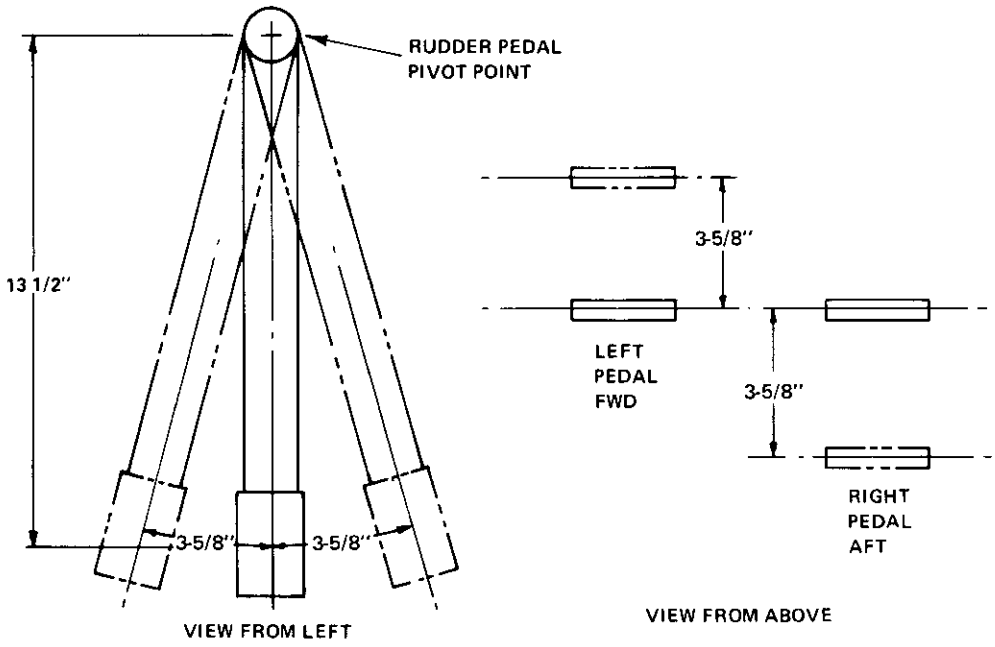

Figure 1-4 RUDDER PEDAL INSTALLATION IN VARIABLE STABILITY T-33 COCKPIT

APPENDIX II

T-33 AERODYNAMIC DATA

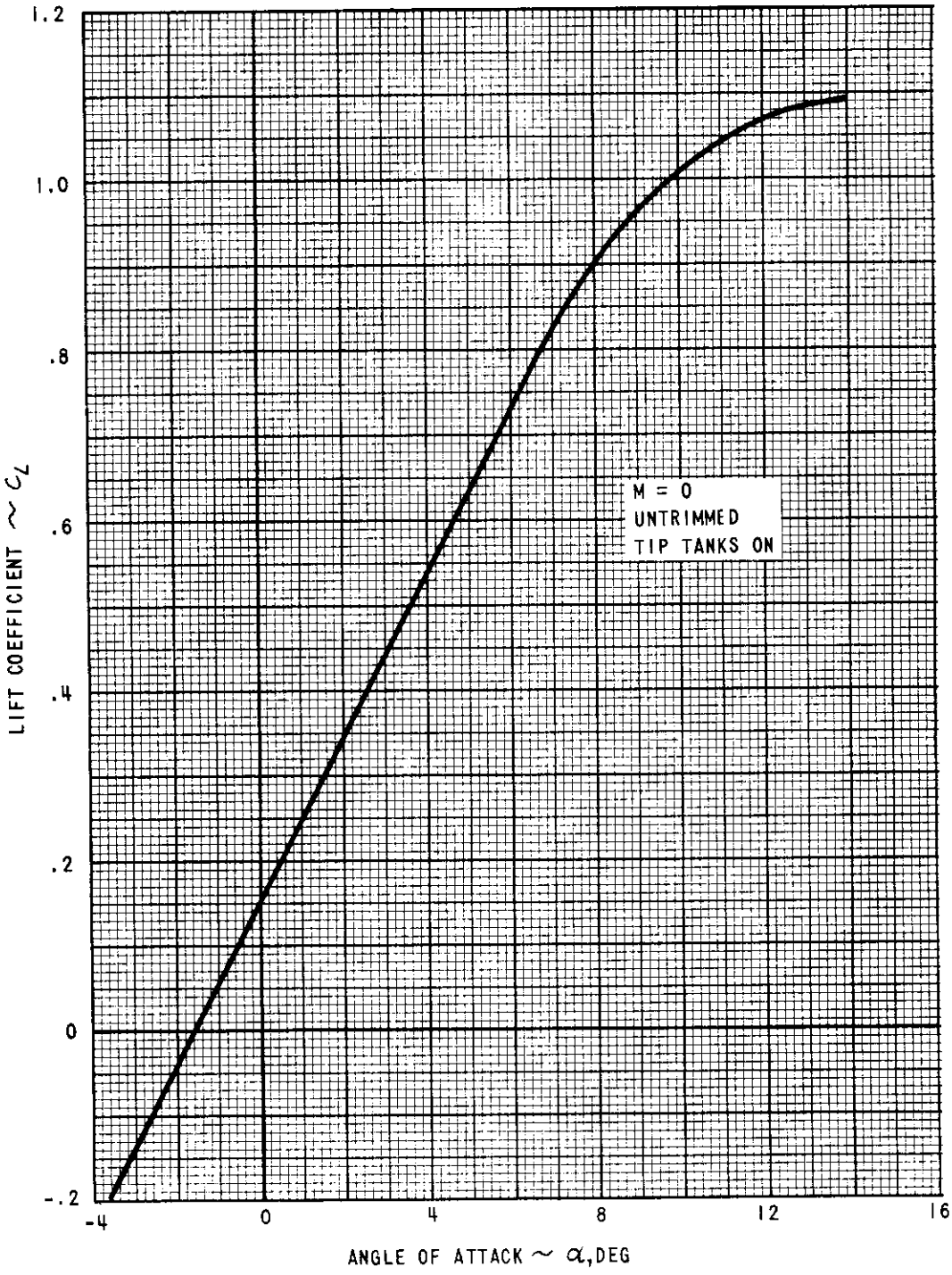

Figure II-1 LIFT COEFFICIENT VS. ANGLE OF ATTACK

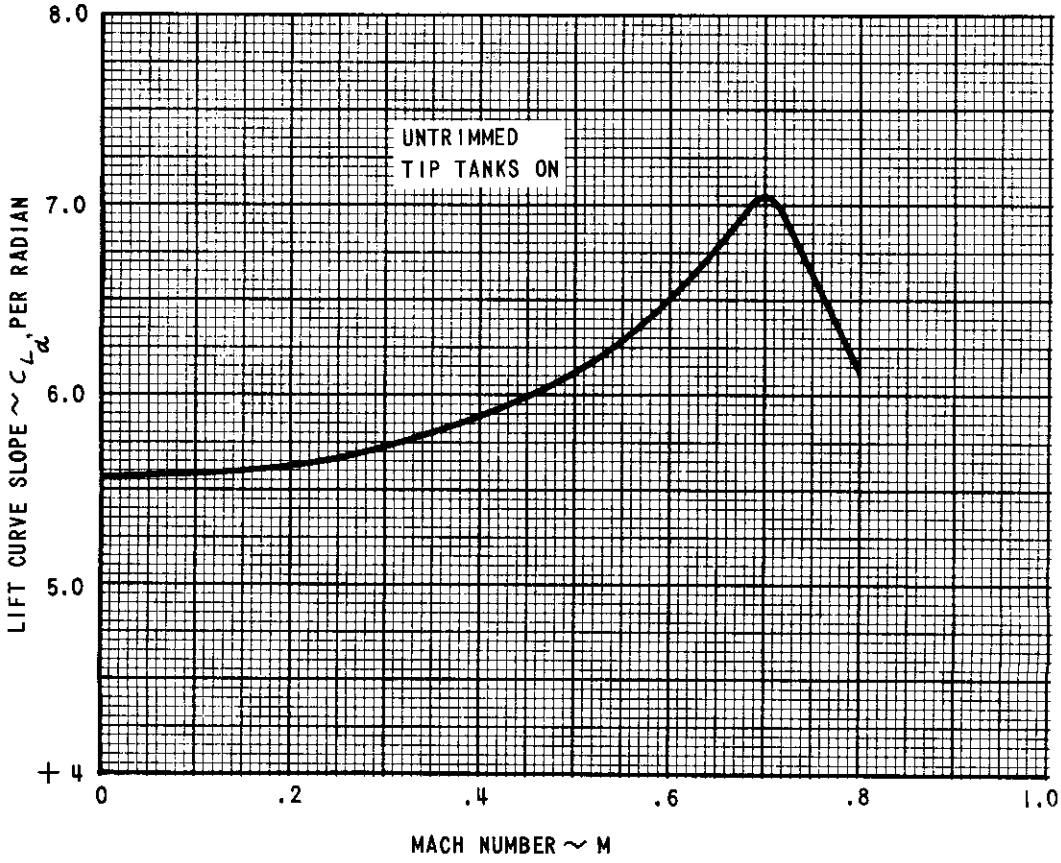

Figure II-2 LIFT CURVE SLOPE VS. MACH NUMBER

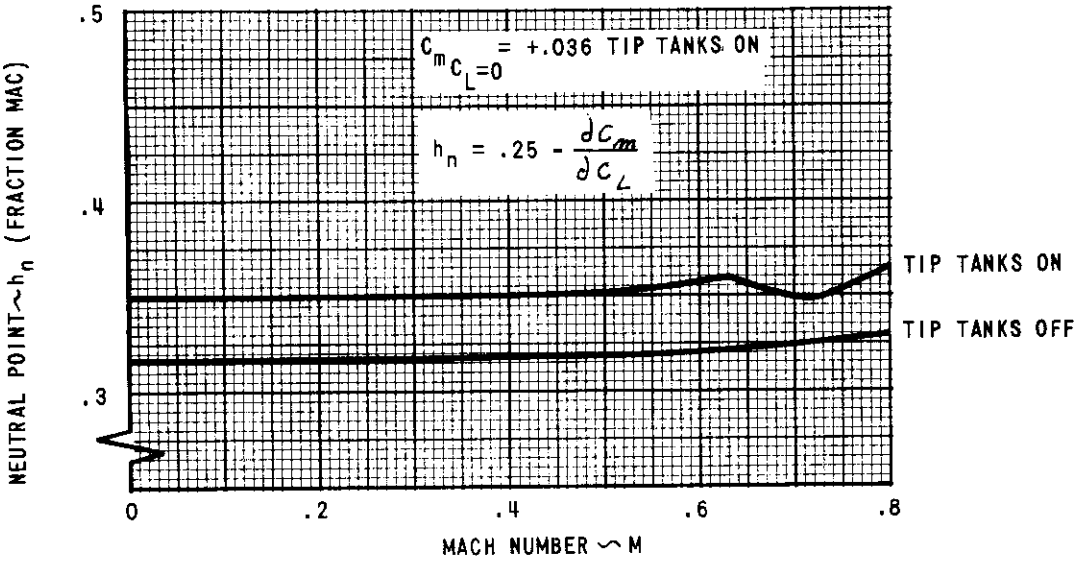

Figure II-3 NEUTRAL POINT

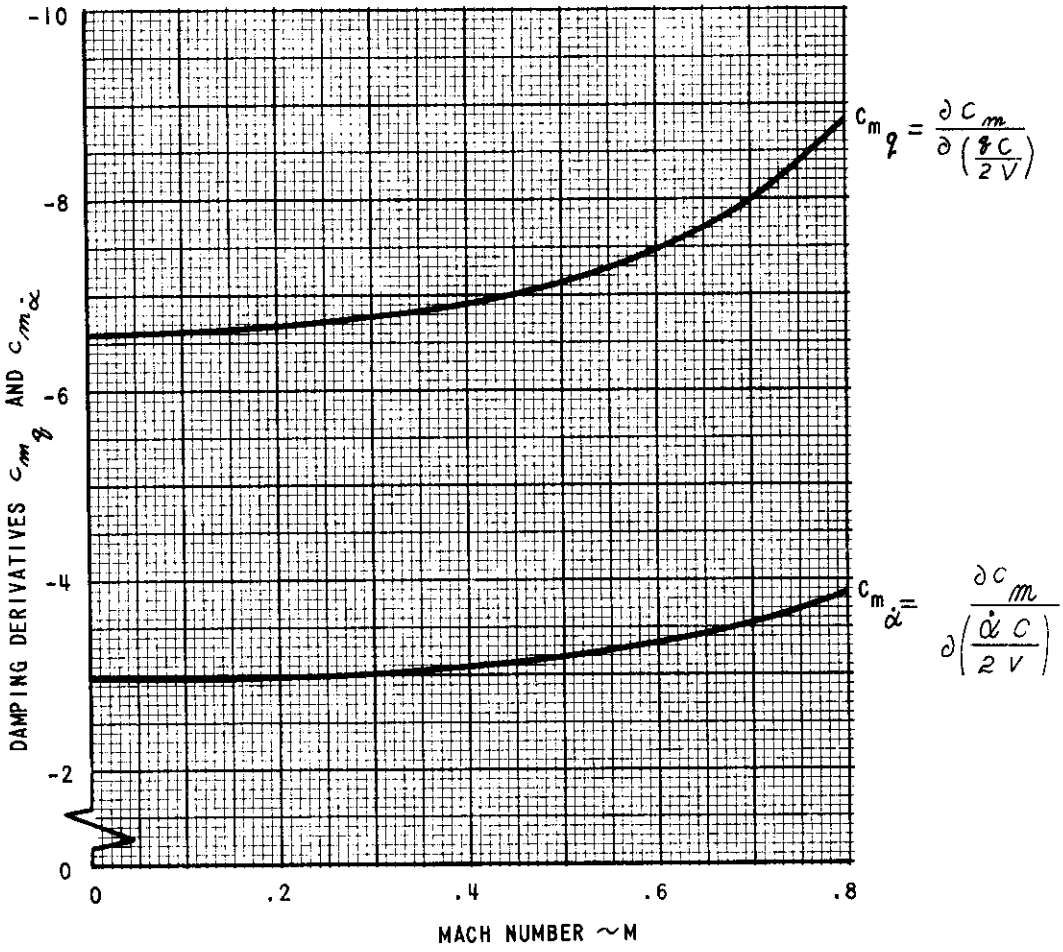

Figure II-4 DAMPING IN PITCH

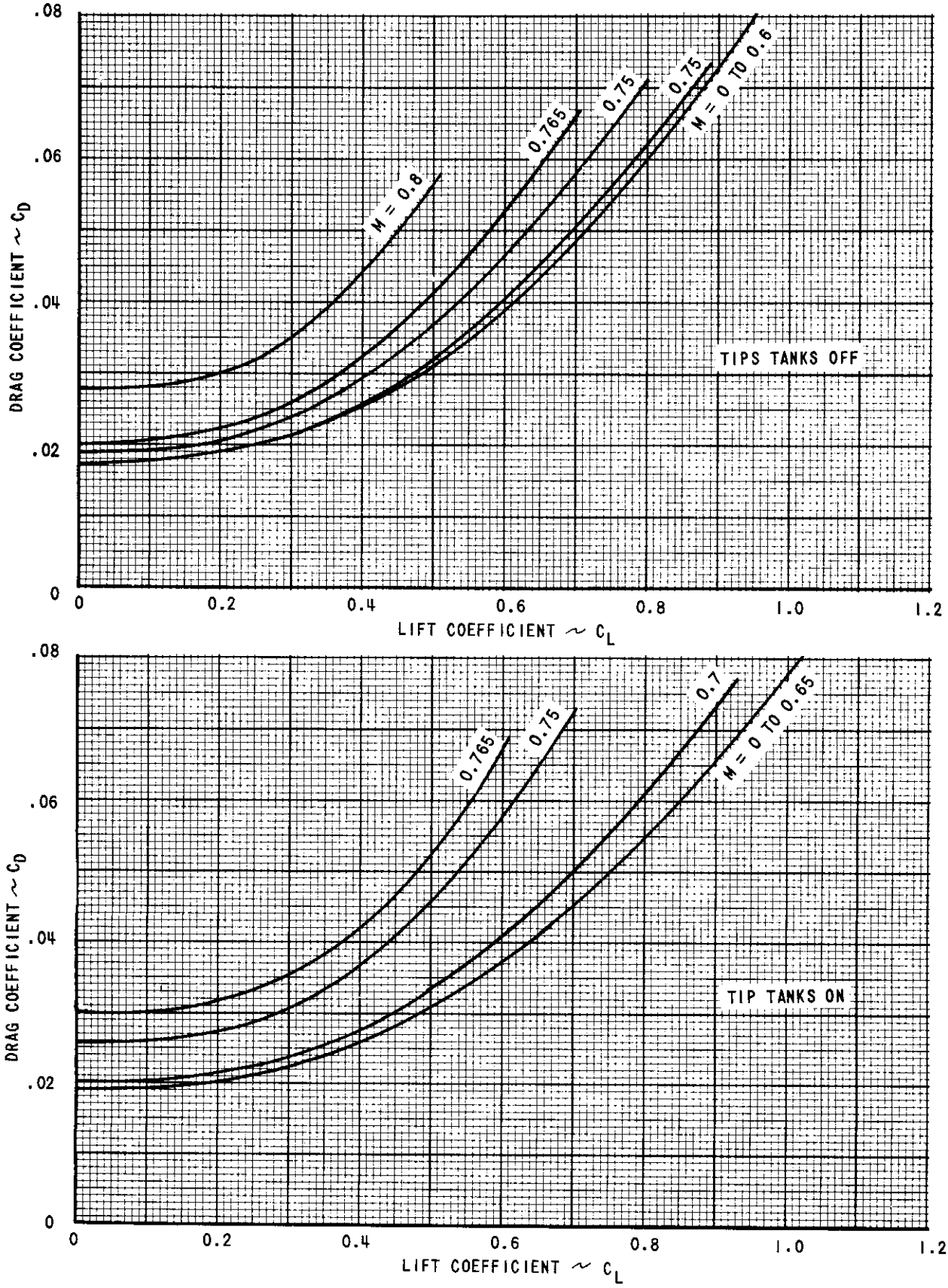

Figure II-5 C_D VS. C_L WITH TIP TANKS ON AND OFF

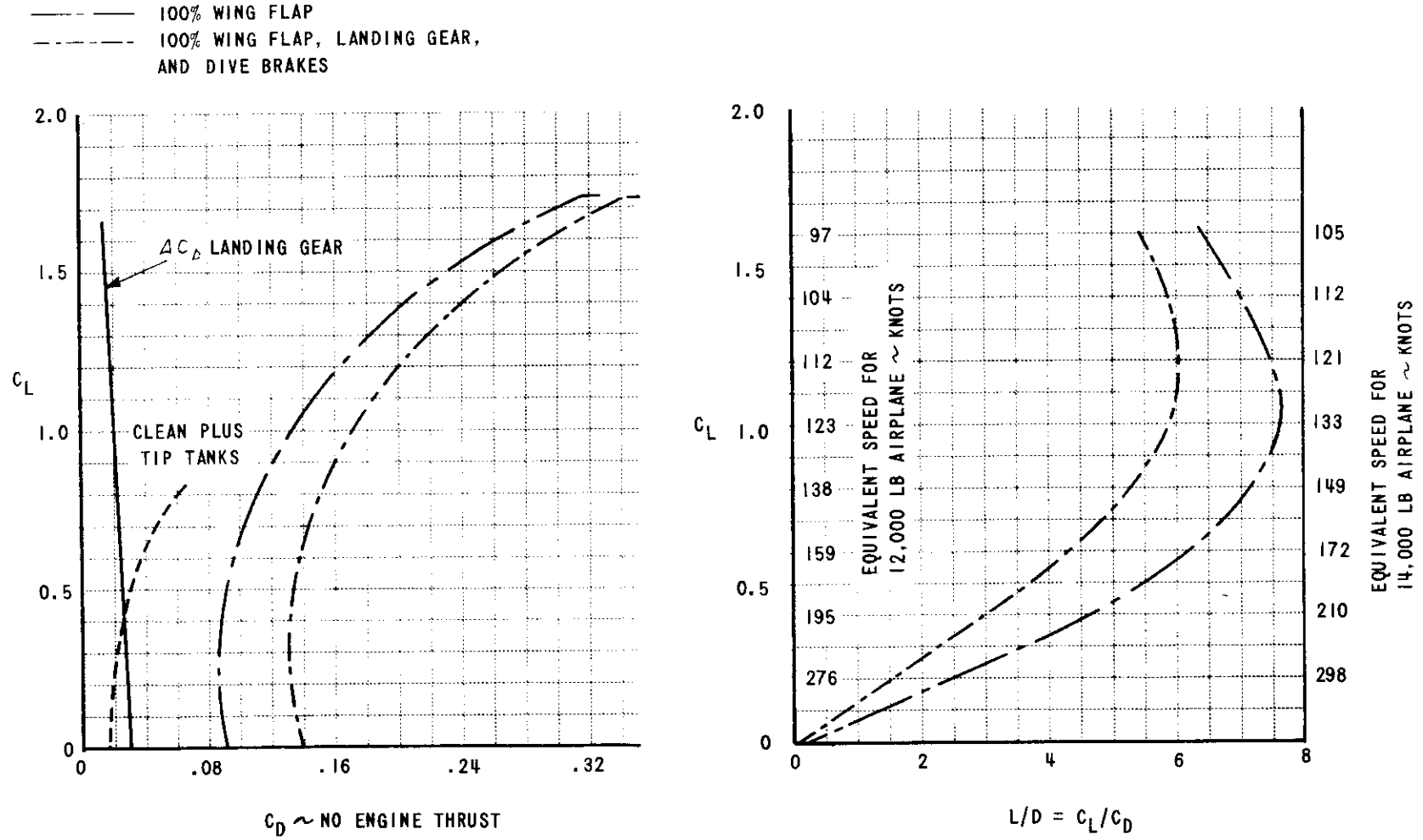

Figure II-6 AERODYNAMIC LIFT-DRAG CHARACTERISTICS OF T-33 WITH TIP TANKS (FROM REF 6)

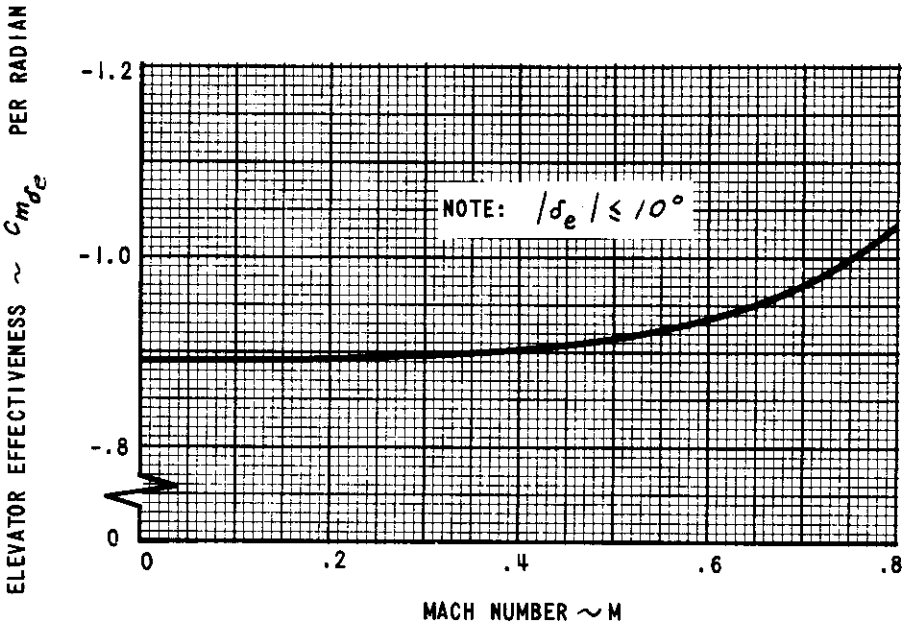

Figure II-7 $C_{m_{\delta_e}}$ VS. M

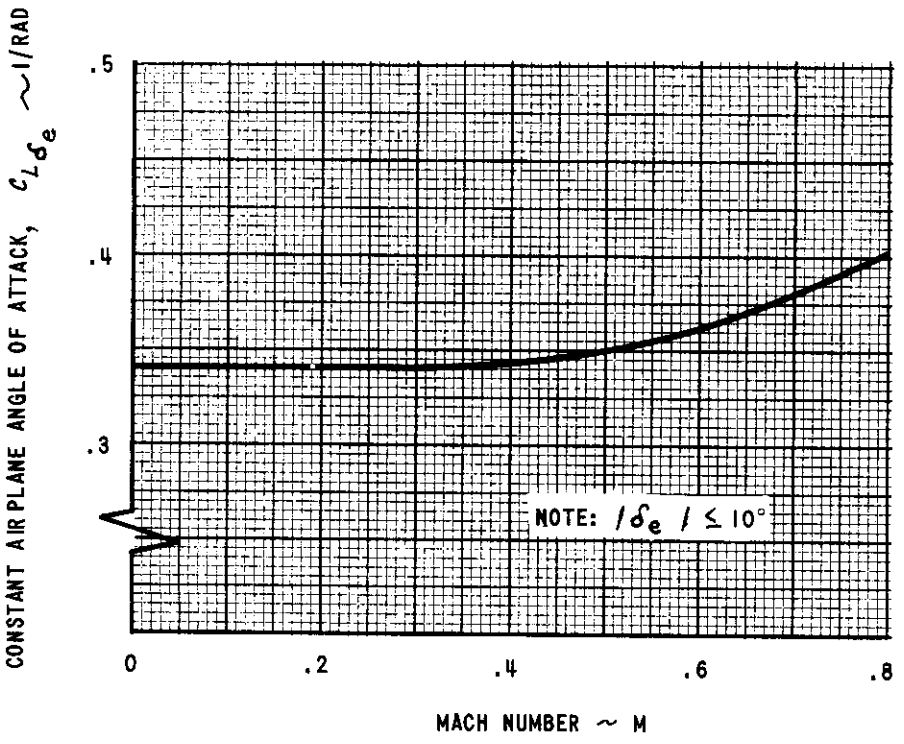

Figure II-8 $C_{L_{\delta_e}}$ VS. M

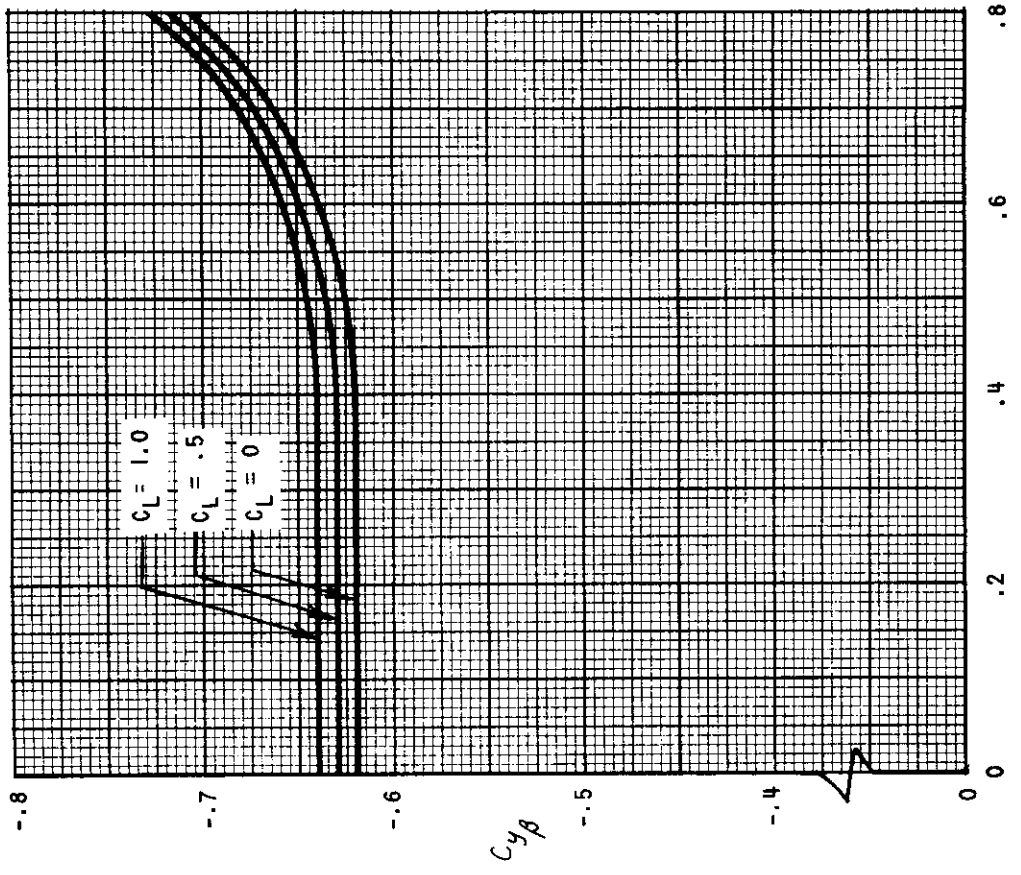

Figure II-10 C_{y_β} VS. M, TIP TANKS ON

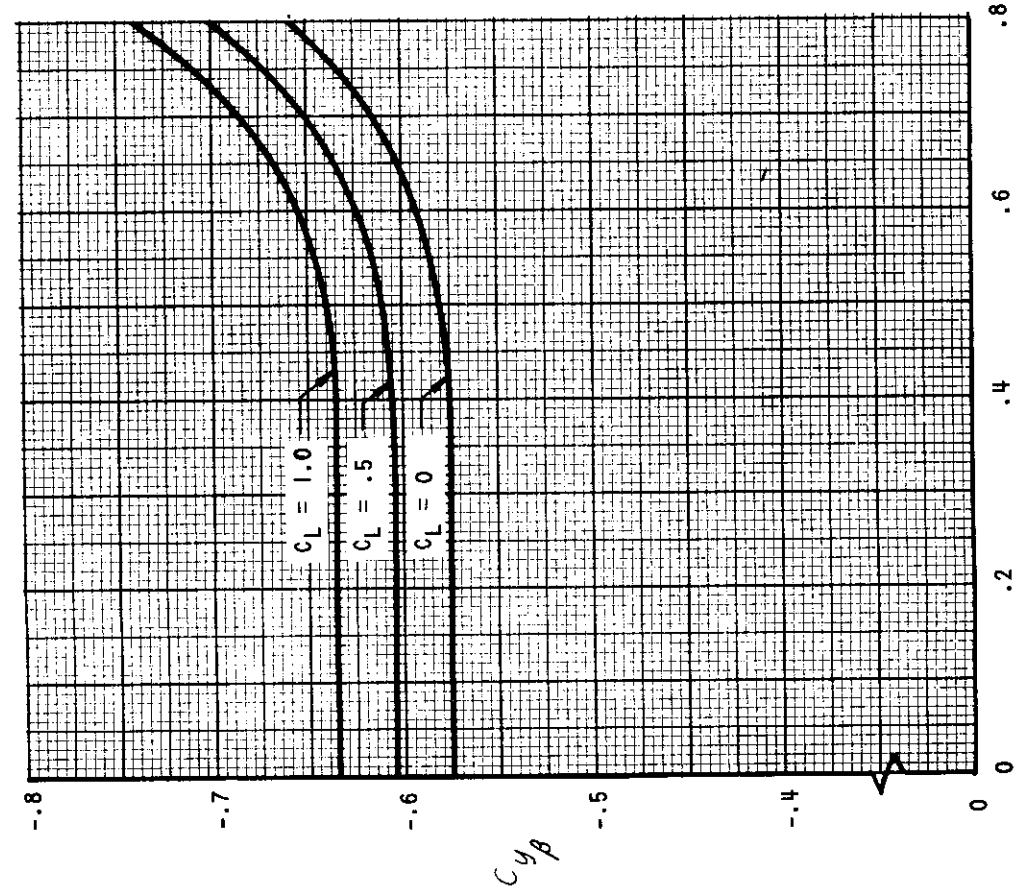

Figure II-9 C_{y_β} VS. M, TIP TANKS OFF

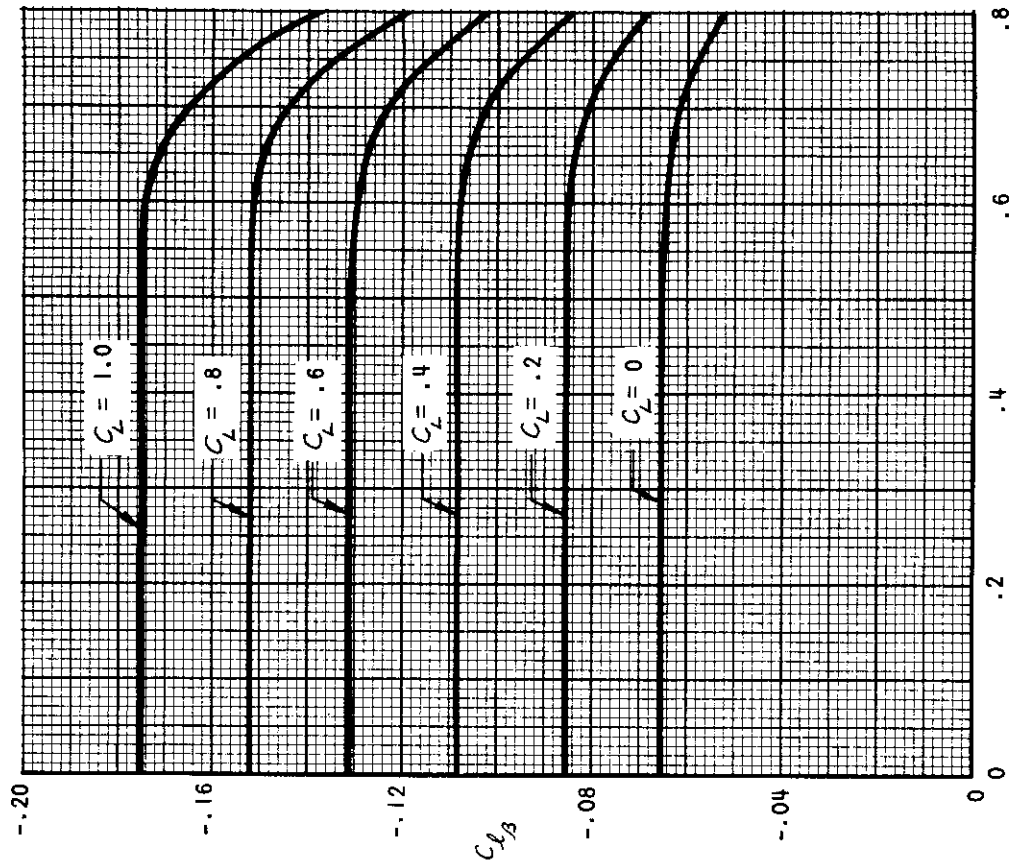

Figure II-12 C_{l_β} VS. M, TIP TANKS ON

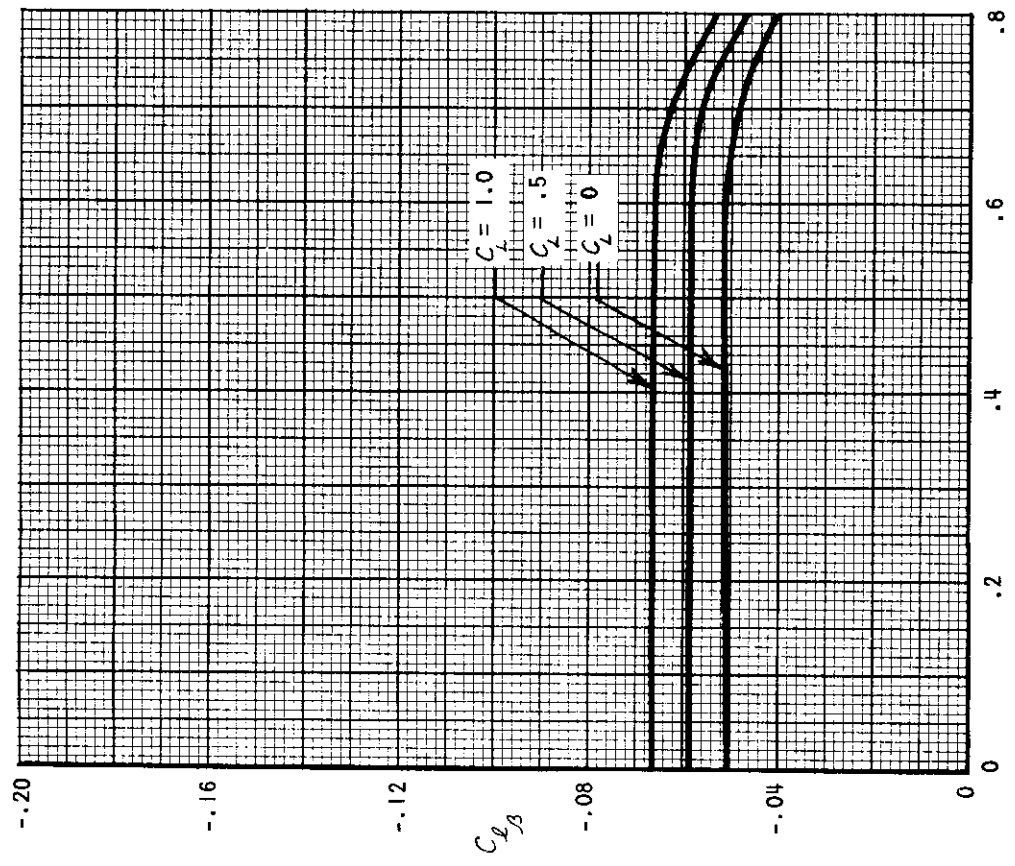

Figure II-11 C_{l_β} VS. M, TIP TANKS OFF

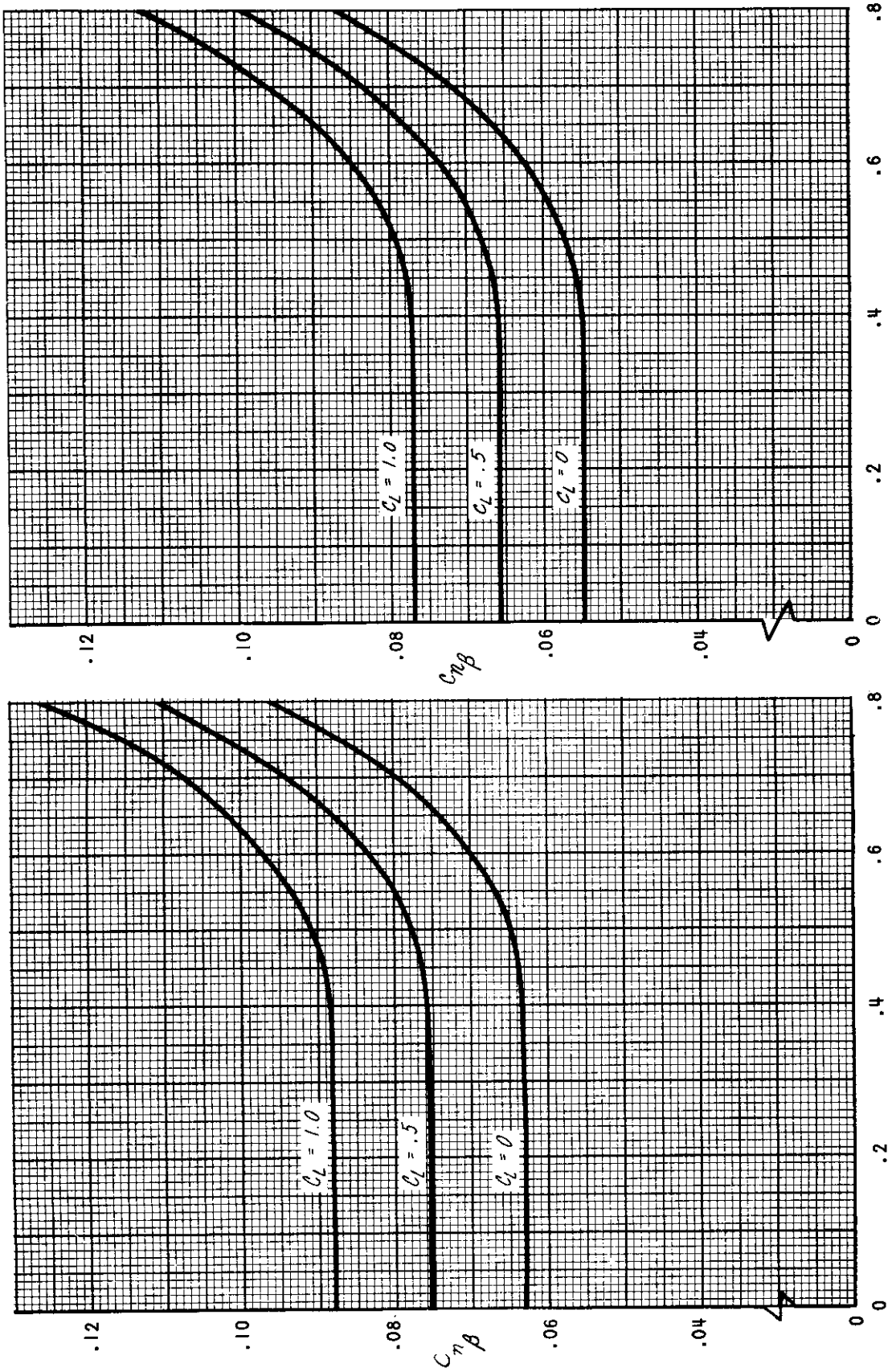

Figure II-13 C_{n_β} VS. M, TIP TANKS OFF

Figure II-14 C_{n_β} VS. M, TIP TANKS ON

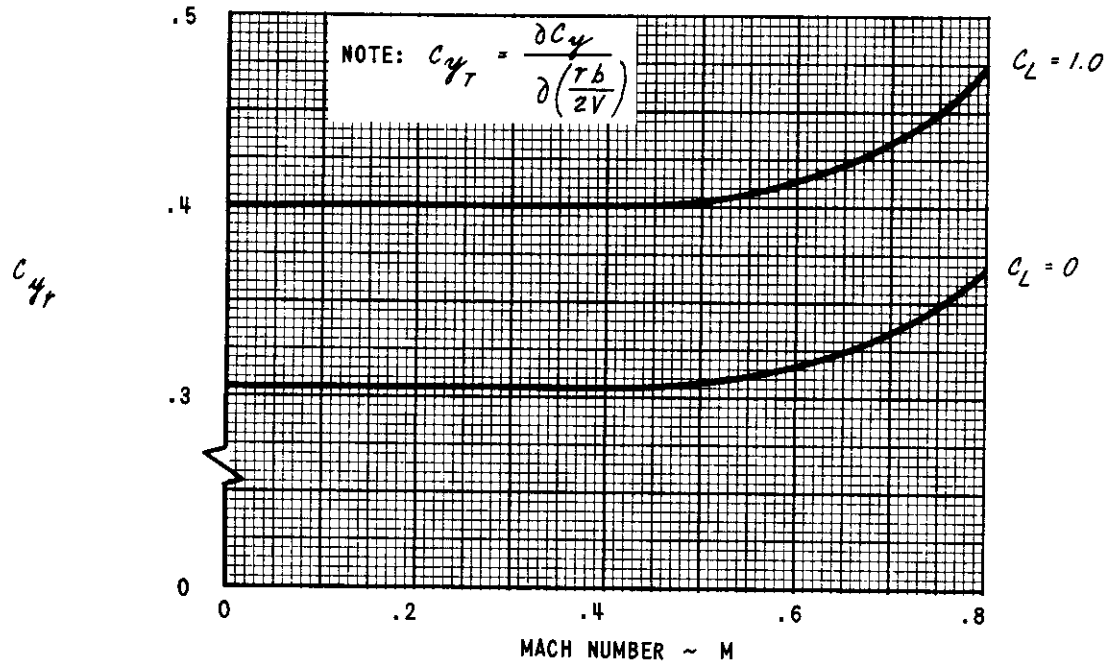

Figure II-15 C_{y_r} VS. M, TIP TANKS ON AND OFF

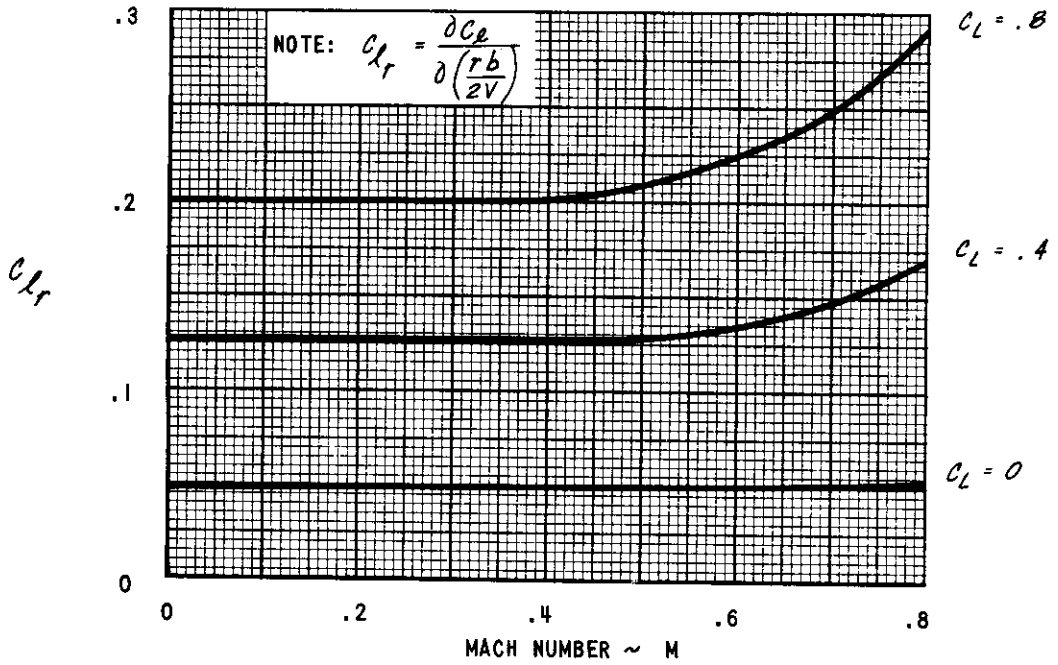

Figure II-16 C_{l_r} VS. M, TIP RANKS ON AND OFF

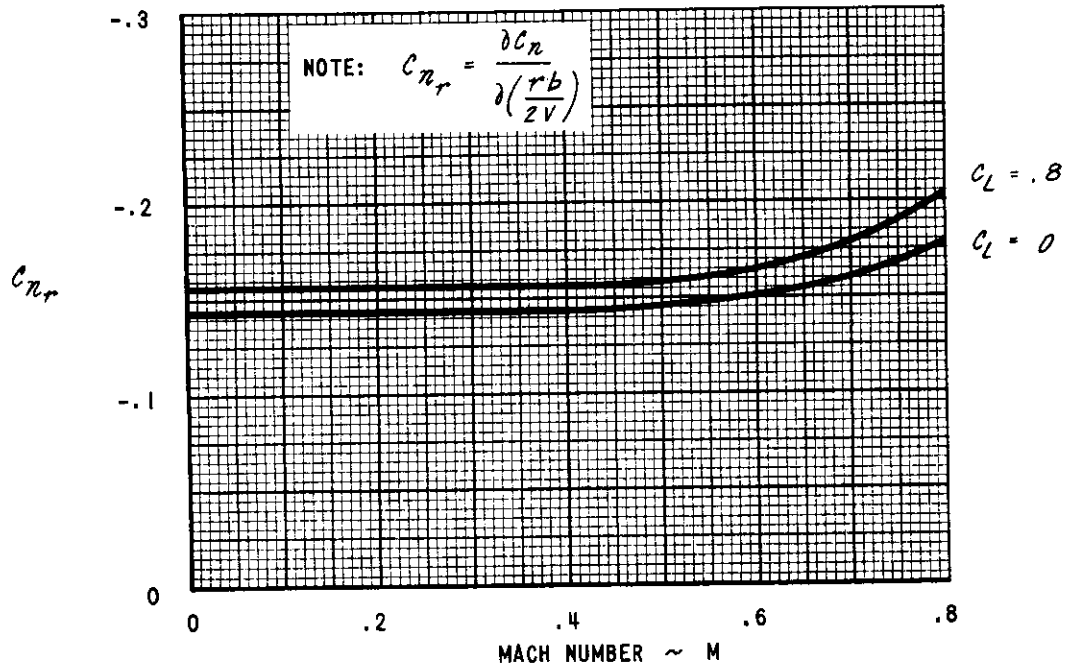

Figure □-17 C_{n_r} VS. M, TIP TANKS ON AND OFF

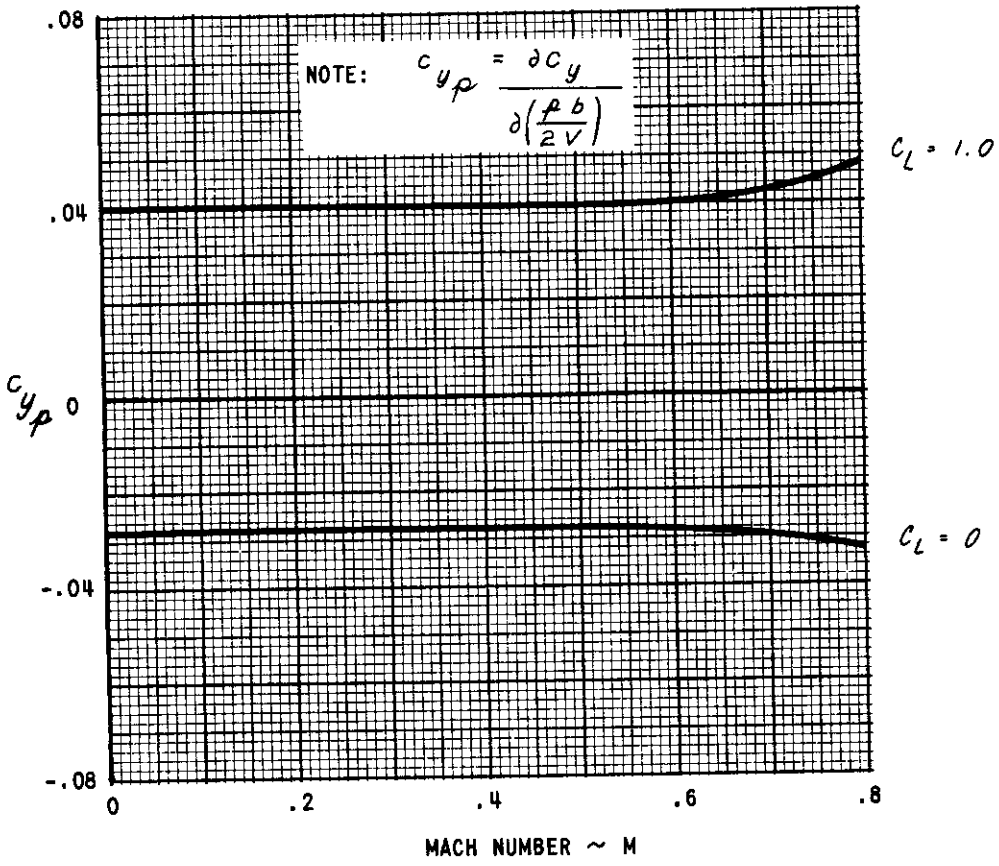

Figure □-18 C_{y_p} VS. M, TIP TANKS ON AND OFF

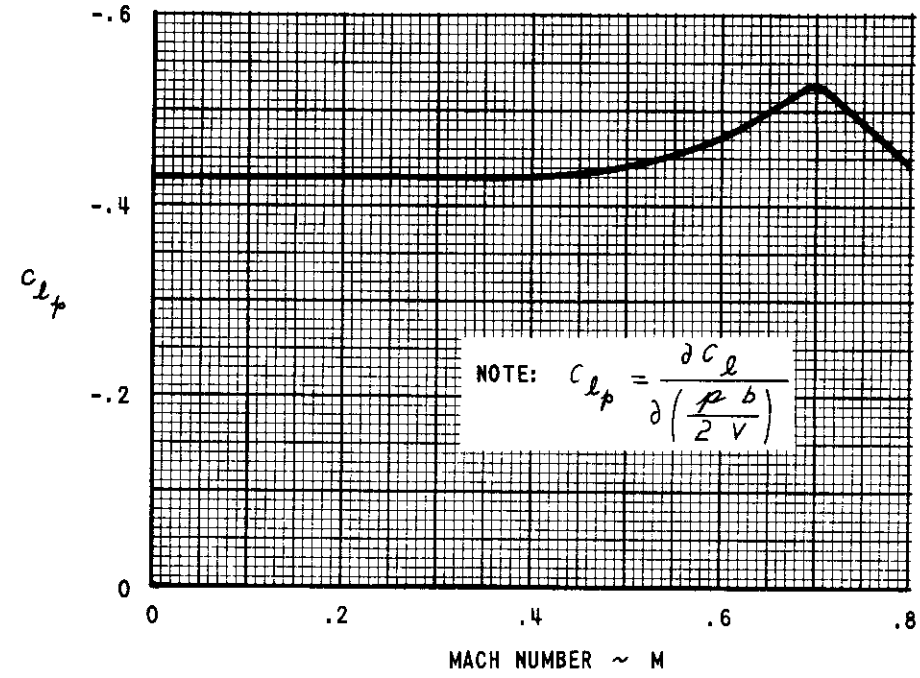

Figure II-19 C_{l_p} VS. M, TIP TANKS OFF

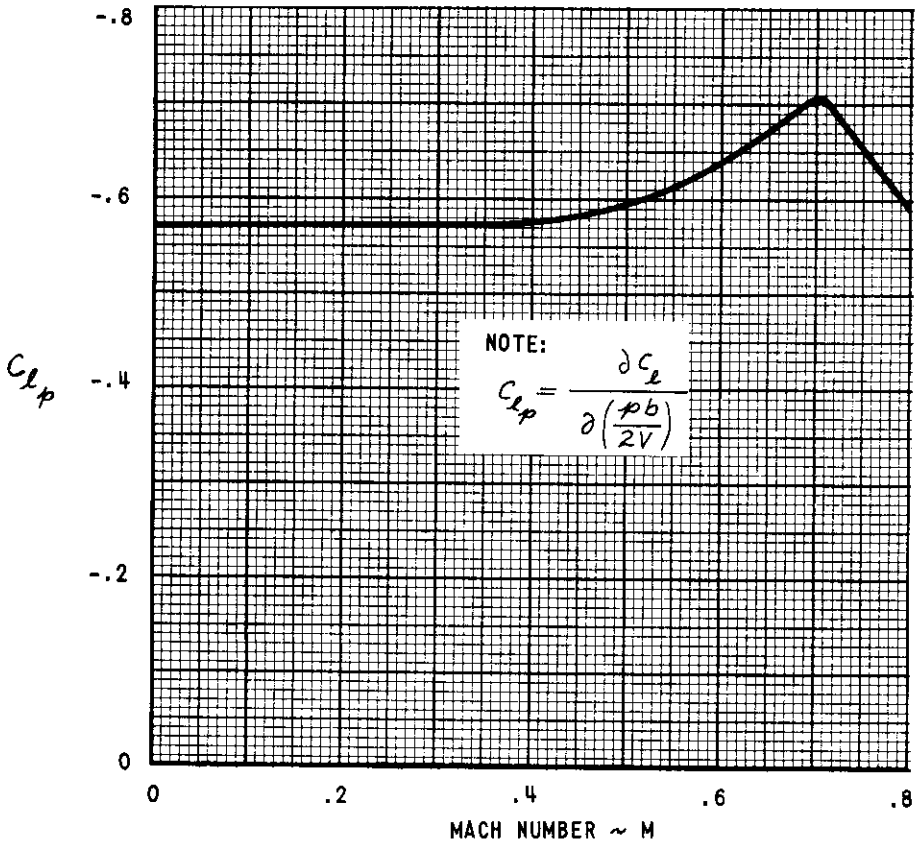

Figure II-20 C_{l_p} VS. M, TIP TANKS ON

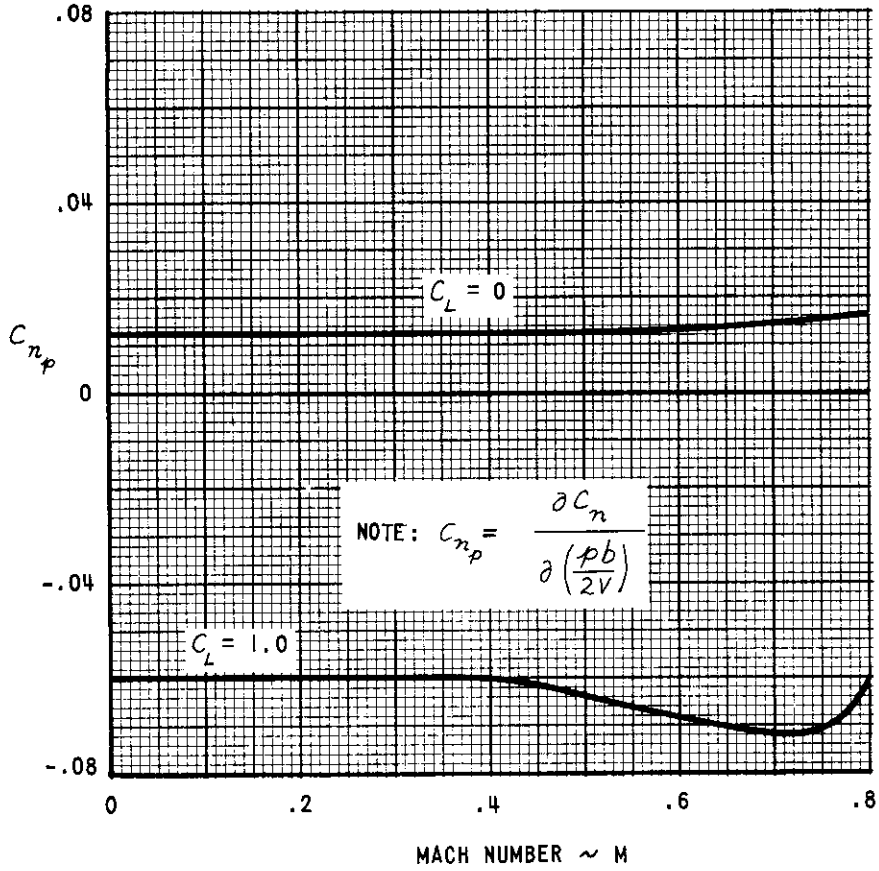

Figure II-21 C_{n_p} VS. M, TIP TANKS ON AND OFF

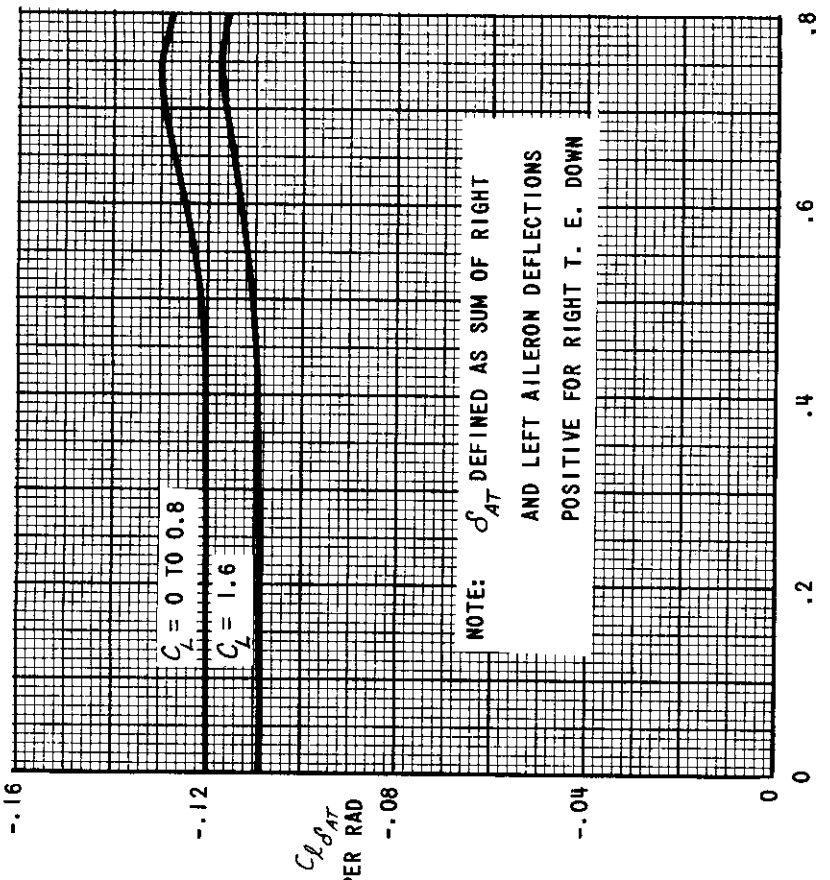

Figure II-22 $C_{l_{\delta_{AT}}}$ VS. M, TIP TANKS OFF

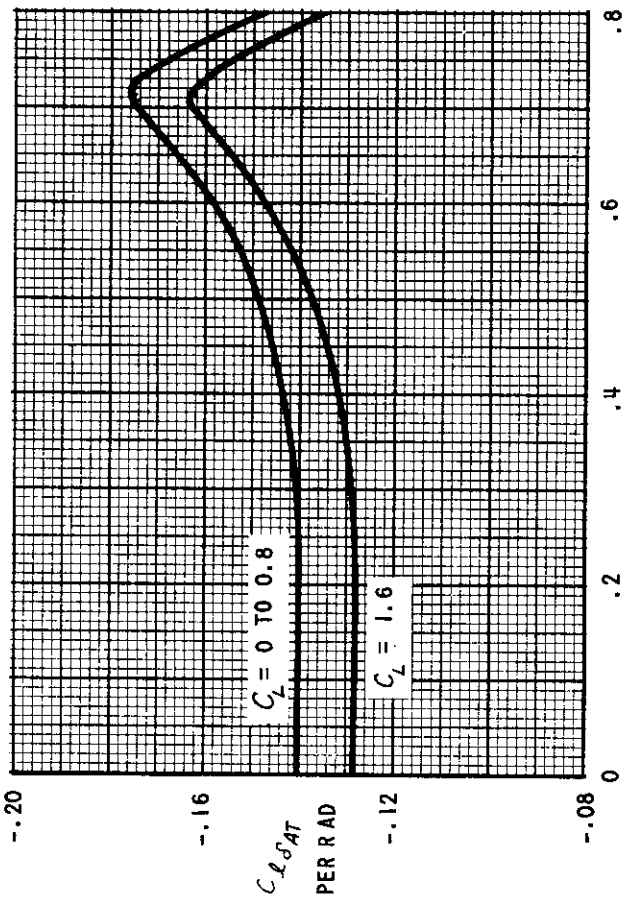

Figure II-23 $C_{l_{\delta_{AT}}}$ VS. M, TIP TANKS ON

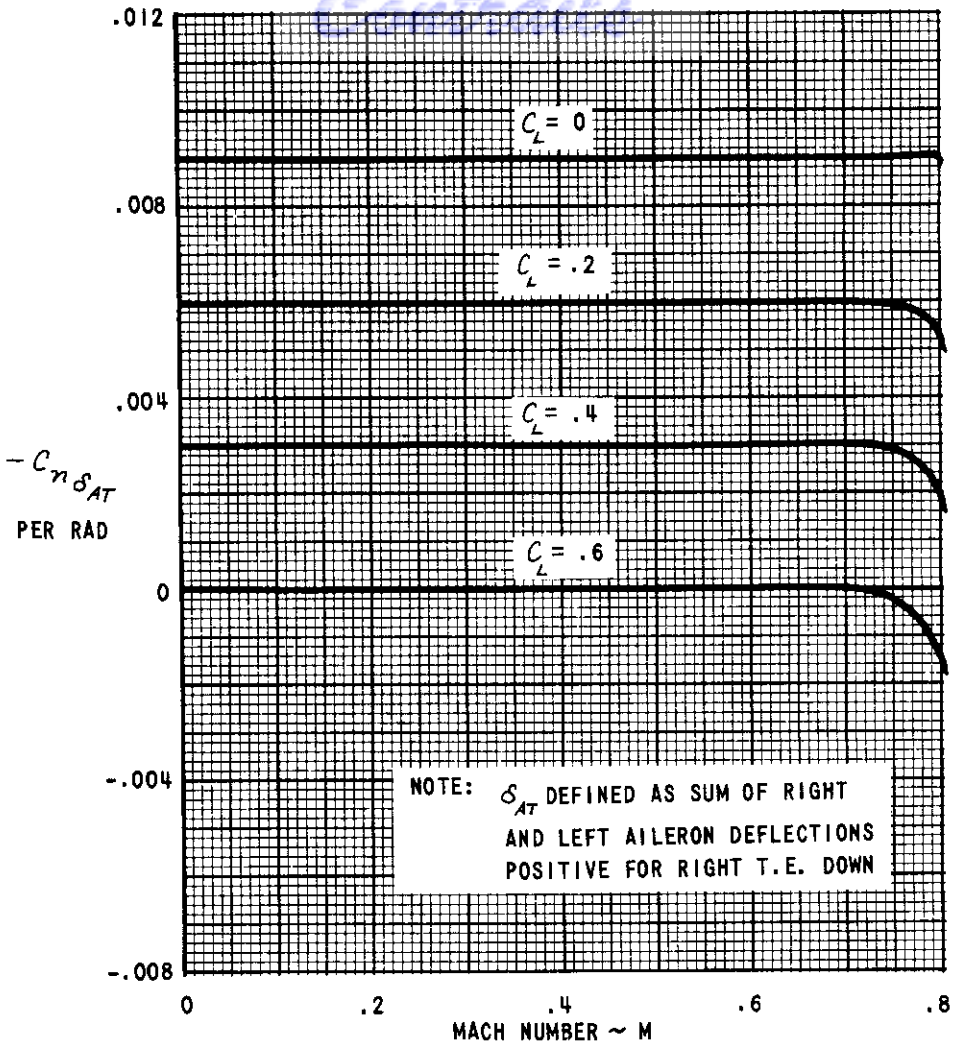

Figure II-24 $C_{n\delta_{AT}}$ VS. M, TIP TANKS OFF

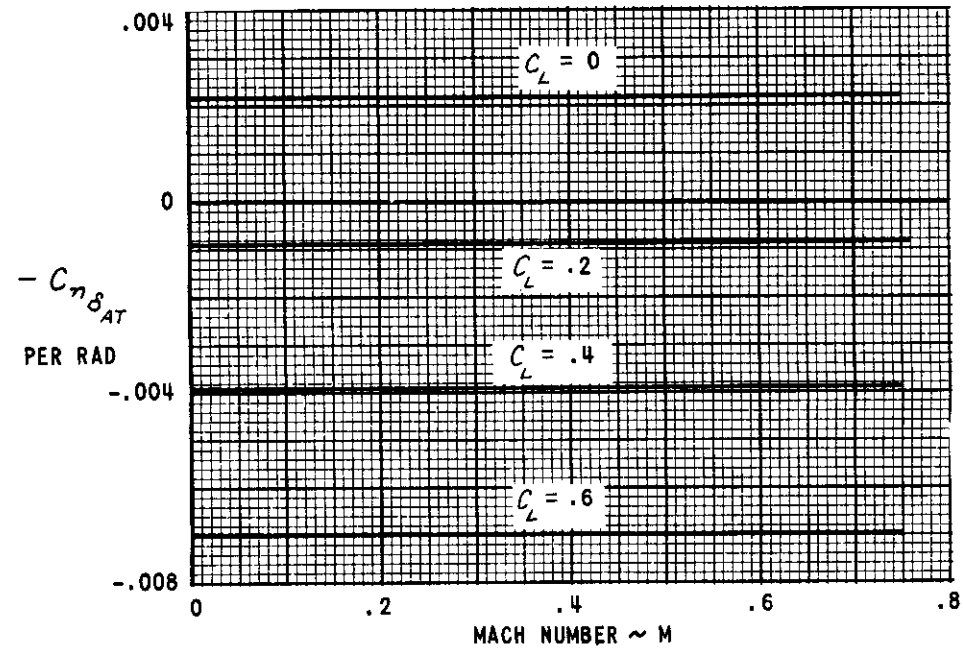

Figure II-25 $C_{n\delta_{AT}}$ VS. M, TIP TANKS ON

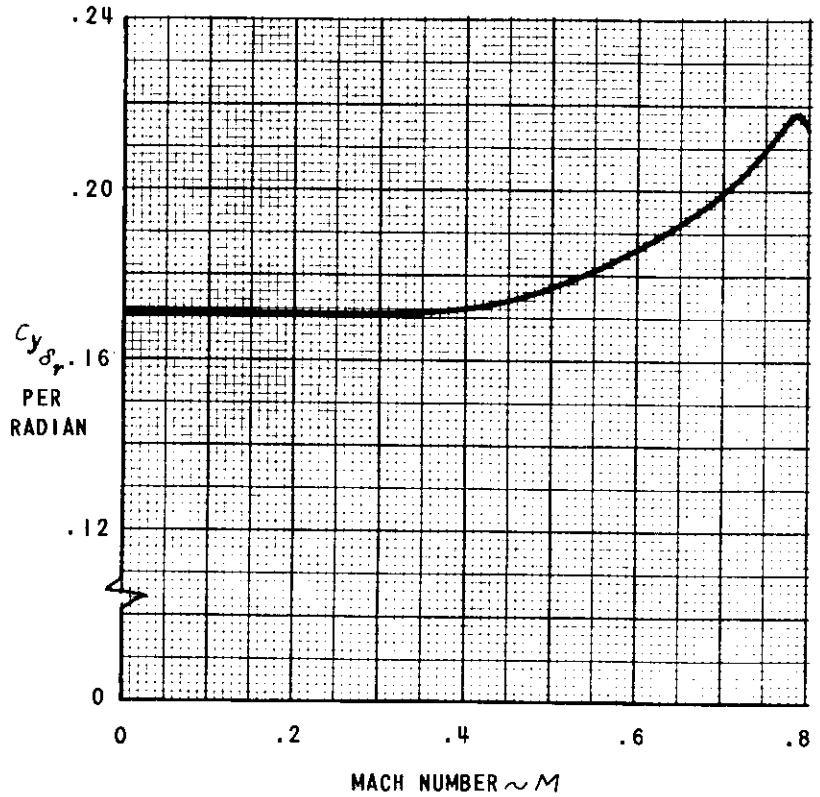

Figure II-26 $C_{y_{\delta_r}}$ VS. M, TIP TANKS ON AND OFF

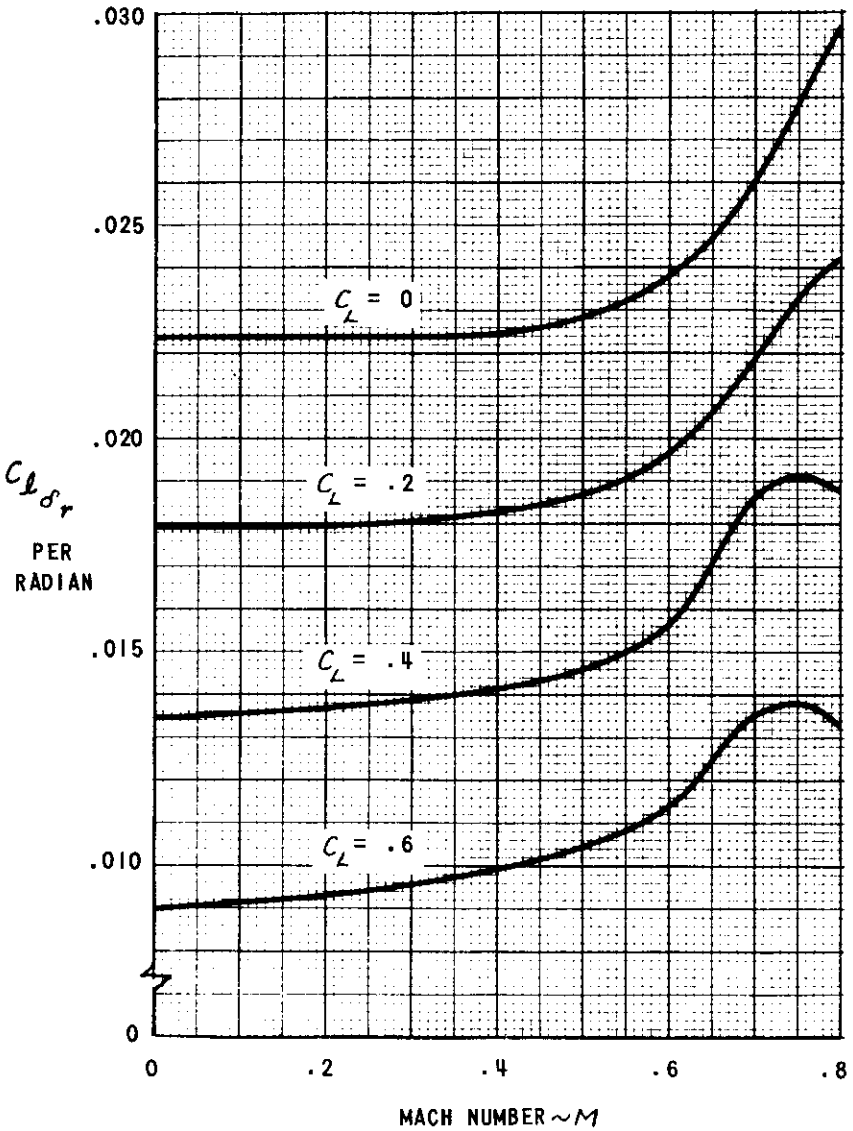

Figure II-27 $C_{l_{\delta_r}}$ VS. M, TIP TANKS ON AND OFF

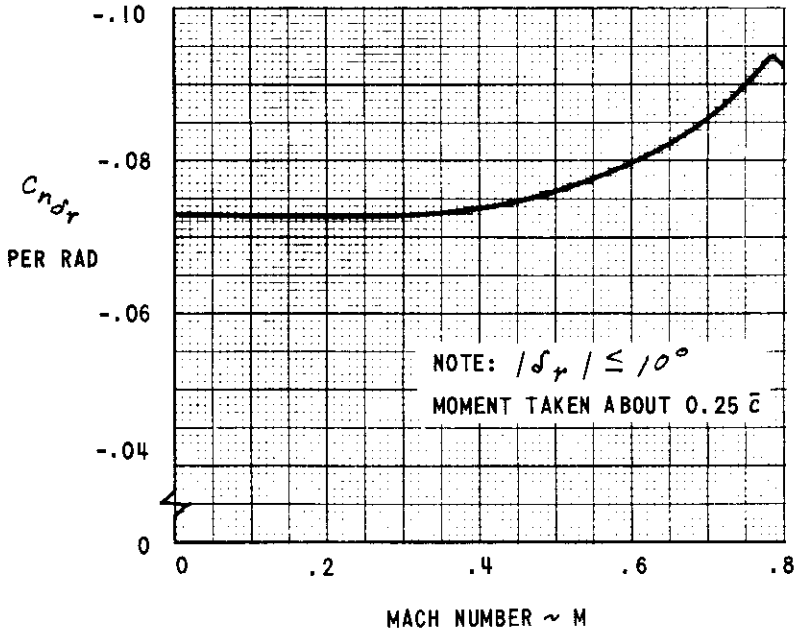

Figure II-28 $C_{n_{\delta_r}}$ VS. M, TIP TANKS ON AND OFF

APPENDIX III

T-33 LATERAL-DIRECTIONAL MODAL PARAMETERS AND
STABILITY DERIVATIVES AS A FUNCTION OF FUEL REMAINING

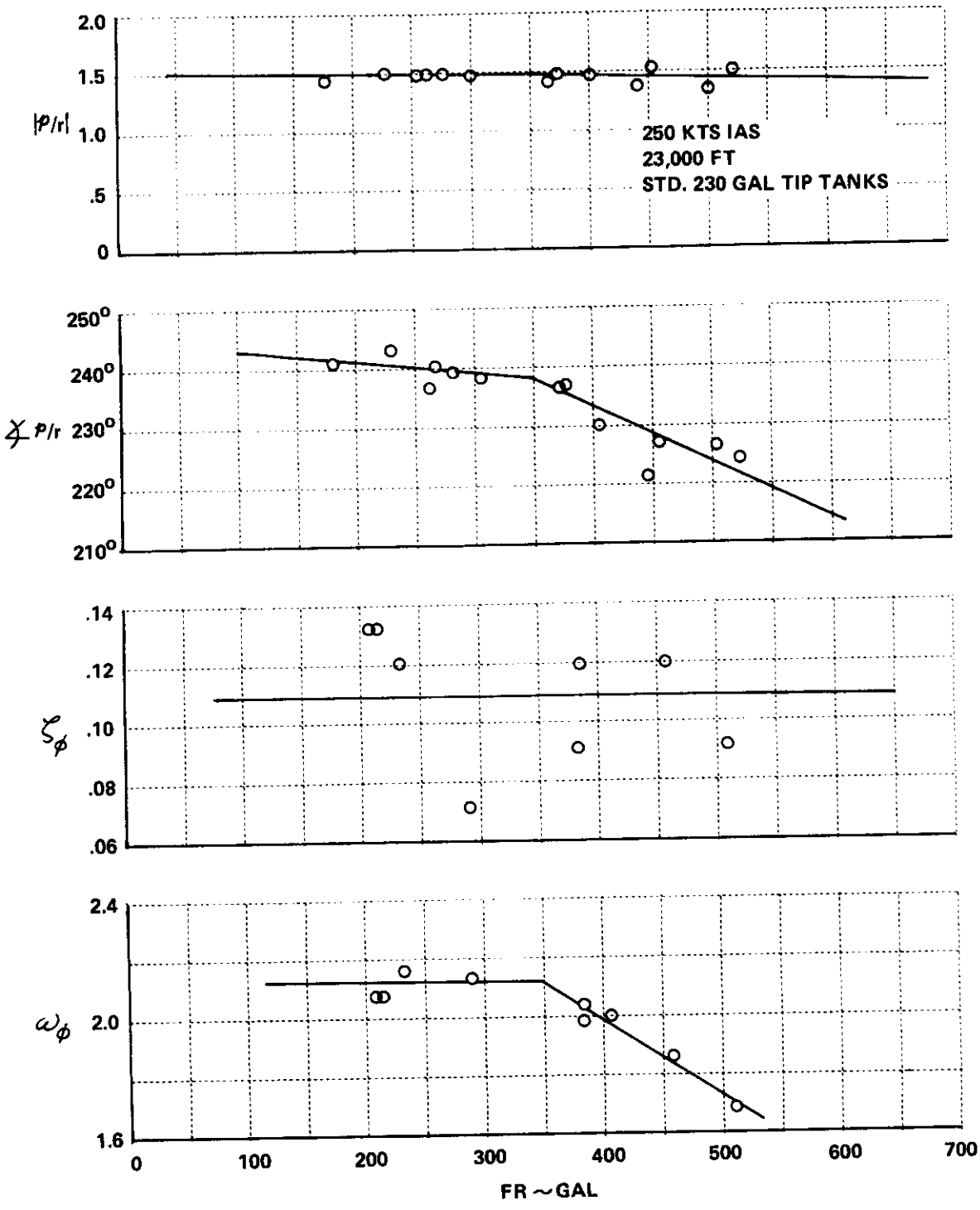

Figure III-1 **LATERAL-DIRECTIONAL MODE CHARACTERISTICS NORMAL T-33 AIRPLANE, 250 KTS, 23,000 FT**

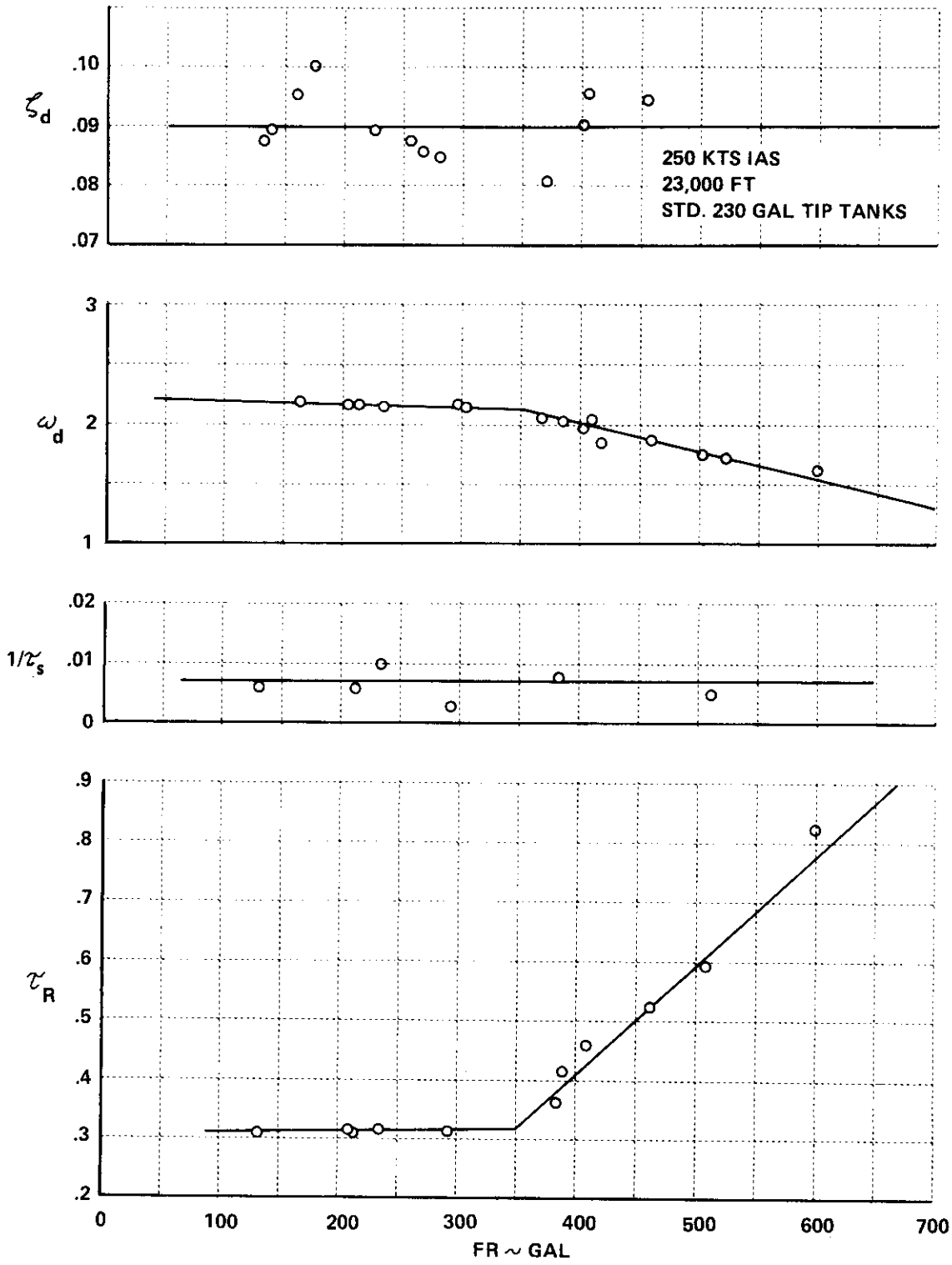

Figure III-2 LATERAL-DIRECTIONAL MODE CHARACTERISTICS
NORMAL T-33 AIRPLANE, 250 KTS, 23,000 FT

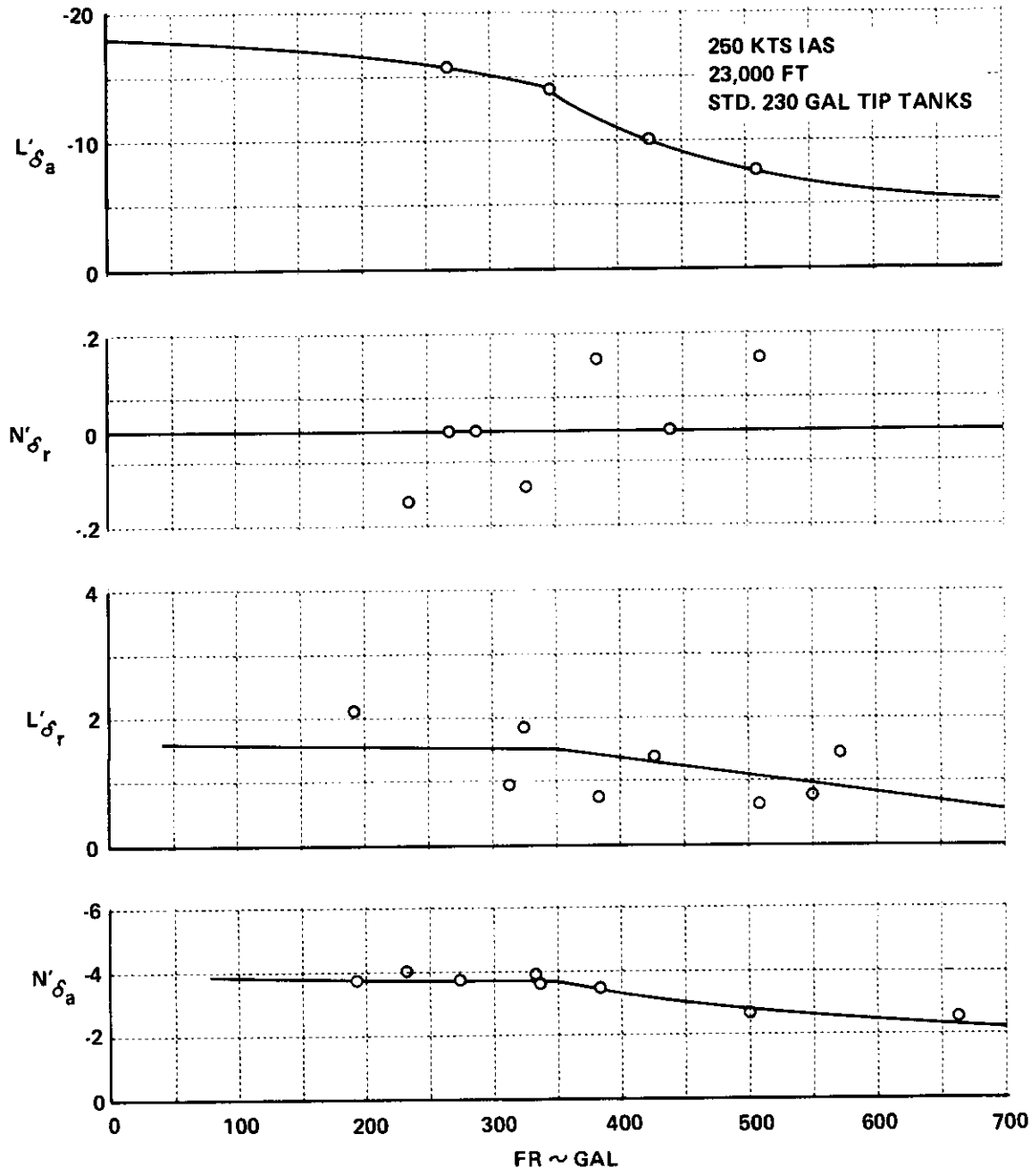

Figure III-3 LATERAL-DIRECTIONAL CONTROL DERIVATIVES
NORMAL T-33 AIRPLANE, 250 KTS, 23,000 FT

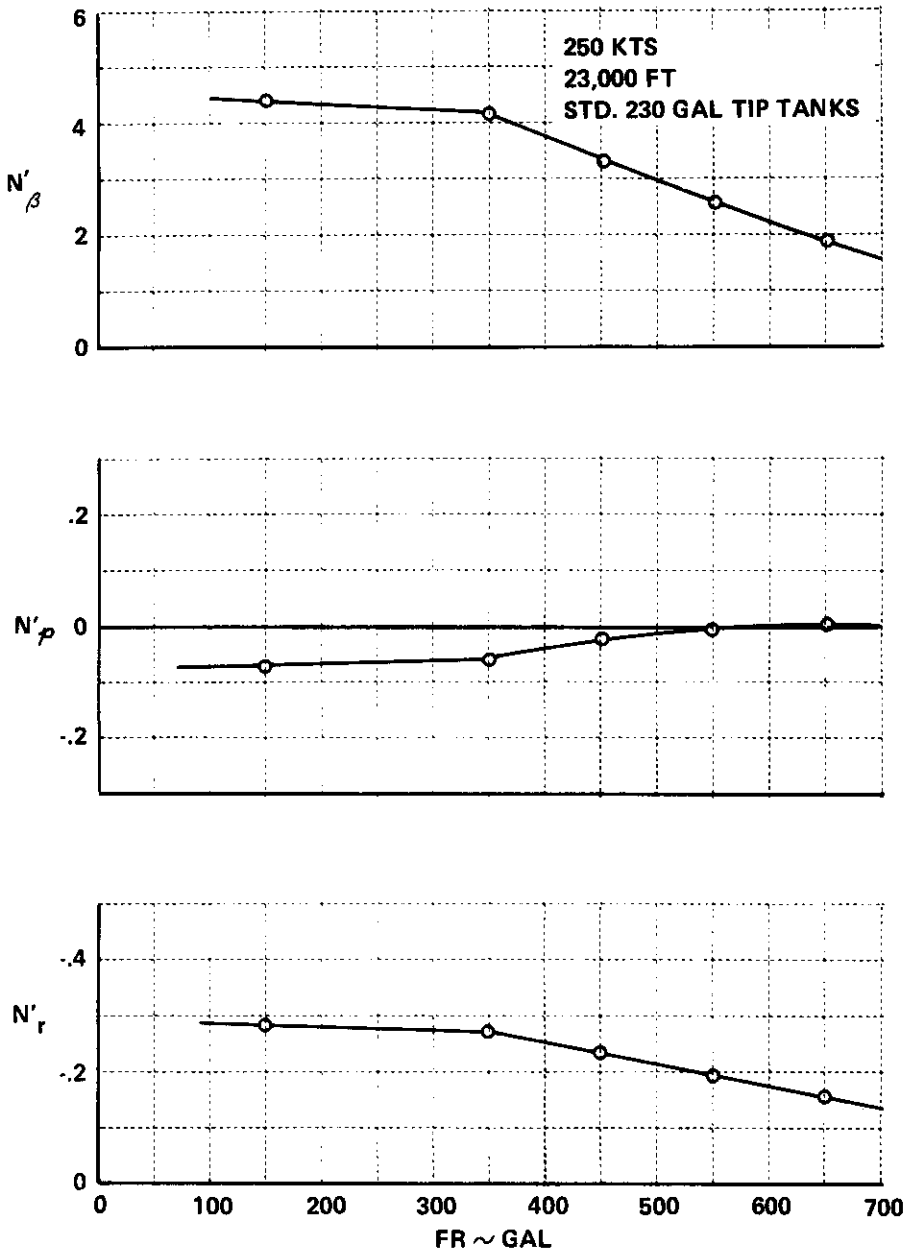

Figure III-4 LATERAL-DIRECTIONAL STABILITY DERIVATIVES NORMAL T-33 AIRPLANE, 250 KTS, 23,000 FT

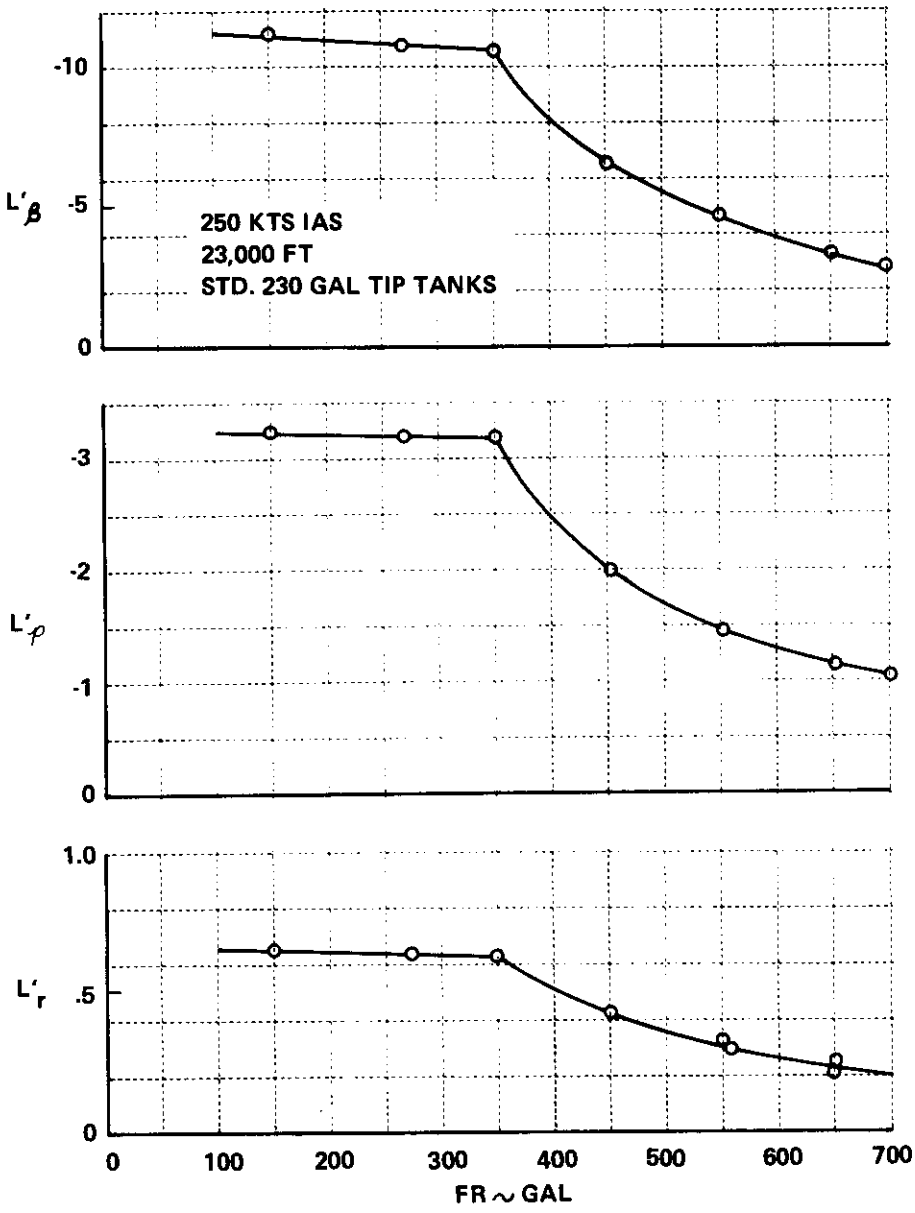

Figure III-5 LATERAL-DIRECTIONAL STABILITY DERIVATIVES NORMAL T-33 AIRPLANE, 250 KTS, 23,000 FT

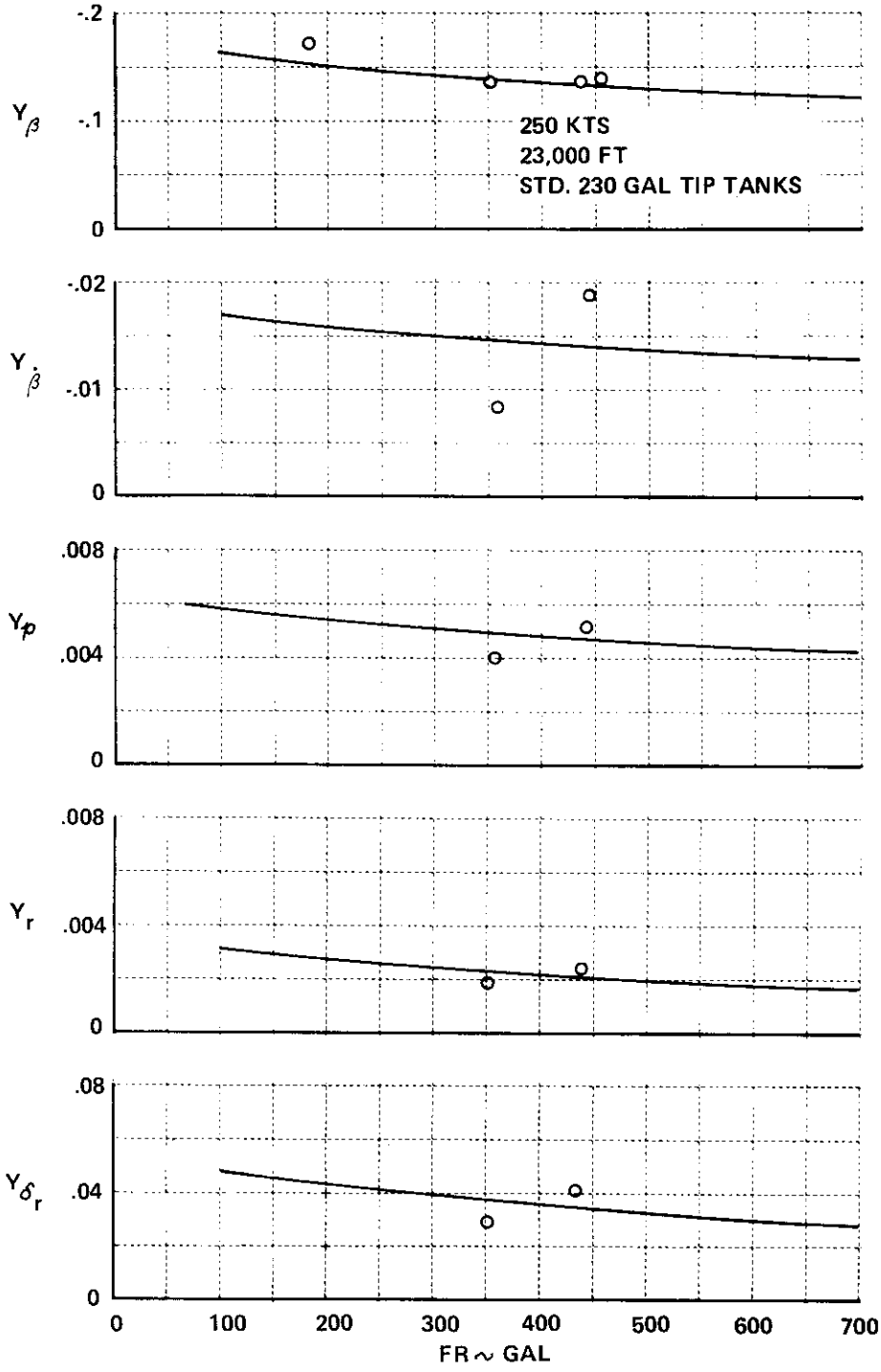

Figure III-6 LATERAL-DIRECTIONAL STABILITY DERIVATIVES NORMAL T-33 AIRPLANE, 250 KTS, 23,000 FT

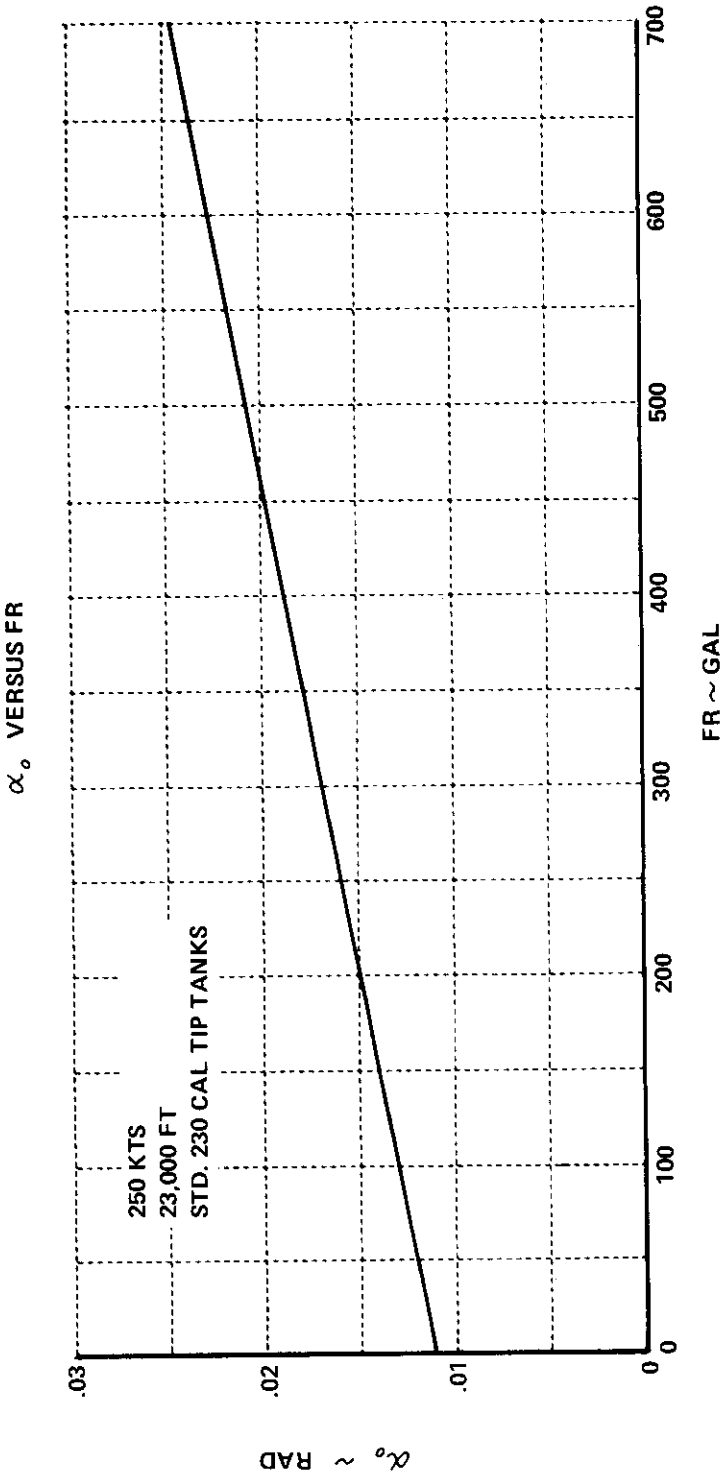

Figure III-7 NORMAL T-33 ANGLE OF ATTACK VS. FUEL REMAINING, 250 KTS, 23,000 FT

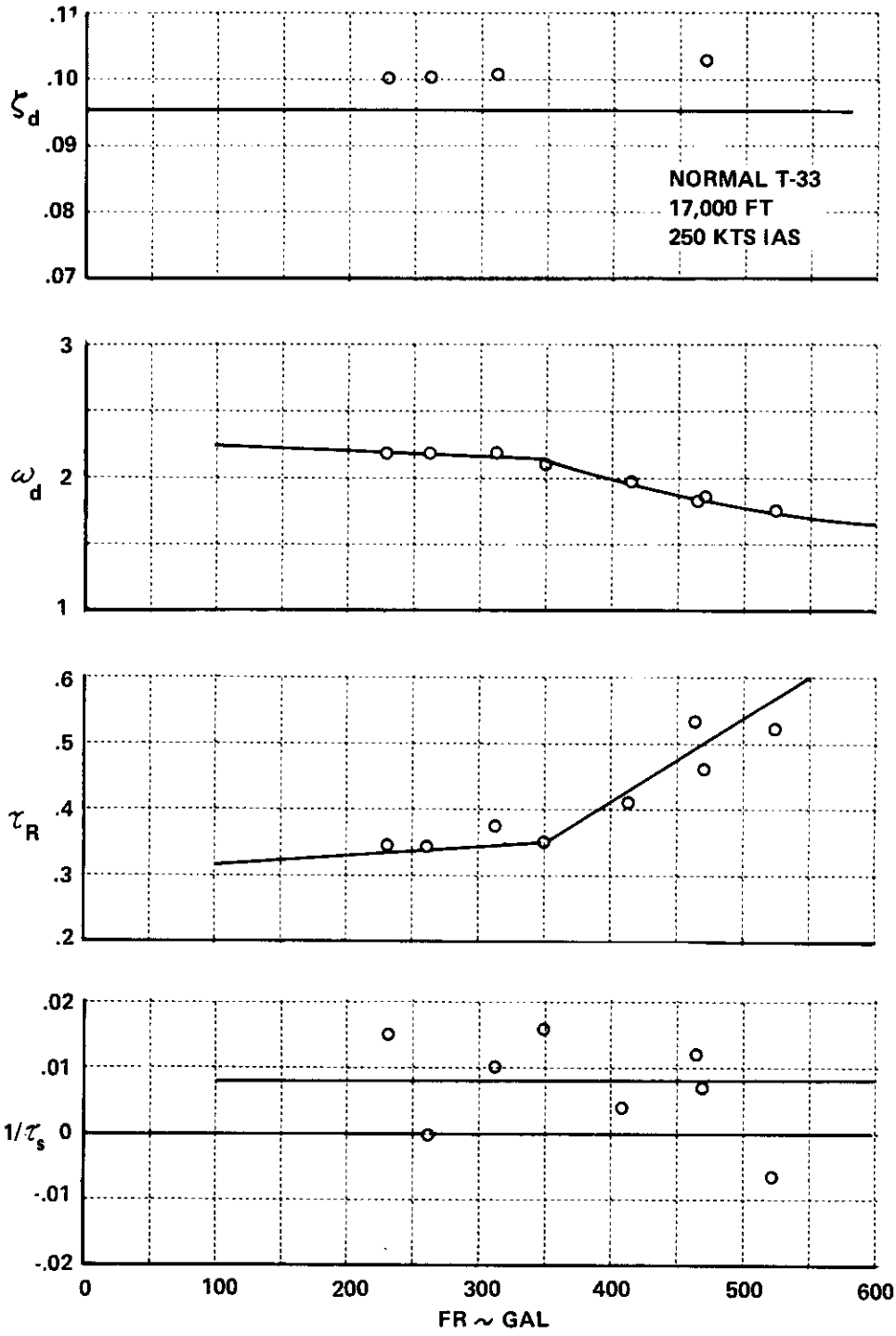

Figure III-8 LATERAL-DIRECTIONAL MODE CHARACTERISTICS
NORMAL T-33, 250 KTS, 17,000 FT

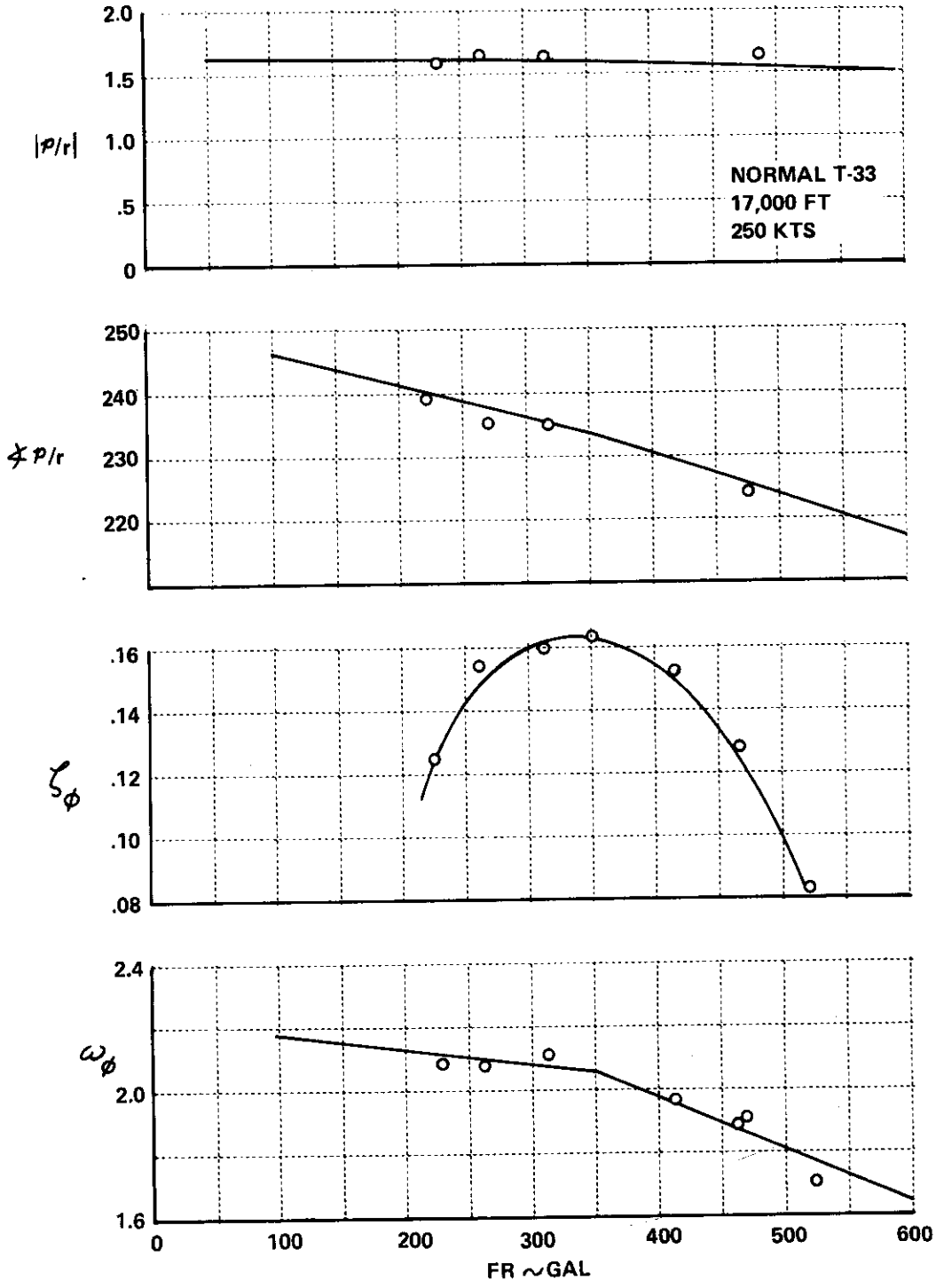

Figure III-9 LATERAL-DIRECTIONAL MODE CHARACTERISTICS
NORMAL T-33, 250 KTS, 17,000 FT

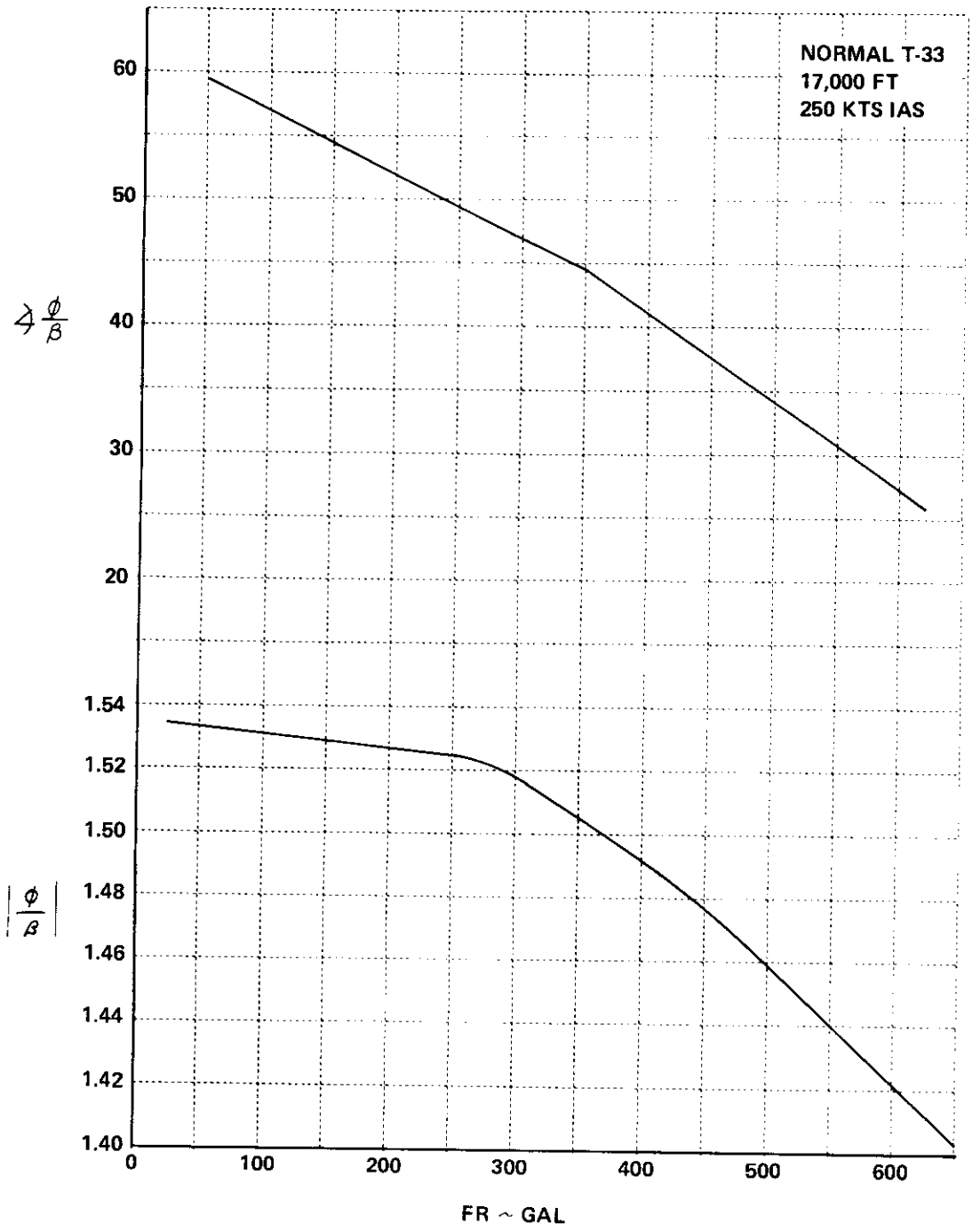

Figure III-10 LATERAL-DIRECTIONAL MODE CHARACTERISTICS
NORMAL T-33 AIRPLANE, 250 KTS, 17,000 FT

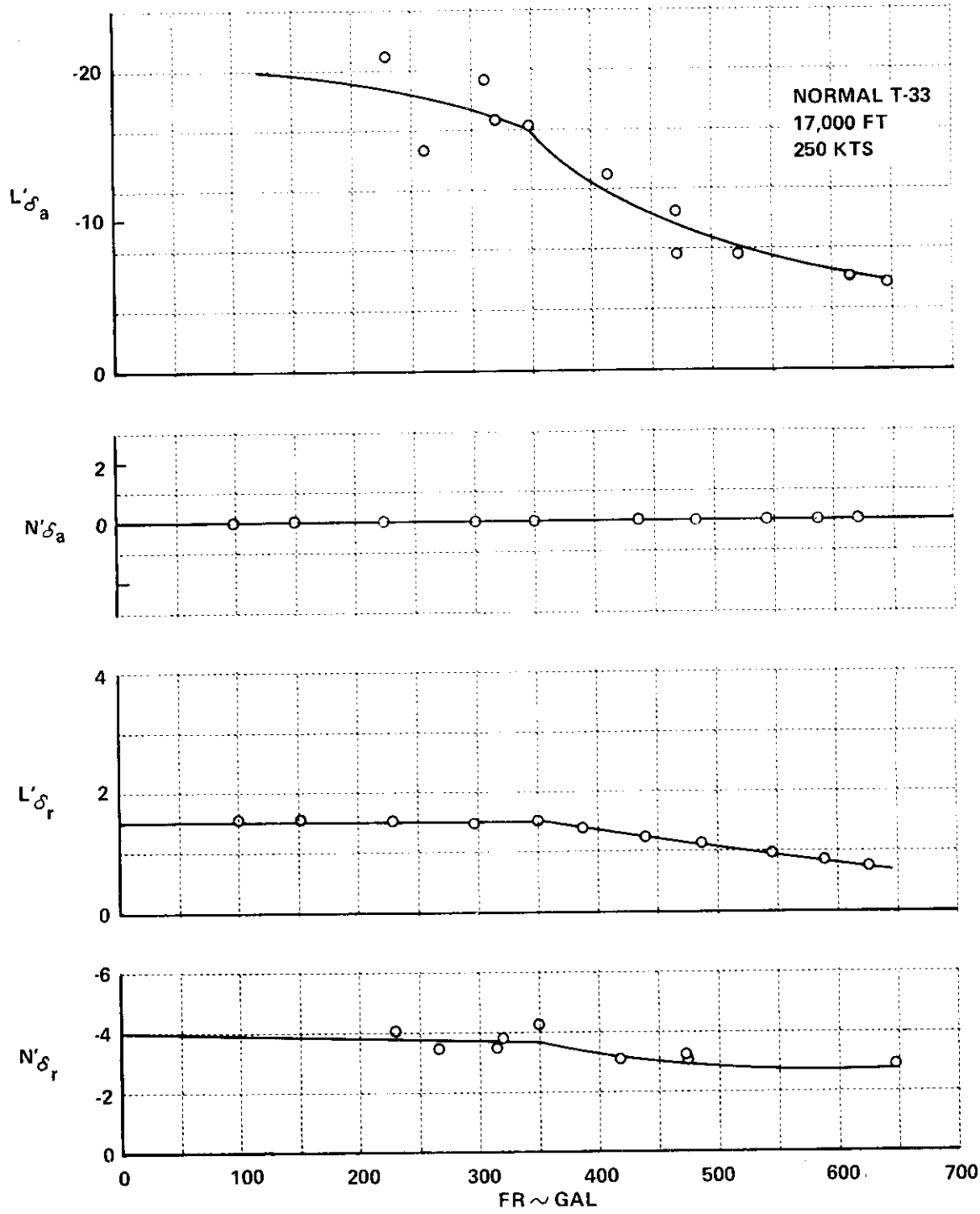

Figure III-11 LATERAL-DIRECTIONAL CONTROL DERIVATIVES
NORMAL T-33, 250 KTS, 17,000 FT

APPENDIX IV

LIST OF T-33 VARIABLE STABILITY SCALE FACTORS

TABLE IV-I

T-33 VARIABLE STABILITY SCALE FACTORS

The entries in the scale factor column are operational amplifier outputs and unless otherwise noted are recorded on both oscillograph and digital recorders.

Parameter	Scale Factor	Plus or minus max value of signal without amplifier overload
α_v	+2°/v	20°
$\Delta\alpha_v$	+1°/v	10°
$\dot{\alpha}_v$	+5°/sec/v	50°/sec
β_v	+1°/v	10°
$\dot{\beta}_v$	+5°/sec/v	50°/sec
$\bar{q}_c$	+0.5 PSI/v	5 PSI
$\Delta\bar{q}_c$	+0.05 PSI/v	0.5 PSI
	(4.42 kt/v @ 250 kt)	(44.2 kt)
$\dot{\bar{q}}_c$	+0.02 PSI/sec/v	0.2 PSI
	(1.81 kt/sec@250 kt)	(18.1 kt/sec)
p	+10°/sec/v	100°/sec
$\dot{p}$	+50°/sec^2/v	500°/sec^2
q	+5°/sec/v	50°/sec
$\dot{q}$	+25°/sec^2/v	250°/sec^2
r	+5°/sec/v	50°/sec
$\dot{r}$	+25°/sec^2/v	250°/sec^2
** θ	+5°/v	50°
ϕ	+10°/v	100°

Parameter	Scale Factor	Plus or minus max value of signal without amplifier overload
N_x	+0.05 g/v	0.5 g
N_y	+0.05 g/v	0.5 g
N_z	+0.5 g/v	5.0 g
Δn_z	+0.5 g/v	5.0 g
δe_{surf}	+2.5°/v	25°
δe_{strut}	-2°/v	20°
* $\delta \ddot{e}_{surf}$	+20,000°/sec^2/v	200,000°/sec^2
$\delta e_{command}$	-2°/v	20°
δa_{total}	+4°/v	40°
$\delta a_{strut\ total}$	-4°/v	40°
* $\delta \ddot{a}_{surf\ total}$	+20,000°/sec^2/v	200,000°/sec^2
$\delta a_{command\ total}$	-4°/v	40°
δr_{surf}	+5°/v	50°
δr_{strut}	-5°/v	50°
* $\delta \ddot{r}_{surf}$	+50,000°/sec^2/v	500,000°/sec^2
$\delta r_{command}$	-5°/v	50°
δ_{ES}	1"/v	10"
$\delta_{ES_{command}}$	-2"/v	20"
F_{ES}	+20#/v	200#
* $\Delta \omega_\eta$	0 to 50 rad/sec	-
* ζ	0 to 2.0	-
* $\Delta F_{ES}/\delta_{ES}$	∞#/in to 1#/in	-
δ_{AS}	1"/v	10"
$\delta_{AS_{command}}$	-1"/v	10"
F_{AS}	+10#/v	100#

Parameter	Scale Factor	Plus or minus max value of signal without amplifier overload
* $\Delta\omega_n$	0 to 50 rad/sec	-
* $\Delta\zeta$	0 to 2.0	-
* $\Delta F_{AS}/\delta_{AS}$	∞ #/in to 0.5#/in	-
δ_{RP}	0.5"/v	5"
$\delta_{RP_{command}}$	-0.5"/v	5"
F_{RP}	+50#/v	500#
* $\Delta\omega_n$	0 to 50 rad/sec	-
* $\Delta\zeta$	0 to 2.0	-
* $\Delta F_{RP}/\delta_{RP}$	∞ #/in to 10#/in	-

* NOT recorded - oscillograph or digital.

** The parameter is actually Sin θ but for small excusions $\theta \approx$ Sin θ.

Δ NOT operational amplifier output.

APPENDIX V

FILTER TRANSFER FUNCTIONS

This appendix contains expressions for transfer function and formulae for circuit design for:

1. Active low pass filter, negative gain, second order, -12 dB/octave slope, (η_x, η_y, η_z filters).
2. Active low pass filter, positive gain, second order, -12 dB/octave slope, (random noise filter).
3. Active low pass filter, negative gain, third order, -18 dB/octave slope, (sensor demodulator filter), (digital recorder filter)
4. Active high pass filter, positive gain, second order, +12 dB/octave slope, (random noise filter).
5. Active network, notch filter, positive gain, (α, β, ρ, q, F_{ES}, F_{RP}, F_{AS} channels)
6. Active network - differentiator and low pass filter, (negative gain) (α, β, ρ, q, r, $\bar{q}_c$ channels)

1. ACTIVE LOW PASS FILTER, SECOND ORDER, (-12 dB/OCTAVE SLOPE), (NEGATIVE GAIN)

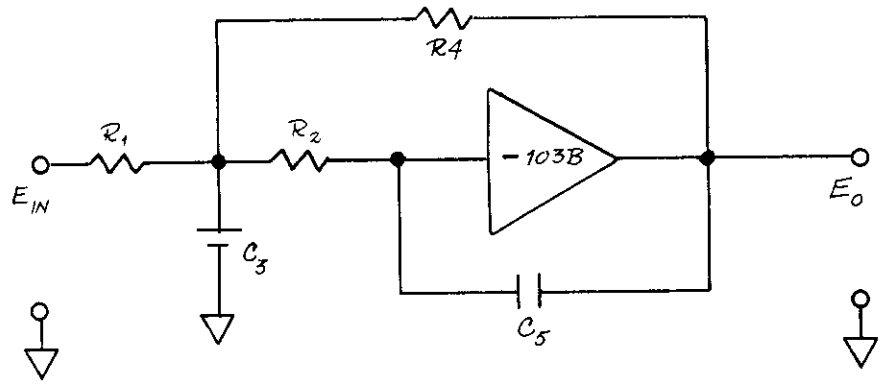

Transfer Function:

$$\frac{E_o}{E_{IN}} = \frac{-\frac{R_4}{R_1}}{s^2\left(R_2 R_4 C_3 C_5\right) + s\left(R_2 C_5 + R_4 C_5 + \frac{R_2 R_4 C_5}{R_1}\right) + 1}$$

$$\frac{E_o}{E_{IN}} = \frac{K}{\frac{s^2}{\omega_n^2} + \frac{2\zeta s}{\omega_n} + 1}$$

Formulas:

$$K = -\frac{R_4}{R_1} \qquad \omega_n = \frac{1}{\sqrt{R_2 R_4 C_3 C_5}}$$

Frequency at which E_o lags E_{IN} by = 90°

$$\zeta = \frac{\omega_n}{2} R_2 C_5 + R_4 C_5 + \frac{R_2 R_4 C_5}{R_1} = \text{damping factor (normally 0.7)}$$

2. ACTIVE LOW PASS FILTER, SECOND ORDER, -12 dB/OCTAVE SLOPE (POSITIVE GAIN)

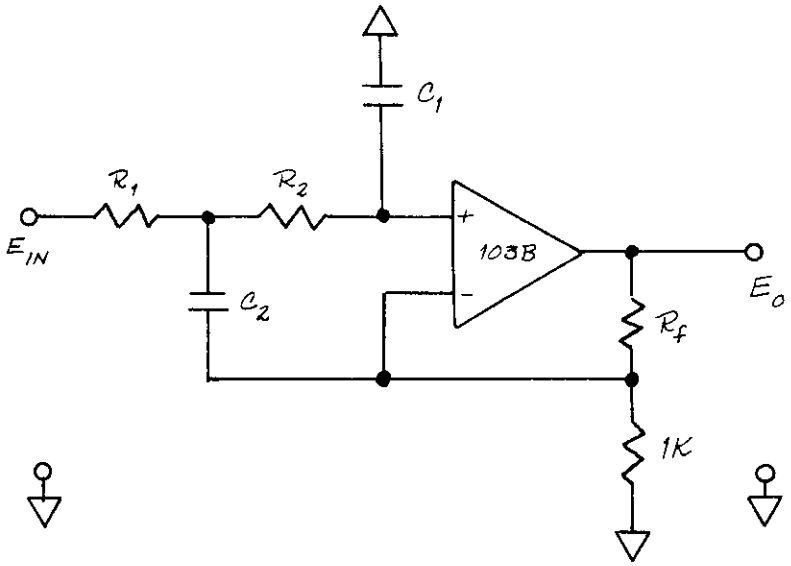

Transfer Function:

$$\frac{E_o}{E_{IN}} = \frac{\frac{R_f + 1K}{1K}}{s^2\left(R_1 R_2 C_1 C_2\right) + sC_1\left(R_1 + R_2\right) + 1}$$

$$\frac{E_o}{E_{IN}} = \frac{K}{\frac{s^2}{\omega_n^2} + \frac{2\zeta s}{\omega_n} + 1}$$

Formulas:

$$K = \frac{R_f + 1K}{1K}$$

$$\omega_n = \frac{1}{\sqrt{R_1 R_2 C_1 C_2}}$$

$$\zeta = \frac{\omega_n}{2} C_1 (R_1 + R_2)$$

3. ACTIVE LOW PASS FILTER, THIRD ORDER, -18 dB/OCTAVE (NEGATIVE GAIN)

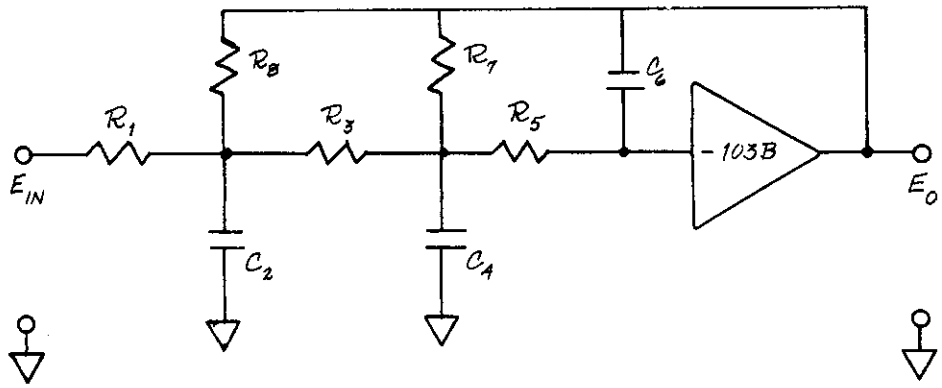

Transfer Function:

$$\frac{E_o}{E_{IN}} = \frac{-b_o}{\frac{a_3 s^3}{\omega_n^3} + \frac{a_2 s^2}{\omega_n^2} + \frac{a_1 s}{\omega_n} + 1} \qquad (1)$$

For Butterworth configuration

$a_3/\omega_n^3 = 1.00$
$a_2/\omega_n^2 = 2.00$
$a_1/\omega_n = 2.00$
$\zeta = 0.5$ damping

See "Synthesis of Passive Networks" by Gwllemin, pg. 591.

L.K. Wadhwa, "Simulation of Third Order Systems With One Operational Amplifier," Proc IRE, Vol. 50, pg. 201-202, February 1962.

$$b_o = \frac{\alpha^2}{(1 + 3\alpha)} \qquad (2)$$

$$\frac{a_1}{\omega_n} = \frac{\alpha}{(1+3\alpha)} RC_2 + (1+\alpha) RC_6 \tag{3}$$

$$\frac{a_2}{\omega_n^2} = \frac{\alpha}{(1+3\alpha)} R^2 C_6 (C_2 + C_4) \tag{4}$$

$$\frac{a_3}{\omega_n^3} = \frac{\alpha^2}{(1+3\alpha)} R_3 C_2 C_4 C_6 \tag{5}$$

$$R_1 = R_3 = R_5 = R \tag{6}$$
$$R_7 = R_8 = \alpha R$$

$$\frac{a_1}{\omega_n} > \frac{\frac{a_3}{\omega_n^3}(1+2\alpha)}{\frac{a_2}{\omega_n^2}(1+3\alpha)} \tag{7}$$

$$T_1 = RC_2$$
$$T_2 = RC_4 \tag{8}$$
$$T_3 = RC_6$$

$$T_1^3 - \frac{\frac{a_1}{\omega_n}(1+3\alpha)}{\alpha} T_1^2 + \frac{\frac{a_2}{\omega_n^2}(1+\alpha)(1+3\alpha)^2}{\alpha^2(1+2\alpha)} T_1 - \frac{\frac{a_3}{\omega_n^3}(1+\alpha)(1+3\alpha)^2}{\alpha^3} = 0 \tag{9}$$

Procedure:

1. Given b_0, a_1/ω_n, a_2/ω_n^2, a_3/ω_n^3, R_1, R_3, R_5, R_7, R_8
   Solve for α from Equation 2.
2. Make check using Equation 7.
3. Solve Equation 9 for T_1.
4. Solve Equation 4, 5 for T_2, T_3 using the value of T_1 from Step 3 where $T_2 = RC_4$, $T_3 = RC_6$, $T_1 = RC_2$
5. Solve for values of C_2, C_4, C_6 from Equation 8 and select physical capacitors with values as close as possible to those calculated.

4. ACTIVE HIGH PASS FILTER, SECOND ORDER, +12 dB/OCTAVE SLOPE (POSITIVE GAIN)

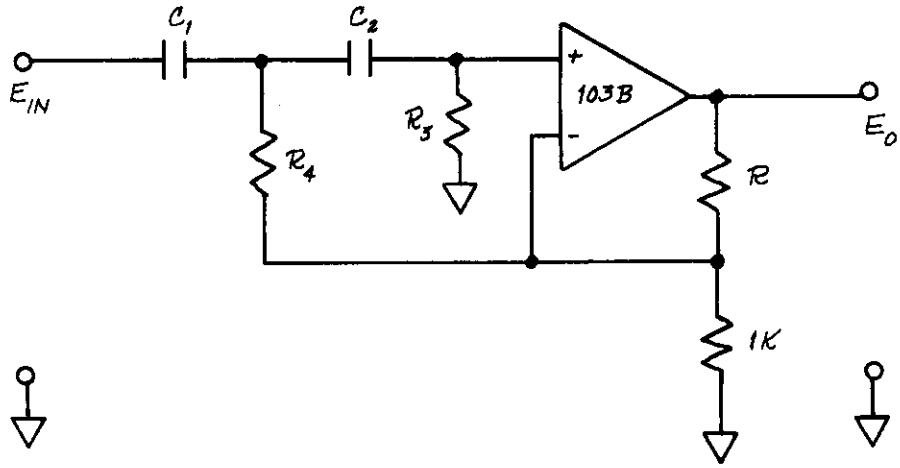

Transfer Function:

$$\frac{E_o}{E_{IN}} = \frac{+\left(\frac{R+1K}{1K}\right) s^2 R_3 R_4 C_1 C_2}{s^2 R_3 R_4 C_1 C_2 + s(C_1 R_4 + C_2 R_4) + 1}$$

$$\frac{E_o}{E_{IN}} = \frac{+K s^2}{\frac{s^2}{\omega_n^2} + \frac{2\zeta s}{\omega_n} + 1}$$

Formulas:

$$K = \left(\frac{R+1K}{1K}\right) R_3 R_4 C_1 C_2$$

$$\omega_n = \frac{1}{\sqrt{R_3 R_4 C_1 C_2}}$$

$$\zeta = \frac{\omega_n}{2} R_4 (C_1 + C_2)$$

5. ACTIVE NETWORK - NOTCH FILTER (POSITIVE GAIN)

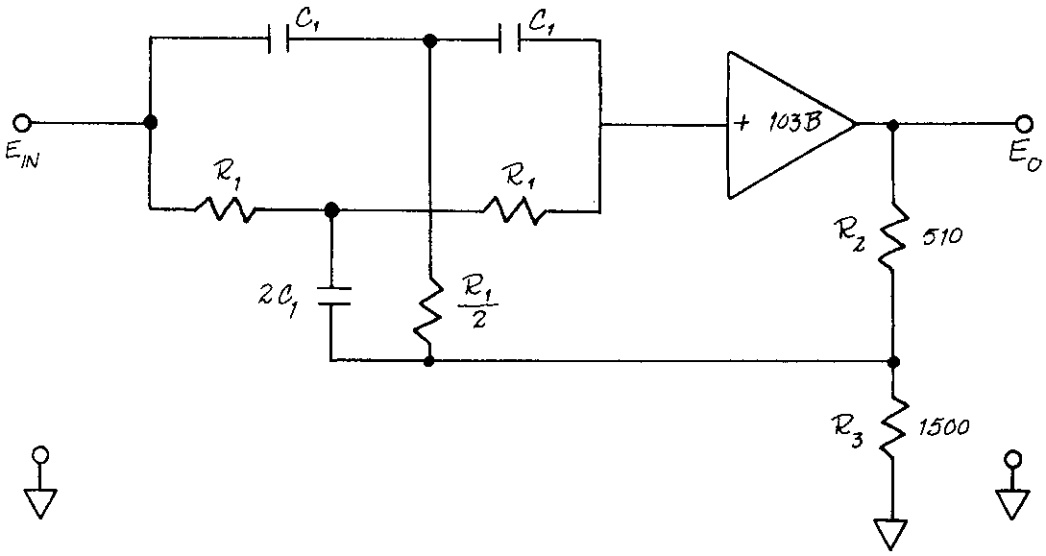

Transfer Function:

$$\frac{E_o}{E_{IN}} = \frac{s^2 R_1^2 C_1^2 + 1}{s^2 R_1^2 C_1^2 + s(4R_1C_1 - 4KR_1C_1) + 1}$$

Formulas:

$$K = \frac{R_3}{R_2 + R_3}$$

$$\zeta = 2 - 2K$$

$$f_{notch} = \frac{1}{2\pi R_1 C_1}$$

Example

$R_2 = 510\Omega$, $R_3 = 1500\Omega$

$$K = \frac{1500}{2010} \approx 0.75$$

$$\zeta = 2 - 2(.75) = 0.5$$

for $K = 0$, $\zeta = 2.0$
(no feedback network)

6. ACTIVE NETWORK - DIFFERENTIATOR AND LOW PASS FILTER (NEGATIVE GAIN)

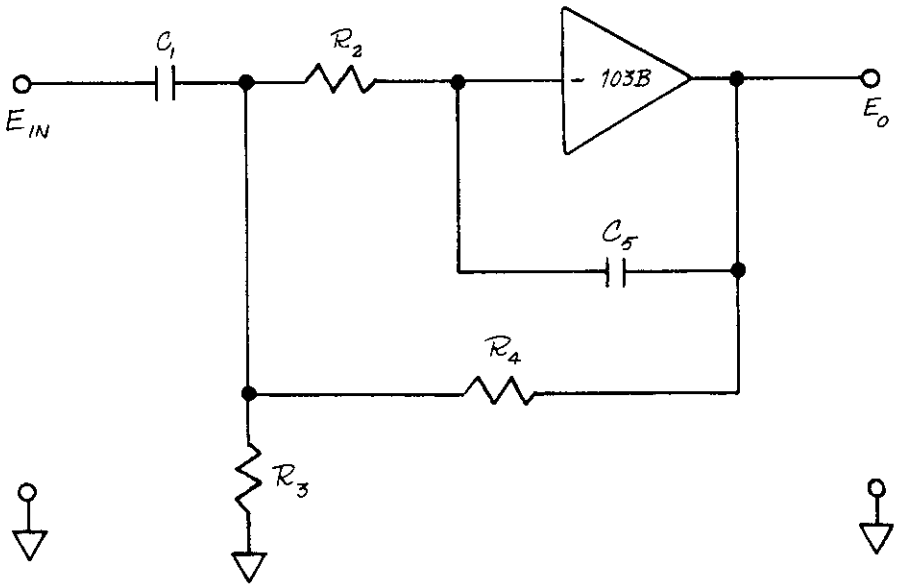

Transfer Function:

$$\frac{E_{OUT}}{E_{IN}} = \frac{-K_S}{\frac{s^2}{\omega_n^2} + \frac{2\zeta s}{\omega_n} + 1}$$

$$= \frac{-sC_1R_4}{s^2(R_2R_4C_1C_5) + s\left(R_2C_5 + R_4C_5 + \frac{R_2R_4C_5}{R_3}\right) + 1}$$

$K = C_1R_4$ = velocity constant

$$\omega_n = \frac{1}{\sqrt{R_2R_4C_1C_5}} \quad \text{rad/sec} = \text{filter cutoff frequency}$$

$$\zeta = \frac{\omega_n}{2}\left(R_2C_5 + R_4C_5 + \frac{R_2R_4C_5}{R_3}\right)$$

The T-33 VSS differentiators-low pass filters have the following component values.

	α, β, p, q, r	$\bar{q}_c$
C_1 =	10.0 μf	10.0 μf
R_2 =	750 Ω	3.01 Ω
R_3 =	Infinity	Infinity
R_4 =	20 K Ω	250 K Ω
C_5 =	1.5 μf	0.33 μf
ω_n =	66.7	20.0
ζ =	1.038	.827
K =	0.2	2.5

$$\omega_n = \frac{1}{\sqrt{R_2 R_4 C_1 C_5}} = \frac{1}{\sqrt{(750)(20\times10^3)(10\times10^{-6})(1.5\times10^{-6})}}$$

$$\omega_n = 66.7 \text{ rad/sec} \qquad f_n = \frac{\omega_n}{2\pi} = 10.6 \text{ cps}$$

$$\zeta = \frac{\omega_n}{2}\left(R_2 C_5 + R_4 C_5 + \frac{R_2 R_4 C_5}{R_3}\right)$$

$$\zeta = \frac{66.7}{2}\left[(750)(1.5\times10^{-6}) + (20\times10^3)(1.5\times10^{-6})\right]$$

$$\zeta = 1.038$$

$$K = (10\times10^{-6})(20\times10^3) = 0.2$$

APPENDIX VI

VSS FREQUENCY RESPONSE PLOTS

This appendix contains frequency response plots and measurement techniques for the various electrical (in some cases electrical-hydraulic) components and subsystems that make up the variable stability system. Most of the data were taken from ground records; however, data on the control surface servo responses were taken from flight records. A list of the plots is given below.

α vane, demodulator and 60 Hz third-order low pass filter.

β probe, demodulator and 60 Hz third order low pass filter.

$\bar{q}_c$ pressure transducer, demodulator, and 60 Hz third-order low pass filter.

r rate gyro, demodulator and 60 Hz third-order low pass filter.

p rate gyro, demodulator and 60 Hz third-order low pass filter.

q rate gyro, demodulator and 60 Hz third-order low pass filter.

n_x accelerometer and second-order low pass filter.

n_y accelerometer and second-order low pass filter.

n_z accelerometer and second-order low pass filter.

Notch Filter, typical response curves.

NOTE: The notch frequency for α, β, p, q, r and $\bar{q}_c$ channels depends upon specific flight program requirements and thus is subject to change.

Differentiator and second-order low pass filter. The α, β, p, q, r differentiators are identical, therefore only information on the α channel and $\bar{q}_c$ channel differentiators is included.

Sensor demodulator filter, third-order, low pass (α, β, p, q, r)

Function generator plot, sin ϕ to ϕ.

ϕ indicator (front cockpit Lear ARU-2B/V) and ϕ recording dynamics.

θ indicator (front cockpit Lear ARU-2B/V) and θ recording dynamics.

ϕ display (ϕ^*) servo.

Horizontal and vertical pointers of the front cockpit altitude indicator Lear ARU-2B/A (vertical and horizontal tracking needles).

Control Surface Servos amplitude and frequency responses.

Measurement technique, α Vane and β Probe and $\bar{q}_c$ Sensor Dynamics

Ordinarily the procedure for obtaining data on the α vane, β probe and $\bar{q}_c$ sensor dynamics due to the electronics associated with the pickoffs, demodulators and demodulator filters would be to apply a physical step change in position to the vane or probe and step change in pressure to pickoff while recording the filter output. There appeared to be no practical way, however, of physically applying a step change of position to the vane or probe or recording the step change in pressure to the $\bar{q}_c$ pickoff. Therefore, a step change in vane, probe, and $\bar{q}_c$ pickoff excitation was done instead.

The assumption was that there would be little or no difference as far as the dynamics is concerned between a step change in the excitation to these sensors and a physical step change (if it could be done) to vane, probe, etc., since the vane and probe are connected directly to the synchro rotors. The step response was then digitally analyzed and amplitude and phase information obtained. These dynamics do not, of course, take into account the dynamics of the vane or probe aligning themselves with the relative wind or the dynamics of the $\bar{q}_c$ pickoff in adjusting to new pressure changes.

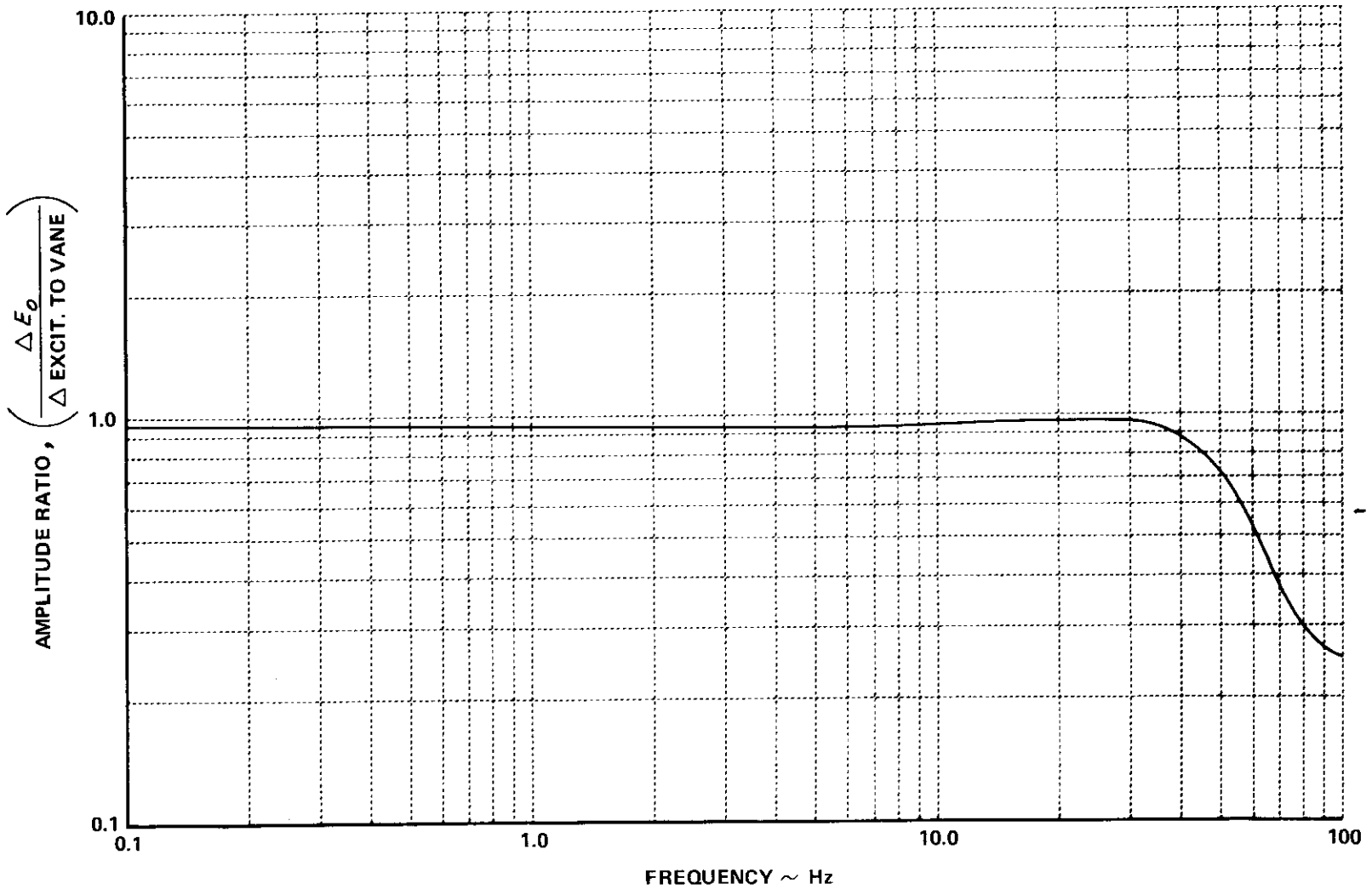

Figure VI-1 α_{VANE} DYNAMICS DUE TO ELECTRONICS OF PICKOFF, DEMODULATOR AND LOW PASS FILTER

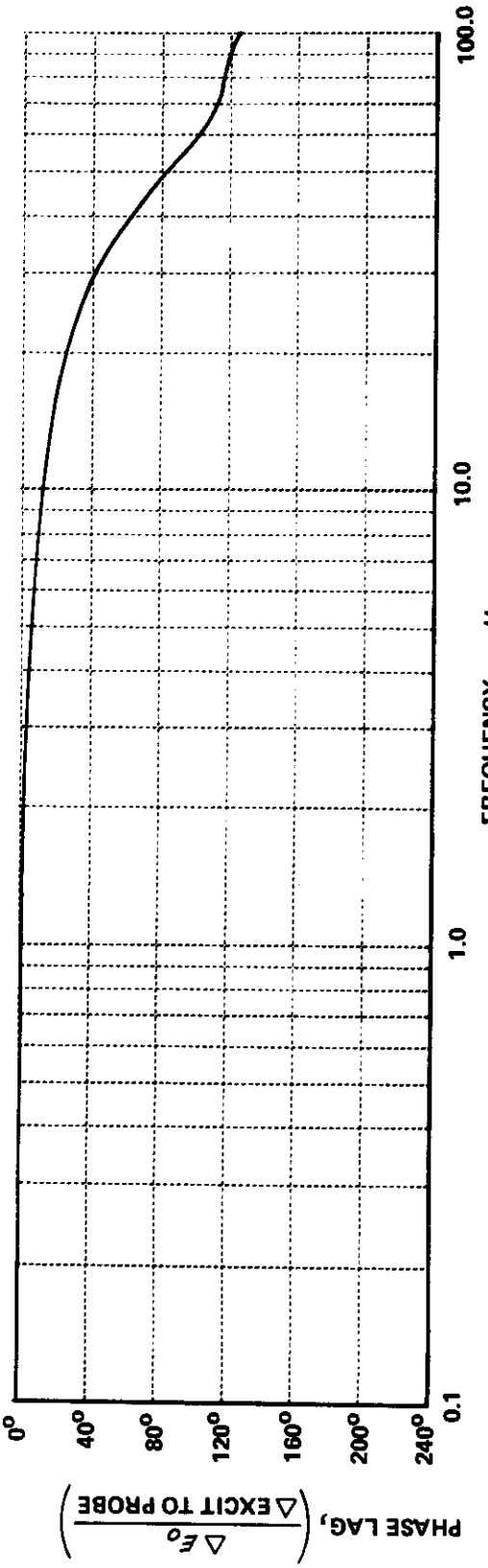

Figure VI-2 α_{VANE} DYNAMICS DUE TO ELECTRONICS OF PICKOFF, DEMODULATOR AND LOW PASS FILTER

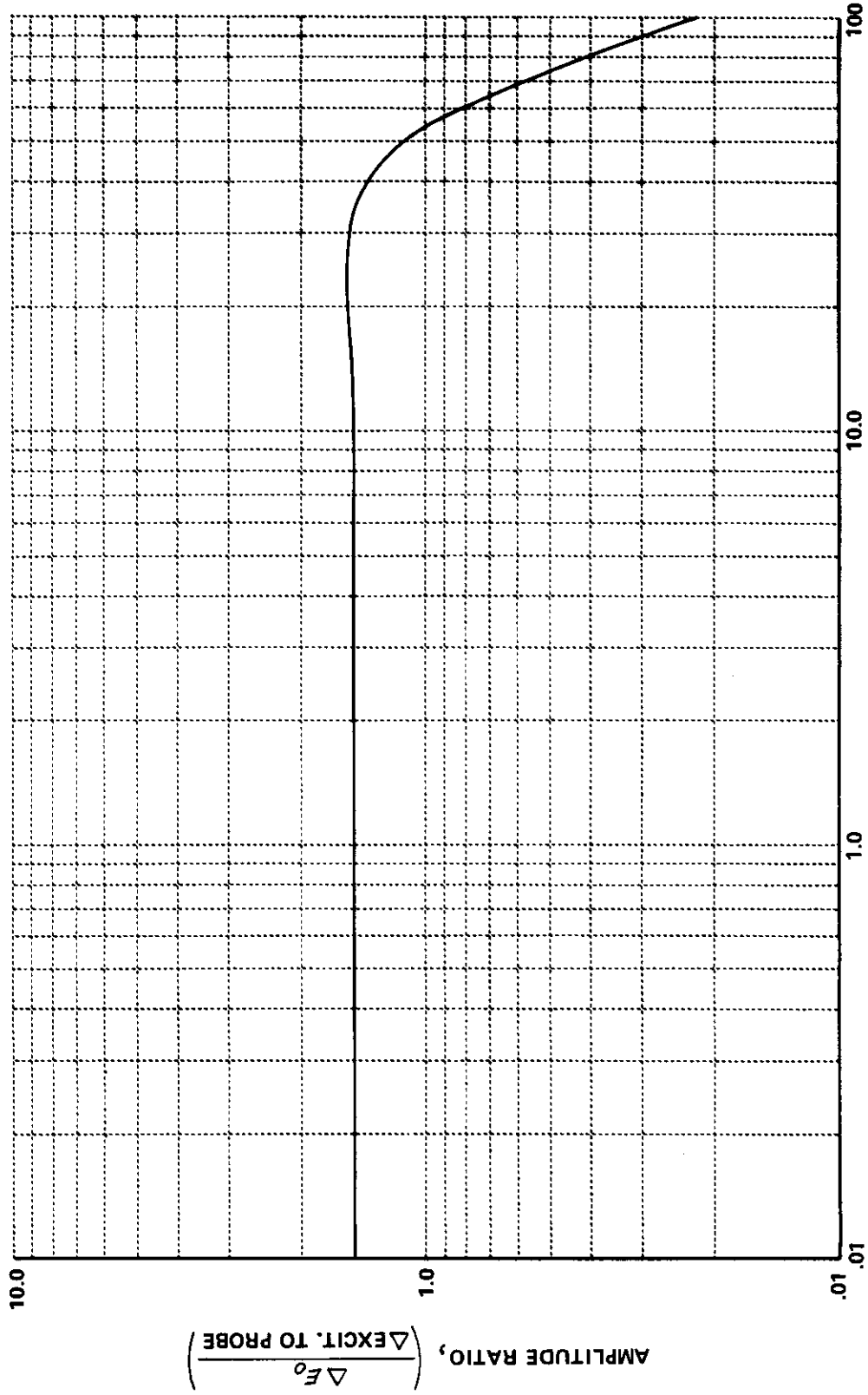

Figure VI-3 β_{PROBE} DYNAMICS DUE TO ELECTRONICS OF PICKOFF, DEMODULATOR AND LOW PASS FILTER

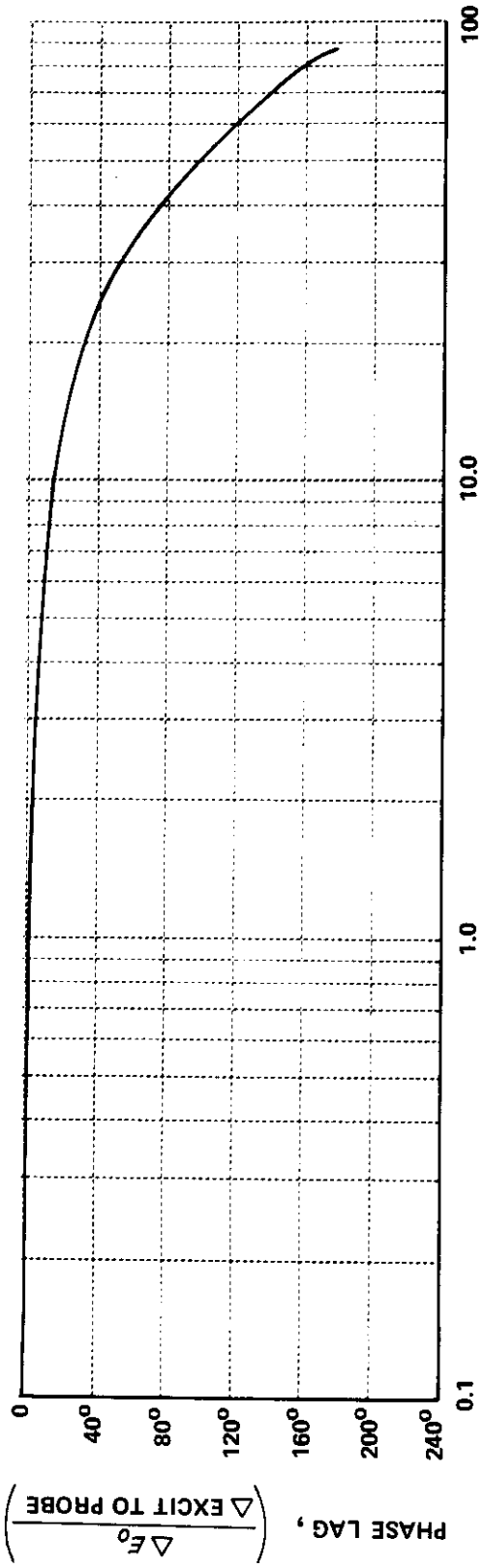

Figure VI-4 β_{PROBE} DYNAMICS DUE TO ELECTRONICS OF PICKOFF, DEMODULATOR AND LOW PASS FILTER

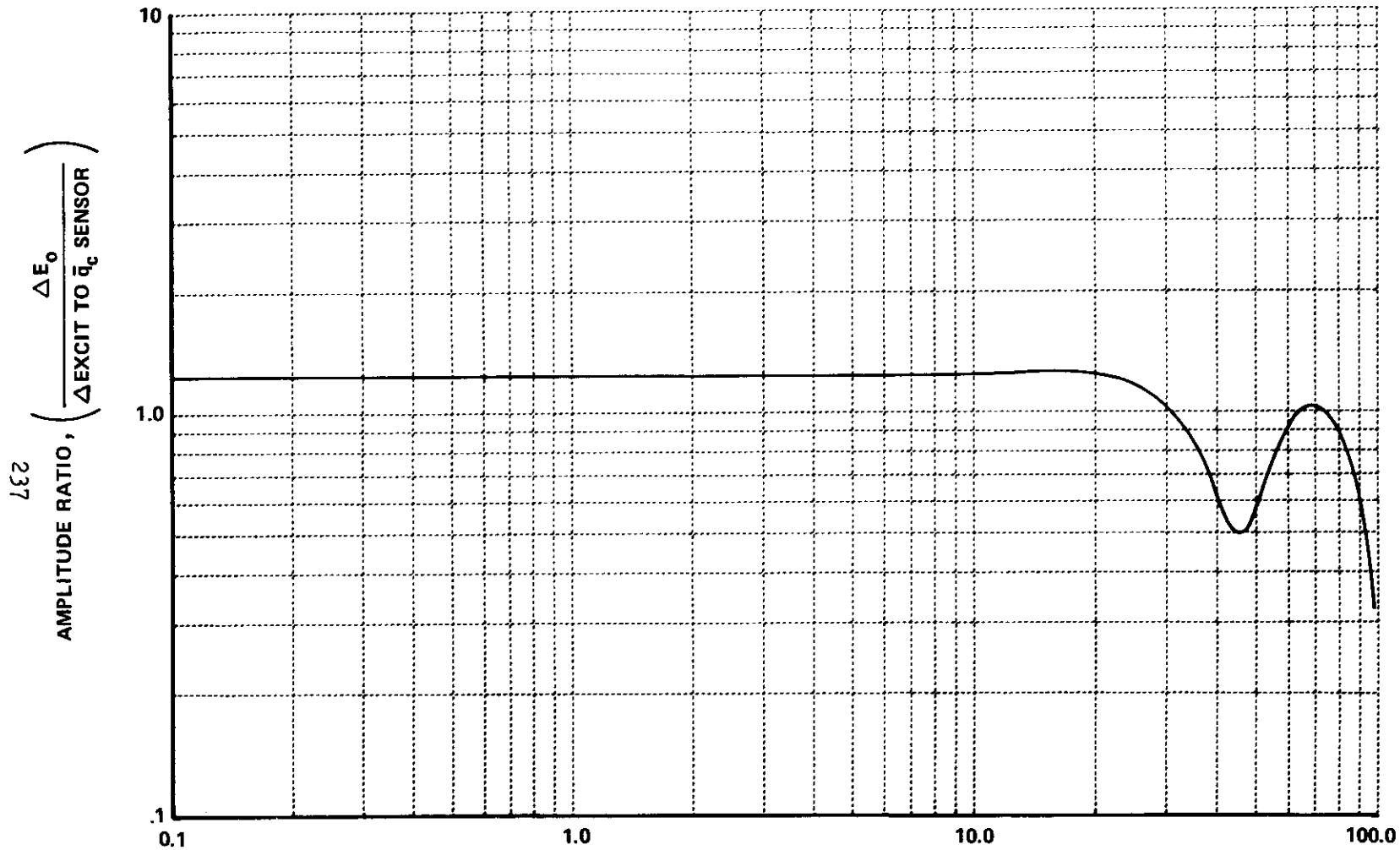

Figure VI-5 $\bar{q}_c$ SENSOR DYNAMICS DUE TO ELECTRONICS OF PICK OFF, DEMODULATOR AND LOW PASS FILTER

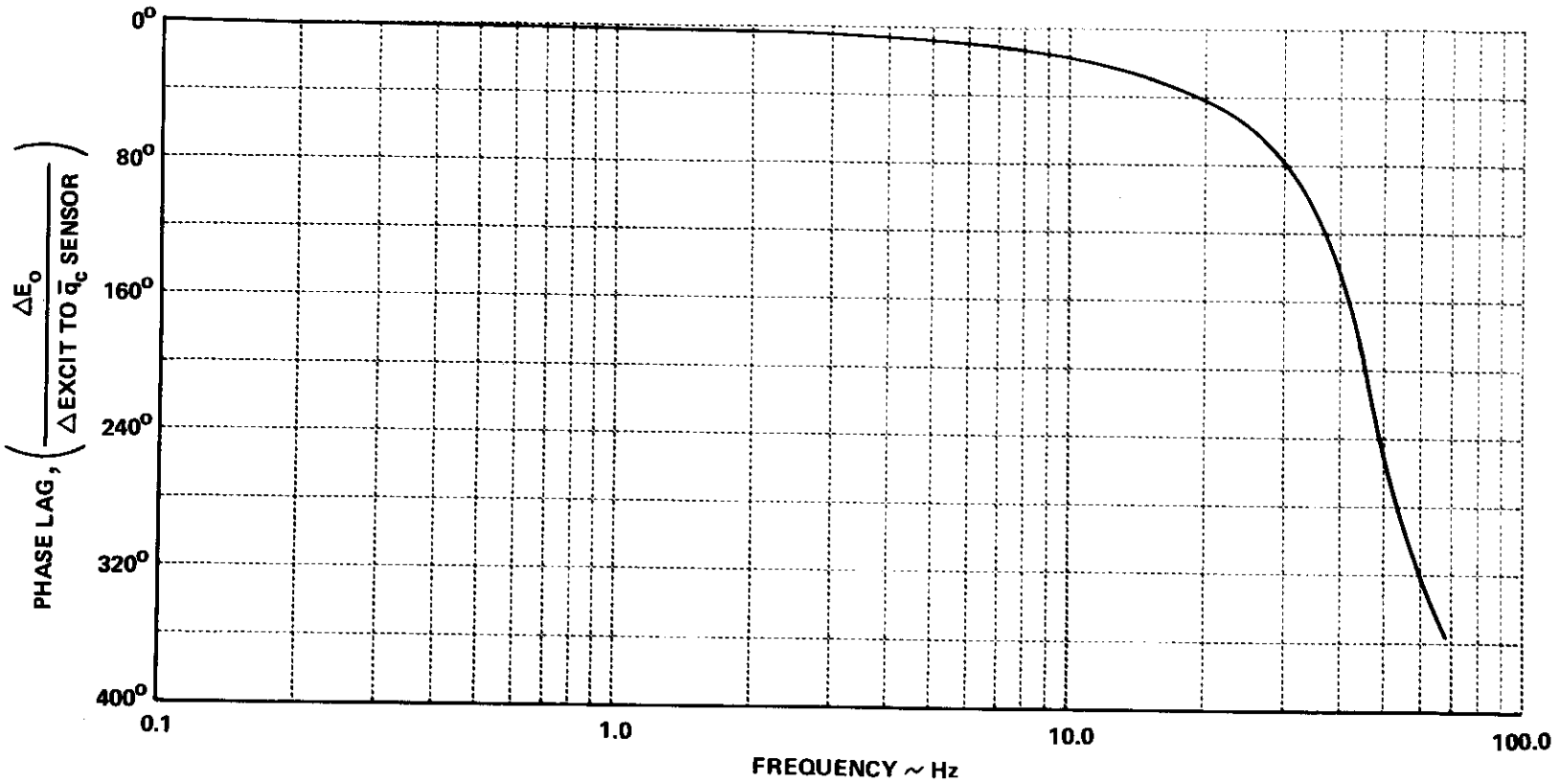

Figure VI-6 $\bar{q}_c$ SENSOR DYNAMICS DUE TO ELECTRONICS OF PICKOFF, DEMODULATOR AND LOW PASS FILTER

Measurement technique, p, q, r Rate Gyro Dynamics

The dynamics of the p, q, and r rate gyros were determined by analyzing the response of the gyros to a step input. The electrical step was applied through the gyro self-test input which torques the gimbal to a predetermined level and the response was recorded at the output of the 80 Hz low pass third-order filter. The step response data were then digitally analyzed and amplitude and phase information obtained.

Manufacturer's Specifications
T-33 RATE GYRO PACKAGE U.S. TIME P/N 400750

	p	q	r
Range	125 deg/sec	40 deg/sec	40 deg/sec
Damping	.7 ±.18	.7 ±.18	.7 ±.18
Natural Frequency	44 Hz	28 Hz	28 Hz
UNITED STATES TIME INC. Part Number	301655	301575	301575

Figure IV-7 shows the physical shape of the three-axis package.

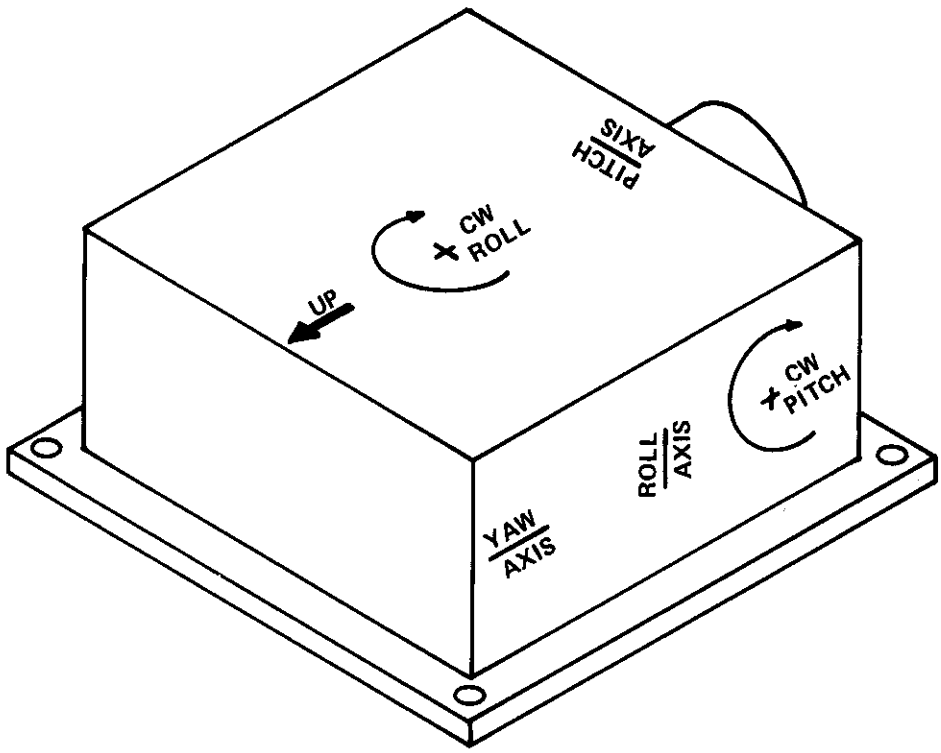

Figure VI-7 U.S. TIME THREE AXIS SELF-TEST RATE GYRO PACKAGE

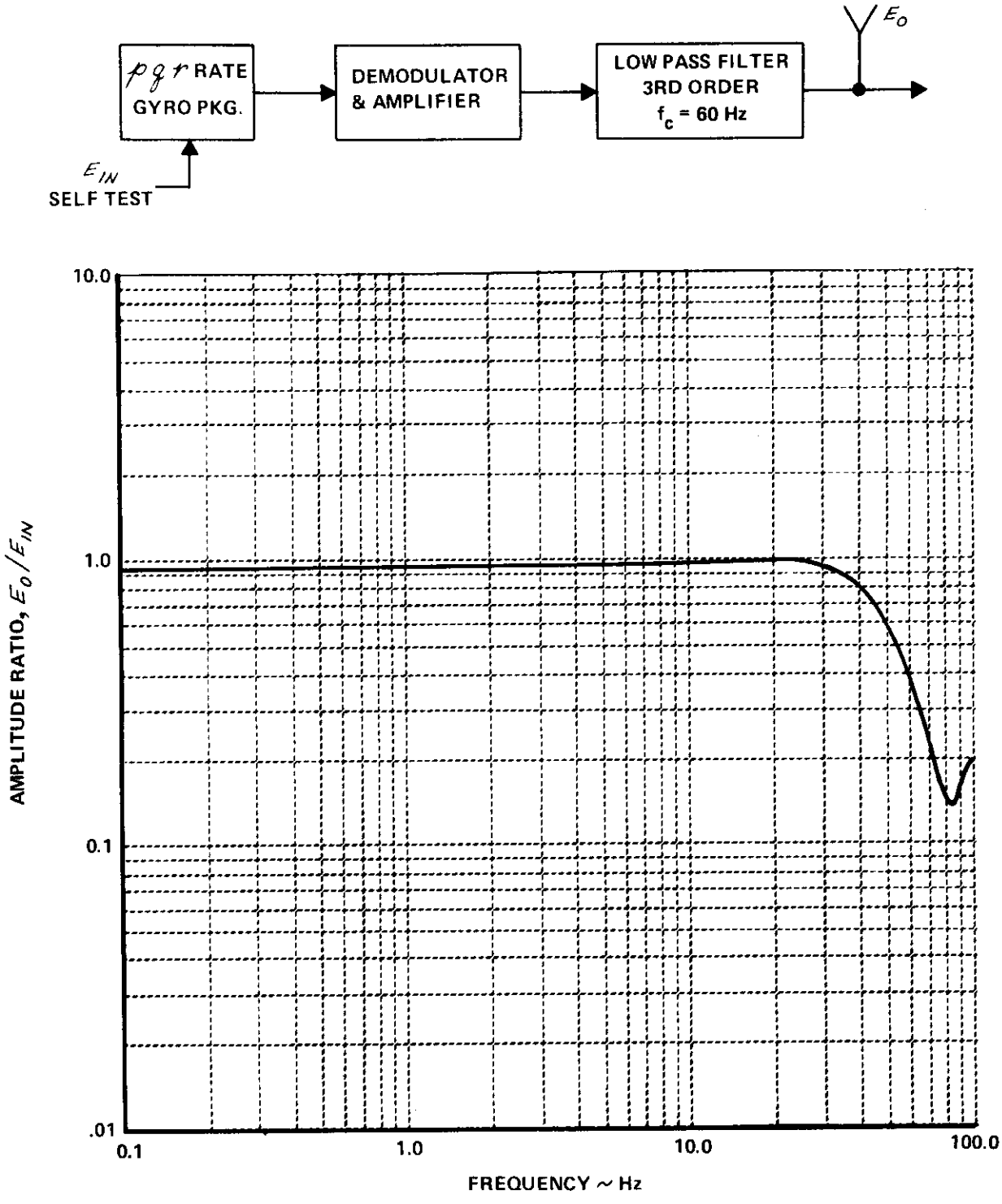

Figure VI-8 p RATE GYRO FREQUENCY RESPONSE PLOT, AMPLITUDE RATIO VERSUS FREQUENCY

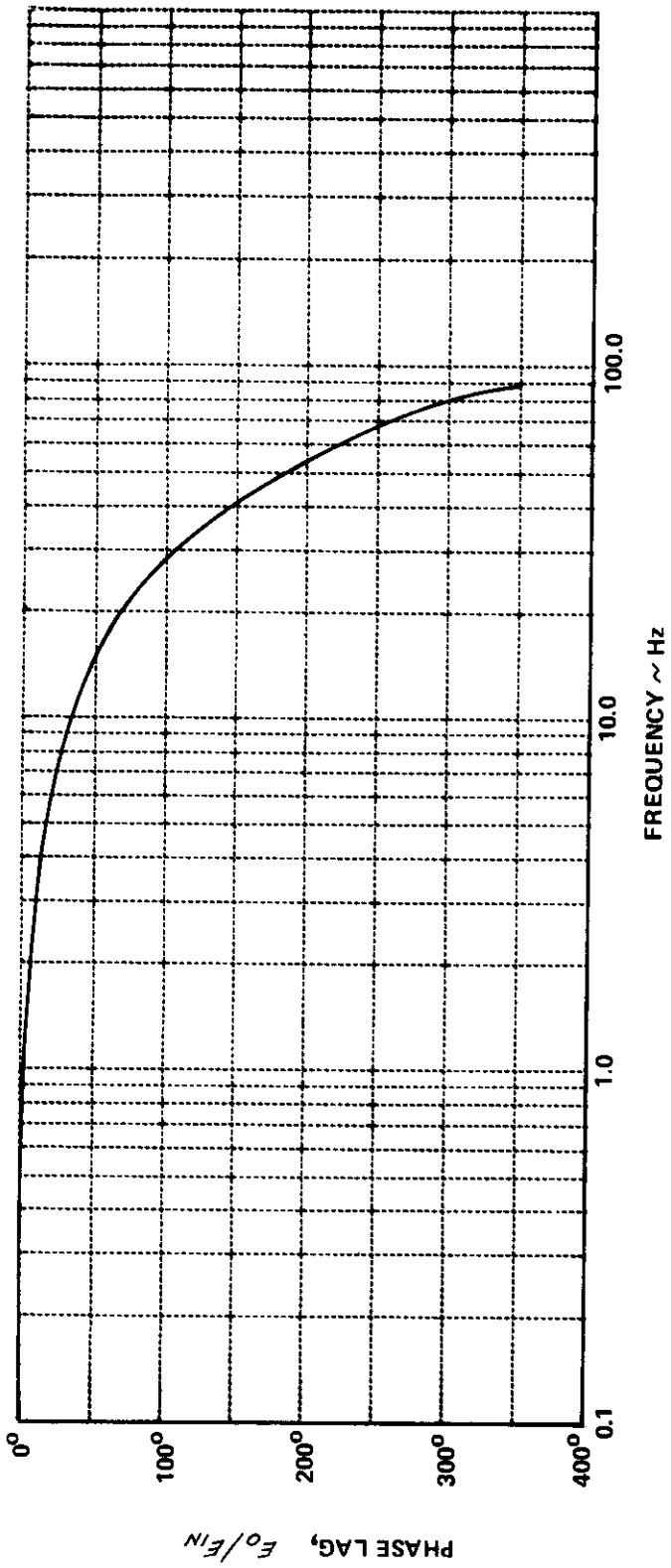

Figure VI-9 $\dot{\rho}$ RATE GYRO FREQUENCY RESPONSE PLOT, PHASE LAG VERSUS FREQUENCY

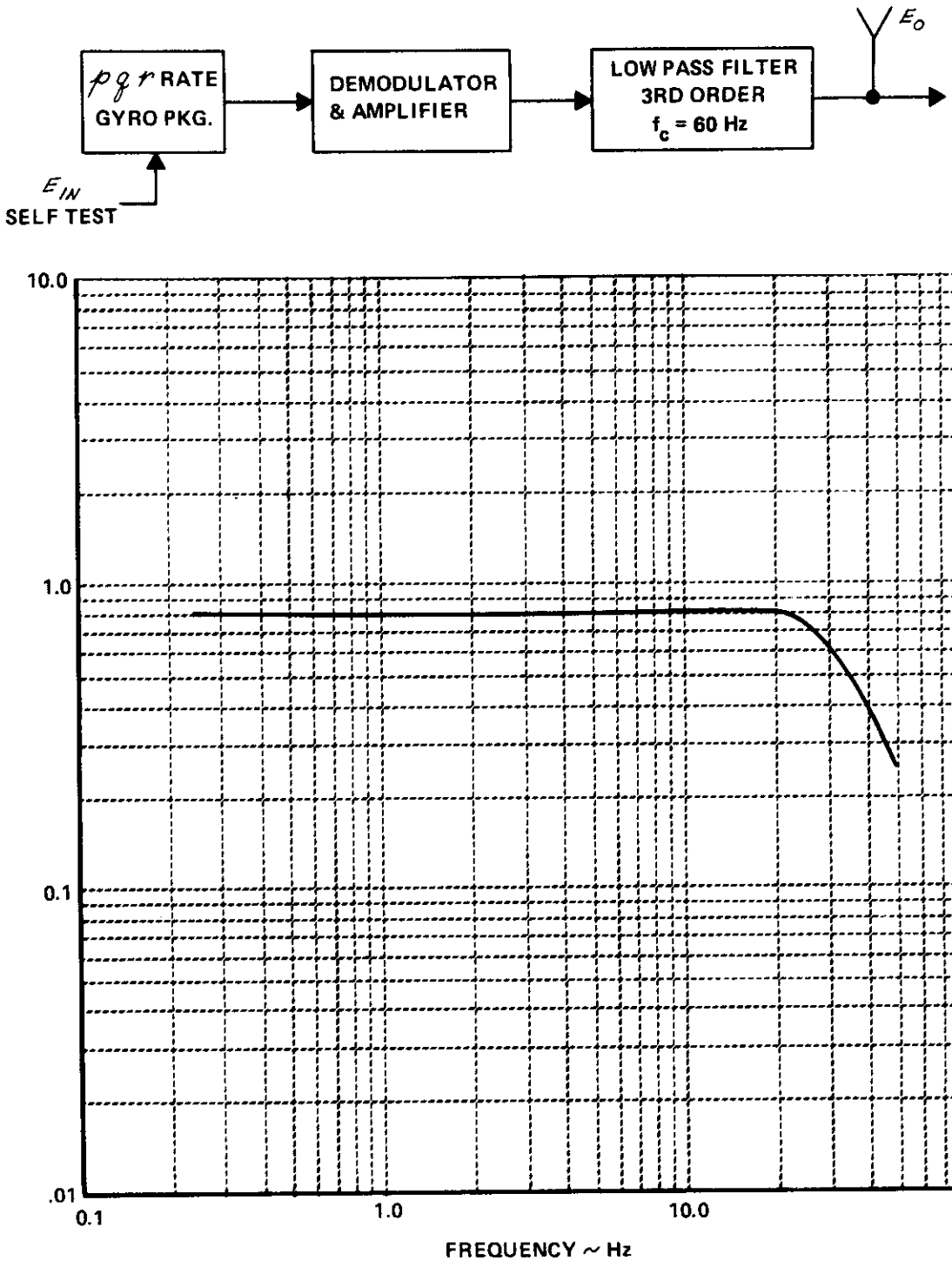

Figure VI-10 q RATE GYRO FREQUENCY RESPONSE PLOT, AMPLITUDE RATIO VERSUS FREQUENCY

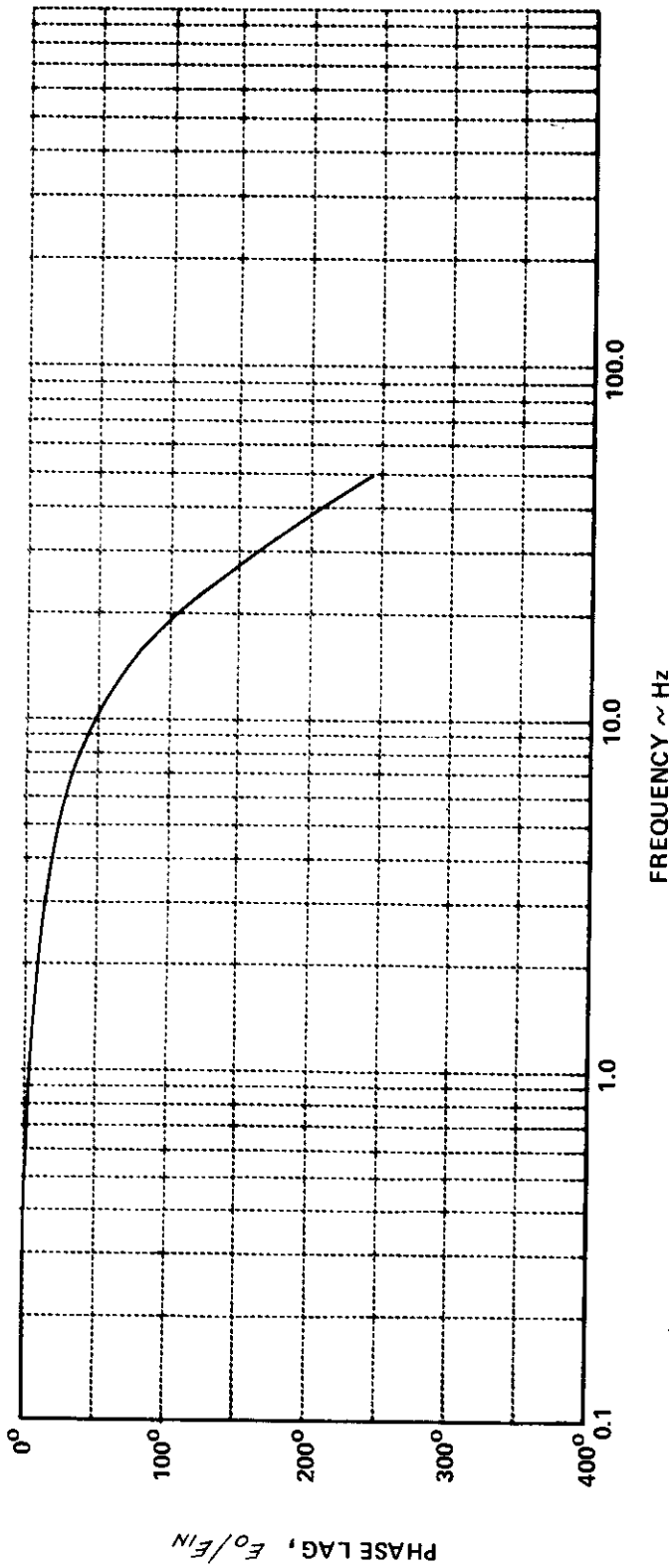

Figure VI-11 $\mathcal{Q}$ RATE GYRO FREQUENCY RESPONSE PLOT, PHASE LAG VERSUS FREQUENCY

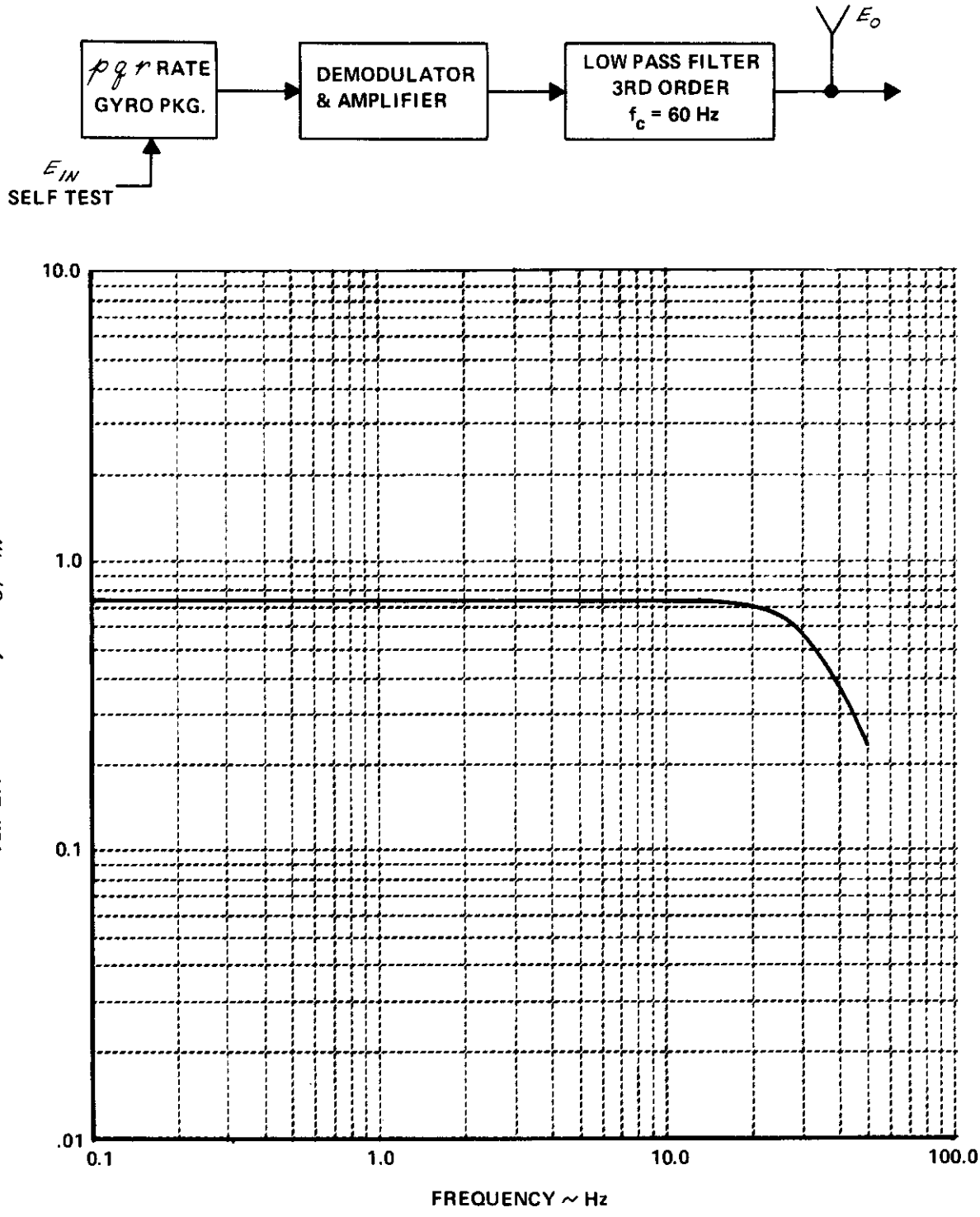

Figure VI-12 r RATE GYRO FREQUENCY RESPONSE PLOT, AMPLITUDE RATIO VERSUS FREQUENCY

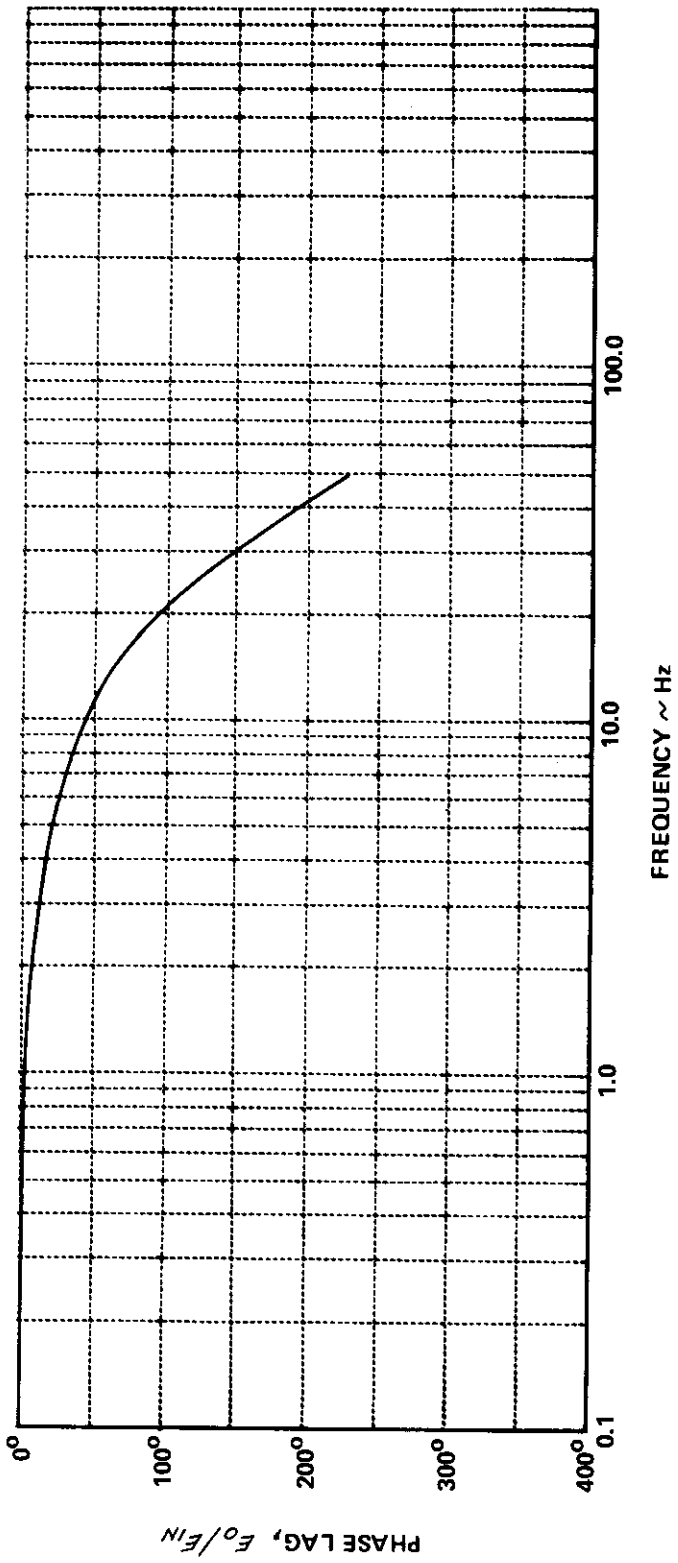

Figure VI-13 RATE GYRO FREQUENCY RESPONSE, PHASE LAG VERSUS FREQUENCY

Measurement Technique, Accelerometer (n_x, n_y, n_z) Dynamics

The dynamics of the n_y and n_z linear accelerometers were determined by digitally analyzing the response of the accelerometer to a step input. The electrical step was applied to the accelerometer self-test input and the response was recorded at the output of the second-order low pass filter. The step response data were digitally analyzed and amplitude and phase information obtained. Data were not taken on the n_x channel since it is identical to the n_y channel.

Amplitude and phase plots are also given for n_z and n_x, n_y second-order low pass filters.

Manufacturer's Specifications

UCI* MODEL MCA-5-6	n_x	n_y	n_z
Range	±1.0 g	±1.0 g	±5.0 g
Damping	.5	.6	.5
Natural Frequency	50 Hz	35 Hz	60 Hz
S/N	285	221	286

Figure VI-14 shows the physical shape of the linear accelerometer package.

*UNICO CONTROLS INC.

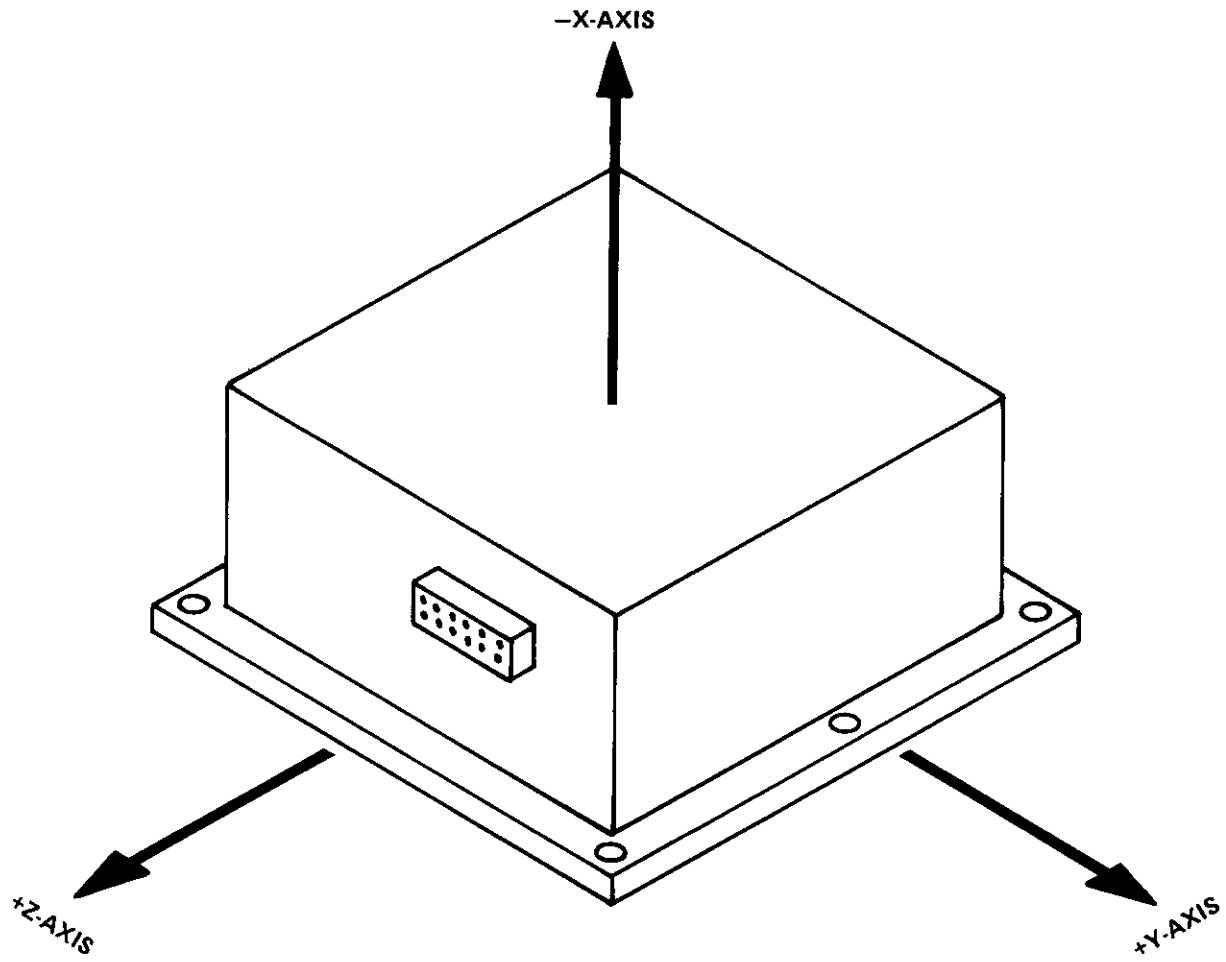

Figure VI-14 3 AXIS LINEAR ACCELEROMETER

Figure VI-15 AMPLITUDE VS FREQUENCY, n_y ACCELEROMETER AND FILTER

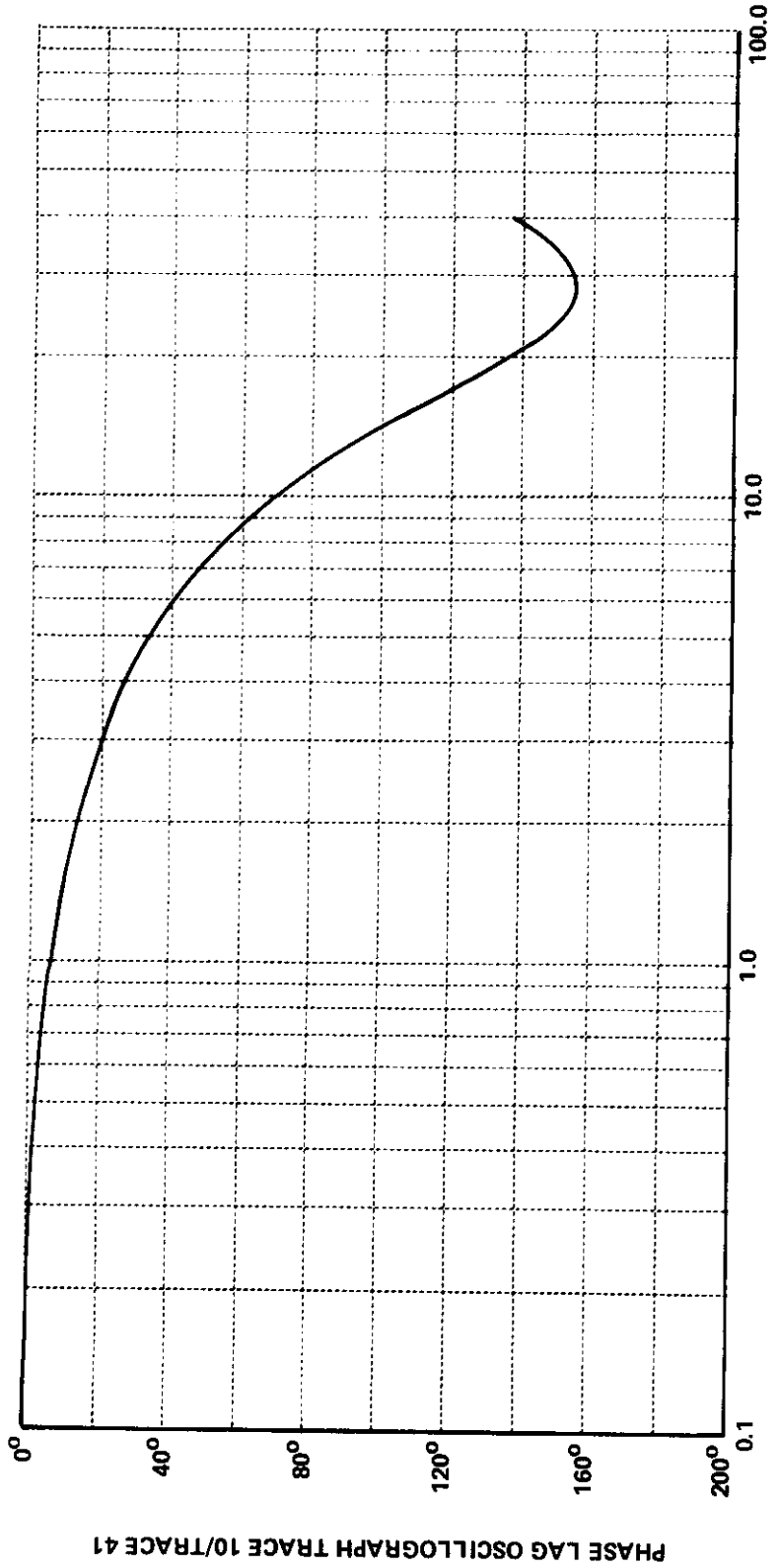

Figure VI-16 PHASE LAG VS FREQUENCY, n_y ACCELEROMETER AND FILTER

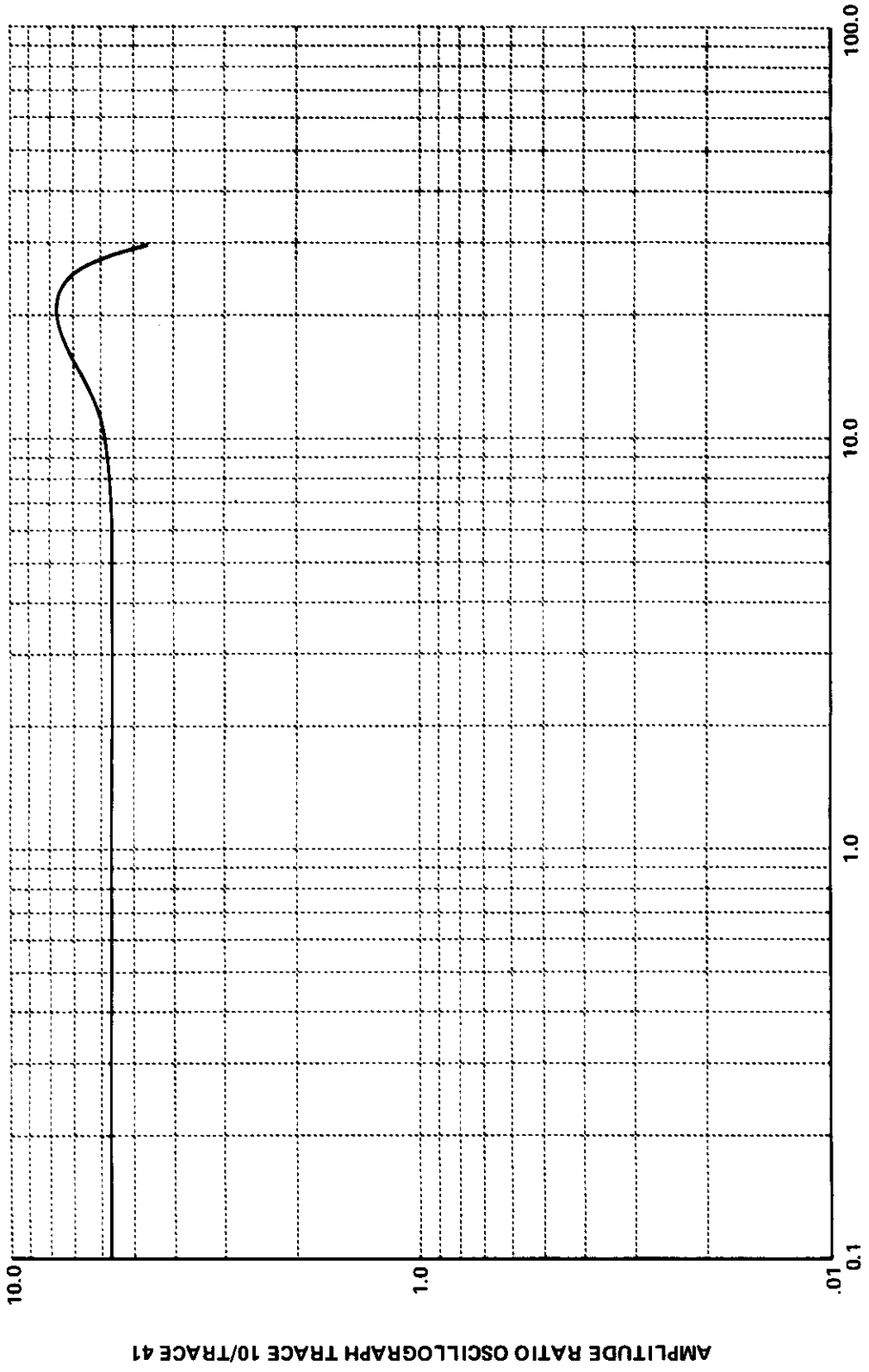

Figure VI-17 AMPLITUDE VS FREQUENCY, n_z ACCELEROMETER AND FILTER

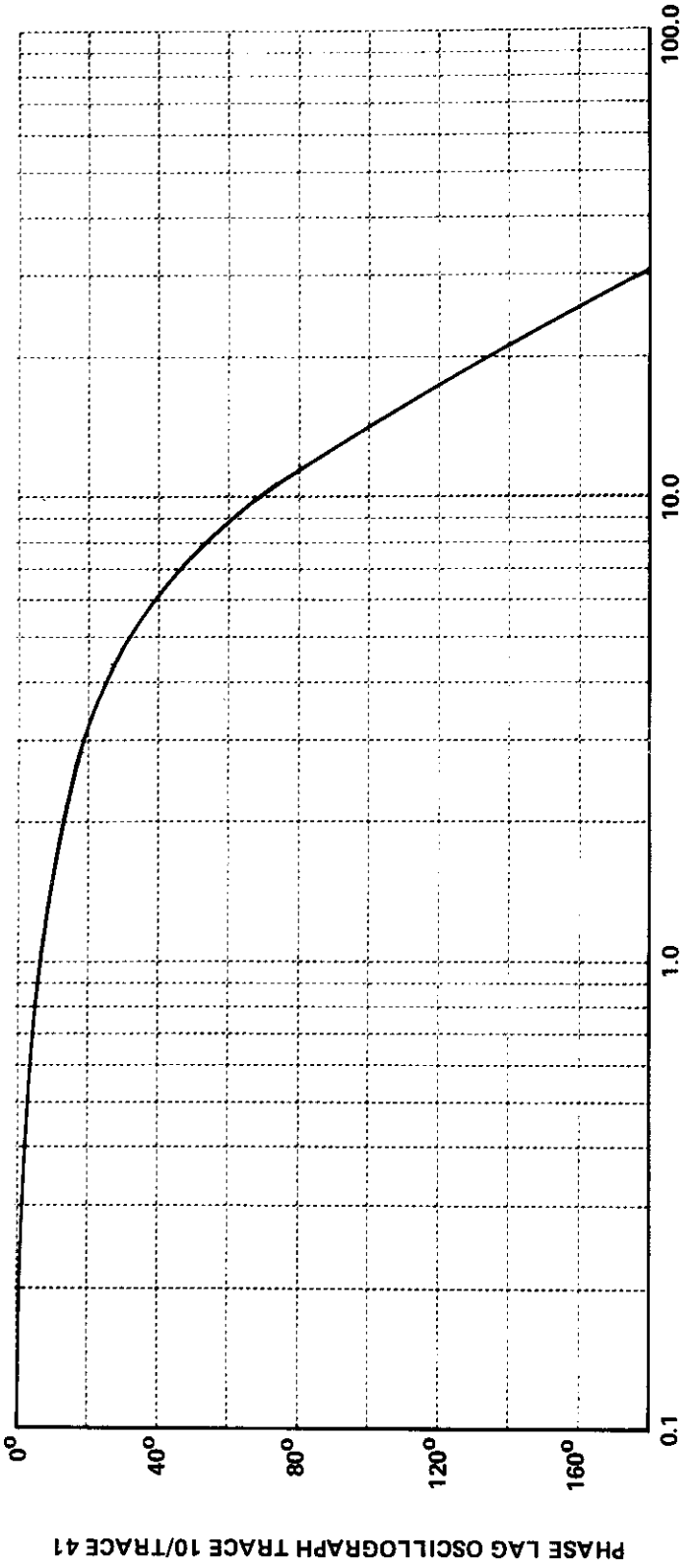

Figure VI-18 PHASE LAG VS FREQUENCY, n_z ACCELEROMETER AND FILTER

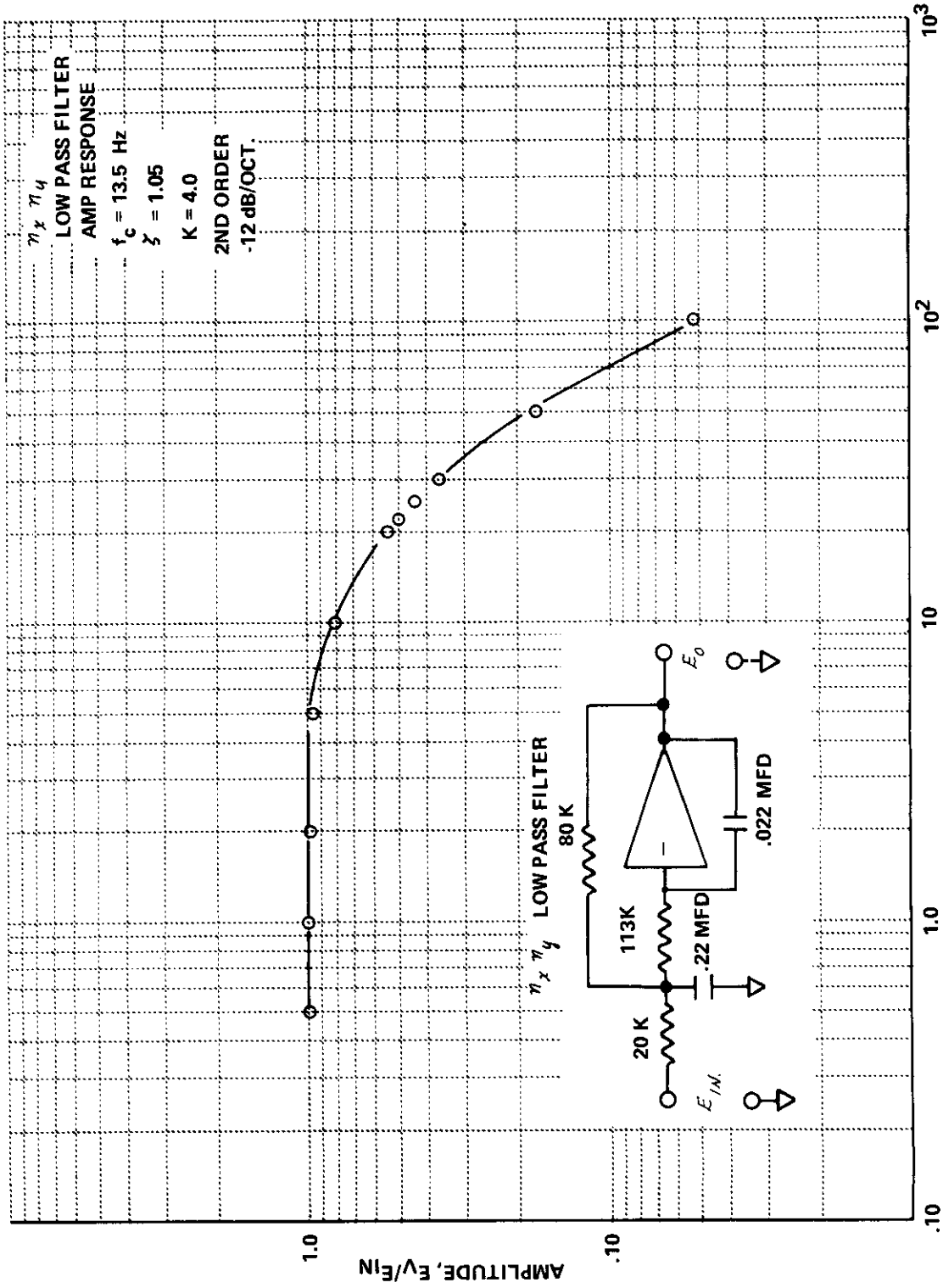

Figure VI-19 AMPLITUDE VS FREQUENCY, η_x,η_y 2ND ORDER LOW PASS FILTER

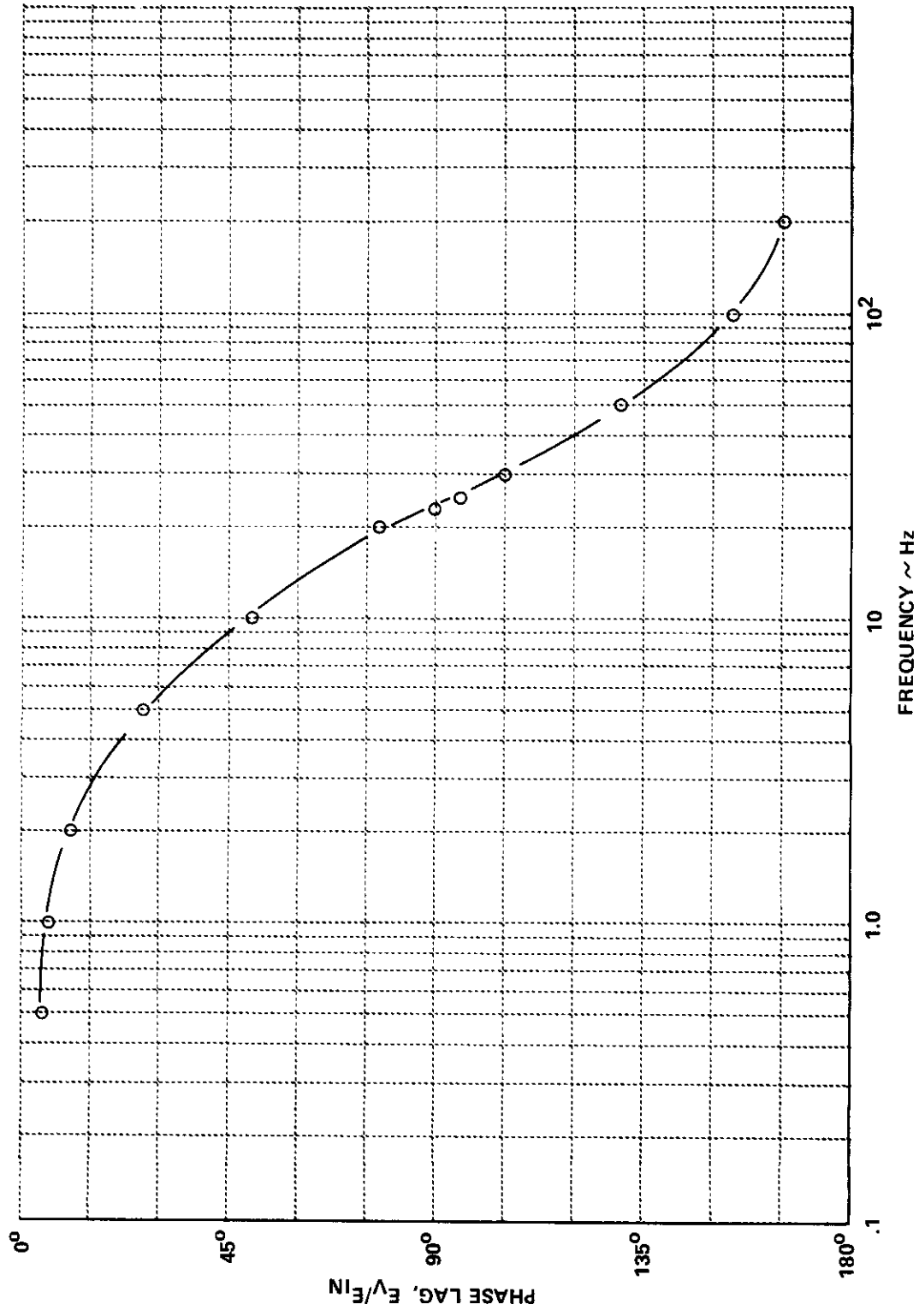

Figure VI-20 PHASE SHIFT VS FREQUENCY, n_x, n_y 2ND ORDER LOW PASS FILTER

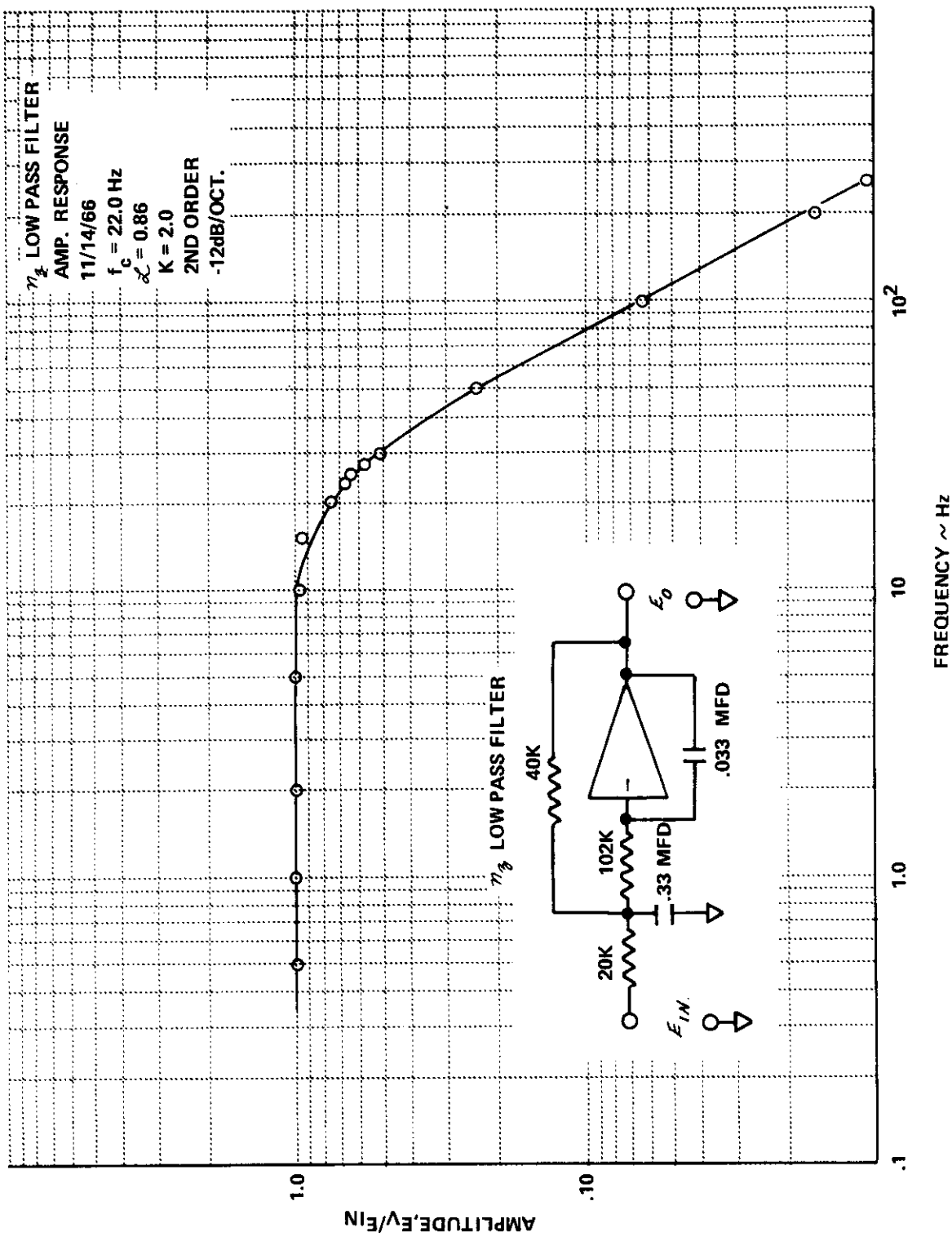

Figure VI-21 AMPLITUDE VS FREQUENCY η_3 2ND ORDER LOW PASS FILTER

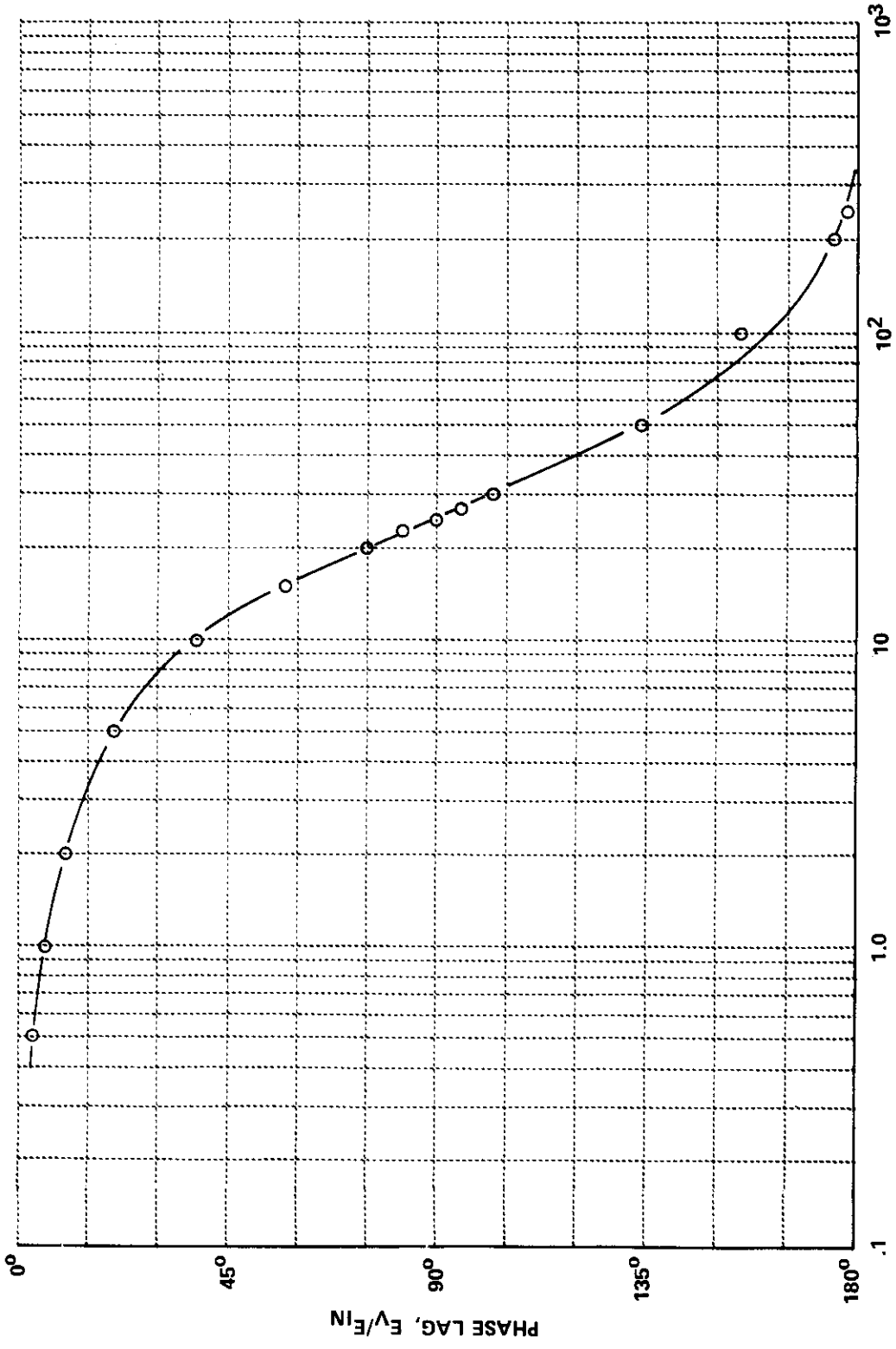

Figure VI-22 PHASE LAG VS FREQUENCY, n_χ 2ND ORDER LOW PASS FILTER

T-33 VSS Notch Filters

The α , β , p , q , r , $\bar{q}_c$, F_{ES} , F_{AS} , F_{RP} channels have (or have provisions for) the insertion of a notch filter in the signal channel; however, since the notch frequency is subject to change depending on flight program requirements only typical amplitude and phase response curves (α channel) are presented here. The α , β , p , q , r and $\bar{q}_c$ signals are recorded after the notch filter and thus the effects of the notch are in the recorded signals. The F_{ES} , F_{AS} and F_{RP} channels are recorded prior to the notch filter.

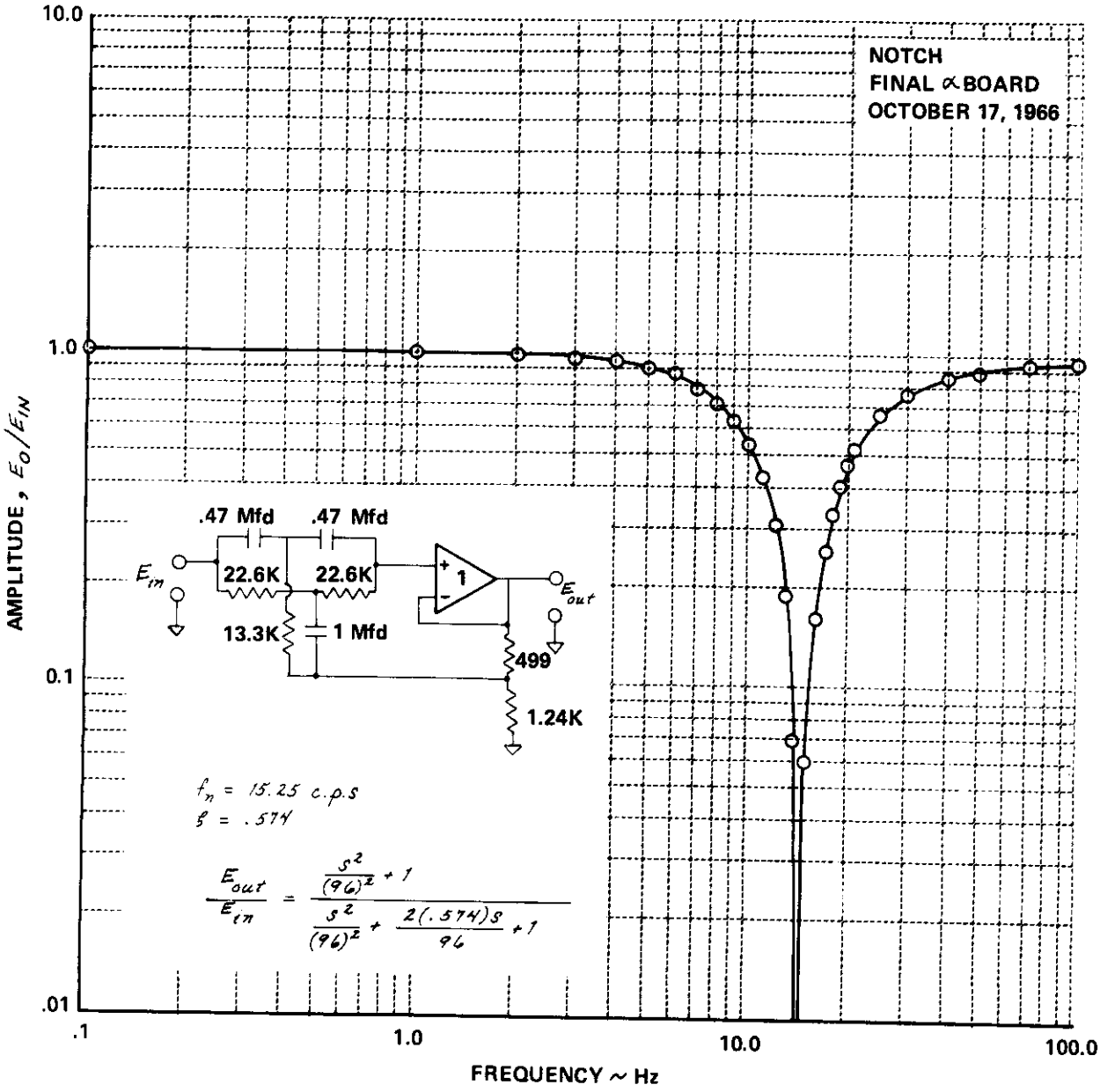

Figure VI-23 AMPLITUDE VS FREQUENCY, ∝ NOTCH FILTER

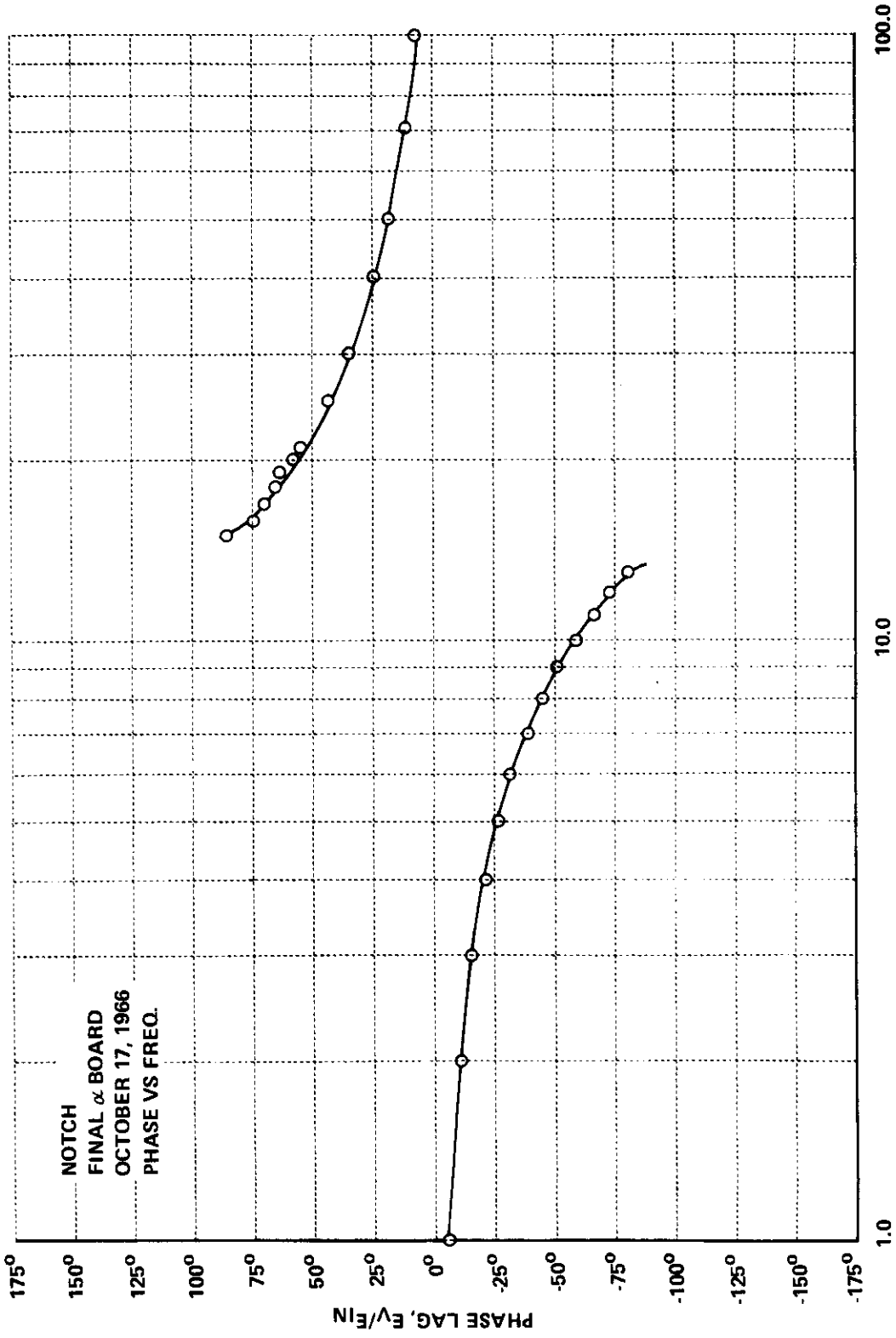

Figure VI-24 PHASE SHIFT VS FREQUENCY, α NOTCH FILTER

T-33 VSS differentiators - Second-Order Low Pass Filter

The α , β , p , q , r channel differentiators are identical, therefore only typical amplitude and phase plots are given (α channel). Data are tabulated for α , β , p , q , r , and the $\bar{q}_c$ differentiator which has different characteristics.

Signal Channel	α, β, p, q, r	$\bar{q}_c$
Filter Corner Frequency (ω_n)	66.7 rad/sec	20 rad/sec
Velocity Constant (K)	0.2	2.5
Filter Damping Factor (ζ)	1.038	0.827

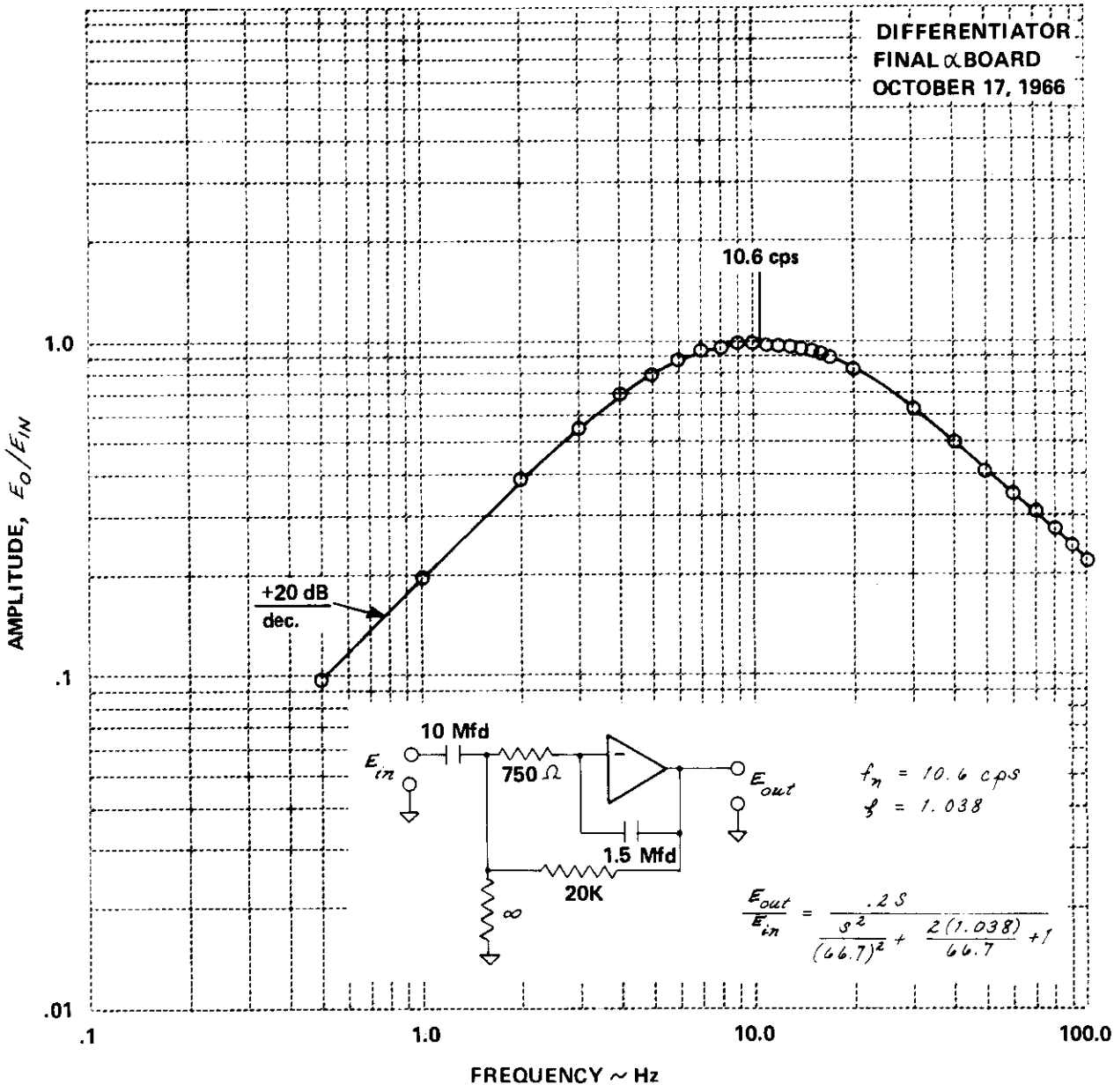

Figure VI-25 AMPLITUDE VS FREQUENCY, ∝ DIFFERENTIATOR CIRCUIT

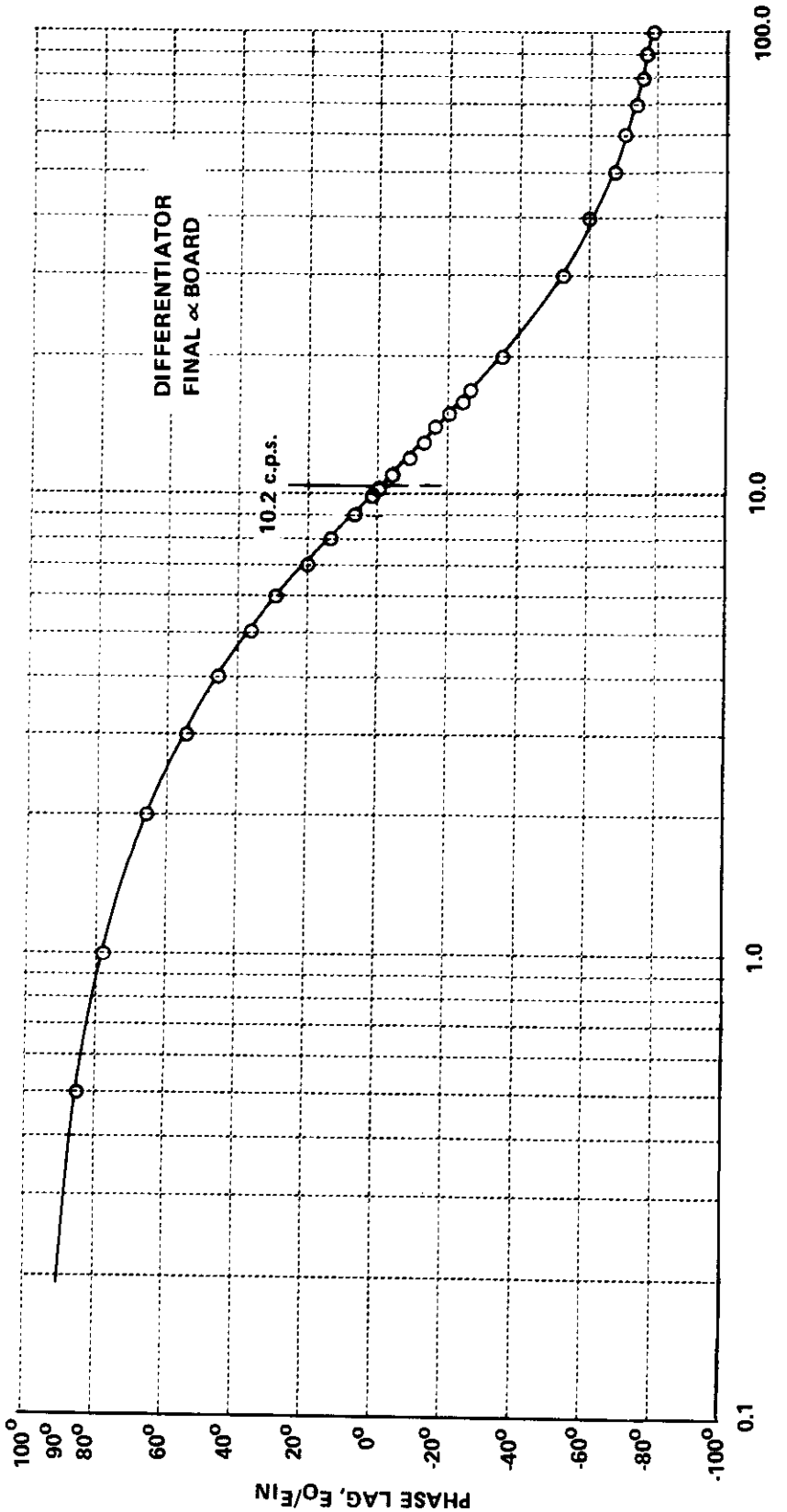

Figure VI-26 PHASE SHIFT VS FREQUENCY, ∝ DIFFERENTIATOR CIRCUIT

T-33 VSS Sensor Demodulator Filters

The α , β , p , q , r and $\bar{q}_c$ demodulator low pass filters are third-order, with approximately 135 degrees phase lag at 60 Hz. The filters are identical and only a typical amplitude and phase plot is presented here. The purpose of these filters is to remove the 800 Hz carrier ripple present due to demodulation of the a.c. type sensor signal. The α , β , p , q , r , and $\bar{q}_c$ signals are recorded on oscillograph and on the digital recorder after filtering of these signals by the low pass, third-order filters takes place.

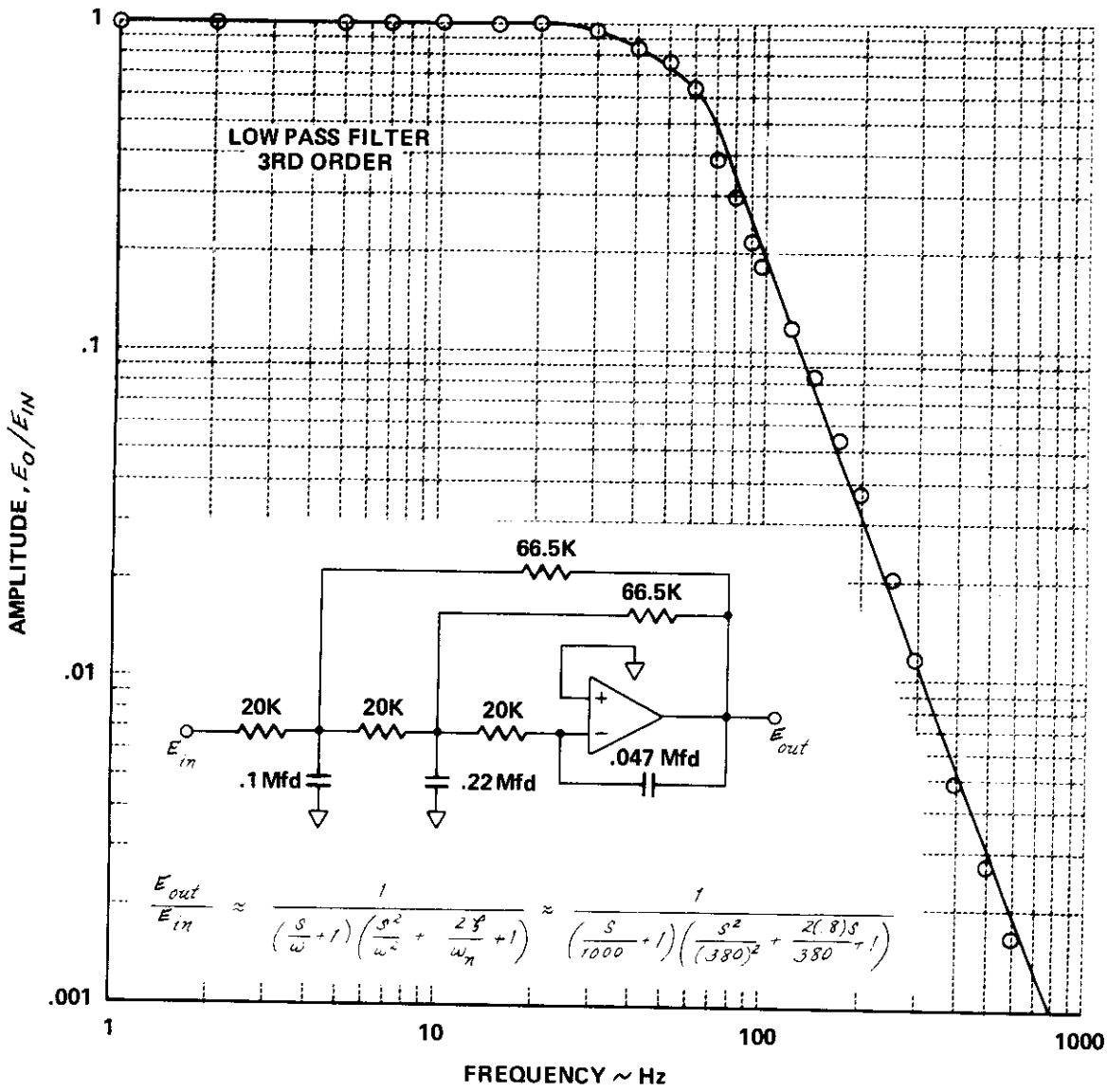

Figure VI-27 AMPLITUDE VS FREQUENCY, LOW PASS FILTER,3RD ORDER

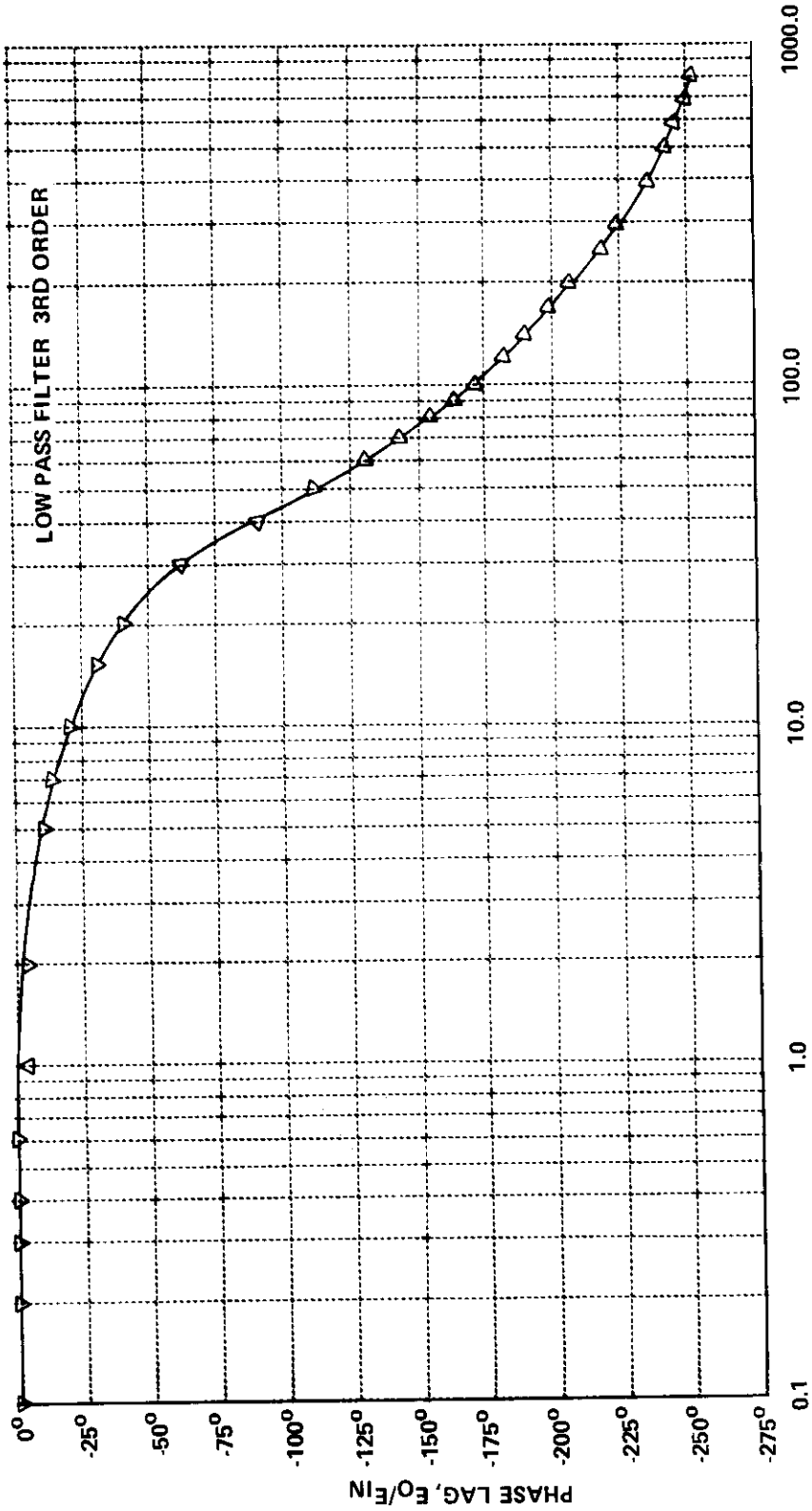

Figure VI-28 PHASE SHIFT VS FREQUENCY, LOW PASS FILTER, 3RD ORDER

Sin ϕ to ϕ Function Generator Plot

The parameter sin ϕ is available in the T-33 VSS for measurement and not ϕ. Therefore, when the variable ϕ is required, a function generator circuit is used to provide it. A similar circuit can be added to change sin ϕ to ϕ if it is required.

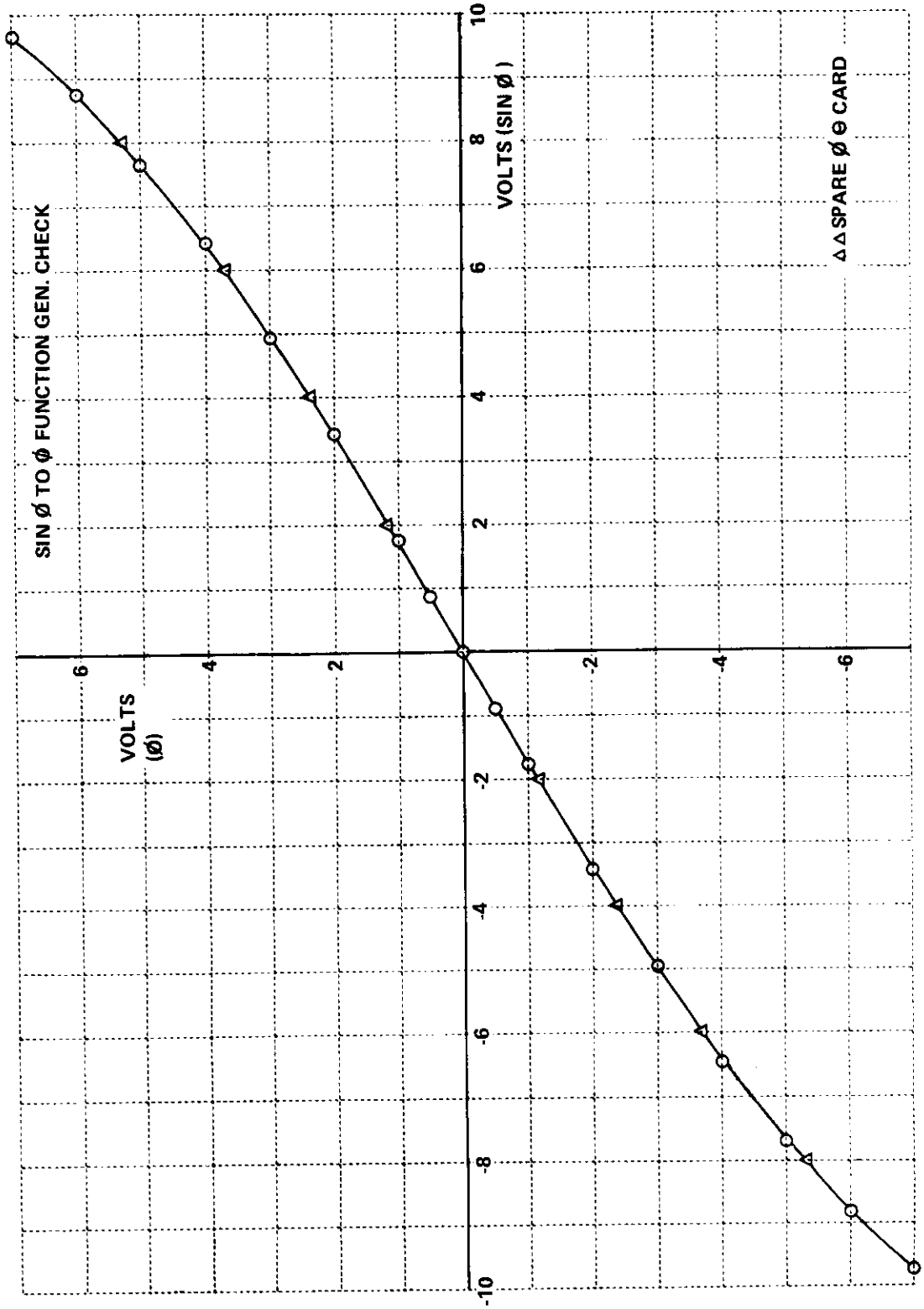

Figure VI-29 FUNCTION GENERATOR PLOT, SIN Ø TO Ø

Measurement Techniques, Bank Angle (ϕ) and Pitch Angle (θ)

Cockpit Indicator Dynamics

To determine the dynamics of the attitude (ϕ, θ display) gyro indicator (Lear Model ARU-2 B/A) step displacements were applied to the indicator by means of two synchros of the type which normally drive the indicator. Excitation was continuously applied to both rotors and a relay switched the indicator from one set of stators to the other. This resulted in a step change in the display the amplitude of which was controlled by the shaft adjustment on the synchros.

A movie camera at 100 frames per second was used to record the indicator step displacement. Also recorded on camera at the same time was an oscilloscope display to indicate when the electrical step change was applied. A running stop watch was also recorded on camera for timing purposes.

Phase and amplitude plots obtained by digitally analyzing the data obtained are presented here.

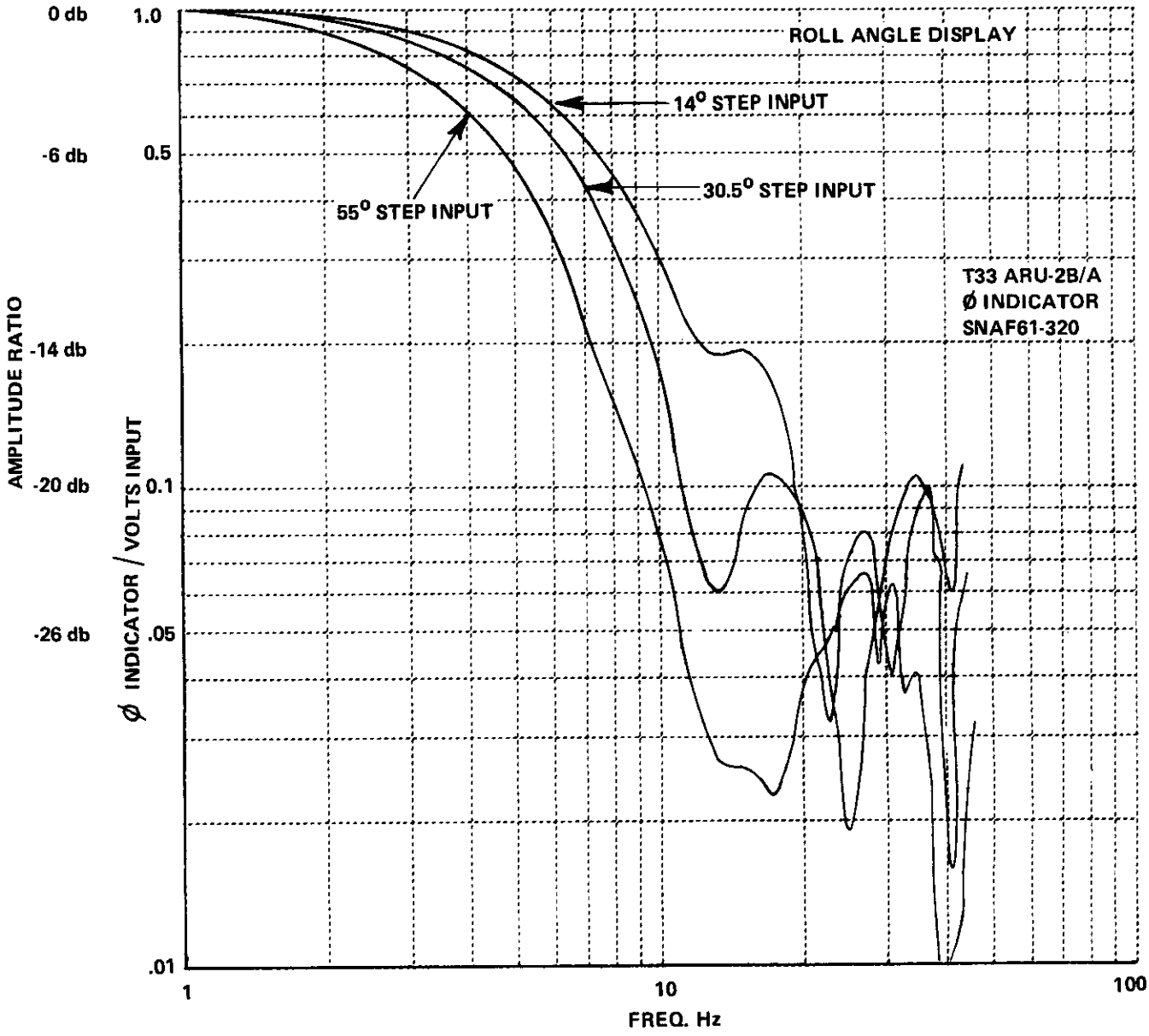

Figure VI-30 AMPLITUDE VS FREQUENCY, T-33 ARU-2B/A

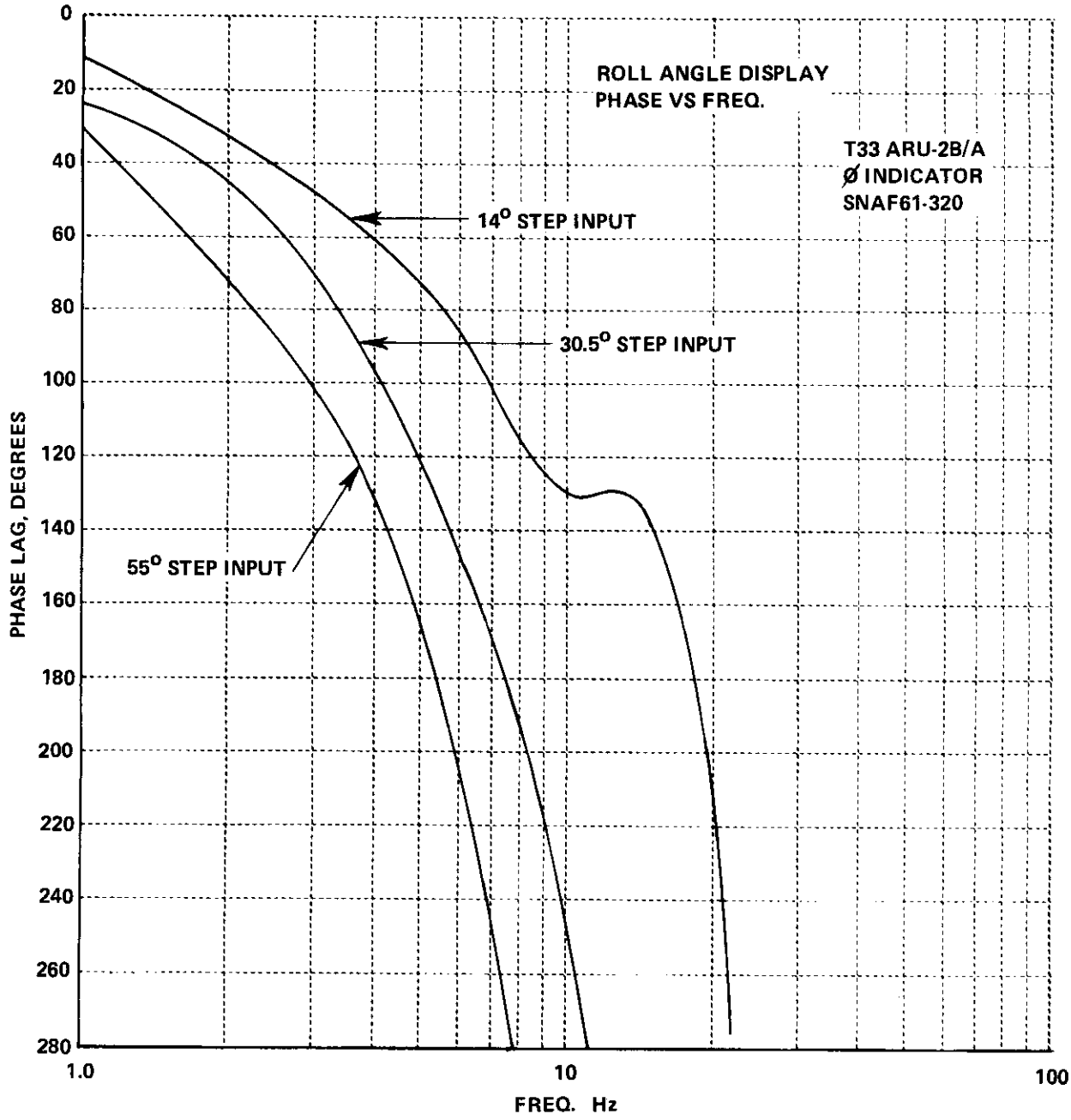

Figure VI-31 PHASE LAG VS FREQUENCY, T33 ARU-2B/A

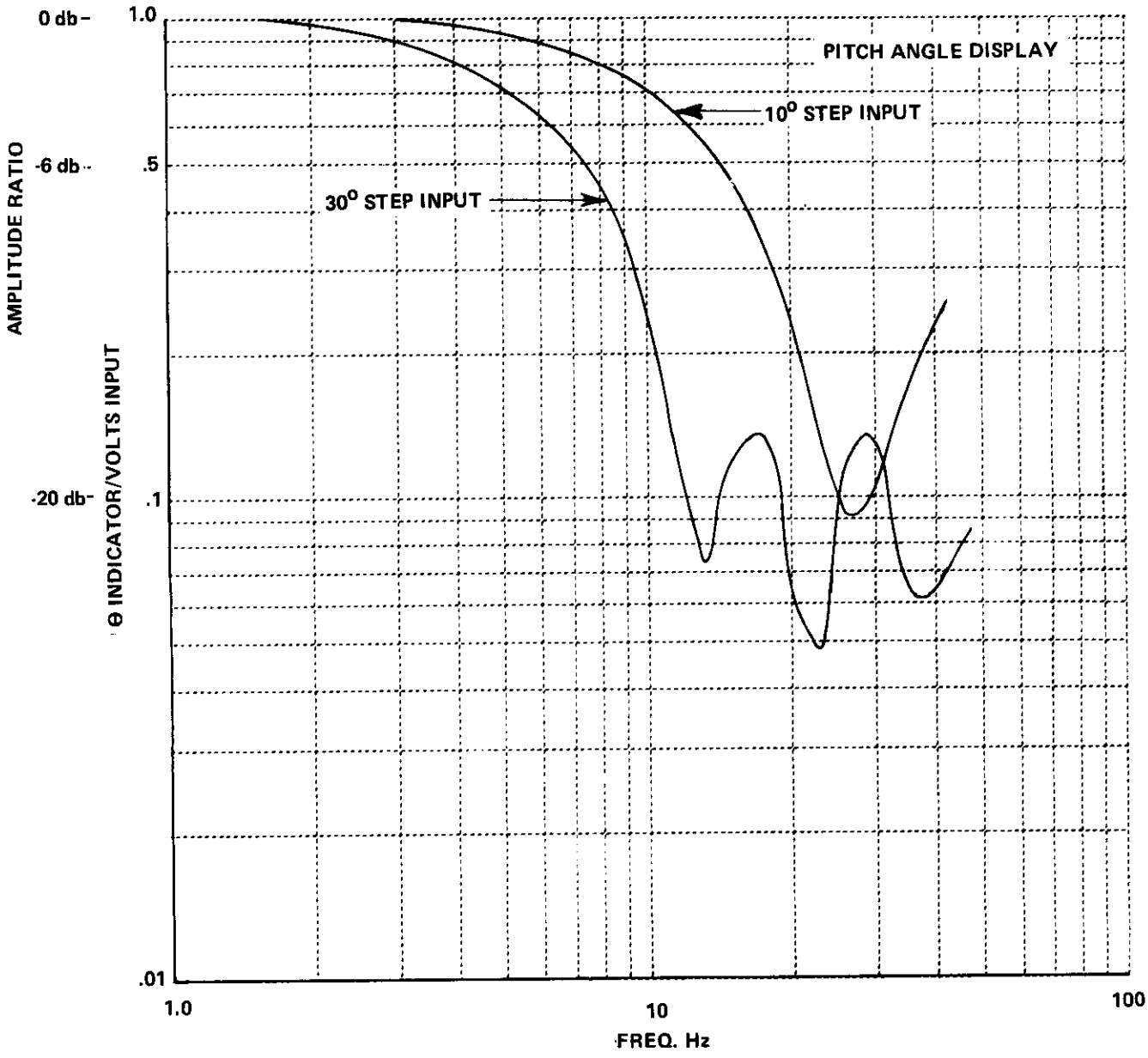

Figure VI-32 AMPLITUDE VS FREQUENCY T33 ARU-2B/A, θ INDICATOR

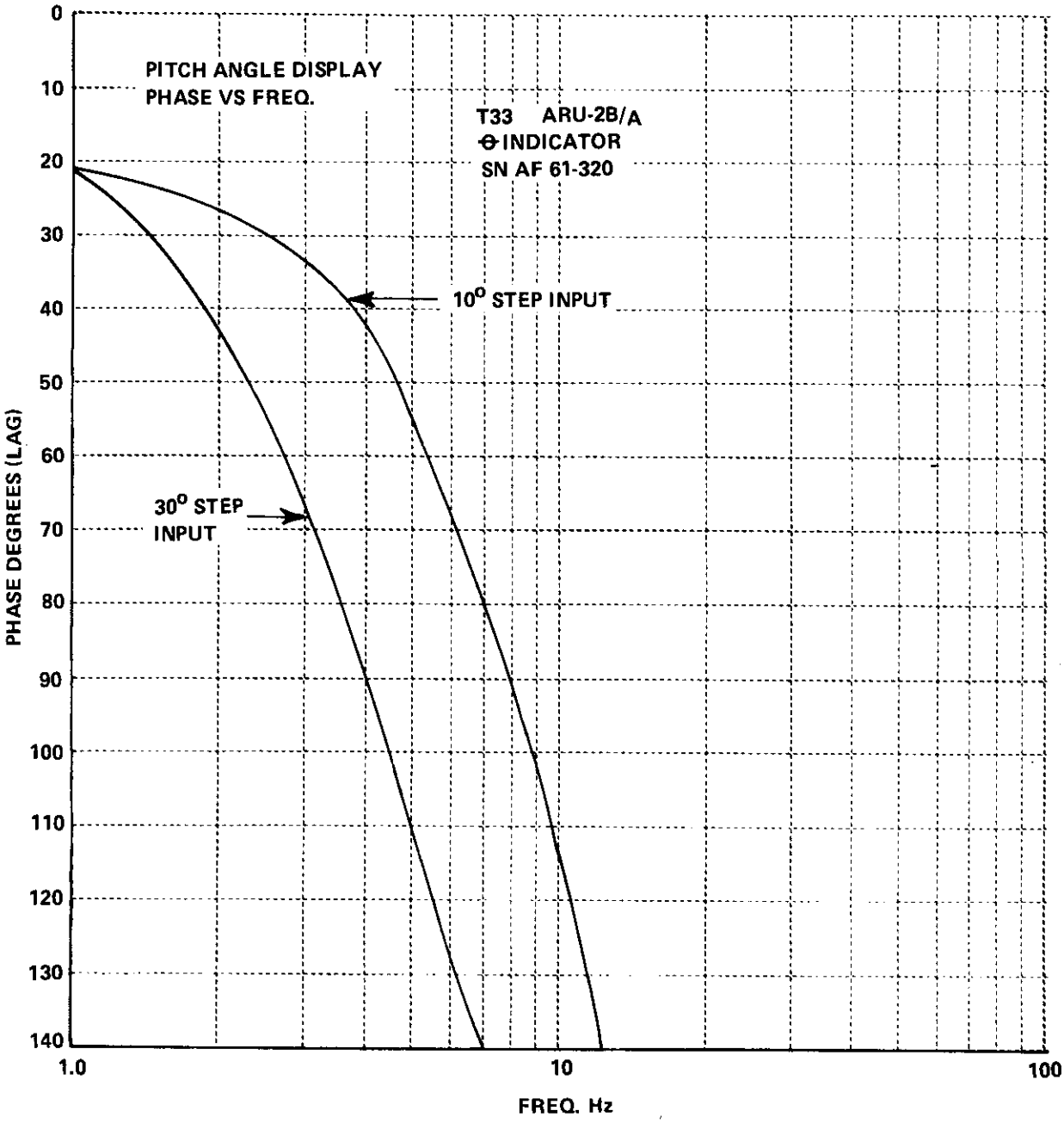

Figure VI-33 PHASE LAG VS FREQUENCY, T33 ARU-2B/A, Θ INDICATOR

ϕ Display (ϕ*) Servo

This servo is used to modify the displayed bank angle signal (front cockpit) by allowing for additional signals to be summed with the true bank angle signal originating in the bank angle gyro.

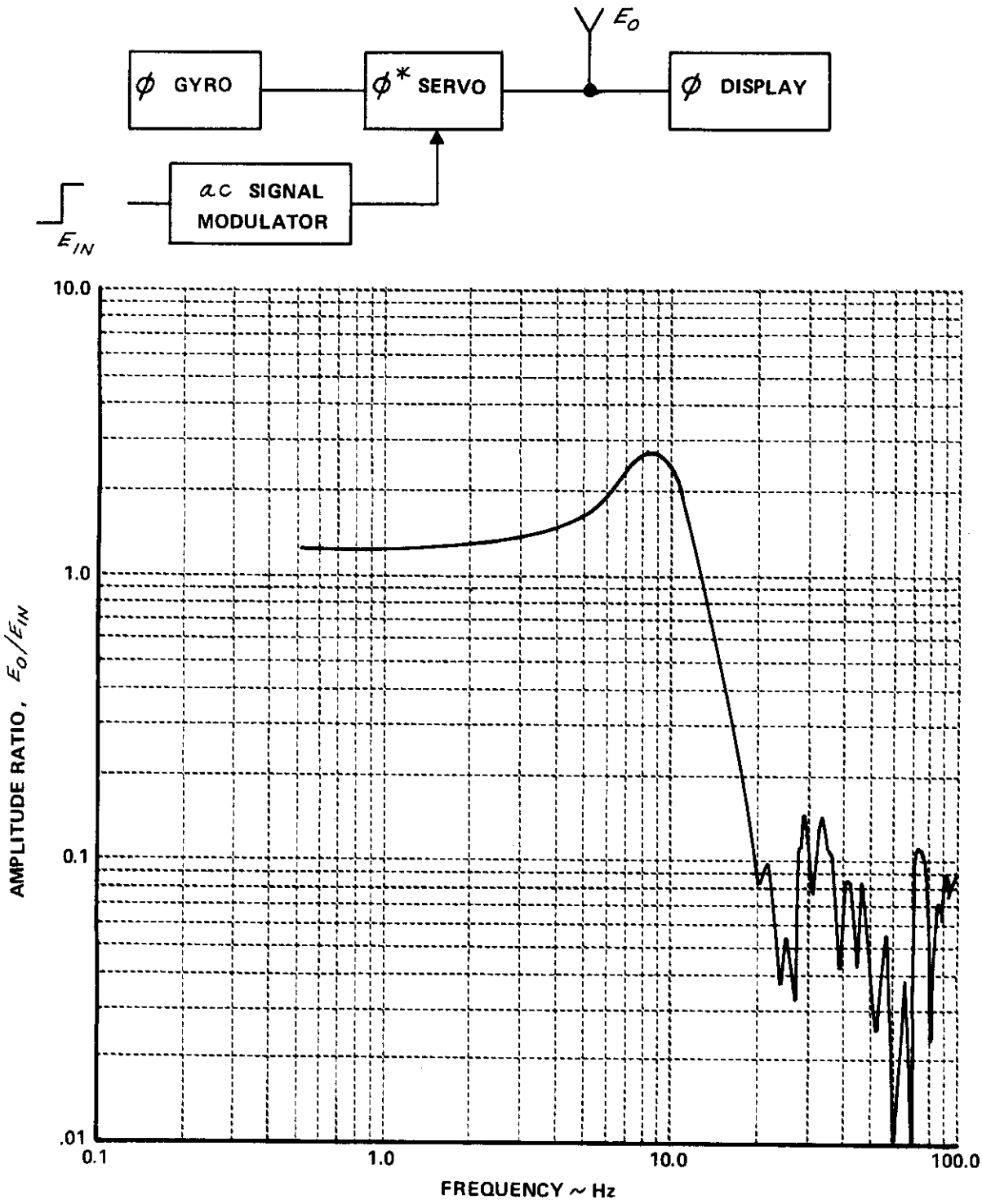

Figure VI-34 AMPLITUDE VS FREQUENCY, ϕ^* SERVO

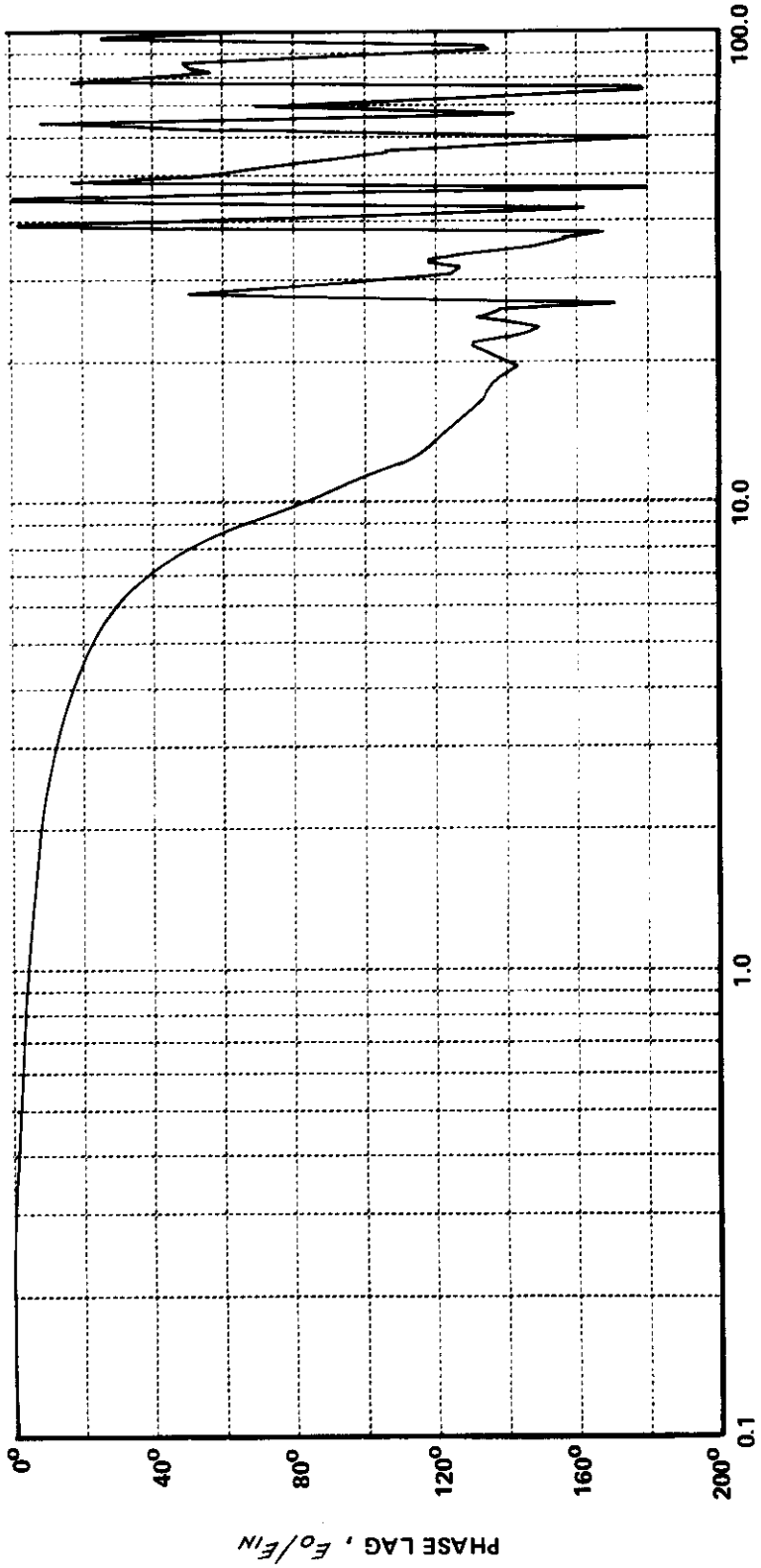

Figure VI-35 PHASE LAG VS FREQUENCY, ϕ* SERVO

Measurement Technique for the Horizontal and Vertical Pointer Dynamics of the Attitude Indicator (Leav ARU-2B/A)

To determine the dynamics of the horizontal and vertical pointers, d.c. voltage step changes were applied to the movements.

A movie camera at 100 frames per second was used to record the indicator step displacement. Also recorded on camera was an oscilloscope display to indicate when the electrical step change was applied. A running stop watch was recorded on camera for timing purposes.

The movie film was projected one frame at a time and amplitude data was measured for enough frames so that an entire step response was obtained. Figures VI-36 and VI-37 present this measured data. Phase and amplitude plots could be obtained by either digitally analyzing the data or by using analog matching techniques.

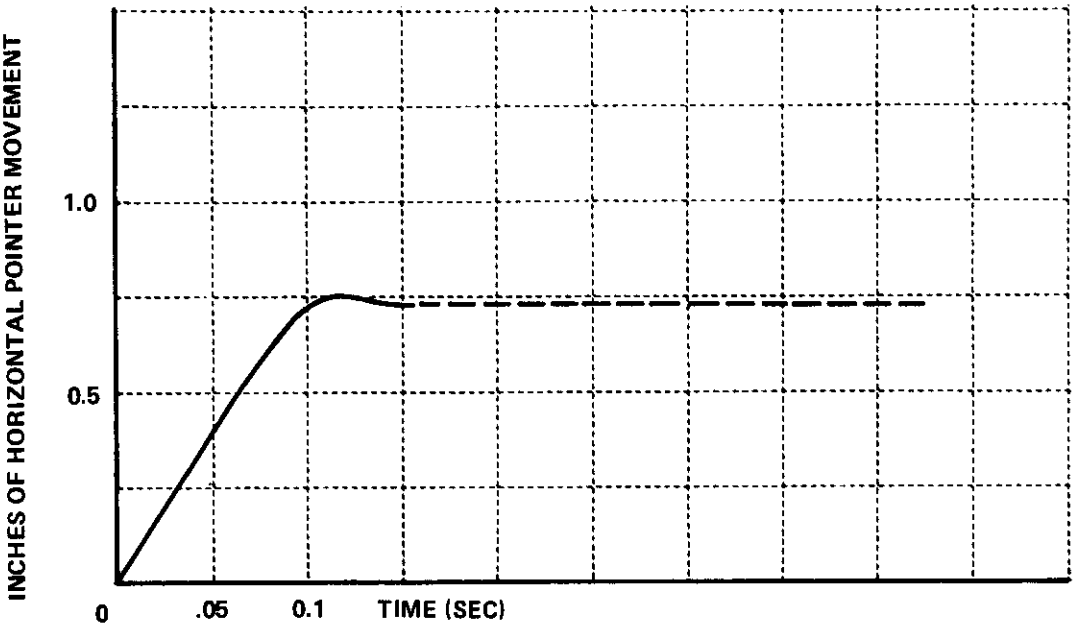

Figure VI-36 HORIZONTAL NEEDLE AMPLITUDE RESPONSE TO STEP INPUT, ATTITUDE INDICATOR ARU-2B/A

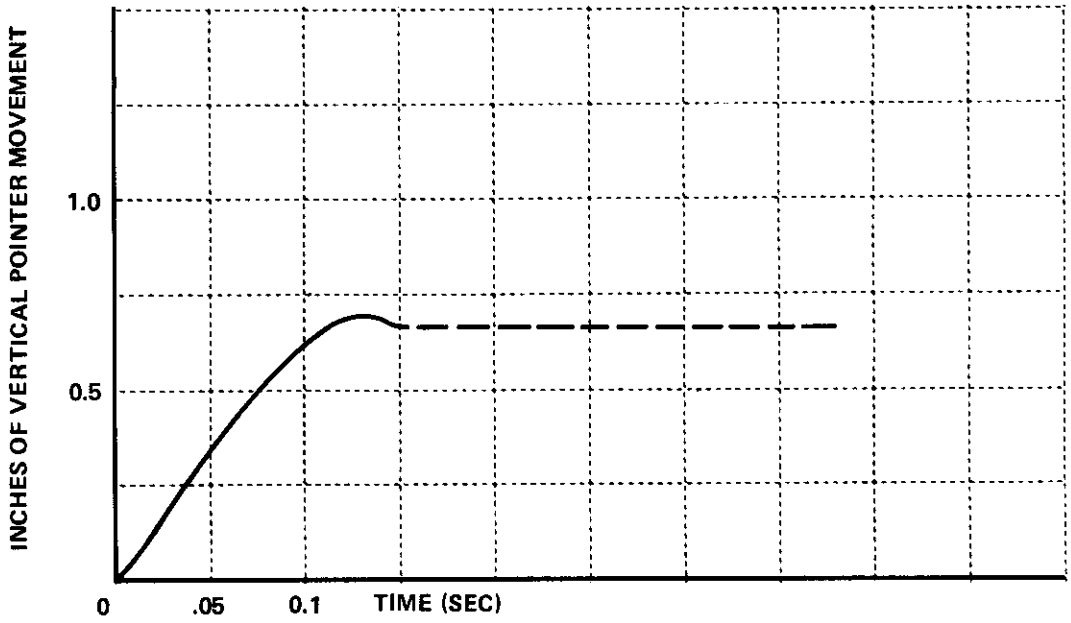

Figure VI-37 VERTICAL NEEDLE AMPLITUDE RESPONSE TO STEP INPUT, ATTITUDE INDICATOR ARU-2B/A

Measurement Technique, Control Surface Servos

Frequency response plots, determined from in-flight step inputs, are given for the elevator, aileron and rudder control surface servos. The data were taken at 250 KIAS and at 5000-7000 foot altitude. The step doublet circuit was used to apply the step inputs. Oscillograph trace deflections were digitally analyzed.

Typical oscillograph recordings (without the recording filters) of in-flight step responses of the elevator, aileron and rudder control surface are given.

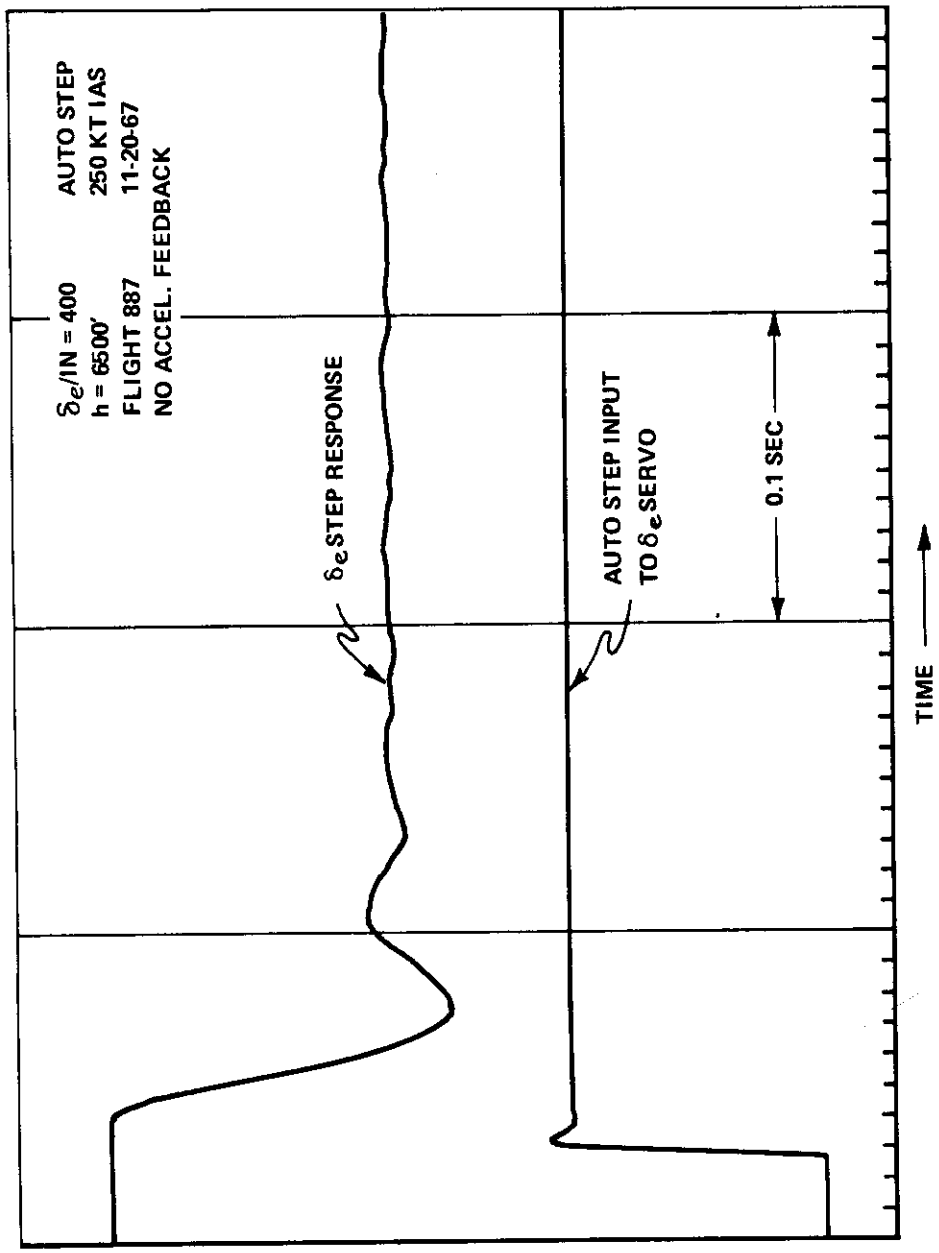

Figure VI-38 δ_e CONTROL SURFACE SERVO STEP RESPONSE, OSCILLOGRAPH RECORDINGS, NO RECORDING FILTERS

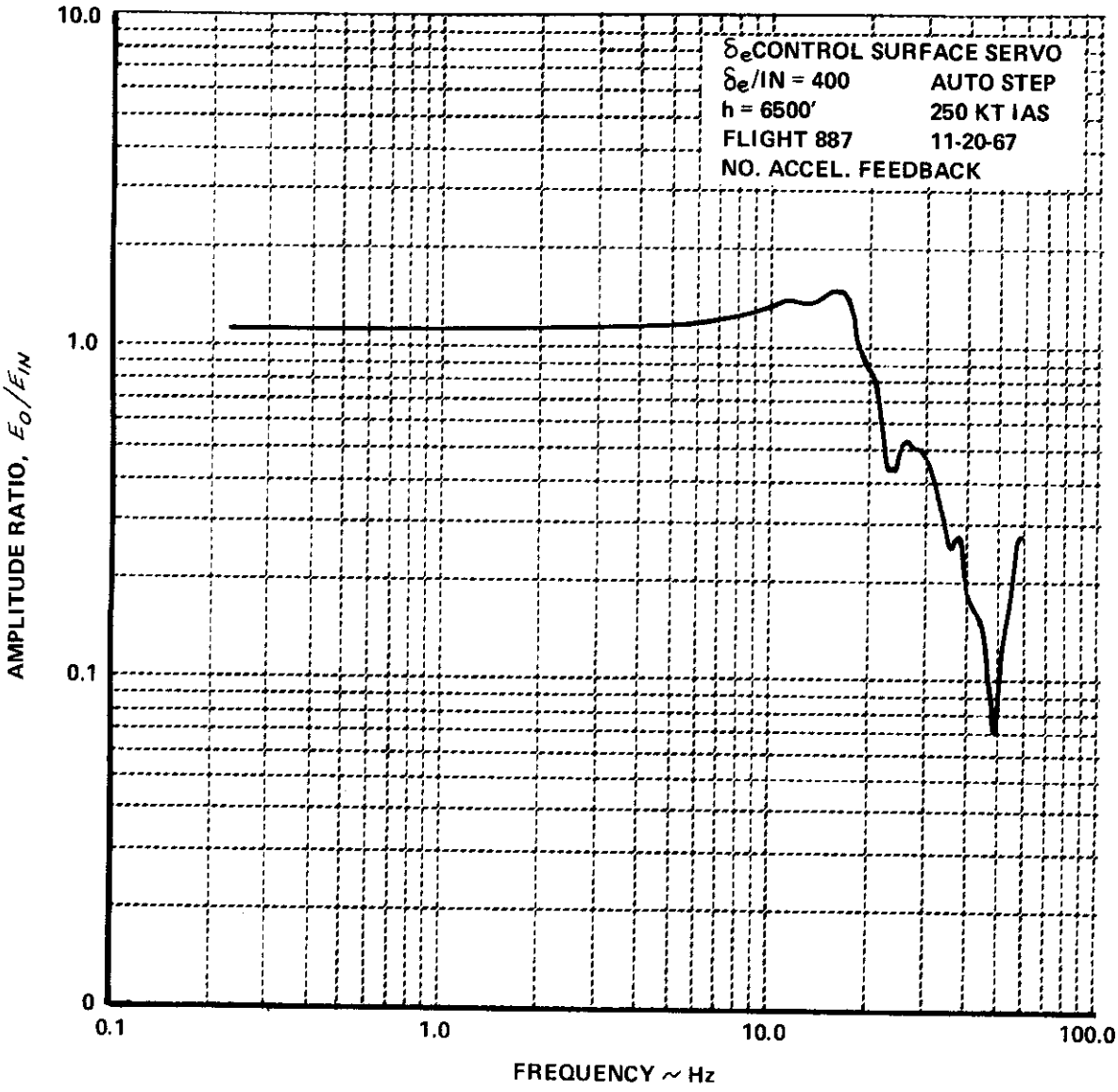

Figure VI-39a ELEVATOR CONTROL SURFACE SERVO RESPONSE, AMPLITUDE VS FREQUENCY

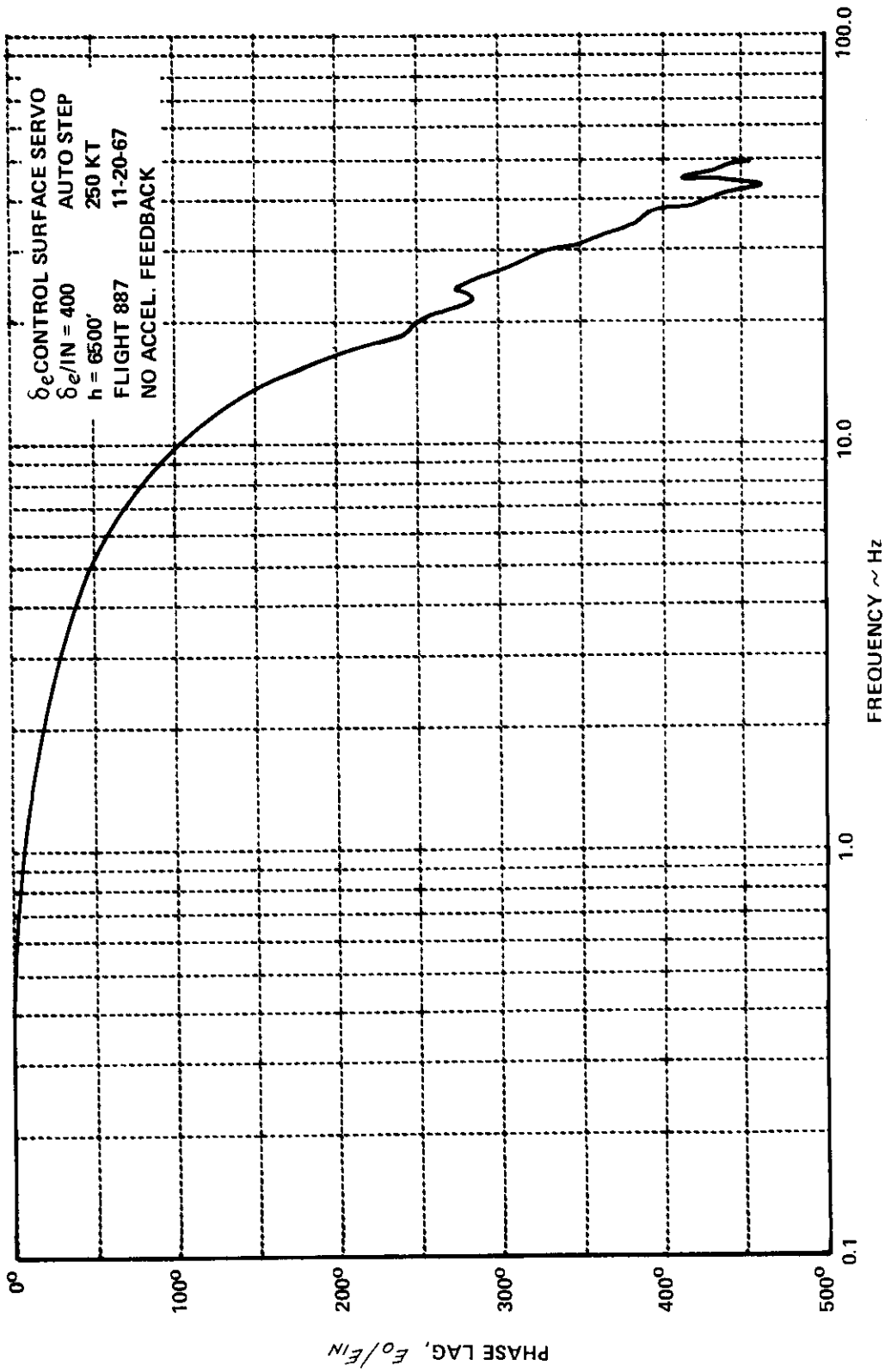

Figure VI-39b ELEVATOR CONTROL SURFACE SERVO RESPONSE , PHASE LAG VERSUS FREQUENCY

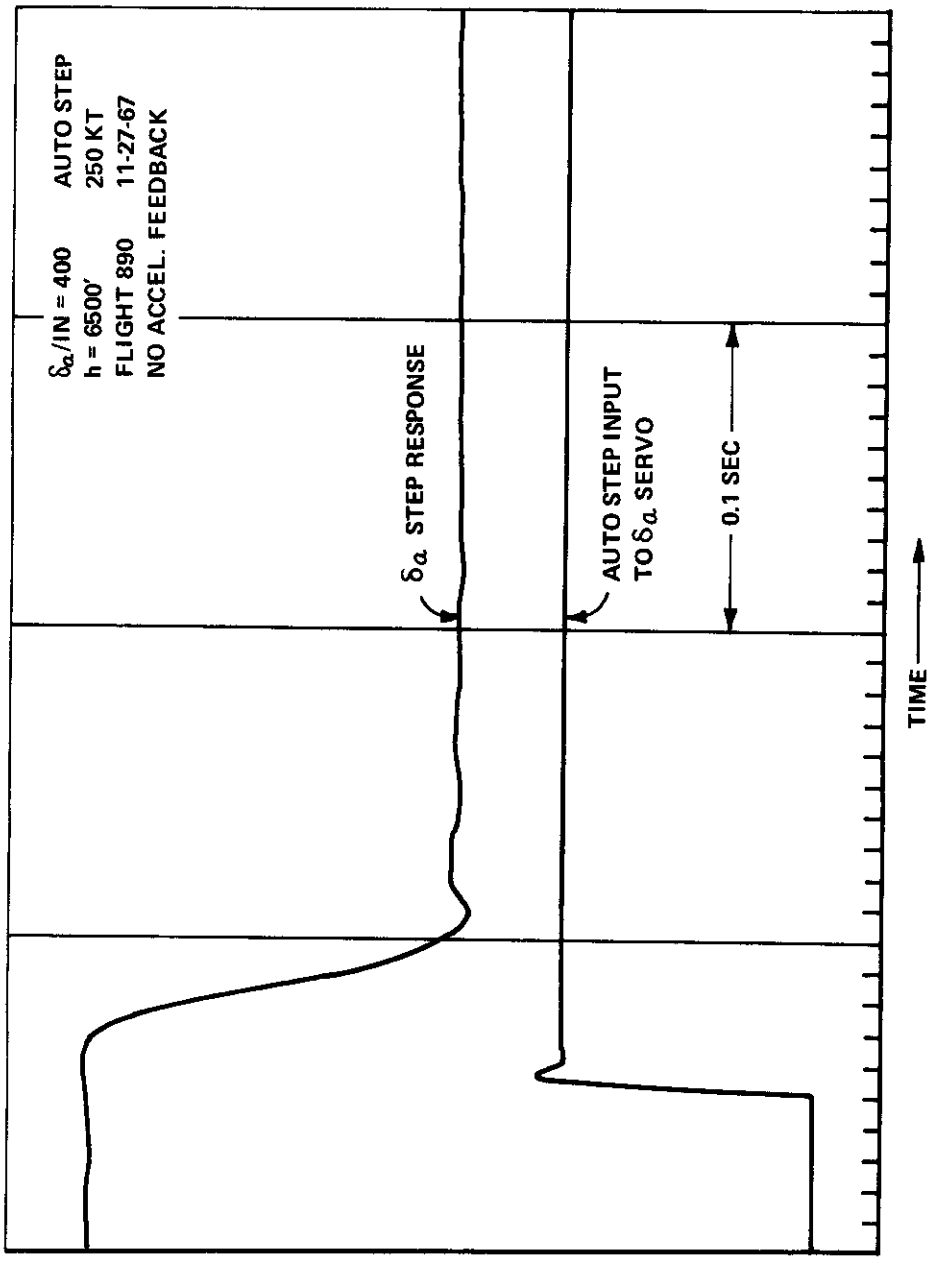

Figure VI-40 δ_a CONTROL SURFACE SERVO STEP RESPONSE, OSCILLOGRAPH RECORDING, NO RECORDING FILTERS

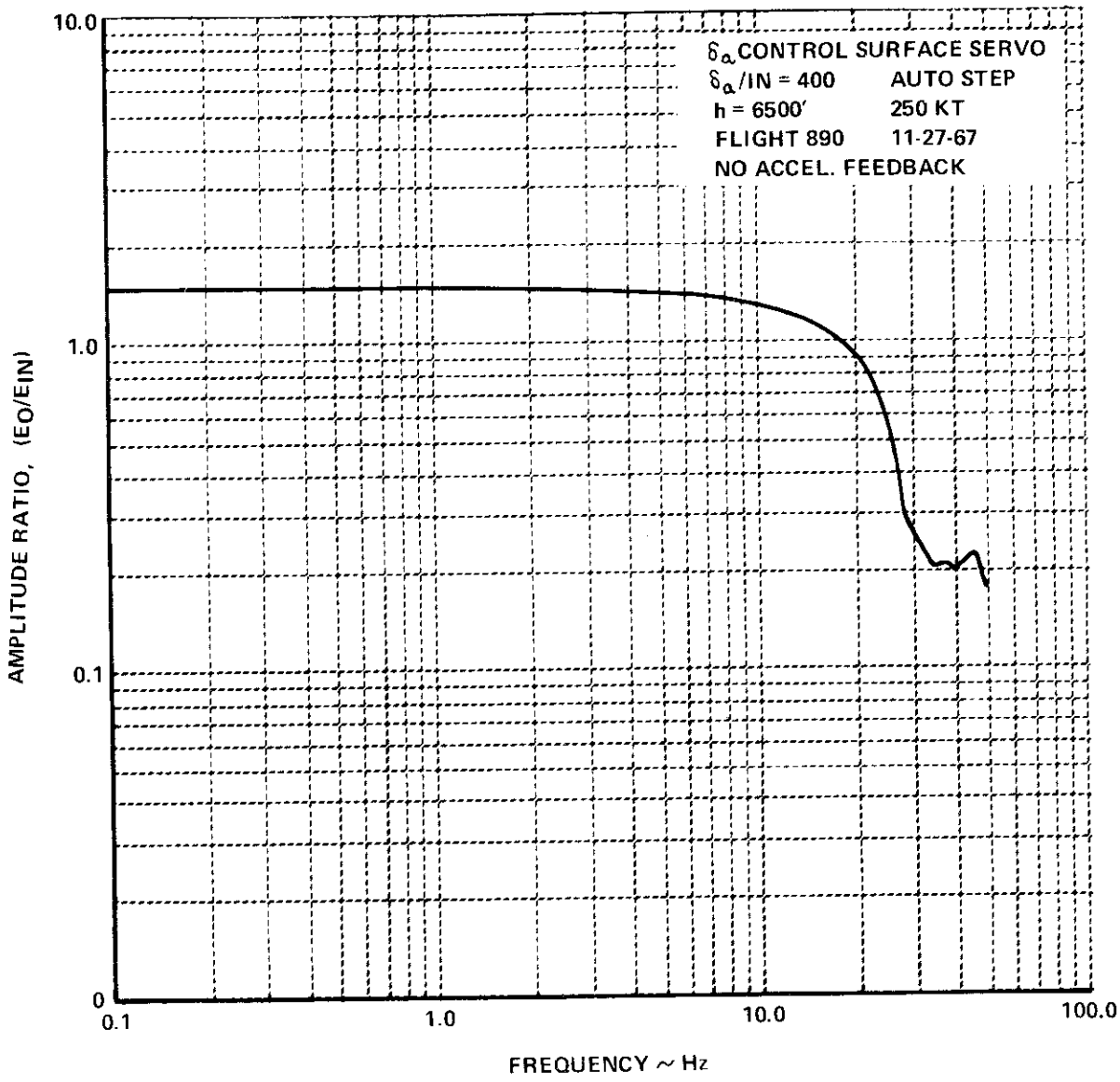

Figure VI-41 AILERON CONTROL SURFACE SERVO RESPONSE, AMPLITUDE VS FREQUENCY

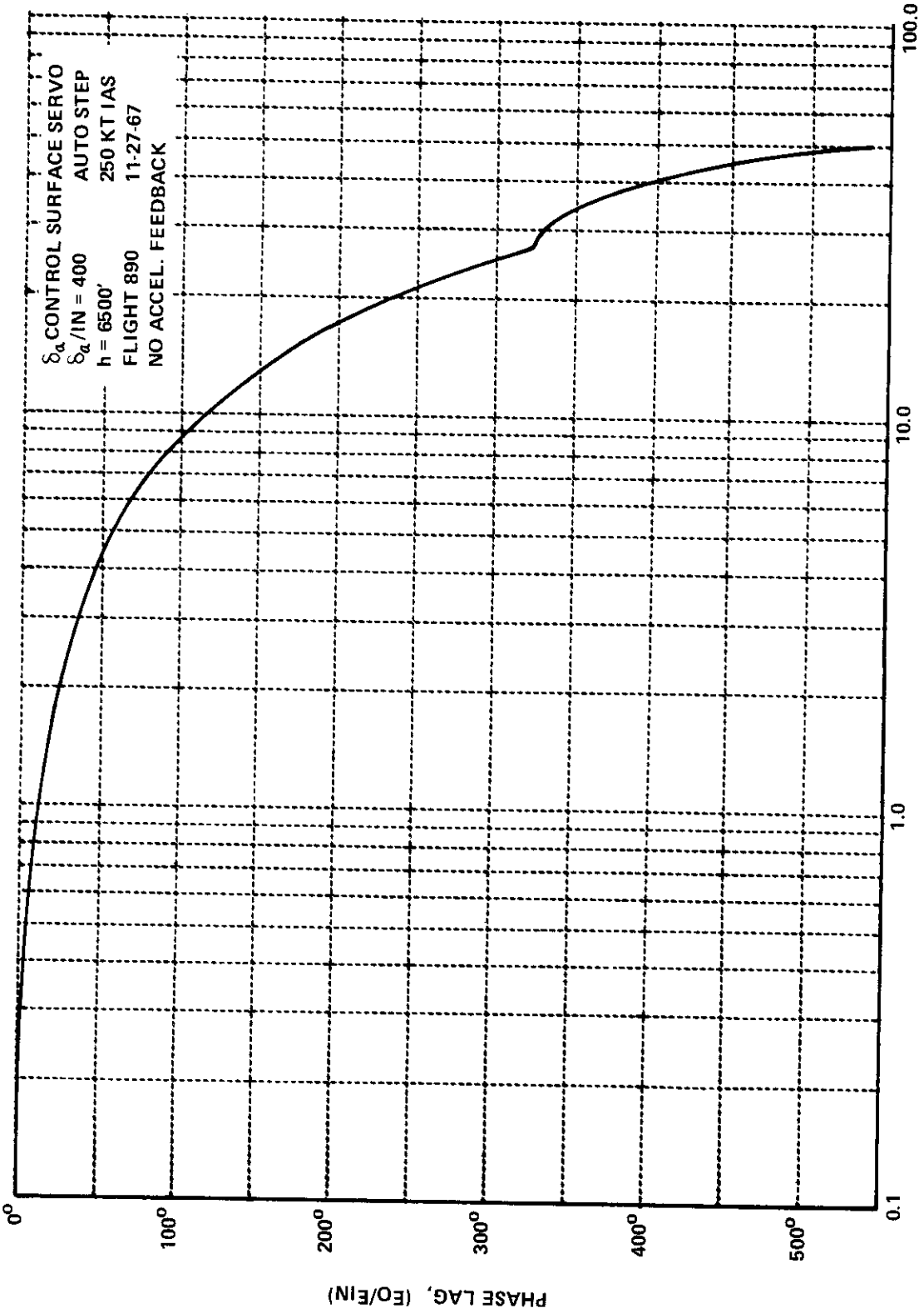

Figure VI-42 AILERON CONTROL SURFACE SERVO RESPONSE, PHASE LAG VS FREQUENCY

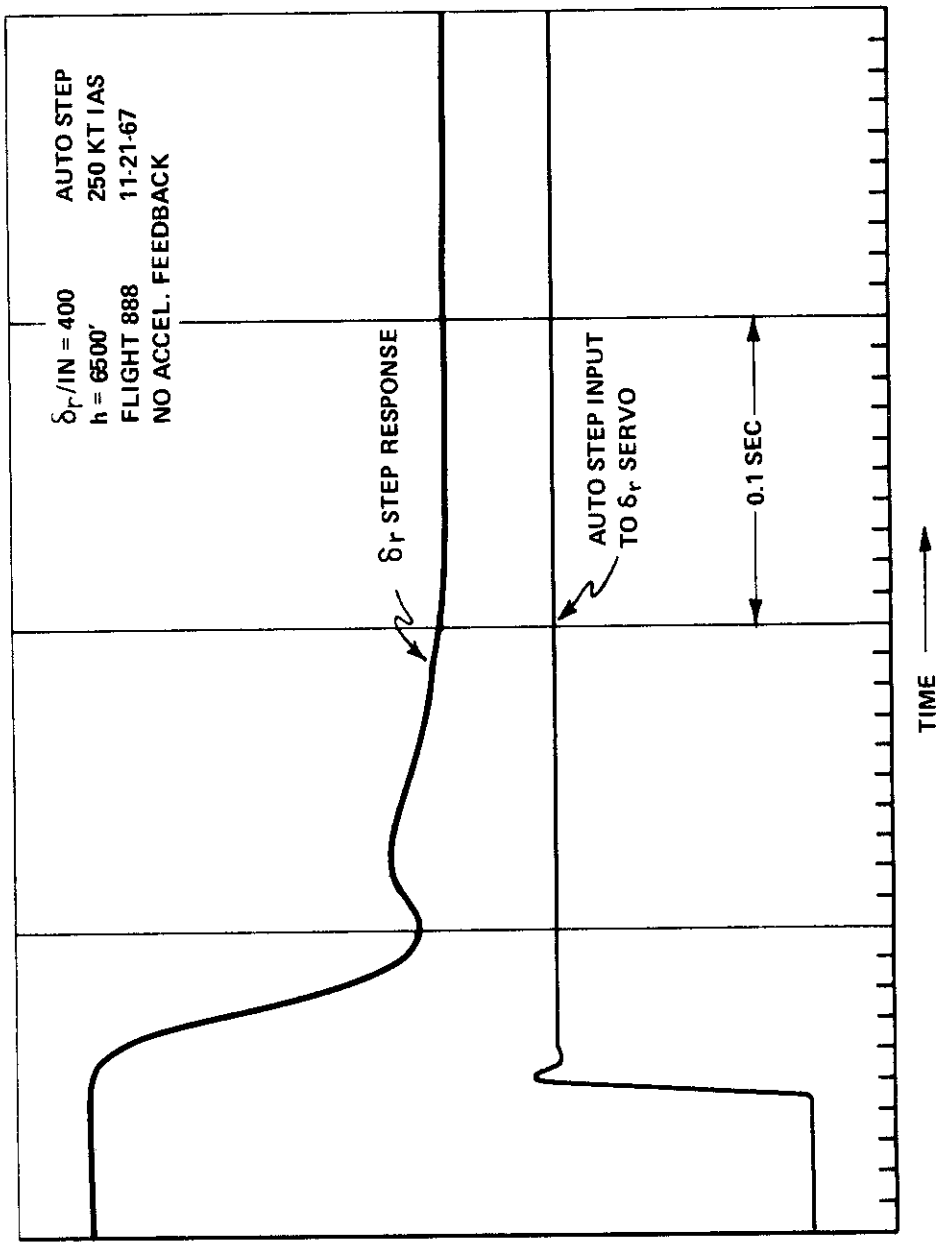

Figure VI-43 δ_r CONTROL SURFACE SERVO STEP RESPONSE, OSCILLOGRAPH RECORDINGS, NO RECORDING FILTERS

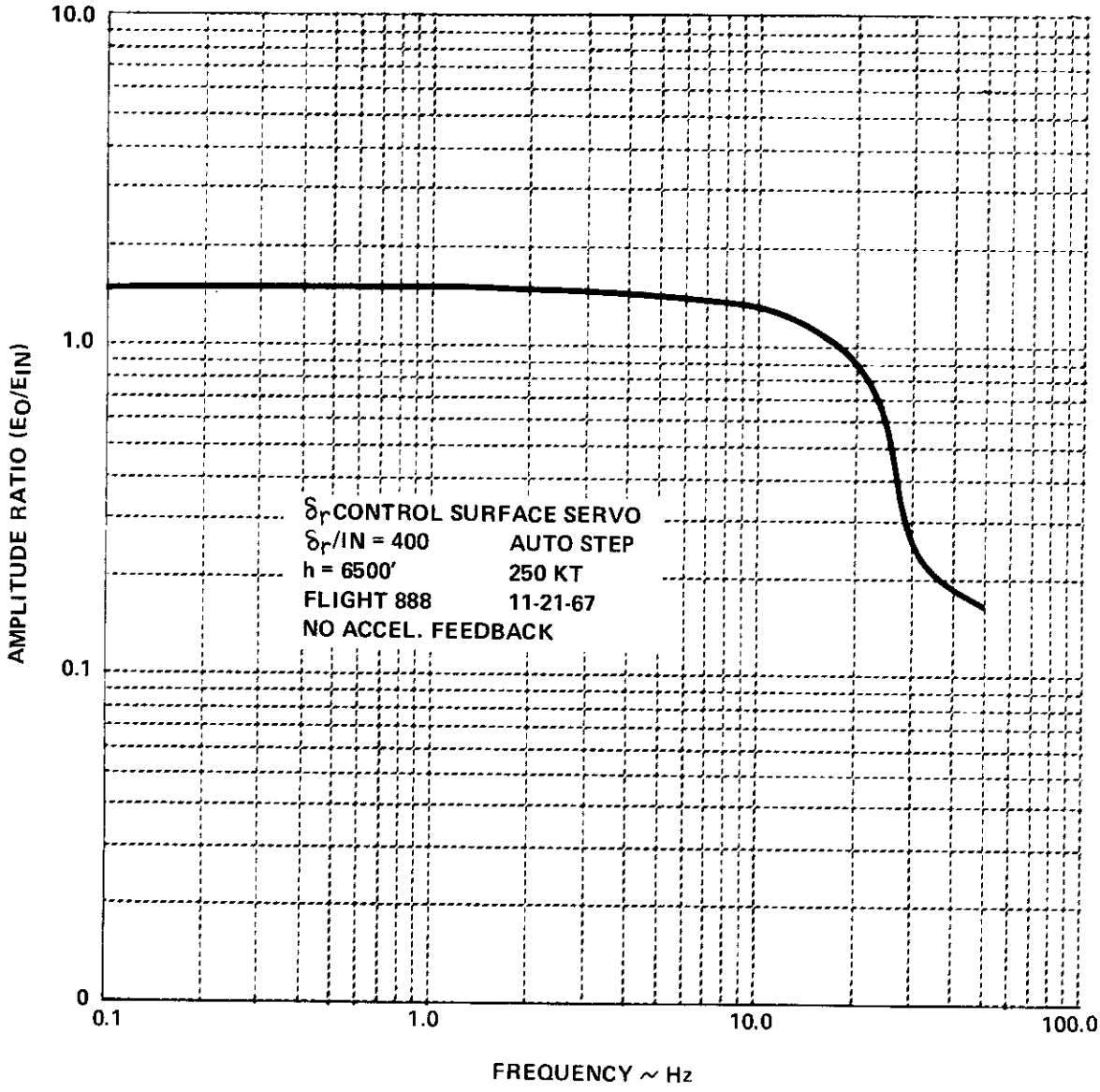

Figure VI-44 RUDDER CONTROL SURFACE SERVO RESPONSE, AMPLITUDE VS FREQUENCY

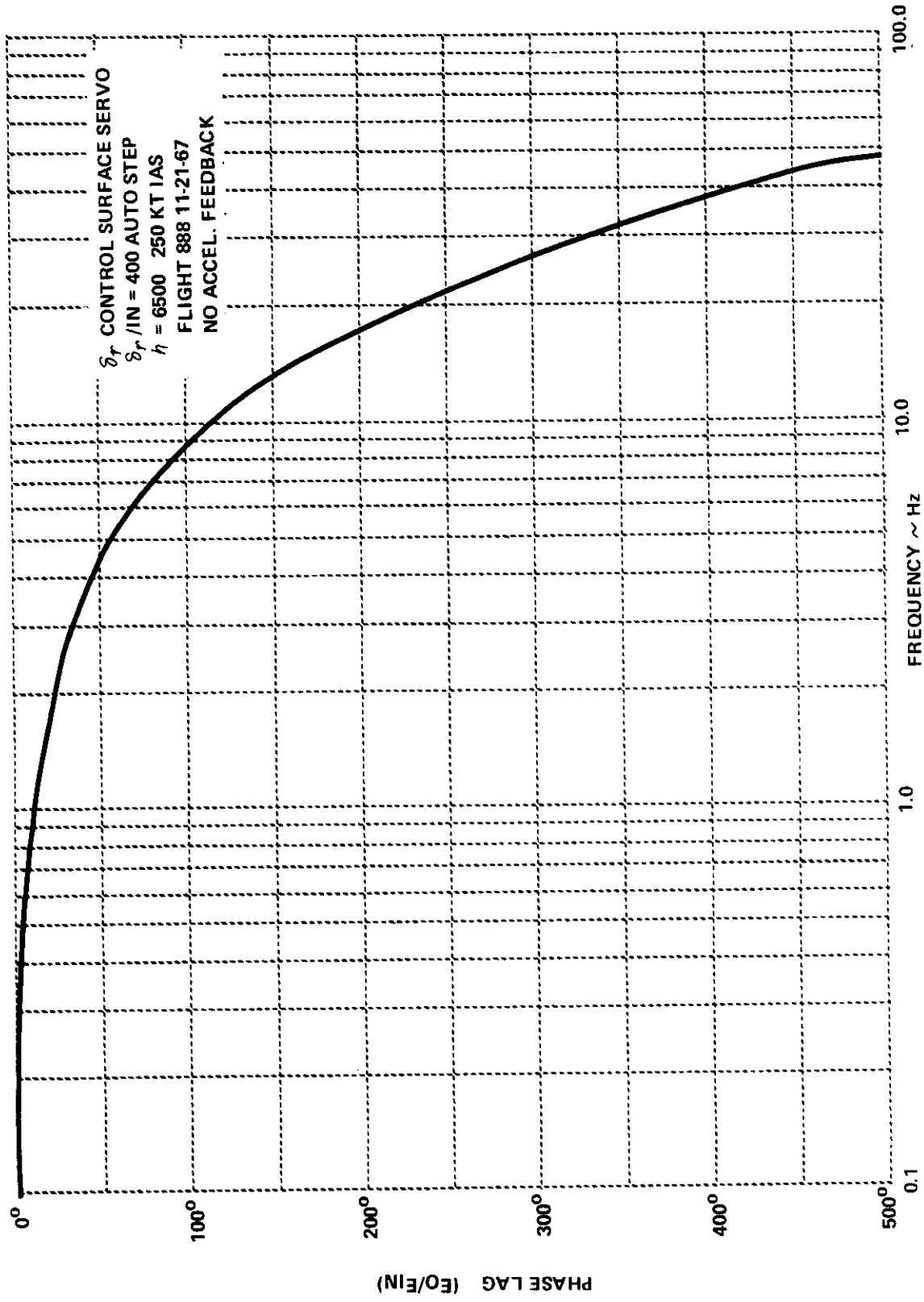

Figure VI-45 RUDDER CONTROL SURFACE SERVO RESPONSE, PHASE LAG VS FREQUENCY

APPENDIX VII
EQUIVALENT FIRST-ORDER TIME CONSTANT TO REPRESENT AN OVERALL VSS CHANNEL LAG

A procedure for estimating an equivalent first-order time constant to represent an overall variable stability channel lag is given.

Most of the variable stability system channels contain a number of components such as sensors, low pass and notch filters, each of which contribute to the overall channel lag.

The most accurate way to determine the response of such a channel is to perform a frequency response test on it so that all the components are included. This should be done whenever possible. However, if the characteristics of the individual components are known, a reasonable approximation can be obtained by summing their effects. This summing process can be done by adding the actual frequency response curves (phase versus frequency) for each component and then converting this to an equivalent first-order lag.

A quicker way to get the total phase lag of all the components in a channel, which should be accurate enough for most applications, is described below.

ESTIMATION OF AN EQUIVALENT LAG TO REPRESENT EACH OF THE INDIVIDUAL COMPONENTS IN A VSS CHANNEL

The dynamics of the components are typically first order $\frac{1}{\tau s+1}$, second order $\frac{\omega_n^2}{s^2+2\zeta\omega_n s+\omega_n^2}$, or higher order with the characteristics of linear phase shift and small amplitude change within the range of frequencies of interest. Plots showing phase angle and amplitude ratio variations with frequency are presented on Figure VII-1 for the first-order and on Figure VII-2 for the second-order systems.

We wish to represent each of these forms of response by a pure lag $e^{-i\omega\tau}$, i.e., linear phase shift given by $\phi = \omega\tau$ and constant unity amplitude ratio. Figures VII-1 and VII-2 show that this is a valid representation in the frequency range $0 < \omega\tau < 0.3$ for the first-order response and $0 < \frac{\omega}{\omega_n} < 0.4$ (or higher, depending on the damping ratio) for the second-order response.

To determine the appropriate value of τ for a first-order system in terms of a pure lag ($\omega\tau = \theta$) we have

$\omega\tau = 1$ when ϕ = 57.3 deg (1 radian) See Figure VII-2

PURE LAG $\bar{e}^{i\tau\omega} = 1 \angle -\tau\omega = 1 \angle \phi_3$

FIRST ORDER $\frac{1}{i\tau\omega+1} = \frac{1}{\sqrt{\tau^2\omega^2+1}} \angle TAN^{-1}(-\tau\omega) = \sqrt{\tau^2\omega^2+1} \angle \phi_2$

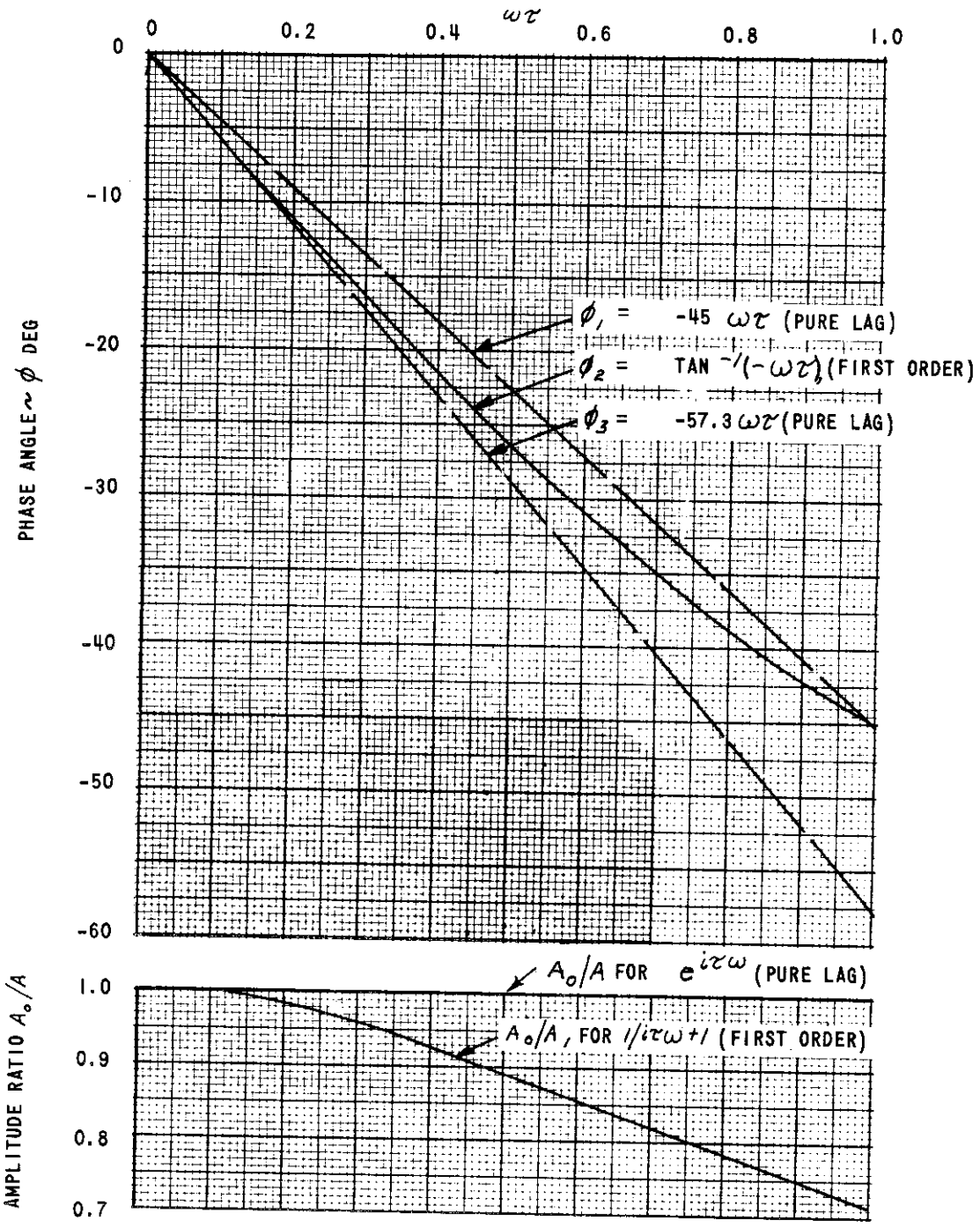

Figure VII-1 VARIATION OF PHASE ANGLE AND AMPLITUDE RATIO WITH FREQUENCY FOR FIRST-ORDER SYSTEM AND "PURE LAGS"

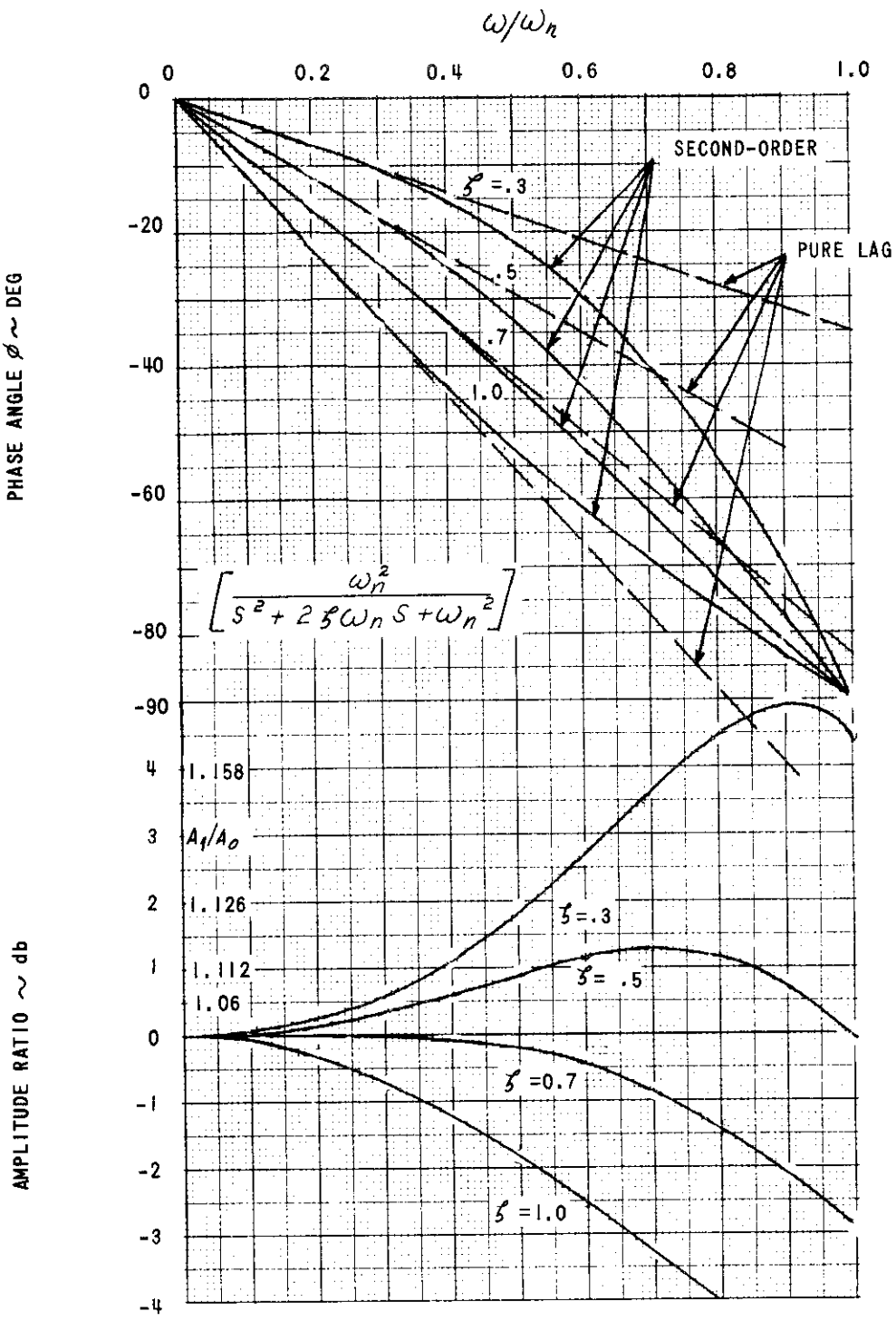

Figure VII-2 VARIATION OF PHASE ANGLE AND AMPLITUDE RATIO WITH FREQUENCY FOR SECOND-ORDER SYSTEM WITH VARIOUS VALUES OF DAMPING RATIO

For a second-order system

$\omega\tau = \frac{\omega}{\omega_n} = 1$ when	$\phi = 35°$	$\zeta = 0.3$
	$\phi = 58°$	$\zeta = 0.5$
	$\phi \doteq 82.5°$	$\zeta = 0.7$
See Figure VII-1	$\phi = 110°$	$\zeta = 1.0$

For higher-order components having a linear phase shift with frequency, the pure lag formula $\omega\tau = \phi$ is also used. More is said about this in the example given for higher-order systems.

Example 1 - First-Order Component

To find the equivalent lag to represent a first-order component having a corner frequency, ω_n, at 10 Hz which will be valid for frequencies upto 1.0 Hz.

For a first-order system, $\omega\tau = 1$ when $\phi = 45°$ and the corresponding ω is the corner frequency ω_n. Solving for the time lag in terms of pure lag we have

$$\omega\tau = 57.3 \text{ deg}$$

$$\tau = \frac{57.3 \text{ deg}}{(10)(2\pi)(57.3)} = 0.0159 \text{ sec}$$

Example 2 - Second-Order Component

To find the equivalent lag to represent a second-order component having a natural frequency, ω_n, to 20 Hz and a damping ratio, ζ, of 0.5 which will be valid up to frequencies of 5 Hz. Figure VII-2 shows the variation of phase angle with frequency for the second-order system response. To match phase variation up to ω = 5 Hz (i.e., $\omega/\omega_n = 5/20 = 0.25$), we will use a tangent to the $\zeta = 0.5$ curve which coincides with the true variation up to at least $\omega/\omega_n = 0.25$. This defines a ϕ at $\omega/\omega_n = 1$ of 58°. Then using the expression $\omega\tau = \phi$, which is the form for our pure lag, we get:

$$\tau_{equivalent} = \frac{\phi}{\omega_n} = \frac{58°}{204360} = 0.00805$$

It will be noticed that for frequencies up to $\omega/\omega_n = 0.25$, the amplitude ratio has departed from unity by only 0.25 dB (i.e., $A/A_o = 1.03$). Thus, the form of pure lag assumed has matched the phase variation almost exactly, and the amplitude to within 3 percent.

Example 3 - Higher-Order Component

To match the response of a higher-order system, or any component for which the frequency response plot has the form of a linear phase shift with approximately zero amplitude attenuation.

To match the equivalent lag form $\omega\tau = \phi$, simply use the slope of the ω versus phase shift line (ϕ) for the higher-order component, so that

$$\tau = \frac{\phi}{\omega \times 360}$$

The disadvantage here is that a frequency response plot of the higher-order component is needed, whereas for the second-order system, only knowledge of the components ω_n and ζ are required, and for the first-order system, only knowledge of the corner frequency of the component is required.

Once the τ for each component in a VSS loop has been determined in the form of a pure lag they can be added ($\tau_{total} = \tau_1 + \tau_2 + \tau_3 + \ldots$) and the total τ expressed in the first order form $\left(\frac{1}{1+\tau s}\right)$ for use in gain compensation equations.

APPENDIX VIII
LIST OF REPORTS RESULTING FROM RESEARCH WORK PERFORMED IN THE VARIABLE STABILITY T-33

Much of the preliminary ground work that resulted in the concept and actual construction of the variable stability T-33 was done at the Cornell Aeronautical Laboratory, Inc. The listing in this appendix includes those reports which were a direct result of work performed in the T-33 up to the publication of this report. FRM 430 (Reference 10) contains a periodically updated listing of publications produced by the Flight Research Department pertaining to variable stability airplanes - their development and research use.

LIST OF T-33 REPORTS

Flight Research Department: Installation of an Automatic Control System in a T-33 Airplane for Variable Stability Research. Part 1 - Preliminary Investigation and Design Studies. WADC-TR 55-156, Part I (CAL Report No. TB-936-F-1), April 1955. Contract No. AF33(616)-2578.

Flight Research Department: Installation of an Automatic Control System in a T-33 Airplane for Variable Stability Research. Part II - Detail Design, Fabrication and Installation. WADC TR 55-156, Part 2 (CAL Report No. TB-936-F-2), September 1956. Contract No. AF33(616)-2578.

Beilman, J.L. and Harper, R.P.: Installation of an Automatic Control System in a T-33 Airplane for Variable Stability Research. Part III - Ground and Flight Checkout. WADC TR 55-156, Part 3 (CAL Report No. TB-936-F-3), August 1957. Contract AF33(616)-2578.

Infanti, N.L.: Augmented Capabilities of the Variable Stability T-33 Airplane for Ground and Flight Handling Qualities Evaluations. CAL Report No. TE-1243-F-1, November 1960. Contract AF33(616)-5823.

Harper, R.P.,Jr.: In-Flight Simulation of the Lateral-Direction Handling Qualities of Entry Vehicles. WADC TR-61-147 (CAL Report No. TE-1243-F-2), February 1961. Contract AF33(616)-5823.

Newell, F.: Wind Tunnel Tests of High Drag Devices on a 10% Scale Model of the T-33 Airplane. CAL Report No. TE-1462-F-1, January 1961. Contract No. AF33(616)-7517.

Newell, F.: Variable L/D Wind Tunnel Data Analysis and System Design. CAL Report No. TE-1462-F-2, January 1961, Contract No. AF33(616)-7517.

Brady, W.: T-33 Variable L/D Project Flutter Model Tests. Addendum to CAL Report No. TE-1462-F-2, April 1961. Contract No. AF33(616)-7517.

Newell, F., Dolbin, B., and Schelhorn, A.: Development and Flight Calibration of a Variable-Drag Device on a Variable Stability T-33 Airplane. ASD-TDR-62-910 (CAL Report No. TE-1462-F-3), August 1963. Contract No. AF33(616)-7517.

Kidd, E.A. and Harper, R.P.: Fixed-Base and In-Flight Simulations of Longitudinal and Lateral-Directional Handling Qualities for Piloted Re-Entry Vehicles. ASD-TDR-61-362 (CAL Report No. TE-1516-F-1), October 1963. Contracts No. AF33(616)-5823 and AF33(616)-7753.

Chalk, C.: Fixed-Base Simulator Investigation of the Effects of L_α and True Speed on Pilot Opinion of Longitudinal Flying Qualities. ASD-TDR-63-399 (CAL Report No. TB-1630-F-1), November 1963. Contract No. AF33(657)-7442.

Newell, F.D.: Simulator Evaluation of Airplane Longitudinal Responses for the Instrument Landing Approach. FDL-TDR-64-84 (CAL Report No. TB-1630-F-2), April 1964. Contract No. AF33(657)-7442.

Chalk, C.: Flight Evaluation of Various Short Period Dynamics at Four Drag Configurations for the Landing Approach Task. FDL-TDR-64-60 (CAL Report No. TB-1630-F-3), April 1964. Contract No. AF33(657)-7442.

Smith, E.H. and DiFranco, D.A.: In-Flight Evaluation of Certain Lateral-Directional Handling Qualities of High-Performance Aircraft. AFFDL-TR-65-97 (CAL Report No. TC-1734-F-1), December 1965. Contract No. AF33(657)-9713.

Newell, F.D.: Ground Simulator Evaluations of Coupled Roll-Spiral Effects on Aircraft Handling Qualities. AFFDL-TR-65-39 (CAL Report No. TC-1921-F-1), March 1965. Contract No. AF33(615)-1253.

Key, D.L.: A Functional Description and Working Data for the Variable Stability System T-33 Airplane. CAL Report No. TC-1921-F-2, October 1965. Contract No. AF33(615)-1253.

DiFranco, D.A.: In-Flight Parameter Identification by the Equations-of-Motion Technique - Application to the Variable Stability T-33 Airplane. CAL Report No. TC-1921-F-3, December 1965. Contract No. AF33(615)-1253.

Chalk, C.: Flight Evaluation of Various Phugoid Dynamics and $1/\tau_{h_1}$ Values for the Landing Approach Task. AFFDL-TR-66-2 (CAL Report No. TC-1921-F-4), February 1966. Contract No. AF33(615)-1253.

Meeker, J.I.: Evaluation of Lateral-Directional Handling Qualities of Piloted Re-Entry Vehicles Utilizing Fixed-Base and In-Flight Evaluations. NASA CR-778 (CAL Report No. TC-1921-F-5), January 1966. Contract No. AF33(615)-1253.

DiFranco, D.A.: Flight Investigation of Longitudinal Short Period Frequency Requirements and PIO Tendencies. AFFDL-TR-66-163 (CAL Report No. TC-2083-F-1), April 1967. Contract No. AF33(615)-2536.

Parrag, Michael L.: Pilot Evaluations in a Ground Simulator of the Effects of Elevator Control System Dynamics in Fighter Aircraft. AFFDL-TR-67-19 (CAL Report No. TC-2083-F-2), July 1967. Contract No. AF33(615)-2536.

Wasserman, R. and Newell, F.D.: In-Flight Investigation of the Effect on PIO of Control System Nonlinearities, Pitch Acceleration and Normal Acceleration Bobweights. AFFDL-TR-69-3 (CAL Report No. BM-2238-F-1), July 1967. Contract No. AF33(615)-3294.

Meeker, J.I. and Hall, G.W.: In-Flight Evaluation of Lateral-Directional Handling Qualities for the Fighter Mission. AFFDL-TR-67-98 (CAL Report No. BM-2238-F-2, July 1967. Contract No. AF33(615)-3294.

DiFranco, D.A. and Saunders, G.H.: An In-Flight Simulation of Handling Qualities of SV-5P (Pilot) Lifting Body With Various Feedback Gains and Rudder to Aileron Interconnect Ratios. (Title Unclassified), AFFDL-TR-67-135 (CAL Report No. BM-2238-F-3), November 1967. Report Confidential. Contract No. AF33(615)-3294.

DiFranco, D.A.: In-Flight Investigation of the Effects of Higher-Order Control System Dynamics on Longitudinal Handling Qualities. AFFDL-TR-68-90 (CAL Report No. BM-2238-F-4), July 1968. Contract No. AF33(615)-3294.

Hall, G. Warren: In-Flight Investigation of Longitudinal Short-Period Handling Characteristics of Wheel-Controlled Airplanes. AFFDL-TR-68-91 (CAL Report No. BM-2238-F-5), July 1968. Contract No. AF33(615)-3294.

Newell, F.D.: Human Transfer Characteristics in Flight and Ground Simulation for the Roll Tracking Task. AFFDL TR-67-30 (CAL Report No. TE-2256-F-1), 1st Revision, January 1968. Contract No. AF33(615)-3605.

Hall, G. Warren: An In-Flight Investigation of Lateral-Directional Dynamics for Cruising Flight. FAA ADS 69-13 (CAL Report No. TB-2710-F-1), December 1969. Contract No. F33615-69-C-1040.

Neal, T.P. and Smith, R.E.: An In-Flight Investigation to Develop Control System Design Criteria for Fighter Airplanes. AFFDL-TR-70-74, Vols. I and II, June 1970.

REFERENCES

1. Key, David L.: "A Functional Description and Working Data for the Variable Stability System T-33 Airplane". CAL Report No. TC-1921-F-2, October 1965.

2. Newell, F. D., B. Dolbin, and A. Schelhorn: "Development and Flight Calibration of a Variable-Drag Device on a Variable Stability T-33 Airplane". CAL Report No. TE-1462-F-3 (ASD-TDR-62-910), August 1963.

3. Neel, R., C. L. Johnson, and R. W. Theriault:" Tests of a 1/5 Scale Wind Tunnel Model of the F-80C Trainer". Lockheed Aerodynamics Laboratory Report No. LAL 127, January 23, 1948.

4. Klawans, B.B., and J. A. White: "A Method Utilizing Data on the Spiral, Roll-Subsidence, and Dutch Roll Modes for Determining Lateral Stability Derivatives From Flight Measurements". NACA Technical Note 4066, August 1957.

5. Bihrle, W., Jr.: "A Handling Qualities Theory for Precise Flight Path Control". AFFDL-TR-65-198, June 1966.

6. Connelly, M.E.: "Simulation Aircraft". Tech. Report NAVTRADEVCEN 7591-R-1, February 1958.

7. Bradley, W. G.: "The In-Flight Calibration of Sideslip Vanes Using the Flat-Turn Technique". C of A Report Aero No. 168, 1964.

8. Shapiro, R.: "Compressible Flow". Volume 1, p.399

9. Alianello, D. and A. Schelhorn: "T-33 Surface Servo Revisions". HQI Memo No. 6, 6 June 1966.

10. Martino, J.A.: "Bibliography of Reports on Variable Stability Aircraft". FRM 423, April 1970.

11. Weingarten, N. and Wasserman, R.: "An Analytical Method to Compute Cockpit and Nose Potentiometer Settings for Lateral-Directional Simulation in the Variable Stability T-33." AFFDL-TR-70-73, August 1970.

UNCLASSIFIED
Security Classification

DOCUMENT CONTROL DATA - R & D

(Security classification of title, body of abstract and indexing annotation must be entered when the overall report is classified)

1. ORIGINATING ACTIVITY *(Corporate author)*
Cornell Aeronautical Laboratory, Inc.
Box 235
Buffalo, New York 14221

2a. REPORT SECURITY CLASSIFICATION
UNCLASSIFIED

2b. GROUP

3. REPORT TITLE
SYSTEM DESCRIPTION AND PERFORMANCE DATA FOR THE USAF/CAL VARIABLE STABILITY T-33 AIRPLANE

4. DESCRIPTIVE NOTES *(Type of report and inclusive dates)*
R&D Final Technical Report

5. AUTHOR(S) *(First name, middle initial, last name)*
Hall, G. Warren and Huber, Ronald W.

6. REPORT DATE
July 1970

7a. TOTAL NO. OF PAGES
300

7b. NO. OF REFS
11

8a. CONTRACT OR GRANT NO.
F33615-69-C-1664

b. PROJECT NO.
8219

c. Task No. 82190

d.

9a. ORIGINATOR'S REPORT NUMBER(S)
CAL Report No. BM-2821-F-2

9b. OTHER REPORT NO(S) *(Any other numbers that may be assigned this report)*
AFFDL-TR-70-71

10. DISTRIBUTION STATEMENT
This document is subject to special export controls and each transmittal to foreign governments or foreign nationals may be made only with prior approval of the Air Force Flight Dynamics Laboratory (FDCC) W-PAFB, Ohio 45433.

11. SUPPLEMENTARY NOTES
The distribution of this report is limited because it contains information that has or could have future application to military systems.

12. SPONSORING MILITARY ACTIVITY
Air Force Flight Dynamics Laboratory (FDCC)
Wright-Patterson Air Force Base, Ohio45433

13. ABSTRACT

The USAF/CAL variable stability T-33 airplane is a jet trainer which has been extensively modified for use as a research vehicle. A response-feedback system allows the normal T-33 derivatives to be augmented so that handling qualities of existing airplanes, future airplanes, or hypothetical configurations may be simulated in flight or in a fixed-base ground simulator. This report has been prepared in an attempt to provide an updated functional description of the variable stability T-33. The information is presented for setting up a simulation program and for performing calibration procedures. A brief description of the equipment and airplane systems is also included.

DD FORM 1 NOV 65 1473

UNCLASSIFIED
Security Classification

14. KEY WORDS	LINK A		LINK B		LINK C	
	ROLE	WT	ROLE	WT	ROLE	WT
Variable Stability Airplane Response-Feedback Flight Control System Flight Data Recording Equipment In-Flight Simulator Fixed-Base Simulator						